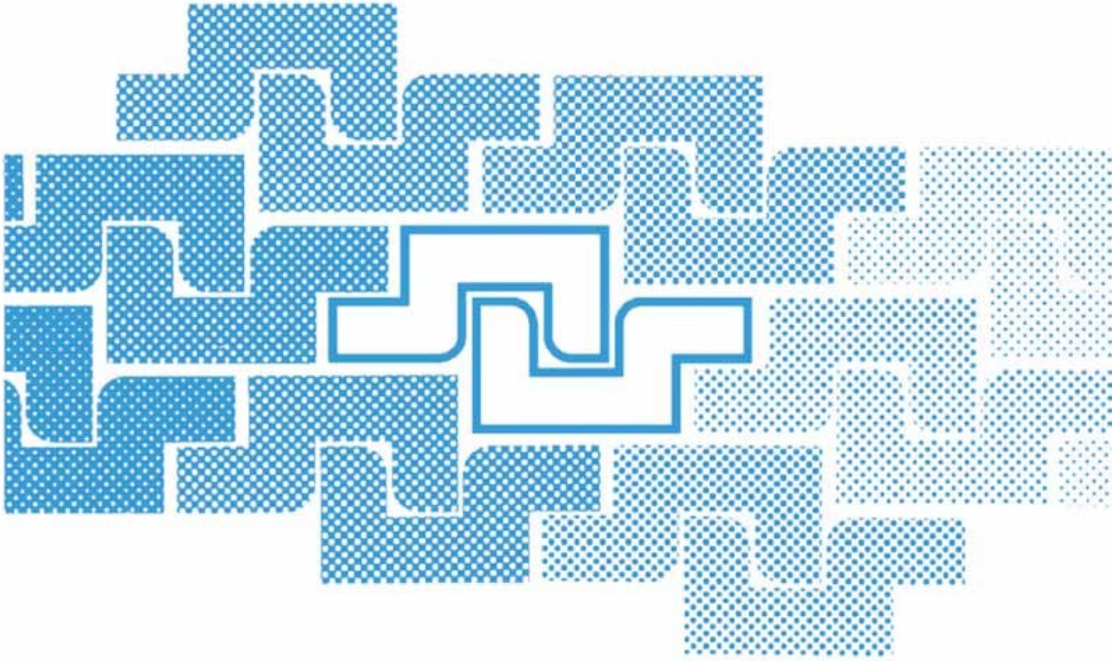

Nonlinear Waves: Classical and Quantum Aspects

Edited by

Fatkhulla Kh. Abdullaev and
Vladimir V. Konotop

NATO Science Series

II. Mathematics, Physics and Chemistry – Vol. 153

Nonlinear Waves: Classical and Quantum Aspects

NATO Science Series

A Series presenting the results of scientific meetings supported under the NATO Science Programme.

The Series is published by IOS Press, Amsterdam, and Kluwer Academic Publishers in conjunction with the NATO Scientific Affairs Division

Sub-Series

I. Life and Behavioural Sciences	IOS Press
II. Mathematics, Physics and Chemistry	Kluwer Academic Publishers
III. Computer and Systems Science	IOS Press
IV. Earth and Environmental Sciences	Kluwer Academic Publishers
V. Science and Technology Policy	IOS Press

The NATO Science Series continues the series of books published formerly as the NATO ASI Series.

The NATO Science Programme offers support for collaboration in civil science between scientists of countries of the Euro-Atlantic Partnership Council. The types of scientific meeting generally supported are "Advanced Study Institutes" and "Advanced Research Workshops", although other types of meeting are supported from time to time. The NATO Science Series collects together the results of these meetings. The meetings are co-organized bij scientists from NATO countries and scientists from NATO's Partner countries – countries of the CIS and Central and Eastern Europe.

Advanced Study Institutes are high-level tutorial courses offering in-depth study of latest advances in a field.
Advanced Research Workshops are expert meetings aimed at critical assessment of a field, and identification of directions for future action.

As a consequence of the restructuring of the NATO Science Programme in 1999, the NATO Science Series has been re-organised and there are currently Five Sub-series as noted above. Please consult the following web sites for information on previous volumes published in the Series, as well as details of earlier Sub-series.

http://www.nato.int/science
http://www.wkap.nl
http://www.iospress.nl
http://www.wtv-books.de/nato-pco.htm

Series II: Mathematics, Physics and Chemistry – Vol. 153

Nonlinear Waves: Classical and Quantum Aspects

edited by

Fatkhulla Kh. Abdullaev

Physical-Technical Institute,
Uzbek Academy of Sciences,
Tashkent, Uzbekistan

and

Vladimir V. Konotop

Centro de Fisica Teórica e Computacional,
Universidade de Lisboa, Portugal
Departamento de Física,
Faculdade de Ciências,
Universidade de Lisboa, Portugal

KLUWER ACADEMIC PUBLISHERS
NEW YORK, BOSTON, DORDRECHT, LONDON, MOSCOW

eBook ISBN: 1-4020-2190-9
Print ISBN: 1-4020-2188-7

Created in the United States of America

Visit Springer's eBookstore at: http://ebooks.kluweronline.com
and the Springer Global Website Online at: http://www.springeronline.com

Contents

Preface

After the discovery of a solitary wave by J.S. Russel almost one and half century ago and later implementation of the soliton conception into the modern physics by Zabusky and Kruskal in 1967, the topic continues to be intensively investigated. Initially the main interest in the soliton theory was related to the hydrodynamics, then to plasma physics and to nonlinear optics. Now the focus is shifted toward the condensed matter physics and biophysics. One of the latest intriguing subjects of the nonlinear science is a theory of nonlinear waves in the Bose-Einstein condensates (BEC's).

The soliton theory is an interdisciplinary topic, where many ideas from mathematical physics, statistical mechanics, nonlinear optics, solid state physics and quantum theory mutually benefit each others. Many of applications of the theory in different areas are based on similar model equations and thus allow unified theoretical approaches. Since the most of the systems are intrinsically quantum, like in linear physics, the nonlinear phenomena have two well pronounced levels of description: classical (or mean filed) one and quantum one. There are also other common features of practical applications of the soliton theory to different systems. They are inevitable presence of noise or thermal fluctuations, effect of disorder, interplay among different physical phenomena including nonlinearity, dispersion, and periodicity or discreteness, etc.

The Estoril Workshop "*Nonlinear Waves: Classical and Quantum Aspects*" (July 13-17, 2003) was focused on various aspects of the nonlinear wave theory and its particular applications. The topics discussed on the Workshop are related to the BEC theory, nonlinear optical phenomena, and discrete nonlinear systems.

The main objective was to explore analogies between the problems occurring in the different areas. Probably the most important example is given by the mean field Gross-Pitaevskii (GP) equation which has a form of the multidimensional nonlinear Schrödinger (NLS) equation with a trap potential, and as such is similar to standard models of the nonlinear optics of the Kerr media. On the other hand, in a number

of cases (in the so-called tight-biding approximation) the GP equation is reduced to a discrete NLS equation (which is a differential-difference equation, also called lattice). Thus, experience acquired on the earlier stages of the development of the nonlinear optics and the lattice theory appears to be very useful for the analysis of the BEC problems.

The first part of the book contains contributions having interdisciplinary character or devoted mainly to mathematical aspects of the nonlinear evolution equations. It starts with the algebro-geometric integration of the GP equation (Enolski) and an analytical method for describing N-soliton interactions (Gerdjikov). Next, different mechanisms of the dynamical stabilization of nonlinear waves by periodic in time modulations of a trap potential, nonlinearity, and dispersion, as well their applications to the nonlinear optics and BEC problems, are analyzed (Abdullaev). A new concept of the nonlinear physics, referred to as dissipative solitons, is described by Akhmediev, Soto-Crespo and Ankiewicz. In the subsequent contributions a large variety of remarkable structures – solitons and vortices – which are relevant to the meanfiled theory of BEC's are presented for cases of a periodic (Baizakov, Malomed and Salerno) and harmonic (Crasovan *et. al.*) potentials. Białynicki-Birula and Sowiński describe a model, the logarithmic nonlinear Schrödinger equation, allowing a number of exact results, a rather rear event in the nonlinear science. An issue of recent interest, the effect of geometry on wave propagation with applications to the theory of photonic crystals is discussed by Gaididei *et al.* Next, the effect of nonlocality on the dynamics of breathers and kinks (Alfimov, Pierantozzi and Vázquez) and new phenomena described in terms of the fractional calculus (Vázquez) are presented. The dynamical behavior of matter coupled to gravity is considered in the contribution by Christodoulakis *et al.* De Lillo and Sanchini discuss various stochastic effects which can be obtained within the framework of the Eckhaus equation. Grecu and Visinescu study various aspects of the modulational instability of nonlinear systems. Collisions between nonlinear Schrödinger solitons and bound quantum states in localized one-dimensional potentials are investigated by Ludu. The study of oscillator-wave interaction is presented in the article by Damgov and Trenchev.

The second part is devoted to a number of latest experimental and theoretical results in the physics of BEC's, a field which received a great deal of attention during the last years. The chapter begins with a brief review on unified approach to BEC from the point of view of the nonlinear quantum mechanics with main emphasis on fundamental problems of superfluidity and BEC in optical lattices (Pitaevskii), and with basics of statistical mechanics of quantum integrable systems within the frame-

work of the approximation of a hard core Bose-gas (Wadati, Kato and Iida). Next, a number of exciting experimental results on BEC's in optical lattices obtained in the Florence (Fort and Fallani) and Pisa (Morsch and Arimondo) experimental groups are reported. Superfluid-insulator transition, expansion of BEC's in moving optical lattices, Landau-Zener tunneling and instabilities are some of them. Theoretical investigations of BEC's embedded in optical lattices, presented in this chapter, deal with the problem of quantum bound states and matter waves delocalization (Salerno), with the use of Feschbach resonance for generation of soliton trains (Brazhnyi and Konotop), and with nonlinear periodic waves in two-component BEC's (Kostov *et al*). Finally, a study of creation and evolution of shock waves in BEC's is reported (Kamchatnov, Gammal and Kraenkel).

The third part is devoted to propagation of electromagnetic waves in different physical systems. As it was already mentioned, the related problems have many similarities with the dynamics of matter waves in BEC systems. Here a waveguide structure plays the role of a trap, while the Kerr nonlinearity plays the role of the effective nonlinearity induced by elastic interactions between two atoms. Nonlinear photonics and BEC in optical lattices also share many common properties. The chapter starts with the study of light propagation in 2D nonlinear photonic structures with defects (Aceves and Dohnal), in quantum dot ensembles (Maimistov), and in surface polaritonic crystals (Darmanyan, Nevière and Zayats). Light propagation in the media with cubic-quintic nonlinearities, including generation of sophisticated coherent structures like pulsed beams, vortices and vortex solitons, as well as instabilities, are presented by Michinel, Paz-Alonso and Salgueiro and by Skarka, Aleksic and Berezhiani. This part of the book contains also reports on propagation of extremely short pulses on the basis of Maxwell-Duffing equations (Kazantzeva), various aspects of statistics of soliton propagation in optical fibers (Boscolo, Derevyanko and Turitsyn; Villarroel), some exactly solvable models for the nonlinear electrodynamics (Shvartsburg).

In the last part of the book classical and quantum aspects of dynamics of anharmonic lattices are are discussed. Consideration is focused on the topics as follows: the quantum breathers in a Hubbard model (Eilbeck and Palmero); the relation between the energy localization in solids and molecules and the first order phase transition (Takeno and Suzuki); propagation of discrete solitons in long disordered Ablowitz-Ladik and Toda chains (Garnier); ultrafast electron transfer in different systems (Aubry). Also the chapter contains recent experimental results demonstrating that self-trapping is a common feature in hydrogen bonded systems (Edler and Hamm); discussion of a concept of quantum anharmonic phonons

and their properties for the Fermi-Pasta-Ulam chain (Szeftel); new results on the perturbation theory for discrete solitons of the perturbed Ablowitz-Ladik model (Doktorov, Matsuka and Rothos); analysis of possibility of the existence of traveling waves in the discrete sine-Gordon and Klein-Gordon equations (Rothos and Feckan; Zolotaryuk); solitary wave dynamics in perturbed ladder lattices (Vakhnenko); application of discrete solitons to the array of BEC's with varying atomic scattering length (Tsoy *et al*); new exact results on functional presentation of the Volterra hierarchy (Vekslerchik) and on Heisenberg chains (Serikbaev *et al*; Rahimov *et al*).

In conclusion the book contains a panoramic view of rapidly developing areas of the nonlinear science – physics of matter waves, nonlinear optics and photonics, and nonlinear discrete systems. The review character of a number of contributions make this book to be interesting for postgraduate students starting a research while the original results reported will be of interest for experts working in the respective fields.

Acknowledgments

Sponsorship generously provided by the NATO Science Committee (Grant no NATO ARW979291) has made the Workshop possible. We express our gratitude to the NATO Science Committee, the main sponsor of the ARW. It is our pleasure to acknowledge partial financial support received from Fundação para a Ciência e a Tecnologia (Ministério da Ciência e do Ensino Superior de Portugal) and Fundação Luso – Americana. We also would like to express our thanks to Faculdade de Ciências da Universidade de Lisboa, its Centro de Física Teórica e Computacional and Departamento de Física for permanent support and help with technical arrangements. We also acknowledge Camara Municipal de Cascais for the help in organization the workshop. Special thanks goes to V.A. Brazhnyi and A. Spire for their assistance in local organization which significantly contributed to the success of the workshop, and to the staff of Kluwer Academic Publishers for technical help in preparation of this volue. One of the editors (VVK) is particularly grateful to his wife S. Konotop for indispensable permanent help during the organization of the workshop and the completion of the Proceedings.

Fatkhulla Abdullaev, Tashkent, January 31, 2004

Vladimir Konotop, Lisbon, January 31, 2004

Contributing Authors

Abdullaev, F. Kh.
Physical-Technical Institute, Uzbek Academy of Sciences, Mavlyanova str. 2-b, 700084 Tashkent, Uzbekistan.

Aceves, A. B.
Department of Mathematics, University of New Mexico, Albuquerque, NM 87131, USA

Akhmediev, N.
Optical Sciences Centre, Research School of Physical Sciences and Engineering, The Australian National University, Canberra ACT 0200, Australia

Aleksic, N. B.
Laboratoire POMA, UMR 6136 CNRS, Universite d'Angers, 49045 Angers, France

Alfimov, G. L.
Lukin's Research Institute of Physical Problems, Zelenograd, Moscow, 103460, Russia

Ankiewicz, A.
Applied Photonics Group, Research School of Physical Sciences and Engineering, The Australian National University, Canberra ACT 0200, Australia

Aubry, S.
Laboratoire Léon Brillouin (CEA-CNRS), CEA Saclay 91191 - Gif-sur-Yvette Cedex, France

Baizakov, B. B.
Dipartimento di Fisica "E.R. Caianiello" and Istituto Nazionale di Fisica della Materia (INFM), Universitá di Salerno, I-84081 Baronissi (SA), Italy

Berezhiani, V. I.
Laboratoire POMA, UMR 6136 CNRS Universite d'Angers, 49045 Angers, France

Białynicki-Birula, I.
Center for Theoretical Physics, Polish Academy of Sciences Lotników 32/46, 02-668 Warszawa, Poland

Bishop, A. R.
Theoretical Division and Center for Nonlinear Studies, Los Alamos National Laboratory, Los Alamos, NM 87545, USA

Boscolo, S.
Photonics Research Group, School of Engineering and Applied Science, Aston University, Birmingham B4 7ET, UK

Brazhnyi, V. A.
Centro de Física Teórica e Computacional, Universidade de Lisboa, Complexo Interdisciplinar, Av. Prof. Gama Pinto 2, Lisbon 1649-003, Portugal

Büttner, H.
Physikalisches Institut, Universität Bayreuth, Bayreuth D-95440, Germany

Christiansen, P. L.
Informatics and Mathematical Modelling, The Technical University of Denmark, DK-2800 Lyngby, Denmark

Crasovan, L.-C.
ICFO-Institut de Ciencies Fotoniques, and Department of Signal Theory and Communications, Universitat Politecnica de Catalunya, 08034 Barcelona, Spain, and Department of Theoretical Physics, Institute of Atomic Physics, P.O.Box MG-6, Bucharest, Romania

Damgov, V.
Space Research Institute at the Bulgarian Academy of Sciences, 6 Moskowska str., P.O.Box 799, 1000 Sofia, Bulgaria

Darmanyan, S. A.
International Research Centre for Experimental Physics, The Queen's University of Belfast, Belfast BT7 1NN, United Kingdom, and Institute of Spectroscopy, Russian Academy of Sciences, Troitsk, Moscow region, Russia

De Lillo, S.
Dipartimento di Matematica e Informatica, Università di Perugia - Via Vanvitelli, 1 - 06123 Perugia, and Istituto Nazionale di Fisica Nucleare, Sezione di Perugia - Via Pascoli,1 - 06123 Perugia

Derevyanko, S. A.
Photonics Research Group, School of Engineering and Applied Science, Aston University, Birmingham B4 7ET, UK

Doktorov, E. V.
B.I. Stepanov Institute of Physics, 220072 Minsk, Belarus

Dohnal, T.
Department of Mathematics, University of New Mexico, Albuquerque, NM 87131, USA

Edler, J.
Physikalisch-Chemisches Institut, Universität Zürich, Winterthurerstrasse 190, CH-8057 Zürich, Switzerland

Eilbeck, J. C.
Department of Mathematics, Heriot-Watt University Riccarton, Edinburgh, EH14 4AS, UK

Enolskii, V. S.
Dipartimento di Scienze Fisiche "E.R.Caianiello" via S.Allende, 84081 Baronissi (SA) Italy

Fallani, L.
LENS, Dipartimento di Fisica, Università di Firenze and Istituto Nazionale per la Fisica della Materia, via Nello Carrara 1, I-50019 Sesto Fiorentino (Firenze), Italy

Feckan, M.
Department of Mathematical Analysis Comenius University, Mlynská dolina, 842 48 Bratislava, and Mathematical Institute, Slovak Academy of Sciences, Stefánikova 49, 814 73 Bratislava, Slovakia

Fort, C.
LENS, Dipartimento di Fisica, Università di Firenze and Istituto Nazionale per la Fisica della Materia, via Nello Carrara 1, I-50019 Sesto Fiorentino (Firenze), Italy

Gaididei, Yu. B.
Bogolyubov Institute for Theoretical Physics, Metrologichna str. 14 B, 01413, Kiev, Ukraine

Gammal, A.
Instituto de Física, Universidade de São Paulo 05315-970, C.P.66318 São Paulo, Brazil

Garnier, J.
Laboratoire de Statistique et Probabilités, Université Paul Sabatier, 118 Route de Narbonne, 31062 Toulouse Cedex 4, France

Gerdjikov, V. S.
Department of Physics "E. R. Caianiello", University of Salerno, I-84081 Baronissi (SA), Italy and Institute for Nuclear Research and Nuclear Energy, Bulgarian Academy of Sciences, 1784 Sofia, Bulgaria

Grecu, D.
Department of Theoretical Physics National Institute of Physics and Nuclear Engineering P.O.Box MG-6, Bucharest, Romania

Hamm, P.
Physikalisch-Chemisches Institut, Universität Zürich, Winterthurerstrasse 190, CH-8057 Zürich, Switzerland

Iida, T.
Department of Physics, Graduate School of Sciences, University of Tokyo, 7-3-1 Hongo, Bunkyo-ku, Tokyo 113-0033, Japan

Kamchatnov, A. M.
Institute of Spectroscopy, Russian Academy of Sciences, Troitsk 142190, Moscow Region, Russia

Kato, Go
Department of Physics, Graduate School of Sciences, University of Tokyo, 7-3-1 Hongo, Bunkyo-ku, Tokyo 113-0033, Japan

Kazantseva, E. V.
Department of Solid State Physics, Moscow Engineering Physics Institute, Kashirskoe sh. 31, Moscow, 115409 Russia

Kevrekidis, P. G.
Department of Mathematics and Statistics, University of Massachusetts, Amherst MA 01003-4515, USA

Konotop, V. V.
Centro de Física Teórica e Computacional, Departamento de Física, Universidade de Lisboa, Av. Professor Gama Pinto 2, Lisboa 1649-003, Portugal, and Departamento de Física, Universidade de Lisboa, Campo Grande, Ed. C8, Piso 6, Lisboa 1749-016, Portugal

Kostov, N. A.
Institute for Electronics, Bulgarian Academy of Sciences, 1784 Sofia, Bulgaria

Kraenkel, R. A.
Instituto de Física Teórica, Universidade Estadual Paulista-UNESP, Rua Pamplona 145, 01405-900 São Paulo, Brazil

Ludu, A.
Northwestern State University Dept. Chemistry and Physics, Natchitoches, LA 71497 USA

Maimistov, A. I.
Moscow Engineering Physics Institute, Kashirskoe sh. 31, 115409 Moscow, Russia

Malomed, B. A.
Department of Interdisciplinary Studies, Faculty of Engineering, Tel Aviv University, Tel-Aviv 69978, Israel

Matsuka, N. P.
Institute of Mathematics, 220072 Minsk, Belarus

Mihalache, D.
ICFO-Institut de Ciencies Fotoniques, and Department of Signal Theory and Communications, Universitat Politecnica de Catalunya, 08034 Barcelona, Spain

Michinel, H.
Area de Optica, Facultade de Ciencias de Ourense, Universidade de Vigo, As Lagoas s/n, Ourense, ES-32005 Spain.

Myrzakul, K.
Institute of Physics and Technology, 480082, Alma-Ata-82, Kazakhstan

Myrzakulov, R.
Institute of Physics and Technology, 480082, Alma-Ata-82, Kazakhstan

Nevière, M.
Institut Fresnel, Faculté des Sciences et Techniques de Saint Jérome, 13397-262 Marseille Cedex 20, France

Palmero, F.
Nonlinear Physics Group. Departamento de Física Aplicada I. ETSI Informática, Universidad de Sevilla Avda Reina Mercedes s/n, 41012 Sevilla, Spain

Paz-Alonso, M. J.
Area de Optica, Facultade de Ciencias de Ourense, Universidade de Vigo, As Lagoas s/n, Ourense, ES-32005 Spain

Pérez-García, V. M.
Departamento de Matemáticas, E.T.S.I. Industriales, Universidad de Castilla-La Mancha, 13071 Ciudad Real, Spain

Pierantozzi, T.
Departamento de Matemática Aplicada, Facultad de Informatica, Universidad Complutense, 28040, Madrid, Spain.

Pitaevskii, L. P.
Dipartimento di Fisica, Università di Trento and Istituto Nazionale per la Fisica della Materia, CRS-BEC, 38050 Trento, Italy, and Kapitza Institute for Physical Problems, 119334 Moscow, Russia

Rahimov, F. K.
Institute of Physics and Technology, 480082, Alma-Ata-82, Kazakhstan

Rothos, V. M.
School of Mathematical Sciences, Queen Mary College, University of London, Mile End London E1 4NS, UK

Salerno, M.
Dipartimento di Fisica "E.R. Caianiello" and Istituto Nazionale di Fisica della Materia (INFM), Universitá di Salerno, I-84081 Baronissi (SA), Italy

Salgueiro, J. R.
Area de Optica, Facultade de Ciencias de Ourense, Universidade de Vigo, As Lagoas s/n, Ourense, ES-32005 Spain

Sanchini, G.
Dipartimento di Matematica e Informatica, Università di Perugia - Via Vanvitelli,1 - 06123 Perugia, and Istituto Nazionale di Fisica Nucleare, Sezione di Perugia - Via Pascoli,1 - 06123 Perugia

Serikbaev, N. S.
Institute of Physics and Technology, 480082, Alma-Ata-82, Kazakhstan

Shvartsburg, A.
Central Design Bureau for Unique Instrumentation Russian Academy of Sciences, p/o 117342, Butlerov Str. 15, Moscow, Russia

Skarka, V.
Laboratoire POMA, UMR 6136 CNRS Universite d'Angers, 49045 Angers, France

Soto-Crespo, J. M.
Instituto de Optica, C.S.I.C., Serrano 121, 28006 Madrid, Spain

Sowiński, T.
Center for Theoretical Physics, Polish Academy of Sciences Lotników 32/46, 02-668 Warszawa, Poland

Suzuki, T.
National Research Institute for Metals, Tsukuba 305-0047, Japan

Szeftel, J.
Université Paris 7, Laboratoire de Physique Théorique de la Matière Condensée, case 7020, 2 Place Jussieu, 75251 Paris Cedex 05, France

Takeno, S.
Institute for Innovative Science and Technology, Nagasaki Institute of Applied Science, Nagasaki 851-0193, Japan

Trenchev, P.
Space Research Institute at the Bulgarian Academy of Sciences, 6 Moskowska str., P.O.Box 799, 1000 Sofia, Bulgaria

Tsoy, E. N.
Physical-Technical Institute of the Uzbek Academy of Sciences, Mavlyanov st., 2-B, Tashkent, 700084, Uzbekistan

Turitsyn, S. K.
Photonics Research Group, School of Engineering and Applied Science, Aston University, Birmingham B4 7ET, UK

Torner, L.
ICFO-Institut de Ciencies Fotoniques, and Department of Signal Theory and Communications, Universitat Politecnica de Catalunya, 08034 Barcelona, Spain

Torres, J. P.
ICFO-Institut de Ciencies Fotoniques, and Department of Signal Theory and Communications, Universitat Politecnica de Catalunya, 08034 Barcelona, Spain

Vakhnenko, O. O.
Bogolyubov Institute for Theoretical Physics, Kyïv UA-03143, Ukraine

Vázquez, L.
Departamento de Matemática Aplicada, Facultad de Informatica, Universidad Complutense, 28040, Madrid, Spain, and Centro de Astrobiologia (CSIC -INTA), 28850, Torrejón de Ardoz, Madrid, Spain

Vekslerchik, V. E.
Institute for Radiophysics and Electronics, Kharkov 61085, Ukraine, and Universidad de Castilla-La Mancha, 13071 Ciudad Real, Spain

Villarroel, J.
Faculty of Sciences, University of Salamanca, Plaza de la Merced 37008 Salamanca, Spain

Visinescu, A.
Department of Theoretical Physics National Institute of Physics and Nuclear Engineering P.O.Box MG-6, Bucharest, Romania

Wadati, M.
Department of Physics, Graduate School of Sciences, University of Tokyo, 7-3-1 Hongo, Bunkyo-ku, Tokyo 113-0033, Japan

Zayats, A.V.
School of Mathematics and Physics, The Queen's University of Belfast, Belfast BT7 1NN, United Kingdom

Zolotaryuk, Ya.
Bogolyubov Institute for Theoretical Physics, National Academy of Sciences of Ukraine Kiev 03143, Ukraine

I

NONLINEAR SYSTEMS: GENERAL TOPICS

TOWARDS ALGEBRO-GEOMETRIC INTEGRATION OF THE GROSS–PITAEVSKII EQUATION

V.Z. Enolskii
Dipartimento di Scienze Fisiche "E.R.Caianiello" via S.Allende, 84081 Baronissi (SA) Italy
vze@ma.hw.ac.uk

Abstract We are discussing various possibilities to construct algebro-geometric solutions of the Gross-Pitaevskii equation on the basis of application of the apparatus of completely integrable systems and theory of Abelian functions. In this context algebro-geometric solutions of Schrödinger equation with finite-gap potential were considered as well the solutions in trigonal Abelian functions of the two-component Vector Nonlinear Schrödinger Equation (or Manakov system).

Keywords: integrable partial differential equations, Scrödinger equation, finite-gap potentials, vector non-linear Schrödinger equation, Manakov system

1. Introduction

The discovery of Bose-Einstein condensation (BEC) in alkali gases "can be considered as one of the most beautiful results of experimental physics in our century" [18]. It is understood now that all the low temperature properties of BEC (see e.g. [8]) are well described by the Gross-Pitaevskii equation [11, 17]. However this equation is nonlinear and only for special classes of potentials certain exact solutions have been found (see, for example, in the same volume [13]). The aim of this communication is to discuss possibilities to enlarge the set of exact solutions of the Gross-Pitaevskii equation on the basis of application of the apparatus of completely integrable systems and theory of Abelian functions (see e.g. [3]). The main idea is to apply to the problem the well known algebro-geometric solutions of Schrödinger equation with finite-gap potential and solutions in trigonal Abelian functions of the two-component Vector Nonlinear Schrödinger Equation (or Manakov system)

F. Kh. Abdullaev and V. V. Konotop (eds.), Nonlinear Waves: Classical and Quantum Aspects, 3–14.

which were recently found. The results reported are based on articles [4] and [10].

2. Utilization of the Schrödinger equation

The Gross-Pitaevskii equation with potential $V(x, y, z, t)$ has the form

$$\mathrm{i}\,\frac{\partial\Psi}{\partial t} = -\Delta_3\Psi + V(x, y, z, t)\Psi + g|\Psi|^2\Psi,$$

where Δ_3 is 3-dimensional Laplace operator and g is a constant. To find a simplest family of solutions to the equation we consider one-dimensional Schrödinger equation

$$\begin{aligned}\mathrm{i}\,\frac{\partial\Psi}{\partial t} &= -\partial_x^2\Psi + U(x,t)\Psi = \\ &= -\partial_x^2\Psi + (U(x,t) - g|\Psi|^2)\Psi + g|\Psi|^2\Psi.\end{aligned}$$

Therefore if the potential is of the form

$$V(x,t) = U(x,t) - g|\Psi(x,t)|^2,$$

then the Gross-Pitaevskii equation has a solution $\Psi(x,t)$.

Let us consider further two one-dimensional Schrödinger equations

$$\begin{aligned}\mathrm{i}\,\frac{\partial}{\partial t}\Psi_1 &= -\partial_x^2\Psi_1 + U_1(x,t)\Psi_1,\\ \mathrm{i}\,\frac{\partial}{\partial t}\Psi_2 &= -\partial_y^2\Psi_2 + U_2(y,t)\Psi_2.\end{aligned}$$

The function

$$\Psi(x, y, t) = \Psi_1(x,t)\Psi_2(y,t)$$

satisfies the equation

$$\mathrm{i}\,\frac{\partial\Psi}{\partial t} = -\Delta_2\Psi + V(x, y, t)\Psi + g|\Psi|^2\Psi,$$

where

$$V(x, y, t) = U_1(x,t) + U_2(y,t) - g|\Psi_1(x,t)|^2|\Psi_2(y,t)|^2.$$

Therefore if the potential is of the form

$$V(x, y, t) = U_1(x,t) + U_2(y,t) - g|\Psi_1(x,t)|^2|\Psi_2(y,t)|^2,$$

then the two-dimensional Gross-Pitaevskii equation has a solution

$$\Psi(x, y, t) = \Psi(x,t)\Psi_2(y,t).$$

D-dimensional solutions of the Gross-Pitaevskii equation can be constructed in a similar way.

This elementary result allows us to use the well known finite-gap potentials and appropriate eigenfunctions of the Schrödinger operators in order to build for the Gross-Pitaevskii equation a large family of solutions in terms of the Abelian functions. These Abelian functions depend on the moduli of the appropriate Riemann surface which we consider as the parameters of our solutions. We hope that the set of parameters is big enough to describe many physically interesting situations of the BEC phenomenon.

3. Solutions in terms of hyperelliptic functions

In this section we describe algebro-geometric solutions to the one dimensional Schrödinger equation with finite-gap potentials, for more details, see e.g. [3].

Let X be the hyperelliptic curve given by the equation

$$\mu^2 = \sum_{i=0}^{2g+1} a_i \lambda^i = 4 \prod_{k=1}^{2g+1} (\lambda - e_k), \tag{1}$$

realized as a two sheeted covering over the Riemann sphere branched in the points $(e_k, 0)$, $k \in \mathcal{G} = \{1, \dots, 2g+1\}$, with $e_j \neq e_k$ for $j \neq k$, and at infinity, $e_{2g+2} = \infty$. Notice we do not require the e_k to be real. However, when they are real, we find it convenient to order them according to $e_1 < e_2 < \ldots < e_{2g+1}$, i. e., in the opposite way as compared to the Weierstrass ordering, see Fig. 1.

Given a canonical homology basis $(\mathfrak{a}_1, \dots, \mathfrak{a}_g; \mathfrak{b}_1, \dots, \mathfrak{b}_g)$ as shown in Fig. 1. Denote holomorphic differentials (first kind) $\mathrm{d}\boldsymbol{u}^t = (\mathrm{d}u_1, \dots, \mathrm{d}u_g)$, where $\mathrm{d}u_k = \lambda^{k-1}/\mu$ and their $\mathfrak{a}$ and $\mathfrak{b}$-periods as

$$A = \Big(\oint_{\mathfrak{a}_k} \mathrm{d}u_i \Big)_{i,k=1,\dots,g}, \; B = \Big(\oint_{\mathfrak{b}_k} \mathrm{d}u_i \Big)_{i,k=1,\dots,g}. \tag{2}$$

Let $\mathcal{H}_g = \{\tau^t = \tau, \quad \mathrm{Im}\,\tau \geq 0\}$ be the Siegel half space of degree g, where $\tau = A^{-1}B$ is the period matrix. The hyperelliptic θ–function, $\theta :\ \mathrm{Jac}(V) \times \mathcal{H}_g \to \mathbb{C}$, with characteristics

$$[\varepsilon] = \begin{bmatrix} \boldsymbol{\varepsilon}'^t \\ \boldsymbol{\varepsilon}^t \end{bmatrix} = \begin{bmatrix} \varepsilon'_1 & \dots & \varepsilon'_g \\ \varepsilon_1 & \dots & \varepsilon_g \end{bmatrix} \in \mathbb{R}^{2g}$$

is defined as the Fourier series

$$\theta[\varepsilon](\boldsymbol{v}|\tau) = \sum_{\boldsymbol{m} \in \mathbb{Z}^g} \exp \pi \mathrm{i} \left\{ (\boldsymbol{m} + \boldsymbol{\varepsilon}')^t \tau (\boldsymbol{m} + \boldsymbol{\varepsilon}') + 2(\boldsymbol{v} + \boldsymbol{\varepsilon})^t (\boldsymbol{m} + \boldsymbol{\varepsilon}') \right\}$$

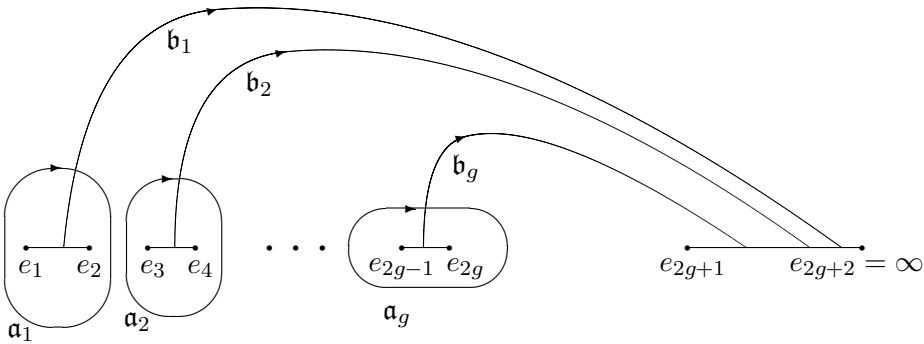

Figure 1. A homology basis on a Riemann surface of the hyperelliptic curve of genus g with real branching points $e_1, \dots, e_{2g+2} = \infty$ (upper sheet). The cuts are drawn from e_{2i-1} to e_{2i} for $i = 1, \dots, g+1$. The $\mathfrak{b}$-cycles are completed on the lower sheet (the picture on lower sheet is just flipped horizontally).

and has the periodicity properties

$$\theta[\varepsilon](\boldsymbol{v} + \boldsymbol{n} + \tau\boldsymbol{n}'|\tau) = \exp\bigl\{-2\,\mathrm{i}\,\pi\boldsymbol{n}'^{t}(\boldsymbol{v} + \frac{1}{2}\tau\boldsymbol{n}')\bigr\}\exp\bigl\{2\,\mathrm{i}\,\pi(\boldsymbol{n}^{t}\boldsymbol{\varepsilon}' - \boldsymbol{n}'^{t}\boldsymbol{\varepsilon})\bigr\}\theta[\varepsilon](\boldsymbol{v}|\tau).$$

We are considering here only half-integer characteristics, $\varepsilon'_k, \varepsilon_l = 0$ or $\frac{1}{2}$ for any $k, l = 1, \dots, g$. Even characteristic $[\varepsilon]$ is nonsingular if $\theta[\varepsilon](\mathbf{0}) \neq 0$. Odd characteristic is nonsingular if the gradient $\frac{\partial}{\partial v_k}\theta(\boldsymbol{v})\big|_{\boldsymbol{z}=0}$ has nonzero components.

The remarkable role of θ-functions in the spectral theory of the Schrödinger equation was discovered by Its and Matveev, 1975 [12]. Consider the spectral problem

$$\left\{\frac{\partial^2}{\partial x^2} - u(x)\right\}\Psi(x;\lambda) = \lambda\Psi(x;\lambda),$$

where $u(x)$ is smooth and real potential, $\Psi(x;\lambda)$ is an eigenfunction, and λ is the spectral parameter. Suppose that the spectrum consists of $n+1$ continuous segments $[\lambda_1, \lambda_2], \dots, [\lambda_{2n+1}, \infty]$. Then the smooth and real potential and the corresponding eigenfunction $\Psi(x;\lambda,\mu)$ are given

by the formulae

$$u(x) = -2\frac{\mathrm{d}^2}{\mathrm{d}x^2}\log\theta(\mathrm{i}\boldsymbol{U}x|\tau) + c \tag{3}$$

$$\Psi(x;\lambda,\mu) = C\frac{\theta\left(\int\limits_{(\infty,\infty)}^{(\lambda,\mu)}\mathrm{d}\boldsymbol{v} + \mathrm{i}\boldsymbol{U}x\big|\tau\right)}{\theta\left(\mathrm{i}\boldsymbol{U}x\big|\tau\right)}\exp\left\{\mathrm{i}\,x\int\limits_{(\lambda_0,\mu_0)}^{(\lambda,\mu)}\mathrm{d}\Omega(\lambda,\mu)\right\}, \tag{4}$$

where the constant C is chosen to provide the normalization condition,

$$|\Psi(x,\lambda)|^2 = 1,$$

while the constant c is expressible in terms of periods of certain meromorphic differentials of the Riemann surface X. The real function of λ

$$k(\lambda) = \int\limits_{(\lambda_0,\mu_0)}^{(\lambda,\mu)}\mathrm{d}\Omega(\lambda,\mu),$$

has a sense of quasi-momentum.

The θ-functional expressions for the potential and of the Gross-Pitaevskii equation takes the form

$$\mathcal{U}(x) = -2\frac{\mathrm{d}^2}{\mathrm{d}x^2}\log\theta(\mathrm{i}\boldsymbol{U}x|\tau) - gC^2\left|\frac{\theta\left(\int\limits_{(\infty,\infty)}^{(\lambda,\mu)}\mathrm{d}\boldsymbol{v} + \mathrm{i}\boldsymbol{U}x\big|\tau\right)}{\theta\left(\boldsymbol{U}_2x + \boldsymbol{U}_0\big|\tau\right)}\right|^2,$$

while the solution coincides with the Bloch function (4).

A special interest for the problem present a superposition of two elliptic solitons. To this end we consider a genus two hyperelliptic curve with two zones almost contracted, but one is much larger then another. A typical form of potential $u(x)$, where the more contracted zone is below the of less contracted one is shown on the Fig. 2. We remark that this plot was computed in terms of 2-dimensional θ-functions in conditions of slow convergence of complete hyperelliptic integrals. To improve convergence we were using the method of arithmetic-geometric mean for the genus two hyperelliptic integrals the interest to which was recently renewed [5]. Solutions of this kind was also obtained earlier in [15] by dressing method.

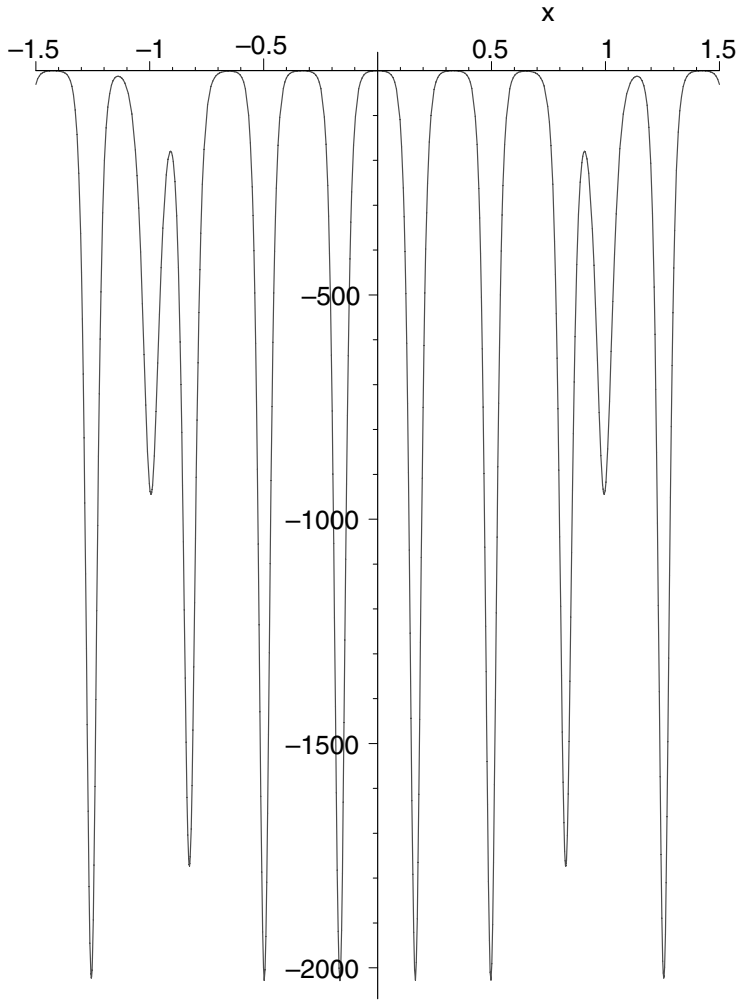

Figure 2. Hyperelliptic two-gap potentials with two contracted zones. A zone being contracted with accuracy to 10^{-8} is placed below zone which is contracted with accuracy to 10^{-2}. The boundaries of zone are $-13-10^{-8}, -13, -8.01. -8, 16$.

We are working to show that parameters in (4) can be chosen in such a way that the train of peaks with bigger period will be canceled and certain periodic part will remains. The remaining periodic function $\mathcal{U}$ can be interpreted as a periodic potential of the Gross-Pitaevskii equation, while the Bloch function of the Schrödinger equation will present the solution itself. The work is in progress [4].

4. Two component Gross-Pitaevskii equation and the Manakov system

In this section we shall discuss a derivation of the algebro-geometric solution for the two-component Gross-Pitaevskii equation with the potential $\mathcal{U}(x)$

$$\begin{aligned} \mathrm{i}\,\frac{\partial\Psi_1}{\partial t}+\frac{\partial^2\Psi_1}{\partial x^2}+2\left(|\Psi_1|^2+|\Psi_2|^2\right)\Psi_1+\mathcal{U}(x)\Psi_1 &= 0,\\ \mathrm{i}\,\frac{\partial\Psi_2}{\partial t}+\frac{\partial^2\Psi_2}{\partial x^2}+2\left(|\Psi_1|^2+|\Psi_2|^2\right)\Psi_2+\mathcal{U}(x)\Psi_2 &= 0. \end{aligned}$$

To do that we shall use special solutions of the Vector Nonlinear Schrödinger equation

$$\begin{aligned} \mathrm{i}\,\frac{\partial\Psi_1}{\partial t}+\frac{\partial^2\Psi_1}{\partial x^2}+2\left(|\Psi_1|^2+|\Psi_2|^2\right)\Psi_1=0,\\ \mathrm{i}\,\frac{\partial\Psi_2}{\partial t}+\frac{\partial^2\Psi_2}{\partial x^2}+2\left(|\Psi_1|^2+|\Psi_2|^2\right)\Psi_2=0. \end{aligned} \tag{5}$$

It was proven by Manakov [16] that this system is completely integrable and, in consequence, the equations (5) are now known as the *Manakov system*.

Periodic and quasi-periodic solutions of the Manakov system expressed in terms of explicit θ-functional formulae have been quoted by several authors [14, 1], while the special case of reduction to a dynamical system with two degree of freedom was studied in [7].

Recently a general class of periodic and quasi-periodic solutions of this equation was derived in [10]. The formulae obtained are well algorithmized and reduce the whole calculation to θ-functions, holomorphic differentials and integrals. That is of importance for applications because in the case considered the solution is parametrized by a class of trigonal curves, which is not well studied.

The procedure to compute algebro-geometric solutions described in [10] is described below. On the all stages one can use Maple software "algcurves" written on the base of [9] and no additional programming is needed to construct the solution.

Fix positive integer $n \in \{2,3,\ldots\}$ and a polynomial in two variables or algebraic curve X

$$\begin{aligned} f(z,w) = (w+\frac{\mathrm{i}}{2}(2z)^n)(w-\frac{\mathrm{i}}{2}(2z)^n)^2\\ +(w-\frac{\mathrm{i}}{2}(2z)^n)P_{n-1}(z)+\mathrm{i}\,P_{n-2}(z)=0, \end{aligned}$$

with arbitrary real polynomials $P_{n-2}(z)$ and $P_{n-1}(z)$ of variable z of degrees $n-2$ and $n-1$ correspondingly.

The geometric genus g of the curve X when the polynomials P_{n-2} and P_{n-1} are in general position be $g = 2n-3$. The curve X can be realized as a 3-sheeted covering of the extended complex plane with regular points at infinities. Therefore there are 3 infinities $\infty_1, \infty_2, \infty_3$, and the curve X is not branched at these infinities.

The homology basis of the curve can be represented for arbitrary genus as the set of vertical cuts connected different sheets and $\mathfrak{a}$-cycles going around the cuts. The cuts connect pair-wisely branch points which are found as zeros of the discriminant of the curve. It can be shown that all zeros of the discriminant are simple and therefore the ramification index be $1/2$ for this class of curves. For the case $g = 3$ the homology basis is shown in Fig. 3; here, the solid, dashed and dash-dotted lines connecting points e_1 to e_2 etc. are cuts connecting the first to second, second to third and third to first sheets respectively. See caption for further comments. The homology basis for higher genera can be plotted analogously.

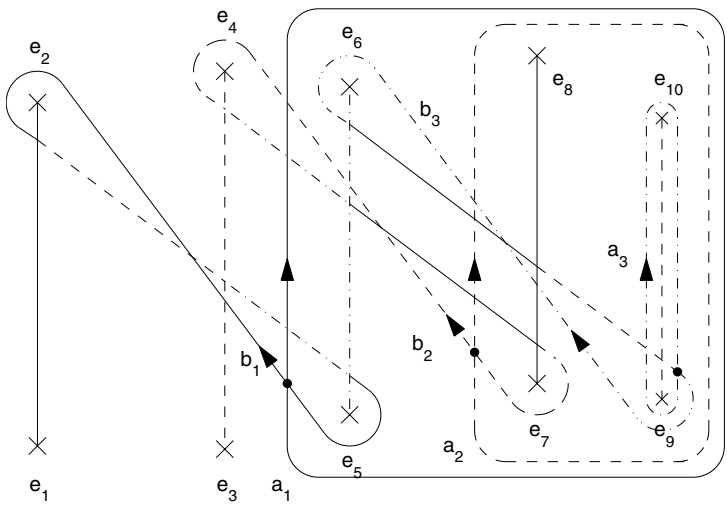

Figure 3. Basis of cycles of the curve X of genus 3. The solid, dashed and dash-dotted lines denote paths on the first, second and third sheets respectively. Correspondingly the solid to dashed line, dashed to dot-dashed line, and dot-dashed to solid lines illustrate trajectories passing through these cuts. The cuts are similarly encoded for clarity.

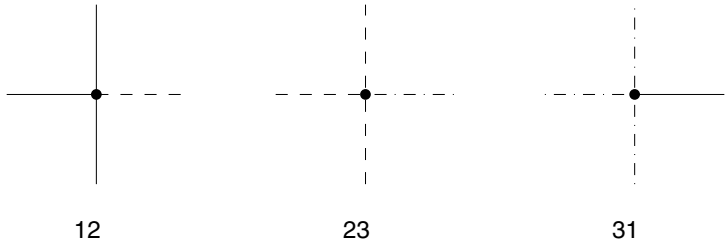

Figure 4. Contours passing from sheet 1 to sheet 2, from sheet 2 to sheet 3 and from sheet 3 to sheet 1.

For the next step compute the vector of holomorphic differentials $\mathrm{d}\boldsymbol{u}(Q) = (\mathrm{d}u_1(Q), \dots, \mathrm{d}u_g(Q))^T$.

$$\mathrm{d}u_i(Q) = \frac{z^i}{\frac{\partial}{\partial w} f(z,w)}\,\mathrm{d}z, \quad i = 0, \dots, n-3,$$
$$\mathrm{d}u_j(Q) = \frac{z^{n-2-j}\left(w - \frac{\mathrm{i}}{2}(2z)^n\right)}{\frac{\partial}{\partial w} f(z,w)}\,\mathrm{d}z, \quad j = n-2, \dots, 2n-3.$$

Compute further the vector of normalized holomorphic differentials

$$\mathrm{d}\boldsymbol{v}(Q) = A^{-1}\mathrm{d}\boldsymbol{u}(Q),$$

where A is the matrix of $\mathfrak{a}$-periods like in (2).

Compute auxiliary winding vectors $\boldsymbol{V}^{(i)}, \boldsymbol{W}^{(i)}, \boldsymbol{Z}^{(i)}$, $i = 1, 2, 3$ from expansions of holomorphic integrals at infinities:

$$\int_Q^P \mathrm{d}\boldsymbol{v}\bigg|_{P\to\infty_i} = O(1) + \boldsymbol{V}^{(i)}\xi + \boldsymbol{W}^{(i)}\xi^2 + \boldsymbol{Z}^{(i)}\xi^3 + \dots, \quad i = 1, 2, 3.$$

Then set for main winding vectors

$$\boldsymbol{V} = \mathrm{i}\,\boldsymbol{V}^{(1)} - \mathrm{i}\,\boldsymbol{V}^{(2)} - \mathrm{i}\,\boldsymbol{V}^{(3)}, \quad \boldsymbol{W} = 4\,\mathrm{i}\,\boldsymbol{W}^{(1)} - 4\,\mathrm{i}\,\boldsymbol{W}^{(2)} - 4\,\mathrm{i}\,\boldsymbol{W}^{(3)}.$$

Compute vectors $\boldsymbol{r}_{2,3}$

$$\boldsymbol{r}_{2,3} = \int_{\infty_1}^{\infty_{2,3}} \mathrm{d}\boldsymbol{v},$$

which are non-complete holomorphic integrals and therefore no problems with convergence appear.

Introduce θ-functions as in the case of hyperelliptic curve.

Compute the following 6 constants. They all are expressible in terms of winding vectors and θ-functions and their derivatives in special points $\boldsymbol{r}_{2,3}$ which are already defined. Namely we have

$$\begin{aligned}
E_{1,2} &= \mathrm{i}\,(\partial_{\boldsymbol{V}^{(1)}} - \partial_{\boldsymbol{V}^{(2,3)}})\ln\theta[\varepsilon](\boldsymbol{r}_{2,3}) \\
&\quad - \mathrm{i}\,\partial_{\boldsymbol{V}^{(3,2)}}\ln\left[\theta[\varepsilon](\boldsymbol{r}_{3,2})\theta[\varepsilon](\boldsymbol{r}_{2,3}-\boldsymbol{r}_{3,2})\right] - \mathrm{i}\,c_1^{(2,3)} - \mathrm{i}\,c_1^{(1)}, \\
N_{1,2} &= 4\,\mathrm{i}\,(\partial_{\boldsymbol{W}^{(1)}} - \partial_{\boldsymbol{W}^{(2,3)}})\ln\theta[\varepsilon](\boldsymbol{r}_{2,3}) \\
&\quad - 4\,\mathrm{i}\,\partial_{\boldsymbol{W}^{(3,2)}}\ln\left[\theta[\varepsilon](\boldsymbol{r}_{3,2})\theta[\varepsilon](\boldsymbol{r}_{2,3}-\boldsymbol{r}_{3,2})\right] \\
&\quad - 2\,\mathrm{i}\left(\partial^2_{\boldsymbol{V}^{(1)},\boldsymbol{V}^{(2,3)}} - \partial^2_{\boldsymbol{V}^{(2,3)},\boldsymbol{V}^{(1)}}\right)\ln\theta[\varepsilon](\boldsymbol{r}_{2,3}) \\
&\quad + 2\,\mathrm{i}\,\partial^2_{\boldsymbol{V}^{(3,2)},\boldsymbol{V}^{(2,3)}}\ln\left[\frac{\theta[\varepsilon](\boldsymbol{r}_{3,2})}{\theta[\varepsilon](\boldsymbol{r}_{2,3}-\boldsymbol{r}_{3,2})}\right] - \mathrm{i}\,c_2^{(2,3)} - \mathrm{i}\,c_2^{(1)}, \\
\delta_{2,3} &= \frac{\mathrm{i}}{\theta[\varepsilon](\boldsymbol{r}_{2,3})}\sqrt{\partial_{\boldsymbol{V}^{(2,3)}}\theta[\varepsilon](\boldsymbol{0})}\sqrt{\partial_{\boldsymbol{V}^{(1)}}\theta[\varepsilon](\boldsymbol{0})},
\end{aligned}$$

where $[\varepsilon]$ be non-singular odd characteristic, for example,

$$\begin{bmatrix} 1/2 & \dots & 0 \\ 1/2 & \dots & 0 \end{bmatrix},$$

$\partial_{\boldsymbol{V}}$, $\partial_{\boldsymbol{W}}$ and $\partial_{\boldsymbol{Z}}$ are directional derivatives,

$$\partial_{\boldsymbol{V}} = \sum_{k=1}^{g} V_k \frac{\partial}{\partial v_k}, \quad \partial^2_{\boldsymbol{V},\boldsymbol{W}} = \sum_{k=1}^{g}\sum_{l=1}^{g} V_k W_l \frac{\partial^2}{\partial v_k \partial v_l}, \quad \text{etc.}$$

and

$$\begin{aligned}
c_1^{(i)} &= -\frac{\partial_{\boldsymbol{W}^{(i)}}\theta[\varepsilon](\boldsymbol{0})}{\partial_{\boldsymbol{V}^{(i)}}\theta[\varepsilon](\boldsymbol{0})}, \\
c_2^{(i)} &= -\left(\frac{\partial_{\boldsymbol{W}^{(i)}}\theta[\varepsilon](\boldsymbol{0})}{\partial_{\boldsymbol{V}^{(i)}}\theta[\varepsilon](\boldsymbol{0})}\right)^2 + \frac{1}{3}\frac{\partial^3_{\boldsymbol{V}^{(i)}}\theta[\varepsilon](\boldsymbol{0})}{\partial_{\boldsymbol{V}^{(i)}}\theta[\varepsilon](\boldsymbol{0})} + \frac{\partial_{\boldsymbol{Z}^{(i)}}\theta[\varepsilon](\boldsymbol{0})}{\partial_{\boldsymbol{V}^{(i)}}\theta[\varepsilon](\boldsymbol{0})},
\end{aligned}$$

where $i = 1, 2, 3$.

We remark that the above 6 constants are fundamental: expression for the constants $c_2^{(i)}$ coincide with accuracy to a trivial multiplier with values of the holomorphic projective connection at infinities. The first and second logarithmic derivatives can be expressed in terms of multidimensional Kleinian ζ and $\wp$-function which classical and modern treatment of hyperelliptic case can be found in [2] and [6] correspondingly.

The algebro-geometric solution is of the form

$$\begin{aligned}
\Psi_{1,2}(x,t) &= 2\,\mathrm{i}\,\alpha_{1,2}\frac{\theta\left(\boldsymbol{V}x + \boldsymbol{W}t - \boldsymbol{D} + \boldsymbol{r}_{2,3}|\tau\right)}{\theta\left(\boldsymbol{V}x + \boldsymbol{W}t|\tau\right)}\exp\left\{-E_{1,2}x + N_{1,2}t\right\}, \\
\alpha_{1,2} &= \delta_{2,3}\exp\left\{\mathrm{i}\ \arg\left(\frac{\theta(\boldsymbol{D}|\tau)}{\theta(\boldsymbol{r}_{2,3}-\boldsymbol{D}|\tau)}\right)\right\},
\end{aligned}$$

where $\boldsymbol{D}$ is arbitrary vector satisfying condition $\theta(\boldsymbol{D}|\tau) \neq 0$.

The strategy of application of algebro-geometric solution of the Manakov system given above to the Gross-Pitaevskii equation could be the same as in the case of Schrödinger equation already described. The quantity $\mathcal{U} = |\Psi_1|^2 + |\Psi_2|^2$ can be considered as a potential. Then the solution obtained has the following property: when the underlying algebraic curve X is of the genus one, which corresponds to $n = 2$ then the solution is independent in time and can considered as x-dependent potential. This potential which can be made elliptic periodic at certain values of the parameters of the solution. Then we consider a curve of higher genus, $g \geq 3$ which yield quasi-periodic solutions of the background of the background of the elliptic periodic solution. Such solution of the Manakov system can be interpreted as a solution of the Gross-Pitaevskii equation with periodic potential. The work is in progress.

Acknowledgements

The author is grateful to the Department of Physics "E.R.Caianiello" for the hospitality, and the University of Salerno for providing research grant in 2002 where the most of this work was done. Informatics and Modelling of the Technical University of Denmark and the MIDIT centre are also acknowledged for funding of the research visit in October-November 2003 within Grant 21-02-0500 from the Danish Research Counsel when this paper was completed.

References

[1] M. R. Adams, J. Harnad, and J. Hurtubise. *Commun. Math. Phys.*, **134**, 555–585, 1990.

[2] H. F. Baker. *Abel's theorem and the allied theory of theta functions*. Cambridge Univ. Press, Cambridge, 1897, reprinted 1995.

[3] E. D. Belokolos, A. I. Bobenko, V. Z. Enolskii, A. R. Its, and V. B. Matveev. *Algebro Geometrical Approach to Nonlinear Integrable Equations*. Springer, Berlin, 1994.

[4] E. D. Belokolos, J. C. Eilbeck, V. Z. Enolskii, and M. Salerno. Algebro-geometric solutions to the Gross-Pitaevskii equation in the optical lattice, *in preparation*.

[5] J.-B. Bost and J.-F. Mestre. *Gaz.Math.S.M.F.*, **38**, 34–64, 1989.

[6] V. M. Buchstaber, V. Z. Enolskii, and D. V. Leykin. *Kleinian functions, hyperelliptic Jacobians and applications*. In S. P. Novikov and I. M. Krichever, editors, *Reviews in Mathematics and Mathematical Physics*, **10**, 2, 1–125, London, 1997. Gordon and Breach.

[7] P. L. Christiansen, J. C. Eilbeck, V. Z. Enolskii, and N. A. Kostov. *Proc. R. Soc. Lond. A*, **456**, 2263–2281, 2000.

[8] F. Dalfovo, S. Giorgini, L. P. Pitaevskii, and S. Stringari. *Rev. Mod. Phys.*, **71** 463, 1999.

[9] B. Deconinck and M. van Hoeij. *Physica D*, **152-153**, 28–46, 2001.

[10] J N Elgin, V Z Enolskii, and A R Its. Effective integration of the nonlinear vector Schrödinger equation. *in preparation*, 2003.

[11] E. P. Gross. *Nuovo Cimento*, **20**, 454, 1961.

[12] A. R. Its and V. B. Matveev. *Teor. Mat. Fiz.*, **23**, 51–67, 1975.

[13] N. A. Kostov, V. Z. Enolskii, V. S. Gerdjikov, V.V. Konotop, and M. Salerno. Two-component Bose-Einstein condensates in optical lattices. *in this volume* also *arXiv:cond-mat/0307156* (2003).

[14] I. M. Krichever. *Russian. Math. Surveys*, **32**, 180–208, 1977.

[15] E. A. Kuznetsov and A. V. Mikhailov. *Soviet Physics JETP*, **40**, 855–859, 1974.

[16] S. V. Manakov. *Soviet JETP*, **38**, 248–253, 1974.

[17] L. P. Pitaevskii. *Sov. Phys. JETP*, **13**, 451–454, 1961.

[18] L. P. Pitaevskii. In D. Nielson and R. Bishop, editors, *Recent Progress in Many-Body Theories*, page 3, Singapore, 1998. World Scientific.

ON MODELING ADIABATIC N-SOLITON INTERACTIONS

Effects of perturbations

V.S. Gerdjikov

Department of Physics "E. R. Caianiello", University of Salerno, I-84081 Baronissi (SA), Italy and Institute for Nuclear Research and Nuclear Energy, Bulgarian Academy of Sciences, 1784 Sofia, Bulgaria

gerjikov@inrne.bas.bg

Abstract The complex Toda chain (CTC) is known to describe the N-soliton train interactions in adiabatic approximation for several nonlinear evolution equations: the nonlinear Schrödinger equation (NLS), the modified NLS, higher NLS. We briefly review and extend the results in order to treat several types of perturbations of the above-mentioned equations. In particular we consider analytically the effects of quadratic and periodic external potentials as perturbations. We also briefly analyze the Hamiltonian properties of the CTC.

Keywords: Soliton interactions, nonlinear waves, Hamiltonian mechanics

1. Introduction

Starting with the pioneer paper [1] the analytical and numerical methods for studying soliton interactions substantially developed. Most attention was paid to the N-soliton train interactions for the nonlinear Schrödinger equation (NLS) and its perturbed versions, see [2, 3, 4, 5] and the references therein:

$$iu_t + \frac{1}{2}u_{xx} + |u|^2 u(x,t) = i\epsilon R[u]. \tag{1}$$

Several other nonlinear evolution equations (NLEE) were also studied, among them the modified NLS (MNLS) equation [6, 7, 8, 9, 10]:

$$iu_t + \frac{1}{2}u_{xx} + i\alpha(|u|^2 u(x,t))_x + |u|^2 u(x,t) = iR[u]; \tag{2}$$

F. Kh. Abdullaev and V. V. Konotop (eds.), Nonlinear Waves: Classical and Quantum Aspects, 15–28.

one of the higher NLS (HNLS) equations [11]:

$$iu_t + \frac{1}{2}u_{xx} + |u|^2 u(x,t) + \frac{i\epsilon_3}{2}(u_{xxx} + 6|u|^2 u_x) = iR[u]; \qquad (3)$$

Here ϵ_3 is a (small) constant and by $R[u]$ we have denoted possible perturbation terms, specific for each of the above equations.

By N-soliton train we mean a solution fixed up by the initial condition:

$$u(x, t=0) = \sum_{k=1}^{N} u_k^{1\mathrm{s}}(x, t=0), \qquad (4)$$

where $u_k^{1\mathrm{s}}(x,t)$ is a generic one-soliton solution of the corresponding NLEE; for the NLS-type equations the k-th soliton is parametrized by four parameters: amplitude ν_k, velocity μ_k, center of mass position ξ_k and phase δ_k. The adiabatic approximation uses as small parameter $\varepsilon_0 \ll 1$ the soliton overlap; in our cases this overlap falls off exponentially with the distance between the solitons. Then the soliton parameters must satisfy [1]:

$$|\nu_k - \nu_0| \ll \nu_0, \quad |\mu_k - \mu_0| \ll \mu_0, \quad |\nu_k - \nu_0||\xi_{k+1,0} - \xi_{k,0}| \gg 1, \qquad (5)$$

where $\nu_0 = \frac{1}{N}\sum_{k=1}^{N} \nu_k$, and $\mu_0 = \frac{1}{N}\sum_{k=1}^{N} \mu_k$ are the average amplitude and velocity respectively. In fact we have two different scales:

$$|\nu_k - \nu_0| \simeq \varepsilon_0^{1/2}, \qquad |\mu_k - \mu_0| \simeq \varepsilon_0^{1/2}, \qquad |\xi_{k+1,0} - \xi_{k,0}| \simeq \varepsilon_0^{-1}.$$

One can expect that the approximation holds only for such times t for which the set of $4N$ parameters of the soliton train satisfy (5).

The equations (1) – (3) have several points in common. First of all they all find a number of applications to nonlinear optics. Second, for $R[u] \equiv 0$ they are all integrable via the inverse scattering method, see [12, 13]. Therefore they allow exact N-soliton solutions. Thirdly, for all of them the corresponding N-soliton train dynamics in the adiabatic approximation is modelled by a complex generalization of the Toda chain (TC) [14]:

$$\frac{\mathrm{d}^2 Q_j}{\mathrm{d}t^2} = 16\nu_0^2 f_0^2 \left(e^{Q_{j+1}-Q_j} - e^{Q_j - Q_{j-1}}\right), \qquad j = 1, \ldots, N, \qquad (6)$$

where Q_j and the constant f_0 for the HNLS are defined in eqs. (10), (11) below; for the MNLS case $f_0 = 1$ and Q_j is as in eq. (14). Like for the free-end TC we assume that $e^{-Q_0} \equiv e^{Q_{N+1}} \equiv 0$; however the dynamical variables Q_j are complex-valued expressions of the soliton variables which justifies the name of complex Toda chain (CTC).

It is important to note that the N-soliton train is *not* an N-soliton solution evaluated for $t = 0$; if one tries to describe the spectral data of

the corresponding Lax operator L he will find also nontrivial data related to the continuous spectrum of L. Thus the analytical results from the soliton theory can not be applied. Another reasons for which we will apply the adiabatic approximation rather than the precise analytical methods are due to the fact that we want to treat solitons moving with equal velocities and the effects of possible nonintegrable perturbations $R[u]$. The present paper briefly reviews and extends the results of several previous ones: see Refs. [2, 3, 4, 5, 10, 11, 15] for the NLS and HNLS and Refs. [8, 9] for the MNLS. Recently with the studies of Bose-Einstein condensates it became important to study NLS equation with additional potential term $iR[u] = V(x)u(x,t)$, see [16]. We derive a perturbed CTC model describing the adiabatic N-soliton interactions in the presence of quadratic and periodic potentials $V(x)$.

2. *N*-soliton trains of the NLS and HNLS equations

Here we remind the results for the soliton solutions and N-soliton trains of the NLS and HNLS equations. The dispersion law for the HNLS eq. (3) we analyze below is $f^{\rm HN} = \lambda^2 - 2\epsilon_3\lambda^3$ where ϵ_3 is a (small) constant. The reason for our choice is that eq. (3) also has applications to nonlinear optics [6]. The 1-soliton solution of eq. (3) is:

$$\begin{aligned} u_k^{\rm 1s}(x,t) &= \frac{2\nu_k e^{i\phi_k}}{\cosh z_k}, \\ z_k(x,t) &= 2\nu_k(x-\xi_k(t)), \qquad \xi_k(t) = V_k t + \xi_{k,0} \qquad (7) \\ \phi_k(x,t) &= \frac{v_k}{\nu_k} z_k + \delta_k(t), \qquad \delta_k(t) = W_k t + \delta_{k,0}, \qquad (8) \\ V_k &= \frac{f_{0,k}}{\nu_k}, \qquad W_k = \frac{2}{\nu_k}(\mu_k f_{1,k} - \nu_k f_{0,k}), \qquad (9) \end{aligned}$$

where $f_{0,k}$ and $f_{1,k}$ are related to the dispersion law evaluated at λ_k by $f(\lambda_k) \equiv f(\mu_k + i\nu_k) = f_{0,k} + if_{1,k}$. For the HNLS $f(\lambda) = f^{\rm HN}(\lambda)$ and:

$$V_k = \mu_k - \epsilon_3(3\mu_k^2 - \nu_k^2), \qquad W_k = 2(1 - 4\epsilon_3\mu_k)(\mu_k^2 + \nu_k^2).$$

The analog of Karpman-Solov'iev equations was derived in [11]. Generalized to N-soliton case we again get a CTC of the form:

$$Q_k(t) = 2i\lambda_0\xi_k(t) + 2k\ln(2\nu_0) + i(k\pi - \delta_k(t) - \delta_0), \qquad (10)$$

$$f_0 = \frac{i}{2\nu_0}\left(\frac{{\rm Im}\, f(\lambda_0)}{\nu_0} - \frac{df}{d\lambda}\right)\Big|_{\lambda=\lambda_0} = 1 - 6\epsilon_3\mu_0 - 2i\epsilon_3\nu_0 = |f_0|e^{i\alpha_0} \qquad (11)$$

where $\mu_0 = 1/N \sum_{k=1}^{N} \mu_k$, $\nu_0 = 1/N \sum_{k=1}^{N} \nu_k$, $\delta_0 = 1/N \sum_{k=1}^{N} \delta_k$ and $\lambda_0 = \mu_0 + i\nu_0$.

Remark 1 *For $\epsilon_3 = 0$, $f_0 = 1$ we obtain the results for the NLS case. The factor $16\nu_0^2$ in (6) can be absorbed away by rescaling the time: $t \to \tau = 4\nu_0 t$. If $\epsilon_3 \neq 0$ then the constant f_0^2 is complex. It can be absorbed by redefining Q_k as follows: $Q_k \to \widetilde{Q}_k = Q_k + 2k \ln f_0$. Obviously the argument α_0 of f_0 will play role in determining the conditions on soliton parameters, responsible for the different dynamical regimes, see Sect. 5 below.*

3. *N*-soliton trains of the MNLS equation

The MNLS eq. (2) is solvable by applying the inverse scattering method to the so-called quadratic bundle [7]. The appropriate technique allowing to apply the Karpman-Solov'ev method to the quadratic bundle was developed in [8]. The one-soliton solution is ($\lambda_k = \mu_k + i\nu_k$):

$$u_k^{1s}(z,t) = i\frac{\nu_k}{\alpha}\frac{\lambda_k e^{-z_k} + \bar{\lambda}_k e^{z_k}}{(\lambda e^{z_k} + \bar{\lambda}_k e^{-z_k})^2} e^{i\phi_k}, \quad \phi_k = \frac{\mu_k}{\nu_k} z_k + \delta_k(t), \quad (12)$$

$$z_k = -\frac{\nu_k}{\alpha}\left(x + \frac{\mu_k}{\alpha}t - \xi_{k,0}\right), \quad \delta_k(t) = \frac{1}{2\alpha^2}(\mu_k^2 + \nu_k^2)t + \delta_{k,0}, \quad (13)$$

where we have used the parametrization as in [9]. The CTC model is given by eq. (6) with $f_0 = 1$ where Q_k are expressed in terms of the soliton parameters by [9]:

$$Q_k = -\frac{\nu_0}{\alpha}\xi_k + 4k\ln(\nu_0\sqrt{2}/\alpha) - i\left[k\pi + \frac{\mu_0}{\alpha}\xi_k + \delta_k + \delta_0 + 4S_k\right], \quad (14)$$

$$S_k = 2\sum_{j=1}^{k-1} s_j + s_k, \quad s_k(t) = \frac{1}{2}\arctan\frac{\nu_k}{1+\mu_k}, \quad \delta_0 = \frac{1}{N}\sum_{j=1}^{N}\delta_j. \quad (15)$$

Note that Q_k depends on the soliton phases in a more complicated way. The effects of perturbations to the MNLS eq. will be considered elsewhere.

4. The importance of the CTC model

The fact [14] that the CTC, like the (real) Toda chain (RTC), is a completely integrable Hamiltonian system allows one to analyze analytically the asymptotic behavior of the N-soliton trains. However unlike the RTC, the CTC has richer variety of dynamical regimes [17] such as:

- asymptotically free motion if $v_j \neq v_k$ for $j \neq k$; this is the only dynamical regime possible for RTC;

- N-s bound state if $v_1 = \cdots = v_N$ but $\zeta_k \neq \zeta_j$ for $k \neq j$
- various intermediate (mixed) regimes; e.g., if $v_1 = v_2 > \cdots > v_N$ but $\zeta_k \neq \zeta_j$ for $k \neq j$ then we will have a bound state of the first two solitons while all the others will be asymptotically free;
- singular and degenerate regimes if two or more of the eigenvalues of L become equal, e.g., $\zeta_1 = \zeta_2 \ldots$ and $\zeta_j \neq \zeta_k$ for $2 < j \neq k$.

By $\zeta_k = v_k + iw_k$ above we have denoted the eigenvalues of the Lax matrix L in the Lax representation $L_\tau = [M, L]$ of the CTC where:

$$L = \sum_{k=1}^{N} b_k E_{kk} + \sum_{k=1}^{N-1} a_k (E_{k,k+1} + E_{k+1,k}), \tag{16}$$

$$b_k \equiv -\frac{1}{2}\frac{d\widetilde{Q}_k}{d\tau} = \frac{1}{2} f_0(\mu_k + i\nu_k), \qquad a_k = \frac{1}{2} f_0 \exp((Q_{k+1} - Q_k)/2).$$

The eigenvalues ζ_k of L are time independent. Since now the dynamical variables Q_k are complex-valued, so are ζ_k and the first components $\eta_k = \vec{z}_1^{(k)}$ of the normalized eigenvectors of L:

$$L\vec{z}^{(k)} = \zeta_k \vec{z}^{(k)}, \qquad (\vec{z}^{(k)}, \vec{z}^{(m)}) = \delta_{km}. \tag{17}$$

The set of real and imaginary parts of $\zeta_k = v_k + iw_k$ and $\eta_k = \sigma_k + i\theta_k$ are natural candidates for the set of action-angle variables of the CTC.

Using the CTC model one can determine the asymptotic regime [2, 5] of the N-soliton train given its initial parameters $\mu_k(0)$, $\nu_k(0)$, $\xi_k(0)$, $\delta_k(0)$. Indeed, from these parameters it is easy to calculate the matrix elements b_k and a_k of L at $t = 0$. Then it is a matter of solving an algebraic equation (the characteristic equation for $L|_{t=0}$) to determine the eigenvalues ζ_k and to find out the set of asymptotic velocities $2v_k = 2\mathrm{Re}\,\zeta_k$.

One can use the CTC model also in another way [2, 5]. One can solve the characteristic equation for $L|_{t=0}$ and impose on its roots ζ_k to be all purely imaginary, i.e. all $v_k = 0$. In this way we will find a set of conditions on the initial soliton parameters $\mu_k(0), \nu_k(0), \xi_k(0), \delta_k(0)$ which characterize the region in the soliton parameter space responsible for the N-soliton bound states. Obviously, the problem of describing the sets of soliton parameters responsible for each of the dynamical regimes reduces to solving a set of algebraic equations. Using this method in [5] we have described the set of parameters responsible for the quasi-equidistant propagation. In this regime all N-solitons form a bound state in which the distance between any two neighboring solitons is

$$\xi_{k+1}(t) - \xi_k(t) \simeq r_0 \simeq \mathrm{const}$$

with a very good precision [5]. Such propagation is important for soliton-based fiber optics communications.

We finish this section by showing that the CTC can be considered as a standard *real* Hamiltonian system (see [18]) with $2N$ degrees of freedom. For convenience we first absorb away the factor $16\nu_0^2 f_0^2$ (see remark 1). Then the Hamiltonian and the Poisson brackets are given by:

$$\begin{aligned} H_{\rm CTC} &= \frac{1}{2}\sum_{k=1}^{N}\left((p_{k,0})^2-(p_{k,1})^2\right) \\ &+ \sum_{k=1}^{N-1}\exp\left(\widetilde{Q}_{k+1,0}-\widetilde{Q}_{k,0}\right)\cos\left(\widetilde{Q}_{k+1,1}-\widetilde{Q}_{k,1}\right), \end{aligned} \tag{18}$$

$$\{p_{k,0},\widetilde{Q}_{j,0}\}=-\{p_{k,1},\widetilde{Q}_{j,1}\}=\delta_{kj}, \tag{19}$$

where

$$\widetilde{Q}_k\equiv Q_k+2k\ln f_0=\widetilde{Q}_{k,0}+i\widetilde{Q}_{k,1}, \qquad p_{k,0}+ip_{k,1}=d\widetilde{Q}_k/d\tau.$$

One can check that the equations of motion which follow from (17) and (19) coincide with the real and imaginary parts of (6) with the factor $16\nu_0^2 f_0^2$ absorbed.

5. Dynamical regimes of the HNLS soliton trains

One of the consequences of this formulation is that the Hamiltonian H coincides with $2{\rm Re}\,{\rm tr}\,L^2$. We can express it in terms of the initial soliton parameters and evaluate the energy of the corresponding CTC state. In terms of the scattering data of L the Hamiltonian (17) takes the form:

$$H_{\rm CTC}=2{\rm Re}\,{\rm tr}\,(L)^2=2\sum_{k=1}^{n}(v_k^2-w_k^2). \tag{20}$$

Let us choose the initial soliton parameters so that we have an N-soliton bound state at rest; then $v_k=0$ and the energy of such N-soliton train is negative $E_{\rm BSR}=-\sum_{k=1}^{N}w_k^2<0$. This fact may be used as an argument for the stability of such N-soliton bound states. For the other dynamical regimes v_k are not all equal to zero which allows them to have positive energies.

Let us illustrate our methods for the simplest nontrivial case $N=2$. One way to study the dynamical regimes is to make use of the explicit solution of the CTC. Such solutions for the RTC are well known for all

N, see [17] and the references therein. For $N = 2$ the solution is:

$$\begin{aligned} Q_1(t) &= Q_1(0) - (\zeta_1 + \zeta_2)t + \ln(2r_1r_2) + \ln\cosh Z(t), \\ Q_2(t) &= Q_1(0) - (\zeta_1 + \zeta_2)t + \ln(2r_1r_2) + 2\ln(\zeta_1 - \zeta_2) - \ln\cosh Z(t), \\ Z(t) &= (\zeta_1 - \zeta_2)t - \ln(r_1/r_2), \qquad r_1^2 + r_2^2 = 1, \end{aligned} \tag{21}$$

where ζ_1, ζ_2 are the eigenvalues of L for $N = 2$. For the RTC both the eigenvalues ζ_k, $Q_1(0)$ and the parameters r_k are real and $\zeta_1 \neq \zeta_2$. Each Q_k describes the motion of 'particle' with one degree of freedom. From (21) we can derive the asymptotic behavior of Q_k:

$$\begin{aligned} \lim_{t\to\infty}(Q_k(t) + 2\zeta_{3-k}t) &= Q_1(0) + \ln r_{3-k}^2 + \beta_k, \\ \lim_{t\to-\infty}(Q_k(t) + 2\zeta_k t) &= Q_1(0) + \ln r_k^2 + \beta_k, \\ \beta_1 = 0, \qquad \beta_2 &= \ln 4(\zeta_1 - \zeta_2)^2, \qquad \zeta_1 > \zeta_2. \end{aligned} \tag{22}$$

The two particles always have different asymptotic velocities, which means that the RTC allows only asymptotically free dynamical regime.

Let us now consider the CTC. The first substantial difference with RTC is that now Q_k become complex, i.e. they describe 'particle' with two degrees of freedom (like the NLS solitons). From eq. (10) it follows that the center of mass of the k-th particle (soliton) $\xi_k(t)$ is determined by the real part of Q_k through $\xi_k(t) = (2k\ln(2\nu_0) - \mathrm{Re}\, Q_k(t))/(2\nu_0)$. The second degree of freedom of the k-th 'particle' (soliton) is an internal one and it is described by the phase $\delta_k(t)$ which is determined through $\mathrm{Im}\, Q_k(t)$. Formally the solution to the $N = 2$ CTC is provided by formula (21); however now the parameters ζ_k, $Q_1(0)$ and r_k are complex-valued. The condition $\zeta_1 \neq \zeta_2$ may be also dropped giving rise to singular and degenerate solutions, but in what follows we will keep it.

In order to determine the asymptotic dynamics of CTC we need to evaluate the asymptotics of $\mathrm{Re}\, Q_k(t)$ for $t \to \pm\infty$. The result is:

$$\begin{aligned} \lim_{t\to\infty}(\mathrm{Re}\, Q_k(t) + 2v_{3-k}t) &= \mathrm{Re}\, Q_1(0) + \ln|r_{3-k}|^2 + \mathrm{Re}\,\beta_k, \\ \lim_{t\to-\infty}(\mathrm{Re}\, Q_k(t) + 2v_k t) &= \mathrm{Re}\, Q_1(0) + \ln|r_k|^2 + \mathrm{Re}\,\beta_k, \end{aligned} \tag{23}$$

where β_k are expressed through ζ_k as in (21). Therefore the asymptotic velocities are $2v_k = 2\mathrm{Re}\,\zeta_k$. If these asymptotic velocities are not equal we find the asymptotically free dynamical regime, just like for RTC; in it the distance between both 'particles' grows linearly in time.

However we have also another option in which $v_1 = v_2$ and $w_1 \neq w_2$, so that $\zeta_1 \neq \zeta_2$. Inserting this into eq. (21) we find:

$$Q_1(t) - Q_2(t) = 2\ln\left(\cos(\widetilde{Z}(t))\right) - i\pi - \ln(w_1 - w_2)^2. \tag{24}$$

where $\widetilde{Z}(t) = (\omega_1 - \omega_2)t + i\ln(r_1/r_2)$; i.e., the distance between the particles is a bounded function of t. In other words the particles do not separate asymptotically but form a bound state.

One can also describe analytically the set of soliton parameters responsible for each of the dynamical regimes. We will show how this can be done for the BSR of the two-soliton trains. From the discussion above these sets of parameters are such that $\mathrm{Re}\,(\zeta_1 - \zeta_2) = 0$ where the eigenvalues are the roots of the characteristic equation of $L_0 = L|_{t=0}$:

$$\det(L_0 - \zeta) = \zeta^2 - (b_1 + b_2)\zeta + b_1 b_2 - a_1^2 = 0. \tag{25}$$

What one should do now is to solve (25) and express $\zeta_1 - \zeta_2$ in terms of b_k and a_1. The BSR is obtained provided the discriminant D of (25) is negative:

$$D = (b_1 - b_2)^2 + 4a_1^2 < 0. \tag{26}$$

Now we insert eqs. (10), (11) and (16) into (26) and after some calculations find that (26) is satisfied in the following cases:

i) $\gamma_0 = \alpha_0$ **and** $\delta_2 - \delta_1 = 2(\mu_0 r_0 - \alpha_0)$, where

$$\gamma_0 = \arctan\frac{\Delta\mu}{\Delta\nu}, \qquad \alpha_0 = -\arctan\frac{2\epsilon_3\nu_0}{1 - 6\epsilon_3\mu_0}, \qquad \Delta\nu \neq 0. \tag{27}$$

and $\Delta\mu = \mu_1 - \mu_2$, $\Delta\nu = \nu_1 - \nu_2$.

ii) $\gamma_0 = \alpha_0$ **and** $\delta_2 - \delta_1 = 2(\mu_0 r_0 - \alpha_0) + \pi$, provided $(\Delta\mu)^2 + (\Delta\nu)^2 > 4\nu_0^2 e^{-2\nu_0 r_0}$, where r_0 is the distance between the solitons at $t = 0$.

This idea can be worked out, just like for the NLS case [2, 5], also for $N > 2$. The analyses there becomes more complicated, but always reduces to a set of algebraic constraints on the soliton parameters. In particular, given the initial soliton parameters we can always calculate (at least numerically) the corresponding eigenvalues ζ_k of L_0 which immediately determines the asymptotic regime of the N-soliton train.

Note also that the condition $\gamma_0 = \alpha_0$ requires $\Delta\mu \neq 0$ whenever $\epsilon_3 \neq 0$. For $\epsilon_3 = 0$ this condition simplifies to $\Delta\mu = 0$ and reproduces the results for the NLS soliton trains, see [5].

6. The perturbed NLS and perturbed CTC

From now on for simplicity we will consider the perturbed NLS equation, i.e. we assume $\epsilon_3 = 0$ and $f_0 = 1$. We will consider several specific choices $R^{(p)}[u]$ of perturbations, $p = 1, 2, \ldots$ in (1). In the adiabatic approximation the dynamics of the soliton parameters can be determined by the system, see [1] for $N = 2$ and [2, 5] for $N > 2$:

$$\frac{d\lambda_k}{dt} = -4\nu_0\left(e^{Q_{k+1}-Q_k} - e^{Q_k-Q_{k-1}}\right) + M_k^{(p)} + iN_k^{(p)}, \qquad (28)$$

$$\frac{d\xi_k}{dt} = 2\mu_k + \Xi_k^{(p)}, \qquad \frac{d\delta_k}{dt} = 2(\mu_k^2+\nu_k^2) + X_k^{(p)}, \qquad (29)$$

where $\lambda_k = \mu_k + i\nu_k$ and $X_k^{(p)} = 2\mu_k\Xi_k^{(p)} + D_k^{(p)}$. The right hand sides of Eqs. (28)–(29) are determined by $R_k^{(p)}[u]$ through:

$$N_k^{(p)} = \frac{1}{2}\int_{-\infty}^{\infty}\frac{dz_k}{\cosh z_k}\,\mathrm{Re}\left(R_k^{(p)}[u]e^{-i\phi_k}\right), \qquad (30)$$

$$M_k^{(p)} = \frac{1}{2}\int_{-\infty}^{\infty}\frac{dz_k\,\sinh z_k}{\cosh^2 z_k}\,\mathrm{Im}\left(R_k^{(p)}[u]e^{-i\phi_k}\right), \qquad (31)$$

$$\Xi_k^{(p)} = \frac{1}{4\nu_k^2}\int_{-\infty}^{\infty}\frac{dz_k\,z_k}{\cosh z_k}\,\mathrm{Re}\left(R_k^{(p)}[u]e^{-i\phi_k}\right), \qquad (32)$$

$$D_k^{(p)} = \frac{1}{2\nu_k}\int_{-\infty}^{\infty}\frac{dz_k\,(1-z_k\tanh z_k)}{\cosh z_k}\mathrm{Im}\left(R_k^{(p)}[u]e^{-i\phi_k}\right). \qquad (33)$$

Inserting (28), (29) into (10) we derive:

$$\frac{dQ_k}{dt} = -4\nu_0\lambda_k + \frac{2k}{\nu_0}\mathcal{N}_0^{(p)} + 2i\xi_k\left(\mathcal{M}_0^{(p)} + i\mathcal{N}_0^{(p)}\right) + i\left(2\lambda_0\Xi_k^{(p)} - X_k^{(p)} - \mathcal{X}_0^{(p)}\right), \qquad (34)$$

where

$$\mathcal{N}_0^{(p)} = \frac{1}{N}\sum_{j=1}^{N}N_j^{(p)}, \qquad \mathcal{M}_0^{(p)} = \frac{1}{N}\sum_{j=1}^{N}M_j^{(p)}, \qquad \mathcal{X}_0^{(p)} = \frac{1}{N}\sum_{j=1}^{N}X_j^{(p)}.$$

Deriving eq. (34) we have kept terms of the order $\Delta\nu_k \simeq \mathcal{O}(\sqrt{\epsilon_0})$ and neglected terms of the order $\mathcal{O}(\epsilon_0)$. The perturbations result in that ν_0 and μ_0 may become time-dependent. Indeed, from (28) we get:

$$\frac{d\mu_0}{dt} = \mathcal{M}_0^{(p)}, \qquad \frac{d\nu_0}{dt} = \mathcal{N}_0^{(p)}. \qquad (35)$$

Brief exposition of the approximations used follows. We first will relate the small parameter ϵ_0 with the initial distance $r_0 = |\xi_2 - \xi_1|_{t=0}$ between the two solitons. Assuming $\nu_{1,2} \simeq \nu_0$ we find:

$$\epsilon_0 = \int_{-\infty}^{\infty}dx\left|u_1^{1s}(x,0)u_2^{1s}(x,0)\right| \simeq 8\nu_0 r_0 e^{-2\nu_0 r_0}. \qquad (36)$$

In particular, (36) means that $\epsilon_0 \simeq 0.01$ for $r_0 \simeq 8$ and $\nu_0 = 1/2$.

It is important to note that only the nearest neighbor interactions are to be taken into account. Indeed, we can assume that initially the solitons are ordered in such a way that $\xi_{k+1} - \xi_k \simeq r_0$. One can check [3, 10] that $N_k^{(p)} \simeq M_k^{(p)} \simeq \exp(-2\nu_0|k-p|r_0)$. Therefore the interaction terms between the k-th and $k\pm1$-st solitons will be of the order of $e^{-2\nu_0 r_0}$; the interactions between k-th and $k \pm 2$-nd soliton will of the order of $e^{-4\nu_0 r_0} \ll e^{-2\nu_0 r_0}$.

The terms $\Xi_k^{(0)}$, $X_k^{(0)}$ are of the order of $r_0^a \exp(-2\nu_0 r_0)$, where $a = 0$ or 1. However they can be neglected as compare to $\widetilde{\mu}_k$ and $\widetilde{\nu}_k$, where

$$\widetilde{\mu}_k = \mu_k - \mu_0 \simeq \sqrt{\epsilon_0}, \qquad \widetilde{\nu}_k = \nu_k - \nu_0 \simeq \sqrt{\epsilon_0}. \tag{37}$$

It is easy to see that the corrections to $N_k^{(p)}$, ..., coming from the terms linear in u which may be present in $iR^{(p)}[u]$ depend only on the parameters of the k-th soliton; i.e., they are 'local' in k. The nonlinear in u terms present in $iR^{(p)}[u]$ produce also 'non-local' in k terms in $N_k^{(p)}$, ... For example, assume that $iR^{(p)}[u]$ contains cubic term like $|u|^2u$. We have to insert in it the ansatz (4) and then evaluate the right hand sides of eqs. (30)–(33). Doing this we encounter terms of the form $u_k u_s^* u_p$ and $u_k^* u_s u_p$ where s and p may take any values between 1 and N. One can check, that the corresponding, rather complicated integrals will be of the order of $r_0^a \exp(-2\nu_0(|k-s| + |k-p|)r_0)$, where a is either 0 or 1. In the adiabatic approximation we keep track only of the leading terms $r_0^a \exp(-2\nu_0 r j_0)$. This is possible if: i) $s = p = k$ and then we get 'local' in k terms; ii) $s = k$ and $p = k \pm 1$ or iii) $s = k \pm 1$ and $p = k$. The cases ii) and iii) give rise to 'non-local' in k terms corresponding to nearest neighbor interaction. All other choices for the triple k, s, p leads to higher order terms and are neglected.

In the next subsections we briefly analyze specific types of perturbations, see [3]. In most cases this leads to a perturbed version of the CTC.

6.1 Second order dispersion and nonlinear gain

Consider the NLS eq. (1) with

$$R[u] = c_0 u + c_2 u_{xx} + d_0|u|^2 u, \tag{38}$$

where c_0, c_2 and d_0 are real constants, see [10].

Another important factor is the order of magnitude of the perturbation coefficients c_0, c_2 and d_0 in (38). If we take them to be of the order of ϵ_0 we find that the N-soliton train evolves according to:

$$\frac{d^2 Q_k}{dt^2} = U_{00} + 16\nu_0^2 \left(e^{Q_{k+1}-Q_k} - e^{Q_k - Q_{k-1}}\right), \tag{39}$$

where for $\mu_0 = 0$ we get $U_{00} = -\frac{8i\nu_0^2}{3}\left(3c_0 + 8\nu_0^2 d_0 - 4c_2\nu_0^2\right)$. This form of perturbed CTC (39) can be solved exactly:

$$Q_k(t) = \frac{1}{2}U_{00}t^2 + V_{00}t + Q_k^{(0)}(t),$$

where $Q_k^{(0)}(t)$ is a solution of the unperturbed CTC and V_{00} is an arbitrary constant. In this cases the effect of the perturbation will be an overall motion of the center of mass of the N-soliton train. The relative motion of the solitons will remain the same!

The situation when the coefficients c_0, c_2 and d_0 become larger, e.g., of the order of $\sqrt{\epsilon_0}$ the corresponding dynamical system becomes more complicated and has to be treated separately.

6.2 Quadratic and periodic potentials

Let $iR[u] = V(x)u(x,t)$. Our first choice for $V(x)$ is a quadratic one:

$$V_1(x) = v_2x^2 + v_1x + v_0. \tag{40}$$

Skipping the details we get the results:

$$N_k^{(1)} = 0, \qquad M_k^{(1)} = -v_2\xi_k - \frac{v_1}{2}, \tag{41a}$$

$$\Xi_k^{(1)} = 0, \qquad D_k^{(1)} = v_2\left(\frac{\pi^2}{48\nu_k^2} - \xi_k^2\right) - v_1\xi_k - v_0, \tag{41b}$$

and $X_k^{(1)} = D_k^{(1)}$. As a result the corresponding PCTC takes the form:

$$\frac{d(\mu_k + i\nu_k)}{dt} = -4\nu_0\left(e^{Q_{k+1}-Q_k} - e^{Q_k-Q_{k-1}}\right) - v_2\xi_k - \frac{v_1}{2}, \tag{42}$$

$$\frac{dQ_k}{dt} = -4\nu_0(\mu_k + i\nu_k) - iD_k^{(1)} - \frac{i}{N}\sum_{j=1}^{N} D_j^{(1)}. \tag{43}$$

If we now differentiate (43) and make use of (42) we get:

$$\begin{aligned}\frac{d^2Q_k}{dt^2} &= 16\nu_0^2\left(e^{Q_{k+1}-Q_k} - e^{Q_k-Q_{k-1}}\right) + 4\nu_0\left(v_2\xi_k + \frac{v_1}{2}\right)\\ &- i\frac{dD_k^{(1)}}{dt} - \frac{i}{N}\sum_{j=1}^{N}\frac{dD_j^{(1)}}{dt}.\end{aligned} \tag{44}$$

It is reasonable to assume that $v_2 \simeq \mathcal{O}(\epsilon_0/N)$; this ensures the possibility to have the N-soliton train 'inside' the potential. It also means that

both the exponential terms and the correction terms $M_k^{(1)}$ are of the same order of magnitude.

From eqs. (42) and (43) there follows that $d\nu_0/dt = 0$ and:

$$\frac{d\mu_0}{dt} = -v_2\xi_0 - \frac{v_1}{2}, \qquad \frac{d\xi_0}{dt} = 2\mu_0, \tag{45}$$

where μ_0 is the average velocity and $\xi_0 = \frac{1}{N}\sum_{j=1}^{N}\xi_j$, is the center of mass of the N-soliton train. The system of equations (45) for $v_2 > 0$ has a simple solution

$$\mu_0(t) = \mu_{00}\cos(\Phi(t)), \qquad \xi_0(t) = \sqrt{\frac{2}{v_2}}\mu_{00}\sin(\Phi(t)) - \frac{v_1}{2v_2}, \tag{46}$$

where $\Phi(t) = \sqrt{2v_2}t + \Phi_0$, and μ_{00} and Φ_0 are constants of integration. Therefore the overall effect of such quadratic potential will be to induce a slow periodic motion of the train as a whole.

Another important choice is the periodic potential

$$V_2(x) = V_{(0)}\sin^2(\omega x + \omega_0), \tag{47}$$

where $V_{(0)}$, ω and ω_0 are appropriately chosen constants. NLS equation with such potentials appear in a natural way in the study of Bose-Einstein condensates, see [16]. The corresponding integrals for N_k, M_k, Ξ_k and D_k can be evaluated with the result:

$$N_k^{(2)} = 0, \qquad M_k^{(2)} = -\frac{\omega V_{(0)}}{2}\sin(2\omega\xi_k + 2\omega_0)\frac{Z_k}{\sinh Z_k}, \tag{48}$$

$$\Xi_k^{(2)} = 0, \qquad D_k^{(2)} = \frac{V_{(0)}}{2}\cos(2\omega\xi_k + 2\omega_0)\frac{Z_k^2\cosh Z_k}{\sinh^2 Z_k} - \frac{V_{(0)}}{2}. \tag{49}$$

where $Z_k = \pi\omega/(2\nu_k)$. These results allow one to derive the corresponding perturbed CTC models. Again we find that $d\nu_0/dt = 0$.

7. Analysis of the Perturbed CTC

Next step will be to analyze each of the perturbed systems above and to see to what extent it allows analytical treatment. The idea is to look for the solutions of PCTC in the form:

$$Q_k(t) = Q_k^{(0)}(t) + s_0(t) + s_k(t), \tag{50}$$

where $Q_k^{(0)}(t)$ is a solution of the unperturbed CTC; $s_0(t)$ describes the center of mass motion – i.e. it may depend on t but not on k. Finally, $s_k(t)$ describes the effect of the perturbation on the relative motion of

neighboring solitons. Note that $s_0(t)$ may not be small, but this is the global driving effect of the potential on the Toda chain. One may be able to solve explicitly for $s_0(t)$. For quadratic potential this was done above.

The real-valued potentials do not change the right hand side of the CTC equations for ν_k and ξ_k. The terms $s_k(t)$ are generically small and can be considered as first nontrivial corrections.

The perturbed CTC allows one to study the simultaneous effect of several perturbations by just taking the sum over the relevant values of p in the right hand sides of eqs. (28), (29).

8. Discussion

Like any other model, the predictions of the CTC should be compared with the numerical solutions of the corresponding NLEE. Such comparison for the NLS has been done thoroughly in [2, 3, 5] and excellent match has been found for all dynamical regimes. For the MNLS eq. such comparison has been performed in [9] with a good agreement. For the HNLS and SG equations up to now no such check has been performed.

Thus we have established that the CTC describes the adiabatic N-soliton interactions for several NLEE and

- is valid for NLEE with different dispersion laws $f(\lambda)$;
- is valid for NLEE solvable with substantially different Lax operators.
- Analogous perturbed versions of CTC describe the N-soliton train interactions also for the perturbed MNLS and HNLS equations.
- Recently it was shown [19] that the N-soliton interaction for the Ablowitz-Ladik system can also be modelled by the CTC.

This supports our hypothesis that the CTC is an *universal model* for describing the adiabatic N-soliton interactions. The exponential terms in CTC are related to the exponential decay of solitons. Other aspects of the Hamiltonian formulation of CTC are analyzed in [18].

Acknowledgments

I am grateful to Professors V. V. Konotop, M. Salerno, E. Doktorov and to Dr B. Baizakov and Dr N. Kostov for useful discussions. Financial support in part from Gruppo collegato di INFN at Salerno, Italy and project PRIN 2000 (contract 323/2002) is gratefully acknowledged.

References

[1] V. I. Karpman, V. V. Solov'ev. Physica D **3D**, 487-502, (1981).

[2] V. S. Gerdjikov, D. J. Kaup, I. M. Uzunov, E. G. Evstatiev. Phys. Rev. Lett. **77**, 3943-3946 (1996).

[3] V. S. Gerdjikov, I. M. Uzunov, E. G. Evstatiev, G. L. Diankov. Phys. Rev. E **55**, No 5, 6039-6060 (1997).

[4] J. M. Arnold. JOSA A **15**, 1450-1458 (1998); Phys. Rev. E **60**, 979-986 (1999).

[5] V. S. Gerdjikov, E. G. Evstatiev, D. J. Kaup, G. L. Diankov, I. M. Uzunov. Phys. Lett. A **241**, 323-328 (1998).

[6] Y. Kodama, A. Hasegawa. IEEE J. of Quant. Electron. **QE-23**, 510 - 524 (1987).

[7] V. S. Gerdjikov, M. I. Ivanov, P. P. Kulish. Theor. Math. Phys. **44,** No.3, 342–357, (1980), (In Russian). V. S. Gerdjikov, M. I. Ivanov. Bulgarian J. Phys. **10,** No.1, 13–26; No.2, 130–143, (1983), (In Russian).

[8] V. S. Shchesnovich and E. V. Doktorov, Physica D **129**, 115 (1999); E. V. Doktorov and V. S. Shchesnovich, J. Math. Phys. **36**, 7009 (1995).

[9] V. S. Gerdjikov, E. V. Doktorov, J. Yang. Phys. Rev. E **64**, 056617 (2001).

[10] V. S. Gerdjikov, I. M. Uzunov. Physica D **152-153**, 355-362 (2001).

[11] E. G. Evstatiev. N-soliton interactions of higher NLS equations. Diploma thesis, Sofia University (1995) (unpublished).

[12] V. E. Zakharov, S. V. Manakov, S. P. Novikov, L. I. Pitaevskii. Theory of solitons: the inverse scattering method (Plenum, N.Y.: Consultants Bureau, 1984).

[13] L. A. Takhtadjan and L. D. Faddeev, *Hamiltonian Approach to Soliton Theory.* (Springer Verlag, Berlin, 1986).

[14] S. V. Manakov. *JETPh* **67**, 543 (1974); H. Flaschka. Phys. Rev. **B9**, n. 4, 1924–1925, (1974);

[15] V. S. Gerdjikov. Complex Toda Chain – an Integrable Universal Model for Adiabatic N-soliton Interactions! In: Proc. of the workshop "Nonlinear Physics: Theory and Experiment.II", Gallipoli, June-July 2002; Eds.: M. Ablowitz, M. Boiti, F. Pempinelli, B. Prinari. p. 64-70 (2003).

[16] J. C. Bronski, L. D. Carr, B. Deconinck, J. N. Kutz Phys. Rev. E **63**, 036612 (2001); Phys. Rev. Lett. **86**, 1402-1405 (2001); J. C. Bronski, L. D. Carr, R. Carretero-Gonzales, B. Deconinck, J. N. Kutz, K. Promislow. Phys. Rev. E **64**, 056615 (2001); F. Kh. Abdullaev, B. B. Baizakov, S. A. Darmanyan, V. V. Konotop, M. Salerno. Phys. Rev. A **64**, 043606 (2001).

[17] J. Moser, In *Dynamical Systems, Theory and Applications.* Lecture Notes in Physics, **v. 38**, Springer Verlag, (1975), p. 467. V. S. Gerdjikov, E. G. Evstatiev, R. I. Ivanov. *The complex Toda chains and the simple Lie algebras – solutions and large time asymptotics* J. Phys. A: Math & Gen. **31**, 8221-8232 (1998).

[18] V. S. Gerdjikov, A. Kyuldjiev, G. Marmo, G. Vilasi, *Eur. Phys. J.* **B29**, 177-181 (2002).

[19] E. Doktorov. Private communication; see also E. V. Doktorov, N. P. Matsuka, V. M. Rothos. **nlin.SI/0311010** (2003).

DYNAMICAL STABILIZATION OF NONLINEAR WAVES

Fatkhulla Abdullaev
Physical-Technical Institute, Uzbek Academy of Sciences, Mavlyanova str. 2-b, 700084 Tashkent, Uzbekistan
fatkh@physic.uzsci.net

Abstract Dynamics of solitons in the nonlinear media with rapidly varying parameters are investigated. One-dimensonal and two-dimensional nonlinear Schrödinger equations with a periodic modulation in time of the dispersion, the nonlinearity and the linear potential, are considered. As physical applications we study problems: 1) the stabilization of atomic matter *soliton* in Bose-Einstein condensate (BEC) with a rapidly varying trap potential; 2) the dynamical stabilization of bright soliton in two dimensional BEC by rapidly oscillating atomic scattering length; (the Feshbach resonance or nonlinearity management), 3)the existence of stable two dimensional dispersion-managed soliton.

Keywords: Stabilization of Townes soliton, periodic dispersion, nonlinearity, oscillating trap, nonlinear matter waves, rapid perturbations, Bose-Einstein condensate.

1. Introduction

Recently bright matter wave solitons have been observed in a Bose-Einstein condensate (BEC) [1, 2]. In the experiment described in Ref. [1] propagation in an anisotropic BEC of cigar type geometry was considered. In Ref. [2] the soliton was monitored by projecting the bound state of approximately 5000 atoms into expulsive harmonic potential. The soliton was observed to propagate without changing in its form for distances of order of $\sim$ 1mm [1]. The expulsive harmonic trap used in the experiment, corresponds to an unstable potential for the GP equation and a soliton can exist only as a metastable state in BEC [3, 4]. It is of interest to investigate the dynamics of a bright matter wave soliton in inhomogeneous time dependent systems, in particular possible stabilization of unstable dynamics or complicated dynamics of solitons in BEC.

F. Kh. Abdullaev and V. V. Konotop (eds.), Nonlinear Waves: Classical and Quantum Aspects, 29–44.

An interesting example of such a trap is an optical trap which is rapidly varied in time indeed. We will call such scheme as follows:

a) The management of potential.

Such management of potential is realized for instance for a condensate in a dipole trap formed by a strong off-resonant laser field [5]. A typical model is a trap formed by a harmonic potential with different frequencies which is cut at some energy V_c. Numerical simulations of the condensate dynamics in 1D BEC with a positive scattering length under periodically shaken trap performed in Ref.[5] show existence of splittings of the condensate. The same form of wave equation governs propagation of spatial solitons in periodically modulated parabolic waveguides. This problem appears in investigation of intense light beams in a nonlinear waveguide with inhomogeneous distribution of a transverse refractive index. A typical distribution can be approximated by a quadratic profile. The rapid variation of this profile along the longitudinal direction leads to a rapidly varying quadratic potential in the nonlinear Schrödinger (NLS) equation. Here we will consider the evolution under rapidly varying in time trap potential [6].

The general mathematical problem is to investigate localized states for the nonlinear wave equation with cubic nonlinearity and with rapidly varying (not small) potential of the form $V_0 = f(x)\alpha(t/\epsilon), \epsilon \ll 1$. Also it is of interest to investigate possibilities of stabilization of a soliton by rapid perturbations. For multi dimensional NLS equation under rapidly varying in *space* periodic potential such a problem is discussed in [7]. We derive the averaged equation and show that the dynamics can be described by the effective potential equal to unperturbed potential plus second order corrections of new functional form.

Another possibilities for the 2D soliton stabilization are open due the possibilities of periodic variations of nonlinearity or dispersion coefficients in the 2D Gross-Pitaevskii (GP) equation - i.e. a nonlinearity and a dispersion management schemes.

b) Nonlinearity management for 2D solitons.

The coefficient in front of the cubic termin the GP equation, proportional to the collision scattering length, may be both positive and negative, which corresponds, respectively, to repulsive and attractive interactions between the atoms [8]. In the case of an attractive interaction, a soliton may be formed in an effectively one-dimensional (1D) condensate; however, in 2D and 3D cases the attraction results in the collapse of the condensate (*weak* and *strong* collapse, respectively [9]) if the number of atoms exceeds a critical value [8].

Recently developed experimental techniques [10] make it possible to effectively control the sign of the scattering length using an external

magnetic field because the interaction constant can be changed through the Feshbach resonance [11]. This technique makes it possible to quickly reverse (in time) the sign of the interaction from repulsion to attraction, which gives rise, via the onset of collapse, to an abrupt shrinking of the condensate, followed by a burst of emitted atoms and the formation of a stable residual condensate [10].

A natural generalization of this approach for controlling the strength and sign of the interaction between atoms and, thus, the coefficient in front of the cubic term in the corresponding GP equation, is the application of a magnetic field resonantly coupled to the atoms and consisting, in the general case of dc and ac components. The dynamical behavior of 2D and 3D condensates in this case is then an issue of straightforward physical interest, as it may be readily implemented in experiments. It is noteworthy that, in the 2D case, this issue is similar to a problem which was recently considered in nonlinear optics for (2+1)D spatial solitons (i.e., self-confined cylindrical light beams) propagating across a nonlinear bulk medium with a layered structure, so that the size [12] and, possibly, the sign [13] of the Kerr (nonlinear) coefficient are subject to a periodic variation along the propagation distance (it plays the role of the evolutional variable, instead of time, in the description of optical spatial solitons). The same optical model makes also sense in the (3+1)D case, because it applies to the propagation of "light bullets" (3D spatiotemporal solitons [14]) through the layered medium [13]. We will demonstrate below that the results obtained for the BEC dynamics in the GP equation involving both a dc and ac nonlinearity are indeed similar to findings reported in the framework of the above-mentioned optical model [15, 16, 17, 18].

c)Dispersion management for 2D solitons.

Nonlinear wave propagation in media with periodically varying dispersion is attracting huge interest over the recent years. A prominent example is a dispersion-managed (DM) optical soliton, which is considered to become the major concept in future soliton-based communication systems. It was shown theoretically and experimentally that the strong DM regime provides the undisturbed propagation of pulses over very long distances. DM solitons are robust to the Gordon-Haus timing jitter, which makes them favorable against the standard solitons [19, 20].

Although well studied in the 1D case, the two and three dimensional extensions of this problem are far less explored. The major difference here is that, contrary to the 1D case, the NLS equation in two and three dimensions is unstable against collapse. From the analysis of the nonlinearity management, these one can reasonably expect that the dispersion-management can play balancing role also in the 2D case, and the stable

2D DM soliton can exist. Such a possibility has recently been considered in Ref.[21] by construction of the ground state for the periodic 2D NLS equation based on the averaged variational principle and the techniques of integral inequalities - i.e. the proof of the existence theorem for DM soliton was presented. Analytical and numerical treatment of the problem, however, has not been addressed so far.

Here we derive the analytical expressions for the parameters of a DM soliton in two dimensions [22]. We consider a 2D NLS equation with cubic nonlinearity and periodically varying dispersion coefficient. The time-dependent variational approach (VA) will be used to derive the set of ODEs for soliton parameters. The analytical expressions for the fixed points of VA equations will be derived and the stability of these fixed points will be analyzed.

2. Dynamics of solitons in BEC with rapidly oscillating trap

The dynamics of BEC is described by the time dependent GP equation

$$i\psi_\tau = -\frac{\hbar^2}{2m}\Delta\psi + V_{tr}(r,t)\psi + g_0|\psi|^2\psi, \tag{1}$$

where m is the atom mass, $g = 4\pi\hbar^2 a_s/m$ and a_s is the atomic scattering length. $a_s > 0$ corresponds to the BEC with repulsive interaction between atoms and $a_s\langle 0$ to the attractive interaction. The trap potential is given by $V_{tr} = m\omega^2(y^2+z^2)/2 + \alpha(t)(m\omega_1^2 x^2/2 + V_1(x,t))$, where $V_1(x,t)$ is a bounded potential or the optical lattice potential, $\alpha(t)$ describes the time dependence of the potential. We will specify the form of V_1 later. Below we will consider the condensate of cigar type with $\omega^2 \gg \omega_1^2$. Within such restrictions we can look for the solution of eq.(1) of the form $\psi(x,y,z,t) = R(y,z)\phi(x,t)$, where R satisfies the equation

$$-\frac{\hbar^2}{2m}\Delta R + \frac{m\omega^2}{2}(y^2+z^2)R = \lambda_\rho R,\ \lambda = \hbar\omega.$$

Averaging over the transverse mode R(i.e. multiplying by R^*,

$$|R_0|^2 = \frac{m\omega}{\pi\hbar}\exp(-\frac{m\omega}{\hbar}\rho^2),$$

and integrating over ρ) we obtain the quasi 1D GP for ϕ [23]

$$i\hbar\phi_\tau = -\frac{\hbar^2}{2m}\phi_{xx} + \alpha(\tau)\left(\frac{m\omega_1^2 x^2}{2} + V_1(x,\tau)\right)\phi + G|\phi|^2\phi, \tag{2}$$

where $G = g\int |R|^4 dxdy/\int |R|^2 dxdy = (2\hbar|a_s|\omega)$. In the dimensionless variables

$$t = \omega\tau/2,\ x = x/l,\ l = \sqrt{\frac{\hbar}{m\omega}},\ u = \sqrt{2|a_s|}\phi,$$

we have the governing equation

$$iu_t + \beta u_{xx} + 2\sigma|u|^2 u = \alpha(t)f(x)u. \tag{3}$$

where we will suppose a periodic modulation of the trap

$$\alpha(t) = \alpha_0 + \alpha_1 \sin(\Omega t). \tag{4}$$

For example for $V_{tr} = m\omega_1^2 x^2/2$ we have $\alpha_0 f(x) = (\omega_1/\omega)^2 x^2$. We introduced the parameter $\beta = \pm 1$ in order to have opportunity to use the results obtained for optical beam propagation. For the BEC system $\beta = 1$. As well as $\sigma = \pm 1$ corresponds to the attractive and repulsive two body interactions respectively.

The field $u(x,t)$ can be represented in the form of sum of slowly and rapidly varying parts $U(x,t)$ and $\xi(x,t)$

$$u(x,t) = U(x,t) + \xi(x,t). \tag{5}$$

For obtaining the equation for an averaged field we will apply the asymptotic procedure suggested in [7], namely we will present the rapidly varying part of the field as expansion on Fourier series

$$\xi = A\sin(\Omega t) + B\cos(\Omega t) + C\sin(2\Omega t) + D\cos(2\Omega t) + ... \tag{6}$$

where A, B, C, D are functions of (x,t) that are slowly varying in the scale $O(1)$ functions. By substituting the equations (5),(6) into (3) we obtain the next set of equations for the slowly varying field and the coefficients of the expansion for the rapidly varying component

$$\begin{aligned} iU_t + \beta U_{xx} + 2|U|^2 U + U^*(A^2 + B^2 + C^2 + D^2) + +2U(|A|^2 + \\ |B|^2 + |C|^2 + |D|^2) + (BCA^* - |A|^2 D + ACB^* + |B|^2 D + \\ +ABC^* + \frac{A^2 D^*}{2} = \alpha f(x)U + \frac{\alpha_1}{2} f(x)A \end{aligned} \tag{7}$$

$$\begin{aligned} iA_t - i\Omega B + \beta A_{xx} + 4|U|^2 A + 2U^*(BC - AD) + 2U^2 A^* + ... \\ = \alpha_1 f(x)U - \frac{\alpha_1}{2} f(x)D, \end{aligned} \tag{8}$$

$$i\Omega A + iB_t + \beta B_{xx} + 4|U|^2 B + 2U^2 B^* + 2U^*(AC + BD) + ... = \frac{\alpha_1}{2} f(x) C, \quad (9)$$

$$iC_t - 2i\Omega D + \beta C_{xx} + 4|U|^2 C + 2U^* AB + ... = \frac{\alpha_1}{2} f(x) B, \quad (10)$$

$$2i\Omega C + iD_t + \beta D_{xx} + 4|U|^2 D + U^*(B^2 - A^2) + ... = -\frac{\alpha_1}{2} f(x) A. \quad (11)$$

The parameters α_1, Ω are assumed $\gg 1$. As we can find from this system, the coefficients can be represented in the form of expansion

$$A = \frac{a_1}{\Omega^2} + \frac{a_2}{\Omega^4},\ B = \frac{b_1}{\Omega} + \frac{b_2}{\Omega^3},$$
$$C = \frac{c_1}{\Omega^3} + \frac{c_2}{\Omega^5},\ D = \frac{d_1}{\Omega^2} + \frac{d_2}{\Omega^4}. \quad (12)$$

For the coefficients of expansion we have the expressions

$$a_1 = -i\alpha_1 f(x) U_t - \alpha_1 (f(x)U)_{xx}) - 2\alpha_1 f(x)|U|^2 U + \alpha_0 \alpha_1 f^2(x) U,$$
$$b_1 = i\alpha_1 f(x) U, \qquad d_1 = \frac{\alpha_1^2 f(x)^2}{4} U, \qquad c_1 = ... \quad (13)$$

From (6),(11),(12) we obtain the averaged equation for U

$$iU_t + \beta U_{xx} + 2|U|^2 U = \alpha_0 f(x) U - i\frac{\epsilon^2}{2} f^2(x) U_t$$
$$-\beta \frac{\epsilon^2}{2} f(x)(f(x)U)_{xx} - 2\epsilon^2 f^2(x)|U|^2 U + \frac{\epsilon^2 \alpha_0}{2} f^2(x) U. \quad (14)$$

Here $\epsilon = \alpha_1/\Omega$.

This equation has the conserved quantity - the number of atoms

$$\int_{-\infty}^{\infty} dx \left(1 + \frac{\epsilon^2 f^2(x)}{2}\right) |U|^2 = \text{const}. \quad (15)$$

So, it is useful to introduce the new field V by

$$V = \left(1 + \frac{\epsilon^2 f^2(x)}{2}\right)^{1/2} U. \quad (16)$$

Substituting (16) into (13) and keeping the terms of order ϵ^2 we obtain the equation

$$iV_t + \beta V_{xx} + 2|V|^2 V = (\alpha_0 f(x) + \frac{\epsilon^2}{2}\beta[f_x(x)]^2)V + O(\epsilon^4). \qquad (17)$$

The averaged equation has the form of a modified NLS equation with a slowly varying potential

$$W(x) = \alpha_0 f(x) + \frac{\epsilon^2}{2}\beta[f_x(x)]^2. \qquad (18)$$

This result shows that the soliton dynamics can have more complicated character than in the case of BEC with slowly varying parameters. We can expect here the stabilization of the unstable dynamics of a soliton by rapidly varying perturbation. It is a direct analogy with the stabilization of systems with a few degrees of freedom under rapidly oscillating perturbation [24].

3. Stable two dimensional bright soliton under Feschbach resonance management

In the case of a high-frequency modulation, there is a possibility to apply the averaging method directly to the 2D Gross-Pitaevskii equation, without using the VA. Note that direct averaging was applied to the 2D nonlinear Schrödinger equation (NLS) with a potential rapidly varying in *space*, rather than in time, in Ref. [7], where the main results were a renormalization of the parameters of the 2D NLS equation and a shift of the collapse threshold. As we will see below, a rapid temporal modulation of the nonlinear term in the GP equation leads to new effects, which do not reduce to a renormalization. Namely, new nonlinear-dispersive and higher-order nonlinear terms will appear in the corresponding effective NLS equation [see Eq. (23) below]. These terms essentially affect the dynamics of the collapsing condensate.

Assuming that the ac frequency ω is large, we rewrite the 2D GP equation in a more general form,

$$i\partial\psi/\partial t + \Delta\psi + \lambda(\omega t)|\psi|^2\psi = 0, \qquad (19)$$

where Δ is the 2D Laplacian. To derive an equation governing the slow variations of the field, we use the multiscale approach, writing the solution as an expansion in powers of $\varepsilon = 1/\omega$ and introducing the slow temporal variables, $T_k \equiv \omega^{-k}t$, $k = 0, 1, 2...$, while the fast time is $\zeta \equiv \omega t$. Thus, the solution is sought for as

$$\psi(r,t) = A(r,T_k) + \omega^{-1}u_1(\zeta,A) + \omega^{-2}u_2(\zeta,A) + ..., \qquad (20)$$

with $\langle u_k \rangle = 0$, where $\langle ... \rangle$ stands for the average over the period of the rapid modulation, and we assume that $\lambda_0 = +1$ (i.e., the dc part of the nonlinear coefficient corresponds to attraction between the atoms).

Following a procedure developed, for a similar problem, in Ref. [25], we first find the first and second corrections,

$$u_1 = -i[\mu_1 - \langle \mu_1 \rangle]|A|^2 A, \tag{21}$$

$$u_2 = [\mu_2 - \langle \mu_2 \rangle][2i|A|^2 A_t + iA^2 A_t^* + \Delta(|A|^2 A)] - |A|^4 A \left[\frac{1}{2}[(\mu_1 - \langle \mu_1 \rangle)^2 - 2M] + \langle \lambda \rangle (\mu_2 - \langle \mu_2 \rangle) \right]. \tag{22}$$

Here

$$\mu_2 = \int_0^\zeta (\mu_1 - \langle \mu_1 \rangle) ds, \qquad \mu_1 \equiv \int_0^\zeta [\lambda(\tau) - \langle \lambda_1 \rangle] \, d\tau$$

$$M = (1/2)(\langle \mu_1^2 \rangle - \langle \mu_1 \rangle^2) = (1/2)(\langle \lambda^2 \rangle - 1)$$

(recall we have set $|\lambda_0| = 1$). Using these results, we obtain the following evolution equation for the slowly varying field $A(x, T_0)$, derived at the order ω^{-2}:

$$i\frac{\partial A}{\partial t} + \Delta A + |A|^2 A + 2M \left(\frac{\epsilon}{\omega} \right)^2 [|A|^6 A - 3|A|^4 \Delta A + 2|A|^2 \Delta(|A|^2 A) + A^2 \Delta(|A|^2 A^*)] = 0. \tag{23}$$

We stress that Eq. (23) is valid in both 2D and 3D cases. In either case, it can be represented in the quasi-Hamiltonian form,

$$\left[1 + 6M \left(\frac{\epsilon}{\omega} \right)^2 |A|^4 \right] \frac{\partial A}{\partial t} = -i \frac{\delta H_q}{\delta A^*}, \tag{24}$$

$$H_q = \int dV \left[|\nabla A|^2 - 2M \left(\frac{\epsilon}{\omega} \right)^2 |A|^8 - \frac{1}{2} |A|^4 + 4M \left(\frac{\epsilon}{\omega} \right)^2 \left| \nabla \left(|A|^2 A \right) \right|^2 \right], \tag{25}$$

where dV is the infinitesimal volume in the 2D or 3D space. To cast this result in a canonical Hamiltonian representation, one needs to properly define the corresponding symplectic structure (Poisson's brackets), which is not our aim here. However, we notice that, as it immediately follows from Eq. (24) and the reality of the (quasi-)Hamiltonian (25), H_q is an integral of motion, i.e., $dH_q/dt = 0$.

For a further analysis of the 2D case, we apply a modulation theory developed in Ref. [26]. According to this theory, the solution is searched for in the form of a modulated Townes soliton. The (above-mentioned) Townes soliton is a solution to the 2D NLS equation in the form $\psi(r,t) = e^{it}R_T(r)$, where the function $R_T(r)$ satisfies the boundary value problem

$$R_T'' + r^{-1}R_T' - R_T + R_T^3 = 0, \quad R_T'(0) = 0, \quad R_T(\infty) = 0. \tag{26}$$

For this solution, the norm N and the Hamiltonian H take the well-known values, $N_T = 1.862$, $H_T = 0$.

The averaged variational equation (23) indicates an increase of the critical number of atoms for the collapse, as opposed to the classical value N_T. Using the relation (20), we find

$$N_{\rm crit} = \int_0^\infty |\psi|^2 r dr = N_T + 2M\left(\frac{\epsilon}{\omega}\right)^2 I_6,$$

where $I_6 = 11.178$. This increase in the critical number of atoms is similar to the well-known energy enhancement of dispersion-managed solitons in optical fibers with periodically modulated dispersion.

Another nontrivial perturbative effect is the appearance of a nonzero value of the phase *chirp* inside the stationary soliton. We define the mean value of the chirp as

$$b = \frac{\int_0^\infty {\rm Im}\left(\frac{\partial\psi}{\partial r}\psi^*\right) r dr}{\int_0^\infty r^2 dr|\psi|^2}.$$

Making use of the expression (21) for the first correction, we find

$$b = -\frac{\epsilon}{\omega} BM\left(\mu_1 - \langle\mu_1\rangle\right),$$

$$B \equiv 3\frac{\int_0^{+\infty} r dr R^2 (R')^2 - (0.25)\int_0^{+\infty} dr R^4}{\int_0^{+\infty} r^2 dr R^2} = 0.596.$$

To develop a general analysis, we assume that the solution with the number of atoms close to the critical value may be approximated as a modulated Townes soliton, i.e.

$$A(r,t) \approx [a(t)]^{-1} R_T(r/a(t)) e^{iS}, \; S = \sigma(t) + \frac{\dot{a}r^2}{4a}, \; \dot{\sigma} = a^{-2} \tag{27}$$

with some function $a(t)$ (where the overdot stands for d/dt). If the initial power is close to the critical value, i.e., when $|N - N_c| \ll N_c$ and the perturbation is conservative,i.e.

$${\rm Im}\int dV[A^* F(A)] = 0$$

as in our case, a method worked out in Ref. [26] makes it possible to derive an evolution equation for the function $a(t)$, starting from the approximation (27). The equation of modulation theory for width is

$$a^3 a_{tt} = -\beta_0 + \frac{\epsilon^2}{4M_0\omega^2} f_1(t), \tag{28}$$

where

$$\beta_0 = \beta(0) - \frac{\epsilon^2 f_1(0)}{4M_0\omega^2},\ \beta(0) = \frac{(N - N_c)}{M_0},$$

and $M_0 \equiv (1/4)\int_0^\infty r^3 dr R_T^2 \approx 0.55$. The auxiliary function is given by

$$f_1(t) = 2a(t)\mathrm{Re}\left[\frac{1}{2\pi}\int dxdy F(A_T)e^{-iS}(R_T + \rho\nabla R_T(\rho))\right]. \tag{29}$$

In the lowest-order approximation, the equation takes the form (for the harmonic modulation)

$$\frac{d^2a}{dt^2} = -\frac{\Lambda_1}{a^3} + \frac{C\epsilon^2}{\omega^2 a^7}, \tag{30}$$

where $\Lambda_1 = (N - N_c)/M_0 - C\epsilon^2/(\omega^2 a_0^4)$ and C is

$$C \equiv \frac{3}{M_0}\int_0^\infty d\rho\left[2\rho R_T^4 (R_T')^2 - \rho^2 R_T^3 (R_T')^3 - \frac{1}{8}\rho R_T^8\right] \approx 39. \tag{31}$$

Thus the averaged equation predicts the *arrest* of collapse by the rapid modulations of the nonlinear term in the 2D GP equation.

Let us estimate the value of the fixed point for the numerical simulations performed in Ref.[15]. In this work the stable propagation of soliton has been observed for two step modulation of the nonlinear coefficient in 2D NLSE. The modulation of the nonlinear coefficient was $\lambda = 1 + \epsilon$ if $T > t > 0$, and $\lambda = 1 - \epsilon$ for $2T > t > T$. The parameters in the numerical simulations has been taken as $T = \epsilon = 0.1, N/(2\pi) = 11.726/(2\pi)$, with the critical number as $N_c = 11.68/(2\pi)$. The map strength M is $M = \epsilon^2 T^2/24$. For this values we have $a_c = 0.49$, that agreed with the value $a_c \approx 0.56$ following from the numerical experiment.

4. Stable two dimensional dispersion-managed soliton

The field dynamics is governed by the 2D NLS equation with periodically varying dispersion [21, 22]

$$iu_t + d(t)\Delta u + |u|^2 u = 0, \tag{32}$$

where $d(t) = d_0 + d_1(t)$ is a periodic function of time, In the strong dispersion-management case it is assumed that $d(t) \sim (1/\epsilon)d(t/\epsilon), \epsilon \ll 1$ and the dispersion averaged over the period is $\langle d(t)\rangle = d_0$. The case $d_0 > 0$ corresponds to the negative dispersion, while $d_0 < 0$ to the positive dispersion.

This equation appears at the consideration of two types of problems: the beam propagation in 2D waveguide arrays with periodically variable coupling between waveguides [27, 28] and the nonlinear matter waves in the Bose-Einstein condensates in 2D optical lattices.

Below we consider the axially symmetric case when $\Delta = \partial^2/\partial r^2 + (1/r)(\partial/\partial r)$, and apply the harmonic modulation for the dispersion-management: $d(t) = d_0 + d_1 \sin(\Omega t)$.

The following analysis of the pulse dynamics under the management of dispersion is based on the variational approach [20, 29]. According to this method a space averaged Lagrangian $\bar{L}$ is derived adopting a suitable ansatz. We use a Gaussian ansatz to calculate $\bar{L} = \int L d\bar{r}$

$$u(r,t) = A(t)\exp\left(-\frac{r^2}{2a^2} + i\frac{b(t)r^2}{2} + i\phi(t)\right), \tag{33}$$

where A, a, b, ϕ are the amplitude, width, chirp and linear phase respectively. The equations for the pulse parameters are then derived from the Euler-Lagrange equations for $\bar{L}$

$$a_t = 2d(t)\beta, \quad \beta_t = \frac{2d(t) - E}{a^3}, \tag{34}$$

where $\beta = ab$, and $E = \int_0^\infty |u|^2 d\bar{r}$ is the energy.

Let us consider the evolution of a pulse (beam) using the division on the fast and slow time scales [30, 31, 32, 33]. The width and chirp of the pulse are then represented as $a(t) = \bar{a} + a_1,\ \beta(t) = \bar{\beta} + \beta_1$, where $\bar{a}, \bar{\beta}$ are slowly varying functions on the scale $1/\epsilon$ and a_1, β_1 are rapidly varying functions. The solutions for a_1, β_1 are

$$a_1 = -\frac{4d_0 d_1}{\bar{a}^3(\omega_0^2 + \Omega^2)}\sin(\Omega t) - \frac{2\Omega d_1 \bar{\beta}}{\omega_0^2 + \Omega^2}\cos(\Omega t), \tag{35}$$

$$\beta_1 = \frac{6\sigma d_1 \bar{\beta}}{\bar{a}^4(\omega_0^2 + \Omega^2)}\sin(\Omega t) - \frac{2d_1\Omega}{\bar{a}^3(\omega_0^2 + \Omega^2)}\cos(\Omega t), \tag{36}$$

where $\omega_0^2 = -6\sigma/\bar{a}^4$, $\sigma = 2d_0 - E$. Note that $\sigma < 0$ for over-critical energy for collapse $E > E_{cr} = 2$, at $d_0 = 1$ given by the VA. The exact value, corresponding to the so called "Townes soliton" is $E_{cr} = 1.862$ [12]. Considering the limit of high frequencies $\Omega^2 \gg \omega_0^2 \sim 1$, for the

averaged parameters of the system we finally get

$$\bar{a}_t = 2\bar{\beta}\left(d_0 + \frac{3d_1^2\sigma}{\Omega^2\bar{a}^4}\right), \tag{37}$$

$$\bar{\beta}_t = \frac{\sigma}{\bar{a}^3} + \frac{12d_1^2 d_0}{\Omega^2\bar{a}^7} + \frac{12\sigma d_1^2\bar{\beta}^2}{\Omega^2\bar{a}^5}. \tag{38}$$

This system has the Hamiltonian

$$H = \frac{\sigma}{2\bar{a}^2} + \frac{2\Lambda^2 d_0}{\bar{a}^6} + \bar{\beta}^2\left(d_0 + \frac{3\Lambda^2\sigma}{\bar{a}^4}\right), \quad \Lambda = \frac{d_1}{\Omega}, \tag{39}$$

and the equations of motion are $\bar{a}_t = \partial H/\partial\bar{\beta}$, $\bar{\beta}_t = -\partial H/\partial\bar{a}$. It follows from this Hamiltonian that the mechanism for collapse suppression originates from the repulsive potential near the small values of width $\sim 1/\bar{a}^6$, which counteracts to the attractive force induced by the nonlinearity $\sim 1/\bar{a}^2$. The exact balance between these forces gives rise to a stable state. This state is oscillatory with the frequency which will be defined later. The stabilization mechanism of a 2D NLSE soliton is similar to that of the inverted pendulum with oscillating pivot point [24]. We should note that averaged dynamics is not potential - a velocity dependent term appears in the interaction potential (see 4th term in (39)). Although this term doesn't contribute to the fixed point, it is important for the description of oscillatory dynamics of 2D DM solitons.

The system (37),(38) has the fixed points

$$\bar{\beta} = 0,\ \bar{a}_c = \left(-\frac{12d_0\Lambda^2}{\sigma}\right)^{1/4}. \tag{40}$$

Note that Λ is proportional to the strength of the dispersion map $D = 2\pi d_1/\Omega$, therefore $\bar{a}_c \sim \sqrt{D}$ in analogy with the estimate for a DM soliton in 1D case. There exists one solution with a stationary width for the anomalous residual dispersion $d_0 > 0, E > 2d_0$.

Let us analyze the stability of fixed points for the anomalous residual dispersion $d_0 > 0$.

We assume $a = a_c + \epsilon a_1$, $\beta = \epsilon\beta_1$. Substituting into Eq.(37) and Eq.(38), and collecting terms of order ϵ we find

$$a_{1,t} = \left(2d_0 + \frac{6\Lambda^2\sigma}{a^4}\right)\beta_1 = M\beta_1, \tag{41}$$

$$\beta_{1,t} = -\left(\frac{3\sigma}{a^4} + \frac{84\Lambda^2 d_0}{a^8}\right)a_1 = -Sa_1. \tag{42}$$

The oscillations of the width and chirp near the fixed points are stable if $MS > 0$, which is always satisfied for $d_0 > 0, E > 2d_0$. The frequency of secondary slow oscillations of a 2D DM soliton is proportional to $\sqrt{MS}$.

The numerical simulations can be performed by two-dimensional fast Fourier transform [34]. The dispersion map has parameters $d_0 = 1,\ d_1 = 3.5,\ \ \Omega = 50$. This choice of parameters corresponds to moderate dispersion-management ($D \simeq 0.45$). The axial section profile of the wave function $|u(r,t)|^2$ as obtained by direct numerical solution of the PDE (32) is presented in Fig.1. As can be seen, rather stable quasi-

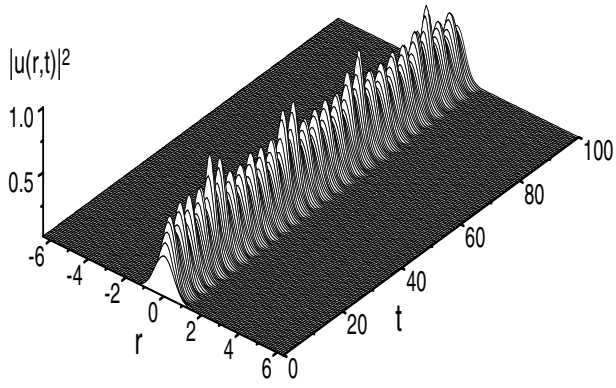

Figure 1. Evolution of a 2D DM soliton according to numerical solution of the equation (32). The wave function is normalized to $N = 2\pi g_0$ with $g_0 = 2.3034$, and the dispersion map is $d_0 = 1,\ d_1 = 3.5,\ \Omega = 50$.

periodic dynamics is realized for a selected parameter settings. Note that would the periodic modulation of the dispersion had not been applied, the initial waveform would have collapsed within $t \sim 3$. The dispersion-management stabilizes the pulse against the collapse or decay, providing undisturbed propagation over very long distances. The agreement between the predictions of the variational equations (34) for the width of a 2D DM soliton and the corresponding result from the full PDE simulations is reported in Fig.2. As can be observed from this figure, the width of a 2D DM soliton performs quasi-periodic motion with the average width of $\bar{a} \simeq 0.8$ according to variational equations, while the PDE simulation yields $\bar{a} \simeq 0.7$. The fixed point for the above set of parameter values, according to eq.(40) is $\bar{a}_c = 0.6635$. The frequencies of slow dynamics given by the VA equations and PDE are also in well agreement (Fig.2). The estimate for the frequency of slow oscillations from Eq.(41) yields $\omega_a = \sqrt{MS} = 3.5$, therefore the period is $T_a = 1.9$. The direct gauge from the Fig.2 shows that $T_a \simeq 2.2$, in reasonable agreement with the above VA estimate.

Let us estimate the value of these parameters for the 2D BEC in the optical lattice [35]. For example, transitions between the 1st and 2nd

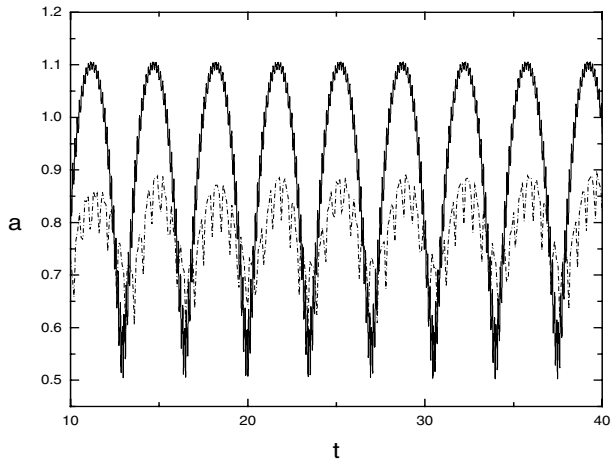

Figure 2. Stable quasi-periodic dynamics of the width of a 2D DM soliton. Solid line - variational equations (34) solved for $E = N/2\pi = 2.3034$, and the initial conditions $a(0) = 1,\ \beta(0) = 0$. Dashed line - full PDE simulations of the equation (32).

bands (at the band edges) in the optical lattice of strength $V_0 = 2.4E_{rec}$ (where $E_{rec} = \hbar^2 k_0^2/2m$ is the recoil energy, $k_0 = 2\pi/\lambda_0$, λ_0 is the laser wavelength), leads to variation of the dispersion coefficient in the range $d(t) = (-2.5 \div 4.5)$ as considered above.

5. Conclusions

We have investigated the propagation of bright matter wave soliton in the Bose-Einstein condensate with trap potential rapidly varying in time. The cases of periodically modulated in time quadratic, bounded and periodic trap potentials have been analyzed. For the repulsive (unstable) trap potential it is shown that there exists a critical value of modulation parameter, when the matter wave soliton is stabilized. Analogous phenomenon of stabilization of unstable fixed points is found for the motion under spatial periodic modulations (optical lattices). For the bounded trap potential it is shown that the effective trap potential can bifurcate from the one well to the triple-well structure; and so, may give rise to the splitting of single attractive BEC into three parts.

We have analytically and numerically studied the dynamical stabilization of two dimensional solitons by means of the Feschbach resonance and dispersion managements.

In this work, we have studied the dynamics of 2D and 3D Bose-Einstein condensates in the case when the scattering length in the Gross-

Pitaevskii equation contains constant and time-variable parts. This may be achieved in the experiment by means of a resonantly tuned ac magnetic field. Using the variational approximation (VA), simulating the GP equation directly, and applying the averaging procedure to the GP equation without the use of VA, we have demonstrated that, in the 2D case, the ac component of the nonlinearity makes it possible to maintain the condensate in a stable self-confined state without external traps, which qualitatively agrees with recent results reported for spatial solitons in nonlinear optics.

We also have demonstrated the possibility to stabilize the 2D soliton with over-critical energy ($E > E_{cr}$) by applying the dispersion-management. The developed theory based on the variational approximation successfully describes the long term evolution of a 2D DM soliton, which is confirmed by direct PDE simulations. We discussed the possible experimental realization of a stable 2D dispersion-managed soliton in Bose-Einsten condensates confined to optical lattices.

Acknowledgments

Author is grateful to B.B. Baizakov, J.G. Caputo, R. Galymzyanov, R.A. Kraenkel, B.A. Malomed, M. Salerno for collaboration. This work has been performed under partial financial support of the Grant of the Fund of Fundamental Researches of the Uzbekistan Academy of Sciences and the NATO linkage grant.

References

[1] K.E. Strecker *et al.,* Nature, **417**, 150 (2002).

[2] L. Khaykovich *et al.,* Science, **296**, 1290 (2002).

[3] L.D. Carr and Y. Castin, Phys.Rev. **A 66**, 063602 (2002).

[4] Y. Nogami and F.M. Toyama, Phys.Rev. **E 49**, 4497 (1994).

[5] R. Dum *et al.,* Phys.Rev.Lett. **80**, 3899 (1998).

[6] F.Kh. Abdullaev and R. Galimzyanov, J. Phys. **B 36**, 1099 (2003).

[7] Yu.S. Kivshar and S.K. Turytsin, Phys.Rev. **E 49**, R2536 (1994).

[8] F. Dalfovo *et al.,* Rev. Mod. Phys. **71**, 463 (1999).

[9] L. Bergé, Phys. Rep. **303**, 259 (1998).

[10] S.L. Cornish *et al.,* Phys. Rev. Lett. **85**, 1795 (2000).

[11] Y. Kagan, E.L. Surkov, and G.V. Shlyapnikov, Phys. Rev.Lett. **79**, 2604 (1997).

[12] L. Bergé *et al.,* Opt. Lett. **25**, 1037 (2000).

[13] I. Towers and B.A. Malomed, J. Opt. Soc. Am. **19**, 537 (2002).

[14] Y. Silberberg, Opt. Lett. **15**, 1281 (1990); B.A. Malomed *et al.,* Phys.Rev. E **56**, 4725 (1997).

[15] L. Berge *et al.,* Opt. Lett. **25**, 1037 (2000).

[16] F.Kh. Abdullaev, J. Bronski, and R. Galimzyanov, eprint:cond-mat/0205464 (2002); Physica D **184**, 319 (2003).

[17] F. Kh. Abdullaev *et al.,* Phys. Rev. A **67**, 013605 (2003).

[18] H. Saito, M. Ueda, Phys. Rev. Lett. **90**, 040403 (2003).

[19] N. J. Smith *et al.,* Electronics Letters, **32**, 54 (1996).

[20] I. Gabitov, S. K. Turitsyn, Opt. Lett. **21**, 327 (1996).

[21] V. Zharnitsky *et al.,* Physica D **152**, 794 (2001).

[22] F.Kh. Abdullaev, B.B. Baizakov, and M. Salerno, Phys.Rev. E **68** in press (2003).

[23] V.M. Perez-Garcia *et al.,* Phys.Rev. **A 56**, 1424 (1997).

[24] L. D. Landau and E. M. Lifshitz, *Mechanics*, (Pergamon Press, Oxford, 1976).

[25] T.S. Yang and W.L. Kath, Opt. Lett. **22**, 985 (1997).

[26] G. Fibich and G.C. Papanicolaou, Phys. Lett. **A 239**, 167 (1998).

[27] U. Peschel and F. Lederer, J. Opt. Soc. Am. B **19**, 544 (2002).

[28] S. A. Darmanyan, Opt. Commun. **90**, 301 (1992).

[29] B. A. Malomed, Progress in Optics, **43**, 69 (2002).

[30] F.Kh. Abdullaev and R.A. Kraenkel, Phys. Lett. A **272**, 395 (2000).

[31] F. Kh. Abdullaev and J. G. Caputo, Phys. Rev. E **58**, 6637 (1998).

[32] S. K. Turitsyn *et al.,* Phys. Rev. E **58**, R48 (1998).

[33] J. Garnier, Opt. Commun. **206**, 411 (2002).

[34] W. H. Press, S. A. Teukolsky, W. T. Vetterling, and B. P. Flannery, *Numerical Recipes. The Art of Scientific Computing.* (Cambridge University Press, 1996).

[35] V. V. Konotop and M. Salerno, Phys. Rev. A **65**, 021602 (2002); H. Pu *et al.,* Phys. Rev. A **67**, 043605 (2003).

SOLITONS AS STRANGE ATTRACTORS

Nail Akhmediev
Optical Sciences Centre, Research School of Physical Sciences and Engineering, The Australian National University, Canberra ACT 0200, Australia

J. M. Soto-Crespo
Instituto de Optica, C.S.I.C., Serrano 121, 28006 Madrid, Spain

A. Ankiewicz
Applied Photonics Group, Research School of Physical Sciences and Engineering, The Australian National University, Canberra ACT 0200, Australia

Abstract We present a detailed study of exploding solitons of the complex cubic-quintic Ginzburg-Landau equation. We show that exploding solitons occur in a vast regions of the parameter space. These are related to the areas where eigenvalues in the linear stability analysis for the ground-state stationary solitons have positive real parts. We also show that this behavior is universal, and that it occurs when we use models with parameter management or add new terms (such as third-order dispersion). The stationary soliton appears to be unstable in these regions and it explodes intermittently, but it attracts the chaotic localized structures around it, thus acting as a 'strange attractor'.

1. Introduction

Solitons in dissipative systems reveal some unusual properties that are unknown for solitons in conservative systems. One well-studied model for dissipative solitons is the cubic-quintic complex Ginzburg-Landau equation (CGLE). This equation contains the basic terms describing the most important physical phenomena occurring in passively mode-locked lasers [1]. The CGLE also serves as a generic equation describing systems near sub-critical bifurcations [2, 3]. It relates to a wide range of dissipative phenomena in physics, such as binary fluid convection [4],

F. Kh. Abdullaev and V. V. Konotop (eds.), Nonlinear Waves: Classical and Quantum Aspects, 45–60.

electro-convection in nematic liquid crystals [5], patterns near electrodes in gas discharges [6] and oscillatory chemical reactions [7].

One of the most recent discoveries related to this model is that of the so-called 'exploding solitons'. These were found in numerical simulations [8, 9] and their existence has been experimentally confirmed in a passively mode-locked solid state laser [10]. These solitons possess the interesting property of exploding at a certain point, breaking down into multiple pieces, and subsequently recovering their original shape. As noted above, exploding solitons can, in principle, be observed in a variety of applications.

Already in the first work on exploding (erupting) solitons [8], it was found that these localized objects exist over a wide range of the system parameters (see Fig. 5 of [8]). A quick comparison with the results of [11] shows that this range of parameters is, if not larger, then at least comparable with the range where stable stationary solitons exist. On the one hand, this remarkable property should make their observation a relatively easy task. On the other hand, we need to find the reasons why it happens.

Some explanations for the existence of exploding solitons and their unusual dynamics have been presented in Ref. [12]. Namely, the stability of the soliton in the laminar stage of evolution, i.e. in the state when the soliton enters its stationary regime of propagation, has been investigated in detail. This study revealed the structure of eigenvalues and eigenfunctions of the stationary soliton that causes the soliton to explode and then return to the same state afterwards.

In this work, we continue these efforts in order to understand, in more detail, the unique behavior and wide range of existence for these exploding solitons. In particular, we find, numerically, the eigenvalues and eigenfunctions of the stationary solitons that have the feature of exploding for a wide interval of values of the parameter ϵ where explosions can occur. Here, we present results showing soliton propagation for parameter values across that range, and show that the qualitative features of the solitons are the same everywhere in that region. The localized solutions of the CGLE can take many forms. Some of them are chaotic, in the sense that the soliton profile changes chaotically in time. Among these chaotic solitons, one class has smooth profiles and does not reveal any drastic changes during evolution [9]. Moreover, the profile stays within certain limits defined by the parameters of the system. Other particular initial conditions that are beyond those limits have a tendency to converge to the chaotic soliton.

Exploding solitons belong to another class of solitons. These change their shapes intermittently and drastically, but return to the laminar

stage after those changes have converted their shapes to irregular profiles. The whole dynamic motion in this case can be considered chaotic. Nevertheless, initial conditions which are beyond the limits of the soliton dynamics again have the tendency to converge to this state. Therefore, those chaotic solitons serve as attractors in the infinite-dimensional phase space, and we can indeed consider them as "strange" attractors.

2. Master equation

The cubic-quintic complex Ginzburg-Landau equation can be written:

$$i\psi_z + \frac{D}{2}\,\psi_{tt} + |\psi|^2\psi + \nu|\psi|^4\psi = i\delta\psi + i\epsilon|\psi|^2\psi + i\beta\psi_{tt} + i\mu|\psi|^4\psi. \quad (1)$$

When used to describe passively mode-locked lasers, z is the cavity round-trip number, t is the retarded time, ψ is the normalized envelope of the field, D is the group velocity dispersion coefficient, with $D = \pm 1$, depending on whether the group velocity dispersion (GVD) is anomalous or normal, respectively, δ is the linear gain-loss coefficient, $i\beta\psi_{tt}$ accounts for spectral filtering ($\beta > 0$),$\epsilon|\psi|^2\psi$ represents the nonlinear gain (which arises,e.g., from saturable absorption), the term with μ represents, if negative, the saturation of the nonlinear gain, while the one with ν corresponds, also if negative, to the saturation of the nonlinear refractive index.

Within a certain range of parameters, equation (1) has soliton solutions that are stationary and stable [15]. Beyond that range, solitons also exist but they are either unstable or have more complicated behavior, and can show pulsating, chaotic or creeping effects [9]. In particular, we found a new soliton instability, of explosive nature, and it is shown in Fig.1. This solution has intervals of almost stationary propagation, but, periodically, the instability develops, producing explosions. The essential features of explosions, observed both theoretically [8, 9] and experimentally [10], are:

1. Explosions occur intermittently. In the continuous model, they happen more or less regularly, but the period changes dramatically with a change of parameters.

2. The explosions have similar features, but are not identical.

3. Explosions happen spontaneously, but additional perturbations can trigger them.

4. One of the basic features of this solution is that the recurrence is back to the soliton solution that is close to the stationary soliton.

Careful study shows that there can be several stationary solutions for the same set of parameters. Exact solutions for them can be found only for a limited range of parameters. In the majority of cases, exact

solutions are unknown but the profiles can be found numerically. Recurrence of an exploding soliton occurs for the soliton which we can call the"ground state". This is the solution with the lowest energy and with a plain "bell-shaped" profile. There could be various reasons for the explosions. If the solution is close to one of the stationary solutions in the laminar regime, then it seems natural to study the stability of that solution. We will study the stability using the technique given below.

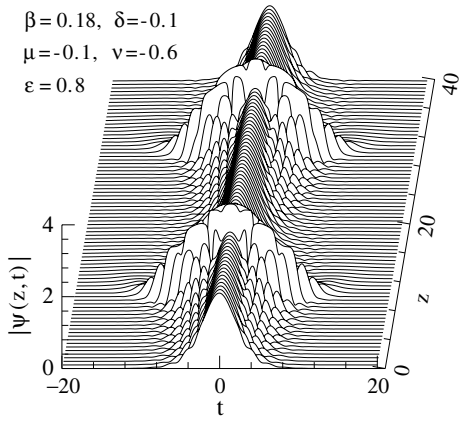

Figure 1. Example of an exploding soliton.

3. Stationary solution and its stability

Let us suppose that the stationary soliton solution of the CGLE is: $\psi(z,t) = \psi_0(t)e^{iqz}$, where $\psi_0(t)$ is a complex function of t with exponentially decaying tails, and that q, its propagation constant, is real. This function can be easily calculated numerically. A technique for finding it has been described, for example, in Ref.[16]. The stationary solution is a singular point of this dynamical system in an infinite-dimensional phase space. Then, the evolution of the solution in the vicinity of this singular point can be described by

$$\psi(z,t) = [\psi_0(t) + f(t)e^{\lambda z} + g(t)e^{\lambda^* z}]e^{iqz}, \tag{2}$$

where $f(t)$ and $g(t)$ are small perturbation functions(we assume $|f,g| \ll |\psi_0|$ for any t), and λ is the associated perturbation growth rate. In general, all λ's are complex numbers and f and g are complex functions. For the soliton solutions of the CGLE, when the dissipative and higher-order terms are small, the stability analysis can be done analytically [13, 14]. However, when the dissipative terms are not small, the analytic approach becomes problematic. Hence, at this stage, we can only rely

on numerical calculations for the eigenvalues and eigenfunctions of the linearized problem. Substituting (2) into the CGLE (1), we obtain:

$$\begin{aligned}(i\lambda - i\delta - q)fe^{\lambda z} + (i\lambda^* - i\delta - q)ge^{\lambda^* z} + (D/2 - i\beta)\, f_{tt}e^{\lambda z} \\ + (D/2 - i\beta)\, g_{tt}e^{\lambda^* z} + 3(\nu - i\mu)|\psi_0|^4(fe^{\lambda z} + ge^{\lambda^* z}) \\ +2(\nu - i\mu)|\psi_0|^2\psi_0^2(f^*e^{\lambda^* z} + g^*e^{\lambda z}) \\ +2(1 - i\epsilon)|\psi_0|^2(fe^{\lambda z} + ge^{\lambda^* z}) + (1 - i\epsilon)\psi_0^2(f^*e^{\lambda^* z} + g^*e^{\lambda z}) = 0\,. \qquad (3)\end{aligned}$$

Separating terms with different functional dependencies on z, we obtain the following two coupled ordinary differential equations:

$$\begin{aligned} Af + Bf_{tt} + Cg^* &= \lambda f, \\ A^*g^* + B^*g^*_{tt} + C^*f &= \lambda g^*, \end{aligned} \qquad (4)$$

where $A = \delta - iq + 2(\epsilon + i)|\psi_0|^2 + 3(\mu + i\nu)|\psi_0|^4$, $B = \beta + i\frac{D}{2}$ and $C = \left[\epsilon + i + 2(\mu + i\nu)|\psi_0|^2\right]\psi_0^2$.

The technique for solving equations (4) numerically has been described in [12]. Here, we use the following parameters for the CGLE: $\mu = -0.1$, $\nu = -0.5$, $\beta = 0.15$ and $\delta = -0.1$, while ϵ varies from 0.3 to 1.7. This interval shows that explosions occur for a wide range of parameters. Higher values of ϵ produce stable soliton solutions, but for lower values, at first fronts dominate and then any solution vanishes on propagation. These parameters are different from those we used in the work [8]. This indicates that not only ϵ, but also other parameters, can change over a wide range and the explosions can still occur.

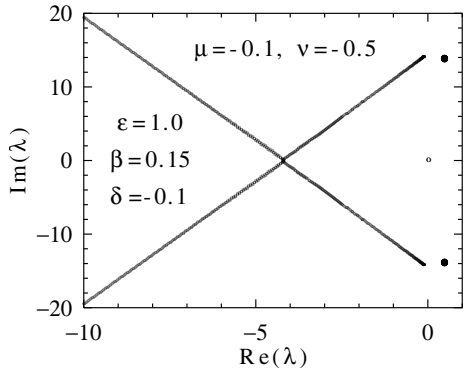

Figure 2. The spectrum of eigenvalues in the complex plane for an exploding soliton.

The complex plane, with the eigenvalues obtained as described in [12], is shown in Fig.2. The total spectrum consists of two complex conjugate eigenvalues with positive real part and a continuous spectrum of complex

conjugate eigenvalues, all with negative real parts. We have also found that the two complex conjugate eigenvalues with positive real part turn out to be degenerate. There are two eigenfunctions corresponding to the same eigenvalue, one is an even function of t and one is odd. The eigenvalue at the origin of the complex plane always exists, but it does not influence any dynamics.

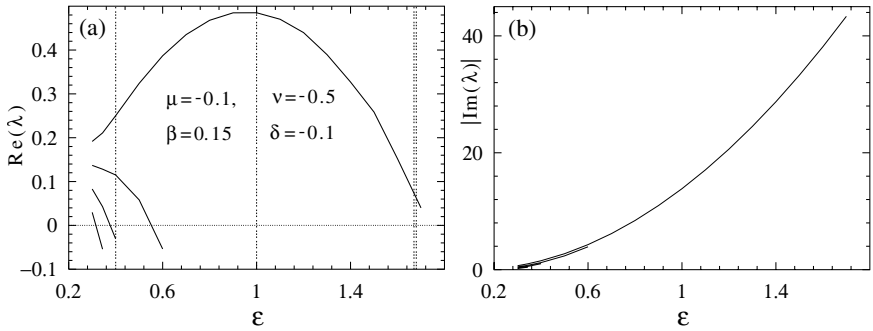

Figure 3. (a) Real and (b) imaginary parts of the discrete eigenvalues (solid lines). At least one eigenvalue has a positive real part throughout the interval $0.3 < \epsilon < 1.7$. Additional eigenvalues of the discrete spectrum appear when $\epsilon < 0.6$. Vertical dashed lines show the values of ϵ in the numerical examples below.

This spectrum does not change qualitatively when we change the parameters of the system in the vicinity of the chosen point. The real and imaginary parts of the discrete eigenvalue are shown in Fig.3a and 3b respectively as functions of ϵ. The real part is much smaller than $|Im(\lambda)|$ when $\epsilon > 0.6$. We can see that, when $\epsilon \approx 1$, the real part has a maximum, and no other eigenvalues appear around this point. The second eigenvalue only appears when ϵ is below 0.6. Hence, we expect that the qualitative behaviour will be the same over a wide range of values of ϵ, from 0.6 to 1.7, where this eigenvalue moves to the left half of the complex plane. Exploding solitons also exist when $0.3 < \epsilon < 0.6$, but their behavior is more complicated in the explosive part of the solution due to the simultaneous existence of several eigenvalues with positive real part.

The whole continuous spectrum of eigenvalues is located on the left half of the complex plane. The corresponding eigenfunctions are much broader than the soliton width. These eigenfunctions are basically continuous waves, of different frequencies and wavenumbers, which are perturbed in the central zone by the soliton. In absence of the soliton, small amplitude radiation waves decay due to δ being negative. This corresponds to the pair of eigenvalues on the r.h.s. edge of the continuous spectrum with real part exactly equal to -0.1. All other eigenvalues of

the continuous spectrum have real parts below -0.1 (i.e. larger than 0.1 in absolute value), due to the influence of spectral filtering on radiation waves of different central frequencies.

An important feature of the spectrum is that each eigenvalue is duplicated, or at least they coincide within the accuracy of our calculations, and on the scale of Fig.2, are completely superimposed. The eigenfunctions corresponding to these eigenvalues are, respectively, even and odd functions of t. For those with positive real part, their corresponding eigenfunctions are shown in Fig.4. Each of these functions is non-zero mainly in the wings of the soliton, where the total gain is positive. These eigenvalues are responsible for the instability of the soliton.

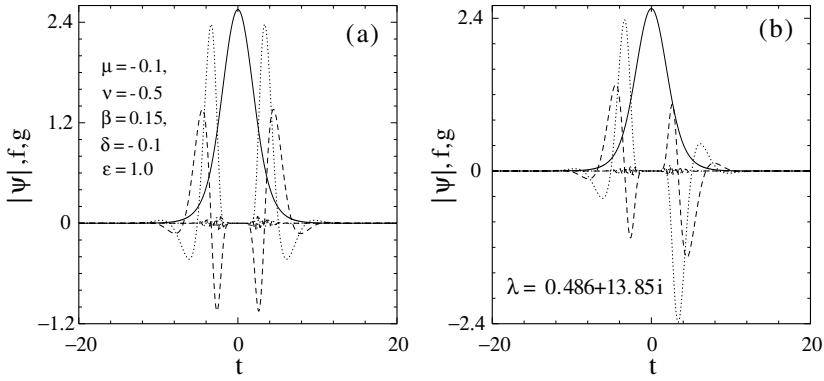

Figure 4. Real (dotted line) and imaginary (dashed line)parts of (a) the even and (b) odd perturbation functions. The solid lines in (a) and (b) show the amplitude of the soliton itself.

4. Dynamics beyond the linear regime

In the presence of eigenvalues with positive real parts, the soliton evolution undergoes the following transformation. Suppose, initially, we have the stationary solution with small perturbations. We note that the real parts of the eigenvalues are relatively small, so that perturbations grow slowly. The imaginary parts of the eigenvalues result in oscillations simultaneously with an increase in the size of the perturbations. We also note that the soliton center is not influenced by this instability, because the eigenfunctions are almost zero in the central part of the soliton.

After the initial linear growth of the perturbation, its amplitude becomes comparable with the soliton amplitude, and the dynamics becomes strongly nonlinear. The nonlinearity mixes all perturbations, creating radiative waves. The amplitudes of radiative waves increase at the expense of the initial perturbation. Consequently, the fraction of the

initial perturbation within them becomes small. The solution at this stage appears to be completely chaotic. However, the solution remains localized, both in amplitude and in width, due to the choice of the system parameters. In particular, the maximum field amplitude is limited due to the fact that μ is negative. In addition, a positive β ensures that the total width in the frequency domain also stays finite, provided that other parameters are within certain ranges. It is also important that the stationary soliton shape is fixed, thus providing the point of return.

As all radiative waves have eigenvalues with negative real parts,they decay and quickly disappear, since the eigenvalues for most of them have much larger negative real parts than the initial perturbation. This means that the solution returns to the state of a stationary soliton with a small perturbation that has an eigenvalue with positive real part. As the real part of the discrete eigenvalue is relatively small, the instability develops again later, thus repeating the whole period of the evolution described above. This process is repeated indefinitely along the z axis.

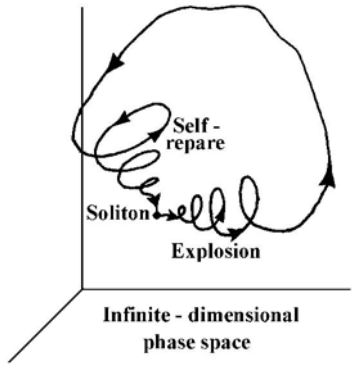

Figure 5. One cycle of evolution of an exploding soliton in an infinite-dimensional phase space.

One cycle of this evolution is shown, schematically, in Fig.5. The fixed point, shown by a black dot in this figure, corresponds to the stationary soliton solution. It can be classified as a stable-unstable focus, because all the eigenvalues in the stability analysis appear as complex-conjugate pairs. We stress here that our system has an infinite number of degrees of freedom, and that the evolution actually occurs in an infinite-dimensional phase space. It cannot be reduced to a finite-dimensional problem, as all the eigenvalues play essential roles in the dynamics. As the fixed point is unstable, the trajectory leaves it in the direction in the phase space defined by the discrete eigenvalues. This motion is exponential as well as oscillatory. After complicated dynamics in the

whole phase space, the trajectory, being homoclinic, returns to the same fixed point but along a different route, as defined by the continuous spectrum. This return is also accompanied by oscillations, as all the eigenvalues in this problem are complex.

This scenario has common features with the one described by Shil'nikov's theorem [17, 18, 19]. The latter is usually applied to a third-order dissipative system or to a higher-order one that can be reduced to a third-order system. In a third-order dissipative dynamical system, the stability of the singular points is described by three eigenvalues. Suppose that a given singular point is a saddle-focus. Then this set of eigenvalues has two complex conjugate eigenvalues with positive real parts and one real negative eigenvalue that is larger in absolute value than the real parts of the other two eigenvalues. We also suppose that there is a homoclinic orbit based on this singular point. Then the evolution of the system close to this homoclinic orbit will be chaotic and will periodically leave and return to this singular point.

Though there is this similarity, the dynamics of an exploding soliton is more involved. Obviously, our system, having an infinite number of degrees of freedom, is much more complicated than any system with three degrees of freedom. Correspondingly, the number of eigenvalues in our case is infinite, rather than just three, and all of them play essential roles in the dynamics. The singular point in our case is a stable - unstable focus rather than saddle-focus. Nevertheless, we have only two identical pairs of eigenvalues with positive real parts responsible for the instability in our system, while the rest of the eigenvalues ensure a quick return to the original state. Besides, the complete phase space in our system is also bounded. As a result, the solution always remains localized, and our system qualitatively behaves the same way as a system described by Shil'nikov's theorem. Specifically, we have a homoclinic orbit that starts and ends at the singular point defined by the exploding soliton, and all nearby trajectories are chaotic.

5. Dynamics over a wide range of parameter ϵ variations

In order to confirm that this explanation is valid in the whole range of positive real part of λ in Fig.3, we investigate, numerically, the soliton evolution in the range of parameters $0.4 < \epsilon < 1.68$. At $\epsilon = 1.68$, the eigenvalue of the perturbation has a large imaginary part that dominates,and the soliton evolves by pulsating periodically, thus repeating its shape and the total energy. This evolution is shown in Fig.5. There are no explosions. Essentially the behaviour is the same when above the

value $\epsilon = 1.68$. At some ϵ above the value 1.7, the real part of the eigenvalue becomes negative. At around $\epsilon \approx 1.8$ the soliton solution becomes stable and any oscillations around the soliton disappear.

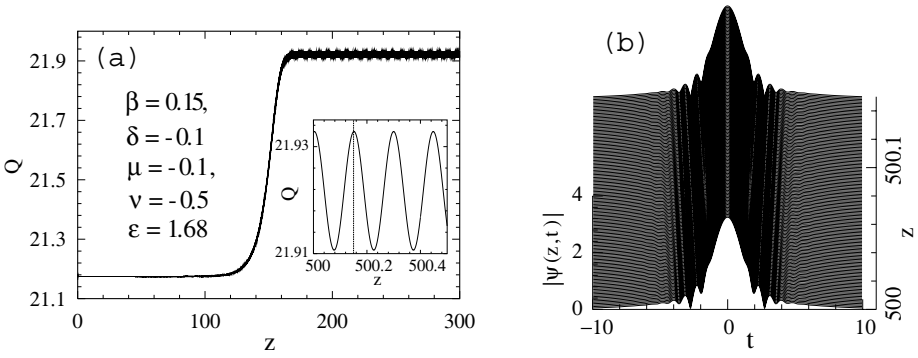

Figure 6. (a) Transition ($z \approx 150$) from stationary to pulsating regime of unstable soliton. The inset shows, on a much-magnified scale,the periodic changes of the soliton energy. (b) Pulsating evolution of the soliton profile during a period, marked in the inset by the co-ordinate axis, and the dashed vertical line.

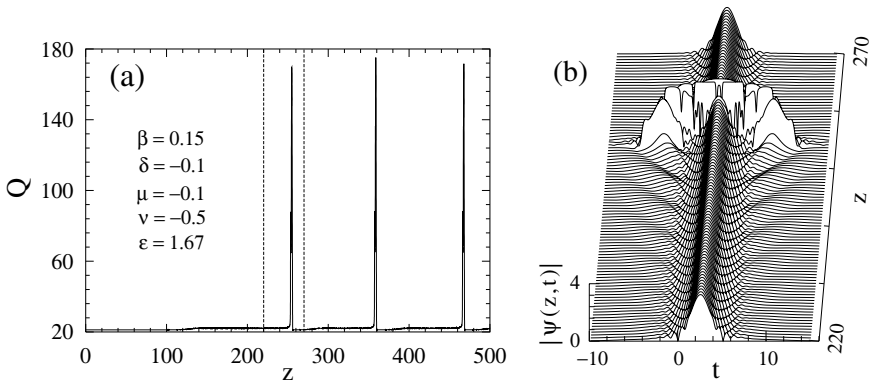

Figure 7. (a) Energy bursts of the soliton at $\epsilon = 1.67$. (b) Explosive evolution of the soliton profile. The dashed vertical lines in (a) correspond to the boundaries of the evolution shown in (b).

A slight change in ϵ, from 1.68 to 1.67, causes drastic changes in the behavior of the soliton. It starts to explode. These explosions occur intermittently, with the distance between the explosions defined by the real part of the eigenvalue. In this particular case, the distance is around $\Delta z \approx 100$. The energy bursts for these explosions are shown in Fig.7a, while one explosion in the soliton profile is shown in Fig.7b. Perturba-

tions start in the soliton wings, since the perturbation function itself is non-zero mainly in the wings. At the final stage, the whole soliton explodes into many pieces, but recovers its shape after the explosion. This behaviour is qualitatively the same at lower values of ϵ. As the real part of the eigenvalue increases up to the point $\epsilon = 1.0$, the distance between the explosions decreases.

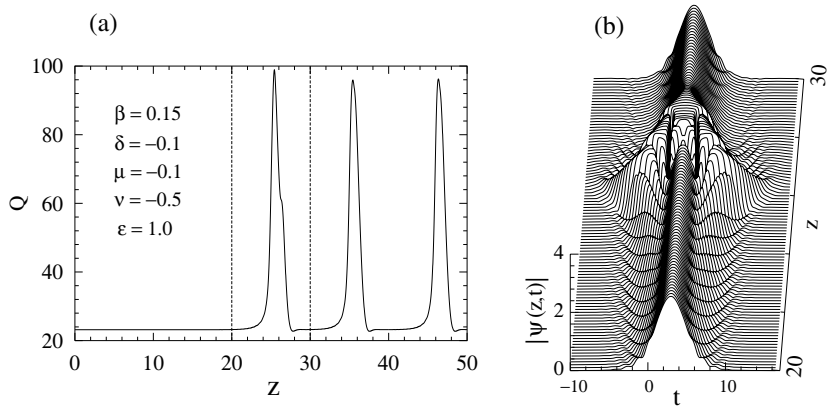

Figure 8. (a) Energy of exploding soliton at $\epsilon = 1.0$. (b) Evolution of the soliton profile for one of the explosions bounded by the vertical lines in (a).

The instability growth rate reaches its maximum at around $\epsilon = 1.0$, as we can see from Fig.3. As a result, the explosions are well-established at this value of ϵ. The frequency of their appearance is also higher because the growth rate is higher, and therefore the instability develops faster. The energy versus z plot for this case is shown in Fig.8a. The input is the unperturbed stationary solution, so, initially it takes a long distance for small perturbations to grow from intrinsic numerical noise. However, after the first explosion, the perturbations are relatively large. Afterwards, explosions occur quite regularly, with the "period" being around $\Delta z \approx 10$. The first explosion is shown separately in Fig.8b. We can clearly see the perturbations and the fact that they do not completely disappear after the explosion, thus causing the process to repeat again.

A further decrease of ϵ to 0.4 results in the appearance of additional discrete eigenvalues with positive real part. We can then expect explosions with more complicated behavior compared with cases involving a single eigenvalue. In addition, for this range of parameters, fronts, rather than pulse solitons, are the dominant structures. The evolution of a soliton for this case is shown in Fig.9. Due to the instability related to the positive velocity of the fronts, the soliton becomes wider and transforms

into fronts with non-zero velocities. These move away from the center of the soliton with constant speed.

The fronts also have instabilities that periodically disturb their smooth profiles. As the eigenfunctions are mainly non-zero on the slopes of the soliton, they have the same structure as half of the eigenfunctions in Fig.4 for each of the fronts. Therefore, the fronts tends to recover in the same way as the exploding solitons. The CW solution that appears between the fronts is stable and its range of its existence increases linearly with z.

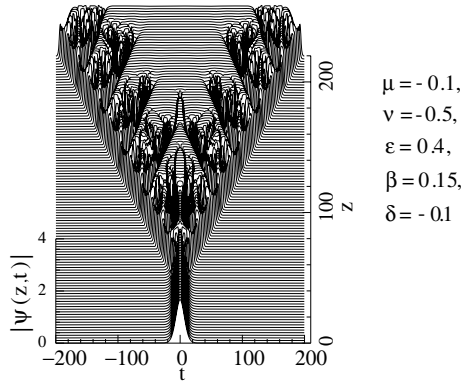

Figure 9. Soliton evolution in the range of parameters where fronts dominate.

Analyzing this last simulation, we can see that the front velocity changes its sign somewhere around $\epsilon = 0.44$. Negative front velocities at higher values of ϵ prevent conversion of the soliton sides into two separating fronts, and also prevent the expansion of the pieces of the soliton explosion. Thus, a localized solution remains localized for all z, even though it is chaotic. This latter effect is an additional reason why exploding solitons serve as strange attractors.

6. Universality of the phenomenon

We now adjust our model to make it closer to the experimental conditions of passively mode-locked lasers. Namely, we take the parameters of the CGLE to be step-wise functions of z, rather than constants, in order to approximate the discreteness of the cavity parameters in the experiment. In the fiber optics field, the dispersion is very often the sole parameter which changes periodically – this situation, where pieces of fiber with various values of dispersion are spliced together, is called 'dispersion management'. It can be used to reduce overall dispersion in a communication link. As we allow all the parameters in the equation,

rather than just the dispersion, to be step-wise functions, we can describe it as a model with 'parameter management'. Numerical results show explosions even in this model with parameter jumps, and they have very similar characteristics to those in the model with constant parameters. Preliminary results are presented in [10]. We also add a new term to the CGLE to account for third-order dispersion, as it is always present in real systems. The latter results in asymmetric explosions, as would be expected. Numerical results for this case are shown in Fig.10.

The existence of explosions in the assorted models that we use in our simulations shows that this phenomenon is not a rarity but is a universal phenomenon. It does appear for a wide range of parameters and for different models of the dissipative system.

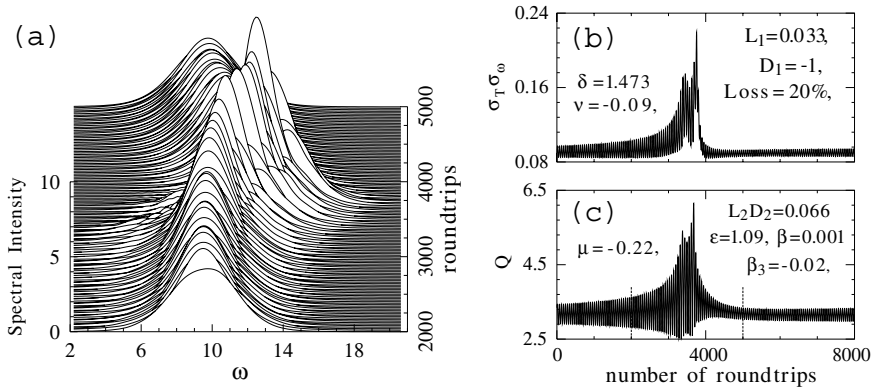

Figure 10. (a) Spectral evolution for a single soliton explosion in the CGLE model with parameter management and third-order dispersion. (b) The product of the widths in the time and frequency domains versus z for this explosion. (c) Energy versus z for the same explosion. The two vertical lines in (c) show the boundaries of evolution given in (a).

We cannot make a direct comparison with similar phenomena that exist in low-dimensional nonlinear dissipative systems. Nonetheless, some analogies can be established. In particular, for one-dimensional maps, there is a phenomenon called intermittency [20, 21]. The iterations for this case show orbits close to being periodic for a longtime (the laminar region), interrupted by bursts of complicated chaotic motion and returning to the laminar regime afterwards. Although there is a resemblance, there are many differences of course, and these relate to the fact that ours is an infinite-dimensional system. Intermittency in low-dimensional systems exists over a small range of parameters close to a saddle-node bifurcation. In our case, explosions exist over a wide range of parameters even far from bifurcations. Hence the explanations must be different.

Another close similarity is a strange attractor in the three-dimensional Lorentz model. The latter is a localized area in the phase space that attracts trajectories from its vicinity. Our exploding soliton is globally chaotic, since each explosion is unique and is not a repetition of a previous one. However, it attracts nearby trajectories in the infinite-dimensional phase space. A great variety of localized initial conditions converge to the exploding soliton solution during evolution. Therefore, the exploding soliton is an attractor similar to a strange attractor in the Lorentz model.

No doubt, the phenomenon of exploding solitons requires further investigation. The most common tool in nonlinear dynamics is a reduction of the dimensionality of the system. This does not seem promising in our case, as we have to operate with the infinite-dimensional system, and such a reduction would qualitatively change the dynamics. As the exploding soliton is close to one of the stationary soliton solutions, and is fundamentally based on it, we apply linear stability analysis to make certain conclusions about the behaviour of exploding solitons. This approach turns out to be successful to some extent, as we can see from the results of this work. Clearly, more studies using other techniques would be desirable.

7. Conclusions

In conclusion, we have presented a study of exploding solitons of the complex cubic-quintic Ginzburg-Landau (CGLE) equation. Linear stability analysis of a stationary solution,which appears in the laminar regime, shows a pair of complex conjugate eigenvalues, with positive real parts, that is responsible for the explosive instability. This pair of eigenvalues exists over a wide range of the parameter ϵ, corresponding to the cubic gain in the system, and this is also true for the explosive instability. We have found that explosions occur, not only in the continuous CGLE model, but also in cases of 'parameter management', i.e. when the equation parameters are step-wise functions of the evolution variable, z. Although the soliton appears to be unstable in these models and explodes intermittently, it attracts the chaotic localized structures around it, acting as a strange attractor.

Acknowledgments

The work of J.M.S.C. was supported by the Dirección General de Enseñanza Superior under contract BFM2000-0806. N. A. acknowledges support from the Australian Research Council, and A.A. from the Australian Photonics CRC.

References

[1] H. Haus, Theory of mode locking with a fast saturable absorber, J. Appl. Phys., **46**, 3049 (1975).

[2] W. van Saarlos and P. C. Hohenberg, Pulses and fronts in the complex Ginzburg-Landau equation near a subcritical bifurcation, Phys. Rev. Lett., **64**, 749 (1990).

[3] R. J. Deissler and H. Brand, Periodic, quasiperiodic and chaotic localized solitons of the quintic complex Ginzburg-Landau equation, Phys. Rev. Lett., **72**, 478 (1994).

[4] P. Kolodner, Drift, shape, and intrinsic destabilization of pulses of traveling-wave convection, Phys. Rev. A **44**, 6448 (1991).

[5] M. Dennin, G. Ahlers and D. S. Cannell, Chaotic Localized States near the Onset of Electroconvection,Phys. Rev. Lett., **77**, 2475 (1996).

[6] K. G. Müller, Structures at the electrodes of gas discharges, Phys. Rev. A, **37**, 4836 (1988).

[7] Y. Kuramoto, Chemical Oscillations, Waves and Turbulence (Springer, Berlin, 1984).

[8] J. M. Soto-Crespo, N. Akhmediev and A. Ankiewicz, Pulsating, creeping and erupting solitons in dissipative systems, Phys. Rev. Lett. **85**, 2937 (2000).

[9] N. Akhmediev, J. M. Soto-Crespo and G. Town, Pulsating solitons, chaotic solitons, period doubling, and pulse coexistence in mode-locked lasers: CGLE approach, Phys. Rev. E, **63** 056602 (2001).

[10] Steven T. Cundiff, J. M. Soto-Crespo and N. Akhmediev, Experimental Evidence for Soliton Explosions, Phys. Rev. Lett., **88**, 073903 (2002).

[11] J. M. Soto-Crespo, N. Akhmediev and V. V. Afanasjev, Stability of the pulse like solutions of the quintic complex Ginzburg-Landau equation, JOSA B, **13**, No 7, 1439 - 1449, (1996).

[12] N. Akhmediev and J. M. Soto-Crespo, Exploding solitons and Shil'nikov's Theorem, Phys. Lett. A, **317**, 287 – 292 (2003).

[13] Kapitula T. Stability criterion for bright solitary waves of the perturbed cubic-quintic Schrödinger equation, *Physica D* **116**, 95 – 120 (1998).

[14] Kapitula T. and Sandstede B.Stability of bright solitary wave solutions to perturbed nonlinear Schrödinger equations, *Physica D* **124**, 58 – 103 (1998);

[15] N. N. Akhmediev and A. Ankiewicz, *Solitons: Nonlinear Pulses and beams*, Chapman and Hall, London, 1997.

[16] J. M. Soto-Crespo, N. Akhmediev and K. Chiang, Simultaneous existence of a multiplicity of stable and unstable solitons in dissipative systems, Phys. Lett. A., **291**, 115 - 123 (2001)

[17] L. P. Shil'nikov, A case of existence of a countable number of periodic motions, Sov. Math. Doklady, **6**, 163 - 166 (1965)

[18] L. P. Shil'nikov, A contribution to the problem ofthe structure of an extended neighborhood of rough equilibrium state of saddle - focus type, Math. USSR - Sbornik, **10**, 91 - 102 (1970).

[19] C. P. Silva, Shil'nikov's theorem - a tutorial, IEEE Transactions on circuits and systems, I: Fundamental theory and applications, **40**, No 10, 675 - 682 (1993).

[20] P. Glendinning, Stability, instability and chaos, Cambridge University Press, 1999, p.324.

[21] P. Bergé, Y. Pomeau, C. Vidal, Order within chaos, towards a deterministic approach to turbulence, John Wiley & Sons, NY, 1984.

MULTIDIMENSIONAL SOLITONS AND VORTICES IN PERIODIC POTENTIALS

B. B. Baizakov, M. Salerno
Dipartimento di Fisica "E.R. Caianiello" and Istituto Nazionale di Fisica della Materia (INFM), Universitá di Salerno, I-84081 Baronissi (SA), Italy

B. A. Malomed
Department of Interdisciplinary Studies, Faculty of Engineering, Tel Aviv University, Tel Aviv 69978, Israel

Abstract The existence of stable solitons and localized vortices in two- and three-dimensional (2D and 3D) media governed by the cubic nonlinear Schrödinger equation with a periodic potential is demonstrated by means of the variational approximation (VA) and in direct simulations. In the 2D case, multi-mode (hexagonal, triangular, and quasi-periodic) potentials are considered (including search for vortex solitons in them), along with the usual square potential. In the 2D and 3D cases, low-dimensional (respectively, quasi-1D and quasi-2D) potentials are considered too. Families of solitons include single- and multi-peaked ones. Solitons of the former type and their stability are well predicted by VA. Collisions of multidimensional solitons in a low-dimensional periodic potential are also studied. Head-on collisions of in-phase solitons lead to their fusion into a collapsing pulse. Solitons colliding in adjacent lattice-induced channels may form a bound state (BS), which then relaxes to a stable asymmetric form. An initially unstable soliton splits into a three-soliton BS. The results apply to Bose-Einstein condensates (BECs) in optical lattices (OLs), and to spatial or spatiotemporal solitons in layered optical media.

Keywords: Soliton, vortex, Bose-Einstein condensate, optical lattice.

1. Introduction

Solitons in multidimensional nonlinear Schrödinger (NLS) equations with a periodic potential have recently attracted considerable interest. In particular, self-trapping of spatial beams in nonlinear photonic crystals is described by a two-dimensional (2D) equation of that type. In this

F. Kh. Abdullaev and V. V. Konotop (eds.), Nonlinear Waves: Classical and Quantum Aspects, 61–80.

case, despite the possibility of collapse [1], simulations reveal robust 2D solitons in the self-focusing model [2]. A similar medium can be created by a grid of laser beams illuminating a photorefractive sample [3].

Similar 2D and 3D models with a periodic potential describe a Bose-Einstein condensate (BEC) trapped in an optical lattice (OL) [4]; in that case, the models are based on the Gross-Pitaevskii (GP) equation, which is quite similar to the NLS one. The application to the BEC in OLs is relevant, as experimental techniques for loading BECs into multidimensional OLs were recently developed [5]. Stable solitons can be supported by an OL even in self-repulsive BECs [6, 7]. In the case of self-attraction, 2D and 3D solitons (including 2D vortices) are stable in the self-focusing model with the OL potential [8], despite the possibility of the collapse.

In the absence of the external potential, stationary soliton solutions to the corresponding self-focusing NLS equation can be easily found, but they are unstable due to the, respectively, weak and strong collapse in the 2D and 3D cases [1]. Alongside the fundamental 2D soliton, in the absence of the OL one can also construct vortex solitons, in the form of

$$u = U(r) \exp\left(-i\mu t + iS\theta\right), \tag{1}$$

where u, t and μ are the wave function, time, and chemical potential in the case of the BEC, or local amplitude of the electromagnetic wave, propagation distance, and (minus) the wavenumber in optics, r and θ are the polar coordinates, $S > 0$ is an integer vorticity ("spin"), and $U(r)$ is a real function, which exponentially decays as $r \to \infty$ and vanishes $\sim r^S$ as $r \to 0$. As well as the fundamental ($S = 0$) soliton, the vortices are unstable in the usual 2D NLS equation (not only against the collapse, but also against perturbations breaking the axial symmetry of the solution). Stable fundamental solitons and vortices have been found in 2D (see reviews [9]) and 3D [10] optical models with non-Kerr nonlinearities, stability conditions for vortex solitons being much tougher than for their fundamental counterparts. On the other hand, it was demonstrated [11] that stable vortices exist in the discrete version of the usual cubic 2D NLS equation (which describes a bundle of nonlinear optical waveguides [3], or BEC trapped in a strong OL field [12]. Note that, unlike the isotropic NLS model, in ones with the axial symmetry broken by the lattice the vorticity is not a dynamical invariant, hence the very existence of such solutions is a nontrivial issue [11].

In the present paper we demonstrate that periodic potentials of the OL type can stabilize 2D and 3D solitons of various types (in particular, both fundamental and vortex solitons are found to be stable in the 2D case). We will investigate the solitons and their stability, using both a

semi-analytical variational approach (VA) and direct numerical methods. In the 2D case we will consider, besides the usual square lattice, also *multi-mode* ones, i.e., hexagonal, triangular, and quasi-crystallic (quasi-periodic) lattices. The existence of stable vortex solitons will be demonstrated, for the first time, in the self-repulsive medium equipped with the 2D lattice.

Of particular interest are stable 2D and 3D solitons in the self- attractive Gross-Pitaevskii (GP) equation with a *low-dimensional* potential, which is uniform in one direction and periodic in the others. Such potentials, capable to support stable *fully localized* solitons, can be induced by a quasi-1D OL in the 2D case, and by a quasi-2D lattice in the 3D case (however, quasi-1D potentials cannot stabilize 3D solitons). A unique peculiarity of the solitons supported by the low-dimensional potential is their motility, as they can move freely in the unconfined direction, which also makes it possible to study collisions between them. We demonstrate that head-on collisions of in-phase solitons lead to their fusion into a collapsing pulse, unless the collision velocity is very large. Solitons colliding in adjacent channels induced by the low-dimensional potential may form a bound state (BS), which initially has a symmetric form. However, the symmetric BS turns out to be unstable, and it relaxes into a stable asymmetric state.

The rest of the paper is organized as follows. The model and variational approximation for the 2D and 3D lattices and solitons in them are introduced in Section 2. New results for solitons in multi-mode lattices are presented in Section 3. The existence of stable vortex solitons in the 2D medium with repulsion, in the presence of the square lattice, is shown in Section 4. Solitons in the low-dimensional potentials, including their stability, collisions between moving solitons, and formation of their bound states, are described in detail in section 5. Conclusion are formulated in Section 6.

2. Basic equations and the variational approach

The rescaled GP equation for the BEC mean-field wave function $u(\mathbf{r}, t)$ is well known [13]:

$$iu_t + \left[\nabla^2 + V(\mathbf{r}) + |u|^2\right] u = 0 \tag{2}$$

(in optical models, it is the NLS equation, t being the propagation distance). The external potential $V(\mathbf{r})$ combines the parabolic-trap and OL terms,

$$V(\mathbf{r}) = \left(\omega^2/2\right) r^2 + \varepsilon[\cos(2x) + \cos(2y) + \cos(2z)], \quad \mathbf{r} \equiv \{x, y, z\}\,, \tag{3}$$

and similar in the 2D case; the OL period is normalized to be π. In optics, the 2D version of the model (without the parabolic trap) describes spatial evolution of a beam in the bulk medium with periodic transverse modulation of the refractive index. Equation (2) conserves two dynamical invariants: the norm (number of atoms in BEC, or the beam's power in the optical model), $N = \int |u(\mathbf{r})|^2 d\mathbf{r}$, and the Hamiltonian.

Stationary soliton solutions to Eq. (2) are sought for as

$$u(\mathbf{r}, t) = \exp(-i\mu t)\, U(\mathbf{r}) \tag{4}$$

with a negative chemical potential μ, cf. Eq. (1). This leads to the stationary counterpart of Eq. (2),

$$\mu U + \left[\nabla^2 + V(\mathbf{r}) + U^2\right] U = 0. \tag{5}$$

Analytical predictions for solitons can be produced by the variational approximation (VA), which was developed in nonlinear optics (see a review [14]), and successfully applied to BECs too [15, 16, 17], including BECs trapped in OL [12] (VA in the 1D version of this model was earlier elaborated for the above-mentioned model of the nonlinear optical waveguide with the transversely modulated refractive index [18]). Following these works, we adopt the Gaussian *ansatz* for fundamental solitons,

$$U(\mathbf{r}) = A \exp\left(-ar^2/2\right), \tag{6}$$

with variational parameters $a > 0$ and A. Note that we set $\varepsilon > 0$ in Eq. (3), hence the central point of the ansatz must be chosen at the minimum of an effective potential, $\mathbf{r} = 0$, that is why we do not introduce an extra parameter for the coordinate of the soliton's center.

Substituting the ansatz (6) into the Lagrangian L corresponding to Eq. (5), we perform spatial integration, and derive equations for a and A in the form of $\partial L/\partial a = \partial L/\partial\left(A^2\right) = 0$. Below, we display variational results, setting $\omega = 0$ in the expression for the potential (3), which implies that the soliton has a size much smaller than that imposed by the parabolic trap.

In the 2D case, the ansatz (6) produces the expression $N = \pi A^2/a$ for the norm, which is used to eliminate A^2. With regard to this, the variational procedure ends up with an equation which determines a in terms of the norm, and another equation that yields the chemical potential/propagation constant:

$$N = 4\pi\left(1 - 2\varepsilon a^{-2} e^{-1/a}\right), \quad \mu = 2\varepsilon\left(2a^{-1} - 1\right) e^{-1/a} - a. \tag{7}$$

Note that, if $\varepsilon = 0$, the first equation in this set yields $N = 4\pi$. In the present notation, it is nothing else but a known variational prediction

for the critical norm in the 2D NLS equation, which simultaneously is a universal value of the norm corresponding to the unstable 2D soliton (*Townes soliton* [1, 24]). With $\varepsilon \neq 0$, Eq. (7) shows that the norm attains a minimum (threshold) value,

$$N_{\rm thr} = 4\pi \left(1 - 8e^{-2}\varepsilon\right), \tag{8}$$

at $a = 1/2$ and

$$\mu = \mu_{\rm thr} \equiv \left(12e^{-2}\varepsilon - 1\right)/2 \, . \tag{9}$$

This means that there is a threshold value of the norm which is necessary to create the 2D soliton; however, the threshold really exists only if it is positive. According to Eq. (8), the threshold exists for a relatively weak lattice, and it vanishes if ε exceeds the value

$$\varepsilon_0 = e^2/8 \approx 0.92 \tag{10}$$

(see Fig. 1a). However, the vanishing of $N_{\rm thr}$ is an unphysical feature, as $N \to 0$ corresponds to the linear limit of the GP equation (2), in which, obviously, no localized state is possible in the absence of the parabolic trap.

In fact, at still smaller values of the OL strength, $e^2/12 < \varepsilon < e^2/8$, Eq. (9) formally predicts that the threshold is attained at positive values of μ, when the soliton cannot exist in reality. Thus, the predictions of the VA for $\varepsilon > e^2/12 \equiv (2/3)\varepsilon_0 \approx 0.62$, which, according to Eq. (8), correspond to $N_{\rm thr} < 4\pi/3 \equiv N_{\rm cr}/3$, are unphysical. This is explained by inapplicability of the simple ansatz (6) in the case of small N. In fact, the soliton is multi-humped in that case, on the contrary to the simple single-humped structure implied by the expression (6), see below.

It also follows from Eq. (7) that the norm cannot exceed the above-mentioned critical value, $N_{\rm cr} = 4\pi$, which means that VA predicts a family of fundamental 2D solitons in the interval

$$N_{\rm thr} = 4\pi \left(1 - 8e^{-2}\varepsilon\right) < N < N_{\rm cr} \equiv 4\pi, \tag{11}$$

as depicted in Fig. 1(a). Numerical simulations of the GP equation (2) reveal a finite threshold at *all values* of ε, as should be expected, see Fig. 1(a). Pulses with an under-threshold value of the norm disintegrate into delocalized quasi-linear Bloch states [19].

The VA make it possible to predict stability of the solitons on the basis of the *Vakhitov-Kolokolov* (VK) criterion [21], which applies if the solution to Eqs. (7) is obtained in the form of $\mu = \mu(N)$: the necessary stability condition is $d\mu/dN < 0$ (of course, the criterion may also be applied to the numerically found family of solitons solutions). A numerical solution of the variational equations (7) produces two different

branches of the dependence $\mu(N)$, see a typical example in Fig. 1(b). An analytical consideration of the near-critical case, $1 - N/4\pi \to +0$, also yields two different solutions:

$$\mu_1(N) \approx -\left(\sqrt{\frac{2\varepsilon}{1-N/4\pi}} + 2\varepsilon\right), \quad \mu_2(N) \approx \left[\ln\left(\frac{1-N/4\pi}{2\varepsilon}\right)\right]^{-1}. \tag{12}$$

Both the numerical and analytical solutions demonstrate that one branch [$\mu_1(N)$ in Eq. (12)] satisfies the VK criterion, and the other one [$\mu_2(N)$ in Eq. (12)] does not. Direct simulations confirm that the variational ansatz satisfying the VK criterion indeed gives rise to a stable soliton, whose form is quite close to the predicted one.

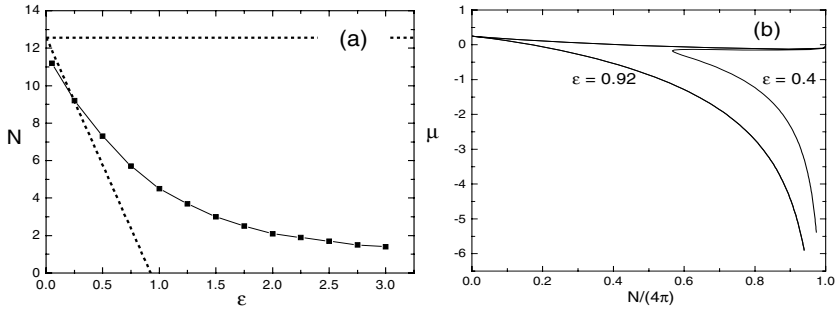

Figure 1. (a) The existence region of 2D solitons in the square lattice, with $V(x,y) = \varepsilon[\cos(2x)+\cos(2y)]$, as predicted by the variational approximation (dashed lines), and as found from direct simulations of Eq. (2) (squares). The upper border found from the numerical simulations is virtually identical to that predicted by the variational approximation, $N = N_{\rm cr} \equiv 4\pi$. As explained in the text, the variational results for $N < N_{\rm cr}/3$ are unphysical. (b) A numerical solution to the variational equations (7) for $\varepsilon = 0.4$ and $\varepsilon = \varepsilon_0 = 0.92$, the latter one being defined by Eq. (10).

Qualitatively, the appearance of the family of stable solitons in the interval $N_{\rm thr} < N < N_{\rm cr}$ in the presence of the lattice can be explained by the fact that it actually creates a nontrivial *band* (in terms of the corresponding values of μ), where the solitons may be stable (in the limit of $\varepsilon \to 0$, the band shrinks to a single point). Note that a band of stable 2D solitons was also found in the OL-supported model with the *positive* scattering length [6].

As it was mentioned above, the ansatz (6) does not take into regard distortion of the soliton's shape by the periodic potential; for this reason, the VA is expected to be accurate if the soliton's size is not essentially larger than the lattice period, which is confirmed by comparison with numerical findings. An example of a single-peak soliton which occupies, essentially, a single cell of the OL is displayed in Fig. 2(a). For such

solitons, the VA accurately predicts their shape and parameters, which is illustrated by Fig. 2(b) showing the soliton's amplitude versus its norm in the square lattice. The variational prediction is almost exact up to $N = N_{\rm thr}$, while pulses with $N < N_{\rm thr}$ disintegrate.

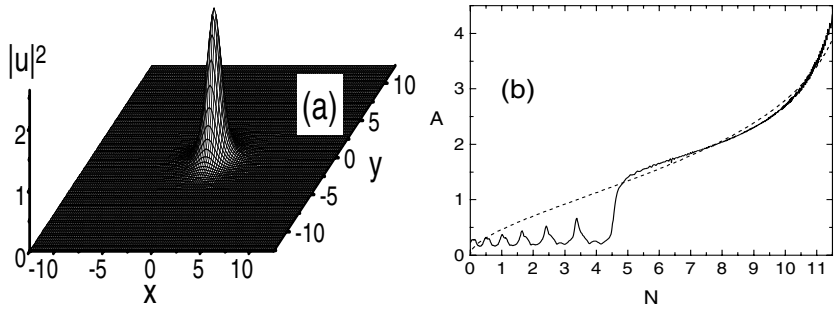

Figure 2. (a) A typical example of the stable 2D soliton (with the norm $N = 3\pi$ in the square lattice of strength $\varepsilon = 0.25$), whose shape is close to that predicted by the variational approximation. (b) The dashed curve is the amplitude of the soliton vs. its norm, as predicted by the variational aproximation. The solid curve is the amplitude of the waveform at the end of direct numerical simulations of the GP equation (2), starting with the initial configuration predicted by the variational approximation to be the soliton. The lattice strength is $\varepsilon = \varepsilon_0 = 0.92$, see Eq. (10). At $N = 4.8$, which is the threshold norm $N_{\rm thr}$ for this value of ε [see Fig. 1(b)], the soliton ceases to exist, the drop in $A(N)$ meaning a transition to a delocalized Bloch state [19].

3. Solitons in multi-mode (hexagonal, triangular, and quasi-periodic) optical lattices

In the case of hexagonal or quasi-crystallic OL potential, the 2D stationary GP equation (5) with self-attraction takes the form

$$\mu U = -\frac{1}{2}\nabla^2 U - \varepsilon \left[\sum_{j=1}^{n} \cos\left(\mathbf{k}_j \mathbf{r}\right)\right] U - U^3. \tag{13}$$

Here, $\{\mathbf{k}_j\}$ is a set of n basis vectors with a common length k (which we again normalize to be 2), and equal angles α between them: $\alpha = 2\pi/n$ if n is odd, and $\alpha = \pi/n$ if n is even. The earlier studied case of the square lattice corresponds to $n = 2$; for the hexagons, $n = 3$, for the Penrose tiling, $n = 5$, etc. The amplitude in front of the periodic or quasi-periodic potential in Eq. (13) is chosen to be negative (with $\varepsilon > 0$); then, the minimum of the potential is located at $\mathbf{r} = 0$.

In the case of the triangular-lattice potential, Eq. (13) is replaced by

$$\mu U = -\frac{1}{2}\nabla^2 U + \varepsilon \left[\sum_{j=1}^{3} \sin\left(\mathbf{k}_j \mathbf{r}\right)\right] U - U^3. \tag{14}$$

In this case, it is more convenient to choose the positive amplitude in front of the potential, which is implied in Eq. (14), on the contrary to Eq. (13). It is easy to see that the minimum of the potential corresponding to the triangular lattice, $U_{\rm tri}\left(\mathbf{r}\right) \equiv \sum_{j=1}^{n} \sin\left(\mathbf{k}_j \mathbf{r}\right)$, is located at a point

$$\mathbf{r}_0 \equiv \left(x_0 = 2\pi/3, y_0 = 0\right), \tag{15}$$

where the potential attains the value

$$\left(U_{\rm tri}\right)_{\rm min} = -3\left(\sqrt{3}/2\right), \tag{16}$$

instead of $\left(U_{\rm hex}\right)_{\rm min} = -3$ at $\mathbf{r}_0 = 0$ in the case of the potential $U_{\rm hex}\left(\mathbf{r}\right) \equiv -\sum_{j=1}^{n} \cos\left(\mathbf{k}_n \mathbf{r}\right)$ corresponding to the hexagonal lattice in Eq. (13).

The stationary equation (13) is derived from the Lagrangian

$$L = \frac{1}{2}\int d\mathbf{r} \left[\mu U^2 - \frac{1}{2}\left(\nabla U\right)^2 + \frac{1}{2}U^4 + U^2 \sum_{j=1}^{n} \cos\left(\mathbf{k}_j \mathbf{r}\right)\right]. \tag{17}$$

We adopt, as before, the simplest isotropic ansatz [cf. Eq. (6)],

$$U = A \exp\left(-\rho R^2/2\right), \tag{18}$$

where A and $\rho > 0$ are the variational parameters.

Substituting the ansatz (18) into Eq. (17), it is easy to calculate the effective Lagrangian for any value of n:

$$L_{\rm eff}\left(A^2, \rho\right) = \frac{\pi}{2}\left[\frac{\mu}{\rho}A^2 - \frac{1}{2}A^2 + \frac{\varepsilon}{4\rho}A^4 + \frac{n}{\rho}A^2 \exp\left(-\frac{1}{\rho}\right)\right]. \tag{19}$$

For the triangular-lattice potential, we should use, instead of (18), the ansatz

$$\phi_{\rm tri} = A \exp\left(-\rho\left|\mathbf{r} - \mathbf{r}_0\right|^2/2\right),$$

where $\mathbf{r}_0$ is taken from Eq. (15). After simple manipulations, in the latter case we arrive again at the expression (19) for the effective Lagrangian, with a formal substitution $n = n_{\rm tri} \equiv 3\left(\sqrt{3}/2\right)$, cf. Eq. (16).

The variational equations, $\partial L_{\rm eff}/\partial\rho = \partial L_{\rm eff}/\partial\left(A^2\right) = 0$, following from the effective Lagrangian, take the following form:

$$\varepsilon A^2 = \rho - 2\mu - 2n\exp\left(-1/\rho\right), \tag{20}$$

$$\mu = -\left(\rho/2\right) - n\left(1 - 2/\rho\right)\exp\left(-1/\rho\right). \tag{21}$$

An additional equation fixes the number of atoms, which for the ansatz (18) is $N \equiv \int d\mathbf{r}\phi^2(\mathbf{r}) = \pi A^2/\rho$. The substitution of the latter expression into Eq. (20) leads to the final variational equation,

$$\varepsilon N = 2\pi \left[1 - 2\left(n/\rho^2\right)\exp\left(-1/\rho\right)\right], \tag{22}$$

from which it is necessary to find $\rho(N)$ for fixed n and ε.

Numerical simulations of the GP equation (2) with the initial waveforms whose parameters satisfy the variational equation (22) confirm the existence of stable 2D solitons, both fundamental and vortex ones, in hexagonal, triangular and quasi-crystallic potentials, which resemble stable fundamental and vortex solitons in the 2D *discrete* NLS equation on triangular and hexagonal ("honeycomb") models, reported in Ref. [22]. Typical examples of the solitons in the hexagonal lattice, found in the present model, are displayed in Fig. 3.

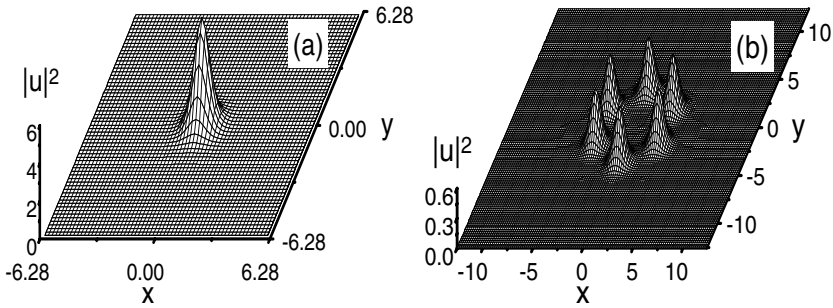

Figure 3. Typical examples of a 2D single-humped fundamental soliton (a) and vortex with $S = 1$ (b), in the hexagonal lattice with $\varepsilon = 1.5$. The norm of both solitons is $N = 2\pi$.

4. Vortex solitons in the repulsive model

The OL potentials can also support stable multidimensional solitons and vortices in the self-repulsive case, the corresponding model being based on the GP equation (2) with the opposite sign in front of the nonlinear term. If the Gaussian waveform with a suitable norm is used to launch direct simulation of this equation, it readily self-traps into a stable soliton, shedding some amount of linear radiation which is absorbed at boundaries of the integration domain.

In fact, the corresponding results for the fundamental 2D solitons were already reported in Ref. [6]. A new result which is presented here is the formation of stable *vortex solitons* in the repulsive model. To this end, we simulated the 2D version of Eq. (2) with the initial condition $u_0(r,\theta) = Ar^S \exp(-ar^2)\exp(iS\theta)$ [cf. Eq. (1)], trying various values

of A and a. Stable vortices with $S \geq 2$ could never be created (the pulse would quickly spread out); however, the initial configurations with $S = 1$ do self-trap into a stable vortex, which features a complex multi-cell organization, see Fig. 4(b); in this figure, a fundamental soliton with the same norm is shown for comparison.

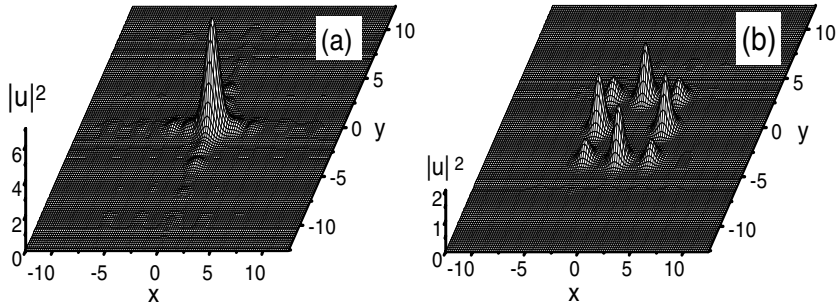

Figure 4. A stable 2D fundamental soliton (a) and vortex with $S = 1$ (b), in the self-repulsive GP equation (2) with the square-lattice potential of the strength $\varepsilon = 4.0$. The initial norm is $N = 4\pi$.

All the above results were obtained for $\omega = 0$ in Eq. (3), i.e., without the parabolic trap. Simulations with $\omega \neq 0$ have demonstrated that the external trap does not affect the 2D and 3D solitons in any conspicuous way, provided that the corresponding harmonic-oscillator length is essentially larger than the lattice period.

5. Solitons in low-dimensional potentials

5.1 The model

The multidimensional solitons considered above were pinned by the lattice. A similar mechanism may stabilize partly mobile solitons in the self-attractive medium equipped with periodic potentials of a lower dimension, viz., quasi-1D (Q1D) and Q2D lattices in the 2D and 3D cases, respectively.

In optics, the corresponding 2D equation in the spatial domain governs the beam propagation in a layered bulk medium along the layers, which is an extension of the 1D multichannel system introduced in Ref. [18], where the potential was induced by transverse modulation of the refractive index (RI). In the temporal domain, the 2D and 3D equations with the Q1D and Q2D potential govern, respectively, the longitudinal propagation of spatiotemporal optical solitons in a layered planar waveguide, or in a bulk medium with the RI periodically modulated in both transverse directions.

The 2D and 3D equations with the low-dimensional potential directly apply to BECs loaded in a Q1D or Q2D lattice. The physical significance of this setting is two-fold: first, in the experiment it is much easier to create a lower-dimensional lattice than a full-dimensional one, both in BECs and in optics, hence the use of such lattices is the most straightforward way to create multidimensional solitons in these media. Second, the solitons created this way can freely move in the unconfined direction, which also suggests a possibility to study their collisions, and to look for their bound states (BSs). As yet, no other way to create multidimensional *mobile* solitons in BECs and their BSs has been proposed. In optics, solitons of this type suggest new applications. Indeed, in optical media with the full-dimensional lattice potential, transfer of a trapped beam from one position to another is difficult, as the necessary external push strongly disturbs the beam [18]. In the lower-dimensional potential, the beam can slide along the free direction, making the transfer easy. In BECs confined by a low-dimensional OL, matter-wave solitons can be driven in the free direction by a weak laser beam.

The normalized form of the self-focusing 2D NLS equation with a Q1D periodic potential of the strength ε is

$$iu_t + u_{xx} + u_{yy} + [\varepsilon \cos(2x) + \chi|u|^2]u = 0, \tag{23}$$

where $\chi = \pm 1$ in the case of the self-attraction/repulsion. In BECs, t is time, while in optics it is the propagation distance [cf. Eq. (2)]. For BECs or spatial optical solitons, x and y are transverse coordinates; for spatiotemporal optical solitons in the 2D waveguide with anomalous chromatic dispersion, y is a temporal variable. The 3D version of Eq. (23) is

$$iu_t + u_{xx} + u_{yy} + u_{zz} + \left\{\varepsilon \left[\cos(2x) + \cos(2y)\right] + \chi|u|^2\right\} u = 0. \tag{24}$$

Besides the Hamiltonian and the norm (the number of atoms in the BEC, or total power/energy of the spatial/spatiotemporal optical soliton), Eqs. (23) and (24) conserve also the momentum along the free direction. The equations are normalized the same way as Eq. (3), so that the period of the potential is π, free parameters being again ε and N.

5.2 The variational approximation

Stationary solutions to Eq. (23) are looked in the form (4), which yields

$$\mu U + U_{xx} + U_{yy} + \left[\varepsilon \cos(2x) + \chi U^2\right] U = 0 \tag{25}$$

[cf. Eq. (5)], and similar in the 3D case. To apply the VA (variational approximation) to Eq. (25), we adopt the *ansatz*

$$U = A \exp\left[-\left(ax^2 + by^2\right)/2\right], \tag{26}$$

or, in the 3D case,

$$U = A \exp\left[-\left(a(x^2 + y^2) + bz^2\right)/2\right]. \tag{27}$$

The corresponding norms are

$$N_{\rm 2D} = \pi A^2/\sqrt{ab}, \quad \text{and} \quad N_{\rm 3D} = \pi^{3/2} A^2/(a\sqrt{b}).$$

Following the procedure of the application of VA to multidimensional solitons [14], we derive variational equations from the Lagrangian of Eq. (25). In the 2D case, they are

$$N\chi = (4\pi/a)\sqrt{a^2 - 2\varepsilon e^{-1/a}}, \ \mu = -a - \varepsilon e^{-1/a}(1 - 3/a), \tag{28}$$

and in the 3D case,

$$N\chi = 2\,(2\pi/a)^{3/2}\sqrt{a^2 - 2\varepsilon e^{-1/a}}, \ \mu = -a/2 - \varepsilon\,(2 - 3/a)\,e^{-1/a}; \tag{29}$$

in both cases, $b = \left(a^2 - 2\varepsilon e^{-1/a}\right)/a$. Evidently, solutions are possible only if $\chi > 0$ (self-attraction).

The 3D solution can be found from Eqs. (29) for any N. On the contrary to this, the 2D solutions exist in the interval [cf. Eq. (11)]

$$N_{\rm thr} \equiv 4\pi\sqrt{1 - \varepsilon/\varepsilon_0} < N < N_{\rm max} \equiv 4\pi \tag{30}$$

[see Fig. 5(a)], where $\varepsilon_0 = e^2/8$ is the same as in Eq. (10), and (formally) $N_{\rm thr} = 0$ if $\varepsilon > \varepsilon_0$. As well as in the case of the square OL considered above, the value $N_{\rm thr}$ is attained at $a = 1/2$, while the corresponding value of the chemical potential is

$$\mu = \mu_{\rm thr}^{\rm (Q1D)} \equiv \left(10e^{-2}\varepsilon - 1\right)/2, \tag{31}$$

cf. Eq. (9). Thus, with the increase of ε, the variational solution becomes unphysical even before $N_{\rm thr}$ vanishes, namely, when the expression (31) becomes positive. Recall that in the case of the square lattice this happened at $\varepsilon = e^2/12 \equiv (2/3)\varepsilon_0$. In the present case, this happens at a somewhat larger value of the OL strength, $\varepsilon = e^2/10 \equiv (4/5)\varepsilon_0$. Direct numerical solutions for stable 2D solitons in the Q1D lattice, displayed in Fig. 5(a), clearly show that, similar to the case of the square lattice [cf. Fig. 1(a)], the actual minimum (threshold) value of the norm necessary for the existence of the solitons is *always* finite.

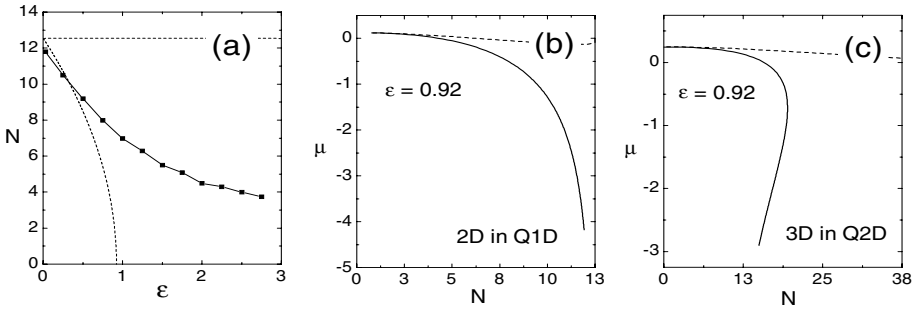

Figure 5. The panel (a) shows the existence limits for stable 2D solitons in the quasi-1D lattice, as predicted by the variational approximation (dashed lines), and as found from direct simulations of the GP equation (23) (squares). The upper limit found from the simulations is virtually identical to that predicted by the variational approximation. The panels (b) and (c) show dependences $\mu(N)$ for 2D and 3D solitons in the quasi-1D and quasi-2D lattices, respectively, as predicted by the variatonal approximation. These dependences determine the stability of the solitons as per the VK criterion.

The results produced by the VA can also be used to predict the stability of the solitons in the present case on the basis of the VK criterion. It follows from Eqs. (28) and (29), and is also evident in Figs. 5(b,c), that the 2D solitons are stable in the existence interval (30). As for the 3D solitons, the criterion shows that, at small ε, they are unstable for any N. Further consideration of the equation (29) predicts that a stability interval of a width $\Delta N \sim \sqrt{\varepsilon - \varepsilon_{\rm cr}^{(3D)}}$ appears around $N_{\rm cr}^{(3D)} \approx 10.1\pi^{3/2}$ if ε exceeds the value $\varepsilon_{\rm cr}^{(3D)} \approx 0.242$.

5.3 Numerical results

In numerical simulations of the model with the low-dimensional OL potential, solitons were generated by the imaginary-time-evolution method [23], starting with the VA-predicted waveforms. Stability was verified by direct simulations of perturbed solitons in real time. Typical examples of the thus found stable 2D and 3D solitons are displayed in Figs. 6 and 7, the 3D ones being nearly isotropic in the (x, y) plane and elongated in the free direction z. As it was already shown above in Fig. 5(a), the existence limits for the stable 2D solitons are essentially different from the VA prediction if N is small; in that case, the discrepancy is due to the fact that the soliton develops a multi-peaked structure [see Fig. 6(b)], which is not accounted for by the simple *ansätze* (26) and (27) adopted above. The *ansätze* can be generalized accordingly; in particular, in the 2D case

this can be done by setting $U = (A + B\cos x)\exp\left[-\left(ax^2 + by^2\right)/2\right]$, but the final result is then quite messy.

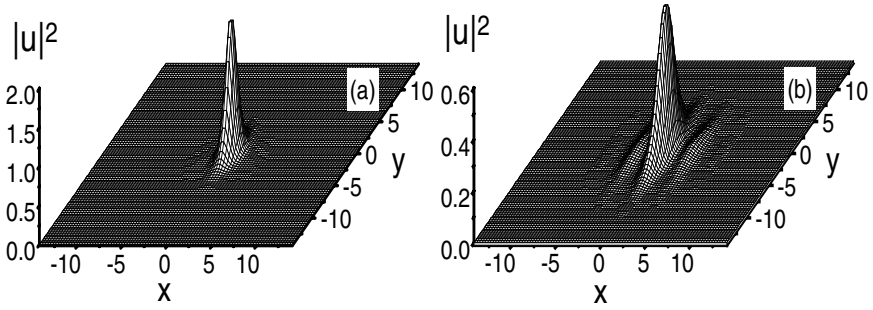

Figure 6. Panels (a) and (b) show typical examples of single- and multi-peaked stable 2D solitons in the quasi-1D potential with $\varepsilon = 2$. The norm of the soliton is $N = 2\pi$ (a) and $N = 1.5\pi$ (b).

The VA predicts that, in the 3D case with the Q1D (rather than Q2D) lattice, all the solitons are VK-unstable. Accordingly, simulations *never* produced stable solitons in this case. This feature can be explained by the fact that, in the free 2D subspace, the soliton is essentially tantamount to the unstable *Townes soliton* [1, 24].

Another relevant remark is that, as it was discussed in detail above, the 2D GP equation (2) with the square lattice gives rise, besides stable fundamental solitons, also to stable vortices [8]. Vortices were found in the present 2D model too, but they always turn out to be unstable.

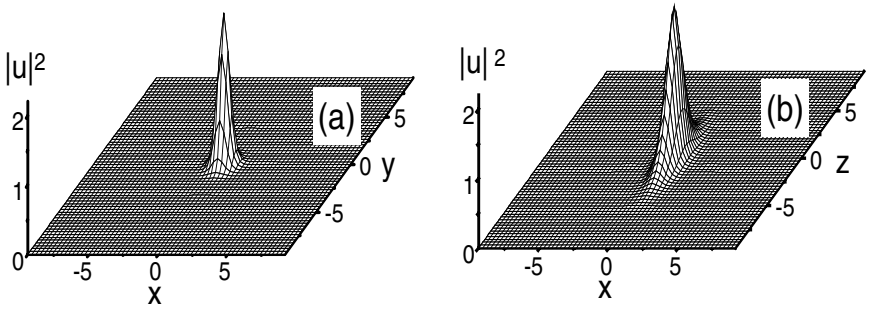

Figure 7. A typical example of a stable single-peaked 3D soliton in the quasi-2D potential ($N = 2\pi$, $\varepsilon = 5.0$) is shown through its $z = 0$ (a) and $y = 0$ (b) cross sections.

We have also investigated the case of self-repulsion ($\chi = -1$) in the underlying GP equations (23) and (24), when the low-dimensional lattice potential cannot support a completely localized pulse. However, adding

the usual parabolic trap, the same as in Eq. (3), readily gives rise to stable states. Actually, these ones are solitons across the lattice and Thomas-Fermi states along the free direction. It is noteworthy that, with $\chi < 0$, these states assume a multi-peaked or single-peaked shape under the action of a weaker or stronger OL potential, respectively, which is *opposite* to what was reported above for the self-attraction case ($\chi > 0$), see Fig. 6. An explanation to this feature is that, in the case of the self-repulsion and $\varepsilon = 0$, no solitons exist at all (even unstable ones, like the above-mentioned Townes soliton).

The influence of the parabolic trap was checked too in the case of $\chi = +1$. If the 2D or 3D soliton is displaced from the central position, it then performs harmonic oscillations along the free direction, completely preserving its integrity. Actually, the *mobility* in the free direction is the most essential difference of these multidimensional solitons from those predicted in other BEC models [6, 7, 8].

5.4 Collisions between solitons, and formation of bound states

It is natural to consider collisions between the solitons which can move freely in the unconfined direction of the low-dimensional lattice potential. Simulations demonstrate that 2D and 3D in-phase solitons colliding head-on with velocities $\pm v$, which are below a critical value $v_{\rm cr}$, *merge* into a single pulse, whose norm exceeds the critical value $N_{\rm max}$ [see Eq. (30)], hence it quickly collapses as shown in Fig. 8(a).

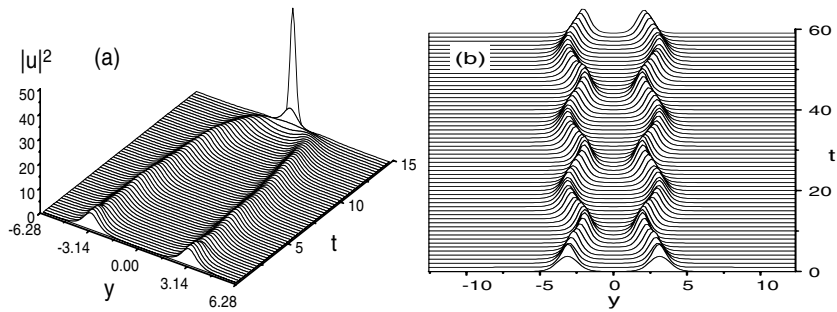

Figure 8. (a) A head-on collision between in-phase 2D solitons results in their merger into a collapsing pulse. In this case, $\varepsilon = 0.92, k = 2, \chi = 1$, and before the collision the solitons were taken with parameters prescribed by the VA: $A = 2.07, a = 1.68, b = 1.07$ for $N/4\pi = 0.8$. (b) Multiple elastic collisions of π out-of-phase solitons in the presence of the weak confining potential, $-\beta y^2$, with $\beta = 0.005$.

If $v > v_{\rm cr}$, the solitons pass through each other (for instance, $v_{\rm cr} = 8.5$ for $\varepsilon = 2.0$ if the norm of each 2D soliton is $N = 2.5\pi$), which is

explained by the fact that the collision time, $\sim 1/v$, is then smaller than the collapse time, $\sim 1/N$. Head-on collisions of π-out-of-phase solitons always results in their bounce. Moreover, two such solitons, placed inside the parabolic trap, perform stable oscillations with periodic elastic collisions, see Fig. 8(b).

In the low-dimensional potential, collisions are also possible between solitons moving in adjacent "tracks" (channels). In that case, they pass each other quasi-elastically if the collision velocity is large. If it is not too large, each soliton captures a small "satellite" in the other channel, see Fig. 9(b).

If the velocity falls below another critical value for given ε, the outcome of the collision in adjacent tracks is altogether different: two solitons form a quiescent symmetric bound state (BS), see Fig. 10(a). Later, the symmetric BS develops an intrinsic instability, spontaneously rearranging itself into a stable *asymmetric* BS [Fig. 10(b)]. This behavior resembles the symmetry-breaking instability of optical solitons in dual-core fibers [25] and the macroscopic quantum-self-trapping effect in BECs confined to a double-well potential [26]. In fact, this result is the first prediction of a stable BS of two solitons in BECs.

Formation of more complex stable BSs of 2D and 3D solitons in the low-dimensional lattices also occurs in a different way: simulations demonstrate that, in both the 2D and 3D cases, VK-*unstable* waveforms predicted by the VA undergo violent evolution, shedding $\simeq 50\%$ of their norm and eventually forming a BS of *three* solitons, with a narrow tall one in the middle, and small-amplitude broad satellites in the adjacent channels [see Fig. 10].

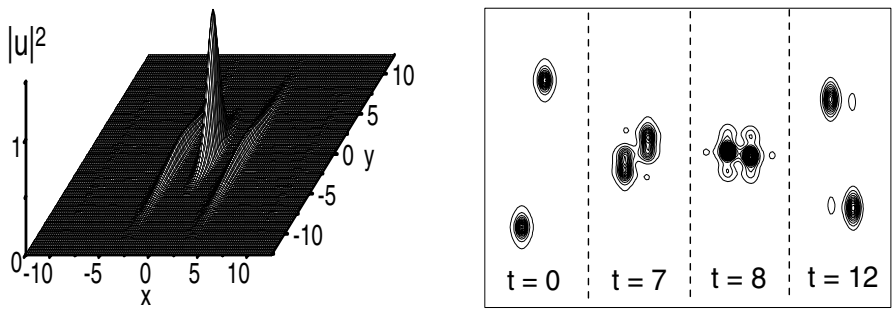

Figure 9. Left panel: a bound state of three solitons developed from the VK-unstable 2D soliton with parameters $A = 0.63$, $a = b = 0.1$, and $\varepsilon = 10$. Half of the initial norm is lost during the formation of the bound state. Right panel: contour plots of 2D solitons colliding at moderate velocities $v = \pm 0.3$ in adjacent tracks of the quasi-1D potential, with the strength $\varepsilon = 1.5$.

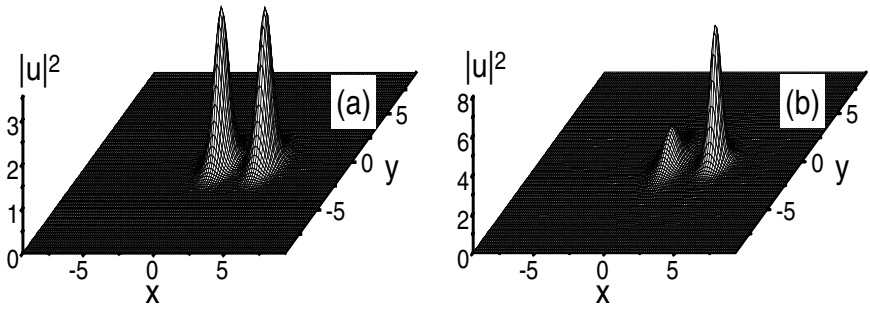

Figure 10. (a) A symmetric bound state (BS) of 2D in-phase solitons formed in adjacent tracks of the quasi-1D lattice, with $\varepsilon = 3$, as a result of the collision between them. (b) Subsequent spontaneous rearrangement of the unstable symmetric BS into a stable asymmetric one. The initial norm and velocities of the solitons are $N = 2\pi$ and $v = \pm 0.1$. In the 3D case, the scenario is quite similar.

6. Conclusion

We have demonstrated that the GP/NLS equation with the cubic nonlinearity and periodic potential, which describes BECs trapped in a 2D or 3D optical lattice (OL), and (in the 2D case) an optical beam in the Kerr medium with a transverse periodic modulation of the refractive index, gives rise to stable solitons. In moderately weak and strong lattices, single-cell and multi-cell solitons were found, the former ones being accurately predicted by the variational approximation. A necessary condition for the formation of 2D solitons is that the initial norm of the field must exceed a minimum (threshold) value (but it must also be smaller than the critical value beyond which the weak collapse sets in). Similar results have been demonstrated for 2D solitons in hexagonal, triangular, and quasi-crystallic lattices. Stable 2D vortex solitons with $S = 1$ were found too, in the cases of both self-attraction (including the hexagonal lattice) and self-repulsion.

We have also shown that the periodic potential whose dimension is smaller by 1 than the full spatial dimension readily supports stable single- and multi-peaked solitons in 2D and 3D self-focusing media (although the quasi-1D potential cannot stabilize 3D solitons), which suggests new settings for experimental search of multidimensional solitons. In this case, stable 2D solitons exist in a finite interval of the values of the norm, while 3D solitons are stable if the lattice strength exceeds a minimum value. In the case of self-repulsion with a parabolic trap, stable localized states are found too. The dependence of their structure on the lattice strength is opposite to that in the case of the self-attraction:

with the increase of the strength, a single-peaked state is changed by a multi-peaked one.

These solitons are the first example of *mobile* multi-dimensional pulses in BECs. Head-on collisions between in-phase solitons may lead to their fusion and collapse, while out-of-phase solitons can collide elastically indefinitely many times. Collision between solitons in adjacent tracks may create a bound state (BS), which then relaxes to an asymmetric stable shape. Three-soliton BSs are created as a result of the evolution of initially unstable solitons.

Finally, we address experimental perspectives. First, an initial pulse occupying a single lattice cell can be created by means of the recently developed technique for patterned loading of BEC into OLs [28], which provides for control over the placement of atoms in lattice sites. On the other hand, an initial waveform spread over multiple cells can be prepared by imposing an OL upon a condensate of a suitable size in the magnetic trap, with subsequent switching off the magnetic field. Varying the norm of the wave function, as supposed in the theory and numerical simulations, can be implemented by variation of the s-wave scattering length via the Feshbach resonance.

Strengths of the OLs necessary to realize the above settings are in the experimentally relevant range [27], $\varepsilon = 0 \div 20$ in units of the recoil energy, $E_{\rm rec} = \hbar^2 k_L^2/(2m)$, where $k_L = 2\pi/\lambda$, and m and λ are the atomic mass and laser wavelength. Relevant units of length and time are, respectively, the cell's size $d \equiv \lambda/2 = 0.425$ μm, and the time $\hbar/E_{\rm rec} = 2m/(\hbar k_L^2) = 50$ μs (for ^{85}Rb atoms and far detuned laser with $\lambda = 850$ nm). Experiments can be performed with ^{7}Li or ^{85}Rb atoms featuring the negative scattering length in the ground state, which is amenable to large variations through the Feshbach resonance.

Acknowledgments

B.B.B. thanks the Physics Department of the University of Salerno, Italy, for a two-year research grant. M. S. acknowledges partial support from the MURST-PRIN-2003 Initiative, and the European grant LOCNET no. HPRN-CT-1999-00163. B.A.M. appreciates a partial financial support from the Israel Science Foundation through the grant No. 8006/03.

References

[1] L. Bergé, Phys. Rep. **303**, 260 (1998).

[2] P. Xie, Z.-Q. Zhang, and X. Zhang, Phys. Rev. E **67**, 026607 (2003); A. Ferrando *et al.*, Opt. Exp. **11**, 452 (2003).

[3] J. Fleischer *et al.*, Phys. Rev. Lett. **90**, 023902 (2003); J. Fleischer *et al.* Nature, **422**, 147 (2003).

[4] C. Jurczak *et al.*, Phys. Rev. Lett. **77**, 1727 (1996); H. Stecher *et al.*, Phys. Rev. A **55**, 545 (1997); D. Jaksch *et al.*, Phys. Rev. Lett. **81**, 3108 (1998); D. I. Choi and Q. Niu, Phys. Rev. Lett. **82**, 2022 (1999); K. P. Marzlin and W. P. Zhang, Phys. Rev. A **59**, 2982 (1999); J. H. Denschlag *et al.*, J. Phys. B **35**, 3095 (2002); Y. B. Band and M. Trippenbach, Phys. Rev. **65**, 053602 (2002); I. Carusotto, D. Embriaco, and G. C. La Rocca, Phys. Rev. A **65**, 053611 (2002); S. Burger *et al.*, Europhys. Lett. **57**, 1 (2002).

[5] M. Greiner *et al.*, Nature **415**, 39 (2002); **419**, 51 (2002); I. Bloch *et al.*, Phil. Trans. R. Soc. L. A **361** 1409 (2003).

[6] B. B. Baizakov, V. V. Konotop, and M. Salerno, J. Phys. B **35**, 5105 (2002).

[7] E. A. Ostrovskaya and Y. S. Kivshar, Phys. Rev. Lett. **90**, 160407 (2003).

[8] B. B. Baizakov, B. A. Malomed, and M. Salerno, Europhys. Lett. **63**, 642 (2003); some similar results for the 2D case have also been obtained by J. Yang and Z. Musslimani, Opt. Lett. **23**, 2094 (2003).

[9] L.-C. Crasovan, B. A. Malomed, and D. Mihalache, Pramana **57**, 1041 (2001); B. A. Malomed *et al.*, *ibid.* **57**, 1061 (2001).

[10] D. Mihalache *et al.*, Phys. Rev. Lett. **88**, 073902 (2002); D. Mihalache *et al.*, Phys. Rev. E **66**, 016613 (2002); D. Mihalache *et al.*, J. Optics A **4**, 615 (2002).

[11] B. A. Malomed and P. G. Kevrekidis, Phys. Rev. E **64**, 026601 (2001); P. G. Kevrekidis *et al.*, J. Phys. B **36**, 3467 (2003).

[12] A. Trombettoni and A. Smerzi, Phys. Rev. Lett. **86**, 2353 (2001); F. Kh. Abdullaev *et al.*, Phys. Rev. A **64**, 043606 (2001).

[13] F. Dalfovo *et al.* Rev. Mod. Phys. **71**, 463 (1999).

[14] B. A. Malomed, Progr. Optics **43**, 69 (2002).

[15] L. D. Carr and Y. Castin, Phys. Rev. A **66**, 363602 (2002).

[16] F. Kh. Abdullaev *et al.* Phys. Rev. A **67**, 013605 (2003).

[17] V. M. Perez-Garcia, V. V. Konotop, and J. J. Garcia-Ripoll, Phys. Rev. E **62**, 4300 (2000); T. Tsurumi and M. Wadati, J. Phys. Soc. Jpn. **70**, 1512 (2001); L. Salasnich, A. Parola and L. Reatto, Phys. Rev. A **65**, 043614 (2002);

[18] B. A. Malomed *et al.*, J. Opt. Soc. Am. B **16**, 1197 (1999).

[19] B. B. Baizakov and M. Salerno, Phys. Rev. A **69**, N1 (2004) (in press).

[20] L. Khaykovich *et al.*, Science **296**, 1290 (2002); K. E. Strecker *et al.*, Nature **417**, 150 (2002).

[21] M. G. Vakhitov and A. A. Kolokolov, Radiophys. Quantum Electron. **16**, 783 (1973).

[22] P. G. Kevrekidis, B. A. Malomed, and Yu. B. Gaididei, Phys. Rev. E **66**, 016609 (2002).

[23] M. L. Chiofalo, S. Succi, and P. Tosi, Phys. Rev. E 62, 7438 (2000).

[24] R. Y. Chiao, E. Garmire, and C. H. Townes, Phys. Rev. Lett. **13**, 479 (1964).

[25] C. Pare and M. Florjańczyk, Phys. Rev. A **41**, 6287 (1990).

[26] A. Smerzi, S. Fantoni, S. Giovanazzi, and S. R. Shenoy, Phys. Rev. Lett. **79**, 4950 (1997); S. Raghavan, A. Smerzi, S. Fantoni, and S. R. Shenoy, Phys. Rev. A59, 620-633 (1999).

[27] M. Cardenas and M. L. Chiofalo, Physica B 322, 116 (2002); M. Greiner *et al.*, Nature **419**, 51 (2002); J. H. Denschlag *et al.*, J. Phys. B **35**, 3095 (2002); Y. B. Band and M. Trippenbach, Phys. Rev. **65**, 053602 (2002); I. Carusotto, D. Embriaco, and G. C. La Rocca, Phys. Rev. A **65**, 053611 (2002); S. Burger *et al.*, Europhys. Lett. **57**, 1 (2002).

[28] S. Peil *et al.*, Phys. Rev. **67**, 051603 (2003).

GLOBALLY-LINKED VORTEX CLUSTERS

Lucian-Cornel Crasovan[1,*], Vadym Vekslerchik[2], Dumitru Mihalache[1,*], Juan P. Torres[1], Víctor M. Pérez-García[2] and Lluis Torner[1]

[1] *ICFO-Institut de Ciencies Fotoniques, and Department of Signal Theory and Communications, Universitat Politecnica de Catalunya, 08034 Barcelona, Spain*

[2] *Departamento de Matemáticas, E.T.S.I. Industriales, Universidad de Castilla-La Mancha, 13071 Ciudad Real, Spain*

Abstract

We show the existence of a rich variety of fully stationary vortex structures made of an increasing number of vortices nested in paraxial wave fields confined by symmetric and asymmetric harmonic trapping potentials in both static and rotating reference frames. In the static reference frame the clusters are built by means of Hermite-Gauss functions, being termed H-clusters, whereas in the rotating frame they are generated by using the Laguerre-Gauss functions, being thus termed L-clusters. These complex vortex-structures consist of globally linked vortices, rather than independent vortices and, in symmetric traps, they feature monopolar global wave front. Nonstationary or flipping circular vortex-clusters can be built in symmetric traps and they feature multipolar phase front. In asymmetric traps, the existing stationary vortex clusters can feature multipolar wave fronts, depending on the ratio of the trap frequencies. In the nonlinear case, corresponding to nonrotating Bose-Einstein condensates, the stationary vortex clusters also exist and some of these highly excited collective states display dynamical stability.

1. Introduction

Singular wave structures, that contain topological wave front dislocations [1], are ubiquitous in many branches of classical and quantum science. Screw dislocations, or vortices, are a common dislocation type. They are spiral phase-ramps around a singularity where the wave phase is undefined and its amplitude vanishes or, in a mathematical

*Also with:Department of Theoretical Physics, Institute of Atomic Physics, P.O.Box MG-6, Bucharest, Romania

F. Kh. Abdullaev and V. V. Konotop (eds.), Nonlinear Waves: Classical and Quantum Aspects, 81–98.

language, they are zeros of complex functions with a nonzero phase circulation around them. Wave packets with nested vortices find applications in fields as diverse as cosmology, biosciences, or solid state physics [2, 3, 4, 5]. As striking examples, they are at the heart of schemes to generate engineered quNits in quantum information systems in higher dimensional Hilbert spaces [6, 7], are believed to be essential for the onset of superfluidity in Bose-Einstein condensates (BECs) [8, 9, 10, 11], or allow tracking the motion of a single atom [12].

A recent study of the motion of vortex lines governed by both linear and nonlinear Schrödinger equations describing the dynamics of atoms in harmonic traps revealed that the topological features of vortex dynamics are to large extent universal [13]. The dynamics of the vortices nested on localized wave packets depends on the evolution of the host beam, and on the interferences and interactions between the vortices [14]. Multiple vortices nested on the same host typically follow dynamical evolutions which might include large vortex-drifts that destroy their initial arrangement, and vortex-pair annihilations that destroy the vortices themselves. Vortex evolutions are particularly complex in strongly nonlinear media, such as BEC, where the vortices can interact with each other. Therefore, a fundamental question arises about whether stationary or quasi-stationary vortex clusters or lattices [16], made of vortices with equal and with opposite topological charges exist. To isolate the pure vortex features from the dynamics solely induced by the evolution of the host wave packet, it is convenient to study wave fields confined by suitable potentials, as in weakly-interacting trapped BEC.

We find that a rich variety of *fully stationary* vortex clusters made of an increasing number of vortices do exist. The important point we put forward is that these clusters are *globally linked*, rather than products of independent vortices. Also, they feature a *monopolar* global wave front. We also show that the clusters exist and are robust in nonlinear systems such as interacting BEC. By contrast, we show that vortex clusters with multipolar global wave fronts nested in wave fields confined by trapping potentials are non-stationary, when the number of vortices and their location are not constant during dynamical evolution, or at best flipping, when the vortices periodically flip their topological charges through extremely sharp Berry trajectories [17]. In the former case, multiple vortex revivals mediated by Freund stationary point bundles [18], that carry the necessary Poincaré-Hopf indices [19], can occur.

The chapter is organized in four parts as follows: Introduction, model and equations, vortex clusters in the non-interacting case and vortex clusters in the interacting case.

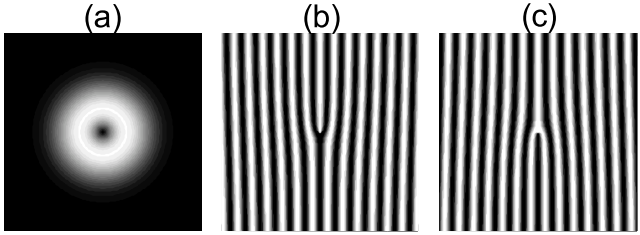

Figure 1. (a) Intensity distribution of a field hosting unit vortices. (b) Interference fringes for the unit positive topological charge and (c) for the vortex with unit negative topological charge.

2. Model and equations

We thus address the slowly-varying evolution of generic wave functions governed by the paraxial wave equation

$$iA_z = \mathcal{L}A + \mathcal{N}(A), \tag{1}$$

where A is a complex field, $\mathcal{L}$ is a two-dimensional linear differential operator containing a trapping potential and $\mathcal{N}(A)$ takes care of any nonlinear contribution. We assume the trapping potential to be harmonic thus $\mathcal{L} = -1/2\left(\partial_x^2 + \partial_y^2\right) + \left(n_x x^2 + n_y y^2\right) + \Omega L_z$. The last term appears in rotating reference frames, $L_z = i\left(x\frac{\partial}{\partial y} - y\frac{\partial}{\partial x}\right)$ being the angular momentum operator and Ω the angular velocity of the rotating frame. The case of a nonrotating frame will correspond to $\Omega = 0$.

To be specific, when $\mathcal{N}(A) \sim |A|^2 A$, this equation models the propagation of a light beam guided in a Kerr nonlinear graded-index medium and the mean-field evolution of a two-dimensional trapped BEC at zero-temperature (where $n_{x,y}$ are proportional to the trap frequencies in appropriate units). When referring to matter-wave phenomena the equation (1) is also termed as the Gross-Pitaevskii (GP) equation.

For convenience, from now on we will split

$$A(x, y; z) = F(x, y; z)V(x, y; z)$$

taking the host packet F as given by the fundamental mode of the trapping potential

$$F(x, y; z) = \exp\left[-\left(\sqrt{\frac{n_x}{2}}x^2 + \sqrt{\frac{n_y}{2}}y^2\right)\right]\exp\left[-i\left(\sqrt{\frac{n_x}{2}} + \sqrt{\frac{n_y}{2}}\right)z\right].$$

In the linear case, the function $V(x, y; z)$ carries all the essential information about the solutions and in particular about vortex dynamics. The

simplest vortex function describing the unit vortices with positive and negative topological charges reads $V(x, y, z = 0) = (x \pm iy) \exp(-x^2 - y^2)$. The intensity distribution and the interference patters for these fields hosting vortices are given in Fig. 1. A characteristic feature of the interference pattern is the existence of a fork-like bifurcation of a fringe. The difference in the number of arms before and after the bifurcation gives us the topological charge of the vortex nested in the bifurcation point. The topological charge tells us the number of multiple of 2π the phase will face on a closed loop around the vortex core. Vortices of opposite charges display bifurcations in different senses when making the interference with the same plane wave.

In what follows we will consider the evolution of polynomial initial data for V corresponding to (multi)vortex solutions of Eq. (1). Such solutions can be expressed as finite series and, as will be clear later, all of them must be periodic or stationary.

3. Vortex clusters in the noninteracting case

3.1 Clusters of product vortices

Let us first consider the linear ($\mathcal{N}(A) = 0$) evolution of vortex-clusters built as products of n independent single-charge vortices: $V(x, y; z = 0) = \prod_{k=1}^{n}[x - x_k + i\sigma_k(y - y_k)]$, where (x_k, y_k) are the locations in the vortex cores in the transverse plane, and $\sigma_k = \pm 1$. None of the above product-vortex clusters is found to be dynamically stationary. On the contrary, the number of vortices and their location is found to vary during evolution, so that the initial vortex structure is destroyed. These results can be illustrated by examining the evolution of the 4-vortex cluster: $V(z = 0) = (x+a+iy)(x-a+iy)(x-iy-ia)(x-iy+ia)$, which contains two vortices with positive topological charge and two vortices with negative charge in a symmetrical geometry. This cluster features a quadrupolar global wave front, as is revealed by calculating the gradient of the wave front Φ far from the cluster core, to obtain $|\nabla\Phi| \sim 1/\rho^3$, where ρ is the polar coordinate, similar to the corresponding electrostatic multipole [20]. Substitution into (1) yields

$$\begin{aligned} V(x, y; z) &= [(x^2 + y^2)(x^2 + y^2 + 2e^{4iz} - 2)]e^{-8iz} \\ &\quad +4ia^2xye^{-4iz} + 1/2(1 - e^{-4iz})^2 - a^4. \end{aligned} \tag{2}$$

One finds three different regimes of evolution, as shown in Fig. 2: Vortex drifts, and vortex-pair annihilations and revivals take place, so that depending on the value of the geometrical parameter a, the total number of vortices, n, hosted in the wave field during propagation can oscillate between: (i) 4 and 8 [see Fig. 2(a)]; (ii) 4, 0 and 8 [see Fig. 2(b)]; (iii)

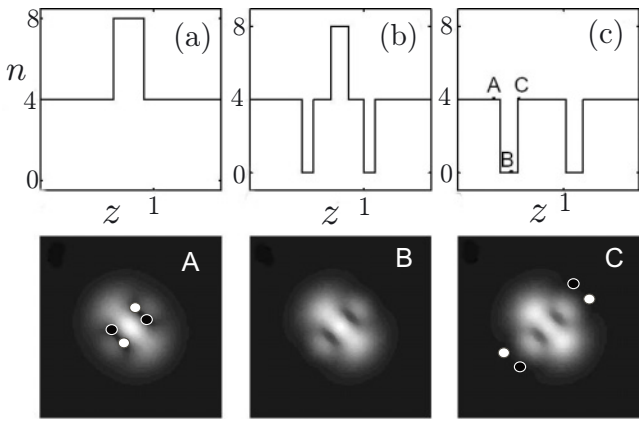

Figure 2. Evolution of a vortex quadrupole, constructed as the product of four single-charge vortices. Upper row: Number of vortices n as a function of z, for different values of the initial quadrupole size. (a) $a = 0.5$, (b) $a = 1.1$ and (c) $a = 1.2$. Bottom row: Intensity snapshots corresponding to points labeled A, B and C in (c). Black-filled circles: positive vortices; white-filled circles: negative vortices.

4 and 0 [see Fig. 2(c)]. When $n = 0$, it is understood that all vortices have annihilated each other. Analogous evolutions were found for octupoles and higher-order multipoles built as product of independent vortices. Only dipoles can be made quasi-stationary, but flipping, when the corresponding vortex twins periodically flip their topological charges [21]. We will show, in the next section, that the vortex dipoles belong to a family of circular quasistationary vortex clusters, for which the constituent vortices periodically flipp the charge. Thus, the main conclusion reached is that the interference between the constituent vortices of all the product-clusters produces beatings between the normal modes of the system, rendering the clusters non-stationary.

3.2 Flipping vortex clusters in symmetric traping potentials

As mentioned above, in symmetric nonrotating traping potentials, one can generate families of circular quasistationary vortex clusters. These vortices of these necklaces are located at the intersection between the circle $x^2+y^2-a^2 = 0$, where $\Re e(V) = 0$, and the lines $y \pm \tan(2k\pi/n)x = 0$, $k \in \mathbb{N}$, where $\Im m(V) = 0$. We can write specific vortex functions for clusters built with $n = 4, 8, 12, \ldots$ vortices ($n = 4k$, $k \in \mathbb{N}$) or for the vortex necklaces with $n = 2, 6, 10, \ldots$ vortices ($n = 2(2k + 1)$, $k \in \mathbb{N}$). The evolution of the vortex function for the $n = 4k$-circular vortex

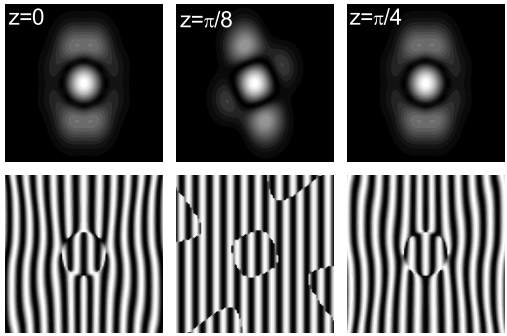

Figure 3. Evolution of the flipping $n = 8$ circular vortex-necklace. Upper row: intensity distribution; lower row: interference fringes.

clusters is given by:

$$V(x,y,z) = (x^2 + y^2 - 1/2)\exp(-4iz) + ixy \prod_{j=1}^{(n-4)/4} (y \pm \tan 2j\pi/n)\exp(-2inz) + (a^2 - 1/2), \quad (3)$$

whereas for the $n = 2(2k+1)$ vortex clusters it is:

$$V(x,y,z) = (x^2 + y^2 - 1/2)\exp(-4iz) + iy \prod_{j=1}^{(n-2)/4} (y \pm \tan 2j\pi/n)\exp(-2inz) + (a^2 - 1/2). \quad (4)$$

Once again, the vortices forming the necklace are intimately linked and do not exhibit a multipolar wave front.

We have chosen, for illustration, the circular vortex cluster with $n = 8$, belonging to the family given by Eq. (3) and a vortex cluster with $n = 6$ belonging to the family built as per Eq. (4). Their field distributions along with the interference fringes at three stages of the evolution are shown in Figs. 3 and 4, respectively. For each case the first and the last frame have the same intensity distribution but different phase portraits. The vortices have flipped the charge through very sharp edge dislocations shown in the middle panel. The charge flipping of the vortices takes place periodically during propagation and, as mentioned above, it is dictated by the beatings between the frequencies of the first two terms in Eqs. (3) and (4).

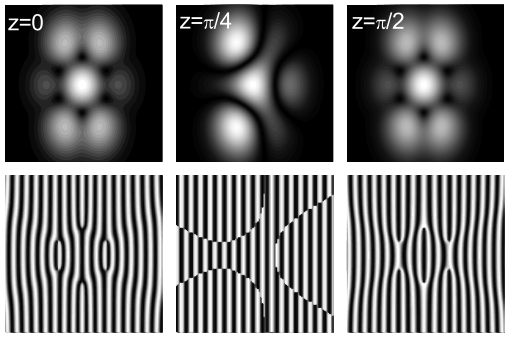

Figure 4. The same as in Fig. 3 but for a $n = 6$ vortex cluster.

3.3 Globally linked vortex-clusters in symmetric traps

(i) The nonrotating case

The key insight we put forward in this paper is that such beatings are not associated to the intrinsic or local properties of the individual vortices, but to the very way the vortices are *globally linked* in the host wave packet. As an example, let us consider the evolution of

$$V(x, y; z = 0) = x^2 + y^2 - a^2 + 2ixy, \tag{5}$$

which contains four vortices located at the same positions and having the same charges as those of the vortex-quadrupole considered above [see Fig. 4(b)]. However, in this cluster the vortices are intimately linked to each other, rather than individually nested in the host F. This fact manifests itself in the global wave front of the cluster, which behaves as $|\nabla\Phi| \sim \cos(2\phi)/\rho + \mathcal{O}(1/\rho^3)$, and thus features a *monopolar* decay almost everywhere. In this case, the vortex evolution is given by

$$V(x, y; z) = (x^2 + y^2 - 1/2 + 2ixy)e^{-4iz} + 1/2 - a^2, \tag{6}$$

an evolution that when the cluster is constructed with $a = 1/\sqrt{2}$ does become fully stationary.

The above 4-vortex cluster is not an isolated case, but rather an example of whole existing families of fully stationary vortex structures made of globally linked vortices. In fact, the solutions of Eq. (1) with

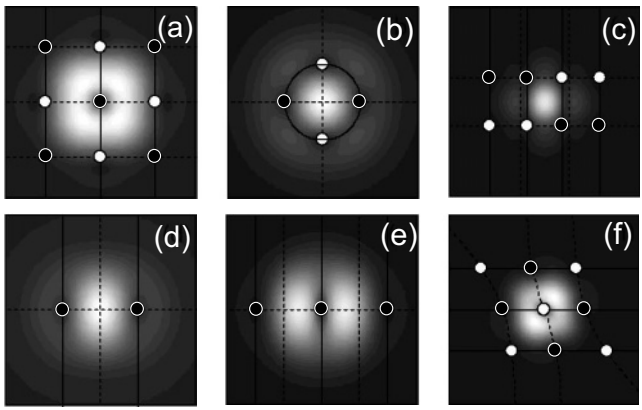

Figure 5. H-cluster zoology. Shown are several examples of stationary vortex matrices and vortex arrays that can be constructed. See text for details. Lines show zero crossings of $\Re e(V)$ (full lines) and $\Im m(V)$ (dashed). Features as in Fig. 2.

$\mathcal{N}(A) = 0$ have the form:

$$A(x, y; z) = \sum_{k,l=0}^{\infty} C_{kl} H_k(x\sqrt{2}) H_l(y\sqrt{2}) e^{-x^2-y^2} e^{-2i(k+l+1)z}, \qquad (7)$$

where H_j are the Hermite polynomials. Therefore, the evolution of initial data of the form $V(x, y; z = 0) = \sum_{k=0}^{n} C_k H_k(\xi) H_{n-k}(\eta)$ for any $C_k \in \mathbb{C}$ and $\xi = x\sqrt{2}, \eta = y\sqrt{2}$, is given by

$$V(x, y; z) = e^{-2inz} \sum_{k=0}^{n} C_k H_k(\xi) H_{n-k}(\eta). \qquad (8)$$

On physical grounds, this simple mathematical result shows that all the stationary clusters are made of globally-linked vortices. Equation (8) allows us to build a variety of structures, to be termed Hermite, or H-clusters, whose key features we discuss in what follows.

Perhaps the simplest type of H-clusters are those with a $n \times n$ *matrix* geometry thus containing n^2 vortices. These clusters can be generated by using as initial data, for example, $V_{n\times n}(x, y; z = 0) = H_n(\xi) + iH_n(\eta)$. In this function the vortex charges alternate throughout the matrix and the vortex locations are dictated by the zeroes of the particular Hermite polynomials involved. In general these vortex matrices are not regular, the distance between vortices varying along the matrix. However, in the particular cases with $n = 2$ and $n = 3$ the matrix is regular. The $n = 3$ case is shown in Fig. 5(a). Notice that a 2×2 matrix cluster can be generated either with $V(x, y; z = 0) = H_2(\xi) + iH_2(\eta)$, or with

$V(x, y; z = 0) = H_2(\xi) + H_2(\eta) + iH_1(\xi)H_1(\eta)$. Actually, this latter possibility generates the stationary 4-vortex cluster discussed earlier [see Fig. 5(b)].

One can also build $m \times n$ ($m \neq n$) stationary vortex matrices. A possible choice for the vortex function generating such a vortex-matrix is $V_{m\times n}(x, y; z = 0) = H_m(\xi) + iH_{|m-n|}(\xi)H_n(\eta)$. As an example we show the 4×2 vortex matrix in Fig. 5(c). In contrast to the $n \times n$ matrices, in the general case the topological charges carried by the vortices of the $m \times n$ matrices do not alternate sign throughout the matrix. An important subclass of the $m \times n$ vortex matrices are the $m \times 1$ cases, to be termed *vortex arrays*. They consist in m co-linearly displaced vortices of the same topological charge. Figures 5(d) and 5(e) show illustrative examples. The simplest array is the vortex-twin shown in Fig. 5(d): A pair of identical vortices that, contrary to the vortex dipole which either undergoes periodic annihilations and revivals or charge flip-flops, can be made fully stationary.

The $n \times n$ matrices are either chargeless for even n, or carry a single net charge for odd values of n, while the $m \times 1$ arrays carry a m total topological charge. In any case, the wave front of all the H-clusters is found *to feature a monopolar* decay ($\sim 1/\rho$) almost everywhere.

More complex H-clusters also exist, and a full classification of all the possibilities falls beyond the scope of this paper. However, an example of one of such exotic H-clusters is displayed in Fig. 5(f), which corresponds to the cluster built with $V(x, y; z = 0) = H_3(\eta)+i(H_3(\xi)+H_1(\eta)H_2(\xi))$. The rich variety of possibilities contained in Eq. (8) is clearly apparent.

(ii) Vortex clusters in rotating reference frame: Spider webs of vortices

The aim of this section is to discuss another type of multivortex configurations in matter and optical waves. Contrary to the case of H-clusters which are rectangular systems of vortices here we deal with the axially symmetric solutions of the GP equation. Such geometry is in some sense more natural in a wide range of situations, as, for example, the case of rotating condensates. To demonstrate the key features of these solutions we will restrict our analytical studies to the linear case leaving analysis of full GP equation to numerical simulations.

Let's rewrite the general GP equation 1 for the interaction-free case in a frame rotating around z-axis with the angular velocity Ω can be written as

$$i\Psi_t = -\frac{1}{2}\Delta\Psi + \frac{1}{2}\omega^2 r^2\Psi + \Omega L_z\Psi \tag{9}$$

where $\Delta = \partial_x^2 + \partial_y^2$ and we have assumed that the trap is axially symmetric, i.e. $n_x = n_y = \omega^2/2$. This model describes the dynamics of

Bose-Einstein condensates stirred by a laser beam rotating with the angular velocity Ω [25].

The main idea is again, as in the case of H-clusters, to use superpositions of stationary solutions of the equation (9). The stationary solutions,

$$\Psi\left(t,\vec{r}\right)=\exp\left(-i\mu t\right)\Psi\left(\vec{r}\right) \tag{10}$$

can be found from the eigenvalue problem which, after separating the gaussian envelope

$$\Psi\left(\vec{r}\right)=\exp\left(-\frac{\omega r^2}{2}\right)\Phi\left(\vec{r}\right) \tag{11}$$

can be written as

$$\mu\Phi=-\frac{1}{2}\Delta\Phi+\omega r\Phi_r+i\Omega\Phi_\theta+\omega\Phi_r. \tag{12}$$

A standard analysis of this equation gives the following result: the eigenvalues of our problem (i.e. the values of μ for which $\Psi\in L_2\left(R^2\right)$) are given by

$$\mu=\mu_{n,m}=(2n+1)\omega+m(\omega-\Omega) \tag{13}$$

where m and n are arbitrary integers. In this case Φ possesses the following structure:

$$\Phi\left(\vec{r}\right)=F_{m,n}(r)(x+iy)^m, \qquad \vec{r}=(x,y), \quad r=|\vec{r}| \tag{14}$$

where $F_{m,n}$ is a polynomial in r^2,

$$F=L_n^m(4\omega r^2), \tag{15}$$

and L_n^m are generalized Laguerre polynomials which solve the equation

$$\xi\frac{d^2F}{d\xi^2}+(m+1-\xi)\frac{dF}{d\xi}+nF=0. \tag{16}$$

Now we can use these stationary solutions to construct ones which describe multivortex configurations of the field. To this end one can use linear combinations of these solutions. Let us consider the simplest linear combination that involves only two such terms:

$$\Psi=\exp\left(-\frac{\omega r^2}{2}\right)\sum_{a=1}^{2}f_a(r)\exp\left(-i\mu_a t+im_a\theta\right) \tag{17}$$

where

$$f_a(r)=r^{m_a}L_{n_a}^{m_a}\left(4\omega r^2\right), \tag{18}$$

$$\mu_a = (2n_a + 1)\,\omega + m_a(\omega - \Omega) \tag{19}$$

and study its zeroes (which correspond to vortices). The complex equation $\Psi = 0$ can be split in two real ones

$$f_1 - \sigma f_2 = 0, \qquad \sigma = \pm 1 \tag{20}$$

and

$$(m_1 - m_2)\,\theta = \pi(\nu + 2\ell) + (\mu_1 - \mu_2)\,t. \tag{21}$$

Here

$$\ell = 1, ..., |\,m_1 - m_2|\,, \qquad \nu = \begin{cases} 0 & \sigma = +1 \\ 1 & \sigma = -1 \end{cases} \tag{22}$$

The right-hand side of (20) is a polynomial in r. So, equation (20) gives us a finite number of values of r. This means that the zeroes of Ψ are located on a few concentric circles. The phase equation (21) shows that at a given moment of time there are $|\,m_1 - m_2|$ zeroes on each circle. To summarize, the set of zeroes can be described as one m-th order zero at the centrum, with $m = \min(m_1, m_2)$, and $2N$ rings, $N = \max(n_1 + m_1, n_2 + m_2)$, each consisting of $|\,m_1 - m_2|$ points (like the nodes of a spider web) rotating with the angular velocity

$$2\frac{n_1 - n_2}{m_1 - m_2}\omega + \omega - \Omega. \tag{23}$$

Of course, these solutions are not stationary in the strict sense of this word (i.e. the field intensity changes in time) but they represent stable patterns undergoing rotation (and periodic changes of their fine structure) that can be seen in experiments and can be viewed as some generalized stationary states. Moreover, in principle, there can be situations when zeroes do not move, but only in the commensurate case, when

$$\frac{\Omega}{\omega} = \frac{\text{integer}}{\text{integer}} \tag{24}$$

which is similar to the GP with anisotropic trap, where the degeneracy of the energy levels occurs only if the trap frequencies are are equal or, more generally, commensurate.

We expect that stationary (in the general sense) rotating spider webs of vortices discussed above will have correspondent stationary solutions in the interacting case and that those solutions are robust (as it is the case of the H-clusters) and we hope that further numerical studies of the full GP equation will confirm this claim.

3.4 Vortex clusters in asymmetric traps

In this section we will present some results concerning the existence of stationary vortex clusters in asymmetric traps. The asymmetric trapping potentials, i.e. those with $n_x \neq n_y$, present more degrees of freedom as comparing to the symmetric ones. As concerning the experimental accessibility to such potentials, at least in the Bose-Einstein condensates, the tuning of the trap frequencies is currently used in order to achieve cigar shaped or pancake shaped condensates. We will consider here the nonintercating case and the results will be compared with those obtained for the symmetric traps in the previous chapters.

The general expression of a stationary solution of Eq. (1) in the nonrotating $\Omega = 0$ and noninteracting limit $\mathcal{N}(A) = 0$ reads:

$$A(x,y;z) = \sum_{k,l}^{\infty} C_{kl} H_k[(2n_x)^{1/4}x] H_l[(2n_y)^{1/4}y] \times e^{-\left(\sqrt{\frac{n_x}{2}}x^2 + \sqrt{\frac{n_y}{2}}y^2\right)} e^{-iE_{k,l}z}, \tag{25}$$

provided that all the terms in this sum have the same eigenvalue $E_{k,l} = \sqrt{2n_x}(k+1/2) + \sqrt{2n_y}(l+1/2)$. Here, as in the previous sections H_j, $j \in \mathbb{N}$ are the Hermite polynomials and $C_{k,l}$ are complex coefficients. Analyzing the above condition one can see that such stationary states can be built only in traps with the frequencies fulfilling $r = \sqrt{\frac{n_y}{n_x}} \in \mathbb{Q}$. A few representative cases of stationary vortex clusters in asymmetric traps are presented in Fig. 6. As can be seen from this figure, a stationary vortex dipole can be built in a trap with $n_x : n_y = 1 : 4$ ($r = 2$). The complex field hosting this vortex dipole is

$$A(x,y,z) = [H_2(x) + iH_1(\sqrt{2}y)] \exp(-x^2/2 - y^2) \exp(-7iz/2)$$

for $n_x = 1/2$ and $n_y = 2$. Moreover, the phase gradient of this field decays at infinity as $|\nabla\Phi| \sim 1/\rho^2$, being thus similar to the electrostatic dipole.

This behavior is different from that of the globally-linked vortex clusters existing in symmetric traps and displaying a monopolar phase front. Another interesting case of stationary vortex ensembles shown in the same Fig. 6 is the mirrored vortex dipole, i.e. two parallel vortex dipoles. This structure exists in asymmetric traps with $r = 2$ and for $n_x = 1/2$ it is hosted by the complex field

$$A(x,y,z) = [H_2(x)H_1(y) + iH_2(\sqrt{2}y)] \exp(-x^2/2 - y^2) \exp(-11iz/2).$$

In asymmetric traps, tuning the ratio of the trap frequencies, one can acquire vortex arrays. i.e. n vortices of alternating topological charges

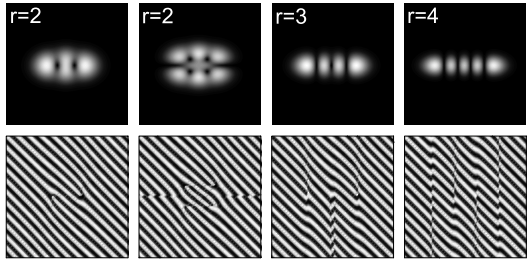

Figure 6. Vortex clusters in asymmetric traps. Shown are the vortex arrays for $r = 2$ (vortex dipole), $r = 3$ and $r = 4$, respectively and the parallel vortex dipoles existing in the $r = 2$ traps.

$(+, -, +, \ldots)$ displaced on a line. The general expression for such vortex arrays in a traps with $r = n$, $n \in \mathbb{N}$ and $n_x = 1/2$ is

$$A_n(x, y, z) = [H_n(x) + iH_1(\sqrt{n}y)] \exp(-x^2/2 - ny^2/2) \exp[-(3n + 1)iz/2].$$

In Fig. 6 we have shown the $(+, -, +)$ vortex array existing for $r = 3$ and the $(+, -, +, -)$ vortex array existing in the case $r = 4$.

4. Vortex clusters in the interacting case

An interesting issue is the existence and stability of vortex-clusters in the presence of nonlinear cubic interactions such as those appearing in the propagation of beams in Kerr media or in the dynamics of BEC. To ease the comparison with BEC literature we choose now $n_x = n_y = 1/2$ and $\mathcal{N}(A) = U|A|^2A$ [26]. In this context the evolution variable is denoted by t instead of z. With this choice of parameters the range of U values experimentally accessible for the two-dimensional case is $0 < U < 10^2 - 10^3$ [27].

We have studied several particular examples to verify that these structures indeed exist and are stable in the nonlinear regime. We have taken as initial data several linear configurations such as a single vortex, dipole systems and the 4-vortex cluster given by Eq. (5) and evolved them for $UN = 10$ ($N = \int |A|^2 d\mathbf{x}$ is the wave function norm) using an standard split-step integrator.

It is found that, although the background performs oscillations and the vortex locations oscillate around their equilibrium positions, the vortex clusters remain stable (see Fig. 7). We have also searched for stationary solutions of Eq. (1), of the form $A(x, y; t) = e^{i\lambda t}\psi(x, y)$. To do so we have used a steepest descent method to minimize the functional

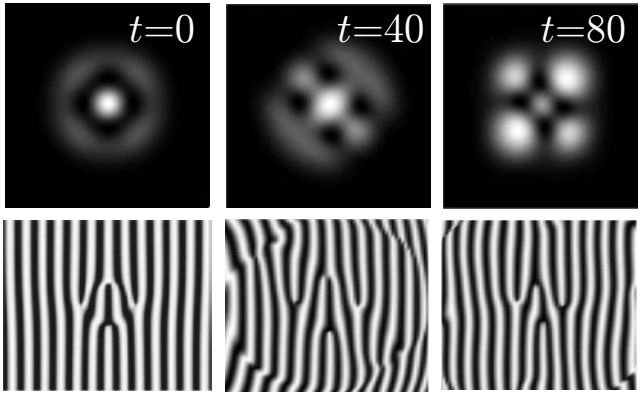

Figure 7. Stable evolution of initial data given by Eq. (5) for $UN = 10$. Upper row: Intensity plots; bottom row: Interference fringes. Spatial region spanned is $[-4, 4] \times [-4, 4]$.

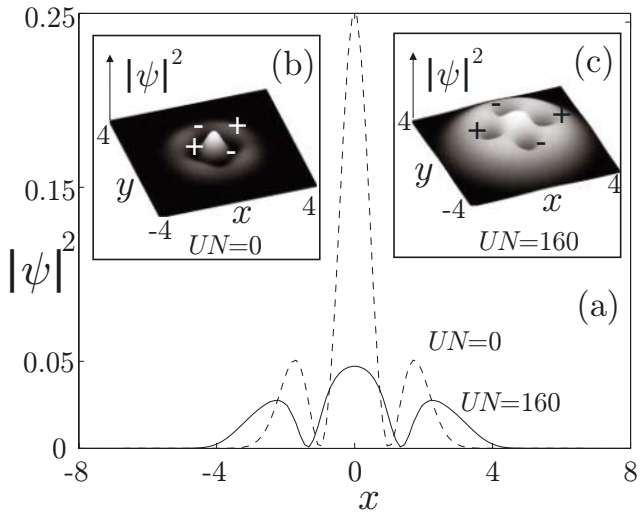

Figure 8. Linear 4-vortex cluster [Eq. (5)] vs. its nonlinear stationary version for $U = 100, \lambda = 8$. (a) Plots of $|\psi(x, y = 0)|^2$ for the linear (dashed line) and nonlinear (solid line) cases. (b,c) Surface plots of $|\psi(x, y)|^2$ for (b) the linear and (c) nonlinear situations. The vortex locations and topological charges are indicated by plus and minus signs.

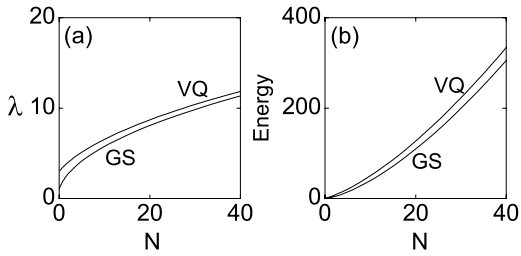

Figure 9. (a) The $\lambda(N)$ and (b) the $E(N)$ dependences for the vortex-quadrupole (labelled here VQ) and the ground state (GS) solutions for $U = 10$.

[28]:

$$F(\psi) = \frac{\int \psi^* \left(-\Delta - \lambda + r^2 + U|\psi|^2\right) \psi d\mathbf{x}}{\int |\psi|^2 d\mathbf{x}}, \tag{26}$$

whose minima (except for $\psi = 0$) coincide with the stationary solutions of Eq. (1) for a given value of λ. For instance, taking as initial data for the minimization process the linear 4-vortex cluster and setting $\lambda = 8.0$ and $U = 100$, we found a stationary 4-vortex cluster solution (see Fig. 8) with norm $N = \int |\psi|^2 d\mathbf{x} \simeq 1.6005$ (thus the product $UN \simeq 160$ which lies into the fully nonlinear regime).

In Fig. 9 we have plotted the chemical potential λ versus the number of atoms N and the energy E versus N for the one-parametric family of vortex quadrupoles along with the corresponding dependences for the ground state solutions. This curves indicate, as expected, that the vortex-quadrupole is an excited state of the atomic ensemble, its energy exceeding always the energy of the ground state (bell-shaped vortex-free state).

These vortex quadrupoles existing in BEC are highly excited collective states of the condensed atoms and, in contrast with their equivalents in optics (spatiotemporal soliton molecules or soliton necklaces) which are highly unstable [29] or, at best metastable [30]-[31], they are very robust under time evolution when small perturbations are added.

These evidences show that the existence of H-clusters in a BEC should be experimentally accessible, at least from the dynamical point of view.

5. Conclusions

In conclusion we have comparatively presented the stationary and flipping vortex clusters existing in trapped wave fields in both noninteracting and interacting limits. For the noninteracting case we have shown that in the nonrotating frame the vortices forming the stationary H-cluster are *globally linked*, rather than product of independent vortices. Similar, in the rotating frames, a rich variety of L-clusters do exist. For commensurate ratios of the trap frequency and the angular velocity of the rotating frame the vortex spider-web is stationary in the rotating reference frame. We have also pointed out that nonsymmetric trapping potentials open new possibilities for building exotic stationary vortex ensembles that cannot be built in symmetric traps. The stationary vortex clusters found in the linear limit have, as a rule, correspondents in the interacting case and the family of nonlinear vortex quadrupoles was investigated in detail, these solutions displaying a remarkable stability on evolution. Following this idea it is possible to generate a variety of additional novel structures with fascinating properties. The exploitation of such intrinsic linking might open new opportunities in classical and quantum systems based on topological light and matter waves. The first challenge is the demonstration of the generation of the clusters, by suitable computer-generated holograms [32] in Optics and phase-imprinting techniques in BEC [33].

Acknowledgments

This work was supported by the Generalitat de Catalunya and Ministerio de Ciencia y Tecnología under grants TIC2000-1010 and BFM2000-0521. L. -C. Crasovan acknowledges NATO support and thanks M. Damian and O. Halmaghi for helpful discussions. D.M. acknowlegdes support from ICREA-Institucio Catalana de Recerca i Estudis Avancats.

References

[1] J. F. Nye and M. V. Berry, Proc. R. Soc. London Ser. A **336**, 165 (1974).

[2] H. J. Lugt, *Vortex Flow in Nature and Technology* (Krieger, Malabar, FL, 1995).

[3] L. M. Pismen, *Vortices in Nonlinear Fields* (Clarendon, Oxford, UK, 1999).

[4] A. Ashkin, Opt. Photon. News **10**(5), 41 (1999); M. E. J. Friese *et al.*, Nature **394**, 348 (1998); M. J. Padgett and L. Allen, Contemp. Phys. **41**(5), 275 (2000); L. Paterson *et al.*, Science **292**, 912 (2001).

[5] P. Galajda and P. Ormos, Appl. Phys. Lett. **78**, 249 (2001).

[6] A. Mair *et al.*, Nature **412**, 313 (2001).

[7] G. Molina-Terriza, J. P. Torres, and L. Torner, Phys. Rev. Lett. **88**, 013601 (2002).

[8] R. J. Donnelly, *Quantized Vortices in Hellium II* (Cambridge University Press, Cambridge, 1991).

[9] M. R. Matthews *et al.*, Phys. Rev. Lett. **83**, 2498 (1999); K. W. Madison *et al.*, Phys. Rev. Lett. **84**, 806 (2000).

[10] D. A. Butts and D. S. Rokhsar, Nature (London) **397**, 327 (1999).

[11] M. Tsubota, K. Kasamatsu and M. Ueda, Phys. Rev. A **65**, 023603 (2002).

[12] O. Horak *et al.*, Phys. Rev. Lett. **88**, 043601 (2002).

[13] I. Bialynicki-Birula, Z. Bialynicka-Birula, and C. Śliwa, Phys. Rev. A **61**, 032110 (2000); I. Bialynicki-Birula and Z. Bialynicka-Birula, Phys. Rev. A **65**, 014101 (2001).

[14] For reviews focused on optical vortices, but relevant to BEC too, see D. Rozas, C. T. Law, and G. A. Swartzlander, J. Opt. Soc. Am. B **14**, 3054 (1997); Yu. S. Kivshar *et al.*, Opt. Commun. **152**, 198 (1998); M. S. Soskin and M. V. Vasnetsov, *Singular Optics*, in Progress in Optics, vol. 42, p. 219, E. Wolf ed., (Elsevier, Amsterdam, 2001).

[15] I. Freund, Opt. Commun. **159**, 99 (1999).

[16] J. R. Abo-Shaeer *et al.*, Science, **292**, 476 (2001).

[17] M. V. Berry, in *Singular Optics*, M. S. Soskin ed., Proc. SPIE 3487, pp. 1-5, 1998.

[18] I. Freund, Opt. Commun. **181**, 19 (2000); I. Freund and D. A. Kessler, Opt. Commun. **187**, 71 (2001).

[19] I. Freund, Opt. Lett. **26**, 545 (2001).

[20] Analogously, vortex monopoles $V(z=0) = x \pm iy$, give $|\nabla\Phi| \sim 1/\rho$, dipoles feature $|\nabla\Phi| \sim 1/\rho^2$, and so on.

[21] G. Molina-Terriza, L. Torner, E. M. Wright, J. J. García-Ripoll, V. M. Pérez-García, Opt. Lett. **26**, 1601 (2001).

[22] L.-C. Crasovan, G. Molina-Terriza, J. P. Torres, L. Torner, V. M. Perez-Garcia, and D. Mihalache, Phys. Rev. E **66**, 036612 (2002).

[23] T. Kobayashi, Physica A **303**, 469 (2002).

[24] I. Freund, Opt. Commun. **199**, 47 (2001).

[25] D. L. Feder, C. W. Clark, and B. I. Scheneider, Phys. Rev. Lett. **82**, 4956 (1999); A. A. Svidzinsky and A. L. Fetter, Phys. Rev. Lett. **84**, 5919 (2000).

[26] With this choice the basis functions are $H_m(x), H_n(y)$ and the "background" $F(x,y,t) = e^{-x^2/2-y^2/2}e^{it/2}$.

[27] See e.g. J. J. García-Ripoll, V. M. Pérez-García, Phys. Rev. A **64**, 013602 (2001).

[28] J. J. García-Ripoll, V. M. Pérez-García, SIAM J. Sci. Comp. **23**, 1315 (2001).

[29] M. Soljacic, S. Sears, and M. Segev, Phys. Rev. Lett. **81**, 4851 (1998); A. S. Desyatnikov and Yu. S. Kivshar, Phys. Rev. Lett. **88**, 053901 (2002).

[30] Ya. V. Kartashov *et al.*, Phys. Rev. Lett. **89**, 273902 (2002); L.-C. Crasovan *et al.*, Phys. Rev. E **67**, 046612 (2003).

[31] V. M. Pérez-García and V. Vekslerchik, Phys. Rev. E **67**, 061804 (2003); Phys. Rev. E **68**, 016617 (2003).

[32] V. Yu. Bazhenov, M. V. Vasnetsov, and M. S. Soskin, JETP Lett. **52**, 429 (1991); N. R. Heckenberg *et al.*, Opt. Lett. **17**, 221 (1992).

[33] J. E. Williams and M. J. Holland, Nature **401**, 568 (1999); L. Dobrek *et al.*, Phys. Rev. A **60**, R3381 (1999); J. Denschlag *et al.*, Science **287**, 97 (2000); G. Andrelczyk *et al.*, Phys. Rev. A **64**, 043601 (2001).

SOLUTIONS OF THE LOGARITHMIC SCHRÖDINGER EQUATION IN A ROTATING HARMONIC TRAP

Iwo Białynicki-Birula and Tomasz Sowiński
Center for Theoretical Physics, Polish Academy of Sciences Lotników 32/46, 02-668 Warszawa, Poland

Abstract We study the influence of the nonlinearity in the Schrödinger equation on the motion of quantum particles in a harmonic trap. In order to obtain exact analytic solutions, we have chosen the logarithmic nonlinearity. The unexpected result of our study is the existence in the presence of nonlinearity of two or even three coexisting Gaussian solutions.

Keywords: nonlinear Schrödinger equation, rotating harmonic trap, logarithmic Schrödinger equation, exact solutions of a nonlinear Schrödinger equation

1. Introduction

The nonlinear Schrödinger equation with the logarithmic nonlinearity (we use the units $\hbar = 1$ and $m = 1$)

$$i\partial_t \psi(\mathbf{r},t) = \left(-\frac{1}{2}\Delta + V(\mathbf{r},t) - b\log(|\psi(\mathbf{r},t)|^2/a^3)\right)\psi(\mathbf{r},t) \qquad (1)$$

was introduced [1] long time ago to seek possible departures of quantum mechanics from the linear regime. The parameter b measures the strength of the nonlinear interaction (positive b means attraction) and a is needed to make the argument of the logarithm dimensionless — it plays no significant role since the change of a results only in an additive constant to the potential. In what follows, we shall absorb the parameter a into the wave function that amounts effectively to putting $a = 1$.

It has been proven in beautiful experiments with neutron beams [14, 15, 9] that the nonlinear effects in quantum mechanics, if they exist at all, are extremely small. The upper limit for the constant b was determined to be $3.3\ 10^{-15}$ eV. Thus, the applicability of the logarithmic

F. Kh. Abdullaev and V. V. Konotop (eds.), Nonlinear Waves: Classical and Quantum Aspects, 99–106.

Schrödinger equation to the time evolution of wave functions seems to have been ruled out. Nevertheless this equation, owing to its unique mathematical properties, has been used in many branches of physics to model the nonlinear behavior of various phenomena. It has been applied in the study of dissipative systems [11], in nuclear physics [10], in optics [12, 5], and even in geophysics [7]. In contrast to the properties of other nonlinear equations, the logarithmic Schrödinger equation in any number of dimensions possesses analytic solutions, called Gaussons in [2]. Gaussons represent localized nonspreading solutions of the Gaussian shape. The internal structure of the Gaussons may also change in time. The existence of these analytic solutions enables one to study in detail the influence of nonlinearities. In this paper we focus our attention on the behavior of the solutions of the logarithmic Schrödinger equation in a rotating harmonic trap. The aim of our study was to see to what extent the nonlinear interaction may change the dynamics and affect the stability of solutions. Perhaps, our results will help to better understand the behavior of the Bose-Einstein condensate in a rotating trap. Previous studies of these problems (for example, [13] and [6]) were often based on the hydrodynamic equations and we plan in the future to express our results in terms of the hydrodynamic variables.

2. Formulation of the problem

The logarithmic Schrödinger equation in a rotating trap has the form

$$i\partial_t\psi(\mathbf{r},t) = \left(-\frac{1}{2}\Delta + \frac{1}{2}\mathbf{r}\cdot\hat{V}(t)\cdot\mathbf{r} - b\log(|\psi(\mathbf{r},t)|^2)\right)\psi(\mathbf{r},t), \qquad (2)$$

where the symmetric 3×3 matrix $\hat{V}(t)$ depends on time due to rotation. In order to simplify the analysis of stability, we assume that the trap is subjected to a uniform rotation and we shall use the coordinate system co-rotating with the trap. In this manner the potential becomes time-independent but due to rotation there appears an additional term in the equation.

$$i\partial_t\psi(\mathbf{r},t) = \left(-\frac{1}{2}\Delta + \frac{1}{2}\mathbf{r}\cdot\hat{V}\cdot\mathbf{r} - b\log(|\psi(\mathbf{r},t)|^2) - \mathbf{\Omega}\cdot\mathbf{M}\right)\psi(\mathbf{r},t), \quad (3)$$

where $\mathbf{\Omega}$ is the vector of angular velocity and $\mathbf{M} = \mathbf{r}\times\mathbf{p}$ is the operator of angular momentum. We shall seek the solutions of Eq. (3) in the Gaussian form

$$\psi(\mathbf{r},t) = N(t)e^{if(t)}\exp\left(-\frac{1}{2}\tilde{\mathbf{r}}\cdot(\hat{A}(t)+i\hat{B}(t))\cdot\tilde{\mathbf{r}}(t) + i\boldsymbol{\pi}(t)\cdot\mathbf{r}\right), \qquad (4)$$

where $\tilde{\mathbf{r}} = \mathbf{r} - \boldsymbol{\xi}(t)$. The time-dependent vectors $\boldsymbol{\xi}(t)$ and $\boldsymbol{\pi}(t)$ specify the position and momentum of the center of mass of the Gaussian wave packet and the time-dependent real symmetric matrices $\hat{A}(t)$ and $\hat{B}(t)$ specify the shape and the internal motion of the wave packet, respectively. The two real functions $N(t)$ and $f(t)$ define the normalization and the overall phase of the Gausson. Substituting this Ansatz into Eq. (3), we arrive at the following set of *ordinary* differential equations for all the functions entering our formula (4)

$$\frac{d\hat{A}(t)}{dt} = \hat{B}(t)\hat{A}(t) + \hat{A}(t)\hat{B}(t) - \left[\hat{\Omega}, \hat{A}(t)\right], \tag{5}$$

$$\frac{d\hat{B}(t)}{dt} = \hat{B}(t)^2 - \hat{A}(t)^2 + \hat{V} + 2b\hat{A}(t) - \left[\hat{\Omega}, \hat{B}(t)\right], \tag{6}$$

$$\frac{d\boldsymbol{\xi}(t)}{dt} = \boldsymbol{\pi}(t) - \boldsymbol{\Omega} \times \boldsymbol{\xi}(t), \tag{7}$$

$$\frac{d\boldsymbol{\pi}(t)}{dt} = -\hat{V}\cdot\boldsymbol{\xi}(t) - \boldsymbol{\Omega} \times \boldsymbol{\pi}(t), \tag{8}$$

$$\frac{dN(t)}{dt} = \frac{1}{2}\mathrm{Tr}\{\hat{B}(t)\}N(t), \tag{9}$$

$$\frac{df(t)}{dt} = -\frac{1}{2}\left(\mathrm{Tr}\{\hat{A}(t)\} + \boldsymbol{\pi}(t)\cdot\boldsymbol{\pi}(t) - \boldsymbol{\xi}(t)\cdot\hat{V}\cdot\boldsymbol{\xi}(t)\right), \tag{10}$$

where the antisymmetric matrix $\hat{\Omega}$ and the components of the angular velocity vector $\boldsymbol{\Omega}$ are related through the formula $\Omega_{ij} = \epsilon_{ijk}\Omega^k$. Note, that the internal motion (described by $\hat{A}(t)$ and $\hat{B}(t)$) completely decouples from the motion of the center of mass (described by $\boldsymbol{\xi}(t)$ and $\boldsymbol{\pi}(t)$). In turn, the equations for the normalization factor and the phase can be integrated after the internal and the center of mass motion has been determined. This decoupling follows from the general theorem [8] and [4] stating that from every solution of a nonlinear Schrödinger equation in a harmonic potential (including time-dependent potential) one may obtain a solution displaced by a classical trajectory fully preserving the shape of the wave function.

3. Solutions and their stability

In what follows, for simplicity, we shall assume that the trap rotates along one of its principal axis. In this case the motion in the direction perpendicular to the rotation plane decouples and we are left with a two-dimensional problem. In the stationary state of our system the center of mass motion must be absent ($\boldsymbol{\xi}(t) = 0, \boldsymbol{\pi}(t) = 0$) The stationary state of the system is described by the wave function characterized by the solution of the following two time-independent equations for two 2×2

matrices A and B

$$0 = \hat{B}\hat{A} + \hat{A}\hat{B} - \left[\hat{\Omega}, \hat{A}\right], \tag{11}$$

$$0 = \hat{B}^2 - \hat{A}^2 + \hat{V} + 2b\hat{A} - \left[\hat{\Omega}, \hat{B}\right]. \tag{12}$$

We shall seek the solutions of these equations in the coordinate frame in which the matrix $\hat{V}$ is diagonal, $\hat{V} = \mathrm{Diag}\{\omega_1^2, \omega_2^2\}$. We assume, for definitness, that $\omega_1 < \omega_2$. It follows from Eqs. (11–12) that in this frame the matrix $\hat{A}$ is also diagonal and the matrix $\hat{B}$ is off-diagonal. Finally, we are left with three equations for two matrix elements α_1, α_2 of $\hat{A}$ and one matrix element β of $\hat{B}$

$$(\alpha_1 + \alpha_2)\beta - (\alpha_1 - \alpha_2)\Omega = 0, \tag{13}$$

$$\beta^2 - \alpha_1^2 + \omega_1^2 + 2b\alpha_1 + 2\beta\Omega = 0, \tag{14}$$

$$\beta^2 - \alpha_2^2 + \omega_2^2 + 2b\alpha_2 - 2\beta\Omega = 0. \tag{15}$$

It follows from Eq. (13) that in the absence of rotation β must vanish and we obtain immediately two physically acceptable solutions of the decoupled quadratic equations for the parameters α

$$\alpha_1 = (\omega_1\sqrt{1 + b^2/\omega_1^2} + b), \tag{16}$$

$$\alpha_2 = (\omega_2\sqrt{1 + b^2/\omega_2^2} + b), \tag{17}$$

$$\beta = 0. \tag{18}$$

The two remaining solutions yield negative values of the α's and must be rejected. Thus, in the absence of rotation the nonlinearity modifies only the size of the Gaussian wave function without introducing any significant changes. Even for negative values of b (nonlinear repulsion), stable solutions described by (16) and (17) always exist, no matter how strong is the repulsion.

Simple analytic formulas can also be obtained in the presence of rotation but without nonlinearity. The formulas for the Gausson parameters read in this case

$$\alpha_1 = \frac{\sqrt{\omega_1^2 + \omega_2^2 + 2\Omega^2 \pm 2\sqrt{(\omega_1^2 - \Omega^2)(\omega_2^2 - \Omega^2)}}}{1 + \sqrt{(\omega_2^2 - \Omega^2)/(\omega_1^2 - \Omega^2)}}, \tag{19}$$

$$\alpha_2 = \frac{\sqrt{\omega_1^2 + \omega_2^2 + 2\Omega^2 \pm 2\sqrt{(\omega_1^2 - \Omega^2)(\omega_2^2 - \Omega^2)}}}{1 + \sqrt{(\omega_1^2 - \Omega^2)/(\omega_2^2 - \Omega^2)}}, \tag{20}$$

$$\beta = \Omega\frac{1 - \sqrt{(\omega_2^2 - \Omega^2)/(\omega_1^2 - \Omega^2)}}{1 + \sqrt{(\omega_2^2 - \Omega^2)/(\omega_1^2 - \Omega^2)}}. \tag{21}$$

The values of α are real in the two regions of stability when $\Omega < \omega_1$ (region 1) and $\Omega > \omega_2$ (region 2). The same regions of stability were obtained in the analysis of the characteristic frequencies in classical or quantum-mechanical center-of-mass motion [4]. In the formulas (19) and (20) the + and – sign is to be chosen for the region 1 and the region 2, respectively.

In the presence of both rotation and nonlinearity the properties of solutions change significantly. The most striking difference is the appearance of additional stationary Gaussian solutions. This is an unexpected result because in the linear theory a purely Gaussian shape always is found for *only one* fundamental state of the system — all other states have polynomial prefactors. We have not been able to find closed expressions for the parameters α and β, so we had to resort to numerical analysis of the solutions of Eqs. (13–15). We present our results in three plots showing the calculated values of the parameters α_1 and α_2 that determine the shape of the Gaussian wave function. These values are plotted as functions of the angular velocity Ω. In all plots we have fixed the trap parameters to be $\omega_1 = \sqrt{2/3}, \omega_2 = \sqrt{4/3}$. We have chosen three values of b to describe the following characteristic cases. In Fig. 1 we plot the values of α's without the nonlinear interaction ($b = 0$). In Fig. 2 we added the attractive nonlinear interaction ($b = 1$) and in Fig. 3 the repulsive nonlinear interaction ($b = -1$).

4. Conclusions

Knowing the exact analytic form of the solutions of our nonlinear Schrödinger equation we were able determine the influence of rotation and nonlinearity on the stability of solutions. The unexpected result of our analysis is that the repulsive interaction *expands* the region of stability. We have to admit, however, that this may be true only for the special form of the nonlinearity: the logarithmic nonlinearity.

References

[1] I. Bialynicki-Birula and J. Mycielski, Wave equations with logarithmic nonlinearities, Bull. Acad. Polon. Sci. Cl. III **23**, 461 (1975).

[2] I. Bialynicki-Birula and J. Mycielski, Nonlinear wave mechanics, Ann. of Phys. (N.Y.), **100**, 62 (1976).

[3] I. Bialynicki-Birula and J. Mycielski, Gaussons: Solitons of the logarithmic Schrödinger equation, Physica Scripta, **20**, 539 (1978).

[4] I. Bialynicki-Birula and Z. Bialynicka-Birula, Center of mass motion in many-body theory of Bose-Einstein condensates, Phys. Rev. A **65**, 063606 (2002).

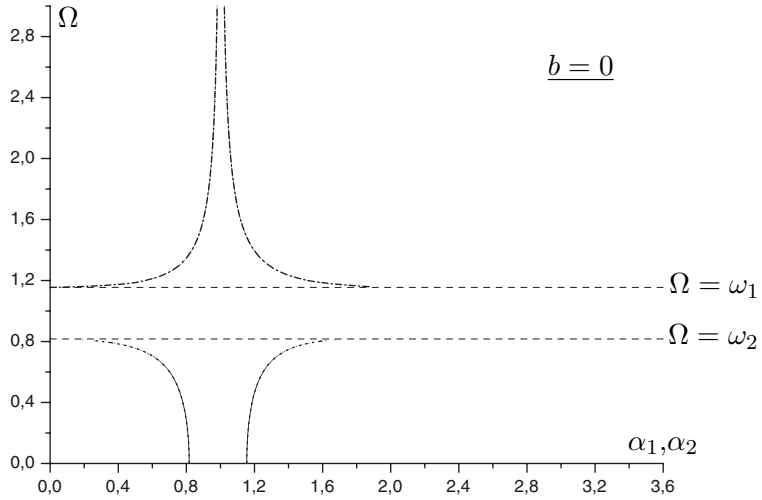

Figure 1. This plot shows the values of α_1 and α_2 in the absence of the nonlinearity. For each value of Ω in the stability regions there is just one Gaussian wave function whose shape is described by the values of α's.

[5] H. Buljan, A. Šiber, M. Soljačic, T. Schwartz, M. Segev, and D. N. Christodoulides, Incoherent white light solitons in logarithmically saturable noninstantaneous nonlinear media, Phys. Rev. E **68**, 036607 (2003).

[6] M. Cozzini, S. Stringari, V. Bretin, P. Rosenbusch, and J. Dalibard, Scissors mode of a rotating Bose-Einstein condensate, Phys. Rev. A **67**, 021602(R) (2003).

[7] S. De Martino, M. Falanga, C. Godano, and G. Lauro, Logarithmic Schrödinger-like equation as a model for magma transport, Europhys. Lett. **63**, 472 (2003).

[8] J. J. García-Ripoll, V. M. Pérez-García, and V. Vekslerchik, Construction of exact solutions by spatial translations in inhomogeneous nonlinear Schrödinger equations, Phys. Rev. E **64**, 056602 (2001).

[9] R. Gähler, A. G. Klein, and A. Zeilinger, Neutron optical tests of nonlinear wave mechanics, Phys. Rev. A **23**, 1611 (1981).

[10] E. F. Hefter, Application of the nolinear Schrödinger equation with a logarithmic inhomogeneous term to nuclear physics, Phys. Rev. **A 32**, 1201 (1985).

[11] E. S. Hernandez and B. Remaud, General properties of Gausson-conserving descriptions of quantal damped motion, Physica **105A**, 130 (1980).

[12] W. Krolikowski, D. Edmundson, and O. Bang, Unified model for partially coherent solitons in logaritmically nonlinear media, Phys. Rev. E **61**, 3122 (2000).

[13] A. Recati, F. Zambelli, and S. Stringari, Overcritical rotation of a trapped Bose-Einstein condensate, Phys. Rev. Lett. **86**, 377 (2001).

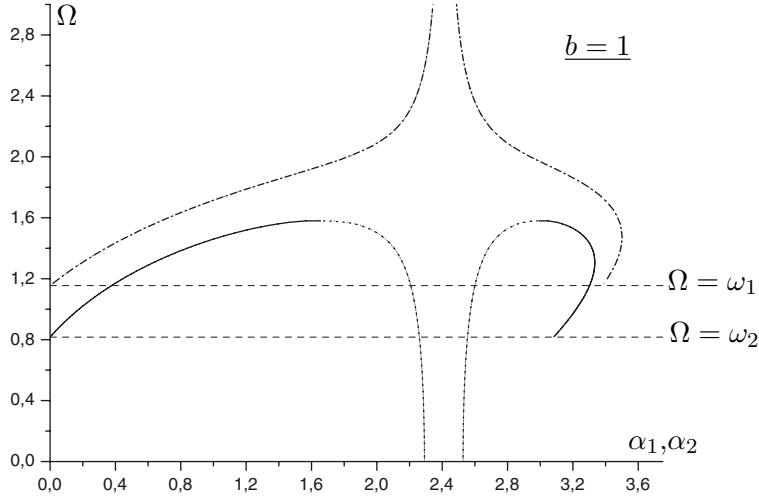

Figure 2. This plot shows the values of α_1 and α_2 in the case of attractive nonlinear interaction. For sufficiently large values of b, as in this case, there are no regions of instability. For small and for large values of Ω there is just one Gaussian wave function but for intermediate values there are two or even three solutions. Matching pairs of α's are distinguished by the lines of the same style: solid, dashed, and dotted.

[14] A. Shimony, Proposed neutron interferomenter test of some nonlinear variants of wave mechanics, Phys. Rev. A **20**, 394 (1979).

[15] C. G. Shull, D. K. Atwood, J. Arthur, and M. A. Horne, Search for a nonlinear variant of the Schrödinger equation by neutron interferometry, Phys. Rev. Lett. **44**, 765 (1980).

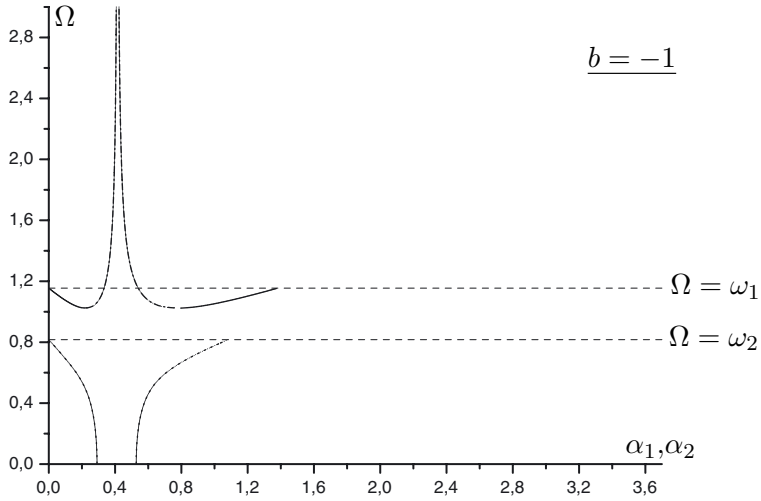

Figure 3. This plot shows the values of α_1 and α_2 in the case of repulsive nonlinear interaction. The upper region of stability is extended now downwards as compared to the case without the nonlinear term. Moreover, there are two solutions (solid and dashed lines) that coexist in the newly established region of stability.

LINEAR AND NONLINEAR BOUND STATES IN CURVED WAVEGUIDES

Yu.B. Gaididei
Bogolyubov Institute for Theoretical Physics, Metrologichna str. 14 B, 01413, Kiev, Ukraine
yg@imm.dtu.dk

P.L. Christiansen
Informatics and Mathematical Modelling, The Technical University of Denmark, DK-2800 Lyngby, Denmark
plc@imm.dtu.dk

P.G. Kevrekidis
Department of Mathematics and Statistics, University of Massachusetts, Amherst MA 01003-4515, USA
kevrekid@math.umass.edu

H. Büttner
Physikalisches Institut, Universität Bayreuth, Bayreuth D-95440, Germany
helmut.buettner@uni-bayreuth.de

A.R. Bishop
Theoretical Division and Center for Nonlinear Studies, Los Alamos National Laboratory, Los Alamos, NM 87545, USA
arb@lanl.gov

Abstract Motivated from curved waveguides embedded in photonic crystals, we examine the effects of geometry in a "quantum channel" of parabolic form. We study the linear case and derive exact as well as approximate expressions for the eigenvalues and eigenfunctions of the linear problem. The analytical results are used as initial conditions in direct numerical

F. Kh. Abdullaev and V. V. Konotop (eds.), Nonlinear Waves: Classical and Quantum Aspects, 107–120.

simulations of the nonlinear problem and localized excitations are found to persist, as well as to have interesting relaxational dynamics.

Keywords: Curvature, Waveguides, Nonlinear Schrödinger Equation

1. Introduction

Localization phenomena are widely recognized as key to understanding the excitation dynamics in many physical contexts such as light propagation, charge and energy transport in condensed-matter physics and biophysics, and Bose-Einstein condensation of dilute atomic gases [1, 2]. Recent advances in micro-structuring technology have made it possible to fabricate various low-dimensional systems with complicated geometry. Examples are photonic crystals with embedded defect structures such as microcavities, waveguides and waveguide bends [2, 3, 4, 5], narrow structures (quantum dots and channels) formed at semiconductor heterostructures [6, 7, 8], magnetic nanodisks, dots and rings [9, 10, 11].

On the other hand, it is well known that the wave equation subject to Dirichlet boundary conditions has bound states in straight channels of variable width [12, 13, 14], and in curved channels of constant cross-section [15, 16]. Spectral and transport characteristics of quantum electron channels [17] and waveguides in photonic crystals [3] are in essential ways modified by the existence of segments with finite curvature. The two-dimensional Laplacian operator supported by an infinite curve which is asymptotically straight has at least one bound state below the threshold of the continuum spectrum, as was recently proved in [18]. The appearance of an effective attractive potential in the wave equation is due to constraining quantum particles from higher to lower dimensional manifolds [19, 20, 21]. Curvature induced bound-state energies and corresponding wave functions were studied in [22].

Until recently there have been few theoretical and numerical studies of the effect of curvature on properties of nonlinear excitations. Nonlinear whispering gallery modes for a nonlinear Maxwell equation in microdisks were investigated in [23]; the excitation of whispering-gallery-type electromagnetic modes by a moving fluxon in an annular Josephson junction was shown in [24]. Nonlinear localized modes in two-dimensional photonic crystal waveguides were studied in [25]. A curved chain of nonlinear oscillators was considered in [26] and it was shown that the interplay of curvature and nonlinearity leads to a symmetry breaking when an asymmetric stationary state becomes energetically more favorable than a symmetric stationary state. Propagation of Bose-Einstein condensates in magnetic waveguides was experimentally demonstrated recently in [27]; single-mode propagation was observed along homoge-

neous segments of the waveguide, while geometric deformations of the microfabricated wires led to strong transverse excitations.

Motivated by the experimental relevance of the above mentioned geometric deformations, in the present work we aim at investigating nonlinear excitations in a prototypical setup incorporating such phenomena. As our case example, we will examine an infinitely narrow curved nonlinear waveguide (channel) embedded in a two-dimensional linear medium (idle region).

Our presentation will proceed as follows: in Section 2, we set up the mathematical model of interest and examine its general properties and equations of motion. In Section 3, we study the linear case and present its explicit solutions for the bound states, as well as for the corresponding eigenvalues. In section 4, we supplement our analysis with numerical results for both the linear and the nonlinear case. Finally, in section 5, we summarize our findings and present our conclusions.

2. Setup and Equations of Motion

Our model is described by the Hamiltonian

$$H = \int_{-\infty}^{\infty} \{|\nabla\psi|^2 - \nu\,(|\psi|^2 - A\frac{1}{2}|\psi|^4)\,\delta(y - f(x))\}dxdy, \tag{1}$$

where $\psi(\vec{r}, t)$ is the complex amplitude function, $\vec{r} = (x, y)$, $\nabla^2 = \partial_x^2 + \partial_y^2$, ν is the energy difference between the quantum channel and the passive region (refractive index difference in the case of photonic crystals and waveguides), the coefficient A characterizes the nonlinearity of the medium, e.g., the nonlinear corrections to the refractive index of the photonic band-gap materials, or self-interaction of the quasi-particles in the quantum channel. The function $y = f(x)$ determines the shape of the channel. From the Hamiltonian, we obtain the equation of motion in the form

$$i\partial_t\psi(\vec{r}, t) + \nabla^2\psi + \nu\,\delta(y - f(x))F(|\psi|^2)\,\psi = 0, \tag{2}$$

where the function $F(|\psi|^2)$ is given by

$$F = 1 - A|\psi|^2. \tag{3}$$

Equation (2) has as integrals of motion the Hamiltonian (1) and the (L^2) norm (referred to e.g., as the number of atoms in BEC or power in nonlinear optics)

$$N = \int_{-\infty}^{\infty} |\psi|^2\,dxdy. \tag{4}$$

It is well known (see *e.g.*, [28]) that if the edges of the Frénet trihedron (the tangent, the principal normal and the binormal) at a given point are considered as the axes of a Cartesian coordinate system, then the equation of the curve in a neighbourhood of this point has the form

$$x = s + \cdots\,,\ y = \frac{\kappa}{2}\, s^2 + \cdots\,,\ z = -\frac{\kappa\,\tau}{6}\, s^3 + \cdots \tag{5}$$

where s is the arclength, κ is the curvature and τ is the torsion of the curve at this point. Thus, if the curvature of the plane curve is not too large one can represent it as a parabola

$$y = \frac{\kappa}{2}\, x^2. \tag{6}$$

In this case Eq. (2) takes the form

$$i\partial_t\psi + \nabla^2\psi + \nu\,\delta(y - \frac{x^2}{2R})F(|\psi|^2)\,\psi = 0, \tag{7}$$

where $R = 1/\kappa$ is the maximum radius of curvature of the curve. It is convenient to use the parabolic coordinates

$$x = \frac{uv}{R}, \quad y = \frac{R}{2} + \frac{1}{2R}(u^2 - v^2). \tag{8}$$

The coordinate lines are two orthogonal families of confocal parabolas, with axes along the y axis. These lines are given by

$$R\frac{x^2}{v^2} = 2y - R + v^2/R, \quad R\frac{x^2}{u^2} = -2y + R + u^2/R$$

or

$$u/\sqrt{R} = \pm\sqrt{y - \frac{R}{2} + \sqrt{(y - \frac{R}{2})^2 + x^2}},$$
$$v/\sqrt{R} = \sqrt{-y + \frac{R}{2} + \sqrt{(y - \frac{R}{2})^2 + x^2}}. \tag{9}$$

The variable u is allowed to range from $-\infty$ to ∞, whereas v is positive. Introducing Eqs. (8) into Eq. (7) and using the properties of parabolic coordinates (see e.g., [29]), we obtain:

$$i\,\frac{1}{R^2}(u^2 + v^2)\,\partial_t\psi + \left(\partial_u^2 + \partial_v^2\right)\psi + \nu\,\delta(v - R)\,F(|\psi|^2)\,\psi = 0. \tag{10}$$

Using the Fourier transform with respect to t,

$$\bar{\psi} = \frac{1}{2\pi}\int\limits_{-\infty}^{\infty} e^{i\omega t}\psi(u, v, t)\,dt, \tag{11}$$

where the bars denote the Fourier transformed quantities, one can represent Eq. (10) in the form

$$-\frac{\omega}{R^2}(u^2+v^2)\,\bar{\psi}+\left(\partial_u^2+\partial_v^2\right)\bar{\psi}+\nu\,\delta(v-R)\,\overline{F(|\psi|^2)\,\psi}(u,v)=0. \quad (12)$$

Equation (10) can, in turn, be expressed in the form of the integral equation

$$\bar{\psi}(u,v,\omega)=\nu\int\limits_{-\infty}^{\infty}du'\int\limits_{0}^{\infty}dv'\,G\left(u,v;u',v'\right)\,\delta(v'-R)\,\overline{F(|\psi|^2)\psi}(u',v',\omega), \quad (13)$$

where the Green's function $G\left(u,v;u',v'\right)$ satisfies the equation

$$\left(\partial_u^2+\partial_v^2\right)\,G-\frac{\omega}{R^2}(u^2+v^2)\,G=-\delta(u-u')\,\delta(v-v'), \quad (14)$$

and has the form

$$G\left(u,v;u',v'\right)=\frac{\sqrt{\pi}}{2}\sum_{n=0}^{\infty}F_n(u)\,F_n(u')\,\{V_n(v)\,U_n(v')\,\theta(v'-v) +U_n(v)\,V_n(v')\,\theta(v-v')\}. \quad (15)$$

Here

$$F_n(u)=a_n\,e^{-\sqrt{\omega}u^2/2R}\,H_n\left(u\,\omega^{1/4}\,R^{-1/2}\right),\quad n=0,1,2,..., \quad (16)$$

where $H_n\left(z\right)$ is the Hermite polynomial [30], $a_n=\left(\frac{\omega^{1/2}}{R\,\pi}\right)^{1/4}\frac{1}{(2^n\,n!)^{1/2}}$ is the normalization constant, and

$$V_n(v)=V\left(n+\frac{1}{2},v\,\sqrt{2}\,\omega^{1/4}\,R^{-1/2}\right),$$
$$U_n(v)=U\left(n+\frac{1}{2},v\,\sqrt{2}\,\omega^{1/4}\,R^{-1/2}\right), \quad (17)$$

with $V(a,x)$ and $U(a,x)$ being the Weber parabolic cylinder functions [30].

It can then be seen from Eqs. (13) and (14) that the Fourier transformed channel wave function

$$\bar{\phi}(u,\omega)\equiv\bar{\psi}(u,v,\omega)\Big|_{v=R}, \quad (18)$$

satisfies the equation

$$\bar{\phi}(u,\omega) = \nu\,\omega^{-1/4}\,\frac{\sqrt{\pi\,R}}{2}\sum_{n=0}^{\infty}\int_{-\infty}^{\infty} F_n(u)\,F_n(u') \times V_n(R)\,U_n(R)\,\overline{F(|\phi|^2)\,\phi}(u',\omega)\,du', \tag{19}$$

or equivalently the equation

$$\nu\,\omega^{-1/4}\,\frac{\sqrt{\pi\,R}}{2}\,\overline{F(|\phi|^2)\,\phi}(u,\omega) = \sum_{n=0}^{\infty}\int_{-\infty}^{\infty}\frac{F_n(u)\,F_n(u')}{V_n(R)\,U_n(R)}\bar{\phi}(u',\omega)\,du'. \tag{20}$$

The wave function $\bar{\psi}(u,v,\omega)$ may be represented in terms of the channel wave function $\bar{\phi}(u,\omega)$ as follows:

$$\bar{\psi}(u,v,\omega) = \frac{\omega^{1/4}}{\sqrt{R}}\int_{-\infty}^{\infty} du'\,\bar{\phi}(u',\omega)\sum_{n=0}^{\infty} F_n(u)\,F_n(u')\,\frac{V_n(v)}{V_n(R)} \tag{21}$$

for $0 < v < R$ and

$$\bar{\psi}(u,v,\omega) = \frac{\omega^{1/4}}{\sqrt{R}}\int_{-\infty}^{\infty} du'\,\bar{\phi}(u',\omega)\sum_{n=0}^{\infty} F_n(u)\,F_n(u')\,\frac{U_n(v)}{U_n(R)} \tag{22}$$

for $R < v$.

3. Linear case: $A = 0$

In the linear case ($A = 0$), Eq. (20) assumes the form

$$\nu\,\omega^{-1/4}\,\frac{\sqrt{\pi\,R}}{2}\,\overline{\phi}(u,\omega) = \sum_{l=0}^{\infty}\int_{-\infty}^{\infty}\frac{F_l(u)\,F_l(u')}{V_l(R)\,U_l(R)}\bar{\phi}(u',\omega)\,du'. \tag{23}$$

Taking into account that the set of functions $F_n(u)$ is complete and orthonormal, one can rewrite Eq.(23) as

$$\sum_{l=0}^{\infty}\{\nu\,\omega^{-1/4}\,\frac{\sqrt{\pi\,R}}{2}\,U_l\,(R)\;V_l\,(R) - 1\}\,\phi_l = 0, \tag{24}$$

where

$$\phi_l = \int_{-\infty}^{\infty} F_l(u)\,\overline{\phi}(u,\omega)\,du. \tag{25}$$

Thus, we can conclude that the solution of the linear eigenvalue problem can be presented in the form

$$\phi_l = \delta_{kn}\, \mathcal{N}_n \tag{26}$$

$$\nu \sqrt{\frac{R}{\lambda_n}}\, U\left(n+\frac{1}{2}, \sqrt{2\lambda_n R}\right)\, V\left(n+\frac{1}{2}, \sqrt{2\lambda_n R}\right) = \frac{2}{\sqrt{\pi}}. \tag{27}$$

Eq. (27) determines the frequency ($\omega_n = \lambda_n^2$) of the n-th eigenstate and Eq. (26) with $\mathcal{N}_n$ being a normalization constant and δ_{kn} being the Kronecker delta, yields its amplitude.

Introducing Eqs. (25) and (26) into Eqs. (21)-(22) we obtain that the eigenfunction $\Phi_n(u,v) \equiv \bar{\psi}(u,v,\omega_n)$, which corresponds to the eigenvalue given by Eq. (27), can be expressed as:

$$\Phi_n(u,v) = \mathcal{N}_n\, F_n(u)\, \left(\frac{V_n(v)}{V_n(R)} \theta(R-v) + \frac{U_n(v)}{U_n(R)}\, \theta(v-R) \right). \tag{28}$$

For even values of n: $n = 2m$ ($m = 0, 1, 2, ..$), Eq. (27) always has a solution and for $\nu R \to 0$ and the eigenvalue is given by

$$\lambda_{2m} \approx \left(\frac{\Gamma(m+\frac{1}{2})}{m!} \right)^2 \frac{\nu^2 R}{4(1+\nu R)^2}. \tag{29}$$

For $n = 2m+1$, $m = 0, 1, 2, ...$ the bound state exists only for $\nu R \geq 1$ and near the lower bound the energy of the bound state is given by

$$\lambda_{2m+1} \approx \left(\frac{m!}{2\,\Gamma(m+\frac{3}{2})} \right)^2 \frac{(\nu\, R - 1)^2}{\nu^2\, R^3}. \tag{30}$$

In the limit of large radius of curvature R and moderate n, i.e., $\nu R \gg n + \frac{1}{2}$, we obtain from Eq. (27) that the eigenvalues λ_n are determined by

$$\lambda_n = \frac{\nu}{2} \left(1 - \frac{2n+1}{\nu R} \right). \tag{31}$$

Thus the bound state energy decreases when the curvature of the chain increases and in the limit $R \to \infty$ we obtain the straight-line result: $\lambda = \nu/2$.

It is interesting to return to the Cartesian coordinates and to consider the shape of the bound state wave function. Let us consider the case

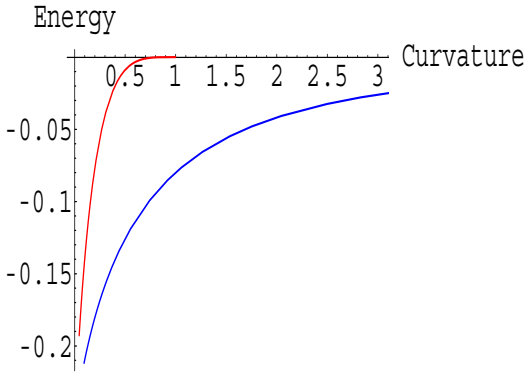

Figure 1 Bound state energy ($-\lambda_n^2$) vs. curvature ($\kappa = 1/R$): $n = 0$ (lower curve), $n = 1$ (upper curve). The dependence of the energy as a function of the curvature is obtained through the solution of Eq. (27).

$n = 0$. It can be seen that

$$\Phi_0 = \mathcal{N}_0\, e^{-\lambda_0 y}\left(\text{erfc}\left(\sqrt{\lambda_0 R}\right)\theta\left(y - \frac{x^2}{2R}\right)\right.$$
$$\left. +\text{erfc}\left(v\sqrt{\lambda_0}\right)\theta\left(\frac{x^2}{2R} - y\right)\right), \qquad (32)$$

where the function $v(x, y)$ is given by Eq. (8). When $R \to \infty$ (straight waveguide) the wave function is localized in the y-direction only. However, for finite R the function is localized both in x- and y-directions. The localization length in the x-direction is proportional to R. The expression of Eq. (31) will also be used as a starting point in our direct numerical simulations of Eq. (10); see section 4 below.

4. Numerical Results

We start by demonstrating the results of the linear case of Eqs. (27) and (31). The eigenvalue (energy) of the linear case as a function of curvature is shown in Fig. 1, while the lowest energy, bound state wavefunction of the linear problem is given in Fig. 2.

In order to demonstrate that this linear bound state persists in the nonlinear limit we have performed full dynamical evolution simulations of Eq. (7), with an initial condition of the form expressed in Eq. (31), and demonstrated in Fig. 2. We note in passing that similar results have been obtained with a variety of initial conditions. In particular, we show typical numerical simulation results in Fig. 3 for $R = 10$, $\nu = A = 1$.

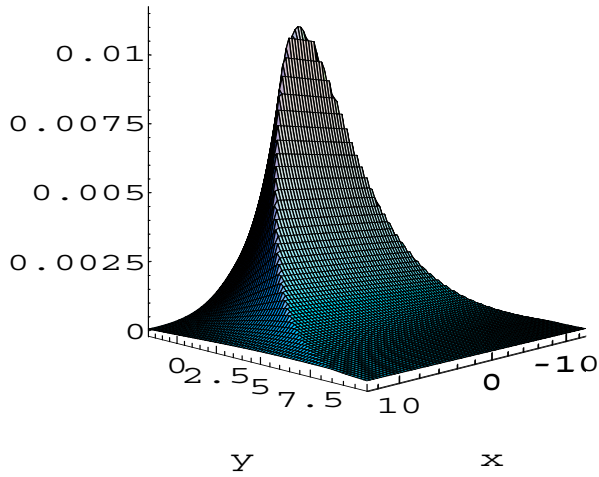

Figure 2 The wave function of the lowest bound state of the linear problem ($A = 0$) is shown in the figure for $R = 10$, $\nu = 1$ (obtained through Eq. (31)).

Notice that the δ function was represented as

$$\delta(s) = \sqrt{\frac{1}{\pi\epsilon}} \exp\left(-\frac{s^2}{2\epsilon}\right) \tag{33}$$

with $\epsilon = 0.05$. The contour plot of Fig. 3 shows the result after a numerical evolution of 100 time units of Eq. (7). The dynamical development indicates that after an initial transient the original linear profile slightly reshapes itself into the nonlinear solution depicted in Fig. 3. In the process, some radiation waves ("phonons") are shed, that are absorbed by the absorbing boundary conditions used in a layer close to the end of the domain (our computational box is of size 25×25).

Beyond the proof-of-principle simulations for various initial conditions, we also attempted to examine the dynamics of the nonlinear excitations of the channel. This was done using the following numerical protocol: after obtaining a quasi-relaxed nonlinear localized mode for the channel of the form $y = x^2/(2R)$, we moved the channel to a new position, namely $y = (x-1)^2/(2R)$. Notice that similar in spirit experiments have recently been carried in Bose-Einstein condensates [31], where the magnetic trap confining the condensate is displaced to a new position and the ensuing dynamics of the condensate are observed. The position of the center of mass of the initial condition profile was approximately obtained (using a trapezoidal approximation to the relevant two-dimensional integrals) as $(x(t=0), y(t=0)) = (0.178, 0.862)$. The new bottom of the channel (hence the point to which the center of mass

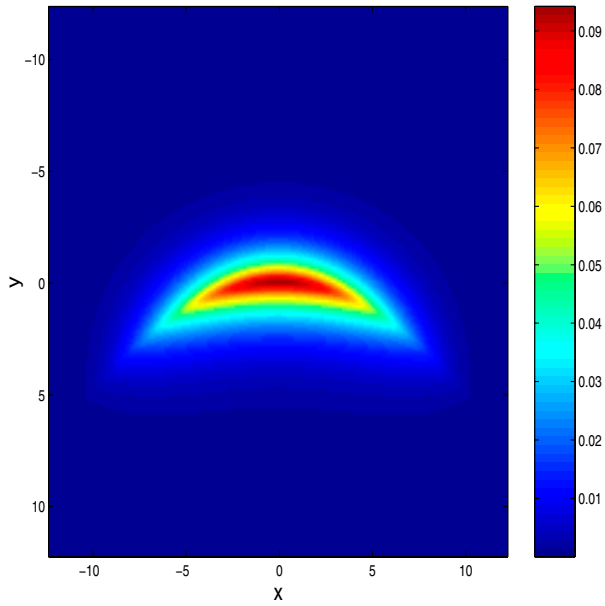

Figure 3. Contour plot of the solution of the partial differential equation of Eq. (7) with $f(x) = x^2/(2R)$, $R = 10$, $\nu = A = 1$ and initial condition given by the linear profile of Eq. (31).

should approach) in this case is $(x, y) = (1, 0)$. In Fig. 4, the process of relaxation to this new equilibrium is shown as a function of time for a very long dynamical simulation of t up to 1000 time units. In this run, we observe (after an initial transient) a slow relaxation towards the new minimum of the potential well. Notice that despite the *Hamiltonian* nature of the model, the excitation of an "internal mode" of the nonlinear wave [32] can be dissipated due to mechanisms of coupling to extended wave, phonon modes, such as the ones reported in [33].

5. Summary

In summary, we have shown that:

- In two-dimensional media with a curved *infinitely thin* waveguide (quantum channel) there exist bound states for linear and nonlinear self-interacting excitations;
- The finite curvature of the waveguide provides a stabilizing effect on otherwise unstable localized states of repelling excitations;
- The binding energy of both linear and nonlinear localized excitations decreases when the curvature of the waveguide increases.

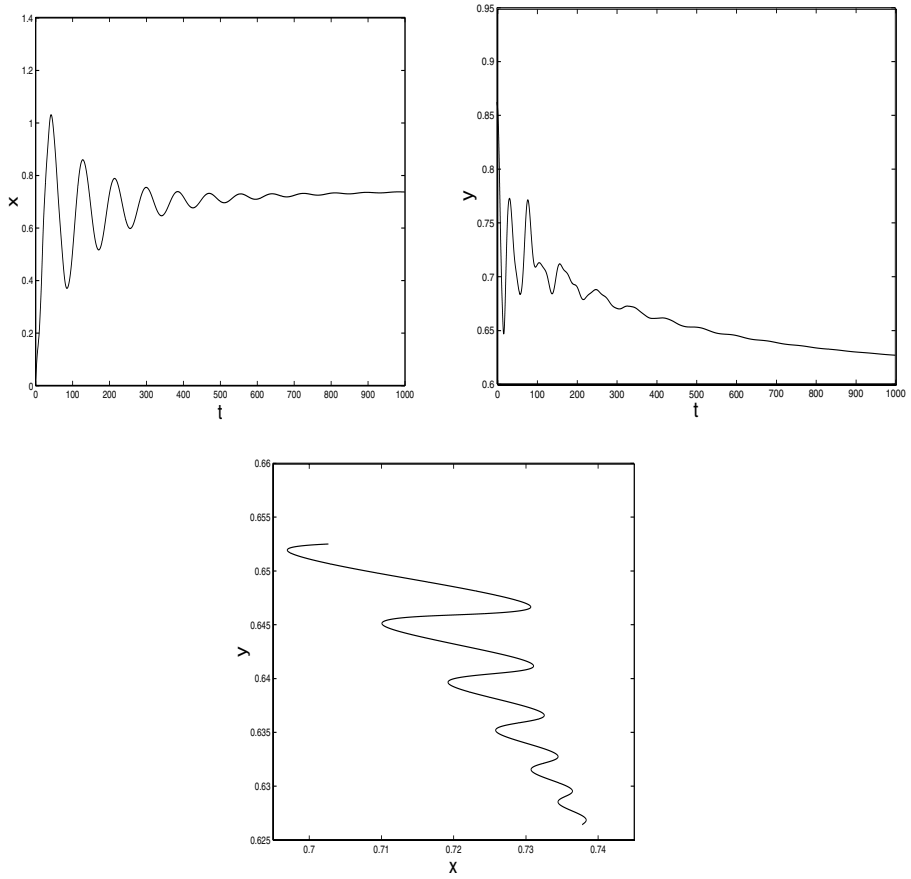

Figure 4. The top left panel shows, for times between t=500 and t=1000, the time evolution of the x-coordinate of the center of mass of the nonlinear excitation. Similarly, the top right panel shows the y-coordinate of the center of mass. Finally, the bottom panel shows the time evolution of the center of mass in the $x - y$ plane (the motion proceeds from the top left to the bottom right as time evolves).

- Such linear bound states as the ones found here persist in the nonlinear dynamical problem as localized excitations. These have been found to be robust for different initial conditions and are centered at the minimum (point of largest curvature) of the parabola. When, the mode is initialized away from this minimum, it slowly relaxes to it.

A number of future interesting and potentially relevant (e.g., to the embedding of a waveguide in a two-dimensional photonic crystal) questions have arisen in this study that warrant future investigations. The detailed numerical study of the stability of the nonlinear localized modes identified here is, naturally, one such topic. Another direction that could be of further interest is the examination of a case of a finite (rather than infinitesimal) width channel [which can be computational achieved e.g., by allowing the parameter ϵ of Eq. (33) to vary towards larger values]. The examination of thresholds for genuinely two-dimensional instabilities, such as e.g., the transverse or the snaking instability, would be of particular relevance within the latter context.

Such studies are currently in progress and will be reported in future publications.

Acknowledgments

Yu.B.G. thanks the Informatics and Mathematical Modelling, Technical University of Denmark for a Guest professorship. Yu.B.G acknowledges support from Deutsche Zentrum für Luft- und Raumfart e.V., Internationales Büro des Bundesministeriums für Forschung und Technologie, Bonn, in the frame of a bilateral scientific cooperation between Ukraine and Germany, project No. UKR-02/011. This work was supported by a UMass FRG, NSF-DMS-0204585 and the Eppley Foundation for Research (PGK)

References

[1] *N*onlinear Science at the Dawn of the 21st Century, Eds P.L. Christiansen, M.P. Sørensen, A.C. Scott, Lecture Notes in Physics (Springer,Berlin, Heidelberg, New York,2000); *L*ocalization and Energy transfer in Nonlinear Systems, Eds L. Vázquez, R.S. Mackay, M.P.Zorzano (World Scientific, Singapore, 2003).

[2] *P*hotonic Crystals and Light Localization in the 21st Century, C. M. Soukoulis (ed.), NATO Science Series C**563**, (Kluwer Academic Dordrecht, Boston, London, 2001).

[3] A. Mekis, J.C. Chen, I. Kurland, S. Fan, P.R. Villeneuve, and J.D. Joannopoulos, Phys. Rev. Lett. **77**, 3787 (1996).

[4] S. Noda, A. Alongkarn, and M. Imada, Nature (London), **407**, 608 (2000).

[5] Yu.S. Kivshar, P.G. Kevrekidis and S. Takeno, Phys. Lett. A, **307**, 287 (2003).

[6] B.J. van Wees, H. van Houten, C.W.J. Beenakker, J.G. Williamson, L.P. Kouwenhoven, D. van der Marel, and C.T. Foxon, Phys. Rev. Lett. **60**, 848 (1988).

[7] *N*anostructure Physics and Fabrication, Eds M.A. Reed and W.P. Kirks, (Academic Press, New York,1989).

[8] K. Ismail, S. Washburn, and K. Y. Lee, Appl. Phys. Lett. **59**, 1998 (1991).

[9] R. Pulwey, M. Rahm, J. Biberger, and D. Weiss, IEEE Transactions on magnetics **37,** 2076 (2001).

[10] T. Shinjo, T. Okuno, R. Hassdorf, K. Shigeto, and T. Ono, Science, **289**, 930 (2000).

[11] M. Klaui, C. A. F. Vaz, J. Rothman, J. A. C. Bland, W. Wernsdorfer, G. Faini, and E. Cambril, Phys. Rev. Lett. **90**, 097202 (2003).

[12] R.L. Schult, D.G. Ravenhall and H.W. Wyld, Phys. Rev. B**39**, 5476 (1989).

[13] K.F. Berggren and Z.L. Ji, Phys. Rev. B**43**, 4760 (1991).

[14] M. Andrews and C.M. Savage , Phys. Rev. A **50**, 4535 (1994).

[15] P. Exner and P. Seba, J. Math. Phys. **30**, 2574 (1989).

[16] J. Goldstone and R.L Jaffe, Phys. Rev. B **45**,14100 (1992).

[17] Yu. B. Gaididei and O.O. Vakhnenko, J. Phys.: Condens. Matter **6**, 32229 (1994); O.O. Vakhnenko, Phys. Rev. B**52**, 17386 (1995).

[18] P. Exner and T. Ichinose, J. Phys. A **34**, 1439 (2001).

[19] R.C.T. da Costa, Phys. Rev. A **23**, 1982 (1981).

[20] P.C. Schuster and R.L. Jaffe, e-print hep-th/0302216.

[21] P. Exner and D. Krejcirik, J. Phys. A: Math. Gen. **34**, 5969 (2001).

[22] M. Encinosa and B. Etemadi, Phys. Rev. A **58**, 77 (1998); M. Encinosa and L. Mott, Phys. Rev. A **68**, 014102 (2003).

[23] T. Harayama, P. Davis and K. S. Ikeda, Phys. Rev. Lett. **82**, 3803 (1999).

[24] A. Wallraff, A.V. Ustinov, V.V. Kurin, I.A. Shereshevsky, and N.K. Vdovicheva, Phys. Rev. Lett. **84**, 151 (2000).

[25] S.F. Mingaleev, Yu.S. Kivshar, and R.A. Sammut, Phys. Rev. E **62**, 5777 (2000); S.F. Mingaleev and Yuri S. Kivshar Phys. Rev. Lett. **86**, 5474 (2001).

[26] Yu. B. Gaididei, S.F. Mingaleev and P.L. Christiansen, Phys. Rev. E **62** R53 (2000); J. Phys.:Condens. Matter **13**,1 (2001).

[27] A.E. Leanhardt, A.P. Chikkatur, D. Kielpinski, Y. Shin, T.L. Gustavson, W. Ketterle, and D.E. Pritchard, Phys. Rev. Lett. **89**, 040401 (2002).

[28] *E*ncylopaedia of Mathematics, vol. 3 (Kluwer Academic Publishers, Dordrecht, Boston, London, 1989), p. 159.

[29] D. Jones, *Generalized Functions* (McGraw-Hill Publishing Company, London 1966).

[30] M. Abramowitz and I. Stegun, *Handbook of Mathematical Functions* (Dover Publications, Inc., New York, 1972).

[31] A. Smerzi, A. Trombettoni, P.G. Kevrekidis and A.R. Bishop, Phys. Rev. Lett. **89**, 170402 (2002); F.S. Cataliotti, L. Fallani, F. Ferlaino, C. Fort, P. Maddaloni and M. Inguscio, New. J. Phys. **5**, 71 (2003).

[32] Yu.S. Kivshar, D.E. Pelinovsky, Thierry Cretegny, and Michel Peyrard, Phys. Rev. Lett. **80**, 5032 (1998); P.G. Kevrekidis and C.K.R.T. Jones, Phys. Rev. E **61**, 3114 (2000).

[33] M. Johansson and S. Aubry, Phys. Rev. E **61**, 5864 (2000); P.G. Kevrekidis and M.I. Weinstein, Physica D **142**, 113 (2000); P.G. Kevrekidis and M.I. Weinstein, Math. Comp. Simul. **62**, 65 (2003).

NUMERICAL STUDY OF A NONLOCAL SINE-GORDON EQUATION

G. Alfimov*
Lukin's Research Institute of Physical Problems, Zelenograd, Moscow, 103460, Russia
alfimov@nonlin.msk.ru

T. Pierantozzi
Departamento de Matemática Aplicada, Facultad de Informatica,
Universidad Complutense, 28040, Madrid, Spain
Teresa_Pierantozzi@mat.ucm.es

L. Vázquez
Departamento de Matemática Aplicada, Facultad de Informatica,
Universidad Complutense, 28040, Madrid, Spain;
Centro de Astrobiologia (CSIC -INTA), 28850, Torrejón de Ardoz, Madrid, Spain
lvazquez@fdi.ucm.es

Abstract For the nonlocal sine-Gordon equation $u_{tt} - Hu_x + \sin u = 0$, where H is the Hilbert transform, a family of breather-like solutions is found numerically. These objects are quite robust and even can be developed from some bell-shaped initial data. Also it is shown that the interactions between the elementary entities which describes this nonlocal equation are not elastic, so it hardly can be integrable.

Keywords: Nonlocal equations, sine-Gordon, breathers.

1. Introduction

The nonlocal equation

$$u_{tt} - Hu_x + \sin u = 0, \tag{1}$$

*On sabbatical leave in: Departamento de Matemática Aplicada, Facultad de Informatica, Universidad Complutense, 28040, Madrid, Spain

F. Kh. Abdullaev and V. V. Konotop (eds.), Nonlinear Waves: Classical and Quantum Aspects, 121–128.

where H is the Hilbert transform

$$Hf(x) \equiv \frac{1}{\pi}\text{v.p.}\int_{-\infty}^{\infty}\frac{f(x')dx}{x'-x},$$

appears in various physical applications (see e.g. [1, 2]) as a nonlocal analogue of the classical sine-Gordon equation

$$u_{tt} - u_{xx} + \sin u = 0 \tag{2}$$

It is well known that Eq.(2) is completely integrable and its exact solutions can be constructed by means of some regular procedure. The two important particular solutions of Eq.(2) are *travelling* 2π*-kink* (antikink) solution

$$u(t,x) = 4\arctan\exp\left\{\pm\frac{c-ct}{\sqrt{1-c^2}}\right\}, \quad c^2<1 \tag{3}$$

and *breather* solution

$$u_\omega(t,x) = 4\arctan\frac{\sqrt{1-\omega^2}\cos\omega t}{\omega\cosh\sqrt{1-\omega^2}x}, \quad 0<\omega<1 \tag{4}$$

Eq.(1) is much less studied. The energy integral for Eq.(1) is

$$\mathcal{H} = \int_{-\infty}^{\infty}\left\{\frac{1}{2}u_t^2 - \frac{1}{2}uHu_x + 1 - \cos u\right\}dx; \quad \frac{d\mathcal{H}}{dt} = 0; \tag{5}$$

Also it is known that Eq.(1) admits some exact solutions. They are: the steady-state 2π-kink (antikink) solution [1]

$$u(t,x) = \pi \pm 2\arctan x, \tag{6}$$

the travelling 4π-kink (antikink) solution [3]

$$u(t,x) = \pm 4\arctan(x \pm t), \tag{7}$$

and some periodic travelling structures [4]. Not all the exact solutions of (1) have their counterparts among the solutions of (2) (an example is the solution (7)). One should mention also that the steady-state solutions of (1), $u_t(t,x) \equiv 0$, are related to the solutions $v(\tau,\xi)$ of the so-called sine-Hilbert equation [5]

$$\frac{1}{\pi}\text{v.p.}\int_{-\infty}^{\infty}\frac{v_\tau(\tau,\xi')d\xi'}{\xi'-\xi} = \sin v(\tau,\xi) \tag{8}$$

which also is completely integrable. For some of these solutions the spectral stability problem can be solved, completely and explicitly [6].

In this communication, we report on a new family of objects described by Eq.(1) which are analogues of the breather solutions (4) of the sine-Gordon equation (i.e. periodic in time and localized in space). However, since our structures were obtained numerically, their periodicity and localization cannot be claimed rigorously in the mathematical sense. Anyway, we suppose that in physical applications these objects can be treated as periodic in time and localized in space. It is important that these entities are quite robust and can be developed as a result of evolution of initial states of rather different shape.

2. The construction of the breathers

In order to construct the breather solutions we used the approach called sometimes *the rotating wave approximation* [7]. It can be sketched as follows. Let us suppose that the breather solution can be described well by one temporal harmonics only i.e.

$$u(t,x) \sim u_0(x)\cos\omega t \tag{9}$$

where ω (the parameter) is the temporal frequency of the solution. Substituting (9) into the equation (1) and collecting the terms corresponding to $\cos\omega t$ we obtain the following equation for the amplitude $u_0(x)$

$$H\frac{du_0}{dx} + \omega^2 u_0 - 2\mathrm{J}_1(u_0) = 0 \tag{10}$$

where $\mathrm{J}_1(\xi)$ is the Bessel function. Eq.(10) can be solved numerically. The next step of the analysis consists in numerical simulations of Eq.(1) starting with initial profile given by $u_0(x)$. If necessary, the approximation (9) can be improved by adding more terms, corresponding to $\cos 3t$, $\cos 5t$ etc.

Eq.(10) was solved using a numerical procedure based on inverse power method algorithm [8]. Fig.1 represents some solutions of Eq.(10). All of these solutions are even, positive, and have power-decay asymptotics as $x \to \infty$ [9]:

$$u_0(x) \sim C/x^2, \quad x \to \pm\infty \tag{11}$$

This contrasts with the situation which takes place in the local case where the typical decay of breather profile is exponential but not algebraic. It worth noting that as ω tends to unity, the amplitude of $u_0(x)$ tends to zero.

The second part of the investigation implies numerical simulations for Eq.(1). Here the results can be summarized as follows:

(i) The solutions of Eq.(10) provide *good approximations* of the initial profiles for periodic breather-like pulsations, if ω is reasonably close to

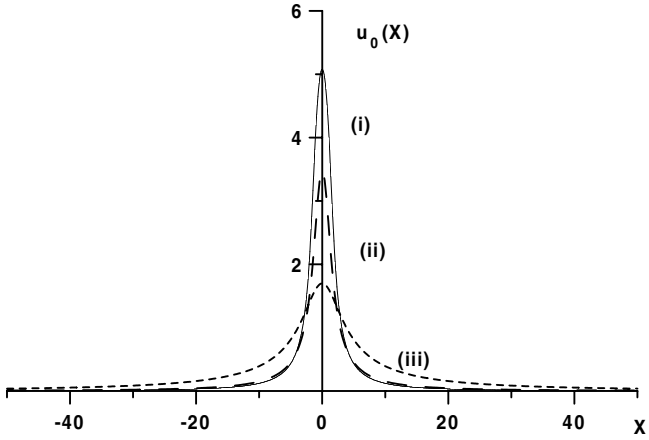

Figure 1. The solutions of Eq.(10) for (i) $\omega = 0.6$; (ii) $\omega = 0.8$; (iii) $\omega = 0.95$.

1. An example is shown in Fig.2. In this figure the evolution of the initial data $u(0,x) = u_0(x)$, $u_t(0,x) = 0$, where $u_0(x)$ is the solution of Eq.(10) for $\omega = 0.8$, is depicted.

(ii) These breather-like objects are quite *robust*. We suppose that these objects are stable (at least within some range of ω), although we did not study linear stability problem with time-dependent potential for these solutions. Moreover, these breather-like objects even can emerge from the initial data which have no relation with the structure appeared (for example, sech-shaped or similar ones). Fig.3 represents evolution of the initial data $u(0,x) = 3/\cosh 0.2x$, $u_t(0,x) = 0$. The object which appears in the simulation and is shown in this figure is close to the breather from the family described above with the frequency $\omega \approx 0.65$.

(iii) There exists *a minimum value of energy* for the breather to be generated. It corresponds to the limit $\omega \to 1$ when the amplitude of the breather tends to zero. Asymptotic analysis of Eq.(10) for $\omega \to 1$ shows that this value of energy is

$$\mathcal{H}_0 = 4\int_{-\infty}^{\infty} U^2(\eta)d\eta \approx 9.876 \tag{12}$$

where $U(\eta)$ is the localized solution of the equation

$$HU_\eta - U + U^3 = 0 \tag{13}$$

(see e.g.[10]). This statement was confirmed by numerical simulations: no breather has emerged if the initial energy of the sech-shape pulse was below this value.

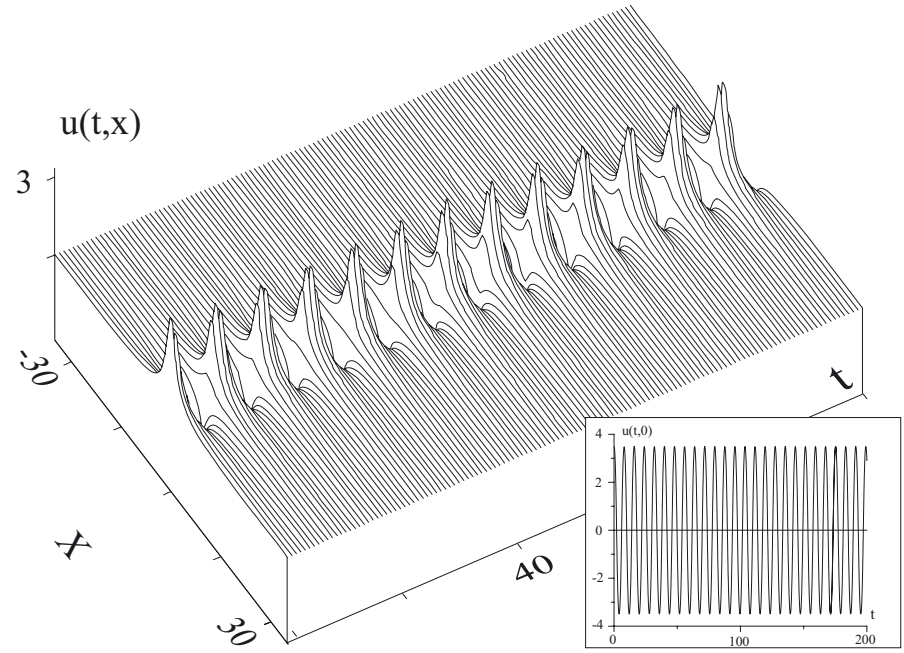

Figure 2. Evolution of the initial profile $u_0(x)$, the solution of Eq.(10), $\omega = 0.8$.

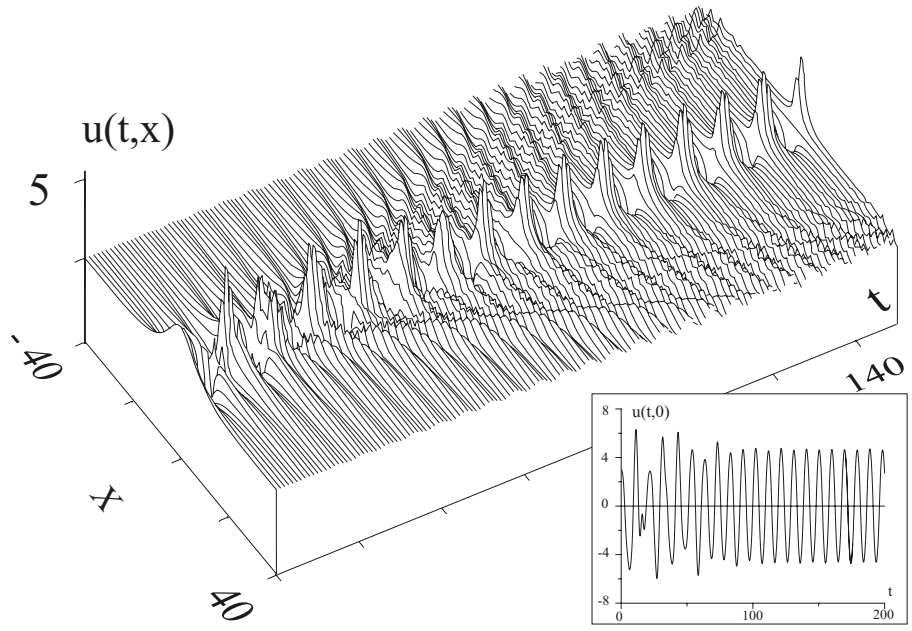

Figure 3. Evolution of initial data $u(0,x) = 3/\cosh 0.2x$, $u_t(0,x) = 0$.

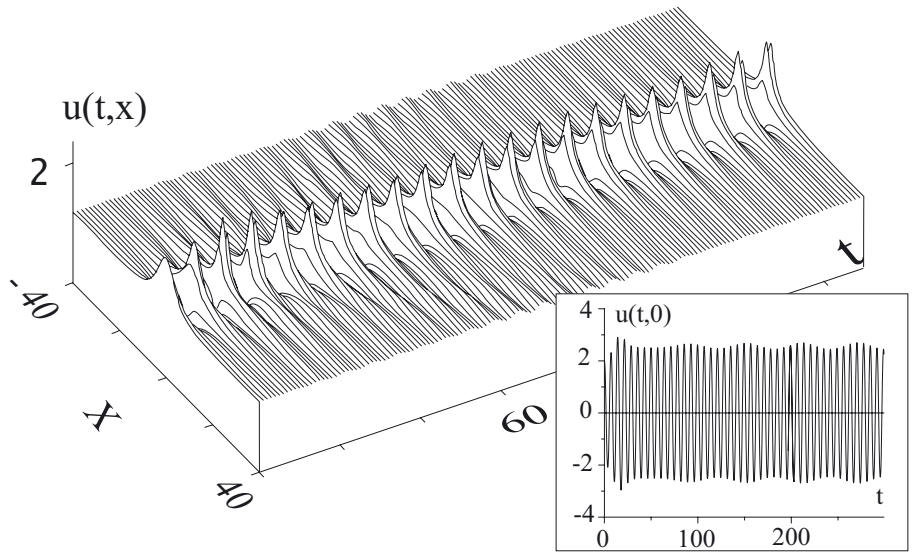

Figure 4. Evolution of initial data $u(0,x) = 2/\cosh 0.3x$, $u_t(0,x) = 0$.

(iv) Apart from the periodic breather-like structures, Eq.(1) covers *quasiperiodic* localized structures. They can be described as "fast" periodic breather-like pulsations with slowly modulated envelope. The period of the envelope modulation is considerably greater than the period of the "fast" oscillations. One of these structures is shown in Fig.4. The initial data in this case are $u(0,x) = 2/\cosh 0.3x$, $u_t(0,x) = 0$. The solutions with such a behavior can be regarded as analogues of exact sine-Gordon quasiperiodic breathers.

3. Kink-antikink interactions

The presence of a number of exact solutions of Eq.(1) and the connections of Eq.(1) with integrable sine-Gordon and sine-Hilbert equations bring up the question about the integrability of Eq.(1). It is known that one of indirect indications to integrability of an equation is elastic character of interaction between entities which it describes. To clarify this issue for Eq.(1) we performed numerical simulations of interaction between the travelling 4π-kink and antikink (7) (see Fig.5) and between the 4π-kink (7) and two steady-state 2π-antikinks (6) (see Fig.6). It follows from these figures that the objects involved are destroyed in the course of interactions and, correspondingly, Eq.(1) hardly can be integrable.

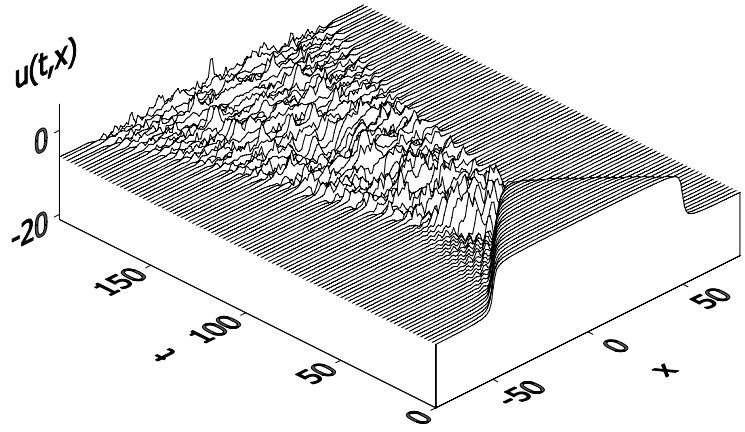

Figure 5. The interaction between the 4π-kink and the 4π-antikink.

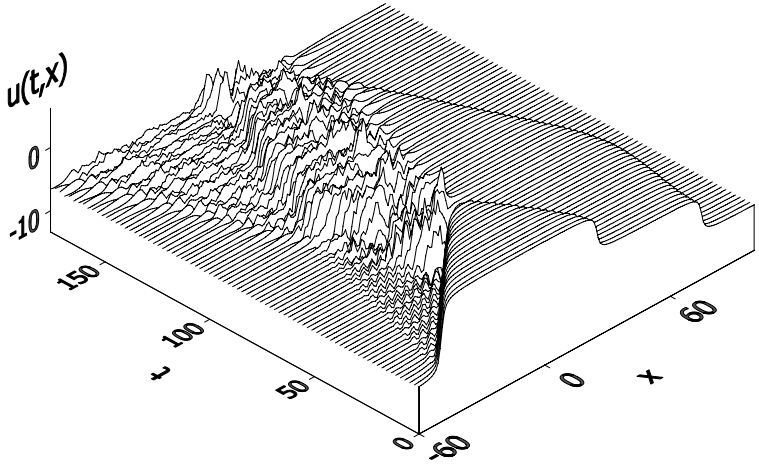

Figure 6. The interaction between the 4π-kink and two steady-state 2π-antikinks.

Acknowledgments

G.A. acknowledges the financial support from Spanish Ministry of Education, Culture and Sport through a sabbatical program SAB2000-0340. T.P. thanks the predoctoral fellowship of the European Network COSYC of SENS (HPRN-CT-2000-00158). L.V. thanks the partial support of the Ministerio de Ciencia y Technologia of Spain under grant BFM 2002-02359.

References

[1] A. Gurevich. Phys. Rev. B, **46**, 3187 (1992);

[2] R.G. Mints and I.B. Snapiro. Phys. Rev. B, **49** 6188 (1994).

[3] Yu.M. Aliev and V.P. Silin. Phys. Lett. A, **177** 259 (1993).

[4] G.L. Alfimov and V.P. Silin. J. Exp. Theor. Phys. **79** 369 (1994).

[5] M.J. Ablowitz and P.A. Clarkson. Solitons, nonlinear evolution equations and inverse scattering. C.U.P., 1991.

[6] G.L. Alfimov and V.P. Silin. J. Exp. Theor. Phys., **81** p.915 (1995).

[7] S. Flach and C.R. Willis, Phys. Rep., **295**, 181 (1998).

[8] A. Eydeland and J. Spruck *Nonlinear Diffusion Equations and Their Equilibrium States, ed. W.-M.Ni et al*, Math.Sci.Res.Inst.Publ., **13**, 273, (1988).

[9] J.L. Bona, Yi.A. Li., J. Math. Pures Appl., **76**, 377, (1997).

[10] G.L. Alfimov, D. Usero, L. Vázquez, J.Phys.A: Math.Gen., **33**, 6707, (2000).

A FRUITFUL INTERPLAY: FROM NONLOCALITY TO FRACTIONAL CALCULUS

L.Vázquez
Departamento de Matemática Aplicada, Facultad de Informatica,
Universidad Complutense, E-28040, Madrid, Spain;
Centro de Astrobiologia (CSIC -INTA), E-28850, Torrejón de Ardoz, Madrid, Spain
lvazquez@fdi.ucm.es

Abstract The Fractional Calculus represents a natural instrument to model nonlocal phenomena either in space or time. From Physics and Chemistry to Biology, there are many processes that involve different space/time scales. In many problems of the above context the dynamics of the system can be formulated by fractional differential equations which include the nonlocal effects. We give a panoramic view of the problem and show some examples.

Keywords: Nonlocality, Fractional derivative, Diffunors, Diffusion process, Generalized Dirac equation

1. Nonlocal Equations

In the context of the field theory, we have the *local theories* associated to the local couplings where the interaction terms are built up from field quantities referring to the same space-time point. On the other hand, we have the *nonlocal theories* defined by nonlocal couplings where the interaction takes place over a "region" of the space-time characterized by a prescribed function [1].

Up to 1994 a very extensive review about the nonlinear nonlocal wave equations with applications to hydrodynamics, magnetohydrodynamics and plasma can be found in the book of Naumkin and Shishmarev [2].

As an illustration of the nonlocal effects, in [3]-[4] a nonlocal generalization of the standard sine-Gordon equation was studied

$$u_{tt} - u_{xx} = 2\cos\frac{u(x,t)}{2}\int dy f(x-y)\sin\frac{u(y,t)}{2} \qquad (1)$$

F. Kh. Abdullaev and V. V. Konotop (eds.), Nonlinear Waves: Classical and Quantum Aspects, 129–133.

This equation can be associated with DNA models as well as the Frenkel-Kontorova model including long–range interaction. When the kernel defined by $f(x-y)$ is the Dirac Delta we have the classical sine-Gordon equation; thus it is difficult to analyze the nonlocal model using a perturbative approach from the local case. The model (1) has static solutions with zero topological charge that do not exist in the local limit. They could be interpreted as frozen breathers originated by the space averaging of the nonlocality. Other nonlocal wave equations had been studied in [5]-[7].

2. Fractional Calculus

There are different definitions of the fractional derivatives but all of them coincide in the integer case (see e.g. [8]-[10] and [15]). The fractional derivative of a function is not determined by the behavior of the function at a single point, but depends on the values of the function over a entire interval. As an example, we have the following definitions of time and space fractional derivatives:

- *Thetime fractional derivative* of order $\alpha > 0$ for a sufficiently well-behaved *causal* function $u(t)$ is defined as follows

$$\frac{d^\alpha}{dt^\alpha}u(t) = \frac{1}{\Gamma(m-\alpha)}\int_0^t (t-\tau)^{1-\alpha-m}\, u^{(m)}(\tau)d\tau \qquad (2)$$

  where $m = 1, 2, ...,$ and $0 \leq m-1 < \alpha \leq m$. This definition requires the absolute integrability of the derivative of order m.

- *The symmetric space fractional derivative* [10] of order $\alpha > 0$ of a sufficiently well-behaved function $u(x), x \in \mathbb{R}$, is defined as the pseudo-differential operator characterized in its Fourier representation by

$$\frac{d^\alpha}{d \mid x \mid^\alpha}u(x) \longrightarrow - \mid \kappa \mid^\alpha \hat{u}(\kappa) \qquad (3)$$

  being $\kappa \in \mathbb{R}$.

3. Framework of Applications

The Fractional Calculus offers a unifying framework for different contexts according to the following basic remarks:

- The freedom in the definition of fractional derivatives allow us to incorporate different types of information.

- The fractional derivatives show algebraic scale properties with non-integer exponents what is relevant in the data analysis.

- A new formulation for the damped systems is possible by using the fractional derivatives [11]-[12].
- The fractional derivatives allow a natural interpolation among differential equations of very different properties as the classical wave and heat equations:

$$\frac{\partial^\alpha}{\partial t^\alpha}\Psi - \frac{\partial^2}{\partial x^2}\Psi = 0 \tag{4}$$

  where $1 \leq \alpha \leq 2$.
- The fractional derivative of a function is given by a definite integral, thus it depends on the values of the function over the entire interval. In this context, the fractional derivatives are suitable for the modelling of systems with long range interactions in space and/or time (memory) and processes with many scales of space ans/or time involved.

The applications range in a wide spectrum of areas [13]-[16]: material sciences(viscoelasticity, polymers,..), circuits, diffusion processes, Biology, Economy, Geology, Astrobiology, traffic problems, data analysis,...etc

4. Internal Degrees of Freedom

It is well known the approach of Dirac to obtain his famous equation from the Klein-Gordon equation [1]. The free Dirac equation can be considered as the square root of the Klein-Gordon equation. In a more general context Morinaga and Nono [17] analyzed the integer s-root of the partial differential equations of the form

$$\sum_{|I|=s} a_I \frac{\partial^{|I|}}{\partial x^I}\phi = \phi \tag{5}$$

The $s-$root is the first order system

$$\sum_{i=1}^{n} \alpha_i \frac{\partial \Phi}{\partial x_i} = \Phi \tag{6}$$

where $\alpha_1, ...\alpha_n$ are matrices. From the physical point of view the α_k describe internal degrees of freedom of the associated system.

In the above context, a natural generalization is to consider the fractional diffusion equations with internal degrees of freedom [18]-[19]. They can be obtained as the s-roots of the standard scalar linear diffusion

equation. Thus, we have a possible definition of the square root of the standard diffusion equation (SDE) in one space dimension, $u_t - u_{xx} = 0$, as follows:

$$\left(A\frac{\partial^{1/2}}{\partial t^{1/2}} + B\frac{\partial}{\partial x} \right) \psi(x,t) = 0 \tag{7}$$

where A and B are matrices satisfying the conditions:

$$A^2 = I \quad , \quad B^2 = -I \tag{8}$$

$$\{A, B\} \equiv AB + BA = 0. \tag{9}$$

Here $\psi(x,t)$ is a multicomponent function with at least two scalar space-time components. Also, every scalar component satisfies the SDE. Such solutions can be interpreted as *probability distributions with internal structure associated to internal degrees of freedom of the system.* We could name them **diffunors** in analogy with the spinors in Quantum Mechanics.

We have two possible realizations of the above algebra in terms of real matrices 2×2 associated to the Pauli matrices:

$$A = \begin{pmatrix} 1 & 0 \\ 0 & -1 \end{pmatrix} \quad , \quad B = \begin{pmatrix} 0 & 1 \\ -1 & 0 \end{pmatrix} \tag{10}$$

and

$$A = \begin{pmatrix} 0 & 1 \\ 1 & 0 \end{pmatrix} \quad , \quad B = \begin{pmatrix} 0 & 1 \\ -1 & 0 \end{pmatrix} \tag{11}$$

Other realizations involving complex bi-dimensional matrices are possible, but taking into account the meaning of the reference diffusion equation we only consider the real representations.

The solutions of (7) are related to the SDE in a simple way. As an illustration, let us consider the representation (10), i.e.

$$\psi(x,t) = \begin{pmatrix} \varphi(x,t) \\ \chi(x,t) \end{pmatrix}$$

such that $\chi(x,t) = \pm\varphi(x,t)$. We have two general independent solutions of (7):

$$\varphi(x,t) \begin{pmatrix} 1 \\ 1 \end{pmatrix} \quad \text{and} \quad \varphi(x,t) \begin{pmatrix} 1 \\ -1 \end{pmatrix} \tag{12}$$

where $\varphi(x,t)$ is a solution of SDE. The solutions (12) represent two possible probability distributions depending not only on the space and

time coordinates, but also on the internal degrees of freedom. This effect could model the diffusion of particles with internal structure.

The equation (7) is not time reversible but it is invariant under space reflection as the underlying SDE. More precisely, in the representation given by (10) a possible representation of the **parity operator** is $P = AP^0$, such that $P^0 : x \longrightarrow -x$.

Acknowledgments

This work has been partially supported by the Ministerio de Ciencia y Tecnología of Spain under grant BFM2002-02359.

References

[1] S.S. Schweber, *An Introduction to Relativistic Quantum Field Theory*. Ed. Harper and Row (1964).

[2] P. I. Naumkin and I.A. Shishmarev, *Nonlinear Nonlocal Equations in the Theory of Waves*. A.M.S. Vol. **133** (1994).

[3] L. Vázquez, W.A.B. Evans and G. Rickayzen, Phys. Lett. A **189**, 454-459 (1994)

[4] M.D. Cunha, V.V. Konotop and L. Vázquez, Phys. Lett. A **221**, 317 (1996).

[5] G.L. Alfimov and V.P. Silin, J. Exp. Theor. Phys. **79**, 369 (1994).

[6] G.L. Alfimov and V.P. Silin, J. Exp. Theor. Phys. **81**, 915 (1995).

[7] G.L. Alfimov, D. Usero and L. Vázquez, J. Phys. A: Math. Gen. **33**, 6707 (2000).

[8] B. Ross (Ed.) *Fractional Calculus and its Applications*. Lecture Notes in Mathematics **457**. Springer-Verlag (1975).

[9] S.G. Samko, A.A. Kilbas and O.I. Marichev, *Fractional Integrals and Derivatives: Theory and Applications*, Gordon and Breach (1993).

[10] F. Mainardi, *Fractals and Fractional Calculus in Continuum Mechanics*. Eds. A. Carpinteri and F. Mainardi, CISM Courses and Lectures **378**, Springer-Verlag, 291-348 (1997).

[11] G. Turchetti, D. Usero and L. Vázquez, Tamsui Oxford J. Math. Sciences **18**, 31 (2002).

[12] D. Usero and L. Vázquez, *Localization and Energy Transfer in Nonlinear Systems*. Eds. L. Vázquez, R.S. MacKay and M.P. Zorzano, World Scientific, 296-303 (2003).

[13] R.T. Baillie and M.L. King (Eds.), *Fractional Differencing and Long Memory Processes*. J. Econometrics **73**, 1 (1996)

[14] D. Helbing, H.J. Herrmann, M. Schreckenberg and D.E. Wolf (Eds.), *Traffic and Granular Flow 99*, Springer Verlag (2000).

[15] R. Hilfer, *Applications of Fractional Calculus in Physics*, World Scientific (2000).

[16] G. Horneck, Christa Baumtark-Khan (Eds.), *Astrobiology: The Quest for the Conditions of Life*, Springer Verlag (2002).

[17] K. Morinaga and T. Nono, J. Sci. Hiroshima Univ.(A) **16**, 13-41 (1952).

[18] L. Vázquez, J. Comp. Math. **21**, 491 (2003)

[19] L. Vázquez and R. Vilela-Mendes, Applied Math. and Comp. **141**, 125 (2003)

ON 3 + 1 DIMENSIONAL FRIEDMAN-ROBERTSON-WALKER UNIVERSES WITH MATTER

T. Christodoulakis
Nuclear and Particle Physics Section, Physics Department, University of Athens
Panepistimiopolis, Ilisia, Athens 15771, Greece
tchris@cc.uoa.gr

C. Helias
Nuclear and Particle Physics Section, Physics Department, University of Athens
Panepistimiopolis, Ilisia, Athens 15771, Greece

P.G. Kevrekidis
Department of Mathematics and Statistics, University of Massachusetts,
Amherst MA 01003-4515, USA
kevrekid@math.umass.edu

I.G. Kevrekidis
Department of Chemical Engineering, Princeton University, Princeton, NJ 08544
yannis@princeton.edu

G. Papadopoulos
Nuclear and Particle Physics Section, Physics Department, University of Athens
Panepistimiopolis, Ilisia, Athens 15771, Greece
gpapado@cc.uoa.gr

Abstract We examine the dynamical behavior of matter coupled to gravity in the context of a linear Klein-Gordon equation coupled to a Friedman-Robertson-Walker metric. The resulting ordinary differential equations can be decoupled, the effect of gravity being traced in rendering the equation for the scalar field nonlinear. We obtain regular (in the mass-

F. Kh. Abdullaev and V. V. Konotop (eds.), Nonlinear Waves: Classical and Quantum Aspects, 135–143.

less case) and asymptotic (in the massive case) solutions for the resulting matter field and discuss their ensuing finite time blowup in the light of earlier findings. Finally, some potentially interesting connections of these blowups with features of focusing in the theory of nonlinear partial differential equations are outlined, suggesting the potential relevance of a nonlinear theory of quantum cosmology.

Keywords: Focusing, FRW metric, nonlinear ODEs

In the past two decades there has been an extensive interest in 3-dimensional gravity, particular after the demonstration of the fact that its quantum version is solvable [1] and that it contains black hole solutions [2].

The idea of examining cosmological models in this context was, however, of interest before [3, 4, 5], as well as after [6, 7] these findings. In most of these studies [3, 4, 5, 7, 8], the Friedman-Robertson-Walker (FRW) metric was used and the resulting equations were ordinary differential equation governing the time-evolution of the scale factor of the relevant metric and the evolution of the matter and/or radiation field coupled to it.

On a slightly different track, one can list the works of [6, 9, 10] (see also references therein and the review of [11]), where the metric scale factors were allowed to be temporally *as well as* spatially variable, and the resulting partial-differential equations (PDEs) were studied to obtain collapse type solutions.

In this brief report, we will restrict ourselves to the former type of considerations but in a 3+1 dimensional setting. We believe that the study of such simple models of ordinary differential equations of geometry coupled with matter is a starting point that may be used to shed light to more complicated cosmological models. From such simple playgrounds, explicit solutions can be obtained and analyzed; these can then be tested in more complex settings. In this view, our work can be considered as being in the same track as those of e.g., [4, 7, 8]. Moreover, we consider the present work to be a first towards building a bridge between conventional cosmology and nonlinear dynamical systems.

We start by fixing the spatial dependence of the metric tensor to be of the FRW type (in co-moving coordinates and with a "cosmological" time choice)

$$ds^2 = -dt^2 + a^2(t)\left(\frac{1}{1-kr^2}dr^2 + r^2 d\theta^2 + r^2 \sin^2\theta d\phi^2\right) \qquad (1)$$

and coupling gravity to the simplest possible model for matter, namely a linear Klein-Gordon (KG) type equation for a massive scalar. In the metric of Eq. (1), a is the scale factor while k describes the curvature of

the spatial slice and can be normalized to the values $-1, 0, 1$ in the hyperbolic, flat and elliptic case respectively. Previously such models were examined in a more complicated setting (most often in 2+1 dimensions) where either equations of state [7] or special scalar field potentials [4] were used to obtain closed form solutions.

Here, we will examine the simplest possible (physically relevant) scalar field potential $V(\phi) = m^2\phi^2/2$, which gives rise to a linear (in ϕ) equation for the scalar coupled to gravity. In particular the Einstein-Klein-Gordon field equations in this case read:

$$-3\frac{k+\dot{a}^2}{a^2} + \rho_\phi = 0 \tag{2}$$

$$\frac{k+\dot{a}^2+2a\ddot{a}}{a^2} + p_\phi = 0 \tag{3}$$

$$\ddot{\phi} + m^2\phi + \frac{3\dot{a}}{a}\dot{\phi} = 0 \tag{4}$$

where the energy density and the pressure associated with the scalar field are given respectively by (see e.g., [7])

$$\rho_\phi = \frac{1}{2}(\dot{\phi}^2 + m^2\phi^2) \equiv \frac{1}{2}\dot{\phi}^2 + V(\phi), \tag{5}$$

$$p_\phi = \frac{1}{2}(\dot{\phi}^2 - m^2\phi^2) \equiv \frac{1}{2}\dot{\phi}^2 - V(\phi). \tag{6}$$

Note that the first is the quadratic constraint $G^0_0 = T^0_0$; the second is the only independent spatial equation $G^1_1 = T^1_1$ while the last is the dynamical equation for the scalar field, i.e., the Klein-Gordon equation. G and T denote the Einstein curvature tensor and the energy-momentum tensor respectively.

In the above equations the dot denotes temporal derivative. Naturally, Eqs. (2)-(4) are not linearly independent as the linear combination of the derivative of the first and of the second can be used to obtain the third.

We first examine the spatially flat case of $k = 0$, and use it as a guide. In this setting one immediately observes that from Eqs. (2) and (4), two separate expressions for $\dot{a}/a$ can be obtained, hence equating them, a second-order ordinary differential equation (ODE) emerges for the scalar field ϕ in the form:

$$\frac{3}{2}\dot{\phi}^2\left(m^2\phi^2 + \dot{\phi}^2\right) = \left(m^2\phi + \ddot{\phi}\right)^2. \tag{7}$$

Notice that this is the only case (among the ones that we will examine) in which the resulting ODE is of 2nd order. In the remaining cases,

the ODE is of 3rd order. Moreover, it is worth commenting on the nature of this ODE: in particular, the resulting equation is *nonlinear*. Hence, even though the inclusion of matter is realized through a linear dynamical equation, in the setting of even the simplest cosmological models, the coupling of matter to gravity induces the emergence of a nonlinear equation; it is as if the "trace" of gravity, when the equation for the scalar field is decoupled from it, remains in the nonlinear self-interaction of the resulting ODE for the matter field.

As the simplest possible case among the ones with $k = 0$, we examine the massless case, i.e., $m = 0$. In the latter setting, we obtain the solutions (up to a constant shift) of the form:

$$\phi = \pm\sqrt{\frac{2}{3}}\log(t^\star - t) \tag{8}$$

which in turn results in a power law dependence of the scale factor of the form $a \sim (t^\star - t)^{1/3}$. Hence, a blowup (focusing) type effect occurs at $t = t^\star$ in a logarithmic fashion for the scalar and the corresponding scale factor shrinks to 0 with a power law dependence. Such dependencies are reminiscent of the critical blowup in prototypical nonlinear PDEs with focusing solutions (for a spatio-temporally dependent field ψ) such as the nonlinear Schrödinger equation [12, 13, 14]

$$i\psi_t = -\Delta\psi - |\psi|^{2\sigma}\psi. \tag{9}$$

Δ stands for the Laplacian and σ the power of the nonlinearity. For $d\sigma < 2$, no focusing solutions occur (d is the dimensionality of the Laplacian); when $d\sigma = 2$, logarithmically slow focusing phenomena take place (in the corresponding "proper time" see [12, 13, 14]), while when $d\sigma > 2$, the so-called strong collapse occurs, where the focusing happens with a power law dependence [13, 14]. Hence, the *critical* case of the nonlinear focusing phenomena in equation (9) shares some of the collapse characteristics of the present model.

We now turn to the massive case (still for $k = 0$). In the latter, we can no longer solve the problem analytically. However, we can directly observe that if we adopt a solution of logarithmic dependence of the form of Eq. (8) in this case as well, the massive terms diverge much more slowly (at worst as $(\log(t^\star - t))^2/(t^\star - t)^2$, as opposed to the $(t^\star - t)^{-4}$ divergence of the dominant (massless) terms). This signifies that asymptotic self-similarity will ensue from this case and the logarithmic dependence will eventually set in and dominate the asymptotic behavior leading to collapse. An example of this is shown in Fig. 1, where a numerical simulation of Eq. (7) clearly indicates the logarithmic focusing of the scalar field for as $t \to 1.38$. This asymptotic type of self-similarity

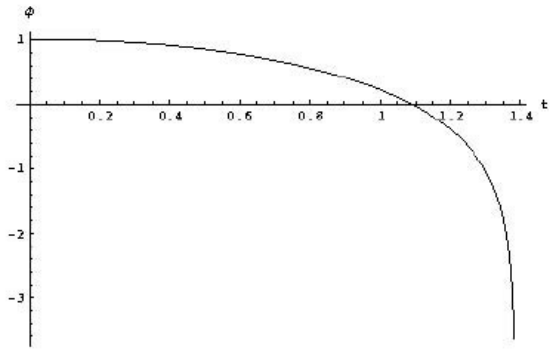

Figure 1. Logarithmic blowup of the scalar field as a function of time in the massive case (for $m = 1$), starting with $\phi(0) = 1$, $\dot{\phi}(0) = 0$. The blowup occurs for $t \approx 1.38$.

occurs quite often in cosmology, as can be seen for example in [15] (and references therein). Another comment worth making about this case is that it appears as if the massive case is asymptoting to the results for the massless one. It should be noted that this solution indicates, as it ought to, a true curvature singularity of the system from a physical point of view. Indeed, since the scale factor $a(t)$ vanishes as t approaches $t^\star$, the curvature scalar $R^{\lambda\mu\nu\kappa}R_{\lambda\mu\nu\kappa}$ blows up. It should also be noted that as the collapse is approached, the matter density also tends to ∞ leading to a matter-dominated universe.

We now turn to the case with $k \neq 0$. In this case also, the reduction that leads to an equation only for the scalar field can be performed. However, due to the more complex nature of the equations, this reduction no longer leads to a second order ODE but rather to a third order one. In particular, in this case the reduction (after differentiating (4) and substituting the result, as well as (2) and (4), in (3)) results in

$$6\dddot{\phi}\dot{\phi} - 8\ddot{\phi}^2 - 10m^2\phi\ddot{\phi} - 6\dot{\phi}^4 + 6m^2\dot{\phi}^2 + 3m^2\phi^2\dot{\phi}^2 - 2m^4\phi^2 = 0 \quad (10)$$

It is interesting to note then that the massless case once again shares the exact same, finite time blowup solutions of Eq. (8). One can then once again use the same argument for the massive case to identify such solutions as the dominant asymptotic behavior for $m \neq 0$, since these terms blowup as $(t^\star - t)^{-4}$ in Eq. (10), while the rest of the terms diverge with a rate of (at most) $O(t^\star - t)^{-2}$. Numerical integration of Eq. (10) for various initial conditions and various masses confirms the theoretical prediction of finite time collapse. It appears however that the mass of the scalar affects the time at which collapse will occur ($t^\star$) (see e.g., Fig. 2).

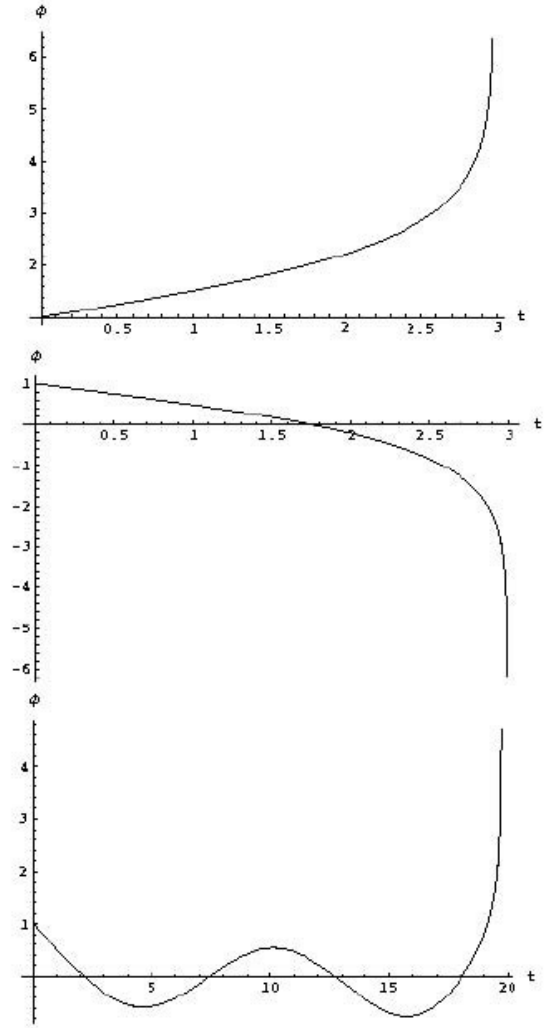

Figure 2. Logarithmic blowup of the scalar field as a function of time in the massive case (for $m = 0.1$), starting with $\phi(0) = 1$, $\dot{\phi}(0) = 0.5$, $\ddot{\phi}(0) = 0$ (top panel) and $\phi(0) = 1$, $\dot{\phi}(0) = -0.5$, $\ddot{\phi}(0) = 0$ (middle panel). The blowup occurs for $t \approx 3$ in these cases. A case with a larger mass ($m = 0.6$) is shown in the bottom panel. In this case, the blowup occurs at later times (in this case for $t \approx 20$).

It is also worth noting that in the context of Eq. (10), the steady state $\phi = 0$ appears to be linearly stable since for small perturbations $\sim \epsilon \exp(\omega t)$, collecting the leading order behavior ($\mathrm{O}(\epsilon^2)$), one obtains the algebraic stability equation of the form:

$$(\omega^2 + m^2)^2 = 0. \tag{11}$$

Eq. (11) has double imaginary roots:

$$\omega = \pm im \tag{12}$$

which, in turn, denote marginal stability. Notice that the same situation occurs in the critical case of Eq. (9). However, the nonlinear term of the form $-6\dot{\phi}^4$ asymptotically dominates and gives rise to a nonlinearity-induced instability leading to logarithmic blowup. This (blowup), in fact, is to be expected since the incompleteness of geodesics in 3+1-dimensional spacetimes [16], established using general techniques of differential topology in [17, 18], has been shown under quite general conditions [19] to lead to divergence of physically observable properties.

In conclusion, in this work, we have examined the coupling of $3+1$-dimensional gravity to a scalar field satisfying a linear Klein-Gordon equation. We have found that it is possible to *decouple* the equation for the massive scalar from the one for the scale factor of the FRW metric used in this work at the "expense" of obtaining a nonlinear ordinary differential equation for the scalar. The "memory" of the coupling to gravity has been encapsulated in the nonlinear nature of the resulting equation. Closed form solutions of the resulting equation can be obtained in the massless case and exhibit logarithmic divergence of the scalar field as a function of time (and power-law vanishing of the scale factor). It is then observed that these solutions persist as dominant asymptotic behavior in the case where $m \neq 0$. These results are corroborated by numerical integration of the nonlinear ODEs in the massive case. Even though slightly different methods have been used for the cases where the space is flat ($k = 0$) and when $k \neq 0$, the same principal conclusions have been drawn in all cases.

This phenomenon of decoupling persists even in the case of more general, anisotropic Bianchi models [20]. In all these cases, special solutions to the ensuing decoupled non-linear ODE exist and they also exhibit blowup behavior.

Finally, we return to the analogy of the logarithmic focusing of the solutions in this simple model (where spatial dependence was a priori fixed in the metric) with the logarithmic blowup in the critical case of a prototypical nonlinear partial differential equation, namely the nonlinear Schrödinger equation, that sustains focusing solutions. It would

be particularly interesting to examine whether the inclusion of spatial dependence can lead to an equation of this type (through appropriate envelope wave expansions, given that NLS is the envelope equation for nonlinear wave equations of the Klein-Gordon type). In particular, if, in the presence of the spatial dependence, the reduction to a *nonlinear partial differential equation* for the scalar field provides a nonlinear KG equation, then it will be natural to expect that the reduction to NLS and the ensuing focusing solutions will carry through. If such a program succeeds, it may appear natural to consider the NLS as prototypical model for a "nonlinear quantum cosmology".

G.O. Papadopoulos is currently a scholar of the Greek State Scholarships Foundation (I.K.Y.) and acknowledges the relevant financial support. T Christodoulakis and G.O. Papadopoulos, acknowledge support by the University of Athens, Special Account for the Research Grant-No. 70/4/5000 This work was also partially supported by a University of Massachusetts Faculty Research Grant and NSF-DMS-0204585 (PGK), as well as the AFOSR (Dynamics and Control, IGK).

References

[1] E. Witten, Nucl. Phys. B **311**, 46 (1988).

[2] M. Bañados, C. Teitelboim and J. Zanelli, Phys. Rev. Lett. **69**, 1849 (1992); M. Bañados, M. Henneaux, C. Teitelboim and J. Zanelli, Phys. Rev. D **48**, 1506 (1993).

[3] S. Giddings, J. Abbott and K. Kuchar, Gen. Rel. Grav. **16**, 751 (1984).

[4] J.D. Barrow, A.B. Burd and D. Lancaster, Class. Quantum. Grav. **3**, 551 (1986).

[5] N.J. Cornish and N.E. Frankel, Phys. Rev. D **43**, 2555 (1991).

[6] M.W. Choptuik, gr-qc/9803075.

[7] N. Cruz and C. Martínez, Class. Quantum Grav. **17**, 2867 (2000).

[8] F. Williams and P.G. Kevrekidis, Class. Quantum Grav. **20**, L177 (2003).

[9] T. Koike, T. Hara and S. Adachi, Phys. Rev. Lett. **74**, 5170 (1995).

[10] A.M. Abrahams and C.R. Evans, Phys. Rev. Lett. **70**, 2980 (1993).

[11] C. Gundlach, gr-qc/9712084.

[12] M.J. Landman, G.C. Papanicolaou, C. Sulem and P.L. Sulem, Phys. Rev. A **38**, 3837 (1988).

[13] C. Sulem and P.-L. Sulem, *The Nonlinear Schrödinger equation*, Springer-Verlag (New York, 1999).

[14] C.I. Siettos, I.G. Kevrekidis and P.G. Kevrekidis, Nonlinearity **16**, 497 (2003).

[15] B.J. Carr and A.A. Coley, Class. Quantum Grav. **16**, R31 (1999).

[16] S.W. Hawking and R. Penrose, Proc. R. Soc. A **314**, 529 (1969).

[17] S.W. Hawking and G.F.R. Ellis, *The Large Scale Structure of Space-Time*, Cambridge University Press (Cambridge, 1973).

[18] F.J. Tipler, G.F.R. Ellis and C. Clarke, *General Relativity and Gravitation*, ed. A Held, pp 97-206, Plenum (New York, 1978).

[19] C. Clarke, Commun. Math. Phys. **41**, 65 (1975); C. Clarke and J. Isenberg, Proc. 9th Int. Conf. on General Relativity and Gravitation ed. E Schmutzer, Cambridge University Press (Cambridge, 1982).

[20] T. Christodoulakis *et al.* (in preparation).

STOCHASTIC EFFECTS ON THE ECKHAUS EQUATION

Silvana De Lillo and Giampaolo Sanchini
Dipartimento di Matematica e Informatica, Università di Perugia - Via Vanvitelli, 1 - 06123 Perugia, and Istituto Nazionale di Fisica Nucleare, Sezione di Perugia - Via Pascoli,1 - 06123 Perugia
silvana.delillo@pg.infn.it
giampaolo.sanchini@pg.infn.it

Abstract The random-force driven Eckhaus equation is studied in the case of a long range correlated noise. The ensemble average of the Kink solution is obtained, and some relevant correlation functions are obtained.

Keywords: Eckhaus, Soliton, Kink.

1. Introduction

We study the statistical properties of the random-force-driven Eckhaus PDE [1]

$$i\psi_t + \psi_{xx} + 2(|\psi|^2)_x\psi + |\psi|^4\psi = if(t)\psi_x, \qquad \psi = \psi(x,t) \tag{1}$$

where $f(t)$ is a gaussian random noise. The right hand side of (1) is a multiplicative external forcing term of the drift type. Due to the random term, the system (1) experiences fluctuations; it is of interest to study the statistical average $\langle\psi(x,t)\rangle$ and its long time behaviour. The brackets $\langle .,. \rangle$ denotes the average taken over all the possible realizations of the random process $f(t)$. The gaussian function $f(t)$ is characterized by the average $\langle f(t)\rangle = 0$ and by the two time correlation function

$$\big\langle f(t), f(t')\big\rangle = \mu(t-t'). \tag{2}$$

It will be considered the case of a noise with a long–range correlation (see [2]), defined by

$$\mu = D\left|t-t'\right|^{-\gamma}, \qquad \left|t-t'\right| \geq d, \quad \text{with} \quad J = \int_0^d \mu(|s|)ds < \infty \tag{3}$$

F. Kh. Abdullaev and V. V. Konotop (eds.), Nonlinear Waves: Classical and Quantum Aspects, 145–150.

where $D > 0$ is the noise intensity and $\gamma > 0$ is a positive constant (the diffusion coefficient).

2. Solution

By the change of variables

$$\begin{cases} U(X,T) = \psi(x,t) \\ X = x + W(t), \quad W(t) = \int_0^t f(t')dt', \quad T = t \end{cases} \tag{4}$$

equation (1) becomes the homogeneous Eckhaus equation [1]

$$iU_t + U_{xx} + 2(|U|^2)_x U + |U|^4 U = 0. \tag{5}$$

The function $W(t)$ in (5) is also a Gaussian process, with zero average, that is

$$\langle W(t) \rangle = 0 \tag{6}$$

and with variance given by

$$\sigma^2(t) = \langle W(t), W(t) \rangle = \int_0^t dt' \int_0^t \mu(t' - t'')dt'' \tag{7}$$

by using (3)we obtain:

$$\sigma^2(t) = \frac{2Dt^{2-\gamma}}{(\gamma-1)(\gamma-2)} > 0, \quad \gamma < 1 \quad \text{or} \quad \gamma > 2, \tag{8}$$

$$\sigma^2(t) \underset{t \text{ large}}{\cong} 2Dt \ln t, \quad \gamma = 1 \tag{9}$$

$$\sigma^2(t) \underset{t \text{ large}}{\cong} 2\left(\frac{D}{d} + J\right)t, \quad \gamma = 2 \tag{10}$$

The above expressions imply that as t grows, $\sigma^2(t)$ is increasing more the linearly in the region $\gamma \leq 1$ and increasing linearly for $\gamma = 2$; it is instead a decreasing function of t in the region $\gamma > 2$. The range $1 < \gamma < 2$ is excluded by our considerations since in this region the variance becomes negative, thus lacking its physical sense. It is also worth noticing that the case $\gamma \leq 1$ is usually associated with anomalous diffusion [2]. The case $\gamma \geq 2$ is instead related to normal diffusion.

In our analysis we introduce, for simplicity, the function

$$\tilde{G}(k,t) = e^{ikW(t)} \tag{11}$$

and its statistical average which, as a consequence of the Gaussian property (6), is given by

$$\langle \tilde{G}(k,t) \rangle = \exp\left[-\frac{1}{2}k^2\sigma^2(t)\right]. \tag{12}$$

In order to study the statistical average of the original function $\langle\psi(x,t)\rangle$ we introduce the Fourier transform of $\psi(x,t)$

$$\tilde{F}(k,t) = \int \psi(x,t)e^{-ikx}dx, \tag{13}$$

with

$$\psi(x,t) = \frac{1}{2\pi}\int \tilde{F}(k,t)e^{ikx}dk. \tag{14}$$

Using (4) and (12), then (13) becomes

$$\tilde{F}(k,t) = \int U(X,t)e^{-ikX}e^{ikW(t)}dX = \tilde{U}(k,t)\tilde{G}(k,t). \tag{15}$$

Thus

$$\langle\tilde{F}(k,t)\rangle = \tilde{U}(k,t)\langle\tilde{G}(k,t)\rangle, \tag{16}$$

where $\tilde{U}(k,t)$ is the Fourier transform of $U(X,t)$. From (14) and (16) we get

$$\begin{aligned}\langle\psi(x,t)\rangle &= \frac{1}{2\pi}\int\left\langle\tilde{F}(k,t)\right\rangle e^{ikx}dk \\ &= \frac{1}{\sqrt{2\pi\sigma^2(t)}}\int U(y,t)\exp\left(-\frac{(x-y)^2}{2\sigma^2(t)}\right)dy \end{aligned}\tag{17}$$

valid for any Gaussian process $f(t)$.

3. Statistical properties

Before considering any explicit solution of the Eckhaus equation, we consider the correlation of the system with the noise

$$\langle\psi(x,t_1),f(t_2)\rangle = \frac{1}{2\pi}\int dyU(x-y,t_1)\int e^{iky}\langle e^{ikW(t_1)},f(t_2)\rangle dk, \tag{18}$$

where (13), (16) and (11) have been used. In order to solve (18), we study the term in brackets of the right hand side, namely

$$\langle e^{ikW(t_1)},f(t_2)\rangle = ik\langle W(t_1),f(t_2)\rangle\exp\left[-\frac{1}{2}k^2\sigma^2(t)\right]. \tag{19}$$

Finally from (18) and (19) we get

$$\langle\psi(x,t_1),f(t_2)\rangle = C(t_1,t_2)\int\frac{\partial}{\partial y}U(x-y,t_1)\exp\left[-\frac{y^2}{2\sigma^2(t_1)}\right]dy, \tag{20}$$

where

$$C(t_1, t_2) = \frac{\langle W(t_1), f(t_2)\rangle}{\sqrt{2\pi\sigma^2(t_1)}}. \tag{21}$$

In order to evaluate (21) in our case we must compute the correlation $\langle W(t_1), f(t_2)\rangle$.

If $t_1 < t_2$ $(\gamma \neq 1)$, when $\gamma < 1$ and $\gamma > 2$, we have

$$\langle W(t_1), f(t_2)\rangle = \int_0^{t_1} \frac{D}{(t_2 - t')^\gamma} dt' = \frac{D}{\gamma - 1}\left[t_2^{1-\gamma} - (t_2 - t_1)^{1-\gamma}\right]. \tag{22}$$

If $t_1 > t_2$, when $\gamma < 1$ and $\gamma > 2$, we have

$$\begin{aligned}\langle W(t_1), f(t_2)\rangle &= \int_0^{t_2} \frac{D}{(t_2 - t')^\gamma} dt' + \int_{t_2}^{t_1} \frac{D}{(t' - t_2)^\gamma} dt' \\ &= \frac{D}{\gamma - 1}\left[t_2^{1-\gamma} + (t_1 - t_2)^{1-\gamma}\right].\end{aligned} \tag{23}$$

Eqs. (22) and (23) imply that the correlation (20) becomes negative in the case $\gamma < 1$ (anomalous diffusion). We therefore concentrate our attention on the normal diffusion case . Consequently, by (21),(22) and (23) we get for $t_1 < t_2$,

$$C(t_1, t_2) = \frac{1}{2}\sqrt{\frac{D(\gamma - 2)}{\pi(\gamma - 1)}} t_1^{\frac{\gamma}{2}-1}\left[t_2^{1-\gamma} - (t_2 - t_1)^{1-\gamma}\right], \tag{24}$$

analogously for $t_1 > t_2$

$$C(t_1, t_2) = \frac{1}{2}\sqrt{\frac{D(\gamma - 2)}{\pi(\gamma - 1)}} t_1^{\frac{\gamma}{2}-1}\left[t_2^{1-\gamma} + (t_1 - t_2)^{1-\gamma}\right]. \tag{25}$$

(24) shows that for as $t_1 < t_2$, the correlation between the noise and the field is negative, eventually approaching zero as t_2 grows. The negative value is understood as a violation of the causality principle: the value of the noise at a given time (t_2) cannot influence the field at a previous time (t_1). The correlation is instead increasing according to (25) as t_1 grows (t_2 fixed)implying that the influence of the noise at a given time on the system at a later time is growing due to the long range correlation of the noise. These two different behaviours are shown in Fig. 1 and Fig. 2, respectively.

In order to study the two time autocorrelation of system, it is convenient to work in the Fourier space, where the correlation function via

(15) is given by

$$\left\langle \tilde{F}(k,t), \tilde{F}(-k,t) \right\rangle = \int U(y,t) e^{-iky} dy \int U(z,t+s) e^{-ikz} \times \left\langle e^{ikW(t)}, e^{-ikW(t+s)} \right\rangle dz = \Phi(t,t+s) \tilde{U}(k,t) \tilde{U}(-k,t+s), \tag{26}$$

with

$$\Phi(t,t+s) = \exp\left\{ -\frac{1}{2} k^2 \left[\sigma^2(t) + \sigma^2(t+s) - 2 \langle W(t), W(t+s) \rangle \right] \right\}. \tag{27}$$

After evaluating the product $\langle W(t), W(t+s) \rangle$ we finally get

$$\Phi(t,t+s) = \exp\left\{ -\frac{D k^2 s^{2-\gamma}}{(\gamma-1)(\gamma-2)} \right\}, \tag{28}$$

which shows a correlation exponentially vanishing as s grows. We now consider the one-soliton (Kink) solution $U_s(X,t)$ of the Eckhaus equation (5)

$$U_s(X,t) = \frac{p^{1/2} \exp\left[\frac{1}{2} iv(X - wt) + i\alpha \right]}{\sqrt{1 + \exp\left[-2p(X - x_0 - vt) \right]}}. \tag{29}$$

where p and v are real, positive parameters and is $w = \frac{1}{2} v - 2p^2/v$. From (20) and (29) we have the statistical average of the kink as

$$\langle \psi_s(x,t) \rangle = \frac{1}{\sqrt{\pi}} e^{-i\alpha_1 t} e^{i\alpha_2 x} \int \frac{\exp\left[-\left(z^2 + i\alpha_2 \sqrt{2\sigma^2(t)} z \right) \right] dz}{\left[1 + \exp\left(-2p \left(x - \sqrt{2\sigma^2(t)} z - vt \right) \right) \right]^{1/2}}. \tag{30}$$

with $z = \frac{(x-y)}{\sqrt{2\sigma^2(t)}}$ and $\alpha_1 = \frac{1}{2} vw, \quad \alpha_2 = \frac{1}{2} v$.

The results of analytical and numerical evaluations show that the average $\langle \psi_s(x,t) \rangle$ is a growing function of the time which eventually collapses as $t \longrightarrow +\infty$ in the case of anomalous diffusion ($\gamma < 1$). In the normal diffusion case ($\gamma > 2$), the average is instead decreasing eventually, approaching zero as $t \longrightarrow +\infty$. The two different behaviours are shown in Figs. 3 and 4, respectively.

References

[1] F. Calogero, and S. De Lillo, The Eckhaus PDE $i\psi_t + \psi_{xx} + 2(|\psi|^2)_x \psi + |\psi|^4 \psi = 0$. *Inverse Problems*, **3**, 633-681 (1987).

[2] T. Iizuka, Anomalous diffusion of solitons in random systems. *Phys. Lett. A*, **181**, 39-42 (1993).

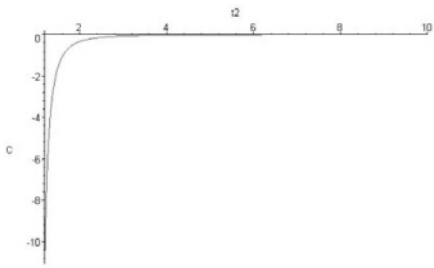

Figure 1. Case $t_1 < t_2$ (with a fixed value of $t_1 = 1$) for $\gamma = 3$ ($D = 5$).

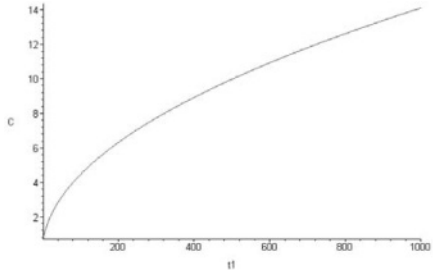

Figure 2. Case $t_1 > t_2$ (with a fixed value of $t_2 = 1$) for $\gamma = 3$ ($D = 5$).

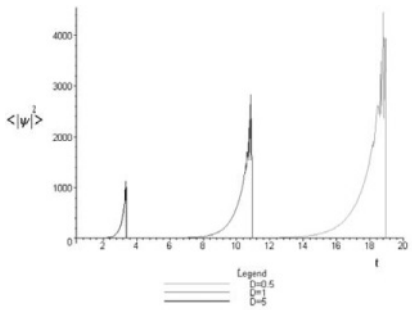

Figure 3. The statistical average $\langle|\psi_s(x,t)|^2\rangle$ for the *Soliton of the first kind* for $\gamma = 0.5$.

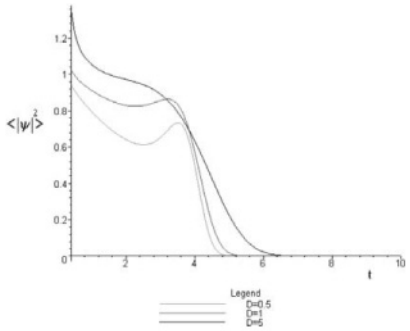

Figure 4. The statistical average $\langle|\psi_s(x,t)|^2\rangle$ for the *Soliton of the first kind* for $\gamma = 3$.

MODULATIONAL INSTABILITY OF SOME NONLINEAR CONTINUUM AND DISCRETE MODELS

D. Grecu and Anca Visinescu

Department of Theoretical Physics National Institute of Physics and Nuclear Engineering P.O.Box MG-6, Bucharest, Romania

dgrecu@theor1.theory.nipne.ro

Abstract The statistical approach of the modulational instability is reviewed for several nonlinear systems: the nonlinear Schrödinger equation, the discrete self-trapping equation and the Manakov system. An integral stability equation is deduced from a linearized kinetic equation for the two-point correlation function. This is solved for several choices of the unperturbed initial spectral function.

Keywords: Modulational instability, nonlinear Schrödinger equation, Manakov system, discrete systems.

1. Introduction

Modulational instability (also known as the Benjamin-Feir instability) is a general phenomenon which takes place when a quasi-monochromatic wave is propagating in a dispersive and weakly nonlinear media. Discovered in the middle of sixties by Lighthill [1], Benjamin and Feir [2] and Bespalov and Talanov [3] is now a standard chapter of nonlinear physics, being studied and observed in almost any domain (hydrodynamics, nonlinear optics, plasma physics, condensed matter, etc.) (see [4]-[7] where more references can be found). Two distinct ways to study this phenomenon are possible. The first, the most common one, is a deterministic approach in which small modulations of the amplitude of a plane wave solution (a Stokes wave) are considered. Two side bands around the carrier wave appear and they reinforce each other by nonlinear interaction. In the second a statistical approach is considered in which the accent is on the wave-wave energy transfer due to weak nonlinear couplings in a nearly homogeneous random media [8]-[9]. A kinetic equation for a two-point correlation function is written down, and a

F. Kh. Abdullaev and V. V. Konotop (eds.), Nonlinear Waves: Classical and Quantum Aspects, 151–156.

linear stability analysis around an unperturbed initial condition (which takes into account the correlation properties of the random medium) is performed.

In the present paper we shall summarize some of our results concerning the Statistical Approach of Modulational Instability (SAMI) for several systems [10]-[12], namely:

- nonlinear Schrödinger (NLS) equation

$$i\frac{\partial A}{\partial t} + \lambda\frac{\partial^2 A}{\partial x^2} + \mu|A|^2 A = 0. \tag{1}$$

- discrete self-trapping (DST) equation

$$i\frac{da_n}{dt} - \omega_0 a_n + \lambda(a_{n+1} + a_{n-1}) + \mu|a_n|^2 a_n = 0. \tag{2}$$

- Manakov system (MS)

$$\begin{aligned} i\frac{\partial A}{\partial t} + \lambda\frac{\partial^2 A}{\partial x^2} + \mu(|A|^2 + |B|^2)A = 0 \\ i\frac{\partial B}{\partial t} + \lambda\frac{\partial^2 B}{\partial x^2} + \mu(|A|^2 + |B|^2)B = 0. \end{aligned} \tag{3}$$

2. SAMI for NLS equation

We shall begin by discussing SAMI for NLS equation (1). The first step is to find a kinetic equation for the two-point correlation function $\rho(x_1, x_2) =< A(x_1)A^*(x_2) >$. Here $< ... >$ denotes an ensemble average. Using a Gaussian approximation to decouple four-point correlation functions we get

$$i\frac{\partial \rho}{\partial t} + \lambda\left(\frac{\partial^2}{\partial x_1^2} - \frac{\partial^2}{\partial x_2^2}\right)\rho + 2\mu\left[\overline{a^2}(x_1) - \overline{a^2}(x_2)\right]\rho(x_1, x_2) = 0, \tag{4}$$

where $\overline{a^2}(x) =< A(x)A^*(x) >$ is the average mean square amplitude.

The next step is to introduce the new coordinates $X = \frac{x_1+x_2}{2}$ and $x = x_1 - x_2$ and the Fourier transform $F(k, X)$ of $\rho(x, X)$ with respect to the relative coordinate x. The equation (4) becomes

$$\frac{\partial F}{\partial t} + 2\lambda k\frac{\partial F}{\partial x} + 4\mu\sum_{n=0}^{\infty}\frac{(-1)^n}{2^{2n+1}(2n+1)!}\frac{\partial^{2n+1}F}{\partial k^{2n+1}}\frac{\partial^{2n+1}\overline{a^2}}{\partial X^{2n+1}} = 0. \tag{5}$$

A linear stability analysis around an unperturbed solution $F_0(k)$, independent of X ($F_0(k)$ plays the same role as the Stokes wave in a deterministic approach) will be done. We write

$$F(k, X) = F_0(k) + \epsilon F_1(k, X) \qquad \overline{a^2}(X) = \overline{a_0^2} + \epsilon\overline{a_1^2}(X) \tag{6}$$

where $\overline{a_0^2} = \int_{-\infty}^{+\infty} F_0(k)dk$, $\overline{a_1^2} = \int_{-\infty}^{+\infty} F_1(k,X)dk$. Then a linear evolution equation for $F_1(k,X,t)$ is found, namely

$$\frac{\partial F_1}{\partial t} + 2\lambda k \frac{\partial F_1}{\partial x} + 4\mu \sum_{n=0}^{\infty} \frac{(-1)^n}{2^{2n+1}(2n+1)!} \frac{\partial^{2n+1} F_0}{\partial k^{2n+1}} \frac{\partial^{2n+1} \overline{a_1^2}}{\partial X^{2n+1}} = 0. \quad (7)$$

Looking for plane wave solutions

$$F_1(k,X) = f_1(k) e^{i(KX - \Omega t)} \quad (8)$$

the following integral stability equation is easily obtained

$$1 + \frac{\nu}{K\lambda} \int_{-\infty}^{+\infty} \frac{F_0(k+\frac{K}{2}) - F_0(k-\frac{K}{2})}{k - i\omega} dk = 0, \quad (9)$$

considering Ω purely imaginary ($\Omega = i\Omega_i$) and denoting $\omega = \frac{\Omega_i}{2\lambda K}$.

Different forms for the initial condition $F_0(k)$ can be considered. For a δ-spectrum, $F_0(k) = \overline{a_0^2}\delta(k)$, and from (9) we get

$$\Omega_i = 4\lambda K \sqrt{\frac{\mu}{\lambda}\overline{a_0^2} - \frac{K^2}{4}}. \quad (10)$$

An instability exists if both μ, λ have the same sign (the focusing case of NLS equation), and if $K < 2(\frac{\mu}{\lambda}\overline{a_0^2})^{\frac{1}{2}}$, i.e. in the long wave-length limit. This is an unphysical situation, but it represents an useful limit to which all the other cases can be compared. From the point of view of modulational instability it represents the most favorable case.

Other initial conditions were discussed in [12]. We give here the results only for a Lorentzian spectrum $F_0(k) = \frac{\overline{a_0^2}}{\pi} \frac{p}{k^2+p^2}$, with the following result

$$\Omega_i = 2K\lambda \left(\sqrt{\frac{\nu}{\lambda}\overline{a_0^2} - \frac{K^2}{4}} - p \right). \quad (11)$$

On this expression it if easily seen the effect of the statistical properties of the medium on the development of the modulational instability. If p is too large (larger than the square root) the instability is suppressed. But large p corresponds to short-range correlations in the x-space. The conclusion is that the modulational instability can develop in a medium if and only if a certain long-range correlation exists.

3. SAMI for DST equation

For the DST equation (2) the same steps as for the NLS equation has to be followed. We shall mention here only the differences between the two cases, a full discussion being given in our recent paper [10].

One considers a chain of N molecules with cyclic boundary conditions. We introduce the new discrete variables $M = \frac{1}{2}(n_1+n_2)$, and $m = n_1-n_2$ and the Fourier transform $F(k,M)$ where k is restricted to the first Brillouin zone $(-\pi,\pi)$. We see that $F(k,M)$ is a periodic function of k, with period 2π. The kinetic equation satisfied by $F(k,M)$ is

$$i\frac{\partial F}{\partial t} + 4\lambda \sin k \sinh \frac{1}{2}\frac{\partial F}{\partial M} \tag{12}$$
$$+4\mu \sum_{j=1}^{\infty} \frac{(-1)^{j-1}}{(2j-1)!2^{2j-1}} \left(\frac{\partial^{2j-1}\overline{a_0^2}(M)}{\partial M^{2j-1}}\right)\left(\frac{\partial^{2j-1}F(k,M)}{\partial k^{2j-1}}\right) = 0.$$

A linear stability analysis leads to the following integral stability eq.

$$1 + \frac{\mu}{4\pi\lambda \sin\frac{K}{2}} \int_{-\pi}^{\pi} \frac{F_0(k+\frac{K}{2}) - F_0(k-\frac{K}{2})}{\sin k - \frac{\Omega}{4\lambda \sin\frac{K}{2}}} dk = 0. \tag{13}$$

For $F_0(k)$ a δ-spectrum we get $(K>0)$

$$\Omega_i = 4\lambda \sin\frac{K}{2}\sqrt{\frac{\mu}{\lambda}\overline{a_0^2} - \sin^2\frac{K}{2}}\,. \tag{14}$$

For a Lorentzian like spectrum $F_0(k) = \overline{a_0^2}\frac{p\sqrt{1+p^2}}{\sin^2\frac{k}{2}+p^2}$ which satisfies the periodicity condition, we obtain

$$\Omega_i = 4\lambda \sin\frac{K}{2}\left(\sqrt{\frac{\mu}{\lambda}\overline{a_0^2} - \sin^2\frac{K}{2}} - 2p\frac{1+\cos\frac{K}{2}+\cos K}{1+\cos\frac{K}{2}}\right). \tag{15}$$

4. SAMI for Manakov system

In this section preliminary results concerning SAMI for Manakov's system (3) will be presented. The calculations become more complicated because we have to deal with four two-point correlation functions $\rho_{AA}, \rho_{AB}, \rho_{BA}, \rho_{BB}$ where $\rho_{\alpha\beta} =< \alpha(x_1)\beta^*(x_2) >, \quad \alpha,\beta = A,B$. Assuming a Gaussian decoupling approximation, kinetic equations for these correlation functions can be written down; for the diagonal $\rho_{\alpha\alpha}$ it writes

$$i\frac{\partial}{\partial t}\rho_{\alpha\alpha} + \lambda\left(\frac{\partial^2}{\partial x_1^2} - \frac{\partial^2}{\partial x_2^2}\right)\rho_{\alpha\alpha} + \mu\left[\overline{\alpha\beta}(x_1)\rho_{\beta\alpha} - \overline{\beta\alpha}(x_2)\rho_{\alpha\beta}\right] +$$

$$\mu\left[2\left(\overline{\alpha^2}(x_1) - \overline{\alpha^2}(x_2)\right) + \left(\overline{\beta^2}(x_1) - \overline{\beta^2}(x_2)\right)\right]\rho_{\alpha\alpha} = 0. \tag{16}$$

Here $\overline{\alpha\beta}(x) =< \alpha(x)\beta^*(x) >$. Next, Fourier transforming these equations with respect to the relative coordinate $x = x_1 - x_2$, kinetic equations for $F_{\alpha\beta}(k, X, t)$ are obtained. For $F_{\alpha\alpha}$ this is given by

$$i\frac{\partial}{\partial t}F_{\alpha\alpha}(k,X,t) + 2ik\lambda\frac{\partial}{\partial X}F_{\alpha\alpha}(k,X,t) +$$

$$i\mu\sum_{j=1}^{\infty}\frac{2(-1)^j}{2^{2j+1}(2j+1)!}\left[2\frac{\partial^{2j+1}\overline{\alpha^2}(X)}{\partial X^{2j+1}} + \frac{\partial^{2j+1}\overline{\beta^2}(X)}{\partial X^{2j+1}}\right]\frac{\partial^{2j+1}F_{\alpha\alpha}}{\partial k^{2j+1}} \quad (17)$$

$$+\mu\sum_{j=0}^{\infty}\frac{(i)^j}{2^j j!}\left[\frac{\partial^j\overline{\alpha\beta}(X)}{\partial X^j}\frac{\partial^j F_{\beta\alpha}}{\partial k^j} - (-1)^j\frac{\partial^j\overline{\beta\alpha}(X)}{\partial X^j}\frac{\partial^j F_{\alpha\beta}}{\partial k^j}\right] = 0.$$

In a linear approximation.

$$F_{\alpha\beta}(k,X,t) = f_{\alpha\beta}(k) + \epsilon\,\mathcal{F}_{\alpha\beta}(k,X,t) \quad (18)$$

$$\overline{\alpha^2}(X,t) = \overline{\alpha_0^2} + \epsilon\overline{\alpha_1^2}(X,t)$$

where $\overline{\alpha_0^2} = \int_{-\infty}^{+\infty} f_{\alpha\alpha}(k)dk$ and $\overline{\alpha_1^2}(X,t) = \int_{-\infty}^{+\infty}\mathcal{F}_{\alpha\beta}(k,X,t)dk$. Linear evolution equations for $\mathcal{F}_{\alpha\beta}$ are easily obtained. Looking for plane wave solutions

$$\mathcal{F}_{\alpha\beta}(k,X,t) = g_{\alpha\beta}(k)e^{i(KX-\Omega t)} \quad (19)$$

$$\overline{(\alpha\beta)_1}(X,t) = e^{i(KX-\Omega t)}\int_{-\infty}^{+\infty} g_{\alpha\beta}(k)dk = G_{\alpha\beta}e^{i(KX-\Omega t)}$$

a linear homogeneous system for $G_{\alpha\beta}$ is obtained. Even for a δ-spectrum initial condition $f_{\alpha\beta} = \overline{(\alpha\beta)}_0\delta(k)$ the compatibility condition of this system is a 4x4 determinant, depending on four independent parameters $(\overline{\alpha\beta})_0$. Therefore we shall simplify the problem assuming $(\overline{\alpha\beta})_0 = \overline{a_0^2}$ anyone α and β are (an "absolute democracy" assumption). Also we shall take $\mu = 2\lambda = 1$ (canonical form of Manakov system). Then the homogeneous linear system takes the simpler form

$$\left(\omega^2 + \frac{K^2}{4} - 2\overline{a_0^2}\right) - \overline{a_0^2}G_{\beta\beta}$$

$$-\overline{a_0^2}(i\frac{\omega}{K} + \frac{1}{2})G_{\alpha\beta} + \overline{a_0^2}(i\frac{\omega}{K} - \frac{1}{2})G_{\beta\alpha} = 0 \quad (20)$$

$$\left(\omega^2 + \frac{K^2}{4} - \overline{a_0^2}\right)G_{\alpha\beta} = \overline{a_0^2}(i\frac{\omega}{K} + \frac{3}{2})G_{\alpha\alpha} - \overline{a_0^2}(i\frac{\omega}{K} - \frac{3}{2})G_{\beta\beta}$$

This is easily solved and the only acceptable solution is

$$\Omega_i = K\sqrt{4\overline{a_0^2} - \frac{K^2}{4}}. \quad (21)$$

Compared with the result obtained for NLS case we see that the region of instability is larger in this case $K < 4(\overline{a_0^2})^{\frac{1}{2}}$. For a Lorentzian spectrum with a similar assumption of "complete democracy" we get

$$\Omega_i = K\left[\sqrt{4\overline{a_0^2} - \frac{K^2}{4}} - p\right]. \tag{22}$$

More details will be published elsewhere.

Acknowledgments

On of the authors (DG) would like to thank Prof. V. Konotop and the Organizing Committee for financial support. This work is supported by the program CERES/66.

References

[1] M. J. Lightill, J. Inst. Math. Appl. **1**, 269 (1965)

[2] T. B. Benjamin, J. F. Feir, J. Fluid. Mech. **27**, 417 (1967)

[3] V. I. Bespalov, V. I. Talanov, Pisma JETP, **3**, 417 (1966)

[4] R. K. Dodd, J. C. Eilbeck, J. D. Gibbon, H. C. Morris, "Solitons and Nonlinear Wave Equations" (Acad. Press, 1982)

[5] M. Remoissenet, "Waves Called Solitons. Concepts and Experiments" (Springer, 1999)

[6] A. C. Newell, ed. "Nonlinear Wave Motion" (Am.Math.Soc. Providence, 1974)

[7] F. Kh. Abdulaev, S. A. Darmanyan, J. Garnier, in "Progress in Optics", (ed. E. Wolf, Elsevier), **44**, 303 (2002)

[8] I. E. Alber, Proc. Roy. Soc. London A **365**, 525 (1978)

[9] M. Onorato, A. Osborne, M. Serio, R. Fedele, nlin.CD/0202026;

[10] A. Visinescu, D. Grecu, Eur. Phys. J. B **34**, 225 (2003)

[11] A. Visinescu, D. Grecu, Proc. Int. Math. NAS Ukraine (2004), in press

[12] D. Grecu, A. Visinescu, Proc. First South-East Eur. Symp. "Interdisciplinary Approach in Fractal Analysis" (May, 2003, Bucharest), p. 158

SCATTERING OF NLS SOLITONS WITH BOUND QUANTUM STATES

Andrei Ludu
Deptartment of Chemistry and Physics Northwestern State University, Natchitoches, LA 71497 USA
ludua@nsula.edu.edu

Abstract Inelastic collision between NLS3 solitons and bound quantum states in strong localized one-dimensional potentials are investigated.

1. Introduction

There are three basic microscopic models approaching nonlinear quantum mechanics of compact systems, and all three converge towards the same type of nonlinear dynamics described by the Gross-Pitaevski equation (GP). One model is provided by nonlinear extension of traditional geometric collective models, that is introduction of large amplitude collective excitation of the surface of the system as solitons. A second model is provided by nonlinear Hamiltonian hydrodynamics in terms of mass and current densities with nonlocal potential. The last approach is provided by recent studies in BEC dynamics [1] with application in nuclear clusters and alpha resonances [2]. The one-dimensional toy-model presented in this contribution analyzes the collision of NLS one- or many-soliton states with bounded quantum states in a localized potential well or barrier. Our hypothesis is that the overall dynamics of the system is provided by the GP equation which describes a Bose gas with a two-body attractive δ-function interaction. We consider the asymptotic states of the free compound system outside the potential as being described by the NLS equation for which we have analytic solutions in the form of modulated solitons traveling with constant shape and constant speed. The advantage of solitons compared to orthodox quantum wave packets (or plane waves) is that such "quantized" solitons are bounded, square integrable and stable in time. Inside the potential the same GP equation is governing the system, but if the potential is deep (or high) enough,

F. Kh. Abdullaev and V. V. Konotop (eds.), Nonlinear Waves: Classical and Quantum Aspects, 157–162.

and if the excitation functions are small enough we can neglect the nonlinear term inside, and the GP equation reduces to standard Schrödinger equation (SE) with exact time dependent, or stationary analytic solutions. We match boundary condition at the ends of the potential region and we normalize the whole wave function. In this way one can estimate reflection and transmission coefficients for solitons in different reaction channels, and we put into evidence adiabatic excitation of resonant states inside the potential zone. Applications of such systems can be found in BEC systems, α-particle nuclear matter, clusters, nonlinear dynamical lattices, fiber optics with inclusions or defects, etc.

This nonlinear quantum model consists in the collision between a compound quasi-classical system (the projectile) described by an incoming NLS soliton, and a target in a bounded quantum state described by one internal degree of freedom. Contrary to orthodox quantum mechanics case [3] we consider the projectile to be a soliton and not a plane wave. There are advantages (non dispersive effect of wavefunction, internal degrees of freedom of complex projectile and its coupling with the target degrees of freedom, normed wave-functions, simpler calculations) as well as disadvantages (not orthodox quantum mechanics approach: target is a traditional quantum system, projectile is a quasi-classical condensate approximation).

2. Quantized solitary waves

If we consider the projectile constructed by N identical particles interacting via a δ-function potential, a quantization of the solitary wave solutions to the second-quantized description reproduces the weak-coupling limit of the known quantum mechanical result. The Hamiltonian

$$H[\Phi] = \frac{\hbar^2}{2m}\Phi_x\Phi_x^* + V(x)\Phi\Phi^* - \frac{k}{2}(\Phi_x\Phi_x^*)^2, \tag{1}$$

can be expressed in terms of a complex scalar field Φ where k is a strength parameter, and $V(x)$ is the external potential. In a two-dimensional theory, the Euler-Lagrange equation of motion for the "collective" wave function $\Phi(x,t)$ is the GP equation

$$i\hbar\Phi_t = -\frac{\hbar^2}{2m}\Phi_{xx} + V(x)\Phi - k(\Phi^*\Phi)\Phi, \tag{2}$$

where subscripts represent partial differentiation. Therefore, although the underlying fundamental quantum mechanics is linear, the "macroscopic wavefunction" of the system, as emergent entity, is governed by a nonlinear equation. In the following we consider the target to be described by a very localized potential with compact support included

in the interval $x \in [-\frac{a}{2}, \frac{a}{2}]$. Consequently, outside of this domain the potential $V(x)$ is zero, and the GP Eq.(2) reduces to the NLS equation

$$i\hbar\Phi_t = -\frac{\hbar^2}{2m}\Phi_{xx} - k(\Phi^*\Phi)\Phi, \tag{3}$$

which describes the free asymptotic motion of the compound projectile. For $k > 0$ this NLS admits a family of solitary waves solutions. The one-soliton solution of Eq.(3) $\Phi_1(x,t)$ depends on four independent parameters, namely amplitude A, phase velocity q, initial position x_0, and constant phase χ

$$\Phi_1 = Ae^{i[p(x-x_0)+qt+\chi]}\mathrm{sech}\,\frac{x-x_0-Vt}{L}, \tag{4}$$

where the wave vector p, the group (soliton) velocity V and half-width of the wavefunction L are given by

$$p = \frac{\sqrt{m(A^2k-2q\hbar)}}{\hbar}, \quad V = \sqrt{\frac{A^2k-2q\hbar}{m}}, \quad L = \frac{\hbar}{A\sqrt{km}}. \tag{5}$$

We note that in order to have a soliton solution we need $A^2k > 2q\hbar$. One particular feature of the NLS Eq.(4) is that both positive (soliton) or negative amplitude (anti-soliton) can move in either directions. Moreover, there is no direct relation between the half-width of the soliton and its velocity like in the KdV, or MKdV cases, since this soliton depends on 3 free parameters. From Eq.(4) we obtain the norm of the wavefunction, which is related to the number of particles in the projectile N

$$||\Phi_1||^2 = N = \int_{-\infty}^{\infty}\Phi\Phi^*dx = \sqrt{\frac{2\hbar|A|}{\sqrt{km}}}, \tag{6}$$

which is constant in time. The NLS equation provides norm conservation in time, so the quantum mechanical probabilistic formalism is preserved. Identical solitons move with the same speed so they never collide, while different solitons have different shapes (A, L) and travel with different speeds. The energy of the Eq.(4) state is given by

$$E_1 = \frac{<\Phi_1|H|\Phi_1>}{<\Phi_1|\Phi_1>} = \int_{-\infty}^{\infty}\left(\frac{\hbar^2}{2m}\Phi_{1x}\Phi_{1x}^* - \frac{k}{2}(\Phi_1\Phi_1^*)^2\right)dx = \frac{A^2k}{3} - \hbar q. \tag{7}$$

The first term in in the last result of Eq.(3) is soliton internal energy of excitation, while the second one is its kinetic energy. In the linear limit ($k \to 0$) Eq.(3) approaches the SE equation, the wave function

aproaches a plane wave with $p_0 = \sqrt{-2q_0/\hbar}$, the phase speed becomes $V \to p_0\hbar/\sqrt{m}$, the norm blows up to infinity, and the energy approaches the linear wave kinetic energy, $E_1 \to -\hbar q_0$.

For the target system we consider the example of a finite symmetric rectangular potential well/barrier of depth $\pm V_0$, and width a. Inside this region, if the potential strength V_0 is strong enough compared to the amplitude of the wavefunction, we can neglect the nonlinear term and reduce eq.(3) to the orthodox Schrödinger equation $i\hbar\Psi_{b,t} = -\frac{\hbar^2}{2m}\Psi_{b,xx} + V(x)\Psi_b$ valid for $x \in [-a/2, a/2]$ and $|E_b| < |V_0|$, with its general bounded solution

$$\Psi_b(x,t) = \int_{-V_0}^{\infty} [C_1(\epsilon)e^{i\sqrt{2m|V_0-E_b|/\hbar^2}x} + C_2(\epsilon)e^{-i\sqrt{2m|V_0-E_b|/\hbar^2}x}]e^{-\frac{iE_bt}{\hbar}}d\epsilon, \tag{8}$$

The GP→SE approximation inside the potential region is now valid if $\|\Psi_b\| \ll \sqrt{\frac{m}{k}}\frac{V_0}{\hbar}$ which is automatically fulfilled if the target potential intensity is large enough and/or the strength parameter of the field is small. In order to solve the collision problem we need one more approximation, namely the soliton velocity should be enough small to allow the establishing equilibrium inside the potential zone, that is using the adiabatic approximation inside the potential. From the uncertainty relations this happens if the necessary time for the soliton to cross the target, L/V, is larger than $\hbar\triangle E_b$, that is the change in target's energy. This condition is accomplished if the constant phase shift of the Schrödinger state in the potential zone is almost zero (that is if the wave function is as asymmetric as possible) and/or if the kinetic energy of the incoming soliton is of the same order of magnitude with its internal energy, namely $\hbar q \simeq A^2 k$.

3. Inelastic soliton-resonant state collision

The soliton-bounded state collision problem can be solved for any elastic or inelastic channel. For the elastic collision we have a total of 15 free parameter (4 from each soliton: incident, reflected, and transmitted), and 3 parameters from the stationary state. We use 8 constrains: 4 boundary conditions for the continuity of the logarithmic derivative of wave functions, 1 general normalizing condition over the whole axis, and 3 equations from energy conservation. This situation still leaves room for 7 free parameters which can be chosen for example as: energy of the reaction, the 3 constant phases of solitons, and initial positions of the solitons. However, the elastic collision channel is closed for the stationary states of the particle in the well. The wavefunction inside the well has exponential time variation at the ends, while the solitons

boundary effects can never be reduced to sinusoidal variation. If one needs to match soliton-type of boundary conditions one needs to work in the adiabatic approximation, where the energy $E_b(t)$ in the well has a (slow) variation in time compared to the speed of solitons.

Consequently, we study this problem for the inelastic collision in the adiabatic approximation. Because of space limitations we present here only the reflectionless situation. In this case we have 11 parameters, and 7 equations, so we have 4 free parameters. We choose arbitrary position for the incoming soliton, arbitrary initial energy and arbitrary phases, so the problem is still underdetermined. We have to fulfill the following boundary conditions: $\|\Phi_{in}\|^2 + \|\Phi_T\|^2 + \|\Psi\|^2 = 1$, $\Phi_{in}^{(j)}(-a/2,t) = \Psi^{(j)}(-a/2,t)$, and $\Phi_T^{(j)}(a/2,t) = \Psi^{(j)}(a/2,t)$ where $j = 0,1$ represents the matching of the wavefunction and its first derivative, and T represents the transmitted soliton, of parameters A_T, q_T, and $x_{0,T}$. We introduce the nonlinear transmission coefficient to be the transmitted soliton wavefunction norm over the incoming soliton norm, calculated in the asymptotic limit. The traditional transmission coefficient behavior for a linear plane wave scattered by a rectangular barrier shows resonances in the transmission coefficient at specific energies when the wavelength of the wave function is a integer sub-multiple of the potential barrier (or well) width. In the limit of high energies (very small wavelength) the problem becomes quasi-classical and the transmission coefficient approaches asympotic the value 1 for all energies. In the case of the NLS soliton the transmission coefficient has a different behavior. For width of the soliton smaller or larger than the potential box we have very small transmission coefficient, and we note that such a quasi-classical system behaves rather like a band-pass filter for space scales. On the top of this restricted window of transmission we obtained a fine structure of resonances which are related to the radiation tail of the soliton-perturbation collision [4].

In Fig. 1 we present analytic calculation of an example of a collision between a left-incoming soliton and a potential well of very small width compare to soliton width, $a \ll L$. During this collision new bounded states are excited in the potential valley, and a transmitted soliton is generated. After this collision, both solitons still have the same amplitude and width, while the phase velocity of the transmitted soliton is smaller on behalf of the lost energy in the collision. The excited states inside the potential trap do not decay, and the total shift in the energy of the bounded state is given by

$$\triangle E_b = \frac{\hbar A \tan(\alpha)}{a} \sqrt{\frac{k}{m}}, \tag{9}$$

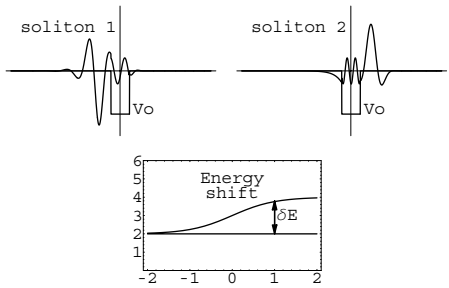

Figure 1. Soliton in inelastic reflectionless collision with a stationary state in a rectangular well. The final energy of the bounded state increases as a tanh function.

where α is the induced phase shift in the transmitted soliton. The energy jump is related to topological soliton-like perturbation that leaves the system excited. In the reflection case we use two-soliton solution for the left part of the system, with the two peaks moving with opposite velocities. The total momentum of the system is zero in this case. These situations do not represent all scattering channels of the NLS soliton with the potential box. We have analyzed collisions between wider solitons and narrower potential well, and we obtained after the collision a series of smaller emerging solitons are generated in both directions [4]. The study of this type of interactions for other potential profiles (Morse, Pöschel-Teller, etc.) as well as a possible algebraic scattering approach based on q-deformed spaces for the nonlinear space of wave-functions are the subject of a future study.

Acknowledgments

This work was supported by the National Science Foundation under NSF grants No. 0140274 and DMS-0306887. The author wants to thank Drs. A. Temple, and P. Withey for their encouragement and support.

References

[1] A. Griffin, W. D. Snoke and S. Stringari, *Bose-Einstein Condensation,* Cambridge University Press, Cambridge 1995.

[2] M. Brenner *et al*, *Alpha-particle structure on the surface of the atomic nucleus.* Proc. of the Intl. Workshop on Fission Dynamics, Luso, Portugal, 2000.

[3] A. Messiah, *Quantum Mechanics.* North-Holland, Amsterdam, 1962.

[4] A. Ludu, *Nonlinear Physics at Microscopic Scale.* Proc. of Computational and Group Theoretical Methods in Nuclear Physics, Playa del Carmen, Mexico, February 2003. Eds. Hirsch, Jorge and Pittel, Sttuart, World Scientific, Singapore (in print).

"OSCILLATOR-WAVE" MODEL: MULTIPLE ATTRACTORS AND STRONG STABILITY

Vladimir Damgov and Plamen Trenchev
Space Research Institute at the Bulgarian Academy of Sciences, 6 Moskowska str., P.O.Box 799, 1000 Sofia, Bulgaria
vdamgov@bas.bg; ptrenchev@space.bas.bg

Abstract A generalized model of an oscillator, subjected to the influence of an external wave is considered. It is shown that the systems of diverse physical background, which this model encompasses by their nature, should belong to the broader, proposed in our previous works, class of "kick-excited self-adaptive dynamical systems" [1,2,3]. The theoretical treatment includes an analytic approach to the conditions for emergence of small and large amplitudes, i.e. weak and strong non-linearity of the system. Derived also are generalized conditions for the transition of systems of this "oscillator-wave" type to non-regular and chaotic behaviour.

1. Introduction

The works [1-5] present the class of kick-excited self-adaptive dynamical systems. In these works are provided numeric and analytic proofs for the behavior and the principal properties of dynamic systems subjected to the influence of an external non-linear exciting force. The considerations are based on a generalized pendulum model the non-linearity of the external influence being introduced through particularly selected functional dependencies.

Here we consider the generalized "oscillator-wave" model and show that the inhomogeneous external influence is realized naturally and does not require any specific conditions. Systems covered by the "oscillation-wave" model immanently belong to the generalized class of kick-excited self-adaptive dynamical systems. Attempting maximal clarity of the sequence of presentation we consider the excitation of oscillations in a

F. Kh. Abdullaev and V. V. Konotop (eds.), Nonlinear Waves: Classical and Quantum Aspects, 163–171.

non-linear oscillator of the "pendulum" type under the influence of an incoming (fall) wave. We will show that under certain condition in the system will arise non-attenuated oscillations with a frequency close to the system's natural frequency and an amplitude which belongs to a defined discrete spectrum of possible amplitudes. The model under consideration is remarkable for the occurrence of the following objective regularities: the phenomenon of "discrete" ("quantized") oscillation excitation in macro-dynamical systems having multiple branch attractors and strong self-adaptive stability.

2. Model of the interaction of an oscillator with an electromagnetic wave: approach applicable for small amplitudes of the system oscillations

Let us consider the interaction of an electromagnetic wave with a weakly dissipative non-linear oscillator. Let the electric charge q having mass m oscillate along the x-axis under the influence of a non-linear returning force around a certain fixed point. The electromagnetic wave also propagates along the x-axis and has a longitudinal electric field component E. The equation of motion for the charge interacting with the wave can be represented as:

$$m(\ddot{x} + 2\delta_d \dot{x} + \omega_o^2 \sin x) = Eq \sin(\nu t - kx), \tag{1}$$

where $2\delta_d$ is the damping coefficient, ω_o is the natural frequency of small oscillations of the charge, ν is the wave frequency and k is the wave number. The case considered is: $\nu \gg \omega_o$.

We assume that the excitation of charge oscillations by the influence of the wave does not perturb significantly the symmetry of the charge's motion around its equilibrium position and the coordinate of the charge changes according to the law

$$x = a \sin\theta, \quad \theta = \omega t + \alpha, \quad a = a(t), \quad \alpha = \alpha(t) \tag{2}$$

Substituting the solution (2) in the right hand side of Eq. (1) we obtain

$$Eq \sin(\nu t - ka \sin\theta) = Eq \sum_{n=-\infty}^{\infty} J_n(ka) \sin(\nu t - n\theta).$$

Letting $\dot{x} = a\omega\cos\theta, \quad \dot{a}\sin\theta + \dot{\alpha}a\cos\theta = 0$ in accordance with the Krylov-Bogolyubov-Mitropolskii method [6] we obtain to first order:

$$\begin{cases} \dfrac{da}{dt} = -2\delta_d a + \dfrac{F_o}{\omega}\displaystyle\sum_{n=-\infty}^{\infty} J_n(ka)\sin(\nu t - n\theta)\cos\theta \\ \dfrac{d\alpha}{dt} = \dfrac{\Omega^2 - \omega^2}{2\omega} - \dfrac{F_o}{\omega}\displaystyle\sum_{n=-\infty}^{\infty} J_n(ka)\sin(\nu t - n\theta)\cos\theta \end{cases} \tag{3}$$

where Ω is the frequency of free oscillations having an amplitude a,

$$\Omega^2 = \frac{2J_1(a)}{a}\omega_o^2 \cong \omega_o^2\left[1 - \frac{a^2}{8} + O(a^4)\right] \tag{4}$$

$J_n(\cdot)$ are Bessel functions of the first kind, $F_o = \frac{Eq}{m}$.

The excitation of continuous oscillations with a frequency $\omega = \omega_s$ close to the oscillator's natural frequency is only possible under the condition $\frac{2\pi}{\lambda}a > 1$ where λ is the wavelength of the influencing wave. As result of the interaction of the oscillator with the wave a frequency components appears in the force spectrum that is close to its natural oscillation frequency. Then the action of these spectral components becomes dominant and the right-hand side of Eq. (1) attains the form:

$$\frac{Eq}{m}\sum_{n=-\infty}^{\infty} J_n(ka)\sin(\nu t - n\theta) = F_o\left\{J_{\frac{\nu}{\omega}-1}(ka)\sin\left[\omega t - (\frac{\nu}{\omega} - 1)\alpha\right] - J_{\frac{\nu}{\omega}+1}(ka)\sin\left[\omega t + (\frac{\nu}{\omega} + 1)\alpha\right]\right\} \tag{5}$$

Under the condition $\nu > \omega$ the resonance area of the nonlinear oscillator can be entered by several spectral components of the exciting wave each of which could excite the oscillator into stationary oscillations with amplitude belonging to a discrete sequence of possible amplitudes. For fixed parameters of the oscillator and the wave the excitation of oscillations with amplitude from the possible sequence of amplitudes is determined by the initial conditions. In accordance with relation (4) the values of the discrete sequence of stationary amplitudes can be calculated by the formula:

$$a_{s0} = \sqrt{8\left(1 - \frac{\nu^2}{s^2\omega_o^2}\right)} \cong 4\sqrt{1 - \frac{\nu}{s\omega_o}}, \quad s = 1, 2, 3, ... \tag{6}$$

Averaging the right-hand side of Eqs. (3) and taking into account (5), we determine:

$$\begin{cases} \dfrac{da_s}{dt} = -\delta_d a + \dfrac{F_o}{2\omega_s}\left[J_{s-1}(ka_s) + J_{s+1}(ka_s)\right]\sin(pt-\gamma_s) \\ \dfrac{d\alpha_s}{dt} = \dfrac{\Omega^2-\omega_S^2}{2\omega_s} - \dfrac{F_o}{2\omega_s a_s}\left[J_{s-1}(ka_s) - J_{s+1}(ka_s)\right]\cos(pt-\gamma_s) \end{cases} \tag{7}$$

where $p = \nu - \frac{\nu}{\omega_s} \ll \omega_s$, $\gamma_s = \frac{\nu}{\omega_s}\alpha_s$, $\omega_s = \frac{v}{s}$.

In accordance with the familiar recurrence relations for Bessel functions, Eqs. (7) can be represented in the form:

$$\begin{cases} \dfrac{da_s}{dt} = -\delta_d a_s - \dfrac{vF_o}{\omega_s^2 k a_s} J_s(ka_s)\sin(pt-\gamma_s) \\ \dfrac{d\alpha_s}{dt} = \dfrac{\Omega_s^2-\omega_s^2}{2\omega_s} - \dfrac{F_o}{\omega_s a_s} J_s'(ka_s)\cos(pt-\gamma_s) \end{cases} \tag{8}$$

In the case of stationary oscillations ($\frac{da_s}{dt} = 0$ and $\frac{d\alpha_s}{dt} = 0$) from Eqs. (8) we find

$$\tan\gamma_s = \frac{2\delta_d a_s \omega_s^2 k}{(\Omega_s^2-\omega_s^2)\nu}\frac{J_s'(ka_s)}{J_s(ka_s)}$$

The connection between the intensity of the wave's longitudinal component and the amplitude of oscillations has the form:

$$F_o^2 = \left[\frac{a_{so}^2\omega_s^2\delta_d k}{vJ_s(ka_{so})}\right]^2 + \left[\frac{a_{so}(\Omega_s^2-\omega_s^2)}{2J_s'(ka_{so})}\right]^2 \tag{9}$$

For high intensities of the wave Eq. (9) can be represented as:

$$F_o \cong \frac{a_{so}^2\omega_s^2(a_s-a_{so})}{8J_s'(ka_s)}$$

The first term in formula (9) represents the minimal threshold value F_o of the wave's intensity. If the intensity of the wave is smaller than this threshold value only the excitation of forced oscillations with frequency equal to the wave's frequency is possible. For wave intensities above the threshold value depending on the initial conditions, the oscillator's motion is realized with one of the amplitudes from the discrete sequence (6). When $\nu > \omega_o$ each amplitude is realized for oscillation frequency close to the oscillator's natural frequency Ω_s. Using the approach, developed in [3], it is not difficult to show that for fixed values of the frequency ν and the amplitude F_o of the external force the oscillator's motion with amplitude from the discrete sequence (6) is stable.

The performed analysis shows that the continuous wave having a frequency much larger than the frequency of a given oscillator can excite

in it oscillations with a frequency close to its natural frequency and an amplitude belonging to a discrete set of possible stable amplitudes.

The settling of certain particular amplitude depends on the initial conditions. When the motion becomes stationary the amplitude's value practically does not depend on the wave's intensity when the latter changes over a significant range above a certain threshold value. This is reminiscent of Einstein's explanation of the photoelectric effect using Planck's quantization hypothesis. In this case the absorption is also independent of the incoming wave's intensity. Besides, the absorbed frequencies can be expressed as integer multiples of a certain basic frequency reminding of resonance phenomena.

3. General conditions for transition to irregular behavior in an oscillator under wave action

The model system under consideration is presented by the following system of equations

$$\begin{cases} \dot{x}_1 = x_2 \\ \dot{x}_2 = -\sin x_1 + \mu[F_o \sin(\theta - \rho x_1) - \delta_d x_2] \\ \dot{\theta} = v \end{cases} \tag{10}$$

where $[x_1, x_2, \theta(t)] \in \mathbb{R}^3$, the dot denotes an operation of differentiation by the time t, $F_o$and ν are correspondingly the amplitude and the frequency parameter of the external acting wave, δ_d reflects the dissipation in the system, $0 < \mu \ll 1$ is a small parameter.

Proceeding from the non-perturbed system (μ=0),

$$\dot{x}_1 = x_2, \qquad \dot{x}_2 = -\sin x_1$$

i.e. from the system with Hamiltonian function $H = \frac{x_2^2}{2} + 1 - \cos x_1$, the phase space divides into two domains and a separating boundary (separatrix), where qualitatively different phenomena occur: I domain, $0 < H < 2$; II separatrix, $H = 2$ and III domain (a regime of rotation), $H > 2$.

The solution in the so outlined domains can be presented in the form as follows.

I domain, notating $\kappa = \frac{H}{2}$:

$$\begin{cases} x_1 = 2\arcsin[\kappa\,\mathrm{sn}(t - t_o, \kappa)], & N = 0, \pm1, \pm2, \pm3, ... \\ x_2 = 2\kappa\,\mathrm{cn}(t - t_o, \kappa), & t_o = \mathrm{const} \end{cases}$$

and as well

$$\begin{cases} x_1 = -2\arcsin[\kappa\,\mathrm{sn}(t - t_o, \kappa)] + 2\pi N, \\ x_2 = -2\kappa\,\mathrm{cn}(t - t_o, \kappa), \end{cases}$$

II separatrix:

$$\begin{cases} x_1 = 2\arcsin[\tanh(t-t_o)] + 2\pi N, \\ x_2 = \dfrac{2}{\cosh(t-t_o)}, \end{cases}$$

and as well

$$\begin{cases} x_1 = -2\arcsin[\tanh(t-t_o)] + 2\pi N, \\ x_2 = -\dfrac{2}{\cosh(t-t_o)}, \end{cases}$$

III domain (a regime with rotation), notating $\kappa^2 = \frac{2}{H}$:

$$\begin{cases} x_1 = 2\arcsin\left[\mathrm{sn}\left(\dfrac{t-t_o}{\kappa}, \kappa\right)\right] + 2\pi N, \\ x_2 = \dfrac{2}{\kappa}\,\mathrm{dn}\left(\dfrac{t-t_o}{\kappa}, \kappa\right), \end{cases}$$

and as well

$$\begin{cases} x_1 = -2\arcsin\left[\mathrm{sn}\left(\dfrac{t-t_o}{\kappa}, \kappa\right)\right] + 2\pi N, \\ x_2 = -\dfrac{2}{\kappa}\,\mathrm{dn}\left(\dfrac{t-t_o}{\kappa}, \kappa\right). \end{cases}$$

Let us consider the system dynamics in the domain of the separatrix (the homoclinic trajectory). We work with the solution

$$x_o = \begin{pmatrix} x_{o1} \\ x_{o2} \end{pmatrix} = \begin{pmatrix} 2\arcsin[\tanh(t-t_o)] \\ 2/\cosh(t-t_o) \end{pmatrix}.$$

We can write

$$\begin{aligned} \frac{d}{dt}x &\equiv \begin{pmatrix} dx_1/dt \\ dx_2/dt \end{pmatrix} = f_o(x) + \mu f_1(x,t) \\ &\equiv \begin{pmatrix} x_2 \\ -\sin x_{o1} \end{pmatrix} + \mu \begin{pmatrix} 0 \\ F_o\sin(\theta - \rho x_1) - \delta_d x_2 \end{pmatrix}, \end{aligned}$$

where in the right-hand side of the equation the initial approximation stands $x_o = \begin{pmatrix} x_{o1} \\ x_{o2} \end{pmatrix}$ for $x_1 = \begin{pmatrix} x_1 \\ x_2 \end{pmatrix}$. Hence

$$\begin{aligned} f_o \times f_1 \equiv f_o \wedge f_1 &= \begin{pmatrix} x_{o2} \\ -\sin x_{o1} \end{pmatrix} \wedge \begin{pmatrix} 0 \\ F_o\sin(\theta - \rho x_{o1}) - \delta_d x_{o2} \end{pmatrix} \\ &= \frac{2F_o}{\cosh(t-t_o)}\sin\{\theta - 2\rho\arcsin[\tanh(t-t_o)]\} - \frac{4\delta_d}{\cosh^2(t-t_o)}. \end{aligned}$$

For the system under consideration the Melnikov distance [6] can be expressed:

$$D(t_o,t_o) = -\int\limits_{-\infty}^{\infty} f_o \wedge f_1 dt = \int\limits_{-\infty}^{\infty} \left\{ \frac{2F_o}{\cosh(t-t_o)} \right.$$
$$\left. \times \sin\left[\theta - 2\rho \arcsin\left(\tanh(t-t_o)\right)\right] + \frac{4\delta_d}{\cosh^2(t-t_o)} \right\} dt \quad (11)$$

Irregular (chaotic) behaviour occurs for the areas where $D(t_o,t_o)$ passes through zero. For the practice the case of $\rho = 1$ is the most interesting.

Substituting θ as $\theta = \nu t + \theta_o = \nu(t-t_o) + (\nu t_o + \theta_o)$, Eq. (11) becomes

$$D(t_o,t_o) = \int\limits_{-\infty}^{\infty} \left\{ -\frac{2F_o}{\cosh(t)} \sin[\nu t + (\nu t_o + \theta_o)][1 - 2\tanh^2(t)] \right.$$
$$\left. + \frac{2F_o}{\cosh(t)} \cos[\nu t + (\nu t_o + \theta_o)] \frac{2\sinh(t)}{\cosh^2(t)} + \frac{4\delta_d}{\cosh^2(t)} \right\} dt$$
$$= -2F_o \sin(\nu t_o + \theta_o) \int\limits_{-\infty}^{\infty} \cos\nu\tau \frac{(1-\sinh^2\tau)}{\cosh^3\tau} d\tau$$
$$-2F_o \sin(\nu t_o + \theta_o)^2 \int\limits_{-\infty}^{\infty} \sin\nu\tau \frac{\sinh\tau}{\cosh^3\tau} d\tau + 4\delta_d \int\limits_{-\infty}^{\infty} \frac{d\tau}{\cosh^2\tau} \quad (12)$$

The integrals in (12) are evaluated as follows:

$$\int\limits_{-\infty}^{\infty} \cos\nu\tau \frac{(1-\sinh^2\tau)}{\cosh^3\tau} d\tau = \frac{\nu^2\pi}{\cosh\frac{\nu\pi}{2}},$$
$$\int\limits_{-\infty}^{\infty} \sin\nu\tau \frac{\sinh\tau}{\cosh^3\tau} d\tau = \frac{\nu^2\pi}{2\sinh\frac{\nu\pi}{2}}, \qquad \int\limits_{-\infty}^{\infty} \frac{d\tau}{\cosh^2\tau} = 2$$

According to these expressions Eq. (12) is rewritten as

$$D(t_o,t_o) = -2\pi\nu^2 F_o \left(\frac{1}{\cosh\frac{\nu\pi}{2}} + \frac{1}{\sinh\frac{\nu\pi}{2}} \right) \sin(\nu t_o + \theta_o) + 8\delta_d$$

or finally

$$D(t_o,t_o) = -\frac{4\pi\nu^2 F_o e^{\nu\frac{\pi}{2}}}{\sinh\nu\pi} \sin(\nu t_o + \theta_o) + 8\delta_d.$$

Under the condition $D(t_o, t_o) = 0$ and taking into account that $\delta_d > 0$ and $|\sin(\nu t_o + \theta_o)| < 1$, the general condition for transmission to irregular (chaotic) behaviour in nonlinear oscillator under the wave action takes the form

$$2\delta_d \sinh(|\nu|\,\pi) < \pi\nu^2\,|F_o|\,e^{\nu\frac{\pi}{2}}.$$

Obviously this condition is fulfilled in some domains of the space (δ_d, F_o, ν).

It is necessary to note that the solution of Eq. (10) strongly depends on the choice of initial conditions. Besides, the homoclinic bifurcation is one of the first bifurcations that occur in the transition from regular to irregular motion in the system under consideration. The latter is related with the condition for overcoming the strong self-adaptive mechanism of the system internal stability [1-3]. It is necessary also to emphasis that the homoclinic tangency implies formation of a very complicated fractal boundary for the basins of attraction [1, 5].

4. Conclusion

The analysis shows the following two essential features of the system considered.

1. There exists a discrete set of possible stationary stable amplitudes.

2. There exists a threshold value for the amplitude such that for values above it the discrete states are stable.

Regardless of its simplicity, the "oscillator-wave" model obviously reflects a number of processes in the micro- and macroworld. The model is manifested naturally in different material media and harmonizes with the modern ideas about the world into and out of us as a totality of particles and fields. Also, it takes into account the wide extension of the oscillating processes in Nature. In the presence of particle flows and fields of different nature, the model realizes (materializes) widely in Nature in a very natural way. In one way or another, the model has been considered by a number of authors, but the most essential feature of behaviour – the "quantization" phenomenon, has escaped their attention.

References

[1] V.N. Damgov. Nonlinear and Parametric Phenomena in Radio-Physical Systems". "Prof. Marin Drinov" Academic Publishers, Sofia, 2000.

[2] V. Damgov and Pl. Trenchev. Class of Kick-Excited Self-Adaptive Dynamical Systems: "Quantized" Oscillation Excitation. - "Chaos, Solitons and Fractals", Oxford 2003, vol. 17, No 1, pp. 11-40.

[3] V.N. Damgov and I. Popov. "Discrete" Oscillations and Multiple Attractors in Kick-Excited Systems. Discrete Dynamics in Nature and Society (International Multidisciplinary Research and Review Journal), vol.4, pp. 99-124, (2000)

[4] V.N. Damgov, Modeling Systems and Mechanisms of Oscillation Excitation. Earth, Moon and Planets 61, 87-117 (1993)

[5] V.N. Damgov, and D. B. Douboshinsky, The Wave Nature and Dynamical Quantization of the Solar System. Earth, Moon and Planets, 1992, v.56, No.2, pp. 233-242

[6] A. J. Lichtenberg and M.A. Liberman, Regular and Stochastic Motion, Springer-Verlag, New York (1983)

II

BOSE-EINSTEIN CONDENSATES AND MATTER WAVES

BOSE-EINSTEIN CONDENSATION: THE ODD NONLINEAR QUANTUM MECHANICS

L.P. Pitaevskii

Dipartimento di Fisica, Università di Trento and Istituto Nazionale per la Fisica della Materia, CRS-BEC, 38050 Trento, Italy, and Kapitza Institute for Physical Problems, 119334 Moscow, Russia.

Abstract The non-linear Gross-Pitaevskii (GP) equation plays an important role in the mean-field theory of the Bose-Einstein condensation and has interesting mathematical properties. In this lecture we consider two non-trivial problems related to physical interpretation of the solutions of the GP equation: the superfluidity of a BEC gas in an optical lattice and the superfluidity of a 1D Bose-gas, with special attention to the role of grey solitons.

1. Introduction

In this lecture we consider the behavior of Bose-Einstein condensates (BEC) in external periodic potentials, created by light beams of laser sources.

A quantum-mechanical description of particles in a periodic field was developed many years ago by F. Bloch. Most of the experiments into past, however, were done with fermions, i.e. electrons in the periodic lattice of crystals.

In the case of condensates made of cold trapped atoms, the periodic potential can be created by using light (laser) beams. With respect to "natural" lattices, this "artificial" optical potential has many advantages: its period is macroscopically large and can be varied, its intensity can be varied and it has no defects, it is possible to create one- and two-dimensional structures, which are difficult to build in solids.

F. Kh. Abdullaev and V. V. Konotop (eds.), Nonlinear Waves: Classical and Quantum Aspects, 175–192.

2. Optical lattice

Let us consider a condensate in a monochromatic electric field. One can write the field in the form

$$\mathbf{E}(\mathbf{r},t) = \mathbf{E}_0(\mathbf{r})e^{-i\omega t} + c.c. \,. \tag{1}$$

The averaged (with respect to time) force acting on an atom is

$$\mathbf{f}(\mathbf{r}) = \frac{\alpha(\omega)}{2}\nabla\overline{E^2} = \alpha(\omega)\nabla|E_0|^2, \tag{2}$$

where $\alpha(\omega)$ - is the atomic polarizability and $\overline{E^2}$ is the time average of E^2. This equation is valid if the frequency ω is far enough from the absorption line of the atom at frequency ω_0. Then $\alpha(\omega)$ is real. On the other hand, it is profitable to work near enough to ω_0, where polarizability is large. Thus the frequency must satisfy the conditions

$$\omega_0 \gg |\omega - \omega_0| \gg \Gamma, \tag{3}$$

where Γ is the absorption line width. Notice, that BEC is convenient from this point of view, because absorption lines in the condensate are very narrow.

Under the condition (3) the polarizability can be approximately written as

$$\alpha(\omega) \approx \frac{A}{\omega_0 - \omega}, \tag{4}$$

with $A > 0$. This means that for $\omega < \omega_0$ ("red detuning") atoms are driven into strong field regions, while for $\omega > \omega_0$ ("blue detuning") they attracted into low field regions.

The force (2) corresponds to the mean potential energy:

$$U_{opt}(\mathbf{r}) = -\alpha(\omega)|E_0|^2. \tag{5}$$

One can create a one-dimensional (1D) periodic potential by using a standing laser wave. In such a wave $|E_0|^2 \sim \sin^2(qz)$, where q is the wave vector. In this case one usually writes the potential energy as

$$U_{opt}(z) = sE_r \sin^2(qz) \,, \tag{6}$$

where s is a dimensionless parameter, proportional to the intensity of the laser beam, and E_r is the "recoil energy", i.e. the energy acquired by an atom of mass m after absorbing a photon with momentum $\hbar q$:

$$E_r = \frac{\hbar^2 q^2}{2m} \,. \tag{7}$$

In most of the recent experiments one has $s < 20$. The potential (6) is periodic with period $d = \pi/q$. Correspondingly, the period of reciprocal lattice is $2q$. A three-dimensional optical lattice can be created by three standing laser waves in the three directions of space:

$$U_{opt}(\mathbf{r}) = sE_r[\sin^2(qx) + \sin^2(qy) + \sin^2(qz)] \; . \tag{8}$$

3. Bose-Einstein condensate in a periodic lattice. Ground state

A Bose-Einstein condensed system is characterized by the presence of a macroscopically large number of atoms in one quantum state. Let us consider the second quantization operator of atoms $\hat{\psi}(r,t)$. Its quantum properties are expressed by the commutation relation

$$\hat{\psi}(\mathbf{r},t)\hat{\psi}^{\dagger}(\mathbf{r}',t) - \hat{\psi}^{\dagger}(\mathbf{r}',t)\hat{\psi}(\mathbf{r},t) = \delta\left(\mathbf{r}-\mathbf{r}'\right). \tag{9}$$

Let us separate from $\hat{\psi}(r,t)$ the part $\hat{\psi}_0(r,t)$, which corresponds to annihilation of atoms in the macroscopically occupied state, where the condensation occurs. Matrix elements of $\hat{\psi}_0$ are macroscopically large. This means that one can neglect the non-commutativity of $\hat{\psi}_0$ and $\hat{\psi}_0^{\dagger}$ and replace $\hat{\psi}_0$ with a classical field $\psi_0(r,t)$. The function $\psi_0(r,t)$ is called the order parameter or the wave function of the condensate. This procedure has a deep physical meaning. In fact this replacement is analogous to the transition from quantum electrodynamics to the classical description of electromagnetism. We know that this is justified if one has a big number of photons in approximately the same quantum state. In this case the non-commutativity of the field operators is not important and one can describe the electromagnetic field using classical functions, i.e. the electric and the magnetic fields, which obey the Maxwell equations. In our case the presence of a big number of atoms in a single state (Bose-Einstein condensate) permits to introduce the classical function $\psi_0(r,t)$. (We will omit the index "0" below.)

If the gas is dilute enough, it can be described with good accuracy by the mean-field approximation. This corresponds to the lower order approximation of the Bogoliubov theory of a uniform dilute Bose-gas [1]. In this approximation all atoms are in the condensate at $T = 0$. Thus the gas density is

$$n(\mathbf{r},t) = |\psi(\mathbf{r},t)|^2. \tag{10}$$

The function $\psi(r,t)$ satisfies the non-linear equation [2, 3]

$$i\hbar\frac{\partial}{\partial t}\psi(\mathbf{r},t) = \left(-\frac{\hbar^2\nabla^2}{2m} + V_{ext}(\mathbf{r},t) + g \mid \psi(\mathbf{r},t) \mid^2\right)\psi(\mathbf{r},t) \; . \tag{11}$$

The non-linear term in this equation describes the interaction between of atoms of the condensate. The coupling constant g is fixed by the s-wave scattering length a through:

$$g = 4\pi\hbar^2 a/m \quad . \tag{12}$$

It is possible to say that the atom moves in a mean field, created by other atoms, which is proportional to the density.

Equation (11) for the condensate wave function ψ plays a role analogous to the Maxwell equations in classical electrodynamics. One can say that the condensate wave function represents the classical limit of the de Broglie wave , where the corpuscular aspect of matter is no longer important. Still, differently from the Maxwell equations, Eq.(11) contains the quantum constant $\hbar$ explicitly. The reason for this difference is due to the different relation between energy ϵ and momentum p in the case of photons and atoms, which implies a different relation between the frequency $\omega = \epsilon/\hbar$ and the wave vector $k = p/\hbar$ of the corresponding classical waves. For photons the relation $\epsilon = cp$ provides the classical dispersion relation $\omega = ck$. For atoms the relation $\epsilon = p^2/2m$ instead yields the dispersion law $\omega = \hbar k^2/2m$, containing explicitly $\hbar$. This implies, in particular, that the coherence phenomena, like interference, depend on the value of the Planck constant.

The condensate function is a complex one, $\psi = |\psi|\, e^{i\varphi}$, and its phase φ defines the superfluid velocity:

$$\mathbf{v}_s = \frac{\hbar}{m}\nabla\varphi. \tag{13}$$

In a stationary state the wave function depends on time according to $\psi(\mathbf{r}, t) = \psi(\mathbf{r}) \exp(-i\mu t/\hbar)$, where μ is the chemical potential for a given state.

In this paper we consider mainly the 1D potential (6). Thus we assume that ψ has the form $\psi(z) \exp(-i\mu t/\hbar)$. In real experiments, of course, besides the periodic potential, there exists a magnetic trapping potential. However, the trapping in the z-direction is weak and the size of the condensate in this direction is large with compared to the lattice period d. The trapping potential changes slowly on the distance d and we can neglect this axial trapping in first approximation. On the contrary, the "radial" trapping in x and y directions is tight and the radial degrees of freedom are never excited. The wave function can be presented in the form $\psi(\mathbf{r}, t) = \psi_r(r)\psi(z) \exp(-i\mu t/\hbar)$. We will choose $\psi_r(r)$ in a such way that $|\psi(z)|^2 = n(z)$ is the 1D atom density, i.e. the number of

atoms per unit length. Then equation (11) for $\psi(z)$ becomes

$$\left(-\frac{\hbar^2}{2m}\frac{d^2}{dz^2} + sE_r \sin^2(qz) + g_1 \mid \psi(z) \mid^2\right)\psi(z) = \mu\psi(z) \tag{14}$$

where g_1 now is the new "one dimensional" coupling constant, which is proportional to the "three-dimensional "coupling constant g (see [4], § 17.2 for details).

The state,ground wave function is real and periodic, $\psi_0(z) = \psi_0(z+d)$. It can be expanded as a Fourier series:

$$\psi_0(x) = \sum_{l=-\infty}^{\infty} \psi^{(l)} e^{il2qz}, \quad \psi^{(l)} = \psi^{(-l)*} . \tag{15}$$

Equation (15) is an expansion of the ground state with respect to states with values of momenta $p_l = \hbar 2ql$. This statement is well-known in the theory of electrons in a crystal lattice. But it is difficult to check it experimentally in a solid crystal. Conversely, in BEC equation (15) can be checked in direct and relatively simple experiments. It is enough to switch off both trapping and periodic potentials. Then atoms with $l = 0$ will stay at rest. Atoms with p_l will move according to the law

$$z_l(t) = \frac{\hbar l 2q}{m} t . \tag{16}$$

Such an experiment is described in [5]. In Fig. 1 one can see the central peak with $l = 0$ and "split" condensates with $l = \pm 1$. The relative population of the P_1 peaks according to (15) is $|\psi^{(1)}|^2/|\psi^{(0)}|^2$. This ratio depends on the intensity s of the periodic potential and, due to the interactions, on the gas density (see Fig. 2).

4. Quasi-momentum and current.

A system of interactive Bose-Einstein condensed bosons is superfluid. It can move relative to the lattice without friction. The flow as a whole can be described by the "Bloch-like" solutions of (14):

$$\psi_{kb}(z) = e^{ikz} u_{kb}(z) . \tag{17}$$

Here $\hbar k$ is the quasi-momentum, b - the Bloch band index. The function $u_{kb}(z)$ is a complex periodic function of period d. Notice, that the existence of solution of the form (17) of the non-linear equation (14) is quite non-trivial. It is related to the gauge invariance of (14).

The chemical potential, corresponding to the solution (17), is also a function of k and b: $\mu = \mu_b(k)$. (We will omit the Bloch band index b

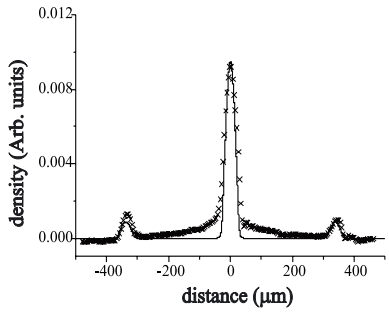

Figure 1. The density profile for the expanded array of condensates for $s = 5$ and $t = 29.5$ ms. From [5].

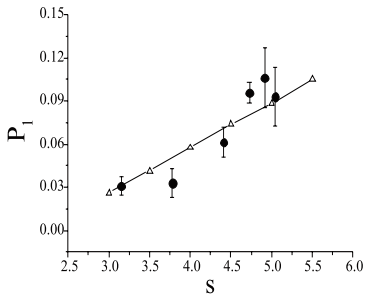

Figure 2. Experimental (solid circles) and theoretical (triangles) values of the population of the $l = 1$ peak with respect to $l = 0$ central peak. From [5].

below.) The ground state energy can be calculated by using the wave function (17). The energy per unit length is

$$E(k) = \frac{1}{L}\int_0^L \left(\frac{\hbar^2}{2m}\left|\frac{d\psi_k}{dz}\right|^2 + sE_r \sin^2(qz) \mid \psi_k \mid^2 + \frac{g_1}{2} \mid \psi_k \mid^4 \right) dz\,, \tag{18}$$

where $\mu(k) = \partial E(k)/\partial n$, $n = N/L$ is the number of atoms per unit of length, L is the lattice length, N is the total number of atoms. Instead the energy $E(k)$ it is sometimes convenient to use the grand canonical energy

$$E_\mu(k) = E(k) - \mu(k)n = E(k) - \mu(k)\int_0^L \mid \psi_k(z) \mid^2 dz/L\,. \tag{19}$$

Then $n = -\partial E_\mu(k)/\partial\mu$. One can obtain the GP equation (14) by minimizing either the functional E with respect ψ at constant n, or the functional E_μ at constant μ.

Let recall that values of k differing by $n2q$, with n integer, are physically equivalent. This means that k can be restricted to the first Brillouin zone: $-q < k < q$. However, it is convenient sometimes not to restrict k to the first zone and to allow k to take arbitrary values by treating $E(k)$ (and $j(k)$ below) as periodic functions with period $2q = 2\pi\hbar/d$.

The wave functions (17) describe stationary states of the system corresponding to a moving condensate. The mass current associated with this motion can be obtained from (11). It has the usual form, the non-linear

term playing no role. In the 1D case one has:

$$j = \frac{i\hbar}{2}\left(\psi\frac{d\psi^*}{dz} - \psi^*\frac{d\psi}{dz}\right) . \tag{20}$$

The current j is constant in a stationary state and does not depend on t and z.

One can calculate j for the Bloch function (17), if one knows the energy $E(k)$. To this aim, let us replace in (14) and in the energy functional (19) the operator $\frac{d}{dz}$ with $\frac{d}{dz} - iA$, where A a constant "vector-potential". Then differentiation gives

$$-m\left[\frac{\partial E_\mu}{\partial \hbar A}\right]_{A=0,\mu} = \frac{i\hbar}{2L}\int_0^L \left[\psi\frac{d\psi^*}{dz} - \psi^*\frac{d\psi}{dz}\right] dz = j . \tag{21}$$

It is important here that one needs not to differentiate wave function ψ. The wave function depends on A, however the variation of the functional with respect to ψ is equal to zero due to (14).

The constant term A in the equation does not change its periodic properties and the modified wave function $\psi(z, A)$ still has the Bloch form. However, one can eliminate the constant A by a guage transformation:

$$\psi = e^{iAz}\psi' . \tag{22}$$

This means, that the modified equation has the same dispersion law $E_\mu(k')$, where $\hbar k'$ is the quasi-momentum corresponding to ψ'. It is obvious from (22) that $\psi(z, A)$ has quasi-momentum $\hbar k = \hbar(k' + A)$. Thus $E_\mu(k, A) = E_\mu(k - A)$ and (21) gives for the current:

$$j(k) = m\left(\frac{\partial E_\mu}{\hbar \partial k}\right)_\mu = m\left(\frac{\partial E}{\hbar \partial k}\right)_n . \tag{23}$$

This equation is well-known in the theory of metals. However its usual derivation is based on the linear Schrödinger equation. It is not clear in the linear theory if the mass current j is defined by $E(k)$ or $\mu(k)$, because in a such theory $E = n\mu$. Therefore we presented here a different derivation, based on the gauge invariance of the Gross-Pitaevskii equation (11). This derivation, of course, is valid also for the linear Schrödinger equation.

It is useful to rewrite (23) in terms of the "group velocity"

$$v_g(k) \equiv \frac{1}{\rho}j(k) = \frac{1}{n}\left(\frac{\partial E}{\partial \hbar k}\right)_n , \tag{24}$$

where $\rho = mn$ is the mean linear mass density. One can find examples of calculations $E_b(k)$ and $v_g(k)$ in [6] (see Fig. 3).

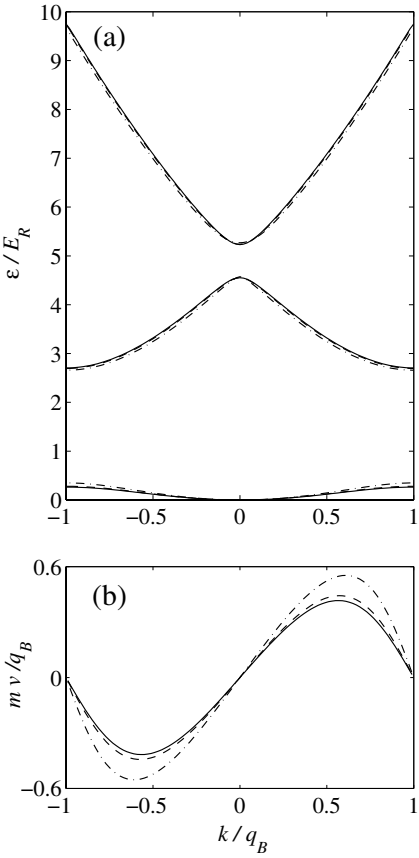

Figure 3 (a) Energy per atom $\epsilon = E(p)/N$ as a function of quasi-momentum p in the three first Bloch bands for $s = 3$, $q_B = \pi/d$. (b) Group velocity in the first Bloch band. From [6].

Equation (23) defines the mass current in the coordinate frame of the lattice. If the lattice moves with velocity v_L, then the mass current in the laboratory frame is given by the general Galileo's transformation:

$$j_{lab} = j(k) + \rho v_L \ . \tag{25}$$

Let us consider now the condensate in the lattice in the presence of a weak spatially uniform force F. In the r.h.s. of eq. (11) one must add a term $-Fz\psi(z,t)$. Even at small F, this term strongly modifies the solution because of its unrestricted increasing at large z. In order to compensate this term, one can look for a solution of (11) in the form of the Bloch function (17), but with a time-dependent quasi-momentum $\hbar k$. Then the term $-\hbar\frac{dk}{dt}z\psi(z,t)$ will appear in the l.h.s. of eq. (11). Both terms in eq. (11) proportional to z will cancel if

$$\frac{d\hbar k}{dt} = F \ . \tag{26}$$

Notice that one needs not to differentiate the periodic part $u_{kr}(z)$ of the Bloch function (17), since the corresponding terms do not contain z and are negligible at small F. Equation (26) again has the same form as in the linear one-particle theory.

The above equations allow one to define the function $v_g(k)$ in a direct experiment [7]. In the experiment, the lattice can be put into motion by detunning the frequencies of two laser beams in the standing wave. In the difference in frequencies is $\delta\omega(t)$, then the lattice moves with the time-dependent velocity $v_L(t) = \delta\omega(t)/q$. In the coordinate frame of the lattice the force of inertia $F = -mdv_L/dt$ acts on the condensate. According to equation (26) the condensate acquires the quasi-momentum

$$\hbar k = -mv_L(t) \; . \tag{27}$$

Then one can switch-off the trap and lattice potential and measure the mean velocity of the condensate, which according to (25) is given by

$$v_m \equiv j_{lab}/\rho = v_L - v_g(mv_L/\hbar) \; . \tag{28}$$

By repeating the experiment for different values of the final velocity v_L, one can extract the $v_g(k)$ function function (see Fig. 4).

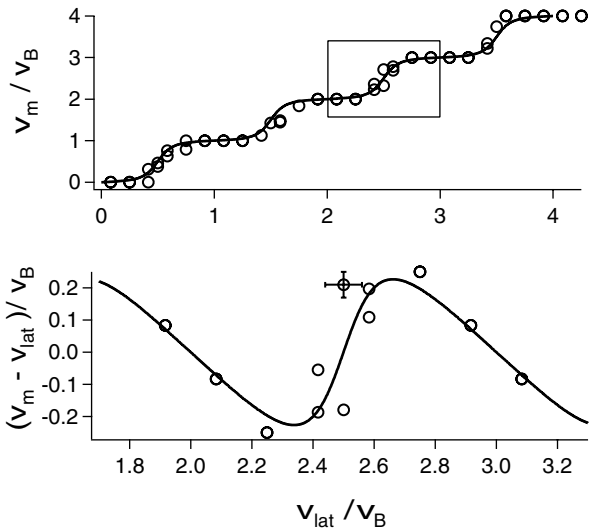

Figure 4. (a) Mean velocity v_m in the laboratory frame as a function of the lattice velocity $v_L \equiv v_{\rm lat}$. (b) Mean velocity $v_m - v_L$ in the rest frame of the lattice as a function of v_L. $v_B = 2\pi\hbar/md$. The solid lines are the theoretical curves for the first Bloch band. From [7].

For small values k one can expand $E(k)$ as

$$E(k) = E_0 + n\frac{\hbar^2 k^2}{2m^*} \ . \tag{29}$$

The quantity m^* has the meaning of the effective mass of the condensate in the lattice. Correspondingly one has

$$v_g(k) = \frac{\hbar}{m^*}k \ . \tag{30}$$

It is not difficult to show that $m^* > m$ in the first Bloch zone. In the next section we will see , that m^* defines the superfluid fraction of the gas.

The chemical potential can be expanded analogously:

$$\mu(k) = \mu_0 + \frac{\hbar^2 k^2}{2m_\mu} \ , \tag{31}$$

where

$$\mu_0 = \frac{\partial E_0}{\partial n}, \quad \frac{1}{m_\mu} = \frac{\partial}{\partial n}\frac{n}{m^*} \ . \tag{32}$$

5. Superfluid density

According to the Landau theory of superfluidity [8], an uniform superfluid at $T = 0$ is "completely superfluid", i.e. the superfluid density is equal to the total density: $\rho_s = \rho$. This is not true for a liquid in inhomogeneous external conditions, for example in the presence of impurities or, as in our case, in the presence of a periodic potential. One has now $\rho_s < \rho$ even at $T = 0$. However, the meaning of this inequality at $T = 0$ is different from the finite temperature case. The normal part density $\rho_n = \rho - \rho_s$ is at rest with respect to the lattice. It is thus meaningless to introduce the normal fluid velocity.

In the Landau theory, the superfluid part is "something that cannot rotate". This results in the following definition of the superfluid density. Let the lattice be "twisted" in a ring of a large radius R. Let the ring slowly rotate with the angular velocity Ω. Then the angular momentum of a normal fluid would be $M = \rho 2\pi R^2 \Omega$. If the fluid is superfluid, then only the normal part rotates and the angular momentum is

$$M = \rho_n 2\pi R^2 \Omega = (\rho - \rho_s)2\pi R^2 \Omega \ . \tag{33}$$

Notice that Andronikashvili measured the superfluid density of superfluid ^{4}He just in the same type of experiment. In [9] ρ_s was measured by this method in inhomogeneous systems of ^{4}He films on Vycor substrate.

To calculate ρ_s for a gas in a lattice we need the Galileo's transformation of the condensate wave function. Let $\psi(z,t) = \psi_k(z)\, e^{-i\mu t/\hbar}$ be the wave function in the lattice frame. Then the wave function in the laboratory frame, where the lattice moves with velocity v_L, is

$$\psi_{lab}(z,t) = e^{imv_L z/\hbar}\psi(z - v_L t, t)\, e^{-imv_L^2 t/2\hbar} \tag{34}$$

(see [10], problem to §17). It is not difficult to check that function (34) satisfies eq. (11) if $\psi_k(z)$ is a solution of eq. (14).

Using equation (17) for ψ_k one finds

$$\psi_{lab}(z,t) = e^{i(k+mv_L/\hbar)z} u_k(z - v_L t) e^{-i[\mu(k)+\hbar k v_L + mv_L^2/2]t/\hbar}\,. \tag{35}$$

Now, let us twist the lattice in a ring. If the radius of the ring R is large enough, one can use (35). In this case z is the coordinate along the ring and $v_L = \Omega R$. To be single-valued, the wave function must be periodic with respect to z:

$$\psi_{lab}(z,t) = \psi_{lab}(z + 2\pi R, t)\ . \tag{36}$$

According to (34) this gives

$$(k + mv_L/\hbar)\, 2\pi R = 2\pi l, \quad l = 0, \pm 1, \ldots\,. \tag{37}$$

In the absence of rotation $l = 0$. This condition must be satisfied also at slow rotation. This gives $\hbar k = -mv_L$, analogously to (27). The mass current can be calculated using (25). Thus at low speed of rotation one has

$$j_{lab} = mnv_L + \frac{m}{\hbar}\left[\frac{\partial E(k)}{\partial k}\right]_{k=-mv_L/\hbar} \approx mnv_L\left(1 - \frac{m}{m^*}\right)\,, \tag{38}$$

and the angular momentum is

$$M = j_{lab} 2\pi R = mn\Omega 2\pi R^2\left(1 - \frac{m}{m^*}\right)\ . \tag{39}$$

The comparison with (33) finally gives the superfluid density

$$\rho_s = mn\frac{m}{m^*} = \rho\frac{m}{m^*}\ . \tag{40}$$

Let us go back to the lattice frame. Equation ρ_s permits to define the superfluid velocity through the formula $j = \rho_s v_s$ which yields

$$v_s = \frac{\hbar}{m}k\,. \tag{41}$$

Equation (40) for the superfluid density has been obtained in a different way in [11] and [12], devoted to properties of superfluid ^{4}He films. However, the authors of the recent papers [13] and [14] claimed that $\rho_s = \rho$ in the absence of interaction. This contradicts (40), inasmuch $m^* \neq m$ also in the absence of interaction [15]. This disagreement motivated us to investigate the problem more carefully. Our result, as we have already mentioned, coincides with [11] and [12]. The disagreement with [13] and [14] is, in our opinion, a result of an arbitrary identification the effective mass of the Bose-Habbard Hamiltonian with free particle mass, made in these papers.

The first experimental confirmation of equation (40) was given in the experiments [16]. The authors observed oscillations of the condensate, confined in a harmonic magnetic trap in the presence of a periodic optical potential. To describe this phenomenon one should develop the theory a bit further.

The wave vector k in the solution (17) is constant. However, one can consider an approximate solution of the form:

$$\psi(z,t) = e^{i\phi(z,t)} u_{k=d\phi/dx}(z) \; , \tag{42}$$

where the phase $\phi(z,t)$ changes slowly on distances of the order of lattice period d. Equation (41) for the superfluid velocity then the form

$$v_s = \frac{\hbar}{m} \frac{\partial}{\partial z} \phi \; . \tag{43}$$

One can derive equations for the density ρ and the superfluid velocity v_s following the Landau considerations [8]. However, one should take into account that in our case the velocity and entropy of the normal part are equal to zero.

The continuity equation is

$$\frac{\partial \rho}{\partial t} + \frac{\partial (\rho_s v_s)}{\partial z} = 0 \; . \tag{44}$$

We write the equation of motion for the superfluid part by assuming that, besides the periodic potential, there is a slowly varying trapping potential $U_{ext}(z)$. Then

$$\frac{\partial v_s}{\partial t} + \frac{\partial}{\partial z} \left[\frac{m}{m_\mu} \frac{v_s^2}{2} + \mu_0(n) + U_{ext}(z) \right] = 0 \; , \tag{45}$$

where we neglected terms of order higher that v_s^2.

With the help of these equations let us consider the oscillations of a condensate as in the experiments [16]. The trapping potential is harmonic, $U_{ext}(z) = m\omega_z^2 z^2/2$. We assume that the effective mass m^* does

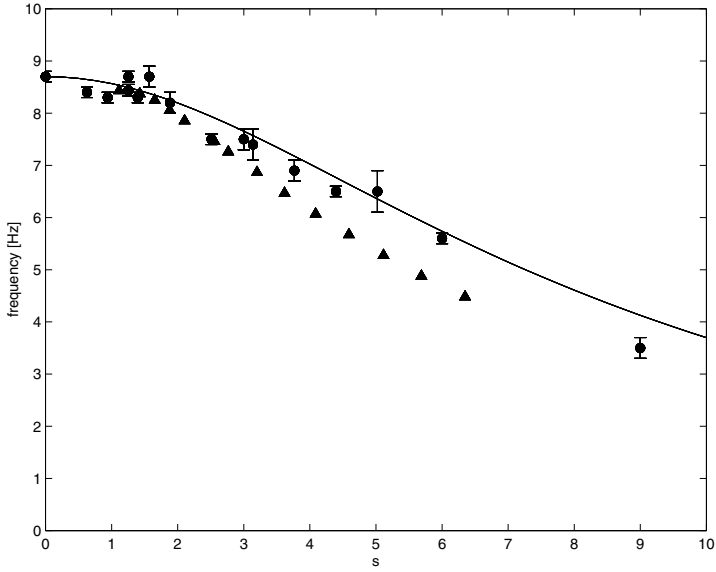

Figure 5. Frequency of the dipole oscillations as a function of the amplitude s of the periodic potential. The solid circles and triangles are, correspondingly, the experimental and theoretical data of [16]. The solid line is the calculations of [17].

not depend on density and therefore on coordinate and time. (In the experiment these dependencies are not important indeed.) Then the linearized system (44) - (45) has solution of the form $\rho(z,t) = \rho_0(z - z_0(t))$, describing oscillations of the condensate as a whole with velocity dz_0/dt. Here $\rho_0(z)$ is the equilibrium density profile of the condensate. It satisfies the equation $\frac{\partial}{\partial z}\left[\mu_0[\rho_0(z)] + U_{ext}(z)\right] = 0$. Equations (44) - (45) then give

$$\frac{dz_0}{dt} = \frac{m}{m^*} v_s \ , \quad \frac{dv_s}{dt} = -m\omega_z^2 z_0 \ . \tag{46}$$

The first equation means that the condensate moves with group velocity $(m/m^*)v_s = v_g$, and not with the superfluid velocity v_s. The frequency of these "dipole" oscillations according to (46) is [16]

$$\omega_D = \sqrt{\frac{m}{m^*}}\omega_z \ . \tag{47}$$

Results of measurements [16] are reported in Fig. 5. The frequency of the dipole oscillations is presented as a function of the amplitude s of the periodic potential and compared with the prediction of equation (47). The values of the effective mass have been calculated in [17].

Notice that, at the maximal value $s = 9$, the ratio m/m^* is about 6. In these conditions atoms can only move by tunneling through the

potential barriers, that separate the minima of the periodic potential. Thus in the experiments the quantum tunneling of a macroscopical body is observed.

The superfluid nature of the condensate is important here. The thermal cloud can not oscillate in such conditions.

6. Solitons and superfluidity in a one-dimensional Bose-gas

6.1 Grey solitons

Let us consider the one-dimensional (1D) GP equation in the absence of periodic potential:

$$\left(-\frac{\hbar^2}{2m}\frac{d^2}{dz^2} + g_1 \mid \psi(z) \mid^2\right)\psi(z) = \mu\psi(z)\ . \tag{48}$$

This equation has an important class of solutions, so called *grey solitons,* that are localized regions of suppressed density moving with constant velocity. Such solitons have been found by Tsuzuki [19]. The corresponding wave function has the form

$$\psi\left(z - vt\right) = \sqrt{n}\left(i\frac{v}{c} + \sqrt{1 - \frac{v^2}{c^2}}\tanh\left[\frac{z - vt}{\sqrt{2}\xi}\sqrt{1 - \frac{v^2}{c^2}}\right]\right) \tag{49}$$

where the velocity v is a parameter defining the solution, $c = \sqrt{g_1 n/m}$ is the sound velocity and $\xi = \hbar/\left(\sqrt{2}mc\right)$ is the "healing length". The density has a minimum at $z = vt$ corresponding to $n_0 = 1/\sqrt{1 - v^2/c}$ and tends to its equilibrium value n at $z \to \pm\infty$. However, the phase of the wave function undergoes a finite change

$$\Delta\varphi = 2\arccos\left(v/c\right) \tag{50}$$

as z varies from $-\infty$ to ∞. The energy of the soliton, calculated with help of (19) is

$$\epsilon = \frac{4}{3}\hbar c n\left(1 - \frac{v^2}{c^2}\right)^{3/2}\ . \tag{51}$$

The problem of the soliton momentum is not trivial. The velocity of soliton at rest should satisfy the canonical equation $v = \partial\varepsilon/\partial p$. Integrating this equation and assuming that $p = 0$ for a rested soliton, one find

$$p = \int_0^v \frac{\partial\epsilon}{\partial v}\frac{d\left(v\right)}{v} = -2\hbar n\left(\frac{v}{c}\sqrt{1 - v^2/c^2} + \arcsin\left(v/c\right)\right). \tag{52}$$

This is a "canonical" momentum, which must be considered as the momentum of a soliton which is treated as an elementary excitation in the Landau meaning. However, p does not coincide with the total momentum of liquid, which is defined as $\tilde{p} = \int\limits_{-\infty}^{\infty} j dz$ with j given in (20). In fact, one finds $\tilde{p} = -2\hbar n(v/c)\sqrt{1 - v^2/c^2}$[20]. For small v (52) gives $p \approx -4\hbar n v/c$, while for $v \to \pm c$ one obtains $p \approx \mp(\pi\hbar n - \varepsilon/c)$. Notice that p runs over the interval

$$-\pi\hbar n \leq p \leq \pi\hbar n. \tag{53}$$

The presence of a soliton violates superfluidity in the usual meaning of word. Let us assume, as in section 5, that our 1D trap is twisted into a ring. In the presence of a soliton the demand, that ψ is single valued, results in the quantization condition

$$\frac{m}{\hbar} \oint \mathbf{v}_s \cdot d\mathbf{l} - \Delta\varphi\,(v) = 2\pi l, \quad l = 0, \pm 1, ... \tag{54}$$

Thus, in the presence of a soliton, the circulation of superfluid velocity is not quantized and depends on the soliton velocity.

6.2 One-dimensional Bose gas

In previous sections we considered condensates which are finite in x and y directions and unrestricted in the z-direction. Our investigations were based on the mean-field theory. However, conditions for the applicability of such an approximation are by no means obvious and the situation changes drastically when the radial size of the condensate becomes less then the average distance between particles.

Such a tight confinement can be reached in a optical lattice created by two perpendicular standing waves [22]. In this geometry one has an array of parallel elongated condensates, which practically have no overlap and can be considered as independent. The length of each condensate was about 15 μm and the diameter about 60 nm. so that they can be considered as one-dimensional.

Strictly speaking, there is no BEC in 1D systems. The presence of BEC means that the one-body density matrix exhibits the non-diagonal long range order, i.e. $n^{(1)}(r) = \left\langle \hat{\Psi}^{\dagger}(\mathbf{r})\hat{\Psi}(0) \right\rangle \to const$ when $r \to \infty$. In a 1D Bose-system at $T = 0$ the density matrix decays according to an algebraic law, due to the divergence of long wave-length fluctuations:

$$n^{(1)}(|z|) \propto |z|^{-\nu}, \quad \nu = \frac{mc}{2\pi\hbar n}. \tag{55}$$

where, as before, c is the velocity of sound and n is the linear density. The mean-field theory is valid, when the decay is slow enough, that is when

$$\nu = \frac{mc}{2\pi\hbar n} \ll 1. \tag{56}$$

This happens if the gas is dense enough. As a condition for the applicability of mean-field theory this is the opposite of that for 3D systems. Vice-versa, when the 1D gas is dilute, the atoms interact as impenetrable particles with an infinitely high repulsive potential. Indeed, the scattering properties of two particles in 1D are determined by their reflection probability. This tends to zero as the wave length of the scattering particles increases. But in the 1D dilute gas the relevant wave length is of the order of $1/n$, and tends to infinity when $n \to 0$.

It was shown by Girardeau [23] that the ground state energy and the spectrum of elementary excitations of a 1D Bose-gas of impenetrable particles coincide with the ones of an ideal Fermi-gas. The repulsion of Fermi particles due to their statistics imitates in this limit the interaction between Bose-particles. Simple calculations give that in this case $c = \pi\hbar n/m$, so that $\nu = 1/2$. The theory for a point interaction with arbitrary strength was developed by Lieb and Liniger[24]. According to this theory, elementary excitations in the system can be described as creation of fermionic "particles" and "holes". However for $\nu < 1/2$ the excitations exhibit interactions similar to the one in a Fermi-liquid. When ν decreases, the "particles" branch of excitations transforms into the Bogoliubov phonon spectrum of an interacting Bose gas, and the "holes" branch transforms into the soliton dispersion written in equations (49) and (52) [25, 26].

It is important that Fermionic spectra do not satisfy the Landau criterion for superfluidity. According to this criterion a body can move in the system without friction if its velocity V is less then the velocity of sound. For a spectrum of fermionic type the body can always create a particle-hole pair with a small energy ε near the Fermi surface with total momentum $2p_F$. Notice that in our 1D spinless gas one has $p_F = \pi\hbar n$, which just coincides with the maximum momentum of the solitons (53). Thus the Landau condition for creation of excitations $V > \min(\varepsilon/p)$ can be satisfied for any V.

One can estimate the drag force for small V. In paper [27] an impurity moving through the gas and interacting with the gas by a weak potential was considered. The energy dissipation and the drag force can be calculated using the dynamic form factor of the gas $S(\omega, k)$. If the potential is $g_i\delta(z - Vt)$, the drag force is

$$F_V = -\frac{g_i^2 n}{\hbar} \int_0^\infty \frac{dk}{2\pi} kS(kV, k) \tag{57}$$

The form-factor has been calculated by generalizing of the Haldane method [28] for the calculation of correlation functions in the case of time-dependent correlations. $S(\omega, k)$ at small ω and finite k is different from zero for $\omega > c\,|\Delta k| \equiv c\,|k - 2p_F/\hbar|$. In this region

$$S(\omega, k) = A\frac{nc}{\hbar}\left(\frac{\hbar}{mc^2}\right)^{1/\nu}\left[\omega^2 - (c\Delta k)^2\right]^{\frac{1}{2\nu}-1} \quad . \tag{58}$$

One can calculate the coefficient A at $\nu = 2$ and $\nu \ll 1$. Integration (57) gives the drag force

$$F_V \propto V^{\left(\frac{1}{\nu}-1\right)}. \tag{59}$$

In the Girardeau limit $\nu = 2$ one has the force $F_V \propto V$ and the Bose gas behaves, from the point of view of friction, as a normal fluid where the drag force is proportional to the velocity. On the contrary, in the mean-field limit the force is very small and the behavior of the system is analogous to the one of a 3D superfluid. However, even in this limit, the presence of the small drag force makes a great difference. Let us imagine that our system is twisted in a ring and that the impurity rotates around the ring with small angular velocity. If the system is superfluid, in the common mean of words, the superfluid part must stay at rest. The presence of a drag force, conversely, means that equilibrium will be reached only when the gas as a whole will rotate with the angular velocity of the impurity. From this point of view the superfluid part of the 1D Bose gas is equal to zero even at $T = 0$.

Notice that the process of dissipation, which in the language of fermionic excitations can be interpreted as the creation of a particle-hole pair, corresponds in the mean-field limit to creation of a phonon and a low-energy soliton. It seems that such a process cannot be described in the mean-field approach.

Acknowledgments

Author thanks G . Astrakharchik, F. Dalfovo, T. Esslinger, V. Konotop, A. Smerzi and S. Stringari for useful discussions.

References

[1] N.N. Bogoliubov, J. Phys. USSR **11**, 23 (1947)

[2] E.P. Gross, Nuovo Cimento **20**, 454 (1961)

[3] L.P. Pitaevskii, Sov. Phys. JETP **13**, 451 (1961)

[4] L.P. Pitaevskii and S. Stringari, *Bose-Einstein Condensation*, Oxford University Press, Oxford (2003)

[5] P. Pedri, L.P. Pitaevskii, S. Stringari, C. Fort, S. Burger, F.S. Cataliotti, P. Maddaloni, F. Minardi, and M. Inguscio, Phys. Rev. Lett. **87**, 220401 (2001)

[6] M. Krämer, C. Menotti, L.P. Pitaevskii, and S. Stringari, e-print cond-mat/0305300, Eur. Phys. J. D **27**, 247 (2003).

[7] O. Morsch, J. Müller, M. Cristiani, D. Ciampini, and E. Arimondo, Phys. Rev. Lett. **87**, 140402 (2001)

[8] L.D. Landau, J. Phys. USSR **5**, 71 (1941)

[9] D.J. Bishop and J.D. Reppy, Phys. Rev. B **22**, 5171 (1980)

[10] L.D. Landau and E.M. Lifshitz, *Quantum mechanics*, Pergamon Press, Oxford (1987).

[11] A. Eggington, J. Low Temp. Phys. **28**, 1 (1977)

[12] V. Ambegaokar, B.I. Halperin, D.R. Nelson, and E.D. Siggia, Phys. Rev. B **21**, 1806 (1980)

[13] S. Rapsch, U. Schollwöck., and W. Zwerger, Europhys. Lett. **46**, 559 (1999)

[14] R. Roth and K. Burnett, Phys. Rev. A, **67**, 031602 (2003)

[15] One can read in [13]: "In the absence of interaction and disorder it is straightforward to show that $\rho_s = 1$ for arbitrary densities n as it should be." Analogously in [14]: "The superfluid fraction is 1 for the noninteracting system..."

[16] F.S. Cataliotti, S. Burger, C. Fort, P. Maddaloni, F. Minardi, A. Trombettoni, A. Smerzi, and M. Inguscio, Science **293**, 843 (2001)

[17] M. Krämer, L. Pitaevskii, and S. Stringari, Phys. Rev. Lett. **88**, 180404 (2002)

[18] E.M. Lifshitz and L.P. Pitaevskii , *Statistical Physics, Part 2*, Pergamon Press, Oxford (1984).

[19] T. Tsuzuki, J. Low Temp. Phys. **4**, 441 (1971)

[20] The difference between p and $\tilde{p}$ is discussed in [21]. However, in this paper the constant of integration in the definition of p has been chosen in a such way that $p \to \pm\varepsilon/c$ at $v \to \pm c$. Then the function $p(v)$ has a discontinuity at $v = 0$. This means, that the soliton cannot reverse the direction of its motion in an inhomogeneous gas or in the presence of a friction. In our opinion this choice is hardly acceptable.

[21] S.I. Shevchenko, Sov. J. Low Temp. Phys. **14**, 553 (1988)

[22] H. Moritz, T. Stöferle, M. Köhl and T. Esslinger, e-print cond-mat/0307607

[23] M. Girardeau, J. Math. Phys. **1**, 516 (1960)

[24] E.H. Lieb and W. Liniger, Phys. Rev. **130**, 1605 (1963)

[25] P.P. Kulish, S.V. Manakov and L.D. Faddev, Teor. Mat. Phys. **28**, 38 (1976)

[26] M. Ishikava and H. Takayama, J. Phys. Soc. Japan, **49**, 1242 (1980)

[27] G. Astrakharchik and L.P. Pitaevskii, e-print cond-mat/0307247

[28] F.D.M. Haldane, Phys. Rev. Lett. **47**, 1840 (1981)

STATISTICAL MECHANICS OF QUANTUM INTEGRABLE SYSTEMS

Miki Wadati, Go Kato and Toshiaki Iida
Department of Physics, Graduate School of Sciences,
University of Tokyo, 7-3-1 Hongo, Bunkyo-ku, Tokyo 113-0033, Japan

Abstract Recent developments in statistical mechanics of quantum integrable systems are reviewed. Those studies are fundamental and have a renewed interest related to newly developing fields such as atomic Bose-Einstein condensations, photonic crystals and quantum computations. After a brief summary of the basic concepts and methods, the following three topics are discussed. First, by the thermal Bethe ansatz (TBA), a hard-core Bose gas is exactly solved. The model includes fully the effect of excluded volume and is identified to be a $c = 1$ conformal field theory. Second, the cluster expansion method based on the periodic boundary condition for the Bethe wavefunction, which we call the Bethe ansatz cluster expansion (BACE) method, is developed for a δ-function gas and the XXX Heisenberg chain. This directly proves the TBA and reveals intrinsic properties of quantum integrable systems. Third, for a δ-function gas, the integral equations for the distribution functions of the quasi-momentum and the quasi-particle energy are solved in the form of power series. In the weak coupling case, the results reproduce those of Bogoliubov theory.

1. Introduction

We define integrable systems. A quantum system is said to be integrable when the system has a sufficient number of independent conserved operators I_j which commute each other:

$$[I_i, I_j] \equiv I_i I_j - I_j I_i = 0. \tag{1}$$

This definition is a natural extension of the well-known Liouville theorem in classical mechanics. In classical mechanics, a system with N degrees of freedom is called to be completely integrable when there exist N independent conserved quantities which are in involution with a proper Poisson bracket, $\{I_i, I_j\}_{\text{P. B.}} = 0$. For such a classical system, the initial value problem can be solved by quadratures.

F. Kh. Abdullaev and V. V. Konotop (eds.), Nonlinear Waves: Classical and Quantum Aspects, 193–207.

One of our favorite models in the study of integrable system is the nonlinear Schrödinger (NLS) model [1]:

$$i\phi_t + \phi_{xx} - 2c|\phi|^2\phi = 0. \tag{2}$$

It maintains solitons, that is, nonlinear waves with particle properties. More rigorously, solitons are defined to be localized waves in completely integrable systems. The model has been applied in various fields of physics such as plasma physics, hydrodynamics and nonlinear optics. A renewed interest in (2) comes from a fact that it is a one-dimensional Gross-Pitaevskii equation which describes the Bose-Einstein condensate. The corresponding quantum models, the first and second quantized versions, are also known to be integrable.

It is interesting that the classical soliton for the attractive case $c < 0$ arises in a limit of the quantum field theory. We denote by $|n, X, t\rangle_v$ the n-particle bound state in the moving frame with the center of mass X and by $\phi^s(x,t)$ a moving bright soliton. An explicit formula is given by [2]

$$\lim_{n\to\infty} {}_v\langle n, X', t|\phi(x)|n+1, X, t\rangle_v \tag{3}$$

$$= \phi^s(x,t)\Big|_{x_0=X} \delta\left(X' - \frac{n+1}{n}X + \frac{1}{n}(x - vt)\right), \tag{4}$$

where, with $\kappa = -c > 0$,

$$\begin{aligned}\phi^s(x,t) =& 2\kappa^{-1/2}\eta \exp\left[-4i(\xi^2 - \eta^2)t - 2i\xi x + i\theta_0\right] \\ & \times \operatorname{sech}\left[2\eta(x - x_0) + 8\xi\eta t\right].\end{aligned} \tag{5}$$

For the repulsive case $c > 0$, this kind of explicit formula which links the macroscopic waveform with the microscopic quantum state has not been found. This problem remains to be solved.

At zero temperature, the properties of quantum integrable systems are analyzed by the Bethe ansatz method [3, 4]. Needless to mention that it is not a hypothesis but is exact; the wavefunction form is assumed and then proved. Such wavefunction is called Bethe wavefunction. As an alternative approach, the inverse scattering method, which was originally developed to solve classical soliton equations, has been extended to the quantum theory. The quantum inverse scattering method provides us a unified framework to treat quantum integrable systems in an algebraic manner [5]. Therefore, it is called algebraic Bethe ansatz while the original Bethe ansatz is referred to as coordinate Bethe ansatz.

For finite temperature, there are two eminent methods; the thermal Bethe ansatz (TBA) method [6] and the quantum transfer matrix (QTM) [7] method. In the former, a form of the entropy is assumed and the equilibrium properties are determined by minimization of the free

energy. The TBA is often called the Yang-Yang method. In the latter, the equivalence of a 1-dimensional quantum system and a 2-dimensional classical system is used. By exchanging "quantum" and "space" directions, we find that the free energy and the correlation length are obtained only from the largest and the second largest eigenvalues of the transfer matrix respectively. Both methods have been successfully applied to various models, but there should be further investigations on their validity and physical significances.

2. Hard-core Bose gas

We begin with an application of the TBA. A simple but non-trivial example of the quantum integrable particle system is given by a one-dimensional hard-core Bose gas. The Hamiltonian for the N particles is

$$H = -\sum_{j=1}^{N} \frac{\hbar^2}{2m} \frac{\partial^2}{\partial x_j^2} + \sum_{i<j} v(x_i - x_j), \tag{6}$$

with the inter-particle potential,

$$\begin{aligned} v(x) &= \infty \qquad && \text{for } |x| < a, \\ &= 0 && \text{for } |x| > a. \end{aligned} \tag{7}$$

Hereafter, we choose $\hbar = 1$ and $2m = 1$ to simplify the expressions. The potential (7) implies that a is the diameter of each "atom".

A two-body problem is solved as follows. The momenta of particle 1 and 2 are written respectively as k_1 and k_2. Without loss of generality, we set $k_1 > k_2$. The eigenfunctions before and after the collision are $e^{i(k_1 x_1 + k_2 x_2)}$ and $e^{i(k_1 x_2 + k_2 x_1) + i\Delta(k_1 - k_2)}$. The connection relation at $x_2 = x_1 + a$ determines the phase shift $\Delta(k)$ due to the collision,

$$\Delta(k) = -\pi s(k) - ak, \qquad\qquad k \equiv k_1 - k_2, \tag{8}$$

where $s(k)$ is the sign function, $s(k) = 1$ for $k > 0$ and $s(k) = -1$ for $k < 0$. This information is enough for the TBA. Substituting a physical phase shift (8) into the bosonic formulation [8], we obtain

$$p = \frac{1}{2\pi\beta} \int dk \, \log\left(1 + e^{-\beta(k^2 - \mu + ap)}\right), \tag{9}$$

$$\frac{N}{L} = \frac{1}{2\pi}\left(1 - a\frac{N}{L}\right) \int dk \, \frac{1}{e^{\beta(k^2 - \mu + ap)} + 1}, \tag{10}$$

$$\frac{E}{L} = \frac{1}{2\pi}\left(1 - a\frac{N}{L}\right) \int dk \, k^2 \frac{1}{e^{\beta(k^2 - \mu + ap)} + 1}, \tag{11}$$

where $\beta = 1/k_{\rm B}T$ and L is a size of the box. Note that the pressure p and the number density $n \equiv N/L$ appear implicitly in the formulae. We also note that the phase shift $\Delta(k)$ is related to the 2-particle scattering matrix $S(k)$ by $S(k) = \exp(i\Delta(k))$.

2.1 Classical limit

In the limit of the classical statistical mechanics, that is, the Boltzmann statistics, (9) and (10) become

$$p = \frac{1}{2\pi\beta}\int dk\, e^{-\beta(k^2-\mu+ap)}, \tag{12}$$

$$\frac{N}{L} = \frac{1}{2\pi}\left(1 - a\frac{N}{L}\right)\int dk\, e^{-\beta(k^2-\mu+ap)}. \tag{13}$$

The comparison of (12) and (13) readily leads to the equation of state,

$$p\beta = \frac{1}{l-a}, \qquad\qquad l = \frac{L}{N}. \tag{14}$$

This is known as the Tonks equation [9, 10], which is exact in classical statistical mechanics. By the same reason, a one-dimensional hard-core gas is sometimes called the Tonks gas. A derivation of this classic result through the TBA is novel and amusing.

2.2 Low-temperature expansions

For further investigation, it is convenient to introduce the "shifted variables",

$$\hat{\mu} = \mu - ap, \qquad\qquad \hat{n} = \frac{1}{l-a} = \frac{n}{1-an}. \tag{15}$$

Physical meanings are the following: ap represents an energy required to make a "space a" per particle against the pressure p. $l-a$ is the average space available for each particle. In terms of these variables, (9) and (10) are

$$p = \frac{1}{2\pi\beta}\int dk\, \log\left(1 + e^{-\beta(k^2-\hat{\mu})}\right), \tag{16}$$

$$\hat{n} = \frac{1}{2\pi}\int dk\, \left(e^{\beta(k^2-\hat{\mu})}+1\right)^{-1}. \tag{17}$$

To evaluate (16) and (17) at low temperatures, we apply the well-known Sommerfeld formula. Solving them consistently, we obtain

$$p = \frac{2}{3\pi}(\pi\hat{n})^3 + \frac{\pi}{6}\frac{(k_{\rm B}T)^2}{\pi\hat{n}} + \frac{\pi^3}{30}\frac{(k_{\rm B}T)^4}{(\pi\hat{n})^5} + \cdots. \tag{18}$$

Note that the limit $a \to 0$ (therefore, $\hat{n} \to n$) is not the free bosons, but the free fermions. Further, the chemical potential μ, the energy E and the specific heat per unit length C are calculated as

$$\mu = (\pi\hat{n})^2 \left(1 + \frac{2}{3}a\hat{n}\right) + \frac{\pi^2}{12}\frac{(k_{\mathrm{B}}T)^2}{(\pi\hat{n})^2}(1 + 2a\hat{n}) + \frac{\pi^4}{36}\frac{(k_{\mathrm{B}}T)^4}{(\pi\hat{n})^6}\left(1 + \frac{6}{5}a\hat{n}\right) + \cdots, \tag{19}$$

$$\frac{E}{L} = \frac{1}{2l}\left[\frac{2}{3}(\pi\hat{n})^2 + \frac{\pi^2}{6}\frac{(k_{\mathrm{B}}T)^2}{(\pi\hat{n})^2} + \frac{\pi^4}{30}\frac{(k_{\mathrm{B}}T)^4}{(\pi\hat{n})^6} + \cdots\right], \tag{20}$$

$$C = \frac{k_{\mathrm{B}}^2}{6l\hat{n}^2}T + \frac{k_{\mathrm{B}}^4}{15l\pi^2\hat{n}^6}T^3 + \cdots. \tag{21}$$

In the above expressions, the effects of excluded volume are seen clearly.

The conformal field theory has been invented to give a consistent description of $(1+1)$-dimensional quantum systems at criticality. As a consequence, it predicts that the linear specific heat has a form,

$$C = \frac{\pi}{3}\frac{k_{\mathrm{B}}^2 c}{v}T, \tag{22}$$

where c is the conformal charge (only in this section). The velocity v in the formula (22) is calculated from (18) as $v^2 = 2\partial p/\partial n = \left(2\pi\hat{n}^2 l\right)^2$. Then, a comparison of (21) and (22) leads to

$$c = 1. \tag{23}$$

This concludes that the one-dimensional hard-core Bose gas obeys the $c = 1$ conformal field theory at $T = 0$ [11].

3. Bethe ansatz cluster expansion method

In statistical mechanics, the cluster expansion method is the most standard in dealing with interacting particle systems. The method was developed to treat imperfect gases [12] and has been extended into the quantum theory by many researchers [13]. In what follows, we formulate the cluster expansion method for quantum integrable systems.

3.1 δ-function Bose gas

We first consider a one-dimensional system of bosons with repulsive δ-function interaction. The Hamiltonian of the system is

$$H_N = -\frac{\hbar^2}{2m}\sum_{j=1}^{N}\frac{\partial^2}{\partial x_j^2} + c\sum_{j\neq l}\delta(x_j - x_l). \tag{24}$$

The coupling constant c is assumed to be positive, and hereafter we set $\hbar = 1$ and $2m = 1$. This many-particle system is a first quantized version of the nonlinear Schrödinger model (2). While the case $c = 0$ is nothing but free bosons, the limit $c = \infty$ reduces to free fermions (impenetrable gas) just as the $a = 0$ limit of the hard-core bosons in the previous section. The correspondence of the impenetrable gas and the hard-core Bose gas will be discussed in § 4.1.

We assume that the system is in a box of length L and satisfies the periodic boundary condition. An important difference from the hard-core bosons is that particles can pass through each other for a finite c. The N-particle wavefunction (Bethe wavefunction) consists of linear combinations of N single particle wavefunctions with the interchange coefficients. The total energy E and the wavenumber (or, equivalently the momentum) k_j are determined by the following relations,

$$E = \sum_j k_j^2, \tag{25}$$

$$k_j L = 2\pi m_j + \sum_{l \neq j} \Delta\left(k_l - k_j\right). \tag{26}$$

Here $\Delta(k)$ is the phase shift due to the two-particle scattering,

$$\Delta(k) = 2 \arctan\left(k/c\right), \tag{27}$$

and m_j are integers (half-integers) for $N =$ odd (even) satisfying $m_j < m_{j+1}$. The relation (26) is derived from the periodic boundary condition imposed on the N-particle wavefunction and is referred to as the Bethe ansatz (BA) equation.

We are interested in calculating the N-particle partition function,

$$Z_N = \mathrm{Tr}\, e^{-\beta H_N}, \qquad \beta = 1/k_{\mathrm{B}}T. \tag{28}$$

The n-particle cluster integral b_n is related to the partition function as

$$\sum_{n \geq 1} b_n z^n = \log\left(\sum_{N \geq 0} Z_N z^N\right), \qquad z = e^{\beta\mu}. \tag{29}$$

By definition, $Z_0 = 1$.

It is remarkable that we can evaluate (28) and (29) explicitly. By use of only the BA equation, the explicit forms of Z_N and b_n are obtained [14]. As far as the authors know, all the cluster integrals $\{b_n\}$ for an interacting system are given explicitly for the first time. An essential step is the replacement of the summations over $\{m_j\}$ by the integrals

over $\{k_j\}$ in the large L limit (the thermodynamic limit). Instead of writing those derivations and expressions, we emphasize two consequences:

(a) The cluster integrals $\{b_n\}$ consist of only a finite number of terms with the effective interaction $K(k) \equiv d\Delta(k)/dk = 2c/(k^2 + c^2)$.

(b) From the explicit forms of $\{b_n\}$, the following nonlinear integral equation (Yang-Yang integral equation) for the distribution function of the quasi-particle energy, $\epsilon(k)$, is derived,

$$\epsilon(k) = k^2 - \mu - \frac{1}{\beta}\int \frac{dq}{2\pi} K(k-q) \log\left(1 + e^{-\beta\epsilon(q)}\right). \tag{30}$$

This directly proves the thermal Bethe ansatz (TBA) method.

3.2 *XXX* Heisenberg model

We consider the spin-half XXX Heisenberg chain whose Hamiltonian is

$$H = -J\sum_{j=1}^{L}\left(S_j^x S_{j+1}^x + S_j^y S_{j+1}^y + S_j^z S_{j+1}^z\right) - h\sum_{j=1}^{L} S_j^z. \tag{31}$$

Here S_j^α, $\alpha = x, y, z$, are the Pauli matrices on the site j, L is the total number of sites, J is the coupling constant and h expresses the external magnetic field. We assume the periodic boundary condition and use a unit which makes $J = 1$. Let M be the number of up-spins. Since M is a conserved quantity, we can analyze the system with a fixed M. The total energy E and Bethe ansatz equation (periodic boundary condition) are respectively given by

$$E + Mh = \sum_{m=1}^{M} \frac{2}{x_m^2 + 1}, \tag{32}$$

$$\left(\frac{x_m + i}{x_m - i}\right)^L = \prod_{m' \neq m} \frac{x_m - x_{m'} + 2i}{x_m - x_{m'} - 2i}. \tag{33}$$

From the viewpoint of the Bethe ansatz cluster expansion method, an interesting aspect is that BA equation (33) has complex solutions which correspond to bound states. Indeed, it is a motivation for studying here the Heisenberg chain. This difficulty, known as the string hypothesis among experts, is removed by a proper choice of the integral path or a careful treatment of the sign of the Jacobian from $\{m_j\}$ to $\{x_m\}$. Remark that in the thermodynamic limit integers m_j can be regarded as continuous variables. Again, we simply write the results of the analysis [15].

(a) The partition function and the free energy are derived only from the BA equation. Those agree with the results of TBA with the string hypothesis.

(b) The following integral equation [16] for the free energy f is obtained,

$$e^f \equiv \left(\mathrm{Tr}\, e^{-\beta H}\right)^{1/L} = u(0) z^{-1/2}, \qquad z = e^{-2\beta h}, \tag{34}$$

$$u(x) = z + 1 + \oint_{0+} \left[\frac{\exp\left(-\dfrac{2J\beta}{(y+i)^2+1}\right)}{x-y-2i} + \frac{\exp\left(-\dfrac{2J\beta}{(y-i)^2+1}\right)}{x-y+2i} \right] \times \frac{z}{u(y)} \frac{dy}{2\pi i}. \tag{35}$$

To conclude this section, we summarize the significances of the Bethe ansatz cluster expansion (BACE) method. First, $\mathrm{Tr}\, e^{-\beta H}$ can be calculated only from the Bethe ansatz equation (periodic boundary condition). Second, the method gives a proof of TBA and is free from the string hypothesis. Third, the BACE method captures some essential features of quantum integrable systems. It is known that if all the S-matrices (scattering matrices) are given we may express the partition function and the cluster integrals in terms of them. This is a general statement. The quantum integrable systems are characterized by factorized S-matrices: N-particle S-matrix is expressed as a product of $N(N-1)/2$ 2-particle S-matrices. Recall that the 2-particle scattering matrix $S(k)$ and the phase shift $\Delta(k)$ are related by $S(k) = \exp(i\Delta(k))$. This special feature of quantum integrable systems is the origin of a fact that there exist only a finite number of terms in each cluster integral.

4. Solutions of the Lieb-Liniger integral equation

We again consider the δ-function Bose gas (24) for the repulsive case $c > 0$. We like to investigate the ground state properties of the system. For a set of momenta $\{k_j\}$, define

$$f(k_j) = 1/\left[L\left(k_{j+1} - k_j\right)\right]. \tag{36}$$

The meaning of $f(k)$ is that for a large system

$$Lf(k)\, dk = \text{number of } k\text{'s in } (k, k+dk). \tag{37}$$

We call it the distribution function of the quasi-momentum. From (26) with (27), we have

$$2c \int_{-K}^{K} \frac{f(p)}{(p-k)^2 + c^2}\, dp = 2\pi f(k) - 1, \tag{38}$$

where K is the cut-off momentum. We introduce new variables

$$k = Kx, \qquad c = K\lambda, \qquad f(Kx) = g(x), \tag{39}$$

and change (38) into a dimensionless form,

$$1 + 2\lambda \int_{-1}^{1} \frac{g(x)}{\lambda^2 + (x-y)^2}\, dx = 2\pi g(y). \tag{40}$$

We refer to (40) as the Lieb-Liniger (LL) integral equationLieb-Liniger integral equation. To express the strength of the interaction, there exist two parameters,

$$\lambda = \frac{c}{K}, \qquad \gamma = \frac{c}{\rho}. \tag{41}$$

In this section, we write the number density as $\rho = N/L$. An interplay of λ and γ turns out to be interesting, in particular, in the weak coupling case.

Contrary to the intuition, the small c case is difficult. A naive discussion leads to a contradiction: As $\lambda \to 0$, the kernel $2\lambda/\left[\lambda^2 + (x-y)^2\right]$ becomes a representation of $2\pi\delta(x-y)$ so that in this limit (40) reads $1 + 2\pi g(y) = 2\pi g(y)$. We should remark that $c = 0$ is a singular point of the theory. We quote a sentence from Lieb-Liniger's paper [4], "There does not seem to be any simple way to get a systematic, reliable expansion of $g(x)$ as $\lambda \to 0$."

In terms of the distribution function $g(x)$, the ground state energy is

$$E_0 = N\rho^2 e(\gamma), \qquad \rho = N/L,$$
$$e(\gamma) = \frac{\gamma^3}{\lambda^3} \int_{-1}^{1} g(x) x^2\, dx, \tag{42}$$

where the number of particle is fixed by

$$\gamma \int_{-1}^{1} g(x)\, dx = \lambda. \tag{43}$$

A method of solutions has been proposed [17]. The method is simple and direct. We substitute power series expansions,

$$g(y) = \sum_{n=0}^{\infty} a_n y^{2n}, \tag{44}$$

$$\frac{1}{\lambda^2 + (x-y)^2} = \sum_{m=0}^{\infty} \sum_{l=[(m+1)/2]}^{\infty} (-1)^{m-l} \binom{l}{m-l} \times \frac{(2x)^{2l-m}}{(\lambda^2 + x^2)^{l+1}} y^m, \tag{45}$$

into (40). Then, the LL integral equation (40) reduces to a set of linear algebraic equations for $\{a_n\}$. We analyze the set of equations for strong and weak coupling cases.

4.1 Large γ (large λ)

This corresponds to the strong coupling case. The algebraic equations for a_0 and a_1 are easily solved to obtain

$$g(x) = a_0 + a_1 x^2, \tag{46}$$

$$a_0 = \left(2\pi - 4 \arctan \frac{1}{\lambda} + \frac{8}{3\pi\lambda^4}\right)^{-1},$$

$$a_1 = -\frac{4}{\lambda^3}\left(2\pi + \frac{4}{3}\frac{1}{\lambda^3}\right)^{-1} \cdot a_0. \tag{47}$$

Using (46) with (49) in (43), we have

$$\lambda = \frac{1}{\pi}\left(\gamma + 2 - \frac{4\pi^2}{3}\frac{\gamma+1}{\gamma(\gamma+2)^2}\right). \tag{48}$$

and therefore

$$a_0 = \frac{\gamma+2}{2\pi\gamma}\left(1 - \frac{2\pi^2}{3\gamma(\gamma+2)}\right), \qquad a_1 = -\frac{\pi}{\gamma(\gamma+2)}. \tag{49}$$

Those improve the results of the previous work [4]. We considered only a_0 and a_1, because the series (44) converges rapidly. It can be shown that the leading term of a_p is $a_p = (-1)^p(2/\pi)\lambda^{-(2p+1)}a_0$, $p \geq 1$, for large λ.

The ground state energy $e(\gamma)$ is calculated from (42),

$$e(\gamma) = \frac{\pi^2}{3}\left(\frac{\gamma}{\gamma+2}\right)^2\left(1 + \frac{32\pi^2}{15(\gamma+2)^3}\right). \tag{50}$$

It is instructive to compare this result with (20) for the hard-core Bose gas. The "physical" phase shift due to the two-particle scattering is

$$\Delta_{\mathrm{B}}(k) = -2\arctan(c/k). \tag{51}$$

Remark that (27) is for the fermion counting and (51) is for the boson counting. By equating (8) and (51) in the low energy limit $k \to 0$, we have

$$a = -2/c. \tag{52}$$

We see that with the relation (52) the first terms of (20) and (50) are exactly same. At first sight, it seems to be strange that the diameter a is negative for the repulsive case $c > 0$. We may interpret this as follows. Recall that, in contrast to the hard-core interaction, particles can pass through each other in the δ-function interaction. This transparency effect amounts to an effectively negative diameter a in the limits $k \to 0$ and $c \to \infty$. Many researchers discuss the equivalence of the $a = 0$ (Tonks-Girardeau gas) [18] and $c = \infty$ (impenetrable gas) cases. The relation (52) explains such equivalence quantitatively.

4.2 Small γ (small λ)

As remarked before, this case is known to be difficult. We solve a set of equations for $a_1, \ldots, a_N$ and take the limit $N \to \infty$ in $\{a_n\}$. The result is

$$a_0 = \frac{1}{2\pi\lambda} + \frac{1}{4\pi}\sum_{m=0}^{\infty}\left[\frac{(2m-1)!!}{(2m)!!}\right]^2, \tag{53}$$

$$a_l = -\frac{1}{2\pi\lambda}\frac{(2l-3)!!}{(2l)!!} - \frac{1}{4\pi}\sum_{m=0}^{\infty}\frac{(2m+1)!!\ (2m-1)!!\ (2l-1)!!}{[(2m)!!]^2\,(2l)!!\ (2l-2m-1)}, \tag{54}$$

and therefore we obtain

$$g(x) = \frac{1}{2\pi\lambda}(1-x^2)^{1/2} - \frac{1}{4\pi}\sum_{l=0}^{\infty}\sum_{m=0}^{\infty}\frac{(2m+1)!!\ (2m-1)!!\ (2l-1)!!}{[(2m)!!]^2\,(2l)!!\ (2l-2m-1)}x^{2l}. \tag{55}$$

In contrast to the large λ case, all a_p are in the same order of λ.

The physical quantities are finite in the expansion with respect to γ (not with respect to λ). The divergent sums cancel out when λ is replaced by γ through the relation (43). For instance, the ground state

energy and the chemical potential are respectively given by

$$e(\gamma) = \gamma - \frac{4}{3\pi}\gamma^{3/2}, \tag{56}$$

$$\mu = \rho^2\left(3e - \gamma\frac{de}{d\gamma}\right) = 2\rho^2\left(\gamma - \frac{1}{\pi}\gamma^{3/2}\right). \tag{57}$$

The above results agree with those of the Bogoliubov theory. Remark that the physical quantities are expressed in the power series of $\gamma^{1/2} = (c/\rho)^{1/2}$. This method can be applied to the Yang-Yang integral equation at $T = 0$ [19].

An intriguing fact is that the LL integral equation appears in a completely different subject, the circular disk condenser [20, 21]. We consider the condenser of the radius 1 whose two plates are separated by a distance λ. Coordinates are taken as follows: the radial distance from the common axis of the disks is taken to be ρ, the distances from the disks to be ζ, ζ', respectively. E. R. Love (1949) found that the potential ϕ due to the disks is

$$\phi(\rho,\zeta,\zeta') = \frac{V_0}{\pi}\int_{-1}^{1}\left\{\left[\rho^2 + (\zeta + it)^2\right]^{-1/2} - \left[\rho^2 + (\zeta' - it)^2\right]^{-1/2}\right\} \times h(t)\,dt, \tag{58}$$

where $h(t)$ is determined by

$$h(t) - \int_{-1}^{1}\frac{ds}{\pi}\frac{\lambda}{\lambda + (s-t)^2}h(s) = 1. \tag{59}$$

The Love equation (59) is exactly the same form as the LL integral equation; to be precise, $h(x)$ in (59) corresponds to $2\pi g(x)$ in (40). For small λ (small separation), the capacitance was calculated as [20]

$$C = \frac{1}{2\pi}\int_{-1}^{1}h(t)\,dt = \frac{1}{4\lambda} + \frac{1}{4\pi}\log\frac{16\pi}{\lambda e} + o(1). \tag{60}$$

This result is originally by G. Kirchhoff (1877).

On the other hand, the solution (55) gives

$$\int_{-1}^{1}g(x)\,dx = \frac{1}{4\lambda} - \frac{1}{2\pi} + \frac{1}{4}\sum_{m=0}^{\infty}\left[\frac{(2m-1)!!}{(2m)!!}\right]^2. \tag{61}$$

We regularize the last term as follows. We set

$$F(k) \equiv \sum_{m=0}^{\infty}\left[\frac{(2m-1)!!}{(2m)!!}\right]^2 k^{2m} = \frac{2}{\pi}K(k). \tag{62}$$

The function $K(k)$ is the complete elliptic integral of the first kind with the modulus k. Since

$$K(k) = \frac{1}{2}\log\left(16/(1-k^2)\right) \qquad \text{as} \qquad k^2 \to 1-0, \tag{63}$$

if we choose $1-k^2 = \lambda/\pi e$, we have

$$\begin{aligned}\int_{-1}^{1} g(x)\,dx &= \frac{1}{4\lambda} - \frac{1}{2\pi} + \frac{1}{4}\frac{2}{\pi}\lim_{k^2\to 1-0} K(k) \\ &= \frac{1}{4\lambda} - \frac{1}{2\pi} + \frac{1}{4\pi}\log\frac{16\pi e}{\lambda},\end{aligned} \tag{64}$$

which agrees with the Kirchhoff formula (60). This kind of regularization seems to be necessary in perturbative calculations. At the same time, a mystery remains that the physical quantities in the power series of γ do not contain the logarithmic terms as we observe in (56) and (57).

In this section, we have discussed only the ground state properties of the δ-function gas. A more delicate problem which we meet in the analysis at finite temperatures is that the $T = 0$ limit and the $c = 0$ limit do not commute, implying $T = c = 0$ is a singular point [22]. The authors believe that there are at least two regimes in c-T (or γ-T) plane characterized by the sign of the chemical potential μ; the fermionic regime ($\mu > 0$) and the bosonic regime ($\mu < 0$). Evaluation of correlation functions may give an additional information on the classification of the regimes [23, 24]. To summarize, for the δ-function Bose gas, TBA describes well the fermionic properties in the strong coupling regime but further investigations are required to clarify the bosonic properties in the weak coupling regime.

Acknowledgments

One of the authors (M.W) would like to thank Professor V. V. Konotop and the organizers of NATO ARW "Nonlinear Waves: Classical and Quantum Aspects", Estoril, Portugal, 13-17 July, 2003 for invitation and hospitality. He also thanks Professor L. Pitaevskii, Professor V. E. Korepin and the participants for stimulating discussions.

References

[1] V. E. Zakharov and A. B. Shabat, Exact theory of two-dimensional self-focusing and one-dimensional self-modulation of waves in nonlinear media, *Sov. Phys. JETP* **34** (1972) 62–9; Interaction between solitons in a stable medium, *ibid.* **37** (1973) 823–8.

[2] M. Wadachi and M. Sakagami, Classical soliton as a limit of the quantum field theory, *J. Phys. Soc. Jpn.* **53** (1984) 1933–8.

M. Wadati, A. Kuniba and T. Konishi, The quantum nonlinear Schödinger model; Gelfand-Levitan equation and classical soliton, *ibid.* **54** (1985) 1710–23.

[3] H. A. Bethe, Zur Theorie der Metalle. I. Eigenwerte und Eigenfunktionen der Linearen Atomkette, *Z. Phys.* **71** (1931) 205–26.

[4] E. Lieb and W. Linger, Exact analysis of interacting Bose gas. I. The general solution and the ground state, *Phys. Rev.* **130** (1963) 1605–16.

[5] V. E. Korepin, N. M. Bogoliubov and A. G. Izergin, *Quantum Inverse Scattering Method and Correlation Functions,* Cambridge University Press, New York, 1993.

[6] C. N. Yang and C. P. Yang, Thermodynamics of a one-dimensional system of bosons with repulsive delta-function interaction, *J. Math. Phys.* **10** (1969) 1115–22.

[7] T. Koma, Thermal Bethe-ansatz method for the one-dimensional Heisenberg model, *Prog. Theor. Phys.* **78** (1987) 1213–18.
M. Inoue and M. Suzuki, The ST-transformation approach to analytic solutions of quantum-systems. II— Transfer-matrix and pfaffian methods—, *ibid.* **79** (1988) 645–64.
M. Wadati and Y. Akutsu, From solitons to knots and links, *Prog. Theor. Phys. Suppl.* **94** (1988) 1–41.
J. Suzuki, Y. Akutsu and M. Wadati, A new approach to quantum spin chains at finite temperature, *J. Phys. Soc. Jpn.* **59** (1990) 2667–80.
J. Suzuki, T. Nagao and M. Wadati, Exactly solvable models and finite size corrections, *Int. J. Mod. Phys.* **B6** (1992) 1119–80.

[8] M. Wadati, Bosonic formulation of the Bethe ansatz method, *J. Phys. Soc. Jpn.* **54** (1985) 3727–33; Thermal Bethe ansatz and fractional statistics, *ibid.* **64** (1995) 1552–6.

[9] L. Tonks, The complete equation of state of one, two and three-dimensional gases of hard elastic spheres, *Phys. Rev.* **50** (1936) 955–63.

[10] D. C. Mattis (ed.), *The Many-Body Problem: An Encyclopedia of Exactly Solved Models in One Dimension,* World Scientific, Singapore, 1993.

[11] M. Wadati and G. Kato, One-dimensional hard-core Bose gas, *Chaos, Solitons & Fractals* **14** (2002) 23–8.

[12] J. E. Mayer and M. G. Mayer, *Statistical Mechanics,* John Wiley & Sons, New York, 1940.

[13] For instance, E. W. Montroll and J. C. Ward, Quantum statistics of interacting particles; general theory and some remarks on properties of an electron gas, *Phys. Fluids* **1** (1958) 55–72.

[14] G. Kato and M. Wadati, Partition function for a one-dimensional δ-function Bose gas, *Phys. Rev.* E **63** (2001) 036106-1–036106-14; Graphical representation of the partition function of a one-dimensional δ-function Bose gas, *J. Math. Phys.* **42** (2001) 4883–93; Explicit calculation of the partition function of a one-dimensional δ-function bose gas, *Chaos, Solitons & Fractals* **12** (2001) 993–1003.

[15] G. Kato and M. Wadati, Direct calculation of thermodynamic quantities for the Heisenberg model, *J. Math. Phys.* **43** (2002) 5060–78.

[16] M. Takahashi, Simplification of thermodynamic Bethe-ansatz equations, preprint cond-mat/0010486 and ISSP Technical Report No. A3579 (2000).

[17] M. Wadati, Solutions of the Lieb-Liniger integral equation, *J. Phys. Soc. Jpn.* **71** (2002) 2657–62.

[18] M. Girardeau, Relationship between systems of impenetrable bosons and fermions in one dimension, *J. Math. Phys.* **1** (1960) 516–23.

[19] T. Iida and M. Wadati, Solutions of the Yang-Yang integral equation at zero-temperature, *J. Phys. Soc. Jpn.* **72** (2003) 1874–80.

[20] V. Hutson, The circular plate condenser at small separations, *Proc. Camb. Phil. Soc.* **59** (1963) 211–24.

[21] The authors noticed the following monograph: M. Gaudin, *La Fonction d'Onde de Bethe*, Masson S. A. , Paris, 1983. Subsection 4.4.2 refers to [20] to obtain (56) in this text.

[22] M. Wadati and G. Kato, Statistical mechanics of a one-dimensional δ-function Bose gas, *J. Phys. Soc. Jpn.* **70** (2001) 1924–30.

[23] K. V. Kheruntsyan, D. M. Gangardt, P. D. Drummond and G. V. Shlyapnikov, Pair correlations in a finite-temperature 1D Bose gas, *Phys. Rev. Lett.* **91** (2003) 040403-1–040403-4.

[24] G. E. Astrakharchik and S. Giorgini, Correlation functions and momentum distribution of one-dimensional Bose systems, *Phys. Rev.* A **68** (2003) 031602-1–031602-4.

BOSE-EINSTEIN CONDENSATES IN AN OPTICAL LATTICE

C. Fort and L. Fallani
LENS, Dipartimento di Fisica, Università di Firenze and Istituto Nazionale per la Fisica della Materia, via Nello Carrara 1, I-50019 Sesto Fiorentino (Firenze), Italy
fort@lens.unifi.it

Abstract We report a series of experiments performed on the dynamics of a Bose-Einstein condensate (BEC) in the presence of a periodic potential realized by means of an optical lattice. BEC allows to finely investigate properties of periodic potentials already known from the solid state physics, but also opens the field of non-linear matter waves in periodical structure where interesting new effects are predicted as for instance the dynamical instability.

Keywords: Bose-Einstein condensates, periodic structure

1. Introduction

The field of Bose-Einstein condensates (BECs) in optical lattices consistently grew up in the last years starting from the first work by M. Kasevich and coworkers on the macroscopic interference of atomic de Broglie waves tunnelling from a vertical array of BECs [1]. Many results have been then reported as the observation of squeezed states in a BEC [2], the realization of a linear array of Josephson junctions [3] with BECs, the observation of Bloch oscillations and Landau-Zener tunnelling [4, 5], the study of the behaviour of atoms located within an optical periodic potential whose amplitude is periodically or randomly modulated [6, 7], and culminating with the observation of the quantum phase transition from a superfluid to a Mott insulator [8]. Recently, the general interest of this field has been extended to a careful study of the loading of BECs in an optical lattice [9] and to the observation of collapse and revival of the matter wave field of a BEC [10].

F. Kh. Abdullaev and V. V. Konotop (eds.), Nonlinear Waves: Classical and Quantum Aspects, 209–222.

In the second section of the paper we report experiments performed in our laboratory on a magnetically trapped condensate moving in the presence of a 1D optical lattice. Low lying collective modes were investigated in the regime of small amplitude oscillations where the system behaves as a superfluid . When the amplitude of the dipole oscillations becomes bigger than a critical value a dynamical transition from the superfluid to an insulator have been observed that can be understood in terms of dynamical instability occurring for a non-linear system in a periodic potential.

The third section of the paper is devoted to the description of an experiment where a BEC freely expands in the presence of a 1D optical lattice. We measured the velocity of the BEC in the lattice as a function of its quasi-momentum finding a perfect agreement with the Bloch theory of a particle in the periodic potential. From the measured Bloch velocity we can extract the effective mass that also affects the shape of the expanded condensate. In particular we access region of negative effective mass where the condensate inside the optical lattice contracts instead of expanding. In this region the mean field interaction increases and the coupling between different expanding directions results in a faster expansion perpendicularly to the optical lattice axis.

2. Dynamics of a BEC in a 1D optical lattice driven by a harmonic potential

In a first series of experiments we have studied the properties of a condensate produced in the combined potential of a harmonic magnetic trap and a 1D optical lattice. BEC in a sample of dilute gas is obtained by first laser cooling the thermal vapour and then by applying an evaporative cooling stage in a magnetic trap [11]. Our ^{87}Rb condensate is produced in the $F = 1, M_F = -1$ atomic state in a harmonic magnetic potential with a cylindrical symmetry, characterized by frequencies $\omega_z = 2\pi \times 9$ Hz and $\omega_\perp = 2\pi \times 90$ Hz respectively along the axial and the radial direction. The condensate contains $\sim 10^5$ atoms. During the evaporation of the atomic sample trapped in the magnetic field we also switch on the periodic potential. The periodic potential is produced with a far detuned laser beam shined along the axial direction and retroreflected in order to realize a standing wave. The laser beam is provided by a commercial Ti-Sa laser working at few nm on the blue side of the D_1 transition of Rb at 795 nm. In this way, the condensate is produced in the of this combined potential: harmonic (magnetic) + periodic in 1D (optical) [12] given by:

$$V = V_{mag} + V_{opt} = \frac{1}{2}m(\omega_z^2 z^2 + \omega_\perp^2(x^2+y^2)) + sE_R\cos^2(k_L z) \qquad (1)$$

where m is the atomic mass, $E_R = \hbar^2 k_L^2/2m$ is the recoil energy one atoms acquires when it absorbs one lattice photon and s is a dimensionless parameter.

Typically the condensate splits into ~ 200 optical wells each containing ~ 500 atoms. We have studied the dynamics of the condensate in this potential by inducing low lying collective modes. In particular we have studied the center-of-mass dipole oscillation of the cloud [3] and the quadrupole and transverse breathing modes corresponding to shape oscillation of the cloud and already extensively studied for a condensate trapped in a pure harmonic potential [13]. In the regime of small amplitude oscillation the system performs a superfluid motion and the characteristic frequencies of the collective modes are shifted towards lower values as a consequence of the presence of the periodic potential.

2.1 Superfluid regime

In this section we report the experimental results concerning the frequencies of the low lying collective modes we investigated as a function of the optical potential depth. In particular we investigate the dipole mode, corresponding to the center-of-mass oscillation of the system, and the quadrupole and transverse breathing modes corresponding to shape oscillations.

We induce the dipole mode by suddenly displacing the minimum of the magnetic harmonic potential along the axial direction. Then we allow the BEC to move in the combined trap and after a variable time we switch off both the magnetic and the optical potential, let the cloud expand for 28 ms and take an absorption image of the BEC. From the expanded cloud picture we extract the center-of-mass position. For small enough displacements of the magnetic potential minimum the BEC performs a harmonic oscillation characterized by a frequency consistently smaller than the frequency of the harmonic potential and depending on the height of the optical potential. In Fig.1 we show the measured dipole frequencies as a function of the lattice height: as the optical potential is increased the frequency shifts down. The new frequencies can be obtained introducing an effective mass as done in [14]. We remind here that in the tight binding regime we also demonstrated that the dipole motion of an array of condensates in the presence of the periodic potential can be described by coupled Josephson equations for the center-of-mass position of the array and the relative phase of two condensates in two adjacent optical wells [3].

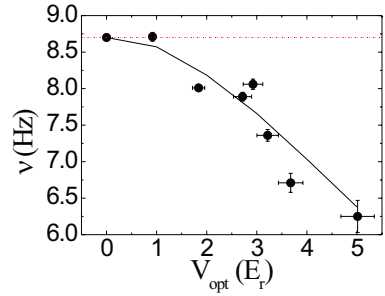

Figure 1. Measured dipole frequency of the condensate performing center-of-mass oscillation in the harmonic magnetic potential in the presence of an optical lattice. The frequency is reported as a function of the optical potential depth (in unit of the recoil energy), the dashed line corresponds to the dipole frequency in the pure harmonic trap while the solid line has been obtained taking into account the periodic potential in order to calculate the effective mass [14].

The quadrupole and transverse breathing mode of the BEC in the combined potential where excited by a resonant modulation of the radial frequency of the trap. This procedure excites modes with zero angular momentum along the symmetry axis of the trap. For an elliptical trap,

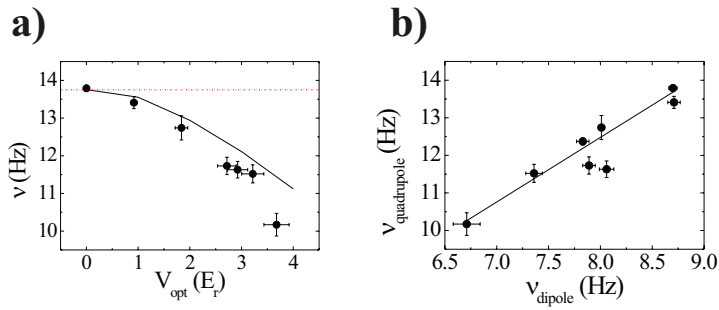

Figure 2. **a)** Measured quadrupole frequency of the condensate trapped in the combined potential (harmonic magnetic trap + 1D optical lattice). The frequency is reported as a function of the optical potential depth (in unit of the recoil energy), the dashed line corresponds to the quadrupole frequency in the pure harmonic trap while the solid line has been obtained taking into account the periodic potential in order to calculate the effective mass [14]. **b)** Frequency of the quadrupole mode as a function of the dipole mode frequency measured for different values of the optical lattice depth from $0E_R$ to $3.7E_R$. The line represents a linear fit giving a slope of 1.57 ± 0.01.

the lowest energy mode of this type corresponds to a deformation of the condensate shape characterized by oscillations of the radial and axial widths with the same frequency but with opposite phases (quadrupole mode). Increasing the frequency another collective mode with zero angular momentum along the symmetry axis can be excited which corresponds to an oscillation of the radial and axial widths with the same frequency and with the same phase (breathing mode). In the Thomas-Fermi regime, for small amplitude oscillations and strongly elongated traps, the two modes are characterized, respectively, by the frequencies $\sqrt{(5/2)}\omega_z$ and $2\omega_\perp$ [16]. In this limit the two frequencies are quite different and the axial and radial excitations are almost decoupled. In the quadrupole mode the axial width oscillates with a much larger amplitude than the radial one. In the transverse breathing mode the situation is reversed and the axial width oscillates with a much smaller amplitude than the radial one. After exciting the collective mode, we let the cloud evolve for a variable time t, then we switch off the combined trap, let the BEC expand for 29 ms and take an absorption image of the expanded cloud along one of the radial directions. From the image we extract the radial and axial radii of the condensate as a function of time t. We use a nonlinear least squares fit of the data with a sine function to obtain the frequencies of the modes with their errors.

Only the quadrupole mode frequency is shifted by the presence of the optical potential (Fig.2a) and scales in the same way as the dipole frequency (Fig.2b), while the transverse breathing mode results unaffected [15]. The experimental findings are consistent with the theoretical predictions of [14] where the modes frequencies have been obtained by generalizing the hydrodynamic equation of superfluids for a weakly interacting Bose gas to include the effects of a periodic potential.

2.2 Dynamical Superfluid-Insulator transition

A non-linear system, as an interacting Bose-Einstein condensate, moving in a periodic potential is expected to experience a dynamical instability when imaginary frequencies arise in its excitation spectrum [17]. The dynamical instability is due to an exponential growth of small perturbations that destroy the condensate. In the tight binding regime, when the lattice height is large enough in order to obtain an array of condensates trapped in the minima of the periodic potential, an analytical theoretical treatment becomes possible [18]. In this regime the dynamical instability can be studied observing the dipole oscillation in the combined trap (harmonic+periodic). The instability takes place when the amplitude of the dipole oscillations or, equivalently, the velocity exceeds a critical value depending on the optical lattice depth. As a

consequence of the transition the system loses the long range coherence (dephasing among condensates trapped in different sites of the periodic potential) and localizes far from the minimum of the magnetic harmonic trap (the center-of-mass motion is inhibited). In this sense a transition from a superfluid to an insulator is expected.

We investigated this transition varying the amplitude of the dipole oscillation of an array of condensates for different values of the optical lattice depth ranging from 3 to 14 E_R [19]. In Fig.3a we show the center-of-mass evolution of an array of condensates moving in a combined trap where the optical lattice depth is 5 E_R for two different displacements of the harmonic trap minimum. For a "small" displacement of 30 μm (open circle in the figure), the system performs a harmonic oscillation, while for a "large" displacement of 120 μm (filled circles) the atomic sample slowly moves towards the center of the magnetic potential.

The imaging of the array of BECs after some expansion directly gives also information about the phase property of the system. The density profile of the expanded cloud corresponds to the interference of the condensates [20, 21]. The interference of a coherent array of condensates shows up in a clear structure of density peaks separated by a distance $d = (2\hbar k_L/m)t_{exp}$ where t_{exp} is the expansion time. In particular the number of visible peaks in the interferogram, as in optics, depends on the radii of the single condensates, and in our regime of parameter we expect to observe only three peaks. On the contrary the interference of condensates with relatively random phase is expected to be a cloud that spreads out without any structure. In Fig.3b we report the data points corresponding to the ratio between the radius of the central peak (R_z) in the interferogram and the distance d taken for the experiments corresponding to Fig.3a. The "small" displacement data (open circles) correspond to a constant dimension of the central peak, actually all over the dynamics the three peak structure remains clearly visible as shown in the density profile shown on the right side of Fig.3b. On the contrary, the "large" displacement data (filled circles) show an increase in the dimension of the central peak during the evolution of the system in the combined trap. In this case the density profile rapidly spreads out as shown in the right side of Fig.3b.

We systematically investigated different values of optical potential depths and displacements in order to identify the critical values corresponding to the transition. In Fig.4 in the plane identified by the optical potential depths versus displacements we report as open circles situations corresponding to a clear harmonic oscillation of the condensates, while the filled circles correspond to experimental observation of the localization of the center-of mass of the atomic cloud. The dashed

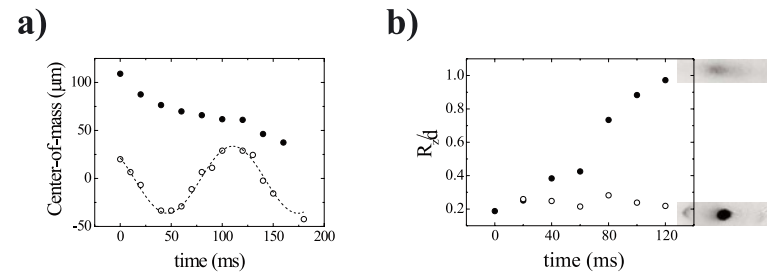

Figure 3. **a)** Position of the center-of-mass of the atomic cloud in the trap for an optical potential height of 5 E_R. Open circles: "small" displacement (30 μm); filled circles: "large" displacement (120 μm). The dashed line is the fit to the small-displacement data with a sine function. **b)** The axial width (R_z) of the interferogram central peak normalized to the peak separation d as a function of time spent in the combined trap after the magnetic trap displacement for an optical barrier height of 5 E_R. Open circles correspond to the "small" displacement of 30 μm; filled circles correspond to the "large' displacement of 120 μm. In the right part of the figure we show the observed density profile at $t = 120$ ms for the two different displacements.

line corresponds to theoretical predictions of the critical displacements based on the model in [18] calculated for our experimental parameters [22]. The theoretical line well distinguish between the two experimental regions corresponding to superfluid/insulator regimes but the transition observed in the experiment is not so sharp as predicted from the theoretical model in [18]. As a matter of fact, we are not able to measure a critical displacement and, moreover the loss of phase coherence along the array of condensates is much less than the predicted one. Close to the transition, even if the center-of-mass no longer oscillates we still observe a residual long range coherence in the array that shows up as an interferogram consisting in the three peak structure. In Fig.5 we show the imaging of the expanded array corresponding to an optical potential depth of 4.5 E_R and a displacement of 50 μm, already in the critical region (see Fig.3a). The interferogram is recognizable even if a structure inside the peaks shows up. This deviations from the 1-D theoretical predictions of [18] can be understood extending to a 3-D theory. In the experiments also the radial degrees of freedom can have a role, as a matter of fact we expect that part of the energy goes into radial modes instead of contributing to the growth of the perturbation causing the superfluid-insulator transition associated to the dynamical instability. On this point a complete 3D simulation can help in understanding the observed behaviour and preliminary results [23] already show a qualitative agreement with our observations.

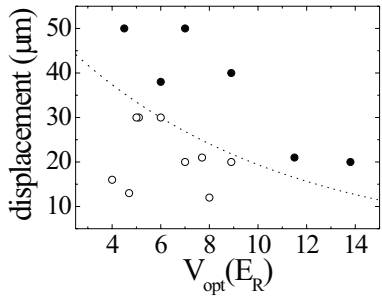

Figure 4. Filled circles represent coherent oscillations (with the three peaks interferogram); empty circles denote pinned motions; the dashed line corresponds to the theoretical value of the critical displacement [18] for the onset of the dynamical instability in our system.

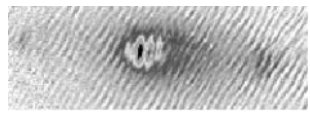

Figure 5. Picture of the expanded array corresponding to an optical potential depth of 4.5 E_R and a displacement of 50 μm. In this condition we do not observe any oscillation of the array but still the system shows a long range phase coherence.

3. Expansion of a BEC in a moving optical lattice

We now discuss a different experiment where we study the expansion of a condensate inside a moving 1D optical lattice [24]. This experiment allows us to load the condensate with different quasi-momenta q in the periodic structure realized by the optical lattice. From the solid state physics it is well known that in the presence of an infinite periodic potential the energy spectrum of the free particle is modified and a band structure arises [25]. In the rest frame of the lattice the eigen-energies of the system are $E_n(q)$, where q is the quasi-momentum and n the band index. According to band theory, the velocity in the n-th band is $v_n = \hbar^{-1}\partial E_n/\partial q$ and the effective mass is $m^* = \hbar^2(\partial^2 E_n/\partial q^2)^{-1}$. The effective mass can be negative for a range of quasi-momentum and this has been recently recognized as a possibility to realize bright solitons in BEC with repulsive interactions [26, 27].

In this experiment we first produce the condensate in a pure harmonic trap, then we switch off the magnetic harmonic potential let the BEC expand for 1 ms and we switch on a moving periodic potential. After 1 ms of expansion the density of the condensate decreases enough to neglect the non linear term in the Gross-Pitaevskii equation describing an interacting BEC. This means that, as a first approximation, we are allowed to consider the BEC as a linear probe of the periodic potential energy spectrum. The moving periodic potential is created by the interference of two counterpropagating laser beams with a slightly different frequency and blue detuned 0.5 nm from the D_2 resonance at 780 nm. The two beams are obtained by the same laser and are controlled by two independent acousto-optic modulators. The resulting light field is a standing wave moving in the laboratory frame with a velocity $v_L = \lambda\Delta\nu/2$ where $\Delta\nu$ is the frequency difference between the two laser beams. In our experiment, we typically vary the optical lattice velocity between 0 and $2v_R$ where $v_R = \hbar k_L/m$ is the recoil velocity of an atom absorbing one lattice photon and k_L corresponds, in the frame of the band theory, to the limit of the Brillouin zone. We switch on the moving optical lattice adiabatically by ramping the intensity of the two laser beams in 2 ms. This ensures we are loading the condensate in a Bloch state of well-defined energy and quasimomentum [9]. We let the condensate expand in the lattice and after a total expansion time of 13 ms we take an absorption image of the cloud along the radial horizontal direction looking at the position and dimensions of the condensate inside the optical lattice. From the position after the expansion, we extract the velocity of the condensate inside the optical lattice. In particular we repeat the experiment for different velocities of the lattice and compare the position of the expanded condensate inside the lattice with the position of the condensate expanded without the optical lattice. Let call this difference in position along the axial direction Δz, then the velocity of the BEC inside the optical lattice is given by $v = \Delta z/\Delta t - v_L$ where Δt is the expansion time inside the lattice.

In Fig.6 we show the results obtained for the velocity of the condensate as a function of the quasimomentum q for two different values of the lattice potential depth. The experimental data points are compared with the theoretical results obtained from the band theory and show a very good agreement. With an adequate sampling of the velocity we can extract the effective mass values given by $\partial v/\partial q$. The results for an optical potential depth of 1.3 E_R are shown in Fig.7. As we increase the lattice velocity (corresponding to increasing the quasimomentum q) the effective mass rapidly increases and between 0.7 q and 0.8 q it first becomes infinite positive and then negative ($q_R = \hbar k_L$).

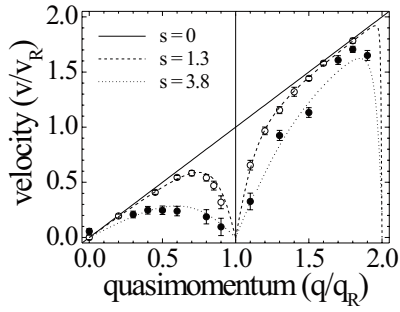

Figure 6. Velocity of the condensate inside the optical lattice as a function of the quasimomentum q in units of the recoil momentum $q_R = \hbar k_L$. The open circles corresponds to data obtained with $V_{opt} = 1.3E_R$ and the filled circles to data obtained with $V_{opt} = 3.8E_R$. The dashed and dotted lines are the correspondent curves given by the band theory.

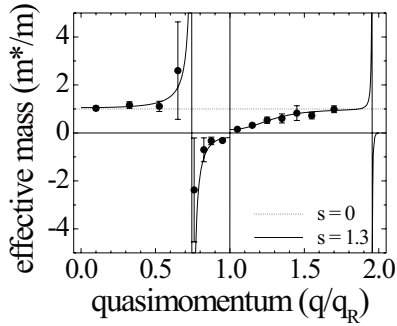

Figure 7. Effective mass of a condensate moving in an optical lattice of $1.3E_R$ as a function of the quasimomentum. The data points correspond to the values extracted from the measured velocity and the solid line is the corresponding theoretical prediction of the band theory.

The consequence of the strong variation of the effective mass is expected to consistently modify the expansion of the condensate along the axial direction [28]. As a matter of fact the effective mass enters the diffusive (kinetic) term in the Gross-Pitaevskii equation.

In Fig.8 we report the radii of the condensate measured as a function of the quasimomentum after the expansion inside the optical lattice compared to numerical predictions based on an effective 1D theoretical

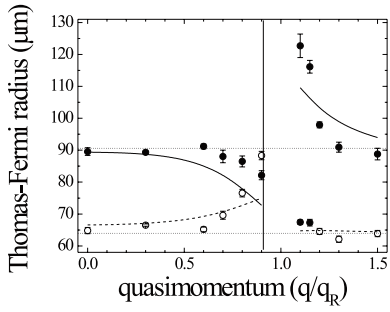

Figure 8. Axial and radial dimensions of the condensate after the expansion in an optical lattice $V_{opt} = 2.9E_R$. The experimental points (filled and open circles) show the Thomas-Fermi radii of the cloud extracted from a 2D fit of the density distribution. The dotted lines show the dimensions of the expanded condensate in the absence of the optical lattice. The continuous and dashed lines are theoretical calculations obtained from the 1D effective model [28, 24].

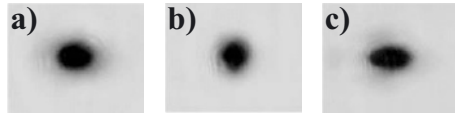

Figure 9. Absorption images of the expanded condensate. From left to right: a) normal expansion of the condensate without lattice; b) axial compression in a lattice of 2.9 E_R and $v_L = 0.9v_R$; c) enhanced axial expansion in a lattice of 2.9 E_R and $v_L = 1.1v_R$.

model [28]. The axial radius (filled circles in Fig.8) decreases until the quasimomentum reaches q_R, this is first due to the increase of the effective mass (causing a slower expansion) and then by the fact the the effective mass becomes negative (causing a contraction of the axial direction during the time spent in the optical lattice). When $q \geq q_R$ the effective mass becomes positive again but with a value smaller then the real mass m. As a consequence the expansion becomes faster in this region of quasimomenta. In Fig.8 we also report the measured values of the radial dimension of the BEC. A deviation from the expansion without optical lattice (dotted line) is observed also in this direction for $q < q_R$, even if this dimension is not directly affected by the presence of the lattice. This is consistent with the theory (dashed line) and can be explained in terms of a coupling between the axial and the radial dynamics. For $q < q_R$ the compression along the lattice direction increases the

mean-field energy and causes a faster radial expansion. Instead, when the condensate is loaded with $q > q_R$, the axial expansion is enhanced ($0 < m^* < m$) and the residual mean-field energy is further reduced, causing a suppression of the non-linear coupling between the axial and radial dynamics. This behaviour is evident in the absorption images reported in Fig.9 where we show the shape of the condensate expanded without optical lattice (image **a)**), and with an optical lattice of 2.9 E_R and respectively quasimomenta $q < q_R$ (**b**)) and $q > q_R$ (**c)**). In the first case a contraction along the axial direction is accompanied by a faster expansion along the radial direction, while in the second case the condensate expands faster in the axial direction.

4. Summary

In this paper we have discussed different experiments devoted to the characterization of the dynamics of a Bose-Einstein condensate in a periodic potential. We have first studied the collective modes of a trapped condensate confined in the combined potential formed by adding to the harmonic magnetic trap the periodic potential due to a 1D optical lattice. The frequencies of collective modes characterized by a motion along the lattice direction are consistently modified [3, 15]. The observed shift can be interpreted in term of a rescaled mass (effective mass) [14]. We have also observed the dynamical instability [19] in the dipole oscillation with large enough amplitude. This phenomenon is peculiar of the interplay between the non-linearity of a trapped condensate and the periodicity introduced by the optical lattice and causes a transition between the superfluid and the insulator regime. The last part of the paper has been devoted to the discussion of an experiment where we have studied the motion of an expanded condensate inside the optical lattice. During the expansion performed by the condensate before switching on the lattice, the mean field energy is mostly converted into kinetic energy allowing us to consider the condensate a linear probe of the energy band structure of the periodic potential. As a matter of fact we were able to measure the velocity of the condensate and its effective mass as a function of the quasi-momentum finding a very good agreement with the single-particle band theory. The non-linear term increases again in the region of negative effective mass where the axial radius of the condensate contracts inside the lattice. This causes a coupling between the axial and the radial direction that evidenced in a modified radial expansion. Loading the condensate in a periodic potential with a negative effective mass is regarded as a possible way to realize bright solitons in repulsive BEC as recently demonstrated in [27].

Acknowledgments

We acknowledge M. Inguscio and F. S. Cataliotti for their fundamental contribution to the experiments reported. We also would like to thank F. Ferlaino and P. Maddaloni for contributing in the first part of our experimental work and J. Catani and M. Zawada for their contribution on the experiment on the expansion of the condensate inside the optical lattice. We also acknowledge useful discussion and theoretical contribution of M. Modugno, P. Massignan, A. Smerzi, A. Trombettoni and C. Menotti. This work has been supported by the EU under Contracts Numbers HPRI-CT 1999-00111 and HPRN-CT-2000-00125, by the MURST through the PRIN2000 Initiatives and by the INFM Progetto di Ricerca Avanzata "Photon Matter" and PAIS2003 "Macroscopic Quantum Phase in Optical Lattices".

References

[1] Anderson B. P., Kasevich M. A., Science **282** 1686 (1998).

[2] Orzel C., Tuchman A. K., Fenselau M. L., Yasuda M., Kasevich M. A., Science **291**, 2386 (2001).

[3] Cataliotti F. S., Burger S., Fort C., Maddaloni P., Minardi F., Trombettoni A., Smerzi A., Inguscio M. Science **293** 843 (2001).

[4] Morsch O., Müller J. H., Cristiani M., Ciampini D., Arimondo E., Phys. Rev. Lett. **87**, 140402 (2001).

[5] Cristiani M., Morsch O., Müller J. H., Ciampini D., Arimondo E., Phys. Rev. A **65**, 063612 (2002).

[6] Steck D. A., Oskay W. H., Raizen M. G., Science **293**, 274 (2001).

[7] Hensinger W. K., Häffner H., Browaeys A., Heckenberg N. R., Helmerson K., McKenzie C., Milburn G. J., Phillips W. D., Rolston S. L., Rubinstein-Dunlop H., Upcroft B., Nature **412**, 52 (2001).

[8] Greiner M., Mandel O., Esslinger T., Hänsch T. W., Bloch I., Nature **415**, 39 (2002).

[9] Denschlag J. H., Simsarian J. E., Häffner H., McKenzie C., Browaeys A., Cho D., Helmerson K., Rolston S. L., Phillips W. D., J. Phys. B At. Mol. Opt. Phys. **35**, 3095 (2002).

[10] Greiner M., Mandel O., Hänsch T. W., Bloch I., Nature **419**, 51 (2002).

[11] Anderson M. H., Ensher J. R., Matthews M. R., Wieman C. E. Cornell E. A., Science, **269** 198 (1995); Davis K. B., Mewes M.-O., Andrews M. R., van Druten N. J., Durfee D. S., Kurn D. M. Ketterle W., Phys. Rev. Lett., **75** 3969 (1995). Bradley C. C., Sackett C. A., Tollett J. J. Hulet R. G., Phys. Rev. Lett., **75** 1687 (1995); **79** 1170 (1997).

[12] Pedri P., Pitaevskii L., Stringari S., Fort C., Burger S., Cataliotti F. S., Maddaloni P., Minardi F., Inguscio M., Phys. Rev. Lett. **87** 220401 (2001).

[13] Jin D. S., Ensher J. R., Matthews M. R., Wieman C. E., Cornell E. A., Phys. Rev. Lett. **77** 420 (1996); Matthews M. R., Hall D. S., Jin D. S., Ensher J. R.,

Wieman C. E., Cornell E. A., Dalfovo F., Minniti C., Stringari S., Phys. Rev. Lett. **81** 243 (1998); Mewes M.-O., Andrews M. R., van Druten N. J., Kurn D. M., Durfee D. S., Townsend C. G., Ketterle W., Phys. Rev. Lett. **77** 988 (1996); Fort C., Prevedelli M., Minardi F., Cataliotti F. S., Ricci L., Tino G. M., Inguscio M., Europhys. Lett. **49** 8 (2000); Chevy F., Bretin V., Rosenbusch P., Madison K.W., Dalibard J., Phys. Rev. Lett. **88** 250402 (2002).

[14] Krämer M., Pitaevskii L., Stringari S., Phys. Rev. Lett. **88** 180404 (2002).

[15] Fort C., Cataliotti F. S., Fallani L., Ferlaino F., Maddaloni P., Inguscio M., Phys. Rev. Lett. **90** 140405 (2003).

[16] Stringari S., Phys. Rev. Lett. **77** 2360 (1996).

[17] Wu B., Niu Q., Phys. Rev. A **64** 061603(R) (2001); Abdullaev F. Kh., Baizakov B. B., Darmanyan S. A., Konotop V. V., Salerno M. Phys. Rev. A **64** 043606 (2001); Konotop V.V., Salerno M. Phys. Rev. A **65** 021602 (2002); Wu B., and Niu Q. cond-mat/0306411 (2003); Menotti C., Smerzi A., Trombettoni A., New Journal of Phys. **5** 112 (2003).

[18] Smerzi A., Trombettoni A.,Kevrekidis P. G., Bishop A. R., Phys. Rev. Lett. **89** 170402 (2002).

[19] Cataliotti F. S., Fallani L., Ferlaino F., Fort C., Maddaloni P., Inguscio M., New Journal of Physics **5** 71 (2003).

[20] Greiner M., Bloch I., Mandel O., Hänsch T. W., Esslinger T., Phys. Rev. Lett. **87** 160405 (2001).

[21] Pedri P., Pitaevskii L., Stringari S., Fort C., Burger S., Cataliotti F. S., Maddaloni P., Minardi F., Inguscio M., Phys. Rev. Lett. **87**, 220401 (2001).

[22] Trombettoni A., private communication.

[23] Modugno M., Nesi F. in preparation.

[24] Fallani L., Cataliotti F. S., Catani J., Fort C., Modugno M., Zawada M., Inguscio M., cond-mat/0303626

[25] Ashcroft N. and Mermin N., *Solis State Physics* (Saunders, Philadelphia, 1976).

[26] Lenz G., Meystre P., Wright E. M., Phys. Rev. A **50**, 1681 (1994); Konotop V., Salerno M., Phys. Rev. A **65**, 021602 (2002); Hilligse K. M., Oberthaler M. K., Marzlin K.-P., Phys. Rev. A **66**, 063605 (2002).

[27] Eiermann B., Treutlein, P. Anker Th., Albiez M., Taglieber, M. Marzlin K.-P., Oberthaler M. K., Phys. Rev. Lett. **91**, 060402 (2003).

[28] Massignan P. and Modugno M., Phys. Rev. A **67**, 023614 (2003).

BOSE-EINSTEIN CONDENSATES IN OPTICAL LATTICES IN THE NONLINEAR REGIME

Oliver Morsch
INFM, Dipartimento di Fisica via Buonarroti 2, I-56127 Pisa, Italy
morsch@df.unipi.it

Ennio Arimondo
INFM, Dipartimento di Fisica via Buonarroti 2, I-56127 Pisa, Italy
arimondo@df.unipi.it

Abstract Bose-Einstein condensates in optical lattices are a valuable tool for investigating the nonlinear dynamics of matter waves in periodic potentials. In this review, we present and discuss recent experiments on the free expansion, nonlinear Landau-Zener tunneling and instabilities of condensates in such potentials.

Keywords: Bose-Einstein condensate, nonlinearity, Landau-Zener tunneling, instability

1. Introduction

Research on Bose-Einstein condensates (BECs) has come a long way since the first realization of BEC in dilute alkali gases in 1995. After the initial - and very exciting - studies of collective modes and sound propagation, the first observation of quantized vortices [1] gave rise to a qualitatively new kind of research on BECs. Likewise, the first demonstration of a BEC loaded into the periodic potential [2] created by two or more interfering laser beams - a so-called optical lattice - inspired a host of theoretical and experimental work on this intriguing system, not least because of its formal resemblance to electrons in a solid state crystal. In this review paper, we will give a summary of recent experiments in Pisa on Bose-Einstein condensates in optical lattices.

F. Kh. Abdullaev and V. V. Konotop (eds.), Nonlinear Waves: Classical and Quantum Aspects, 223–236.

The research field of optical lattices [3] was born shortly after the first optical molasses and magneto-optical traps (MOTs) had been demonstrated in the late 1980s [4, 5]. Initially, optical lattices in the dissipative regime were realized, i.e. on top of the periodic potential felt by the atoms there was also spontaneous scattering of photons which resulted in the Sisyphus cooling mechanism. Later on, Raman sideband-cooling was used to cool the atoms to the vibrational ground states of the potential wells making up the lattice, and in far-detuned lattices with negligible photon scattering rate the dynamics of the atomic matter waves was investigated.

The advent of Bose-Einstein condensates in 1995 opened up new possibilities for optical lattice research. Whilst in the early optical lattice experiments the atoms had to be painstakingly cooled into the vibrational ground states of the wells and the fraction of atoms actually occupying a well was on the order of a few percent, BECs changed all that. Condensate densities exceeding $10^{14}\,\mathrm{cm}^{-3}$ meant that a 3-dimensional lattice with lattice spacing $\approx 400\,\mathrm{nm}$ could be easily loaded with several atoms per lattice site. Since a condensate by definition occupies the lowest quantum state of the magnetic trap in which it is created, by a judicious choice of the loading procedure a BEC can be loaded directly into the ground state of an optical lattice without the need for further cooling.

Another consequence of the high atomic densities in condensates (compared to non-condensed, ultra-cold samples) is the importance of atomic collisions for the dynamics of the BEC. The effect of interactions is usually included into the mathematical description through a mean-field term in the Schrödinger equation, resulting in the Gross-Pitaevskii equation [6]. Depending on the trap frequency and hence the density of the BEC, the effect of this nonlinear term can be rather important with respect to the energy scale of the optical lattice and can lead to new effects in the evolution of the condensate inside the periodic potential. Some of these we shall discuss here.

This paper is organized as follows. After a brief review of the basic concepts and notations related to matter waves in periodic potentials (Sec. 2), we describe the part of our experimental apparatus relevant for the realization of 1D optical lattices (Sec. 3). In Section 4 we then discuss some experiments on BECs in optical lattices in the nonlinear regime: free expansion inside a 1D lattice (Sec. 4.1), nonlinear and asymmetric Landau-Zener tunneling (Sec. 4.2) and instabilities (Sec. 4.3). Finally, we present our conclusions and an outlook on future experiments in Sec. 5.

2. Matter waves in periodic potentials - basic concepts

In order to set the scene for the rest of this paper, in this section we shall briefly remind the reader of some of the basic concepts related to waves in periodic potentials. At this stage, we will concentrate on the linear treatment.

The time-independent Schrödinger equation for a particle of mass m inside a periodic potential of depth V_0 and periodicity d can be written as follows:

$$-\frac{\hbar^2}{2m}\frac{d^2\psi}{dx^2} + V_0 \sin^2(\pi x/d)\psi = E\psi \tag{1}$$

This is formally equivalent to the Mathieu equation, the eigenfunctions of which correspond to energy bands characterized by a band index n and a quasimomentum q [7]. For the purposes of the present article, it will be sufficient to consider only the two lowest energy bands with $n = 0$ and $n = 1$, which we will call ground state and first excited state, respectively. The energy scale of the periodic potential is the lattice energy,recoil $E_{rec} = \hbar^2\pi^2/md^2$, in terms of which we will express the lattice depth V_0 in the following. For small depths V_0/E_{rec}, the energy gap at $q = 1$ between the two lowest bands is $\Delta E \approx V_0/2$.

Two well-known features of the quantum dynamics of particles inside a periodic potential are Bloch oscillations and Landau-Zener tunneling. The former arise when a force is applied to the particles, resulting in a variation of the quasimomentum q. When $q = 1$, which corresponds to the edge of the Brillouin zone, the particles undergo Bragg reflection to $q = -1$ and thus the process of crossing the Brillouin zone starts again. If the group velocity of the particles is measured, it is found that rather than increasing at a constant rate as expected for free particles, it oscillates around the expected straight line $v = at$ with an amplitude depending on the lattice depth.

Up to now, we have assumed that during the acceleration the particles remain in the ground-state energy band of the lattice. If the acceleration a exceeds a critical value $a_c = \frac{d}{4\hbar^2}(\Delta E)^2$, though, the particles can no longer adiabatically follow the ground state and can tunnel into the first excited band when the edge of the Brillouin zone is crossed. The probability r for this Landau-Zener tunneling in a linear model is given by

$$r = \exp(-a_c/a). \tag{2}$$

In the following we shall see that in the presence of a nonlinear term in the Schrödinger equation, the tunneling behaviour can be substantially altered.

3. Experimental realization of BECs in periodic potentials

In order to create a periodic potential, one can make use of the ac Stark shift of a linearly polarized laser beam of intensity I detuned by an amount Δ from an atomic resonance. If two or more such laser beams are superposed, a periodic potential landscape in one, two or three dimensions can be realized. In particular, if two linearly polarized beams with wavelength λ making an angle θ with each other are used, the resulting one dimensional periodic potential is given by

$$V(x) = V_0 \sin^2(\pi x/d), \tag{3}$$

where the lattice spacing $d = \lambda/(2\sin(\theta/2))$. The depth of the potential $V_0 \propto \frac{I}{\Delta}$ can be calculated from the transition strength of the atomic resonance and the intensity and detuning of the laser beam. In our experiments, lattice spacings between $d = 0.39\,\mu$m and $d = 1.6\,\mu$m and lattice depths up to $20\,E_{rec}$ were used [8].

In practice, the two laser beams are derived from the same diode laser, split up into two beams by a beam-splitter and then frequency shifted by two acousto-optic modulators (AOMs). The latter are necessary for fast and controlled switching of the lattice depth, but are also useful for creating a moving or accelerated optical lattice in the following way: If a frequency difference $\delta\nu$ (usually on the order of a few kHz) is introduced between the two AOMs, the resulting periodic potential will move at a velocity $v_{lat} = d\delta\nu$. By linearly chirping $\delta\nu$, an accelerated lattice with $a_{lat} = d\frac{d\delta\nu}{\delta t}$ can be realized.

Our protocol for preparing a BEC in an optical lattice is as follows. After creating a BEC of around 10^4 atoms of ^{87}Rb in a TOP-trap [9], we adiabatically relax the magnetic trap frequency to between 20 Hz and 60 Hz. Thereafter, the intensities of the two laser beams forming the optical lattice are ramped up from 0 to the desired value in $10-50$ ms. In this way, the lattice switch-on is adiabatic with respect to the chemical potential [10] and hence the condensate is in the ground state of the combined harmonic plus periodic potential.

4. Nonlinear effects of BECs in optical lattices

Collisions between the atoms of a BEC can be included into the Schrödinger equation by adding a mean-field term depending on the s-wave scattering length a_s ($a_s = 5.4$ nm for ^{87}Rb), the mass m of the bosons and the local condensate density $|\psi|^2$. The resulting Gross-

Pitaevskii equation for a condensate in a periodic potential then reads

$$i\hbar\frac{\partial\psi}{\partial t} = -\frac{\hbar^2}{2m}\frac{\partial^2\psi}{\partial x^2} + V_0\sin^2\left(\frac{\pi x}{d}\right)\psi + \frac{4\pi\hbar^2 a_s}{m}|\psi|^2\psi. \tag{4}$$

The relative importance of the nonlinear energy scale and the energy scale of the lattice E_{rec} can be expressed through a nonlinear parameter C given by [11]

$$C = \frac{\pi n_0 a_s}{k_L^2}, \tag{5}$$

where $k_L = \pi/d$ is the lattice wavevector and n_0 is the density of the condensate. Depending on the lattice spacing, the number of condensate atoms and the magnetic trap frequency, in our experiments we were able to vary C between $C \approx 0.004$ and $C \approx 0.1$.

In the following we shall describe a number of experiments in which the nonlinear term in the Gross-Pitaevskii equation played an important role in the static and dynamic properties of the condensate inside the optical lattice.

4.1 Free expansion and variation of the chemical potential

The free expansion of a condensate released from a magnetic trap was the subject of the first experiments on Bose-Einstein condensates. In this way, clear evidence for condensation was obtained through the asymmetric expansion of the BEC, and the rate of expansion also made possible a measurement of the chemical potential μ which depends on the nonlinear term in the Gross-Pitaevskii equation.

We conducted similar experiments with BECs expanding freely inside a 1D optical lattice [13]. In these experiments, we loaded a BEC into a lattice as described above. After that, *only* the magnetic trap was switched off and the condensate was imaged after a variable time t_{exp} of free expansion inside the optical lattice. The effect of a deep lattice on the free expansion is clearly evident in the measurements of the condensate dimensions along and perpendicular to the lattice direction shown in Fig. 1. Whilst in the lattice direction the condensate does not expand at all, the expansion in the direction perpendicular to the lattice is noticeably enhanced with respect to the expansion of the condensate in the absence of the optical lattice. The lack of expansion in the lattice direction reflects the fact that the condensate has effectively been split up into several smaller condensates confined in the individual lattice wells, whereas the enhanced expansion in the perpendicular direction is explained by the increase in the chemical potential when the lattice is ramped up.

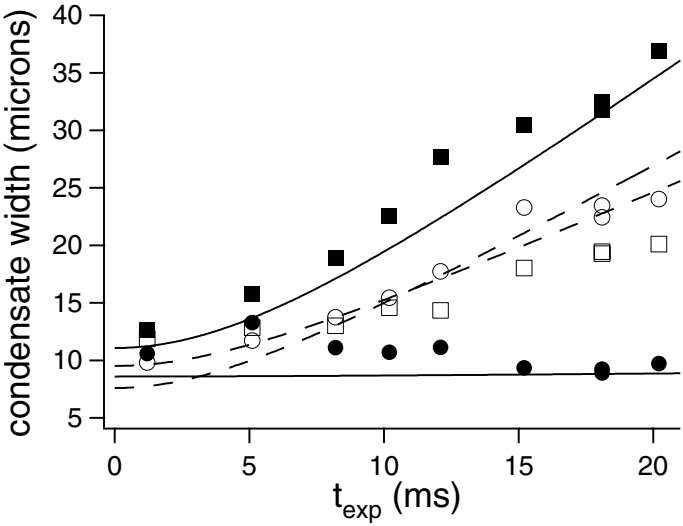

Figure 1. Free expansion of a Bose-Einstein condensate with (full symbols) and without (open symbols) a 1D optical lattice. Shown are the widths along (circles) and perpendicular to the lattice direction (squares) as a function of time after switching off the magnetic trap. When the lattice is present, there is no expansion in the lattice direction, whereas the expansion in the perpendicular direction is enhanced. The solid and dashed lines are theoretical predictions based on the model of [12].

For the central well of the optical lattice, Pedri and co-workers have calculated [14] the (local) chemical potential to be

$$\mu_{local} = \left(\frac{\pi}{2}\right)^{1/5} \left(\frac{V_0}{E_{rec}}\right)^{1/10} \mu_0, \tag{6}$$

where μ_0 is the chemical potential in the absence of the lattice. Measuring the expansion of the condensate for various lattice depths, we were able to deduce the effective chemical potential as a function of V_0. Our measured values agree well with Eqn. (6).

We also note here that in the limit of large lattice depths, our experiments effectively realize an adiabatic transformation between a 3D condensate and an array of 2D condensates. The condition $\mu_{3D} < \hbar\omega_{lat}$ of Ref. [15] (where $\omega_{lat} = 2(E_{rec}/\hbar)\sqrt{V_0/E_{rec}}$ is the harmonic approximation for the oscillation frequency in a lattice well) for the condensates in each well to be in the 2D limit is always satisfied for the small number of atoms in a single well ($\approx 10^3$) present in our experiment. For an array of 2D condensates obtained by creating the condensate in the combined potential of the harmonic trap and the lattice, Burger *et al.* [16]

have shown that in the case of their cigar-shaped condensate (with the long axis along the lattice direction), the transition temperature T_c^{2D} in the presence of the lattice is significantly lower than T_c^{3D} in the 3D case (i.e. in the magnetic trap without the lattice). Calculating the critical temperature T_c^{2D} along the same lines for our system, we find that $T_c^{2D} \approx T_c^{3D}$ due to the larger number of atoms per lattice site in our geometry, and hence we expect no significant change in the condensate fraction in the presence of the lattice. In fact, experimentally we even find a consistently larger condensate fraction after ramping up the lattice. This result indicates that, with an appropriate choice of parameters, a 1D optical lattice could be used to investigate adiabatic transformations between 3D and 2D condensates which could, e.g., be exploited to create condensates from thermal clouds by changing the dimensionality of the system.

4.2 Nonlinear and asymmetric Landau-Zener tunneling

When accelerating a particle inside a periodic potential, Landau-Zener tunneling between energy bands can occur if the critical acceleration for adiabatic following of an energy band is exceeded. In our experiments, we were able to exert a force on the condensate in the rest frame of the lattice by accelerating the latter. In this way, we could study tunneling between the two lowest energy bands of the lattice in a variety of situations. In particular, we were interested in the dependence of the tunneling probability on the value of the nonlinear parameter C defined above. Furthermore, we measured the tunneling rates between the bands for tunneling in both directions and found that in the presence of a strong enough nonlinear term, the two rates were different.

In order to measure the Landau-Zener tunneling rate, we first loaded a Bose-Einstein condensate into our optical lattice and then accelerated the lattice, thus changing the quasimomentum of the condensate. After crossing the edge of the Brillouin zone, we measured the fraction of atoms in the two lowest energy bands (details of this procedure will be discussed later) and hence calculated the tunneling rate. The nonlinear parameter C could be varied both by changing the density of the condensate through the magnetic trap frequency and by choosing different angles between the lattice beams, thus changing the lattice wavevector k_L. Tunneling in the two directions could be measured by either loading the condensate into the lowest energy band, in which case the lattice velocity $v_{lat} = 0$ when the lattice was switched on, or into the first excited band. In the latter case the lattice velocity was set at

$1.5\, v_{rec}$ when switching it on. In this way, in order to conserve energy and momentum the condensate must populate the first excited band at a quasi-momentum half-way between zero and the edge of the first Brillouin zone.

Our results on nonlinear Landau-Zener tunneling from the ground state are reported in [17]. Measuring the tunneling rate as a function of the nonlinear parameter C, we found that when the nonlinearity was large, Landau-Zener tunneling was significantly enhanced. Following Choi and Niu [11], we interpreted our results in terms of an effective potential $V_{eff} = V_0/(1 + 4C)$. As C grows, V_{eff} and hence the effective band-gap $\Delta E_{eff} \approx V_{eff}/2$ decreases, leading to an enhanced tunneling rate. In an intuitive picture, this can be explained as the (repulsive) interaction energy partially cancelling the potential energy of the periodic lattice as the condensate density is locally increased where the lattice potential is low, leading to an apparently smaller periodic energy modulation.

A more surprising result was obtained when comparing the tunneling rates from the ground state band to the first excited band and vice versa. In the linear case one expects these two rates to be the same. In the presence of a nonlinear term, however, this symmetry no longer holds: Whilst the tunneling from the ground to the first excited band is enhanced by the nonlinearity, the inverse is true for the opposite tunneling direction. The asymmetry in the tunneling transition probabilities can be explained qualitatively as follows: The nonlinear term of the Schrödinger equation acts as a perturbation whose strength is proportional to the energy level occupation. If the initial state of the condensate in the lattice corresponds to a filled lower level of the state model, then the lower level is shifted upward in energy while the upper level is left unaffected. This reduces the energy gap between the lower and upper level and enhances the tunneling. On the contrary, if all atoms fill the upper level then the energy of the upper level is increased while the lower level remains unaffected. This enhances the energy gap and reduces the tunneling.

Using a simple two-state model, we calculated the tunneling rates in the two directions as a function of C and found a growing asymmetry when C was increased [18]. We confirmed the presence of a tunneling asymmetry by integrating directly the Gross-Pitaevskii equation (taking into account the full experimental protocol described below), finding qualitative agreement with the prediction of the two-state model.

Experimentally, we investigated the asymmetric tunneling using a procedure similar to the one employed for the measurement of the nonlinear tunneling described above. Initially, the condensate is loaded adiabati-

cally into one of the two bands. Subsequently, the lattice is accelerated in such a way that the condensate crosses the edge of the Brillouin zone once, resulting in a finite probability for tunneling into the other band (higher-lying bands can be safely neglected as their energy separation at the edge of the Brillouin zone is much larger than the band gap). After the tunneling event, the two bands have populations reflecting the Landau-Zener tunneling rate (assuming that, initially, the condensate populated one band exclusively). In order to experimentally determine the number of atoms in the two bands, we then *increase* the lattice depth (from $\approx 2\,E_{rec}$ to $\approx 4\,E_{rec}$) and *decrease* the acceleration (from $\approx 3\,\mathrm{m\,s^{-2}}$ to $\approx 2\,\mathrm{m\,s^{-2}}$). In this way, successive crossings of the band edge will result in a much reduced Landau-Zener tunneling probability (of order a few percent). The fraction of the condensate that after the first tunneling event populated the ground state band will, therefore, remain in that band, whereas the population of the first excited band will undergo tunneling to the second excited band with a large probability (around 90 percent) as the relevant gap is smaller by a factor ≈ 5 for our parameters. Once the atoms have tunneled into the second excited band, they essentially behave as free particles since higher-lying band-gaps are smaller still, so they will no longer be accelerated by the lattice. In summary, using this experimental sequence we selectively accelerate that part of the condensate further that populates the ground state band. In practice, in order to get a good separation between the two condensate parts after a time-of-flight, we accelerate the lattice to a final velocity of $4 - 6\,v_{rec}$ and absorptively image the condensate after 22 ms.

In order to investigate tunneling from the ground state band to the first excited band, we adiabatically ramped up the lattice depth with the lattice at rest and then started the acceleration sequence. Thereafter, the same acceleration sequence as described above is used. For both tunneling directions, the tunneling rate is measured as

$$r = \frac{N_{tunnel}}{N_{tot}}, \tag{7}$$

where N_{tot} is the total number of atoms measured from the absorption picture. For the tunneling from the first excited band to the ground band, N_{tunnel} is the number of atoms accelerated by the lattice, i.e. those detected in the final velocity class $4\,v_{rec}$, whereas for the inverse tunneling direction, N_{tunnel} is the number of atoms detected in the $v = 0$ velocity class.

In a weak magnetic trap and hence a small value of the interaction parameter C, the measured tunneling rates are the same in both di-

rections and agree well with the linear Landau-Zener prediction. By contrast, when C is increased, the two tunneling rates begin to differ. Qualitatively we find agreement with the theoretical predictions of the non-linear Landau-Zener model, whereas quantitatively there are significant deviations. We believe these to be partly due to experimental imperfections. In particular, the sloshing (dipolar oscillations) of the condensate inside the magnetic trap can lead to the condensate not being prepared purely in one band due to non-adiabatic mixing of the bands if the initial quasimomentum is too close to a band-gap. Furthermore, a numerical simulation of the experiment shows that for large values of C, for which the magnetic trap frequency was large, the measured tunneling rates are significantly modified by the presence of the trap. In order to test our theory more quantitatively in BEC systems, the condensate could be held in an optical dipole trap with a small longitudinal trap frequency.

4.3 Instabilities

In our discussion of BECs in periodic potentials, up to now we have tacitly assumed that the effect of the nonlinearity in the Gross-Pitaevskii equation is to change the static and dynamic properties of the BEC in a continuous way: the chemical potential increases with increasing lattice depth, the tunneling rate from the ground state energy band increases with increasing nonlinearity, and an asymmetry between the two tunneling directions arises. Essentially, all these phenomena can be accounted for by rescaling in an appropriate way the system's parameters, i.e. by introducing an effective chemical potential or an (direction-dependent) effective potential depth. In this section, however, we will turn to a different problem which qualitatively changes the condensate dynamics in a drastic way.

When studying the properties of the Gross-Pitaevskii equation with a periodic potential, one finds that its solutions are unstable in the vicinity of the edge of the Brillouin zone [19]. These unstable modes grow exponentially in time with a growth rate that depends on the nonlinear parameter C and the lattice depth. In our experiment, we characterized the onset of the instability by observing the interference pattern of the condensate released after acceleration to a quasimomentum q. In practice, the time-of-flight interference pattern of the condensate released from the lattice then consists of a series of well-defined peaks corresponding to the momentum classes (in multiples of the lattice momentum $2p_{rec} = 2\hbar k_L$), as can be seen in Fig. 2. When the unstable modes grow, the long-range coherence of the condensate is lost and the interference pattern washes out.

In our experiment [21], the time the condensate spends in the 'critical region' where unstable solutions exists is varied through the lattice acceleration. Figure 2 shows typical integrated profiles of the interference patterns for lattice accelerations $a = 5\,\mathrm{m\,s^{-2}}$ and $a = 0.3\,\mathrm{m\,s^{-2}}$. In both cases, the condensate has reached the same point close to the Brillouin zone edge, but because of the longer time it has spent in the unstable region, the interference pattern is almost completely washed out for $a = 0.3\,\mathrm{m\,s^{-2}}$.

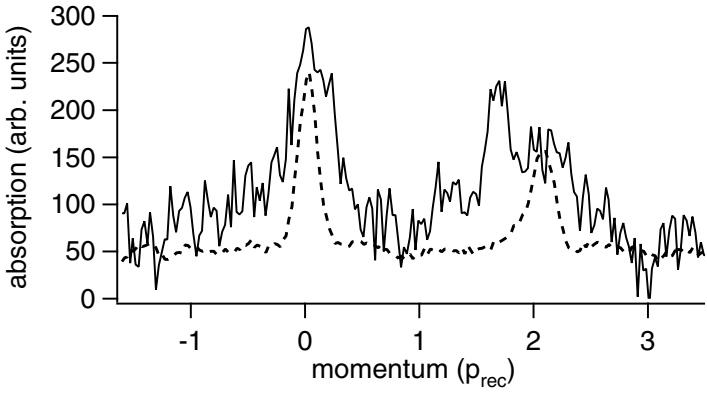

Figure 2. Interference patterns of a condensate close to $q = 1$. The solid and dashed lines correspond to accelerations $a = 0.3\,\mathrm{m\,s^{-2}}$ and $a = 5\,\mathrm{m\,s^{-2}}$, respectively. One clearly sees that for the large acceleration, the pattern is much less distinct than for the large acceleration. The two patterns were re-scaled to give the same peak height for ease of comparison.

In order to characterize our experimental findings more quantitatively, we define two observables for the time-of-flight interference pattern. By integrating the profile in a direction *perpendicular to* the optical lattice direction, we obtain a two-peaked curve for which we can define a visibility (in analogy to spectroscopy) reflecting the phase coherence of the condensate (visibility close to 1 for perfect coherence, visibility $\longrightarrow 0$ for an incoherent condensate). In order to avoid large fluctuations of the visibility due to background noise and shot-to-shot variations of the interference pattern, we have found that a useful definition of the visibility is as follows:

$$visibility = \frac{h_{peak} - h_{middle}}{h_{peak} + h_{middle}}, \tag{8}$$

where h_{peak} is the mean value of the two peaks (both averaged over 1/10 of their separation symmetrically about the positions of the peaks). By averaging the longitudinal profile over 1/3 of the peak separation

symmetrically about the midpoint between the peaks, we obtain h_{middle}. The second observable is the width of a Gaussian fit to the interference pattern integrated *along* the lattice direction over the extent of one of the peaks.

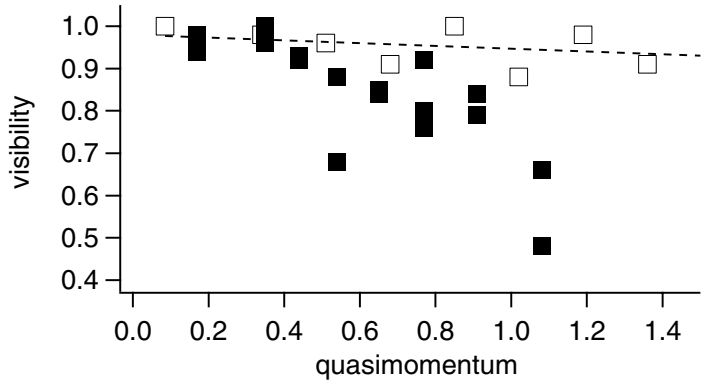

Figure 3. Visibility as a function of quasimomentum (in units of p_{rec}) for two different accelerations. Instabilities close to quasimomentum 1 (corresponding to the edge of the Brillouin zone) lead to a decrease in visibility for $a = 0.3\,\mathrm{m\,s^{-2}}$ (solid symbols). For comparison, the dotted line represents a linear fit to the visibility for the $a = 5\,\mathrm{m\,s^{-2}}$ data (open symbols).

The results of our experiment are exemplified by the two visibility curves in Fig. 3, showing clearly that for an acceleration of $5\,\mathrm{m\,s^{-2}}$, the visibility of the interference pattern remains reasonably stable when the edge of the Brillouin zone is crossed. In contrast, for $a = 0.3\,\mathrm{m\,s^{-2}}$ one clearly sees a drastic change as the quasimomentum approaches the value 1. For this acceleration, the condensate spends a sufficiently long time in the unstable region of the Brillouin zone and hence loses its phase coherence, resulting in a sharp drop of the visibility. At the same time, the radial width of the interference pattern was observed to increase by a factor between 1.5 and 1.7. This increase is evidence for an instability in the transverse direction and may, for instance, be due to solitons in the longitudinal direction decaying into vortices via a snake instability [20]. For the $a = 0.3\,\mathrm{m\,s^{-2}}$ data, the interference patterns for quasimomenta larger than 1 were so diffuse that it was not possible to measure the visibility in a meaningful way.

The experimental results presented above demonstrate that at the edge of the Brillouin zone, a BEC in an optical lattice exhibits unstable behaviour. These instabilities are also reproduced in a 1-D numerical simulation, and our experimental findings also agree qualitatively with

recent 3-D simulations [20]. The fact that we observe a significant effect of the instabilities below accelerations of $\approx 0.5\,\mathrm{m\,s^{-2}}$, for which the condensate spends more than 2 ms in the critical region around the edge of the Brillouin zone (having an extension of around 1/10 of the BZ [19]), indicates that the growth rate of the instability should be of the order of $500\,\mathrm{s^{-1}}$. This agrees reasonably well with a rough estimate of $\approx 300\,\mathrm{s^{-1}}$ derived from a recent work by Wu and Niu [19]. We note here that similar instabilities have been predicted and observed also in other physical systems, such as light propagating in nonlinear crystals [22].

5. Conclusions and outlook

Bose-Einstein condensates in optical lattices are a valuable tool for investigating nonlinear effects of matter waves in periodic potentials. Apart from the work presented in this paper, a number of theoretical and experimental research groups are currently working on, e.g., dispersion management and gap solitons [23]. In the future, one of the challenges will be to make more quantitative measurements of some of the effects presented in the present work. Another very promising line of research is the extension of optical lattice experiments to fermions [24], Bose-Fermi mixtures [25] and also to mixtures of more than one species or isotope of bosons and / or fermions.

Acknowledgments

The experimental and theoretical work reported in this review was carried out by the authors together with M. Anderlini, D. Ciampini, D. Cossart, E. Courtade, M. Jona-Lasinio, N. Malossi, and J.H. Müller. We are grateful to R. Scott, A. Martin and M. Fromhold for useful discussions.

References

[1] K. W. Madison, F. Chevy, W. Wohlleben, and J. Dalibard, Phys. Rev. Lett. **84**, 806 (2000).

[2] B.P. Anderson and M.A. Kasevich, Science **282** 1686 (1998).

[3] For a review of optical lattice research, see D.R. Meacher, Contemp. Phys. **39**, 329 (1998).

[4] S. Chu, L. Hollberg, J. E. Bjorkholm, A. Cable, and A. Ashkin, Phys. Rev. Lett. **55**, 48 (1985).

[5] E. L. Raab, M. Prentiss, A. Cable, S. Chu, and D. E. Pritchard, Phys. Rev. Lett. **59**, 2631 (1987).

[6] For an introduction to the Gross-Pitaevskii equation as applied to BECs, see F. Dalfovo, S. Giorgini, L.P. Pitaevskii, and S. Stringari, Rev. Mod. Phys. **71**, 463 (1999).

[7] C. Kittel, *Introduction to Solid State Physics*, New York: Wiley&Sons , 7th ed. (1996).

[8] M. Cristiani, O. Morsch, J. H. Müller, D. Ciampini, and E. Arimondo, Phys. Rev. A **65**, 063612 (2002).

[9] J.H. Müller, D. Ciampini, O. Morsch, G. Smirne, M. Fazzi, P. Verkerk, F. Fuso, and E. Arimondo, J. Phys. B **33** 4095 (2000).

[10] Y.B. Band, B. Malomed, and M. Trippenbach, Phys. Rev. A **65**, 033607 (2002).

[11] D.-I. Choi and Q. Niu, Phys. Rev. Lett. **82**, 2022 (1999).

[12] Y. Castin and R. Dum, Phys. Rev. Lett. **77**, 5315 (1996).

[13] O. Morsch, M. Cristiani, J. H. Müller, D. Ciampini, and E. Arimondo, Phys. Rev. A **66**, 021601 (2002).

[14] P. Pedri, L. Pitaevskii, S. Stringari, C. Fort, S. Burger, F. S. Cataliotti, P. Maddaloni, F. Minardi, and M. Inguscio, Phys. Rev. Lett. **87**, 220401 (2001).

[15] A. Görlitz, J. M. Vogels, A. E. Leanhardt, C. Raman, T. L. Gustavson, J. R. Abo-Shaeer, A. P. Chikkatur, S. Gupta, S. Inouye, T. Rosenband, and W. Ketterle, Phys. Rev. Lett. **87**, 130402 (2001).

[16] S. Burger, F.S. Cataliotti, C. Fort, P. Maddaloni, F. Minardi, and M. Inguscio, Europhys. Lett. **57**, 1 (2002).

[17] O. Morsch, J. H. Müller, M. Cristiani, D. Ciampini, and E. Arimondo, Phys. Rev. Lett. **87**, 140402 (2001).

[18] M. Jona-Lasinio, O. Morsch, M. Cristiani, N. Malossi, J.H. Müller, E. Courtade, M. Anderlini, and E. Arimondo, e-print: cond-mat/0306210 *(accepted for publication in Phys. Rev. Lett.).*

[19] Biao Wu and Qian Niu, New J. Phys. **5**, 104 (2003).

[20] R.G. Scott, A.M. Martin, T.M. Fromhold, S. Bujkiewicz, F.W. Sheard, and M. Leadbeater, Phys. Rev. Lett. **90**, 110404 (2003).

[21] M. Cristiani, O. Morsch, N. Malossi, M. Jona-Lasinio, M. Anderlini, E. Courtade, and E. Arimondo, e-print: cond-mat/0311160.

[22] Andrey A. Sukhorukov, Dragomir Neshev, Wieslaw Krolikowski, and Yuri S. Kivshar, e-print: nlin.PS/0309075.

[23] B. Eiermann, P. Treutlein, Th. Anker, M. Albiez, M. Taglieber, K.-P. Marzlin, and M. K. Oberthaler, Phys. Rev. Lett. **91**, 060402 (2003).

[24] G. Modugno, F. Ferlaino, R. Heidemann, G. Roati, and M. Inguscio, Phys. Rev. A **68**, 011601 (2003).

[25] H. Ott, E. de Mirandes, F. Ferlaino, G. Roati, G. Modugno, and M. Inguscio, e-print: cond-mat/0311261.

QUANTUM BOUND STATES AND MATTER WAVES DELOCALIZATIONS

Mario Salerno
Dipartimento di Fisica "E.R. Caianiello" and Istituto Nazionale di Fisica della Materia (INFM), Universitá di Salerno, I-84081 Baronissi (SA), Italy
salerno@sa.infn.it

Abstract We discuss localized ground states of the periodic Gross-Pitaevskii equation (GPE) in the framework of a quantum linear Schrödinger equation with effective potential determined in self-consistent manner. We show that depending on the interaction among the atoms being attractive or repulsive, bound states of the linear self-consistent problem are formed in the forbidden zones of the linear spectrum below or above the energy bands. These bound states correspond to exact solitons of the GPE equation. The implication of these results on delocalizing transitions of multidimensional solitons of the GPE is also discussed. In particular we show that the delocalizing transition corresponds to the threshold for the existence of a single bound state in the effective potential.

1. Introduction

One of the most intriguing phenomena occurring in nonlinear systems is the possibility to have stationary localized excitations which undergo a delocalizing transition when the nonlinearity in the system is below a critical threshold and the dimensionality d of the system is greater or equal than a critical value d_c [1, 2, 3] (for the cubic nonlinear Schrödinger equation $d_c = 2$). This phenomenon has been found in different discrete nonlinear systems [1, 3] supporting discrete breathers or intrinsic localized modes (ILM), as well as, in the theory of polaronic states of solids [4]. The occurrence of a delocalizing transition for $d \geq d_c$ is a consequence of the existence of a lower bound in energy (or equivalently in the norm), for a localized excitation to exist [1, 2], e.g. a finite threshold in the electron-phonon coupling constant for polaron formation. This contrasts with the one dimensional (1D) case for which these thresholds do not exist. In this case, indeed, it is possible to transform in

F. Kh. Abdullaev and V. V. Konotop (eds.), Nonlinear Waves: Classical and Quantum Aspects, 237–250.

a reversible manner a small ILM/polaron (i.e. a solution extended on a single lattice cell) into a large ILM/polaron (a solution extended on many lattice cells), by continuously decreasing the nonlinearity in the system (i.e. the electron-phonon constant for polarons). Very recently, the same phenomenon has been found in the continuous multidimensional nonlinear Schrödinger equation (NLS) with periodic potentials [5].

The aim of the present paper is twofold. From one side we show that localized excitations of the periodic nonlinear Schrödinger equation correspond to macroscopic quantum bound states of the linear Schrödinger problem in an effective potential which is determined by means of a self-consistent (SC) procedure. From the other side, we provide a physical interpretation and a theoretical investigation of the delocalizing transition for multidimensional solitons. These problems will be discussed on the physical example of a Bose-Einstein condensate in an optical lattice (OL) described, in the mean field approximation, by the following normalized Gross-Pitaevskii equation [6]

$$i\psi_t = \left[-\nabla^2 + U_{ol}(\mathbf{x}) + \chi|\psi|^2\right]\psi, \tag{1}$$

where χ is the nonlinear parameter, $\mathbf{x}$ denotes three dimensional coordinates and $U_{ol}(\mathbf{x})$ is a periodic potential representing the OL.

Solitonic properties of the GPE in optical lattices were also studied in Refs. [7, 8] for the discrete (tight-binding) case and in Refs. [11]-[14] for the continuous one. Self-consistent approaches were also used as numerical tools to study discrete breathers of the discrete NLS [15] and the stability of gap solitons [16]. The physical implications and the potentiality of the SC approach, however, have not been so far investigated.

The paper is organized as follows. In Section 2 we discuss localized ground states of the periodic Gross-Pitaevskii equation in the framework of a quantum linear Schrödinger equation with effective potential. The effective potential is determined by mean of a self-consistent procedure and the analysis is restricted to the 1D case. As a result, we show that depending on the interaction among the atoms, bound states of the linear self-consistent problem are formed in the forbidden zones of the linear spectrum, below or above the energy bands. These eigenstates are found to be exact solitons of the GPE equation by direct numerical simulations. In Section 3 we discuss the implications of the bound state interpretation on the delocalizing transition observed in higher dimensions [1, 3, 5]. In particular, we consider the case of the GPE with a two-dimensional (2D) optical lattice. Finally, in Section 4 we summarize the main results of the paper.

2. Matter waves as macroscopic quantum bound states

To discuss bound state properties of the localized solutions of the periodic GPE we restrict, for simplicity, to the 1D case (the approach however is of general validity and can be applied to NLS type equations in arbitrary dimensions). Our analysis is based on the simple observation that the stationary localized ground states $\psi_s(x,t) = \psi(x)\exp(-i\mu t)$ of the GPE (and more generally of any NLS-like equation) can be obtained by solving in a self-consistent manner the following linear Schrödinger problem

$$\left[-\nabla^2 + \hat{V}_{eff}(x)\right]\psi = \mu\psi \tag{2}$$

with the effective potential

$$\hat{V}_{eff} = \hat{U}_{ol}(x) + \chi|\hat{\psi}_s(x)|^2. \tag{3}$$

Here μ is the chemical potential (also referred as E in the following), $\hat{U}_{ol} \equiv \varepsilon\cos(2x)$ is the OL and $\chi|\hat{\psi}_s(x)|^2$ represents the potential associated with a given eigenstate of the quantum problem (2). For a self-consistent solution, one starts with a trial wavefunction for ψ_s (typically a Gaussian waveform) calculates the effective potential and solves the corresponding eigenvalue problem (2). Then, one selects a given eigenstate (for example the ground state but not necessarily) as new trial function and iterates the procedure until convergence is reached. The problem is thus reduced to the diagonalization of the quantum Hamiltonian

$$\hat{H} = \hat{H}_0 + \hat{V}_{eff}(x) \tag{4}$$

with $\hat{H}_0 \equiv -\nabla^2$ the kinetic energy operator. This can be effectively done by adopting a discrete coordinate space representation $\{x_n = na\}$, $n = 1, ..., N$, with $a = L/N$ the discretization constant, L the size of the system and N the total number of points. A basis for this space is simply a basis of R^N, i.e. the set of N-component vectors of the type $|n\rangle = (0, ...0, 1, 0, ..., 0)$, with the 1 in the position n. The effective potential is obviously diagonal in this representation i.e. $\langle n|\hat{V}_{eff}|n'\rangle = V_{eff}(na)\delta_{n,n'}$, while $\hat{H}_0$ is diagonal in the reciprocal representation $|k_n\rangle$, ($k_n = 2\pi/Ln$, the two representations being related by the Fourier transform (unitary transformation). The matrix elements of the Hamiltonian $\hat{H}$ can then be constructed as

$$\langle n|\hat{H}|n'\rangle \equiv H_{n,n'} = \langle n|\hat{F}^{-1}\hat{H}_0\hat{F}|n'\rangle + V_{eff}(na)\delta_{n,n'} \tag{5}$$

where $\hat{F}|n\rangle$ denotes the Fourier transform of the vector $|n\rangle$. For an effective construction of these matrix elements one can use the fast Fourier

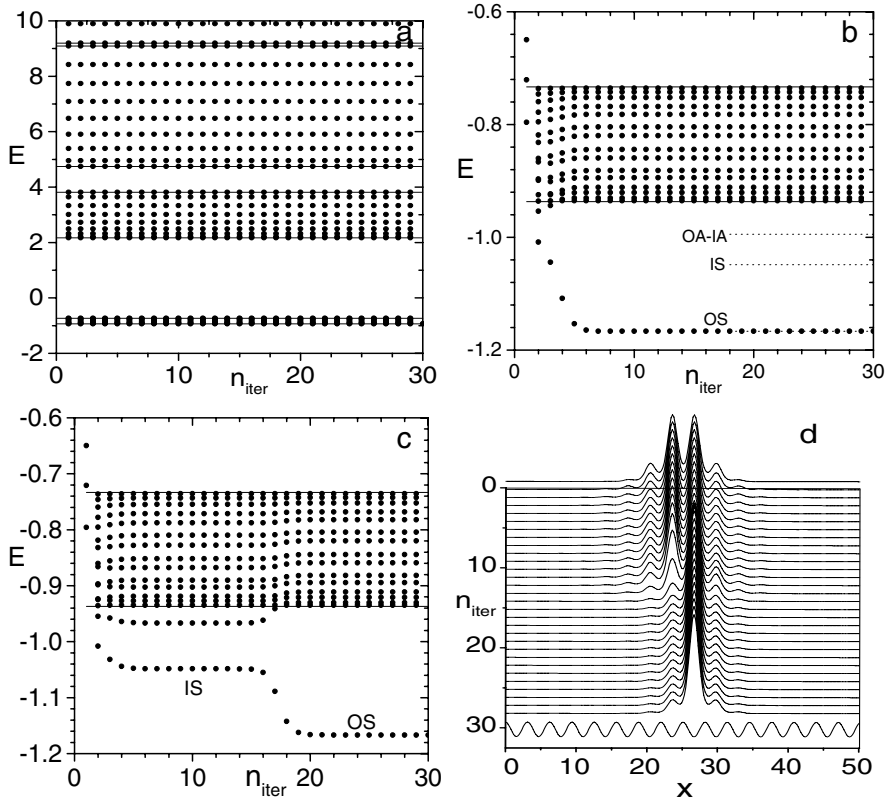

Figure 1. Panel **(a)** Energy spectrum for the effective potential (3) with $A = 3$ and $\chi = 0$ (Mathieu equation). Full lines represent exact values of the band edges of the Mathieu equation while dots are the eigenvalues obtained with the above procedure on a lattice of length $L = 40\pi$, with $N = 512$ points. Panel **(b)** Lowest energy band for the effective potential in Eq. (3) with ψ_s taken as the ground state of the system and for $\chi = -1$ (attractive case). Parameters are fixed as in panel (a). Panel **(c)** The same as in panel (b) but for $\varepsilon = -3$. Panel **(d)** Transition from the metastable IS mode to the OS ground state corresponding to the lower level of panel (c). The optical lattice (scaled by a factor 3) is reported as an help to locate the symmetry center of the solutions. Parameters are fixed as in panel (c).

transform while for the computation of the spectrum one can recourse to standard numerical routines for the diagonalization of real symmetric matrices. To check the method we consider first the linear case ($\chi = 0$) for which the effective potential is $V_{eff} = U_{ol}$ and the eigenvalue problem (2) reduces to the well known Mathieu equation. In Fig. 1a we depict the lowest part of the spectrum from which we see the appearance of the band structure with band edges which exactly correspond to the values obtained for the Mathieu equation (for high energy

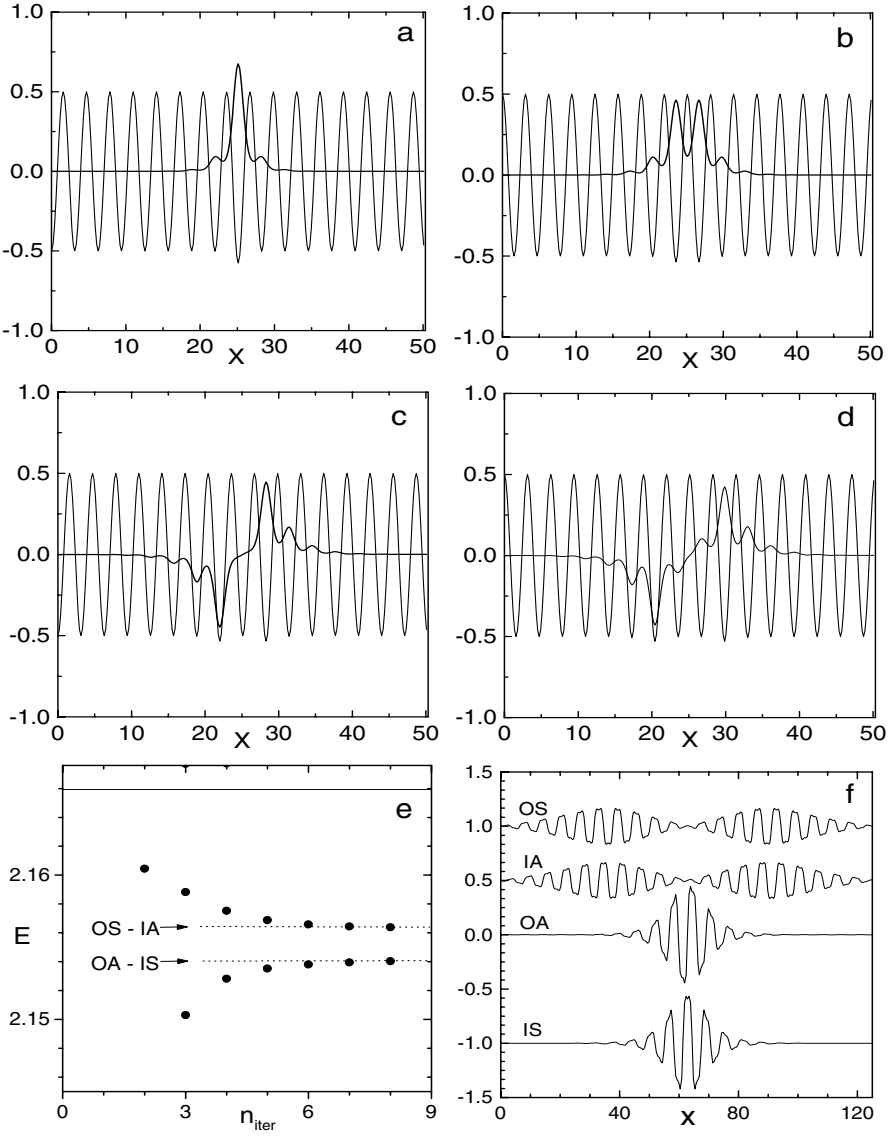

Figure 2. Wavefunctions and corresponding effective potential for the bound states below the lowest bands of Fig 1a for attractive interaction $\chi = -1$. Panel **(a)**. OS mode and corresponding effective potential for $E = -1.1667950$ (ground state) and $\varepsilon = 3$. The effective potential was scaled by a factor of 6 for graphical convenience. Panel **(b)**. Same as (a) for the IS mode at $E = -1.0485745$ and $\varepsilon = -3$. Panel **(c)**. Same as (a) for the OA mode. $E = -0.999261$. Panel **(d)**. Same as (b) for the IA mode. $E = -0.9947127$. **(e)** Energy levels of the OS, IS, OA, IA, modes inside the gap between the first two bands. The continuous line denotes the lower edge of the second band of Fig. 1a while the dotted lines denote the degenerate levels. Parameters are fixed as for corresponding modes in panels a-d. **(f)**. Wavefunctions associated to the levels in panel e. For graphical convenience the IS mode was shifted by -1.0 down while the IA and OS modes were shifted up by 0.5 and 1.0, respectively.

bands to get good accuracy one needs to increase N). Here we are mainly interested in the localized states associated with the lowest two bands (i.e., the ones physically most relevant), for this case the choice of $N = 256$ being adequate for most of the calculations. In Fig. 1b we show how the lowest band of panel 1a is modified by the nonlinear potential $V_{eff}(x) = \varepsilon \cos(2x) + \chi|\psi_0|^2$, where ψ_0 is taken to be the ground state of the system, for the case $\chi < 0$ (negative scattering length). A bound state below the band, rapidly converging to a constant value, is quite evident. Notice that the bound state forms from the lower edge of the band and is accompanied by a rearrangement of the extended states inside the band. The corresponding eigenvector is depicted in Fig.2a together with its effective potential. Notice that the potential has an attractive character (potential well) and the bound state is symmetric around a minima of the OL, i.e., it resembles the onsite-symmetric intrinsic localized mode (ILM) of nonlinear lattices (NL) [17, 18]. In the following we shall call it the onsite symmetric (OS) bound state. By shifting the phase of the OL by π (i.e. by changing the sign of ε) one obtains an eigenstate centered on maxima instead than on minima. This bound state is depicted in Fig. 2b and in analogy with NL we shall call it the intersite symmetric (IS) mode. The corresponding spectrum is reported in Fig. 1c. Notice that the IS mode corresponds to the plateau formed just before the decay into the OS mode occurs, as shown in panel 1d (also note the appearance of an intersite-symmetric (IA) excited level in Fig. 1c which is absorbed into the band in correspondence of the IS-OS decay). We have checked that these bound states coincide with the ones obtained with the approach of Ref. [11] for the same values of energy. The stability of the OS mode and the decay of the IS mode into the OS state was checked by direct numerical integrations of the GPE. To obtain the onsite asymmetric (OA) mode one needs to take the first excited state ψ_1 as effective potential in the SC procedure. This indeed produces an exact soliton solution of the GPE of type OA (see Fig. 2c). Shifting the potential by π produces the intersite asymmetric (IA) mode of Fig. 2d. These solutions have the same energies and are more unstable than the IS mode (they, however, do not decay into the ground state but get mixed with the extended states in the band).

In general, the effective potentials can be taken of the form $\hat{V}_{eff} = \hat{V}_{ol} + \chi|\hat{\psi}_n(x)|$ with ψ_n the n-th eigenstate of the eigenvalue problem in (2). If the energy of ψ_n lies outside the bands a localized mode of the type described above is produced, while if it lies inside a band, extended states which are nonlinear analogues of the Bloch states [13], are produced. From this we conclude that both localized and extended solutions of the GPE are exact quantum eigenstates of the Schrödinger

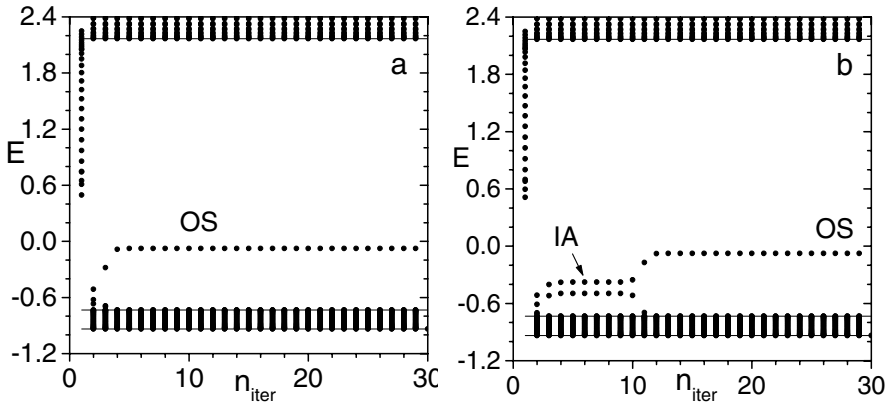

Figure 3. Energy spectrum in correspondence of the localized states above the lowest band of Fig. 1a for repulsive interactions $\chi = 1$. Panel **(a)**. Spectrum associated to the OS mode. Parameters are $\varepsilon = -3, N = 256, L = 40\pi$. Panel **(b)**. Same as panel (a) but for the IA mode with $\varepsilon = 3$. The continuous lines denote exact band edges of the Mathieu equation.

equation with a suitable effective potential. From the above analysis one expects that below each higher energy band eigenstates of the same symmetry type as the ones found for the lowest band should exist. This is precisely what we show in Fig.s 2e, 2f for the energy spectrum and the corresponding eigenstates in the gap below the second band. Notice that the OA and the IS eigenstates are degenerated (the same occurs also to the OS and IA modes). The OA and IS bound states are both very stable while the energy levels of the OA and IS modes, after establishing a plateau similar to the one in Fig 1c, become unstable (the energy oscillates between this level and the lower edge of the second band). The instability of these modes can be understood as an hybridization of the state (being very close to the band edge) with extended states of the second band and is confirmed by direct numerical integration of the PDE system. Similar localized modes can be found also for repulsive interactions ($\chi > 0$), the main difference with the previous case being that now the states appear in the gap above the band edges instead than below. This is shown in Fig. 3 for the lowest energy levels inside the first gap. The corresponding eigenvectors are shown in Fig. 4 together with their effective potentials. Notice that the potential has a local repulsive character (it increases in correspondence of the states) so that these bound states could not exist without the OL.

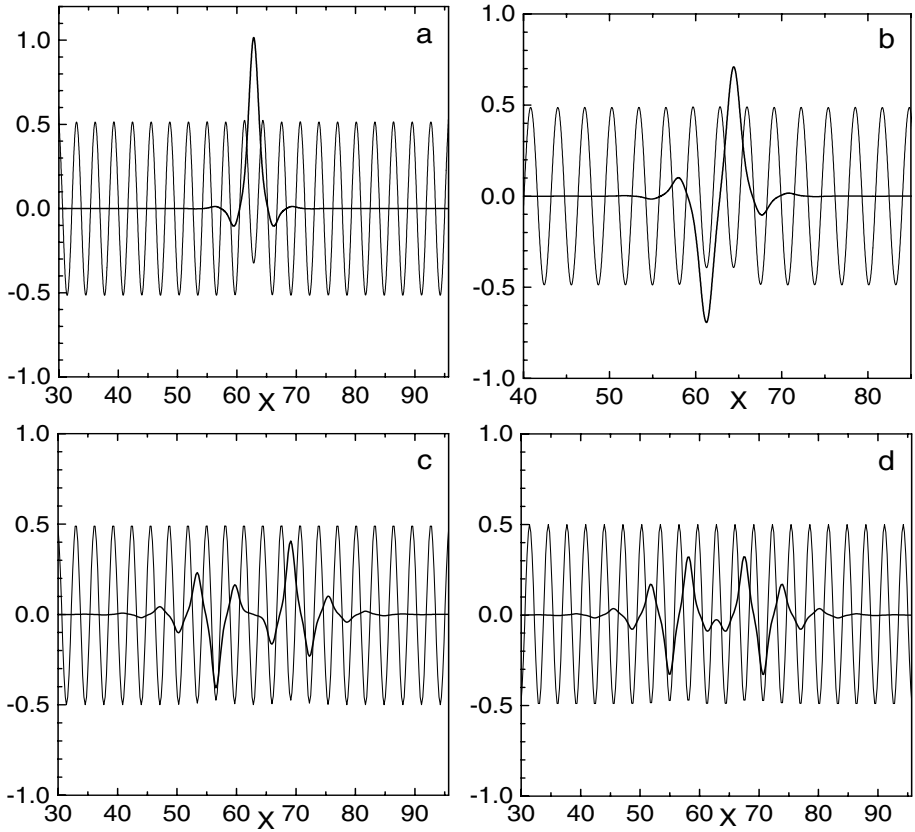

Figure 4. Wavefunctions and effective potentials of the bound states levels of Fig. 4 a,b, for the repulsive case $\chi = 1$. Panel **(a)**. OS mode with corresponding effective potential (thin line). Energy is $E = -0.078355$ and $\varepsilon = -3$. Panel **(b)**. Same as in Panel (a) for the IA mode. $E = -0.376645$, $\varepsilon = 3$. Panel **(c)**. Same as in panel (a) for the OA mode. $E = -0.683070$. Panel **(d)**. Same in panel (b) for the IS mode. $E = -0.691676$. Parameters are fixed as $N = 256$, $L = 40\pi$ for panels (a), (b), and $N = 512$, $L = 40\pi$ for panels (c), (d). The effective potentials have been reduced by a factor of 6 for graphical convenience.

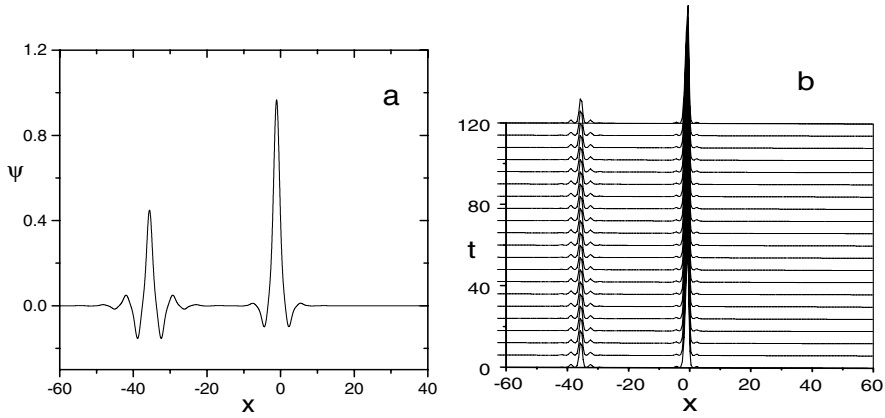

Figure 5. Panel **(a)**. Two soliton bound state of the repulsive GPE obtained from the SC procedure by using as effective potential $V_{eff} = V_{ol} + |\frac{1}{2}\psi_1 - \psi_2|^2$ where ψ_1, ψ_2 denote two eigenfunctions at the top of the first band. Panel **(b)**. Time evolution (modulo square) of the bound state in panel (a) taken as initial condition for the integration of the full GPE.

We remark that localized modes similar to the ones described in this paper were found also in atomic-molecular BEC using an approach based on Wannier functions [19].

Besides localized and extended states, the SC procedure allows to construct full nonlinear bands in reciprocal space. It is worth remarking that more complicated set of solutions of the GPE can be constructed with the SC procedure by taking as effective potentials linear combinations of eigenstates. An example of this is shown in Fig. 5 for the case of repulsive interaction. We see that a linear combination of two eigenstates leads to a bound state with two humps which corresponds to a multi-soliton solution of the GPE (see panel b). We believe this is a general property and we conjecture that *all solutions of the periodic GPE (and more in general of the NLS-like equations with arbitrary potentials) can be obtained with the SC method taking all possible combinations of linear eigenstates as effective potentials.*

3. Delocalizing transitions of matter waves

In this section we discuss the implications of the above bound state interpretation of the soliton ground states of the GPE on the delocalizing transition observed in higher dimensions. The delocalizing transition manifests as an irreversible transformation of a localized solution into an extended state, which occurs for $d \geq 2$, when the strength of the OL, or the nonlinearity in the system, is decreased below some critical

value. In the previous section we have shown that localized states cor-

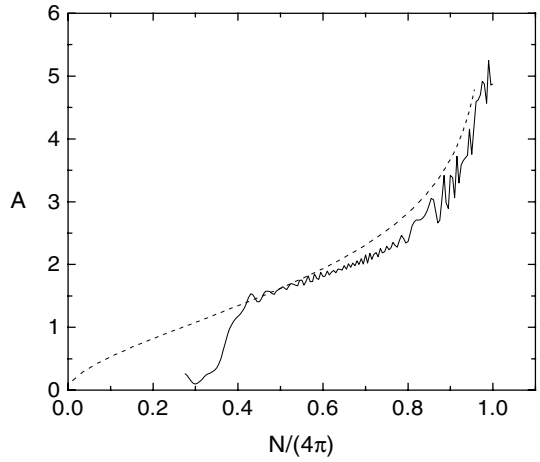

Figure 6. Existence curves of single cell OS solitons as predicted by VA (full line) and as obtained from PDE integrations (dotted line). Notice the existence of a delocalizing transition at $N/4\pi \approx 0.4$.

respond to quantum bound state of the linear Schrödinger equation in a self-consistent potential. Since any 1D potential (bounded from above by and asymptotes to zero) support a bound state (even for an infinitesimal depth of the well) [26] we have that the bound state interpretation implies that no delocalizing transitions can occur in 1D, this being a fact which is well known from numerical simulations. On the other hand, for $d \geq 2$ a finite depth of the well is always required for the formation of a bound state so that a delocalizing transition can exist. According to the above bound state interpretation, the delocalizing transition should occur precisely at the value for which the effective potential becomes unable to support bound states. To check this idea, we consider the GPE with a 2D optical lattice of the form $V_{ol}(x, y) = \varepsilon(\cos(2x) + \cos(2y))$. For simplicity, we also restrict to the case of attractive interaction $\chi < 0$ (the analysis can be easily extended to the repulsive case). In this case, localized solutions of the OS type can be easily constructed by means of a variational analysis (VA) based on a Gaussian ansatz for the soliton profile

$$\psi(x, y, t) = A \exp\left[-\frac{a}{2}(x^2 + y^2)\right] \exp(-i\mu t), \tag{6}$$

where μ is the chemical potential and A, a are the amplitude and width of the solution, respectively. Notice that these parameters are related to the total number of atoms in the condensate by the relation $N =$

$\int_{-\infty}^{\infty} |\psi(x,y,t)|^2 dxdy = \pi A^2/a$. Following the standard procedure of the VA [20, 21], we introduce the effective Lagrangian

$$L = \frac{1}{2}\int_{\infty}^{\infty} \left[|\nabla\psi|^2 - \mu|\psi|^2 - V_{ol}(x,y)|\psi|^2 - \frac{1}{2}\chi|\psi|^4\right] dxdy \qquad (7)$$

and find parameter conditions for which $\delta L = 0$. Substituting the ansatz (6) into the effective Lagrangian (7) and performing the spatial integration with subsequent minimization with respect to variables A and a, we obtain the following variational equations relating the soliton parameters a, A, to the number of atoms, N, the strength of the OL and the chemical potential

$$N = \frac{4\pi}{\chi}\Big(1 - \frac{2\varepsilon}{a^2}e^{-1/a}\Big), \quad \mu = \frac{2\varepsilon}{a}(2-a)e^{-1/a} - a. \qquad (8)$$

From these equations it follows that the existence of solitons in 2D attractive BEC is limited from above by the onset of collapse at the critical norm $N_{col} = 4\pi$ [22]. We also see from Eq.(8) that for a fixed value of the OL strength ε, there exists a minimal norm $N_{min} = \frac{4\pi}{\chi}(1 - 8\varepsilon e^{-2})$ attained at $a = 1/2$, below which the localized solutions do not exist. Notice, however, that the minimal norm vanishes if $\varepsilon > \varepsilon_{cr} = e^2/8 = 0.92$.

In Fig. 6 we show the dependence of the pulse amplitude A versus the number of atoms as predicted by the above VA equations and as obtained from direct PDE simulations for the critical case $\varepsilon_{cr} = 0.92$. From this Figure we see that the VA fails to predict the delocalizing transition observed at lower values of N. In order to investigate the aforementioned nature of the transition, we adopt an effective mass formalism [23, 24] and approximate the original GPE equation with a linear Schrödinger eigenvalue problem with the effective potential

$$V_{eff} = -\chi|\psi_{del}(x,y,t)|^2 \qquad (9)$$

where $\psi_{del}(x,y,t)$ denotes the solution of the nonlinear problem in presence of the optical lattice, evaluated at the delocalizing transition.

The problem then is to investigate the existence of states with negative energy for the following Schrödinger equation

$$(-\nabla^2 + V_{eff} - \mu)\psi(x,y,z) = 0. \qquad (10)$$

For the delocalizing transition reported in Fig. 6 we have that $A_D \approx 1.2$, $\frac{N_D}{4\pi} \approx 0.4$, this giving a VA effective potential of the form

$$V_{eff} = -A_D^2 e^{-a_D(x^2+y^2)}. \qquad (11)$$

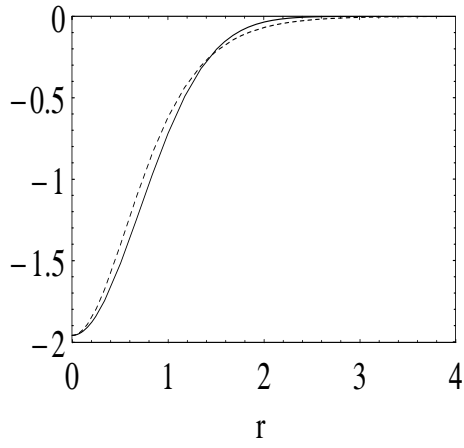

Figure 7. Effective potential of a single cell soliton. The continuous curve refer to the variational potential in Eq. (11) while the dashed one to the Pöschl-Teller potential in Eq. (12) . Parameters $A_D \approx 1.2$, $a_D \approx 0.4$, correspond to the delocalizing transition of Fig. 6.

We could use numerical schemes for Eq. (10) to show that the effective potential is just at the critical threshold for the existence of a single bound state. In the following, however, we provide an analytical estimation of the number of bound states by approximating the effective potential with a solvable potential for which this number is exactly known. To this end we use the following Pöschl-Teller potential [25]

$$V_{PT}(r) = -\frac{A_D^2}{\cosh(r\sqrt{2a_D \log(2)})^2}, \tag{12}$$

to approximate V_{eff} at the delocalizing transition. The parametric form of V_{PT} has been fixed so that V_{PT} has the same amplitude and the same integral value: $2\pi \int_0^\infty r V_{eff}(r) dr$, as V_{eff} . In Fig. 7 V_{eff} and its Pöschl-Teller approximation are depicted for the parameter values corresponding to the delocalizing transition of Fig.6, for which we see that the approximation is quite reasonable (this is true also for other parameters). The number of bound states of the Pöschl-Teller potential is then expressed, for the present parametrization, as [26]

$$n = \left[\frac{1}{4} \left(\sqrt{1 + \frac{2A_D^2}{a_D \log(2)}} + 1 \right) \right] \tag{13}$$

with $[z]$ denoting the integer part of z. From the above values of a_D, A_D, we have that $n = 1.09$, i.e. the delocalizing transition of Fig. 6 is indeed very close to the threshold of existence of a single bound state in the effective potential. The same analysis holds true for other parameter values (for details see Ref.[5]), this confirming the validity of the bound state interpretation.

4. Conclusion

In this paper we have used a self-consistent approach to establish a link between gap solitons of the GPE and quantum bound states of a linear Schröedinger problem with effective potential. This approach has been used to construct localized and extended states as well as more general solutions corresponding to linear combinations of eigenstates, of the GPE with OL. The method converges quite rapidly and provides information also about the stability of the bound states. We remark that this approach can be applicable to arbitrary potentials in arbitrary dimensions d (for $d > 1$, however, the diagonalization problem becomes computationally more expensive). The implications of the bound state interpretation of the soliton solutions of the GPE on the delocalizing transition observed in higher dimensions, have been discussed in detail. In particular, we showed that the delocalizing transition of 2D GPE solitons in OL corresponds to the threshold of existence of a single bound state in the effective potential of the corresponding linear problem. We remark that the connection between localized solutions of the NLS equation and quantum bound states is more general than the present context and is likely to be true also for other physical systems. In particular we mention that similar delocalizing behaviors were observed also for intrinsic localized modes in nonlinear lattices. In these systems, however, the existence of a delocalizing threshold has been explained in mathematical terms as the occurrence of a saddle node bifurcation in parameter space [1]. Our interpretation in terms of bound states provides a complementary physical explanation of the phenomenon.

In a future publication we hope to discuss how to extend the above analysis to the case of ILM solutions of the discrete NLS equation and how to link the above theory to the one of polaronic states in solids.

Acknowledgments

The author wishes to thank Dr. B. Baizakov and Prof. S. De Filippo for interesting discussions. Financial support from the MURST, under a PRIN-2003 Initiative, and from the European grant LOCNET, contract no. HPRN-CT-1999-00163, is also acknowledged.

References

[1] S. Flach, K. Kladko, and R.S. MacKay, Phys. Rev. Lett. **78**, 1207 (1997).

[2] M.I. Weinstein, Nonlinearity **12**, 673 (1999).

[3] G. Kalosakas, K. Ø. Rasmussen, and A.R. Bishop, Phys. Rev. Lett. **89**, 030402 (2002).

[4] G. Kalosakas, S. Aubry, and G.P. Tsironis, Phys. Rev. B **58**, 3094 (1998).

[5] B.B. Baizakov and M. Salerno, Phys. Rev. A (2004) (to appear).

[6] Lev Pitaevskii and Sandro Stringari, *Bose-Einstein Condensation*, Oxford Science Publications, Clarendon Press, Oxford (2003).

[7] A. Trombettoni and A. Smerzi, Phys. Rev. Lett. **86**, 2353 (2001).

[8] F. K. Abdullaev, B. B. Baizakov, S. A. Darmanyan, V. V. Konotop, and M. Salerno, Phys. Rev. A **64**, 043606 (2001).

[9] S. Pötting, O. Zobay, P. Meystre, and E. M. Wright, J. Mod. Opt. **47**, 2653 (2000).

[10] V. V. Konotop and M. Salerno, Phys. Rev. A **65**, 021602 (2002).

[11] G. L. Alfimov, V. V. Konotop, and M. Salerno, Europhys. Lett. **58**, 7 (2002).

[12] N.K. Efremidis and D. N. Christodoulides, Phys. Rev. A **67**, 063608 (2003).

[13] D. Diakonov, L.M. Jensen, C.J. Pethick, H. Smith, Phys.Rev. A **66**, 013604 (2002).

[14] P.J. Louis, E.A. Ostrovskaya C.M. Savage, and Y.S. Kivshar, e-print cond-mat/0208516.

[15] P.G. Kevrekidis, K.O Rasmussen, A.R. Bishop, Phys. Rev. E **61**, 4652 (2000).

[16] Karen Marie Hilligsoe, Markus K. Oberthaler, and Karl-Peter Marzlin, Phys. Rev. A **66**, 063605 (2002).

[17] A.J. Sievers and S. Takeno, Phys.Rev.Lett. **61**, 970 (1988).

[18] O.M. Braun and Yu. S. Kivshar, Phys.Rep. **306**, 2 (1998).

[19] F.Kh. Abdullaev and V.V. Konotop, Phys. Rev. A **68**, 013605 (2003).

[20] D. Anderson, Phys. Rev, **A27**, 1393 (1983).

[21] B. A. Malomed, Progr. Optics **43**, 69 (2002).

[22] F. Kh. Abdullaev, *et al.* Phys. Rev. A **67**, 013605 (2003).

[23] M. J. Steel and W. Zhang, e-print cond-mat/9810284.

[24] H. Pu, L.O. Baksmaty, W. Zhang, N.P. Bigelow, P. Meystre, Phys. Rev. A **67**, 043605 (2003).

[25] G. Pöschl and E. Teller, Z. Phys. **83**, 1439 (1933).

[26] S. Flügge *Practical Quantum Mechanics*, Springer-Verlag, (1994).

CONTROL OF MATTER WAVES IN OPTICAL LATTICES BY FESHBACH RESONANCE

V.A. Brazhnyi and V.V. Konotop
Centro de Fisica Teorica e Computacional, Universidade de Lisboa,
Complexo Interdisciplinar, Av. Prof. Gama Pinto 2, Lisbon 1649-003, Portugal
brazhnyi@cii.fc.ul.pt; konotop@cii.fc.ul.pt

Abstract Using the Feshbach resonance (FR) one can change a scattering length of two-body interactions and thus affect nonlinear dynamics of excitations in a Bose-Einstein condensate. The phenomenon is described by the Gross-Pitaevskii (GP) equation with varying nonlinearity. In this work we discuss the effect of variation of the nonlinearity on excitations in a BEC placed in an optical lattice. More specifically, we describe reductions of a three-dimensional (3D) GP equation to a 1D perturbed nonlinear Schrödinger (NLS) equation for different relations among parameters; discuss periodic solutions of the NLS equation; carry out numerical study of the dynamics of the NLS equation with a periodic and parabolic trap potentials. Special attention is paid to the process of generation of trains of bright and dark matter solitons from initially periodic waves.

Keywords: Bose-Einstein condensate, matter waves, optical lattices, Feshbach resonance, cnoidal waves, solitons.

1. Introduction

The first experiments showed possibility for bosons to condensate in the ground state at ultra-low temperatures [1] originated a large number of theoretical and experimental efforts forwarded to study of Bose-Einstein condensates (BEC's). Recently, realization of BEC's embedded in a periodic potential ([2, 3, 4]) has opened new possibilities to observe and explore matter waves, including dark [5] and bright [6] solitons.

On the other hand it was shown theoretically [7] and confirmed in recent experiments [6, 8] that by changing external magnetic field near the resonant point one can control the magnitude (and even sign) of the scattering length of inter-particle interactions – the so-called Feshbach

F. Kh. Abdullaev and V. V. Konotop (eds.), Nonlinear Waves: Classical and Quantum Aspects, 251–267.

resonance (FR). The obtained results gave origin to theoretical studies of the influence of the varying nonlinearity on dynamics of the matter waves. In particular, it was shown that FR can be employed to generate trains of solitons starting with periodic wave [9], to obtain stable localized solutions [10], and to be used for generation of shock waves [11] in BEC's.

In the present paper we consider dynamics of a BEC in an optical lattice (OL) affected by FR. We start (Sec. 2) with introduction of the mean-field approximation and parameters of the problem. In Sec. 3 we present the listing the main one-dimensional (1D) reductions of the 3D Gross-Pitaevskii (GP) equation depending on the particular choice of the relation among the main scales of the system. In Sec. 4 we discuss the choice of initial conditions and unperturbed periodic solutions describing BEC in an OL. Sec. 5 is devoted to detail study of the effect of FR on the dynamics of the condensate. In conclusion we briefly discuss the results and provide estimates for the parameters allowing experimental realization of the phenomenon.

2. Mean-field approximation and parameters of the problem

The GP equation governing evolution of the wave function $\Psi(\mathbf{r}, t)$ describing a dilute BEC is obtained within the mean-field approximation. It reads [12]

$$i\hbar\frac{\partial\Psi}{\partial t} = -\frac{\hbar^2}{2m}\Delta\Psi + V(\mathbf{r})\Psi + g_0|\Psi|^2\Psi\,. \tag{1}$$

Here we use the standard notations: $g_0 = 4\pi\hbar^2 a_s/m$, a_s is the s-wave scattering length, which can be either positive or negative, and m is the atomic mass. The external potential, $V(\mathbf{r})$, is given by $V(\mathbf{r}) = V_{trap}(\mathbf{r}) + V_{latt}(x)$ where $V_{trap}(\mathbf{r}) = \frac{m}{2}\left(\omega_\perp^2\mathbf{r}_\perp^2 + \omega_0^2 x^2\right)$ is the magnetic trap potential, $\mathbf{r}_\perp = (y, z)$, $\omega_\perp$ and ω_0 are the transverse and axial harmonic oscillator frequencies, and $V_{latt}(x) = E_R u(x)$ is a lattice potential (created by standing laser beams) normalized to the recoil energy, $E_R = \hbar^2 k^2/2m$, where $k = 2\pi/L$. Respectively, $u(x) = u(x + L)$ is a periodic dimensionless function with a period L. The wave function is normalized to the total number of atoms, N: $\int |\Psi|^2 d\mathbf{r} = N$.

We will deal with a cigar-shaped trap where the transverse linear oscillator length, $a_\perp = \sqrt{\hbar/m\omega_\perp}$, is much smaller than the longitudinal one, $a_0 = \sqrt{\hbar/m\omega_0}$: $a_\perp \ll a_0$. Then it is natural to investigate possibilities of reduction of the 3D GP equation to an effective 1D model. By introducing the healing length $\xi = (8\pi n|a_s|)^{-1/2}$, where $n \approx N/a_\perp^2 a_0$ is a mean particle density, one collects four characteristic spatial scales of

the problem at hand $\{a_0, a_\perp, L, \xi\}$, relations among which will define the form of the effective 1D equation. More specifically, we concentrate on the case where relation among these four characteristic lengths can be defined by a small parameter of the system, ϵ, which in the next Section will be used as a keystone of the multiple-scale expansion. The square of the small parameter we define as a ratio between the energy density of two-body interactions, $\sim 4\pi\hbar^2|a_s|n/m$, and a density of the kinetic energy of the transverse excitations, $\sim \hbar^2/2ma_\perp^2$:

$$\epsilon^2 = \frac{a_\perp^2}{\xi^2} \sim \frac{Na_s}{a_0}. \tag{2}$$

Considering relations among the characteristic scales, one can single out four different cases which can be treated by means of the multiple-scale expansion. They are summarized in Table 1. Below, following [13] we consider one of these cases in detail and only outline other possible reductions.

Table 1. Scaling, backgrounds and effective 1D equations describing matter waves in OL's. All variables in evolution equations are dimensionless (see the text).

Case	*Scaling*	$\phi_n(x_0)$	*Equation*
1	$a_\perp \sim L \sim \epsilon\xi \lesssim \epsilon^2 a_0$	$\approx$ Bloch function	$i\psi_t = -(2M)^{-1}\psi_{xx} + 2\sigma\|\psi\|^2\psi$
2	$a_\perp \sim L \sim \epsilon\xi \sim \epsilon a_0$	= Bloch function	$i\psi_t = -(2M)^{-1}\psi_{xx} + 2\sigma\|\psi\|^2\psi$ $+\nu^2x^2\psi$
3	$a_\perp \sim \epsilon L \sim \epsilon\xi \lesssim \epsilon^2 a_0$	$= \pi^{-1/4}e^{-\nu x_0^2/2}$	$i\psi_t = -\psi_{xx} + 2\sigma\|\psi\|^2\psi$ $+U(x)\psi$
4	$a_\perp \sim \epsilon L \sim \epsilon\xi \sim \epsilon a_0$	$\equiv 1$	$i\psi_t = -\psi_{xx} + 2\sigma\|\psi\|^2\psi$ $+U(x)\psi + \nu^2x^2\psi$

3. Effective 1D equations

3.1 Long trap and rapidly varying OL

Let us consider the first case from Table 1, for which $a_\perp \sim L \sim \epsilon\xi \lesssim \epsilon^2 a_0$. It corresponds to the situation when the condensate is rather long and the periodicity modifies the spectrum of the underlying linear system. To this end we introduce dimensionless independent variables $\tilde{t} = \omega_\perp t/2$, $\tilde{x} = x/a_\perp$, $\tilde{\mathbf{r}}_\perp = \mathbf{r}_\perp/a_\perp$, and a renormalized wave function $\tilde{\Psi} = a_\perp|a_s|^{1/2}\Psi$. Then Eq. (1) can be rewritten in the dimensionless

form

$$i\frac{\partial\tilde{\Psi}}{\partial\tilde{t}} = \left(\mathcal{L}_\perp + \mathcal{L}_0 + 8\pi\sigma|\tilde{\Psi}|^2\right)\tilde{\Psi}, \tag{3}$$

$$\mathcal{L}_\perp = -\Delta_\perp + \tilde{r}_\perp^2, \qquad \mathcal{L}_0 = -\frac{\partial^2}{\partial\tilde{x}^2} + \nu^2\tilde{x}^2 + \gamma^2 U(\gamma\tilde{x}). \tag{4}$$

Here σ =sgn(a_s), $\nu = \omega_0/\omega_\perp$ is an aspect ratio of the trap, $U(\gamma\tilde{x}) \equiv u(a_\perp\tilde{x})$ is the new dimensionless periodic function which is varying on a unit scale, and

$$\gamma^2 = \frac{E_R}{\hbar\omega_\perp} \sim \frac{a_\perp^2}{L^2}. \tag{5}$$

Let us consider linear eigenvalue problems associated to (3), (4)

$$\mathcal{L}_0\,\phi_{nq}(\tilde{x}) = \mathcal{E}_{nq}\,\phi_{nq}(\tilde{x}), \qquad \mathcal{L}_\perp\,\xi_{l_1,l_2}(\tilde{\mathbf{r}}_\perp) = \mathcal{E}_{l_1,l_2}\,\xi_{l_1,l_2}(\tilde{\mathbf{r}}_\perp). \tag{6}$$

Here we introduce the indexes n and q for the number of a band and wave vector inside the first Brillouin zone (BZ), and l_1 and l_2 for the two transverse quantum numbers. Strictly speaking the operator $\mathcal{L}_0$ has a discrete spectrum, which however approximates the band spectrum of the first eigenvalue problem in (6) in the limit $\nu \to 0$ ($a_0 \to \infty$). In this case the use of the "band" terminology is justified and $\phi_{nq}(x)$ is approximated by the Bloch function of the respective periodic potential (it will be considered bordering the edge of the first BZ where $q = \pm\pi/L$, and thus the abbreviated notation $\phi_n(x) \equiv \phi_{n\pm\pi/L}(x)$ will be used). All eigenfunctions are considered to be normalized to one. In what follows however, we will be interested in the evolution of the background state ($l_1 = l_2 = 0$) of the transverse component. Thus it will be taken $\xi_{0,0}(\tilde{\mathbf{r}}_\perp) = \pi^{-1/2}e^{-\tilde{r}_\perp^2/2}$, and $\mathcal{E}_{0,0} = 2$.

We look for a solution of Eq.(3) in a form of expansion

$$\tilde{\Psi} = \epsilon\psi_1 + \epsilon^2\psi_2 + \epsilon^3\psi_3 + \cdots, \tag{7}$$

where ψ_j ($j = 1, 2, \ldots$) are functions of $\tilde{\mathbf{r}}_\perp$ and scaled independent variables $t_\alpha = \epsilon^\alpha\tilde{t}$ and $x_\alpha = \epsilon^\alpha\tilde{x}$. Then the leading order of the solution Eq.(7) can be searched in the form of a weakly modulated ground state

$$\psi_1 = \frac{1}{\sqrt{\pi}}\mathcal{A}(x_1, t_2)e^{-i(\mathcal{E}_n+2)t_0}e^{-\tilde{r}_\perp^2/2}\phi_n(x_0). \tag{8}$$

Here $\mathcal{A}(x_1, t_2)$ (as well as $\mathcal{B}_n(x_1, t_2)$ below) is a slowly varying envelope amplitude, where by convention we indicate only the most rapid variables, i.e. $\mathcal{A}(x_1, t_2)$ means that $\mathcal{A}$ depends on all $\{x_1, x_2, \ldots\}$ and $\{t_2, t_3, \ldots\}$.

After substituting expansion (7) into (3), (4) one collects the terms at each order of ϵ, what leads to a set of equations. The first three of them read [$\mathcal{M} = i\partial/\partial t_0 - (\mathcal{L}_0 + \mathcal{L}_\perp)$]:

$$\mathcal{M}\psi_1 = 0, \tag{9}$$

$$\mathcal{M}\psi_2 = 2\frac{\partial^2\psi_1}{\partial x_0 \partial x_1}, \tag{10}$$

$$\mathcal{M}\psi_3 = -i\frac{\partial\psi_1}{\partial t_2} - i\frac{\partial\psi_2}{\partial t_1} - \frac{\partial^2\psi_1}{\partial x_1^2} - 2\frac{\partial^2\psi_2}{\partial x_0\partial x_1} - \frac{\partial^2\psi_1}{\partial x_0\partial x_2} + 8\pi\sigma|\psi_1|^2\psi_1. \tag{11}$$

The first order equation (9) is satisfied by ground state solution (8). A solution of the second order equation (10) is searched in the form

$$\psi_2 = \frac{1}{\sqrt{\pi}} e^{-\tilde{r}_\perp^2/2} e^{-i(\mathcal{E}_n+2)t_0} \sum_{n'\neq n} \mathcal{B}_{n'n}(x_1,t_1)\phi_{n'}(x_0). \tag{12}$$

Applying $\int d\tilde{\mathbf{r}}_\perp dx_0 \bar{\phi}_n \xi_{0,0}$ to Eq. (10) (hereafter an overbar stands for complex conjugation), and taking into account that $\phi_n(x_0)$ borders the forbidden gap and thus is either even or odd, one computes $\partial\mathcal{A}/\partial t_1 = 0$. Thus $\mathcal{A}$ does not depend on t_1, i.e. $\mathcal{A} \equiv \mathcal{A}(x_1, t_2)$. Next, multiplying (10) by $\bar{\phi}_{n_1}\xi_{0,0}$ and integrating over x_0 and $\tilde{\mathbf{r}}_\perp$ one obtains the coefficients $\mathcal{B}_{n_1 n}$ for $n_1 \neq n$

$$\mathcal{B}_{n_1 n} = \frac{\Gamma_{n_1 n}}{\mathcal{E}_{n_1} - \mathcal{E}_n}\frac{\partial\mathcal{A}}{\partial x_1}, \qquad \Gamma_{n_1 n} = -2\int_0^L \bar{\phi}_{n_1}\frac{d}{dx_0}\phi_n dx_0. \tag{13}$$

Finally, applying $\int d\tilde{\mathbf{r}}_\perp dx_0 \bar{\phi}_n \xi_{0,0}$ to (11), we obtain

$$i\frac{\partial\mathcal{A}}{\partial t_2} + \frac{1}{2M_n}\frac{\partial^2\mathcal{A}}{\partial x_1^2} - \chi_n\sigma|\mathcal{A}|^2\mathcal{A} = 0, \tag{14}$$

where

$$\chi_n = 4\int_0^L |\phi_n(x_0)|^4 dx_0, \qquad \frac{1}{2M_n} = 1 + \sum_{n_1\neq n}\frac{|\Gamma_{nn_1}|^2}{\mathcal{E}_{n_1} - \mathcal{E}_n}. \tag{15}$$

By making substitution $\mathcal{A} \to \sqrt{2/\chi_n}\psi$, $t_2 \to t$, $x_1 \to x$, and $M_n \to M$ one obtains a dimensionless 1D nonlinear Schrödinger (NLS) equation

$$i\frac{\partial\psi}{\partial t} + \frac{1}{2M}\frac{\partial^2\psi}{\partial x^2} - 2\sigma|\psi|^2\psi = 0. \tag{16}$$

We emphasize, that the final Eq.(16) does not contain explicitly the parabolic trap potential and OL since they are included in the ground state solution and thus in the coefficients of the obtained equation.

Finally we have to clarify the meaning of the coefficient M_n^{-1}. This can be done, by means of the so-called **kp**-method, known in the solid state physics. Namely, it turns out that in the limit of the band spectrum (i.e. when $a_0/a_\perp \to \infty$) one has $M_n^{-1} = d^2\mathcal{E}_n/dq^2$, i.e. M_n is nothing but the effective mass (see [13]).

3.2 Short trap and rapidly varying OL

By considering another relation among the main parameters of the system one arrives at a different form of the 1D NLS equation. Consider the Case 2 from the Table 1, where $a_\perp \sim L \sim \epsilon\xi \sim \epsilon a_0$ what corresponds to the situation when the condensate size in the axial direction is not large enough and effect of the boundaries on the soliton dynamics cannot be neglected. Like in the first case, the periodicity is of the order of the radial size and modifies the spectrum introducing the effective mass. Mathematically this is expressed by the fact that now $a_0/a_\perp \sim \epsilon$ and thus $\nu^2x^2 = \epsilon^2\tilde{\nu}^2x_1^2$, where $\nu = \epsilon\tilde{\nu}$ and $\tilde{\nu}$ is of unity order. Now one has to redefine the problem (3), (4) as follows

$$i\frac{\partial\tilde{\Psi}}{\partial\tilde{t}} = \left(\mathcal{L}_\perp + \mathcal{L}_0 + \epsilon^2\tilde{\nu}^2(\epsilon\tilde{x})^2 + 8\pi\sigma|\tilde{\Psi}|^2\right)\tilde{\Psi}, \tag{17}$$

$$\mathcal{L}_\perp = -\Delta_\perp + \tilde{r}_\perp^2, \qquad \mathcal{L}_0 = -\frac{\partial^2}{\partial\tilde{x}^2} + \gamma^2U(\gamma\tilde{x}) \tag{18}$$

Next one has to follow the steps described in the preceding subsection, but now with a different operator $\mathcal{L}_0$. This naturally leads to a new background, which is now a solution of a Hill equation and thus is a Bloch function exactly (in the previous case it was only approximated by the Bloch function). Respectively a new term, $\tilde{\nu}^2x_1^2$, appears in the resulting 1D equation:

$$i\psi_t = -\psi_{xx} + \nu^2x^2\psi + 2\sigma|\psi|^2\psi \tag{19}$$

where as before $\{\psi, t, x\}$ stay for $\{\mathcal{A}, t_2, x_1\}$ (see [13, 14], for details).

3.3 Long trap and smooth OL

Let us turn to the next case from the Table 1, where $a_\perp \sim \epsilon L \sim \epsilon\xi \lesssim \epsilon^2 a_0$. The peculiarity now, is that period is of order of the healing length. Thus excitations in a BEC may have scales compared with the lattice period (notice that in this case we again have a potential wide enough, to do not affect significantly wave dynamics). Mathematically this fact

is expressed by the fact that now $\gamma = \epsilon\tilde{\gamma}$, where γ is defined by (5) and $\tilde{\gamma} = (a_\perp/L)(a_0/Na_s)^{1/2}$ is of order one. Then $\gamma^2 U(\gamma\tilde{x}) \equiv \epsilon^2\tilde{U}(x_1)$ where $\tilde{U}(x_1) \equiv \tilde{\gamma}^2 U(\tilde{\gamma}x_1)$. The system (3), (4) takes the form

$$i\frac{\partial\tilde{\Psi}}{\partial\tilde{t}} = \left(\mathcal{L}_\perp + \mathcal{L}_0 + \epsilon^2\tilde{U}(\epsilon\tilde{x}) + 8\pi\sigma|\tilde{\Psi}|^2\right)\tilde{\Psi}, \tag{20}$$

$$\mathcal{L}_\perp = -\Delta_\perp + \tilde{r}_\perp^2, \qquad \mathcal{L}_0 = -\frac{\partial^2}{\partial\tilde{x}^2} + \nu^2\tilde{x}^2. \tag{21}$$

Now the eigenvalue problem for $\mathcal{L}_0$ is solved explicitly giving the Gaussian background $\phi_n(x_0) = \pi^{-1/4}\exp(-x_0^2/2)$, and the final (i.e. already in dimensionless units) 1D equation of motion reads

$$i\psi_t = -\psi_{xx} + U(x)\psi + 2\sigma|\psi|^2\psi. \tag{22}$$

Thus as one could expect in the case at hand the periodic potential appears in the evolution equation in an explicit form. This kind of NLS equation was considered in Ref.[15].

3.4 Short trap and smooth OL

Finally, if one considers condensate not too long and a lattice having the period of order of the healing length, i.e. the situation described in Table 1 as Case 4: $a_\perp \sim \epsilon L \sim \epsilon\xi \sim \epsilon\, a_0$, the both lattice and trap potentials will appear in the final equation of motion. The corresponding problem is formulated now as follows

$$i\frac{\partial\tilde{\Psi}}{\partial\tilde{t}} = \left(\mathcal{L}_\perp + \mathcal{L}_0 + \epsilon^2\tilde{\nu}^2(\epsilon\tilde{x})^2 + \epsilon^2\tilde{U}(\epsilon\tilde{x}) + 8\pi\sigma|\tilde{\Psi}|^2\right)\tilde{\Psi}, \tag{23}$$

$$\mathcal{L}_\perp = -\Delta_\perp + \tilde{r}_\perp^2, \qquad \mathcal{L}_0 = -\frac{\partial^2}{\partial\tilde{x}^2}. \tag{24}$$

The ground state becomes $\phi_n(x_0) \equiv 1$.

Skipping calculations, similar to ones presented in the Case 1, we present the final form of the effective 1D equation

$$i\frac{\partial\psi}{\partial t} = -\frac{\partial^2\psi}{\partial x^2} + \nu^2x^2\psi + U(x)\psi + 2\sigma|\psi|^2\psi \tag{25}$$

where as before the tildes are suppressed.

4. Stationary solution

The Case 1 considered above is the simplest one since it is reduced to the unperturbed NLS equation (16). This allows one obtain rather complete information about the wave function analytically using, say,

the inverse scattering transform (IST), and even to solve the problem explicitly for a number of specific initial conditions (see e.g. [9]). In other cases numerical analysis has to be employed. This rises the problem of a choice of initial conditions adequate to the physical problem one wants to solve. In the present paper we consider effect of the FR, i.e. varying nonlinearity, on a stationary background state. Thus, for the next step we have to solve the problem of finding stationary background distribution, i.e. stationary solutions of the above evolution problems at constant nonlinearity. These last solutions at $t = 0$ will be considered as initial condition for the problem with varying nonlinearity. Considering the Case 2 where NLS equation has the form (19) one can find initial distribution by solving stationary nonlinear problem numerically (see e.g. [14]). The stationary solutions for Case 3 can be found analytically in form of a periodic waves (see e.g. [16]).

In the present paper we are concerned with the Case 4 for which we consider the choice of the stationary solutions in more details.

4.1 Background

In order to find a stationary solution of Eq.(25) we use the ansatz

$$\psi(x,t) = \Phi(x,t)F(x)e^{-i(\omega_{bg}-2\sigma A)t} \tag{26}$$

where $F(x)$ is chosen to solve the nonlinear eigenvalue problem

$$F_{xx} + (\omega_{bg} - \nu^2 x^2)F - 2\sigma A F^3 = 0, \quad F(0) = 1, \quad F_x(0) = 0, \tag{27}$$

ω_{bg} is a spectral parameter and A is a constant. Then $\Phi(x,t)$ solves the equation

$$i\Phi_t + \Phi_{xx} - U(x)\Phi - 2\sigma|\Phi|^2\Phi = R[F,\Phi] \tag{28}$$

with

$$R[F,\Phi] \equiv -2\Phi_x(\ln F)_x + 2\sigma\Phi(|\Phi|^2 - A)(F^2 - 1). \tag{29}$$

It is our aim now, to show, that for relatively small ν, the right hand side of Eq.(28) can be considered as a small perturbation. To this end we expand $F(x)$ in the vicinity of the center of the trap potential:

$$F(x) = 1 + \frac{2\sigma A - \omega_{bg}}{2}x^2 + O(x^4), \qquad \nu x \ll 1. \tag{30}$$

Substituting (30) into (27) and taking into account only the terms of order x^2 one can obtain estimation for the eigenvalue $\omega_{bg} \approx 2\sigma A + \nu^2/2\sigma A$,

which in its turn allows us to rewrite (30) as $F(x) \approx 1 - \nu^2 x^2/(4\sigma A)$. Next we estimate: $(\ln F)_x \sim \nu^2 x$, $(F^2 - 1) \sim \nu^2 x^2$, and rewrite (29) as

$$R[F, \Phi] = \frac{\nu^2}{\sigma A} \left[\Phi_x x - \sigma \Phi (|\Phi|^2 - A) x^2 \right]. \tag{31}$$

Assuming that $\sqrt{A}$ is of order of the amplitude of Φ, i.e. $|\Phi/\sqrt{A}| = O(1)$, in the vicinity of the potential minima ($\nu x \ll 1$) we can neglect the r.h.s. in Eq.(28) and approximate $\Phi(x,t)$ by a solution of the equation

$$i\Phi_t + \Phi_{xx} - U(x)\Phi - 2\sigma|\Phi|^2\Phi = 0. \tag{32}$$

Formally, this result brings us back to the Case 3 from Table 1 (c.f. (22)). There is however a difference from the point of view of dynamics. Eq.(32) will be used to find the initial condition to (25) with varying nonlinearity (see (37), below). It, of course, will not give us an exact solution of the stationary problem, but will allow us to approximate a solution on times less than the time of propagation of a perturbation with the sound velocity along the condensate, τ_ν. In our dimensionless units $\tau_\nu \sim 1/\nu$. Since our main goal is to study the effect of a FR on dynamics, when the respective characteristic times are much less than τ_ν. In that case the initial condition found using (32) can be viewed as an approximation good enough to model the wave dynamics.

4.2 Periodic solutions

Let us now discuss a stationary periodic solution of (32): $\Phi(x,t) = e^{i\omega t}\varphi(x)$, where ω is a frequency and $\varphi(x) = \varphi(x+L)$ is a real periodic function satisfying the equation as follows

$$\varphi_{xx} = (\omega + U(x) + 2\sigma\varphi^2)\varphi. \tag{33}$$

First of all we observe, that Eq.(33) allows one to construct the lattice potential $U(x)$ in an explicit form, when desired wave field $\varphi(x)$ is given apriori (a kind of "inverse engineering"). The only requirement appearing in this way is regular behavior of φ_{xx}/φ. In particular, this is the case of the Jacobi elliptic functions

$$\varphi_{pq}(x) = \sqrt{A}\, pq(\kappa x, m), \tag{34}$$

where we are using standard notations with p=c, d, s and q=n and, hence, the case of the respective trigonometric functions appearing in the limit $m \to 0$. These solutions subject to the proper choice of σ correspond to the lattice potential

$$U(x) = U_0 \mathrm{sn}^2(\kappa x, m). \tag{35}$$

They are summarized in the Table 2. Following Ref.[16], where such solutions were studied in details, we refer to φ_{pq} as trivial-phase solutions.

Table 2. Solutions of type (34), σ must be chosen to make $A > 0$.

pq	A	ω
cn	$(U_0/2 - \kappa^2 m)\sigma$	$\kappa^2(1-2m) + U_0$
dn	$(U_0/2m - \kappa^2)\sigma$	$\kappa^2(m-2) + U_0/m$
sn	$(\kappa^2 m - U_0/2)\sigma$	$\kappa^2(1+m)$

We point out that a general wave field of the form

$$\varphi_{pq}(x) = \Big(A\, pq^{\beta}(\kappa x, m) + B\Big)^{\alpha} \tag{36}$$

with $B > A$, α and β being real and $pq(\kappa x, m)$ being one of the elliptic functions cn , dn or sn can be generated by the proper lattice potential. Some particular case of (36) with $\alpha = 1/2$ and $\beta = 1$ corresponding to the lattice potential (35) were obtained and considered in [16].

5. BEC in OL controlled by FR

Let us now consider management of matter waves by means of FR. In particular, we are interested in change of parameters of a periodic wave transforming it into a sequence of highly localized pulses which can be identified as dark or bright solitons. To this end one has to perturb Eq.(25), however weakly enough in order to do not destroy the periodic wave. This can be achieved by means of FR, i.e. by changing the magnitude of the scattering length, a_s, due to varying magnetic field $B(t)$. A model simulating the process can be chosen as [6], $a_s(t) = a_s(0)\, e^{t/\tau}$, $a_s(0)$ being the initial value of the scattering length far from the resonance, and τ being a FR characteristic time. Assuming that dependence of $a_s(t)$ on time is slow enough (i.e. is governed by $\epsilon^2 t$, where ϵ is given by (2) and t is the real physical time) one can rewrite Eq.(25) in the form

$$i\frac{\partial\psi}{\partial t} + \frac{\partial^2\psi}{\partial x^2} - \nu^2 x^2\psi - U_0 \mathrm{sn}^2(\kappa x, m)\psi - 2\sigma e^{t/\tau}|\psi|^2\psi = 0. \tag{37}$$

Recently the problem of the deformation of the exact solutions subject to the FR was addressed in literature. Model (37) without parabolic

trap, $\nu = 0$, was considered analytically in Ref.[18] and at $\nu = 0$ and $U_0 = 0$ it was studied in Ref.[18]. It was found that by increasing the strength of inter-particle interactions one can generate trains of bright/dark solitons in BEC's with negative/positive scattering length. Analytically the process is described by means of the perturbation technique in the so-called adiabatic approximation. Since various aspects of this technique described in [9, 18], here we concentrate on numerical study of the system (37).

5.1 Deformation of a cn-wave

5.1.1 Evolution problem. First we consider deformation of an cn-wave resulting in creation of a train of bright solitons in a BEC with negative scattering length, $\sigma = -1$, embedded in the OL. Numerical solution of Eq.(37) with initial condition taken in a form $F(x)\varphi_{\rm cn}(x)$, where $F(x)$ is a numerical solution of (27) and $\varphi_{\rm cn}(x)$ is a solution given in the first line of Table 2, is presented in Fig.1. We studied two subsequent regimes. In the time interval $0 \le t \le 2$ the FR was switched on and after that at $2 \le t \le 10$ all potentials and FR were switched off, and the condensate was allowed to expand freely, i.e. being governed by the unperturbed NLS equation.

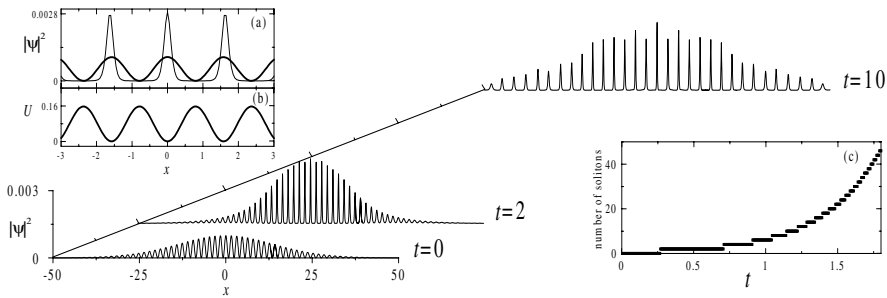

Figure 1. Dynamics of the cn-wave. In the inset (a) thick and thin lines show initial ($t = 0$) and intermediate ($t = 2$) profiles of the wave which are affected by RF and in (b) the potential is shown. Parameters are $\nu = 0.002$, $\tau = 0.2$, $\kappa = 2$, $m = 0.02$. They correspond to $A = 0.001$ and $U_0 = 0.16$. In the inset (c) the number of solitons is shown.

From inset (a) in Fig.1 one can see that growth of the scattering length leads to sharpening of peaks of the initially smooth periodic distribution and to increase of their amplitudes. At an intermediate moment of time (here $t = 2$) we obtain strongly pronounced train of pulses, which can be associated with bright solitons. Strictly speaking the concept of a soliton is well defined in 1D integrable systems, like NLS equation (16). There solitons are associated with the discrete spectrum of the associated

linear spectral problem (see e.g. [19]). In the present paper we also adopt the respective definition of the soliton. That is why, in order to verify numerically, whether created picks of the atomic distribution can be associated with solitons at $t = 2$ (and taking into account typical experimental settings with BEC's) we switch off all external factors. In Fig.1 we can see that the condensate consists of a set of solitary pulses propagating outwards the center without significant changes of their shapes. This behavior supports the fact that we indeed generated train of real bright solitons.

5.1.2 Calculation of the number of bright solitons. In order to use mathematical definition of a soliton, we notice that after switching off all external factors dynamics is governed by the NLS equation [Eq. (16) with $M = 1/2$] which is integrable by means of the IST. Here we do not enter in details of the IST which can be found in numerous monographs on soliton theory (see e.g. [19]). A point important for our analysis is that the number of solitons in a pulse described by the NLS equation coincide with a number of eigenvalues of the Zakharov-Shabat (ZS) spectral problem which can be written as

$$\mathbf{f}_x = \mathbf{U}\mathbf{f}, \qquad \mathbf{f} = \begin{pmatrix} f_1 \\ f_2 \end{pmatrix} \qquad \mathbf{U} = \begin{pmatrix} \frac{\lambda}{2i} & \sqrt{\sigma}\bar{\psi} \\ \sqrt{\sigma}\psi & -\frac{\lambda}{2i} \end{pmatrix}, \tag{38}$$

where constant λ is a spectral parameter.

To calculate a number of solitons we follow Ref. [20] and use piecewise-constant discretization for the ZS spectral problem (see [19]). To this end we truncate the wave function $\psi(x,t)$ outside a sufficiently large ($l \gg a_0$) interval $[-l, l]$. On each elementary subinterval $(x_n - \Delta x/2,\, x_n + \Delta x/2)$, where a point x_n is defined as $x_n = -l + n\Delta x$, $\Delta x = l/K$, and $2K + 1$ is the total number of discretization points of the interval $[-l, l]$, the function $\psi(x,t)$ is chosen to be equal to constant $\psi_n = \psi(x_n, t)$. By direct integration of Eq.(38) on the each elementary subinterval one can write the corresponding solution as follows

$$\mathbf{f}(x_n + \Delta x, \lambda) = \mathbf{T}_n \mathbf{f}(x_n, \lambda). \tag{39}$$

Here the transfer matrix $\mathbf{T}_n(\psi_n, \lambda)$ has the following form [20]

$$\mathbf{T}_n = \begin{pmatrix} \cosh(k_n\Delta x) + \frac{i\lambda}{2k_n}\sinh(k_n\Delta x) & -\frac{i}{k_n}\sinh(k_n\Delta x)\bar{\psi}_n \\ -\frac{i}{k_n}\sinh(k_n\Delta x)\psi_n & \cosh(k_n\Delta x) - \frac{i\lambda}{2k_n}\sinh(k_n\Delta x) \end{pmatrix}$$

where $k_n^2 = -|\psi_n|^2 - \lambda^2/4$.

In order to solve the scattering problem we have to propagate the solution using the transfer matrix what gives the relation $\mathbf{f}(l-\Delta x/2,\lambda) = \mathbf{S}(\lambda)\mathbf{f}(-l-\Delta x/2,\lambda)$, where the scattering matrix $\mathbf{S}(\lambda)$ is defined by

$$\mathbf{S}(\lambda) = \prod_{n=1}^{2K} \mathbf{T}(\psi_n,\lambda). \tag{40}$$

Then the number of zeros of the matrix element $S_{11}(\lambda)$ for definite ψ_n proportional to the number of solitons generated by the pulse $\psi(x)$.

Let us apply this technique to the case of dynamics of the cn-wave shown in Fig.1. On each time step ($\Delta t = 0.005$) in the interval $0 < t \leq 2$ the function $\psi(x,t)$ considered as an initial condition for the respective NLS equation. In Fig.1c one can see that the initial cn-wave does not have solitons while increasing the nonlinear coefficient with time results in growth of the number of solitons.

It should be mentioned that at $t = 2$ the number of solitons calculated by solving spectral problem exceeds the number of solitons visible in Fig.1. This is explained by the fact that peaks in Fig.1 can present bound states consisting of several solitons which move with the same velocities, i.e. multisoliton pulses, and by the fact that small amplitudes solitons cannot be viewed.

5.2 Deformation of a dn-wave

Now let us consider deformation of a dn-wave resulting in creation of a train of bright matter solitons in a BEC with the negative scattering length, $\sigma = -1$. We solve Eq.(37) with initial condition taken as a dn-wave (the second row in Table 2) modulated by the background $F(x)$. The results are shown in Fig. 2.

Increasing the strength of the inter-particle interactions by means of FR as in the previous case each peak starts to grow and becomes thinner. This process gives origing to a train of the bright solitons (see the inset in Fig.2).

In contrast to the previous case, however, in the case of the dn-wave one can generate train of solitons which is less robust. This can be checked by studying free expansion of the condensate after switching off all potentials and fixing nonlinearity for $t > 2.1$. As it is shown in Fig.2 solitons start to move interacting with each other, and finally the train is rapidly destroyed.

5.3 Deformation of a sn-wave

Finally we solve numerically Eq.(37) in the repulsive case $\sigma = 1$ of BEC's with initial condition taken in a form of a sn-wave given by the

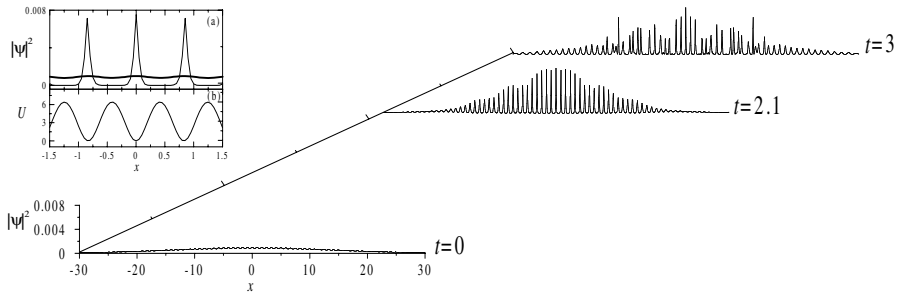

Figure 2. Dynamics of the dn-wave. Dynamics of the cn-wave. In the inset (a) thick and thin lines show initial ($t = 0$) and intermediate ($t = 2.1$) profiles of the wave which are affected by RF and in (b) the potential is shown. Parameters are $\nu = 0.002$, $\tau = 0.2$, $\kappa = 4$, $m = 0.2$. They correspond to $A = 0.001$ and $U_0 = 6.4$.

last row of Table 2, which is modulated by the background $F(x)$ taken as a numerical solution of (27). The initial and final shapes of the condensate density affected by FR as well as the potential shape are shown in Fig.3 a,b.

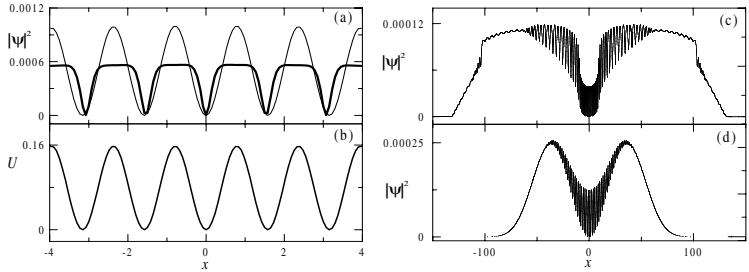

Figure 3. (a) Initial (thin line) and final $t_{fin} = 2.2$ (thick line) profiles of the condensate and (b) potential. Parameters are $\nu = 0.002$, $\tau = 0.2$, $\kappa = 2$, $m = 0.02$. They correspond to $A = 0.001$ and $U_0 = 0.16$ Profiles of the condensate at $t = 9$ with switching off FR, parabolic and periodic potentials (c) at $t = 2.2$ and (d) at $t = 0$.

Fig.3a shows sharpening of the atomic distribution around potential minima. One also observes shifts of the density extrema outwards the minimum of the magnetic trap what is stipulated by the expansion of the condensate due to the grows of repulsive interactions between atoms.

Unfortunately, in this case generated train of excitations is not a sequence of real dark solitons. As in the previous cases this can be verified by switching off FR as well as all potentials and making long time simulation. By fixing magnitude of the nonlinear coefficient at $t = 2.2$ and switching off all potentials we allow condensate to expand freely. At $t = 9$ one can observe (see Fig.3c) the dark solitons are transformed

in an oscillating part of the solution which is located between condensates moving outwards the center, while at the outside part of the new created condensates one can observe formation of the shock waves (we notice that possibility of existence of shock wave in lattices has been reported in Ref. [21], while the use of the FR to generate them was discussed in the recent work [11]). These effects are a consequence of applying FR what can be checked by making simulation with the same initial condition where FR and both potentials were switched off at initial time $t = 0$. A after time $t = 9$ (see Fig.3d) one can see splitting of the condensate in two parts moving in opposite directions. By making reverse experiment of collision of two condensates or living the parabolic potential in the model what leads to oscillatory behavior of the condensates one can observe that two initially separated condensates during collision generate the periodic structure similar to what produced by embedding condensate into the OL.

The fact that obtained sequence of excitations is not a train of real dark solitons can be explained as follows. In the contrast to the process of bright solitons formation the generation of dark solitons requires well defined background which in its turn is strongly affected by both the FR and by the condenstae expansion.

6. Discussion and conclusion

In order to link the above theoretical results with possible experimental settings we estimate the main parameters used in the theory. Let us consider a condensate of $N \approx 10^4$ atoms with initial scattering length $a_s(0) \approx 1$nm. The frequencies of the magnetic trap in the axial and radial directions are $\omega_0 \approx 2\pi \times 1$ Hz, $\omega_\perp \approx 2\pi \times 300$ Hz, what corresponds to the cigar-shaped shape with axial size $a_0 \sim 1\,\mathrm{mm}$ and radial one $a_\perp \sim 10\,\mu\mathrm{m}$. In this case aspect ratio $\omega_0/\omega_\perp \equiv \nu \approx 0.003$ and corresponding small parameter $\epsilon^2 \approx 0.01$. By calculating the real time step as $\Delta t = 2/\omega_\perp \epsilon^2 \approx 100\,\mathrm{ms}$ one can obtain that experimental characteristic time of the FR is about 20 ms, what corresponds to $\tau = 0.2$, and the characteristic time of the appearance of a train of solitons in dimensionless units is approximately 2 what corresponds to the real time $t \approx 0.2\,\mathrm{s}$.

Recent experimental studies [8] have shown that by approaching the resonant point a number of atoms in the condensate start quickly decrease what imposes certain restrictions on the application of FR. This means that the theory is applicable if FR is switched off far enough from the resonant point to preserve the number of particles in the condensate. Another restriction is related to the fact that the transverse Gaussian distribution is also affected by the expansion of the condensate and by

the FR, which are not take into consideration by the theory based on weakly nonlinear expansion.

In conclusion we have investigated formation of the matter bright and dark matter solitons in quasi-1D BEC's embedded in OL by means of FR technique. In particular, for cigar-shaped condensate we have considered the four types of reduction of the initially 3D GP equation to the 1D NLS equation where parabolic and periodic potentials are included into the final NLS equation either explicitly or in the background solution. This was done by using multiple-scale expansion method. Special attention has been paid to the 1D NLS equation in which both parabolic and periodic potentials were included explicitly. It was shown that for small aspect ratio of the condensate initial conditions can be searched as a exact solution of the NLS equation with periodic potential which is modulated by the solution of the NLS equation with only parabolic potential. The general form of the periodic solution of the NLS equation in OL was proposed. The process of formation of the trains of bright/dark solitons by using FR in the presence of parabolic and periodic potentials was studied numerically.

Acknowledgments

We gratefully acknowledge useful comments of L. P. Pitaevskii. VVK. acknowledges support from the European grant, COSYC n.o. HPRN-CT-2000-00158. Work of V.A.B. has been supported by the FCT fellowship SFRH/BPD/5632/2001.

References

[1] M.H. Anderson, J.R. Ensher, M.R. Matthews, C.E. Wieman, and E.A. Cornell, Science, **269**, 198 (1995); K.B. Davis, M.-O. Mewes, M.R. Andrews, N.J. van Druten, D.S. Durfee, D.M. Kurn, and W. Ketterle, Phys. Rev. Lett. **75**, 3969 (1995).

[2] B.P. Anderson and M. Kasevich, Science **282**, 1686 (1998).

[3] M. Greiner, O. Mandel, T. Esslinger, T.W. Hänsch and I. Bloch, Nature **415**, 6867 (2002); M. Greiner, I. Bloch, O. Mandel, T.W. Hänsch and T. Esslinger, Phys. Rev. Lett. **87**, 160405 (2001).

[4] C. Fort, F.S. Cataliotti, L. Fallani, F. Ferlaino, P. Maddaloni, and M. Inguscio, Phys. Rev. Lett. **90**, 140405 (2003); O. Morsch, E. Arimondo: arXiv: cond-mat/0209034.

[5] S. Burger, K. Bongs, S. Dettmer, W. Ertmer, and K. Sengstock , Phys. Rev. Lett. **83**, 5198 (1999); J. Denschlag, J.E. Simsarian, D.L. Feder, C.W. Clark, L.A. Collins, J. Cubizolles, L. Deng, E.W. Hagley, K. Helmerson, W.P. Reinhardt, S.L. Rolston, B.I. Schneider, W.D. Phillips, Science **287**, 97 (2000); B.P. Anderson, P.C. Haljan, C.A. Regal, D.L. Feder, L.A. Collins, C.W. Clark, and E.A. Cornell, Phys. Rev. Lett. **86**, 2926 (2001).

[6] L. Khaykovich, F. Schreck, G. Ferrari, T. Bourdel, J. Cubizolles, L.D. Carr, Y. Castin, and C. Salomon, Science **296**, 1290 (2002); K.E. Strecker, G.B. Partridge, A.G. Truscott, and R.G. Hulet, Nature **417**, 150 (2002).

[7] W. C. Stwalley, Phys. Rev. Lett. **37**, 1628 (1976); E. Tiesinga, B. J. Verhaar, and H. T. C. Stoof, Phys. Rev. A **47**, 4114 (1993); A.J. Moerdijk, B.J. Verhaar, and A. Axelsson, Phys. Rev. A **51**, 4852 (1995).

[8] S. Inouye, M.R. Andrews, J. Stenger, H.-J. Miesner, D.M. Stamper-Kurn, and W. Ketterle, Nature **392**, 151 (1998); J. Stenger, S. Inouye, M. R. Andrews, H.-J. Miesner, D.M. Stamper-Kurn, and W. Ketterle, Phys. Rev. Lett. **82**, 2422 (1999); S.L. Cornish, N.R. Claussen, J.L. Roberts, E.A. Cornell, and C.E. Wieman, Phys. Rev. Lett. **85**, 1795 (2000);

[9] F.Kh. Abdullaev, A.M. Kamchatnov, V.V. Konotop, and V.A. Brazhnyi, Phys. Rev. Let. **90**, 230402 (2003).

[10] P.G. Kevrekidis, G. Theocharis, D.J. Frantzeskakis, and B.A. Malomed, Phys. Rev. Let. **90**, 230401 (2003).

[11] Víctor M. Pérez-García, V.V. Konotop, and V.A. Brazhnyi (submitted); *cond-mat/0311076*.

[12] E.P. Gross, J. Math. Phys. **4**, 195 (1963); L.P. Pitaevskii, Zh. Eksp. Teor. Phys. **4**, 451 (1961); F. Dalfovo, S. Giorgini, L.P. Pitaevskii, and S. Stringari, Rev. Mod. Phys. **71**, 463 (1999).

[13] V.V. Konotop and M. Salerno, Phys. Rev. A **65**, 021602 (2002).

[14] V.A. Brazhnyi and V.V. Konotop, Phys. Rev. A **68**, 043613 (2003).

[15] B.B. Baizakov, V.V. Konotop and M. Salerno, J. Phys. B **35** 5105 (2002).

[16] J.C. Bronski, L.D. Carr, B. Deconinck, and J.N. Kutz, K. Promislow, Phys. Rev. E **63**, 036612 (2001); J.C. Bronski, L.D. Carr, R. Carratero-Gonzalez, B. Deconinck, J.N. Kutz, and K. Promislow, Phys. Rev. E **64**, 056615 (2001).

[17] M. Abramovitz and I.A. Stegun: *Handbook of Mathematical Functions* (Dower, New York, 1965).

[18] V.V. Konotop, *Nonlinear Schrödinger equation with dissipation: Two models for Bose-Einsten condenstaes*, in "*Dissipative solitons*", ed. by N. Akhmeddev (Springer, in press).

[19] L.D. Fadeev, L.A. Takhtajan: *Hamiltonian Methods in the Theory of Solitons*, (Springer Verlag, Berlin, 1987).

[20] G. Boffetta and A.R. Osborne, J. Comput. Phys. **102**, 252 (1992).

[21] F. Kh. Abdullaev, B. B. Baizakov, S. A. Darmanyan, V. V. Konotop, and M. Salerno, Phys. Rev. A **64** 043606 (2001)

TWO-COMPONENT BOSE-EINSTEIN CONDENSATES IN OPTICAL LATTICES

Modulational Instability and Soliton Generation

N. A. Kostov
Institute for Electronics, Bulgarian Academy of Sciences, 1784 Sofia, Bulgaria.
nakostov@ie.bas.bg

V. S. Gerdjikov*, V. Z. Enol'skii, M. Salerno
Dipartimento di Fisica "E.R.Caianiello" and INFM, Universitá di Salerno, I-84081 Baronissi (SA), Italy.
gerjikov@inrne.bas.bg, vze@ma.hw.ac.uk, salerno@sa.infn.it

V. V. Konotop
Centro de Física Teórica e Computacional, Universidade de Lisboa, Complexo Interdisciplinar, Av. Prof. Gama Pinto 2, Lisbon 1649-003, Portugal
konotop@cii.fc.ul.pt

Abstract Coupled nonlinear Schrödinger equations (CNLS) with an external elliptic function potential model a quasi one–dimensional interacting two-component Bose-Einstein condensate trapped in a standing light wave. New stationary solutions of the CNLS with a periodic potential are derived and interpreted as exact Bloch states at the edge of the Brillouin zone. The modulationally unstable solutions lead to formation of localized ground states of the coupled BEC system.

Keywords: Bose-Einstein condensate, optical lattices, modulational instability, soliton generation.

1. Introduction

Recent experiments on dilute-gas Bose-Einstein condensates (BEC's) have generated great interest both from theoretical and experimental

*Permanent address: Institute for Nuclear Research and Nuclear Energy, 1784 Sofia, Bulgaria

F. Kh. Abdullaev and V. V. Konotop (eds.), Nonlinear Waves: Classical and Quantum Aspects, 269–283.

points of view [1]. At ultra-low temperatures the mean-field description for the macroscopic BEC wave-function is constructed using Hartree-Fock approximation and results in the Gross-Pitaevskii (GP) equation [1]. The latter one reduces to the one-dimensional (1D) nonlinear Schrödinger (NLS) equation with an external potential, in particular, when the transverse dimensions of the condensate are much less than its healing length and its longitudinal dimension is of order or much longer than the healing length (see e.g. [2, 3]). This is termed the *quasi-one dimensional* (quasi-1D) regime of the GP equation. In this regime BECs remain phase–coherent, and the governing equations are one-dimensional. Several families of stationary solutions for the cubic NLS with an elliptic function potential were presented in Refs [4, 6]; their stability was examined using analytic and numerical methods [6, 7, 8, 9, 10].

The two-component BEC's is described by GP equations, which in the quasi-1D regime, reduce to coupled nonlinear Schrödinger (CNLS) equations with an external potential [11, 12].

Below we study the stationary solutions of the CNLS with an external potential. Several cases of explicit solutions in terms of elliptic functions are analyzed and their stability properties are studied numerically. We derive a set of stationary solutions with trivial and non trivial phases; some of them were also analyzed independently in Ref. [13]. We extend their results by investigating in more details the solutions of CNLS whose components are expressed through different elliptic functions, see also Section 6. We investigate the possibility that these solutions taken as initial states, may generate localized matter waves (solitons).

2. Basic equations

At very low temperatures, when the mean field approximation is applicable, the evolution of two interacting BEC's is described by two coupled GP equations:

$$i\hbar\frac{\partial\Psi_j}{\partial t} = \left[-\frac{\hbar^2}{2m}\nabla^2 + V_j(\mathbf{r}) + \frac{4\pi\hbar^2}{m}\sum_{l=1,2} a_{jl}|\Psi_l|^2\right]\Psi_j \qquad (1)$$

($j = 1, 2$), see [11, 12]. Here atomic masses of both components are assumed to be equal, $V_j(\mathbf{r})$'s are external trap potentials, and a_{ij} are the scattering lengths of the respective atomic interactions (other notations are standard). If V_j consist of superposition of a magnetic trap providing cigar shape of the condensate (elongated, along the x-axis) and an optical trap inducing a periodic lattice potential along the x-axes we have:

$$V_j(\mathbf{r}) = \frac{m}{2}\omega_j^2[\lambda^2 x^2 + y^2 + z^2] + U(\kappa x),\ U(\kappa x) = U(\kappa(x + L)). \qquad (2)$$

Here λ is the aspect ratio of the condensate, which is assumed to be the same for both components. For cigar-shaped condensates $\lambda \ll 1$ with typical values $10^{-2} \div 10^{-4}$. Although we have assumed equality of the optical potential for both components, in a general case one has to distinguish the linear oscillator frequencies, ω_1 and ω_2, when considering the two components corresponding to the different magnetic moments. For example, in the experimental settings of [14] with ^{87}Rb atoms $\Omega = \omega_2/\omega_1 = \sqrt{2}$. This fact has natural implication on the resulting form of the effective system of coupled 1D NLS equations. Different oscillator frequencies means that two components are located in two different parabolic potentials, and thus their effective densities are different when the number of atoms is equal. Therefore, even at approximately equal s-wave scattering lengths, i.e., for $a_{11} \approx a_{22}$, the two components experience different nonlinearities, proportional to the atomic densities.

Another important fact is that a cigar-shaped BEC can be viewed as a waveguide for matter waves. As such it is characterized by its mode structure. As it is well known (c.f. with the nonlinear optical waveguides [15]) the intrinsic nonlinearity of a BEC results in the mode interaction (and thus energy distribution among modes). If however the nonlinearity is weak enough, the main state of the condensate can be considered as a weakly modulated ground state of the underline linear system. As it is clear that for a two-component BEC the respective small parameter is the ratio between the density energy of two-body interactions, $4\pi\hbar^2 N_j a_{jj}\sqrt{\lambda}/(m a_j^3)$ (here $a_j = \sqrt{\hbar/(m\omega_j)}$ is the linear oscillator length and $N_j = \int |\Psi_j|^2 d\mathbf{r}$ is the number of atoms of the jth component) to the density of the kinetic energy $\hbar^2/(2ma_j^2)$. Thus the small parameter equals $\epsilon = 8\pi N a_{11}\sqrt{\lambda}/a_1 \ll 1$, where $N = N_1 + N_2$ is the total number of atoms. In this situation a self-consistent reduction of the original 3D system (1) to the effective 1D system of the coupled equations can be provided by means of the multiple-scale expansion. Since the details of such a reduction are already known (see [3, 16] for a single component BEC and [5] for the multicomponent case), here we consider basic equations in reduced form and in dimensionless variables.

3. Stationary solutions with non-trivial phases

The rescaled system has the well known form of CNLS equations

$$i\frac{\partial Q_1}{\partial t} + \frac{\partial^2 Q_1}{\partial x^2} + (b_1|Q_1|^2 + b_0|Q_2|^2)Q_1 - V_0 \mathrm{sn}^2(\alpha x, k)Q_1 = 0, \quad (3)$$

$$i\frac{\partial Q_2}{\partial t} + \frac{\partial^2 Q_2}{\partial x^2} + (b_0|Q_1|^2 + b_2|Q_2|^2)Q_2 - V_0 \mathrm{sn}^2(\alpha x, k)Q_2 = 0. \quad (4)$$

They provide a general model with applications in nonlinear optics (see e.g. [15]). We analyze the stationary solutions of these CNLS:

$$Q_j(x,t) = q_j(x)\exp(-i\omega_j t + i\Theta_j(x) + i\kappa_{0,j}), \qquad j = 1,2, \tag{5}$$

where $\kappa_{0,j}$ are constant phases. The real-valued functions q_j and $\Theta_j(x)$ are related by:

$$\Theta_j(x) = \mathcal{C}_j \int_0^x \frac{dx'}{q_j^2(x')}, \qquad j = 1,2, \tag{6}$$

where $\mathcal{C}_j$, are constants of integration.

Following [6] we refer to solutions in the cases $\mathcal{C}_j = 0$ and $\mathcal{C}_j \neq 0$ as to trivial and nontrivial phase solutions, respectively. The nontrivial phase solutions imply nonzero current of the matter – it is proportional to $|q_j(x)|^2\Theta_{jx} = \mathcal{C}_j$, for each of the components – along x-axis, and hence seem to have no direct relation to present experimental setting for BECs (remember that the condensate is confined to a parabolic trap).

An appropriate class of periodic potentials to model the quasi-1D confinement produced by a standing light wave is given by

$$V(\alpha x) = V_0 \mathrm{sn}^2(\alpha x, k), \tag{7}$$

where $\mathrm{sn}(\alpha x, k)$ denotes the Jacobian elliptic sine function with elliptic modulus $0 \leq k \leq 1$. Then, substituting the ansatz (5) in Eqs. (3), (4) and assuming that q_j^2, $j = 1,2$ are quadratic functions of $\mathrm{sn}(\alpha x, k)$:

$$q_j^2 = A_j \mathrm{sn}^2(\alpha x, k) + B_j, \qquad j = 1,2. \tag{8}$$

we find the following set of relations among the solution parameters ω_j, $\mathcal{C}_j$, A_j and B_j and the characteristic of the optical lattice V_0, α and k:

$$A_1 = \frac{(b_2 - b_0)W}{\Delta}, \qquad A_2 = \frac{(b_1 - b_0)W}{\Delta}, \tag{9}$$

$$B_j = -\beta_j A_j, \qquad \mathcal{C}_j^2 = \alpha^2 A_j^2 \beta_j(\beta_j - 1)(1 - \beta_j k^2), \tag{10}$$

$$\omega_j = (1+k^2)\alpha^2 + \frac{W}{\Delta}[\beta_1 b_1(b_2 - b_0) - \beta_2 b_0(b_0 - b_1)] - k^2\alpha^2\beta_j, \tag{11}$$

where $j = 1,2$ and

$$W = V_0 - 2\alpha^2 k^2, \qquad \Delta = \chi_1\chi_2 - \chi^2 = b_1 b_2 - b_0^2. \tag{12}$$

In order that our results (8)–(10) are consistent with the parametrization (5), (6) we must ensure that both $q_j(x)$ and $\Theta_j(x)$ are real-valued; this

means that $C_j^2 \geq 0$ and $q_j^2(x) \geq 0$. This is true provided one of the following pairs of conditions are satisfied:

$$\text{a)} \qquad A_j \geq 0, \quad \beta_j \leq 0, \quad j = 1, 2; \tag{13}$$

$$\text{b)} \qquad A_j \leq 0, \quad 1 \leq \beta_j \leq \frac{1}{k^2}, \quad j = 1, 2; \tag{14}$$

The solutions Q_j in (5) *are periodic in* x provided the parameters satisfy certain condition, see [5].

The solutions for two particular choices of b_1, b_2 and b_0 can be viewed as singular limits of the generic case considered above. The first one $b_0^2 = b_1 b_2$, $b_1 \neq b_2$ corresponds to the case (13); the solution is given by:

$$\begin{aligned} &A_2 = -\frac{b_1}{b_0} A_1, \qquad V_0 = 2k^2\alpha^2, \\ &\omega_1 = (\beta_1 - \beta_2) b_1 A_1 + (1 + k^2)\alpha^2 - \alpha^2 k^2 \beta_1, \\ &\omega_2 = (\beta_1 - \beta_2) b_0 A_2 + (1 + k^2)\alpha^2 - \alpha^2 k^2 \beta_2, \\ &\mathcal{C}_j^2 = \alpha^2 A_j^2 \beta_j (\beta_j - 1)(1 - \beta_j k^2), \qquad B_j = -\beta_j A_j, \qquad j = 1, 2. \end{aligned} \tag{15}$$

The second one $b_1 = b_2 = b$ corresponds to the Manakov system:

$$\begin{aligned} &\omega_j = b(\beta_1 A_1 + \beta_2 A_2) + (1 + k^2)\alpha^2 - \alpha^2 k^2 \beta_j, \\ &\mathcal{C}_j^2 = \alpha^2 A_j^2 \beta_j (\beta_j - 1)(1 - \beta_j k^2), \\ &B_j = -\beta_j A_j, \qquad V_0 = b(A_1 + A_2) + 2k^2\alpha^2, \qquad j = 1, 2. \end{aligned} \tag{16}$$

The constants b_1, b_2 and b_0 in eqs. (3), (4) are assumed to be positive. However our formulae are valid also for negative values of b_1, b_2 and b_0. We have also analyzed [5] the limits of this solution for $k \to 1$ and $k \to 0$.

4. Trivial phase solutions

In this section we consider solutions of (3), (4) with trivial phase, i.e. $C_1 = C_2 = 0$:

$$Q_j(x, t) = e^{-i\omega_j t + i\kappa_{0,j}} q_j(x), \qquad j = 1, 2, \tag{17}$$

and we will look for different possible choices for the functions $q_1(x)$ and $q_2(x)$. This type of solutions in certain cases survive reductions of the constants $b_0^2 = b_1 b_2$ or the limit to the Manakov case: $b_1 = b_2 = b_0$. They are also relevant for processes in BEC and nonlinear optics [15].

In the following we shall consider the $q_i(x)$ to be expressed in terms of Jacobi elliptic functions, i.e. we assume that $q_i(x) = \gamma_i J_i(x)$, where $J_i(x), i = 1, 2$ is one of the Jacobi elliptic function $\mathrm{sn}\,(\alpha x, k)$, $\mathrm{cn}\,(\alpha x, k)$ or $\mathrm{dn}\,(\alpha x, k)$ and γ_i specify the real amplitudes in (17). Note that the

Table 1. Trivial phase solutions in the generic case: $\Delta \equiv b_1 b_2 - b_0^2 \neq 0$. The conditions c_k, $k = 1, \ldots, 4$ are listed in eq. (20).

1	$q_1 = \gamma_1 \mathrm{sn}\,(\alpha x, k)$ $q_2 = \gamma_2 \mathrm{cn}\,(\alpha x, k)$	$\omega_1 = b_0 Y_1 W + \alpha^2(k^2+1)$ $\omega_2 = b_2 Y_1 W + \alpha^2$	$\gamma_1^2 = Y_2 W$ $\gamma_2^2 = -Y_1 W$	c_1
2	$q_1 = \gamma_1 \mathrm{dn}\,(\alpha x, k)$ $q_2 = \gamma_2 \mathrm{sn}\,(\alpha x, k)$	$\omega_1 = b_1 Y_2 W/k^2 + \alpha^2 k^2$ $\omega_2 = b_0 Y_2 W/k^2 + \alpha^2(k^2+1)$	$\gamma_1^2 = -Y_2 W/k^2$ $\gamma_2^2 = Y_1 W$	c_2
3	$q_1 = \gamma_1 \mathrm{dn}\,(\alpha x, k)$ $q_2 = \gamma_2 \mathrm{cn}\,(\alpha x, k)$	$\omega_1 = (b_0 Y_1 + b_1 Y_2/k^2) W + \alpha^2 k^2$ $\omega_2 = (b_2 Y_1 + b_0 Y_2/k^2) W + \alpha^2$	$\gamma_1^2 = -Y_2 W/k^2$ $\gamma_2^2 = -Y_1 W$	c_3
4	$q_1 = \gamma_1 \mathrm{sn}\,(\alpha x, k)$ $q_2 = \gamma_2 \mathrm{sn}\,(\alpha x, k)$	$\omega_1 = \omega_2 = \alpha^2(k^2+1)$	$\gamma_1^2 = Y_2 W$ $\gamma_2^2 = Y_1 W$	c_4
5	$q_1 = \gamma_1 \mathrm{cn}\,(\alpha x, k)$ $q_2 = \gamma_2 \mathrm{cn}\,(\alpha x, k)$	$\omega_1 = \omega_2 = \alpha^2 + W$	$\gamma_1^2 = -Y_2 W$ $\gamma_2^2 = -Y_1 W$	c_3
6	$q_1 = \gamma_1 \mathrm{dn}\,(\alpha x, k)$ $q_2 = \gamma_2 \mathrm{dn}\,(\alpha x, k)$	$\omega_1 = \omega_2 = \alpha^2 k^2 + W/k^2$	$\gamma_1^2 = -Y_2 W/k^2$ $\gamma_2^2 = -Y_1 W/k^2$	c_3

Table 2. Trivial phase solutions in the case: $\Delta \equiv b_1 b_2 - b_0^2 = 0$.

1	$q_1 = \gamma_1 \mathrm{sn}\,(\alpha x, k)$ $q_2 = \gamma_2 \mathrm{cn}\,(\alpha x, k)$	$\omega_1 = \alpha^2(k^2+1) - b_1\gamma_1^2$ $\omega_2 = \alpha^2 - \sqrt{b_1 b_2}\gamma_1^2$	$\gamma_2^2 = \sqrt{b_1/b_2}\gamma_1^2$	$W = 0$
2	$q_1 = \gamma_1 \mathrm{dn}\,(\alpha x, k)$ $q_2 = \gamma_2 \mathrm{sn}\,(\alpha x, k)$	$\omega_1 = \alpha^2 k^2 - b_1\gamma_1^2$ $\omega_2 = \alpha^2(k^2+1) - \sqrt{b_1 b_2}\gamma_1^2$	$\gamma_2^2 = k^2\sqrt{b_1/b_2}\gamma_1^2$	W=0

Table 3. Trivial phase solutions in the case: $b_1 = b_2 = b$.

3	$q_1 = \gamma_1 \mathrm{dn}\,(\alpha x, k)$ $q_2 = \gamma_2 \mathrm{cn}\,(\alpha x, k)$	$\omega_1 = \alpha^2 k^2 + (b_0 + b/k^2) X$ $\omega_2 = \alpha^2 + (b + b_0/k^2) X$	$\gamma_1^2 = -X/k^2$ $\gamma_2^2 = -X$	$W < 0$
4	$q_1 = \gamma_1 \mathrm{sn}\,(\alpha x, k)$ $q_2 = \gamma_2 \mathrm{sn}\,(\alpha x, k)$	$\omega_1 = \omega_2 = \alpha^2(k^2+1)$	$\gamma_1^2 = \gamma_2^2 = X$	$W > 0$
5	$q_1 = \gamma_1 \mathrm{cn}\,(\alpha x, k)$ $q_2 = \gamma_2 \mathrm{cn}\,(\alpha x, k)$	$\omega_1 = \omega_2 = \alpha^2 + W$	$\gamma_1^2 = \gamma_2^2 = -X$	$W < 0$
6	$q_1 = \gamma_1 \mathrm{dn}\,(\alpha x, k)$ $q_2 = \gamma_2 \mathrm{dn}\,(\alpha x, k)$	$\omega_1 = \omega_2 = \alpha^2 k^2 + W/k^2$	$\gamma_1^2 = \gamma_2^2 = -X/k^2$	$W < 0$

CNLS (3), (4) possesses the gauge invariance $Q_j \to Q_j e^{-i\kappa_{0,j}}$. This allows one to fix up the initial phases of both $Q_j(x)$; our choice is to require that $\gamma_j^2 > 0$. We substitute the above ansatz into Eqs. (3), (4) and get a set of algebraic equations for the parameters whose solutions furnish exact ground states of the coupled BEC system.

To illustrate the details of the calculations we start with case 1 in which: $q_1(x) = \gamma_1 \mathrm{sn}\,(\alpha x, k)$, $q_2(x) = \gamma_2 \mathrm{cn}\,(\alpha x, k)$. These functions are solutions of (3) provided the constants satisfy the relations:

$$\begin{aligned} &b_1\gamma_1^2 - b_0\gamma_2^2 - W = 0, \quad b_0\gamma_1^2 - b_2\gamma_2^2 - W = 0, \\ &b_0\gamma_2^2 + \omega_1 - \alpha^2(k^2+1) = 0, \quad b_2\gamma_2^2 + \omega_2 - \alpha^2 = 0. \end{aligned} \tag{18}$$

where W is defined in eq. (12). From this system we can determine 4 of the constants in terms of the others. Let us split these constants into two groups. The first one, $G_1 \simeq \{b_1, b_2, b_0, W, \alpha\}$ are constants determining the equations and the potential and we assume they are fixed. The second group $G_2 \simeq \{\omega_1, \omega_2, \gamma_1, \gamma_2, \}$ characterize the corresponding solution. We solve (18) and express the constants G_2 in terms of G_1.

We have collected all the results for generic choices of b_0, b_1 and b_2 in the Table 1 below using the following notations:

$$Y_1 = \frac{b_0 - b_1}{b_0^2 - b_1 b_2}, \qquad Y_2 = \frac{b_0 - b_2}{b_0^2 - b_1 b_2}, \qquad X = \frac{W}{b_0 + b}. \tag{19}$$

and the conditions:

$$\begin{array}{lllllll} c_1 = W > 0, & Y_2 > 0, & Y_1 < 0, \text{ or } W < 0, & Y_2 < 0, & Y_1 > 0, \\ c_2 = W > 0, & Y_2 < 0, & Y_1 > 0, \text{ or } W < 0, & Y_2 > 0, & Y_1 < 0, \\ c_3 = W > 0, & Y_2 < 0, & Y_1 < 0, \text{ or } W < 0, & Y_2 > 0, & Y_1 > 0, \\ c_4 = W > 0, & Y_2 > 0, & Y_1 > 0, \text{ or } W < 0, & Y_2 < 0, & Y_1 < 0, \end{array} \tag{20}$$

which ensure that $\gamma_1^2 > 0$ and $\gamma_2^2 > 0$.

In the Tables 2 and 3 we treat special situations: i) $b_0^2 = b_1 b_2$ (Table 2 and ii) $b_1 = b_2 = b$ (Table 3). The transition from the generic case to i) is singular. The Manakov case is obtained for $b_0 = b_1 = b_2 = b$ and follows easily from the results in Table 3.

5. Modulational instability of trivial phase solutions and generation of localized matter waves

In this section we discuss the stability of the above solutions from a physical point of view. To this end we remark that all the trivial phase solutions, are periodic functions of period twice the period of the lattice (recall that the period a of potential in Eq. (7) is $a = 2K(k^2)/\alpha$, where $K(k^2)$ is the complete elliptic integral of the first kind). The corresponding wave-number of these solutions is $\mathcal{K} = \pi/a$ which is just the boundary of the Brillouin zone of the uncoupled periodic linear system.

One can check that each component $q_i(x)$ satisfy the Bloch condition

$$q_i(x + R_n) = e^{i\mathcal{K}R_n} q_i(x), \qquad R_n = na, \qquad n \in N, \quad i = 1, 2, \tag{21}$$

i.e. the trivial phase solutions are exact *nonlinear* Bloch states (a nonlinear Bloch state can be defined, in analogy with the linear case, as a state for which Eq. (22) is satisfied). Although nonlinearity does not compromise Bloch property (this being a direct consequence of the translation

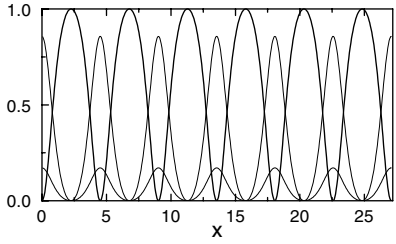

Figure 1. Initial profile of stable a cn-cn solution plotted against the potential profile (thick curve). The thin curves denote the modulo square of q_1 and q_2. The parameters are fixed as: $k^2 = 0.8$, $V_0 = 1$, $\alpha = 1$, $b_0 = 0.5$, $b_1 = 1.0$, $b_2 = 0.6$. The initial amplitudes are $\gamma_1 = 0.414039, \gamma_2 = 0.92582$.

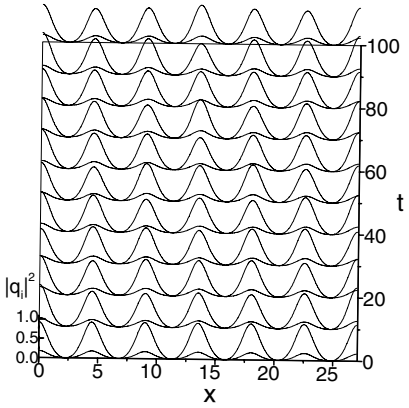

Figure 2. Prospective view of the time evolution of the two components cn-cn solution reported in Fig.1. To check stability the solution was slightly modulated in space with a profile of the form $0.1\cos(0.2x)$. Parameters are fixed as in Fig. 1.

invariance of the lattice), it can drastically influence the stability of the states through a modulational instability mechanism.

The possibility that localized states of soliton type can be generated from modulational instability of Bloch states at the edge of the Brillouin zone was proved, both analytically and numerically, for a single component BEC in optical lattice in the cases of one [3], two and three spatial dimensions [16]. In order to explore the same possibility to occur also in the present periodic two-components system we recourse to numerical simulations. We have integrated Eqs. (3), (4) with an operator splitting method using fast Fourier transform, taking as initial conditions the exact solutions derived above modulated by a long wavelength L ($2\pi/k \ll \pi/L$) and small amplitude sinusoidal profile.

In Fig. 1 we depict the initial profiles of the two components cn-cn solution plotted against the potential profile, while in Fig. 2 we show the time evolution of this solution in presence of a small modulation.

From Fig. 1 we see that the profiles remain stable for long time for both components, indicating that the cn-cn solution is stable against small modulations. The main characteristic features of the modulational instability in the case of small amplitudes, can be understood within the framework of the approach developed in [3, 16]. We assume that the

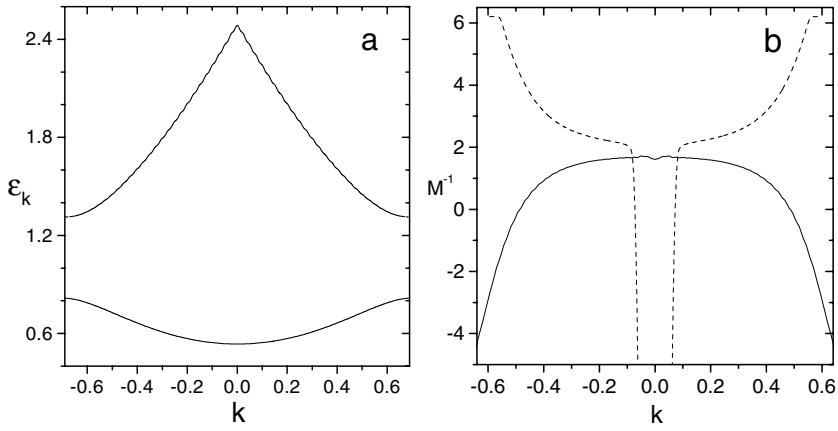

Figure 3. Panel a: Lowest two bands of the linear Schrödinger problem in Eq. (22) in the reduced zone scheme. Panel b: Reciprocal effective masses of the first (continuous curve) and second (dashed curve) band of panel a. The parameter values of the potential are fixed as in Fig. (1). For these parameters the period of the potential is 4.5144 and the edges of the Brillouin zone are ± 0.696 .

perturbations of the nonlinear Bloch states have wavelength much larger than the period of the potential in (3), (4). In analogy with Sec. II, one can look for solutions in the form $Q_j = \phi_j(x_0)\tilde{Q}_j(x_1, t_1)$, where $\phi_j(x_0)$ denote two chosen Bloch functions, $\phi_{n,\kappa}(x_0)$, of the potential $V(\alpha x)$

$$-\frac{d^2\phi_{n,\kappa}(x)}{dx^2} + V(\alpha x)\phi_{n,\kappa}(x) = \mathcal{E}_n(\kappa)\phi_{n,\kappa}(x) \tag{22}$$

with n and κ denoting the number of the zone and the wave vector reduced to the first Brillouin zone, respectively (notice that we adopt again scaled variables). The Bloch functions are chosen to be normalized as follows $\int_0^a |\phi_j(x)|^2 dx = 1$. One can then use these Bloch states as zero order in a multiple scale expansion, in analogy to what done in Sec. II and in Ref. [3]. Here we shall drop details and present just the final system of equations for the amplitudes of the modulation field:

$$i\frac{\partial\tilde{Q}_1}{\partial t} + \frac{1}{2M_1}\frac{\partial^2\tilde{Q}_1}{\partial x^2} + (\tilde{b}_1|\tilde{Q}_1|^2 + \tilde{b}_0|\tilde{Q}_2|^2)\tilde{Q}_1 = 0 \tag{23}$$

$$i\frac{\partial\tilde{Q}_2}{\partial t} + \frac{1}{2M_2}\frac{\partial^2\tilde{Q}_2}{\partial x^2} + (\tilde{b}_0|\tilde{Q}_1|^2 + \tilde{b}_2|\tilde{Q}_2|^2)\tilde{Q}_2 = 0, \tag{24}$$

where we have introduced the following notation: $\frac{1}{M_j} = \frac{d^2\mathcal{E}_n(\kappa)}{d\kappa^2}$ and

$$\tilde{b}_{1,2} = b_{1,2}\int_0^a |\phi_{1,2}(x)|^4 dx, \qquad \tilde{b}_0 = b_0\int_0^a |\phi_1(x)|^2|\phi_2(x)|^2 dx$$

In Fig.(3) we depict the first two bands and the the corresponding reciprocal effective masses of the underlying linear system in Eq. (22). To study modulational instability, we look for a solution of (23), (24) in the form of a weakly modulated constant background

$$\tilde{Q}_j = (\gamma_j + \tilde{\alpha}_j e^{iKx - i\Omega t} + \tilde{\beta}_j e^{-iKx + i\Omega t}) e^{-i\Omega_j t},$$

where $\Omega_1 = \tilde{b}_1\gamma_1^2 + \tilde{b}_0\gamma_2^2$, $\Omega_2 = \tilde{b}_2\gamma_2^2 + \tilde{b}_0\gamma_1^2$, and $|\tilde{\alpha}_j|$, $|\tilde{\beta}_j| \ll |\gamma_j|^2$. Next, we linearize the system with respect to $\tilde{\alpha}_j$, $\tilde{\beta}_j$ and derive the dispersion relation of the resulting linear system in the form

$$\begin{aligned} \Lambda^2 &- (G_1^2 + G_2^2 - 2\tilde{\chi}_1 G_1 - 2\tilde{\chi}_2 G_2)\Lambda \\ &+ G_1 G_2 (G_1 G_2 + 2\tilde{\chi}_1 G_2 + 2\tilde{\chi}_2 G_1 - 4\tilde{\chi}_0^2 + 4\tilde{\chi}_1\tilde{\chi}_2) = 0 \end{aligned} \tag{25}$$

where $\Lambda = \Omega^2$, $G_j = K^2/(2M_j)$, $\tilde{\chi}_j = \gamma_j^2 \tilde{b}_j$ for $j = 1, 2$, and $\tilde{\chi}_0 = \gamma_1\gamma_2\tilde{b}_0$. The respective solution of the coupled nonlinear system (consisting of two nonlinear Bloch waves) is stable if both roots of (25) are positive and unstable otherwise (notice that this analysis gives stability with respect to long wavelengths only).

As a particular example we take the case in which both components belong to the same gap edge, i.e. $M_1 M_2 > 0$ and therefore $G_1 G_2 > 0$. For the stability of the wave the following conditions must be satisfied

$$G_1^2 + G_2^2 - 2\tilde{\chi}_1 G_1 - 2\tilde{\chi}_2 G_2 > 0 \tag{26}$$

$$G_1 G_2 + 2(\tilde{\chi}_1 G_2 + \tilde{\chi}_2 G_1) > 4\tilde{\chi}_0^2 - 4\tilde{\chi}_1\tilde{\chi}_2. \tag{27}$$

Since the cases physically more interesting correspond to positive b_j we have $b_1 b_2 > b_0^2$ and hence $\tilde{\chi} = \tilde{\chi}_1\tilde{\chi}_2 - \tilde{\chi}_0^2$. This implies that either (26) or (27) is satisfied for all K if either $M_{1,2} < 0$ or $M_{1,2} > 0$. In the case $M_{1,2} < 0$ the condition (27) can be viewed as a constrain on the wave amplitude. Indeed, after some simple algebra, one gets that (27) is satisfied for any K if the following equation is satisfied

$$(M_1\tilde{\chi}_1 + M_2\tilde{\chi}_2)^2 < 4(\tilde{\chi}_1\tilde{\chi}_2 - \tilde{\chi}_0^2). \tag{28}$$

In the second case, i.e. when $M_{1,2} > 0$, each of the states is unstable with respect to large wavelength excitations.

Now we can give a qualitative physical interpretation of the result depicted in Figs. 1, 2. As it follows from the explicit form of the solution, both components are described by the states belonging to the same edge of the Brillouin zone. This also can be viewed by the fact that $\Omega_1 = \Omega_2 \approx 0.6$ and thus the frequency of the solution is $\omega + \Omega_{1,2} \approx 1$. Then, from Fig. 3a one concludes that both waves correspond to states at the edge of the Brillouin zone and border the gap from the side of the

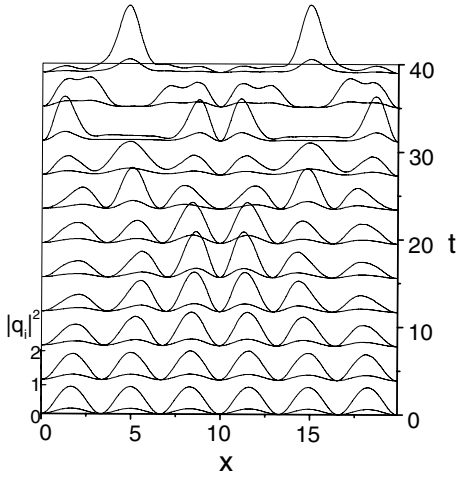

Figure 4. Prospective view of the time evolution of the unstable sn-sn solution. The initial amplitudes are $\gamma_1 = 0.414039$, $\gamma_2 = 0.925820$. Parameters are fixed as in Fig. 1, except for $k^2 = 0.2$. The modulational initial profile is taken as in Fig.2. Coupled soliton components emerge out of the instability.

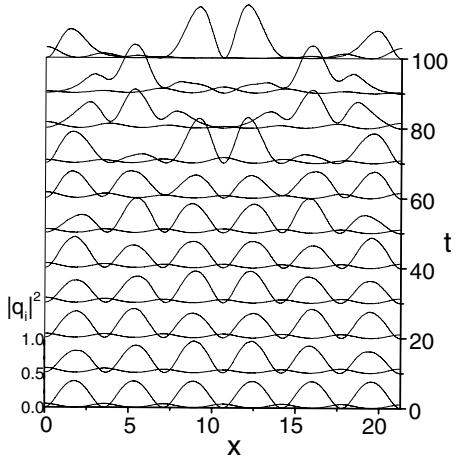

Figure 5. Same as in Fig.4 but for the unstable cn-sn solution. The initial amplitudes are taken as $\gamma_1 = 0.237356$, and $\gamma_2 = 0.627986$. Parameters are fixed as in Fig.1 except for $k^2 = 0.4$ and $b_0 = 0.65$. The unstable sn component dominates and soliton generation is more effective.

negative effective masses (this also follows from the fact that the period of the waves is twice the period of the potential and thus BEC's in the neighbor potential wells have opposite phases). Thus (26) is satisfied.

Next, we consider (28) whose left and right hand sides in the present case can be estimated as ($|M_1| = |M_2| \approx 0.238$, see Fig. 3b) 0.0266 and 0.352 respectively. Thus the stability of the solution observed in numerical simulations is confirmed by our stability analysis.

Let us now consider the case in which two atomic components belong to different edges of the gap, so that $M_1 > 0$ and $M_2 < 0$ (and hence $G_1 > 0$ and $G_2 < 0$) and restrict the consideration to the case $b_j > 0$. Then for the stability of the wave, the following conditions

$$2\tilde{\chi}_1 G_1 < G_1^2 + G_2^2 + 2\chi_2 |G_2|, \quad 2\tilde{\chi}_2 G_1 < G_1 |G_2| + 2\tilde{\chi}_1 |G_2|. \qquad (29)$$

must be satisfied. In this case the first component, having positive effective mass has a self-attractive character, which might dominate the destructive action of the lattice when the matter localizes around the potential maxima. In absence of the second component, this wave would be modulationally unstable, this being well known fact which can be

seen also from Eq. (29) (take $\tilde{\chi}_0$ and G_2 to be equal to zero). On the other hand, the second component, with negative effective mass, has a self-repulsive character, which is compensated by the potential barriers provided its localization occurs around the minima of the lattice potential. This component is stable even in absence of the first harmonic and if its amplitude is large enough (or the amplitude of the first component is small enough) it can help to stabilize the first component, as it follows from (29). More specifically (29) is satisfied for any K if $\gamma_1^2 < \frac{\tilde{b}_2 M_1}{\tilde{b}_1 |M_2|}\gamma_2^2$.

The above analysis is in good qualitative agreement with the results of numerical experiments. In particular, we find that except the cn-cn solution, all other solutions display modulational instability which lead to the formation of localized states. This is clearly seen in Fig. 4 where the time evolution of the unstable sn-sn solution is reported (notice the formation of two localized excitations at time t=40) . As for the previous case, the instability of this solution can be easily understood from the fact that the initial distribution of the matter corresponds to atoms condensed at the maxima of the potential (i.e. a position of unstable equilibrium). Notice that instability develops very quickly (already at time $t = 15$, what is dues large negative effective mass, see Fig. 3 b), out of which two components bright soliton states emerge, as clearly seen at time $t = 40$. The bright soliton consists of two coupled solitons (one for each component) one bigger than the other.

6. Discussions

Here we briefly discuss the above results in comparison with those of Ref [13] in which an n-component NLS-type equation with external potential is considered. The Hamiltonian of the n-component NLS is:

$$H = \int dx \left[\sum_{k=1}^{n} \frac{1}{2\mu_j} \left| \frac{\partial \psi_j}{\partial x} \right|^2 + \frac{1}{2} \sum_{j,p=1}^{n} a_{jp} |\psi_j|^2 |\psi_p|^2 + \sum_{j=1}^{n} V_j(x) |\psi_j|^2 \right].$$

where the integration goes over one period.

One possible class of solutions studied in detail in [13] is obtained with the anzats:

$$\psi_j(x) = n_j(x,t)\psi(x,t), \qquad n_j(x,t) = e^{-i\omega_j t + i\Theta_j(x)}\sqrt{N_j} \tag{30}$$

where $N_j > 0$ and $d\Theta_j/dx = C_j/(N_j|\psi(x)|^2)$. In Ref. [13] four types of non-trivial, as well as trivial phase solutions satisfying (30) and their stability properties are analyzed in details both by analytical and numerical

means. Inserting (30) into H we get the reduced Hamiltonian:

$$H_{\rm red} = \int dx \left[\frac{1}{2} M_0 \left| \frac{\partial \psi}{\partial x} \right|^2 + \frac{1}{2} M_{-1} \frac{1}{|\psi|^2} + V(x)|\psi|^2 + \frac{1}{2} W_0 |\psi|^4 \right], \tag{31}$$

where

$$M_0 = \sum_{j=1}^{n} \frac{1}{N_j \mu_j}, \qquad M_{-1} = \sum_{j=1}^{n} \frac{N_j}{\mu_j}, \qquad W_0 = \sum_{j,p=1}^{n} a_{jp} N_j N_p,$$

which describes the dynamics of the effective field $\psi(x,t)$. The result for the trivial phase solution case leads to $H_{\rm red}$ with $M_{-1} = 0$. This means that the systems of n equations with the anzats (30) reduce to just one equation for $\psi(x,k)$; the remaining $n-1$ equations follow as a consequence of the first one and the set of constraints on the coefficients a_{jl}, N_j, μ_j, ω_j. This argument holds true for our cases 4, 5 and 6.

The class of solutions that describe the multi-component effects should be analyzed by using ansatz more general than (30), such as e.g. in our cases 1, 2 and 3. Their stability properties do not seem to follow from the theorems proved in [13] and deserve additional studies.

Further perspectives of finding stable periodic solutions to the problem of a 2-component condensate could be linked to investigations of finite-gap solutions of Manakov system given in terms of multi-dimensional θ-functions [18] and [19] and to reduction of finite-gap solutions to elliptic functions [20]. Interesting classes of periodic solutions can be also obtained as the result of reduction of the Manakov system to completely integrable two-particle system interacting with fourth order potential [21, 22, 10].

Recently we became aware of Ref. [24] which gives extra evidence for the correctness of our results and their agreement with the ones in [25].

Acknowledgements

V.V.K. acknowledges Prof. Deconinck for discussing results in Ref.[13] prior their publication. V.S.G. and V.Z.E. wish to thank the Department of Physics "E.R.Caianiello" for the hospitality, and the University of Salerno for providing research grant during which most of this work was done. V.V.K acknowledges support from the European grant, COSYC no. HPRN-CT-2000-00158. M.S. acknowledges partial financial support from the MIUR, trough the inter-university project PRIN-2000, and from the European LOCNET grant no. HPRN-CT-1999-00163.

References

[1] F. Dalfovo, S. Giorgini, L. P. Pitaevskii, and S. Stringari, Rev. Mod. Phys. **71**, 463, (1999).

[2] V. M. Pérez-García, H. Michinel, and H. Herrero, Phys. Rev. A **57**, 3837 (1998); H. Michinel, V. M. Pérez-García, and R. de la Fuente, Phys. Rev. A **60** 1513 (1999); L. D. Carr, M. A. Leung , and W. P. Reinhardt, *J. Phys. B***33**, 3983–4001, (2000).

[3] V. V. Konotop and M. Salerno, *Phys. Rev. A***65**, 021602(R), (2002).

[4] F. Barra, P. Gaspard, and S.Rice, *Phys. Rev. E* **61**, 5852–5863, (2000).

[5] N. A. Kostov, V. S. Gerdjikov, V. Z. Enol'skii, V. V. Konotop, and M. Salerno, . *arXiv:cond-mat/0307156* (2003).

[6] J. C. Bronski, L. D. Carr, B. Deconinck, and J. N. Kutz, *Phys. Rev. Lett.*, **86**, 1402–1405, (2001).

[7] L. D. Carr, J. N. Kutz, and W. P. Reinhardt, *Phys. Rev. E* **63**, 066604, (2001).

[8] J. C. Bronski, L. D. Carr, B. Deconinck, J. N. Kutz, and K. Promislow, *Phys. Rev. E* **63**, 036612, (2001).

[9] J. D. Carter, and H. Segur. *nlin.PS/0302041.*

[10] J. C. Eilbeck, V. Z. Enolskii, and N. A. Kostov. J. Math. Phys. **41**, 8236-8248 (2000).

[11] M. Modugno, F. Dalfovo, C. Fort, P. Maddaloni, and F. Minardi, *Phys. Rev. E*, **62**,0663607, 2000.

[12] T. Bush, J. R. Anglin, *Phys. Rev. Lett.*, **87**, 010401, (2001).

[13] B. Deconinck, J. N. Kutz, M. S. Patterson, and B. W. Warner. J. Phys. A: Math. Gen. **36**, 5431-5447 (2003).

[14] P. Maddaloni, M. Modugno, C. Fort, F. Minardi, and M. Inguscio, Phys. Rev. Lett. **85**, 2413 (2000).

[15] G. P. Agrawal, *Nonlinear Fiber Optics.* 2nd ed. (Academic, San Diego, 1995).

[16] B. B. Baizakov, V. V. Konotop, and M. Salerno, *J.Phys. B***35**, 5105–5119, (2002).

[17] M. Abramowitz and I. A. Stegun, *Handbook of mathematical functions*, Dover, (1965).

[18] M. R. Adams, J. Harnad, and J. Hurtubise, *Commun. Math. Phys.*,**155**, 385, (1993).

[19] J.N.Elgin, V.Z.Enolskii, and A.R.Its, Effective integration of the non-linear vector Schrödinger equation, *Preprint* (2003).

[20] E.D. Belokolos, A.I. Bobenko, V.Z. Enolskii, A.R. Its, and V.B. Matveev, *Algebro-Geometrical Approach to Nonlinear integrable Equations*, Springer, Berlin, (1994).

[21] P. L. Christiansen, J. C. Eilbeck, V. Z. Enolskii, and N. A. Kostov, *Proc. R. Soc. Lond. A*, **451**, 685–700, (1995).

[22] P. L. Christiansen, J. C. Eilbeck, V. Z. Enolskii, and N. A. Kostov, *Proc. R. Soc. Lond. A*, **456**, 2263–2281, (2000).

[23] A.C. Sinatra, P. O. Fedichev, Y. Castin, J. Dalibard, and G. V. Shlyapnikov, *Phys. Rev. Lett.* **82**, 251–254, 1999.

[24] E. A. Ostrovskaya and Y. S. Kivshar. arXiv:cond-mat/0309127 (2003).

[25] A. A. Sukhorukov and Y. S. Kivshar. *Phys. Rev. Lett.* **91**, (2003).

SHOCK WAVES IN BOSE-EINSTEIN CONDENSATES

A.M. Kamchatnov
Institute of Spectroscopy, Russian Academy of Sciences
Troitsk 142190,Moscow Region, Russia
kamch@isan.troitsk.ru

A. Gammal
Instituto de Física, Universidade de São Paulo
05315-970, C.P.66318 São Paulo, Brazil
gammal@if.usp.br

R.A. Kraenkel
Instituto de Física Teórica, Universidade Estadual Paulista-UNESP
Rua Pamplona 145, 01405-900 São Paulo, Brazil
kraenkel@ift.unesp.br

Abstract We consider formation of dissipationless shock waves in Bose-Einstein condensates with repulsive interaction between atoms.

Experiments on free expansion of Bose-Einstein condensate (BEC) have shown [1] that evolution of large and smooth distributions of BEC is described very well by hydrodynamic approximation [2] where dispersion and dissipation effects are neglected. At the same time, it is well known from classical compressible gas dynamics that typical initial distributions of density and velocity can lead to wave breaking phenomenon when formal solution of hydrodynamical equations becomes multi-valued. It means that near the wave breaking point one cannot neglect dispersion and/or dissipation effects which prevent formation of a multi-valued region of a solution. If dispersion effects are small but greater than dissipation ones, then the region of strong oscillations is generated in vicinity of wave breaking point [3, 4]. Observation of dark solitons in BEC [5, 6, 7] shows that the main role in dynamics of BEC is played by dispersion and nonlinear effects taken into account by standard

F. Kh. Abdullaev and V. V. Konotop (eds.), Nonlinear Waves: Classical and Quantum Aspects, 285–290.

Gross-Pitaevskii (GP) equation [8]. Hence, there are initial distributions of BEC which can lead to formation of dissipationless shock waves. Here we shall consider such possibility.

The starting point of our consideration is the fact that the sound velocity in BEC is proportional to the square root from its density (see, e.g. [8]). Thus, if we create inhomogeneous BEC with high density hump (with density $\sim \rho_1$) in the center of lower density distribution (with density $\sim \rho_0$), and after that release this central part of BEC, then the high density hump will tend to expand with velocity $\sim \sqrt{\rho_1}$ greater than the sound velocity $\sim \sqrt{\rho_0}$ of propagation of disturbance in lower density BEC. As a result, wave breaking and formation of dissipationless shock wave can occur in this case. Note that initial distribution of this type was realized in the recent experiment [9] where generation of oscillations was also observed. The theory of dissipationless shock waves in media described by one-dimensional (1D) nonlinear Schrödinger (NLS) equation was developed in [10]. Since the GP equation in some cases can be reduced to 1D NLS equation, this theory can be applied to description of dissipationless shock waves in BEC. Here we suggest such description and confirm it by numerical simulations.

We consider BEC confined in a "pancake" trap with the axial frequency ω_z much greater than the transverse one $\omega_x = \omega_y = \omega_\perp$. Let the density of atoms in the central part of BEC be of order of magnitude n_0 and satisfy the condition $n_0 a_s a_z^2 \ll 1$, where $a_s > 0$ is the s-wave scattering length and $a_z = (\hbar/ma_z)^{1/2}$ is the amplitude of quantum oscillations in the axial trap. Then the condensate wavefunction ψ can be factorized as $\psi = \phi(z)\Psi(x,y)$, where $\phi(z) = \pi^{-1/4} a_z^{-1/2} \exp(-z^2/2a_z^2)$ is the ground state wavefunction of axial motion, and $\Psi(x,y,t)$ satisfies the reduced 2D GP equation

$$i\hbar\Psi_t = -\frac{\hbar^2}{2m}(\Psi_{xx} + \Psi_{yy}) + V(x,y)\Psi + g_{2D}|\Psi|^2\Psi, \qquad (1)$$

where $V(x,y)$ is the potential of a transverse trap, $g_{2D} = \frac{2\sqrt{2\pi}\hbar^2 a_s}{ma_z}$ is the effective nonlinear interaction constant, and Ψ is normalized to the number of atoms, $\int |\Psi|^2 dxdy = N$. The initial distribution of density is determined by the potential $V(x,y)$ and consists of wide background with a hump in its center. We assume that the background width is much greater than the hump's width, so that at the initial stage of evolution we can consider an expansion of the central part against the constant background. In a similar way, at the initial stage of evolution, when the radius of the central part does not change considerably, we can neglect the curvature of axially symmetrical distribution and consider its 1D cross section. As a result, we arrive at 1D NLS equation with inhomogeneous

initial distribution of density. To simplify the notation, we introduce dimensionless variables $t' = \omega_z t/2$, $x' = x/a_z$, $u = (2\sqrt{2\pi}a_s a_z/n_0)^{1/2}\Psi$. Then the initial stage of evolution of the wavefunction profile in the x axis cross section is governed by the NLS equation,

$$iu_t + u_{xx} - 2|u|^2 u = 0, \tag{2}$$

where the primes in t' and x' are omitted for convenience of the notation.

Evolution of smooth pulses before the wave breaking point can be described in the hydrodynamic approximation which can be achieved by substitution $u(x,t) = \sqrt{\rho(x,t)}\exp\left(i\int^x v(x',t)dx'\right)$ and separation of the real and imaginary parts. As a result we obtain the system

$$\tfrac{1}{2}\rho_t + (\rho v)_x = 0, \quad \tfrac{1}{2}v_t + vv_x + \rho_x = 0, \tag{3}$$

where we have neglected the so-called "quantum pressure" term with higher space derivatives what is correct until the density distribution has smooth enough profile.

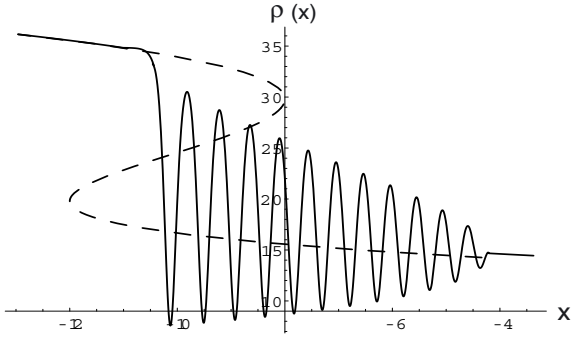

Figure 1. Formation of dissipationless shock wave after wave breaking point according to Whitham modulation theory applied to 1D NLS equation. Dashed line corresponds to multi-valued region arising in hydrodynamic approximation given by Eq. (4) and solid line represents modulated periodic wave given by Eqs. (5) and (6). Both profiles are calculated for $\overline{\lambda} = -10$ at time $t = 1$.

In vicinity of the wave breaking point the solution can be approximated by a cubic function for one Riemann invariant $\lambda_+ = v/2 + \sqrt{\rho}$ of the system (3) and by constant value for another one $\lambda_- = v/2 - \sqrt{\rho}$ (see [10]). After Galileo and scaling transformations the hydrodynamic solution can be written in the form

$$x - (3\lambda_+ + \lambda_-)t = -\lambda_+^3, \quad \lambda_- = \text{const}, \tag{4}$$

and again for $t > 0$ it has a multi-valued region of λ_+.

In framework of Whitham theory of modulations [11, 4] one can obtain an approximate solution of the NLS equation (2) in analytic form where the dissipationless shock wave is presented as a modulated periodic nonlinear wave solution of the NLS equation. The density is expressed in terms of Jacobi elliptic function

$$\begin{aligned}\rho(x,t) =&|u(x,t)|^2 = \tfrac{1}{4}(\lambda_1-\lambda_2-\lambda_3+\lambda_4)^2 + (\lambda_1-\lambda_2)(\lambda_3-\lambda_4)\\ &\times \mathrm{sn}^2[\sqrt{(\lambda_1-\lambda_3)(\lambda_2-\lambda_4)}\xi, m],\end{aligned} \tag{5}$$

where $\xi = x-(\lambda_1+\lambda_2+\lambda_3+\lambda_4)t$, $m = \frac{(\lambda_1-\lambda_2)(\lambda_3-\lambda_4)}{(\lambda_1-\lambda_3)(\lambda_2-\lambda_4)}$, and parameters λ_i, $i = 1,2,3,4$, change slowly along the dissipationless shock. Their dependence on x and t is determined implicitly by the solution

$$x - v_i(\lambda)t = w_i(\lambda), \quad i = 1,2,3; \quad \lambda_4 = \overline{\lambda} = \mathrm{const} \tag{6}$$

of Whitham equations, where Whitham velocities v_i and w_i are given by quite complicated expressions in terms of elliptic integrals (see [10]):

$$w_i = -\tfrac{8}{35}w_i^{(3)} + \tfrac{4}{5}\overline{\lambda}w_i^{(2)} - \tfrac{1}{35}\overline{\lambda}^2 v_i(\lambda) + \tfrac{1}{35}\overline{\lambda}^3, \quad i = 1,2,3, \tag{7}$$

$$w_i^{(k)} = W^{(k)} + (v_i - s_1)\partial_i W^{(k)}, \tag{8}$$

$$W^{(1)} = V = s_1, \quad W^{(2)} = \tfrac{3}{8}s_1^2 - \tfrac{1}{2}s_2, \quad W^{(3)} = \tfrac{5}{16}s_1^3 - \tfrac{3}{4}s_1 s_2 + \tfrac{1}{2}s_3, \tag{9}$$

$$v_i(\lambda) = \left(1 - \frac{L}{\partial_i L}\partial_i\right)V, \quad \partial_i \equiv \partial/\partial\lambda_i, \quad i = 1,2,3,4, \tag{10}$$

where $L = \frac{\mathrm{K}(m)}{\sqrt{(\lambda_1-\lambda_3)(\lambda_2-\lambda_4)}}$ is a wavelength, $\mathrm{K}(m)$ is the complete elliptic integral of the first kind, and s_1, s_2, s_3 are determined by the expressions $s_1 = \sum_i \lambda_i$, $s_2 = \sum_{i<j}\lambda_i\lambda_j$, $s_3 = \sum_{i<j<k}\lambda_i\lambda_j\lambda_k$.

Equations (7) can be solved with respect to λ_i, $i = 1,2,3$, giving them as functions of x and t. Subsequent substitution of these functions $\lambda_i(x,t)$, $i = 1,2,3$, into (5) yields the modulated periodic wave which represents the dissipationless shock wave. The resulting profile of density in dissipationless shock wave is shown in Fig. 1. At one its edge it consists of the train of dark solitons, and at another edge describes small amplitude oscillations propagating with local sound velocity into unperturbed region described by smooth solution of hydrodynamical equations. The modulated periodic wave replaces the multi-valued region shown by dashed line and obtained in hydrodynamic approximation.

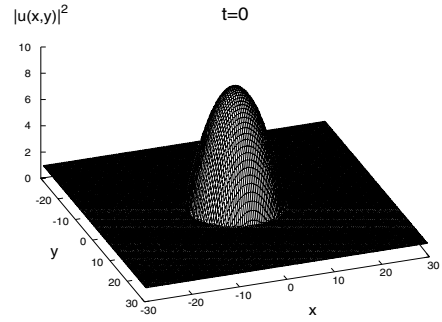

Figure 2. Two-dimensional initial distribution of BEC density with paraboloid hump on constant background given by Eq. (11) with $a = 10$, $\rho_0 = 1$, $\rho_1 = 10$.

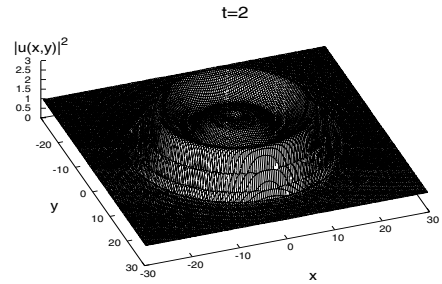

Figure 3. Two-dimensional density distribution of BEC after time $t = 2$ of evolution from initial paraboloid density on constant background according to numerical solution of 2D GP equation.

To check the described above picture of formation of dissipationless shock wave and to extend it to real 2D situation, we have solved numerically Eq. (1) taken in dimensionless form, $iu_t + u_{xx} + u_{yy} - 2|u|^2 u = 0$, with the initial condition

$$\rho(r,0) = \begin{cases} \rho_0 + (\rho_1 - \rho_0)(1 - r^2/a^2), & |r| \le a, \\ \rho_0, & |r| > a, \end{cases} \tag{11}$$

(where $r = (x^2+y^2)^{1/2}$) similar to one studied experimentally [9]. Plot of two-dimensional initial density distribution is shown in Fig. 2 and density distribution after time evolution $t = 2$ is shown in Fig. 3. As we see, the parabolic hump expands with formation of dissipationless shock wave

in the transition layer between high density region to low density one. To see more clearly the evolution of the hump, its cross section profiles are shown in Fig. 4 at different values of time t. Slowly propagating

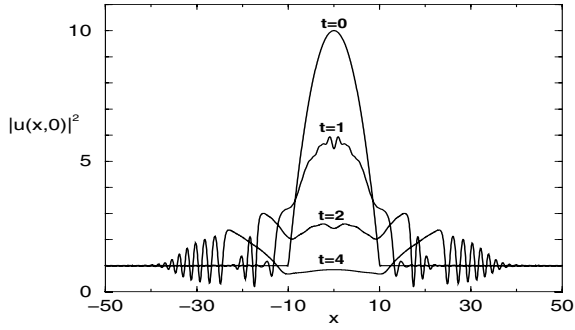

Figure 4. Cross sections of density profile at different evolution time according to numerical solution of 2D GP equation with initial condition (11).

dark solitons are clearly seen as well as small amplitude sound waves propagating into undisturbed low density region. Dissipationless shock wave generated at the right side of the profile coincides qualitatively with results of analytic theory shown in Fig. 1. We believe that oscillations in BEC density profile observed in experiment [9] have the same origin.

This work was supported by FAPESP (Brazil) and CNPq (Brazil). A.M.K. thanks also RFBR (grant 01–01–00696) for partial support.

References

[1] Ernst, U. *et al*, (1998) *Europhys. Lett.* **41,** 1.

[2] Castin, Y., and Dum, R. (1996) *Phys. Rev. Lett.* **77,** 5315.

[3] Gurevich, A.V., and Pitaevskii, L.P. (1973) *Zh. Exp. Teor. Fiz.* **65,** 590.

[4] Kamchatnov, A.M. (2000) *Nonlinear Periodic Waves and Their Modulations,* World Scientific, Singapore.

[5] Burger, S. *et al*, (1999) *Phys. Rev. Lett.* **83,** 5198.

[6] Denschlag, J. *et al*, (2000) *Science,* **287,** 97.

[7] Anderson, B.P. *et al*, (2001) *Phys. Rev. Lett.* **86,** 2926.

[8] Pitaevskii, L., and Stringari, S., (2003) *Bose-Einstein Condensation,* Clarendon Press, Oxford.

[9] E. Cornell, Talk at the NATO Advanced Research Workshop "Nonlinear Waves: Classical and Quantum Aspects", Estoril, July 2003

[10] Kamchatnov, A.M., Kraenkel, R.A., and Umarov, B.A., (2002) *Phys. Rev.* E **66,** 036609.

[11] Whitham, G.B. (1974) *Linear and Nonlinear Waves*, Wiley, N.Y.

III

NONLINEAR OPTICS AND PHOTONICS

STOPPING AND BENDING LIGHT IN 2D PHOTONIC STRUCTURES

Alejandro B. Aceves and Tomáš Dohnal
Department of Mathematics, University of New Mexico, Albuquerque, NM 87131, USA
aceves@math.unm.edu, dohnal@math.unm.edu

Abstract The problem of light propagating through two dimensional photonic structures with a localized defect is addressed. Examples of potential engineering applications of such structures are rerouting of light pulses or optical memory. The governing mathematical model is the system of Coupled Mode Equations (CME) in two spatial dimensions with addition of potentials which account for the defect. As we briefly explain, unlike the one dimensional model of CME without potentials, the two dimensional (x-uniform grating) one does NOT support stable localized pulses as solutions. Because stable pulses are necessary for any physical application, we add grating also in the x direction making, in effect, a true 2D photonic structure, and as we show numerically, this allows for launching of stable pulses. Next, making sensitive assumptions on the shape of the defect, we first give here a derivation of exact linear defect modes, i.e. solutions to the linear system with potentials, and then outline our future study of whether these linear modes persist into the nonlinear regime. Our next future task is to study the interactions of pulses with the nonlinear defect modes.

Keywords: Coupled Mode Equations, planar waveguide, grating, photonic structure, defect mode, stopping light

1. Uniform Grating Structures

1.1 1D Structures - Fiber Gratings

Perhaps the most utilized one dimensional photonic structure is the fiber grating. Here the envelope of the confined transverse (x, y) mode propagates in a medium having a periodic (in z) refractive index profile. Furthermore, the periodicity of the refractive index in the direction of propagation is assumed to be in Bragg resonance with the wavelength of the electric field, thus creating strong back reflection.

F. Kh. Abdullaev and V. V. Konotop (eds.), Nonlinear Waves: Classical and Quantum Aspects, 293–302.

The regime of wave propagation through these gratings that we are interested in is when the coupling between forward and backward propagating modes is of the order of the nonlinear length. A coupled system for the slowly varying envelopes of the electric field can be derived from Maxwell's Equations. The derivation is typically done using a multiple scales expansion under the assumption that the characteristic length scales of the coupling and the nonlinearity are in balance. The dynamics in uniform fiber gratings are then governed by the one dimensional Coupled Mode Equations (see for example chapter 2 of [8])

$$\begin{aligned} i(\partial_t + c_g\partial_z)E_+ + \kappa E_- + \Gamma(|E_+|^2 + 2|E_-|^2)E_+ = 0 \\ i(\partial_t - c_g\partial_z)E_- + \kappa E_+ + \Gamma(|E_-|^2 + 2|E_+|^2)E_- = 0, \end{aligned} \tag{1}$$

where E_+, E_- denote the forward and backward propagating envelopes respectively; and without any loss of generality $c_g, \kappa, \Gamma > 0$.

This system has been studied extensively. Although it is not integrable, Chen and Mills showed in [4] that it supports stable solitary wave solutions with frequency inside the forbidden gap of the linear system ($\Gamma = 0$). These are usually called "**gap solitons**" and in theory they can propagate with velocities ranging between 0 and the speed of light in the corresponding uniform medium. A more general class of solitary wave solutions was presented in [3]. The stability of the solitary waves is not all that surprising because in the more realistic experimental scenario (with frequency close to but outside the gap) (1) can be approximated by the Nonlinear Schrödinger Equation (again chapter 2 of [8]).

Gap solitons were later also demonstrated experimentally, see [5]; but the lowest velocity that has been seen experimentally is about $0.5\frac{c}{n}$. The main difference between the gap solitons and true solitons propagating in bare fibers from the applications point of view is the distance at which solutions converge to these stable pulses. The grating allows for a solution to converge to a stable pulse within centimeters whereas in a bare fiber it happens only after hundreds of meters! This is very important for using periodic structures as optical logic and storing devices.

1.2 2D Structures - Planar Waveguide Gratings

A natural extension to the fiber grating is to go to a waveguide geometry, where the confinement of light is only in one (y) transverse direction. In addition to all the features of waves propagating in fiber gratings we get diffraction in the x direction for the planar waveguide

gratings. The first question to ask is if by balancing coupling between modes, nonlinearity and diffraction, gap solitons exist.

The two dimensional Coupled Mode Equations

$$\begin{aligned} i(\partial_t + c_g\partial_z)E_+ + \kappa E_- + \partial_{x^2}^2 E_+ + \Gamma(|E_+|^2 + 2|E_-|^2)E_+ = 0 \\ i(\partial_t - c_g\partial_z)E_- + \kappa E_+ + \partial_{x^2}^2 E_- + \Gamma(|E_-|^2 + 2|E_+|^2)E_- = 0 \end{aligned} \tag{2}$$

are derived using the assumption that the characteristic length-scale of diffraction is in balance with the length scales listed for (1).

Just like (1), (2) is dispersive, conservative, not integrable and Hamiltonian. It does not, however, support any stable localized pulses as its solutions. In [2] it is shown that for frequencies close to but outside the linear regime gap the system is well approximated by the 2D NLSE. As a consequence, for sufficiently high powers these solutions have a tendency to collapse (point blowup) but a collapse implies broadening of the solution in the Fourier space and eventual overlap of the spectrum with the frequency gap where the NLSE approximation is no longer valid. Therefore, while localized dynamics in the 2D CME does not lead to collapse, it remains unstable and in particular there are no stationary wave solutions. This can be argued more directly using the Hamiltonian structure. The Hamiltonian functional is

$$\begin{aligned} H = \int_{\mathbb{R}}\int_{\mathbb{R}} ic_g\left(E_+^*\partial_z E_+ - E_-^*\partial_z E_-\right) + \kappa\left(E_-E_+^* + E_-^*E_+\right) - \\ |\partial_x E_+|^2 - |\partial_x E_-|^2 + \Gamma\left(\frac{1}{2}|E_+|^4 + 2|E_-|^2|E_+|^2 + \frac{1}{2}|E_-|^4\right)dxdz. \end{aligned}$$

A stationary wave solution would have to be a minimizer of H under the constraint that the total energy (which is conserved) stays constant; $\int\int |E_+|^2 + |E_-|^2 dxdz = \text{const}$. But given a candidate E_+, E_- for the minimizer, we can always perturb it in such a way that we add more x oscillations to increase the negative contribution from the $|\partial_x E_\pm|^2$ terms without changing the L_2 norm of E_+ or E_-. Hence, no minimizer exists. This is an important difference from the 1D case. The nonexistence of stable pulse propagation was seen both in the reduced variational analysis of [1] and in our numerical experiments, where all so far studied localized pulses rapidly diffract in the x direction. How to overcome this is discussed in the next section.

2. Photonic Structures

Because we wish to study capturing and rerouting of light pulses by defects in 2D periodic structures, we also need the pulses to propa-

gate (in a stable fashion) through the uniform periodic medium before they get to the defects. As mentioned in the previous section, periodic structures uniform in x do not allow for such dynamics. That is why we have decided to consider a structure with grating in the x direction as well. This is certainly possible technologically with today's developments in photonic structures. The governing model is obtained from (2) by addition of a positive $x-$periodic potential. Here we choose $P(x) = \delta(1 + \cos(\nu x))$:

$$\begin{aligned} i(\partial_t + c_g\partial_z)E_+ + \kappa E_- + \partial_{x^2}^2 E_+ + P(x)E_+ + \Gamma(|E_+|^2 + 2|E_-|^2)E_+ = 0 \\ i(\partial_t - c_g\partial_z)E_- + \kappa E_+ + \partial_{x^2}^2 E_- + P(x)E_- + \Gamma(|E_-|^2 + 2|E_+|^2)E_- = 0. \end{aligned} \tag{3}$$

To demonstrate existence of localized pulses, we have performed numerical experiments. In our numerics we use the discontinuous Galerkin scheme with a triangular mesh. Here we choose order 6 in space and an additive Runge-Kutta time integrator of order 4. Fig. 1 shows the plot of $|E_+|, |E_-|$ at $t = 1$ for the case $\delta = 10, \nu = 2$ and with the $z-$shape of the initial condition being a sech function and the $x-$shape determined as the solution of the linear eigenvalue problem

$$G'' + (\lambda + \delta(1 + \cos(\nu x))G = 0 \tag{4}$$

corresponding to the eigenvalue $\lambda \approx -15.7951$. This eigenfunction is well localized on the interval $[-\pi, \pi]$. The above eigenvalue problem is the $x-$part of the linear case in (3). Note that the initial pulses $E_+(t = 0) = E_-(t = 0)$ were centered at the origin.

Although no theory is available for finding exact solutions of (3), one can expect some interplay between gap solitons (for the $z-$dependence) and localized Bloch-type waves, which exist for the time independent NLS with a periodic potential (see [7]).

3. Periodic Structures with Defects

The previous sections dealt with uniform periodic structures which accounted for distinct dynamics. An ongoing research trend is the addition of defects to this structure; an example in linear optics is, by inclusion of a one dimensional defect in a 2D or 3D photonic structure, to bend light beams without radiation loss. For a 1D photonic structure like the fiber grating, by a defect we mean a local variation of the $z-$periodic refractive index. Introducing a defect to a fiber grating allows both for convergence to a stable pulse within centimeters and for manipulating the speed or direction of the pulse propagation due to the

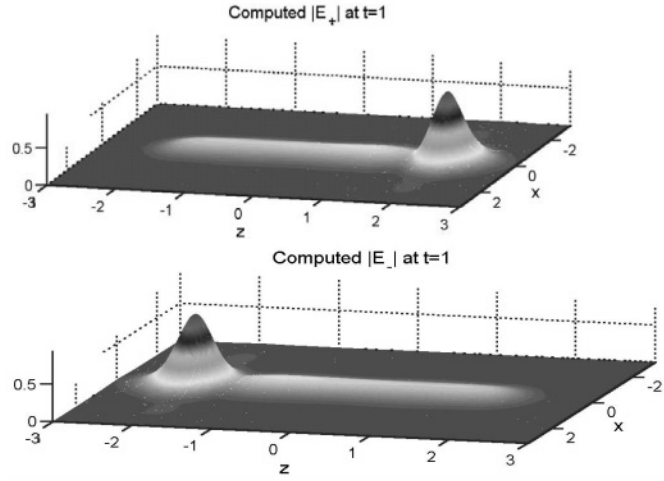

Figure 1. Solution to (3) with $c_g = 2, \kappa = 1, \Gamma = 1$

effective potential well given by the defect. An appropriate balance between spectral properties of the defect, the velocity and the amplitude of the pulse even allows for a complete stopping of the pulse due to the transfer of its energy into a defect mode. This has potential applications for optical memory or optical switches.

A defect in a planar waveguide grating gives even more potential applications. One can imagine rerouting of pulses into various directions according to their amplitude, using these structures in fiber communications to bend light or, once again, for optical memory.

Goodman, Slusher and Weinstein studied fiber gratings with defects in [6] and showed that capturing of gap solitons is possible. The model, they used, is

$$\begin{aligned} i(\partial_t + c_g\partial_z)E_+ + \kappa(z)E_- + V(z)E_+ + \Gamma(|E_+|^2 + 2|E_-|^2)E_+ = 0 \\ i(\partial_t - c_g\partial_z)E_- + \kappa(z)E_+ + V(z)E_- + \Gamma(|E_-|^2 + 2|E_+|^2)E_- = 0. \end{aligned} \tag{5}$$

The authors first studied the linear case, $\Gamma = 0$, and introduced a multiparameter family of defects that support linear bound states (linear defect modes). Their frequency is always in the corresponding frequency gap. Then, by using a perturbative construction, they showed that these defect modes extend into the nonlinear regime. In order to study also large values of the perturbation parameter they did a series of numerical experiments. In these, they managed to verify the principle that a gap soliton interacts most strongly with a defect for which a nonlinear defect

mode exists with the same frequency (resonance) and with equal or less total intensity (energetic accessibility).

In our work we wish to apply similar methods for the 2D case. Our first results now follow.

3.1 Linear Defect Modes for the 2D CME

The model we use for the linear regime in two spatial dimensions (without grating in the $x-$direction) is

$$\begin{aligned} i(\partial_t + c_g\partial_z)E_+ + \kappa(z)E_- + \partial_{x^2}^2 E_+ + (V_1(x) + V_2(z))E_+ = 0 \\ i(\partial_t - c_g\partial_z)E_- + \kappa(z)E_+ + \partial_{x^2}^2 E_- + (V_1(x) + V_2(z))E_- = 0. \end{aligned} \tag{6}$$

Note that even if V_1, V_2 have localized effective support (e.g. sech type functions), $V_1(x) + V_2(z)$ does not model a defect strictly localized in a 2D waveguide. Rather it looks like a cross with each line extending over the whole domain. From an application point of view, this should not be a problem because in a real waveguide (or in numerical simulations) this cross can be truncated at some distance from its center (see Fig. 2). Then our analysis on (6) will apply only on the area spanned by the

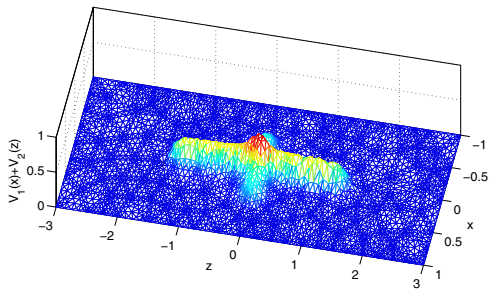

Figure 2. Potential structure used in (6)

cross. We use the potentials V_1, V_2 as given in (6) rather than a more general $V(x, z)$ for simplicity - so that we are able to use separation of variables in (6). Our setup

$$E_\pm = G_\pm(x)F_\pm(z,t) \qquad \text{and} \quad G_+ = G_- =: G$$

gives

$$[i\partial_t + ic_g\sigma_3\partial_z + V_2(z) - \mu + \kappa(z)\sigma_1]\,\vec{F} = 0 \tag{7a}$$

$$G'' + (V_1(x) + \mu)G = 0, \tag{7b}$$

with $\sigma_1 = \begin{pmatrix} 0 & 1 \\ 1 & 0 \end{pmatrix}, \sigma_3 = \begin{pmatrix} 1 & 0 \\ 0 & -1 \end{pmatrix}, \vec{F} = \begin{pmatrix} F_+ \\ F_- \end{pmatrix}$ and μ the separation constant.

If, for the $x-$potential, we set, for example, $V_1(x) = 2\beta^2 \mathrm{sech}^2(\beta x)$, the solution to the eigenvalue problem (7b) has a localized eigenfunction. It is $(G, \mu) = \big(\mathrm{sech}(\beta x), -\beta^2\big)$.

With μ fixed, we now try to solve the equation for $\vec{F}$. This can be complicated or impossible for arbitrary grating $\kappa(z)$ and potential $V_2(z)$ but following the ideas in [6] we can obtain exact solutions for some special cases. If we start in the opposite direction, having a form of the solution $\vec{F}$, the problem is easier. For example, setting

$$\vec{F} = e^{-i\omega t} e^{\frac{i}{c_g}\sigma_3 \int_0^z V_2(\xi)d\xi} \vec{L}(z) \qquad \text{with} \quad \omega \in \mathbb{R}, \quad \vec{L}(z) \in \mathbb{R}^2,$$

the problem reduces to a self-adjoint eigenvalue problem for $(\omega, \vec{L})$:

$$\vec{L}' = \begin{bmatrix} i(\omega - \mu) & u(z) \\ \bar{u}(z) & -i(\omega - \mu) \end{bmatrix} \vec{L} \quad \text{with} \quad u(z) = i\kappa(z) e^{\frac{-2i}{c_g}\int_0^z V_2(\xi)d\xi}. \quad (8)$$

The point spectrum is contained in the frequency gap of the linear regime, i.e. $(\mu - |\kappa_\infty|, \mu + |\kappa_\infty|)$, where $\kappa_\infty = \lim_{|z|\to\infty} \kappa(z)$. Setting $u(z) = -e^{i\phi}\left((\omega - \mu) - ik \tanh\left(\frac{k}{c_g} z\right)\right)$ in (8), there is a simple solution

$$\left(\omega - \mu, \begin{pmatrix} 1 \\ ie^{-i\phi} \end{pmatrix} \mathrm{sech}\left(\frac{k}{c_g} z\right)\right).$$

The corresponding grating and potential are easily found

$$\kappa(z) = e^{i\alpha}\left[(\omega - \mu)^2 + k^2 \tanh^2\left(\frac{k}{c_g} z\right)\right]^{1/2}, \quad \alpha \in \{0, \pi\}$$

$$V_2(z) = \frac{1}{2} \frac{k^2(\omega - \mu)\mathrm{sech}^2\left(\frac{k}{c_g} z\right)}{(\omega - \mu)^2 + k^2 \tanh^2\left(\frac{k}{c_g} z\right)}.$$

The condition for α is to preserve self-adjointness.

Finally, we can express the whole solution $\begin{pmatrix} E_+ \\ E_- \end{pmatrix}$:

$$e^{-i\omega t} \begin{pmatrix} \exp\left(\frac{i}{2} \arctan\left(\frac{k \tanh\left(\frac{k}{c_g} z\right)}{\omega - \mu}\right)\right) \\ ie^{-i\phi} \exp\left(\frac{-i}{2} \arctan\left(\frac{k \tanh\left(\frac{k}{c_g} z\right)}{\omega - \mu}\right)\right) \end{pmatrix} \mathrm{sech}\left(\frac{k}{c_g} z\right) \mathrm{sech}(\beta x),$$

where $\mu = -\beta^2, \phi - \alpha = \frac{3}{2}\pi$.

Fig. 3 shows $|E_+|$ of a numerical solution to (6) with $\kappa(z), V_2(z)$, $V_1(x)$ as given above and the initial condition determined by the above exact solution. The parameters used are $\beta = 7, \omega = -40, k = 4, \phi = \frac{3}{2}\pi$ and $c_g = 1$. The solution is stationary with time invariant modulus.

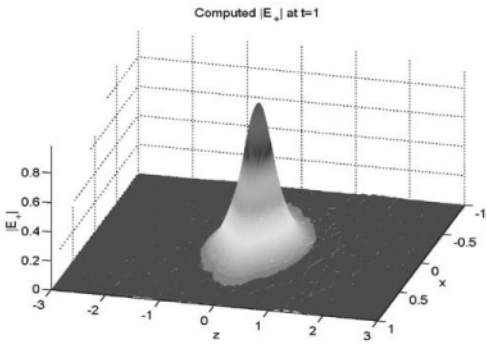

Figure 3. The modulus of a linear defect mode at time $t = 1$

4. Future Work

The linear defect modes, an example of which was given in section 3.1, were not derived for 2D photonic structures, which we have to use in order to achieve stable pulse propagation. Consequently, we will have to change these defect modes to account for the $x-$grating $P(x)$. For each linear frequency ω we will then perform a perturbative construction of a nonlinear defect mode of small total intensity. To continue the bifurcation branch of the mode (and its frequency) for large intensity, we will numerically solve the nonlinear eigenvalue problem

$$\begin{aligned}(\omega + ic_g\partial_z)E_+ + \kappa(z)E_- + \partial_{x^2}^2 E_+ + (V_1(x) + V_2(z) + P(x))E_+ \\ +\Gamma(|E_+|^2 + 2|E_-|^2)E_+ = 0 \\ (\omega - ic_g\partial_z)E_- + \kappa(z)E_+ + \partial_{x^2}^2 E_- + (V_1(x) + V_2(z) + P(x))E_- \\ +\Gamma(|E_-|^2 + 2|E_+|^2)E_- = 0.\end{aligned} \tag{9}$$

It is important to know the temporal frequencies of both the pulse and the defect mode to achieve resonance. Although in the nonlinear case we will probably have to measure the frequency numerically, in the linear case it is easily found from studying the leading exponential tail of each

envelope in (3). Taking G the eigenfunction of (4) and substituting

$$\begin{pmatrix} E_+ \\ E_- \end{pmatrix} = \begin{pmatrix} a \\ b \end{pmatrix} G(x) e^{-\vartheta y} e^{-i\omega t}, \quad \text{where} \quad y = z - pc_g t, \Re(\vartheta) > 0, p \in [0,1]$$

into the linear case of (3), we obtain $\omega = \lambda - ic_g \vartheta p \pm \sqrt{\kappa^2 - c_g^2 \vartheta^2}$.

Next, we realize that although we have numerically shown that photonic structures (grating in both z and x directions - see section 2) allow for propagation of localized pulses, in our results, initial data break into two localized states travelling at high speeds, with the forward (backward) bullet having a predominant E_+ (E_-) component. Referring to the 1D case where for the gap solitons E_+, E_- both co-exist moving in one direction, we wish to determine whether a specific $z-$profile in the initial condition allows for such propagation in our 2D case.

Finally, we will investigate the possibility of trapping these pulses on defects as well as changing direction of their propagation due to the contact with a defect. We expect the same principles of resonance and energetic accessibility to hold as in [6] .

Acknowledgments

The research of A.B. Aceves and T. Dohnal is supported by the Army Research Office Grant DAAD19-03-1-0209. The authors thank Timothy Warburton and Thomas Hagstrom (both University of New Mexico) for assistance with the numerical parts of the research.

References

[1] A.B.Aceves, B.Constantini and C.De Angelis, "Two-dimensional gap solitons in a nonlinear periodic slab waveguide," Journ. of the Opt. Soc. Am B **12**, 1475 (1995).

[2] A.B.Aceves, G.Fibich and B.Ilan, "Gap Solitons in Waveguide Gratings," (to appear in Physica D).

[3] A.B.Aceves and S.Wabnitz, "Self induced transparency solitons in nonlinear refractive media," Physics Letters A **141**, 37 (1989).

[4] W.Chen and D.L.Mills, "Gap solitons and the nonlinear optical response of superlattices," Phys. Rev. Lett. **58**, 160 (1987).

[5] B.J.Eggleton, R.E.Slusher, C.M.de Sterke, P.A.Krug and J.E.Sipe, "Bragg grating solitons," Phys. Rev. Lett. **76**, 1627 (1996).

[6] R.H.Goodman, R.E.Slusher and M.I.Weinstein, "Stopping light on a defect," Journ. of the Opt. Soc. Am B **19**, 1635 (2002).

[7] P.J.Y. Louis, E.A. Ostrovskaya, C.M. Savage and Yu.S. Kivshar, "Bose-Einstein condensates in optical lattices: Band-gap structure and solitons," Phys. Rev. A **67**, 013602 (2003).

[8] R.E.Slusher, B.J.Eggleton, "Nonlinear Photonic Crystals," Springer-Verlag, New York, 2003.

MODEL OF THE TWO LEVEL QUANTUM DOTS ENSEMBLE INTERACTING WITH ULTRA-SHORT PULSE OF COHERENT RADIATION

A. I. Maimistov
Moscow Engineering Physics Institute, Kashirskoe sh. 31, Moscow, 115409 Russia

Abstract Based on a model of strong coupling for two electrons that are localized inside a quantum dot characterized by only two levels of size quantization, a set of equations is derived, which allows one to describe coherent transient processes in an ensemble of isolated dots. Here one considered the case of ultrashort durations of electromagnetic field pulses, when the processes of polarization and population relaxation can be neglected. The resulting set of equations is a generalization of the Maxwell-Bloch equations, which are used in studying the processes occurring under the action of ultrashort electromagnetic pulses. The model obtained is reduced to the model of two-level atoms only if radiation is circularly polarized.

Keywords: Quantum dot, size quantization, two level atoms, ultrashort pulse, electromagnetic field, polariton, solitary wave, coherent phenomena.

1. Introduction

Propagation of ultrashort (and extremely short) pulses of arbitrarily polarized electromagnetic radiation in resonance media has been previously considered in terms of the models of two- or three-level atoms [1, 2, 3, 4] (see also reviews [5, 6]). Interest in new resonance media that can be generally referred to as low-dimensional systems (quantum wells, quantum dots, thin films of atoms at the interface between insulators, and zero-dimensional waveguides) motivated a search for new models.

The majority of investigations in this field were devoted to the transport properties of low-dimensional systems (for example, of a system of coupled quantum dots [7, 8]). However, their optical properties are also considered. The study of optical spectra and exciton states [9, 10, 11] represents a traditional direction of optics of such systems. Nonlinear

F. Kh. Abdullaev and V. V. Konotop (eds.), Nonlinear Waves: Classical and Quantum Aspects, 303–312.

optical properties and, in particular, harmonic generation were considered in [12, 13, 14]. The possibility of the existence of confined states and coherent population transfer in quantum wells were theoretically demonstrated in [15, 16]. The phenomenon of photon echo in low-dimensional systems was studied in [17, 18].

In order to describe coherent phenomena in the optics of quantum dots (QDs), Krasheninnikov et al. [19] suggested a model of a two-level atom whose energy levels correspond to two one-particle states of an electron localized in the QD. This model makes it possible to consider the interactions of the QD electrons with a scalar electromagnetic field of an ultrashort pulse (USP). A system of equations has been derived [20, 21] to describe the evolution of a slowly varying envelope of an arbitrarily polarized ultrashort electromagnetic pulse in a medium whose resonance properties are governed by an ensemble of isolated QDs. Under the assumption that the QD concentration is low, this ensemble is equivalent to a gas of resonance four-level atoms. The equations describing the evolution of the QD state in the USP field can be derived on the basis of a microscopic model of tight binding of electrons in a QD. An increase in the concentration of QDs brings about either electron transport between isolated QDs or excitation transfer, much as the energy is transferred via Frenkel excitons in a molecular crystal. In [22], the model from [20] is generalized to the situation where the interaction between individual QDs occurs via exciton transport between the nearest QDs. This process is accounted for by introducing an exchange term in the Hamiltonian of the ensemble of the QD electrons, which is similar to what is done in transition from the Hubbard model to the t-J model [23]. In this approximation a system of equations for polarization and population of (two-electron) states of the QD chain has been derived. In combination with Maxwell equations, the above equations describe the excitonic wave of excitonic polaritons and a purely excitonic wave; the latter has much lower propagation velocity than that of polaritons. A reduction of this system of equations in the long-wavelength limit and in the approximation of slowly varying variables gives rise to generalized reduced Maxwell-Bloch equations. The latter resemble the equations of the theory of self-induced transparency. However, an additional term appearing in the equations for polarization describes detuning from a precise resonance; this detuning depends linearly on the difference in population.

2. Model of isolated quantum dots

Let us consider a model, in which a quantum dot has only two levels of size quantization: the level ε_a corresponds to the single-particle state

$|a\rangle$ of electrons in the conduction band and the level ε_b corresponds to the single-particle state $|b\rangle$ of electrons in the valence band. Under the action of an ultrashort pulse of electromagnetic radiation, electrons can move from one level to the other, with the spin state of the electron being changed in the process of absorption or emission of a photon.

The Hamiltonian of the system of electrons under consideration can be written as

$$\begin{aligned}\widehat{H} = \varepsilon_c \sum_{j\mu} \widehat{n}_{j\mu} + U_c \sum_j \widehat{n}_{j\uparrow}\widehat{n}_{j\downarrow} + T_c \sum_{j\mu} \left(\widehat{a}^+_{j+1\mu}\widehat{a}_{j\mu} + \widehat{a}^+_{j\mu}\widehat{a}_{j+1\mu}\right) + \\ + \varepsilon_v \sum_{j\mu} \widehat{N}_{j\mu} + U_v \sum_j \widehat{N}_{j\uparrow}\widehat{N}_{j\downarrow} + T_v \sum_{j\mu} \left(\widehat{b}^+_{j+1\mu}\widehat{b}_{j\mu} + \widehat{b}^+_{j\mu}\widehat{b}_{j+1\mu}\right) + \\ + \sum_j \left(V_{1j}\widehat{a}^+_{j\downarrow}\widehat{b}_{j\downarrow} + V_{2j}\widehat{a}^+_{j\uparrow}\widehat{b}_{j\downarrow} + V^*_{1j}\widehat{b}^+_{j\uparrow}\widehat{a}_{j\downarrow} + V^*_{2j}\widehat{b}^+_{j\downarrow}\widehat{a}_{j\uparrow}\right) + \\ + U_{cv} \sum_{j\mu\sigma} \widehat{n}_{j\mu}\widehat{N}_{j\sigma}. \quad (1)\end{aligned}$$

The subscript j numbers all the QDs, and the subscript μ takes the values $\uparrow$ and $\downarrow$. In expression (1), $\widehat{a}^+_{j\mu}$ ($\widehat{b}^+_{j\mu}$) are the operators of creation of the electron with the spin μ in the single-particle state $|a\rangle$ ($|b\rangle$) of the jth QD.

The operators $\widehat{n}_{j\mu} = \widehat{a}^+_{j\mu}\widehat{a}_{j\mu}$ and $\widehat{N}_{j\mu} = \widehat{b}^+_{j\mu}\widehat{b}_{j\mu}$ are the operators of the number of particles in the corresponding states of the jth QD. Here, for simplicity sake, we assume that the electron energies in the valence band and in the conduction band are independent of the QD number, although the spread of the geometrical sizes of the QDs must lead to such dependence, which would correspond to the inhomogeneous broadening of the absorption line of this resonant system. If necessary, this broadening can be easily taken into account in the final equations describing the model being considered. The parameters U_a , U_b , and U_{ab} correspond to the Coulomb repulsion of electrons in the single-particle states $|a\rangle$ and $|b\rangle$ inside the QDs. Coulomb interaction between electrons of adjacent QDs is not taken into account. The quantities T_c and T_v are the tunneling. matrix elements between the nearest neighbor QD sites. The interaction of the electromagnetic field with the electrons is described by the matrix elements V_{1j} and V_{2j}. At the first stage, the effects of tunneling are disregarded.

Since in the general case, equations specifying the evolution of any operator are determined by the Heisenberg equations, it is useful to have the (anti)commutation relations for the creation and annihilation operators of electrons. As shown previously [21], the equations of motion

for the operators $\widehat{P}_{1j} = \widehat{b}^{+}_{j\uparrow}\widehat{a}_{j\downarrow}$, $\widehat{P}_{2j} = \widehat{b}^{+}_{j\downarrow}\widehat{a}_{j\uparrow}$, $\widehat{R}_{1j} = \widehat{n}_{j\downarrow} - \widehat{N}_{j\uparrow}$, $\widehat{R}_{2j} = \widehat{n}_{j\uparrow} - \widehat{N}_{j\downarrow}$, $\widehat{S}_{1j} = \widehat{R}_{2j}\widehat{P}_{1j}$, $\widehat{S}_{2j} = \widehat{R}_{1j}\widehat{P}_{2j}$, $\widehat{N}_{3j} = \widehat{R}_{1j}\widehat{R}_{2j}$, $\widehat{W}_j = \widehat{P}^{+}_{1j}\widehat{P}_{2j} = \widehat{P}_{2j}\widehat{P}^{+}_{1j}$, and $\widehat{K}_j = \widehat{P}_{1j}\widehat{P}_{2j} = \widehat{P}_{2j}\widehat{P}_{1j}$ have the form of the following closed system of equations:

$$i\hbar\frac{\partial}{\partial t}\widehat{P}_{1j} = \Delta\varepsilon\widehat{P}_{1j} + \Delta U\widehat{S}_{1j} - V_{1j}\widehat{R}_{1j}, \tag{2}$$

$$i\hbar\frac{\partial}{\partial t}\widehat{P}_{2j} = \Delta\varepsilon\widehat{P}_{2j} + \Delta U\widehat{S}_{2j} - V_{2j}\widehat{R}_{2j}, \tag{3}$$

$$i\hbar\frac{\partial}{\partial t}\widehat{R}_{1j} = 2\left(V_{1j}\widehat{P}^{+}_{1j} - V^{*}_{1j}\widehat{P}_{1j}\right), \tag{4}$$

$$i\hbar\frac{\partial}{\partial t}\widehat{R}_{2j} = 2\left(V_{2j}\widehat{P}^{+}_{2j} - V^{*}_{2j}\widehat{P}_{2j}\right), \tag{5}$$

$$i\hbar\frac{\partial}{\partial t}\widehat{S}_{1j} = \Delta\varepsilon\widehat{S}_{1j} + \Delta U\widehat{P}_{1j} - V_{1j}\widehat{N}_{3j} + 2V_{2j}\widehat{W}^{+}_{j} - 2V^{*}_{2j}\widehat{K}_{j}, \tag{6}$$

$$i\hbar\frac{\partial}{\partial t}\widehat{S}_{2j} = \Delta\varepsilon\widehat{S}_{2j} + \Delta U\widehat{P}_{2j} - V_{2j}\widehat{N}_{3j} + 2V_{1j}\widehat{W}_{j} - 2V^{*}_{1j}\widehat{K}_{j}, \tag{7}$$

$$i\hbar\frac{\partial}{\partial t}\widehat{N}_{3j} = 2\left(V_{2j}\widehat{S}^{+}_{2j} - V^{*}_{2j}\widehat{S}_{2j}\right) + 2\left(V_{1j}\widehat{S}^{+}_{1j} - V^{*}_{1j}\widehat{S}_{1j}\right), \tag{8}$$

$$i\hbar\frac{\partial}{\partial t}\widehat{W}_{j} = -\left(V_{2j}\widehat{S}^{+}_{1j} - V^{*}_{1j}\widehat{S}_{2j}\right), \tag{9}$$

$$i\hbar\frac{\partial}{\partial t}\widehat{K}_{j} = 2\Delta\varepsilon\widehat{K}_{j} - \left(V_{1j}\widehat{S}_{2j} + V_{2j}\widehat{S}_{1j}\right), \tag{10}$$

where $\Delta\varepsilon = (\varepsilon_c - \varepsilon_b)$, $\Delta U = (U_v - U_{cv}) = (U_c - U_{cv})$. We will suppose that $U_c = U_v \neq U_{cv}$.

Now we can obtain the classical (nonoperator) equations playing the role of the generalized Bloch equations in the case of a two-level quantum dot, if we replace all the operators by their expectation values. It should be noted that the problem of splitting of the products of operators does not appear here.

Let the duration of an ultrashort electromagnetic pulse be such that we can use the reduced Maxwell equations for the slowly varying envelope of an electromagnetic pulse. In this case, we can pass on to the slowly varying complex amplitudes of the average values of the operators entering into (2) - (10) and take the rotating-wave approximation. The site index j of the operators can be omitted also. It is convenient to introduce the following notation:

$$2\left\langle\widehat{P}_{1,2}\right\rangle = p_{1,2}, \quad 2\left\langle\widehat{S}_{1,2}\right\rangle = s_{1,2}, \quad 2\left\langle\widehat{K}\right\rangle = u, \quad 2\left\langle\widehat{W}\right\rangle = w,$$

$$\left\langle\widehat{R}_{1,2}\right\rangle = n_{1,2}, \qquad \left\langle\widehat{N}_{3}\right\rangle = n_{3.}$$

The normalized envelope of the ultrashort electromagnetic pulse is determined by the relation $\mathrm{e}_{1,2} = \mathcal{E}_{1,2}/A_0$, and $2V_{1,2} = \hbar\omega_R \mathrm{e}_{1,2}$, $\Omega = (\Delta\varepsilon - \hbar\omega_0)/\hbar\omega$. Here $\omega_R = 2d_{12}A_0/\hbar$ is the peak Rabi frequency, ω_0 is the wave carrier frequency, d_{12} is the matrix element of the dipole moment operator for the transition between the single-particle states $|a\rangle$ and $|b\rangle$ of the electron in a QD.

The set of normalized generalized Bloch equations has the form

$$
\begin{aligned}
i\frac{\partial}{\partial\tau}p_1 &= \Omega p_1 - \Delta s_1 - \mathrm{e}_1 n_1, \quad i\frac{\partial}{\partial\tau}n_1 = (\mathrm{e}_1 p_1^* - \mathrm{e}_1^* p_1)/2,\\
i\frac{\partial}{\partial\tau}p_2 &= \Omega p_2 - \Delta s_2 - \mathrm{e}_2 n_2, \quad i\frac{\partial}{\partial\tau}n_2 = (\mathrm{e}_2 p_2^* - \mathrm{e}_2^* p_2)/2,\\
i\frac{\partial}{\partial\tau}s_1 &= \Omega s_1 - \Delta p_1 - \mathrm{e}_1 n_3 + \mathrm{e}_2 w^* - \mathrm{e}_2^* u,\\
i\frac{\partial}{\partial\tau}s_2 &= \Omega s_2 - \Delta p_2 - \mathrm{e}_2 n_3 + \mathrm{e}_1 w^* - \mathrm{e}_1^* u,\\
i\frac{\partial}{\partial\tau}n_3 &= (\mathrm{e}_1 s_1^* - \mathrm{e}_1^* s_1)/2 + (\mathrm{e}_2 s_2^* - \mathrm{e}_2^* s_2)/2,\\
i\frac{\partial}{\partial\tau}w &= -(\mathrm{e}_2 s_1^* - \mathrm{e}_1^* s_2)/2\\
i\frac{\partial}{\partial\tau}u &= 2\Omega u - (\mathrm{e}_1 s_2 + \mathrm{e}_2 s_1)/2
\end{aligned}
\tag{11}
$$

These equations must be complemented by the reduced Maxwell equations for normalized circularly polarized components of an electromagnetic wave $\mathrm{e}_{1,2}$

$$
\frac{\partial}{\partial\zeta}\mathrm{e}_a = ip_a \tag{12}
$$

where $a = 1, 2$ is the subscript numbering the components of a circularly polarized USP. In the equations (11) and (12) we used the rescaled variables

$$
\zeta \equiv z/l, \quad \tau \equiv \omega_R(t - z/c) \tag{13}
$$

where l is the normalization length: $l = (4\pi n_A d_{12}^2/c\hbar\omega_R)^{-1}$ and n_A is the the density of QDs. Thus, the set of equations (11) and (12) forms a basis for thr description of coherent transient processes such as the photon echo, free induction decay, optical nutation, and propagation of an ultrashort light pulse through a small-density QDs system.

If the light is circularly polarized, the model under study becomes equivalent to the model of two-level atoms. In the case of arbitrary

light polarization, a four-level model arises that is similar to that considered in [24]. Special cases of stationary solutions of the generalized system of reduced Maxwell-Bloch equations have been obtained in [20]. These solutions exist under the rather unlikely condition that constants of the Coulomb coupling between electrons in different energy states are equal. The direct numerical simulation [20] has shown that the interaction between different circularly polarized USPs is of inelastic nature: the collision gives rise to a change in the propagation velocity and to emission of quasi-harmonic small-amplitude waves at the edges of the colliding high-power pulses.

3. The effect of electron transport

Let us denote the two-particle state of an isolated QD by the ket vector $|n_{a\uparrow}, n_{a\downarrow}; n_{b\uparrow}, n_{b\downarrow}\rangle$, where $n_{a\mu}$ and $n_{b\mu}$ are the numbers of electrons with spin μ. in the single-particle states $|a\rangle$ and $|b\rangle$. In the ground state of the system, in which case each QD is in the state $|0, 0; 1, 1\rangle$, tunneling transitions of electrons between neighboring nodes are forbidden owing to Pauli's exclusion principle. This situation is similar to the absence of conductivity in an intrinsic semiconductor at zero absolute temperature. Exposure to radiation gives rise to non-equilibrium charge carriers and, thus, to photoconductivity. Similarly, the transport of charges can be observed in a system of QDs if the neighboring QDs are in states with a single electron in the one-particle states $|a\rangle$ and $|b\rangle$.

3.1 The *t-J* model

Let the jth QD be in the state $|0, 1; 0, 1\rangle$, which co responds to an exciton located at this point and generated owing to the absorption of a photon with the corresponding spirality. An electron in the state $|a\rangle$ of this QD can execute a transition to the state $|a\rangle$ of the neighboring QD (for example, of the $(j-1)$th QD); thereby, the energy of the entire system would increase by about U_{ab}. Further transitions to the state $|a\rangle$ of the $(j-2)$th QD increase the total energy by a value determined by the Coulomb interaction of spatially separated charges. However, if, immediately after the electron transition from the state $|a\rangle$ of the jth QD to the same state of the $(j-1)$th QD, the electron of the $(j-1)$th QD in the $|b\rangle$ state is transferred to the state $|b\rangle$ of the jth QD, the energy of the system is not changed and remains at the same level as corresponds to a single exciton in the system, with this exciton being transferred from the jth QD to the $(j-1)$th QD. *Such a transfer of excitons is more energetically favorable than charge transport due to the electron tunneling from one site to the neighboring sites in the QD chain.* This process

can be taken into account in the simple model under consideration by introducing the following additional term into Hamiltonian (1) instead of the terms proportional to the matrix elements T_a and T_b:

$$\widehat{H} = J \sum_{j,\ a=1,2} \left(\widehat{P}^{+}_{a\ j+1} \widehat{P}_{a\ j} + \widehat{P}^{+}_{a\ j-1} \widehat{P}_{a\ j} \right) \tag{14}$$

The conventional Hubbard model describing the transport of electrons from one site to another site incorporates (in addition to the energy of the Coulomb interaction between electrons at a site U) a matrix element of electron transition to the neighboring site T_0 which controls the energy-band width in the tight-binding model [25]. The Coulomb repulsion between electrons in a QD U for the typical case of a GaAs-based structure amounts to about 1 meV, whereas T_0 is on the order of 0.05 meV. Since $U/T_0 \gg 1$, an electron system of an ensemble of QDs constitutes an example of a strongly correlated system. Since the energy of the Coulomb repulsion of electrons at the same site is much larger than the intersite-transition parameter T_0 , the states with two electrons at the same site may be disregarded and the Hubbard model may be replaced by the effective Hamiltonian of the t-J model [23] (see review [26]). The constant of the effective exchange interaction J in this model is related to the parameters of the initial Hubbard model by the formula $J = T_0^2/U$. In the model under consideration, two types of electrons are involved. Their internode transitions are characterized by the matrix elements of electron transitions T_a and T_b in the states $|a\rangle$ and $|b\rangle$, respectively. On the basis of analogy to the motion of an electron in the tight-binding model, we may estimate the constant J in (14) as $J = T_a T_b / U_{ab}$.

3.2 The generalized system of reduced Maxwell-Bloch equations

The equations of motion for the operators $\widehat{P}_{a\ j}$, $\widehat{R}_{a\ j}$, $\widehat{S}_{a\ j}$, $\widehat{N}_{3\ j}$, $\widehat{W}_j$ and $\widehat{K}_j$ have the form like the system of equations (2) - (10), but inwhere the matrix elements V_{aj} should be rewriten as $\widetilde{V}_{aj} = V_{aj} + J(\widehat{P}_{a\ j+1} + \widehat{P}_{a\ j-1})$.

In the quasi-classical approximation, in which case the mean product of operators with different site indices are replaced by the product of the mean values of these operators, the corresponding system of equations has the same form as system (2) - (10), with all the operators replaced by the c-numbers. The resulting system of generalized Bloch equations takes the form which is like to (11), where normalized envelopes e_a should be replaced to $\widetilde{\mathrm{e}}_a = \mathrm{e}_a + (J/2\hbar\omega_R)(p_{a\ j+1} + p_{a\ j-1})$. These fields describe

the interaction of an electromagnetic field with electrons in a QD. Thus, it may be assumed that the effect of the exciton transport is reduced to the introduction of a local Lorentz field.

It should be noted that we consider a *polaritonic wave*, i.e., an electromagnetic wave propagating along the QD chain with a velocity differing only slightly from the speed of light owing to the drag of the polarization cloud. To emphasize that this polarization arises when localized excitons come into existence, one can use the term *excitonic polaritons*.

When considering an electromagnetic pulse in the approximation of a slowly varying envelope and phase, it may be additionally assumed that the envelope encompasses a large number of QDs, so that the transition to the continuous approximation is justified; i.e., one may write $p_{a\ j+1} + p_{a\ j-1} \approx 2p_a(z) + a_0^2\partial^2 p_a(z)/\partial z^2$. In this situation, the term $2Jp_a/\hbar$ describes a correction to the Lorentz local field and the second term $a_0^2\partial^2 p_a/\partial z^2$ accounts for the motion of an exciton along the chain. Here a_0 is distance between quantum dots. The effective mass of such an exciton can be defined as $m_*^{-1} = Ja_0^2/\hbar$. In the approximation of heavy excitons ($m_* \longrightarrow \infty$.), a non-local normalized field can be represented as $\widetilde{\mathrm{e}}_a(z) = \mathrm{e}_a(z) + (J/\hbar\omega_R)p(z)$ The equations obtained in this approximation become local.

3.3 A particular solution: a circularly polarized polariton

For the sake of simplicity, let us consider the situation, where the pulse of circularly polarized radiation propagates along the chain. Let us assume that the absorption line is homogeneous one. In the case of a circularly polarized wave one of the components of the normalized enelopes is equal to zero. Let be $\mathrm{e}_2 = 0$. It is easy to verify that $p_2 = s_2 = 0$ in the case under consideration. If the QD system is in the ground state in the absence of the pulse, then $w = u = 0, p_1 = s_1 = p$ and $n_1 = n_2 = n$ at any τ. The remaining equations can now be written as

$$\frac{\partial}{\partial\zeta}\mathrm{e}_1 = ip, \tag{15}$$

$$\frac{\partial}{\partial\tau}p = -i(\Omega - \Delta)p + i\mathrm{e}_1 n + i\beta pn, \tag{16}$$

$$\frac{\partial}{\partial\tau}n_1 = (\mathrm{e}_1 p^* - \mathrm{e}_1^* p)/2i, \tag{17}$$

where $\beta = J/\hbar\omega_R$.

In [22] it was shown that two types of steady-state circularly polarized solitary polaritonic waves can propagate along such chains; these are waves with exponentially and algebraically decaying leading and trailing edges. Previously, a USP with exponentially decaying leading and trailing edges was identified in a problem concerning excitonic self-induced transparency [27]. In the situation considered here, a steady-state pulse with Lorentzian shape and more slowly decaying leading and trailing edges was identified in addition to the above pulse.

4. Conclusion

A simple model of a quantum dot (and ensemble of QDs) interacting with an ultrashort pulse of arbitrarily polarized radiation was considered. The Hamiltonian of two electrons localized in a QD contains a term describing the motion of an exciton along the chain of QDs in addition to the terms accounting for the Coulomb interaction of electrons. On the basis of this Hamiltonian, a system of equations describing the evolution of the state of this chain was derived and discussed. The creation of excitons occurs under the effect of an arbitrarily polarized electromagnetic wave. In the limiting case, this system of equations is reduced to the Bloch equations for two-level atoms with allowance made for the effect of the Lorentz local field. For a circularly polarized wave, two types of solutions were obtained; these solutions correspond to steady-state solitary waves which differ in the characteristics of decay of the electric field at the edges of these pulses. Both types of solutions describe the propagation of a polarization wave dragged by an electromagnetic pulse along the QD chain.

The models under consideration can also be used to study the coherent responses of an ensemble of QDs (even if the number of QDs is small). This can be useful in developing the coherent nonlinear spectroscopy of low-dimensional systems. Some results concerning the refraction of a USP at a thin layer of QDs were reported previously [28]. The model used in [28] can be derived from the model considered in this paper.

Acknowledgments

We are grateful to my colleagues Dr. S.O. Elyutin, and Dr. E.V. Kazantseva for valuable discussions. This study was supported in part by the Russian Foundation for Basic Research, project no. 03-02-16979.

References

[1] L. Allen, J.H. Eberly, *Optical Resonance and Two-Level Atoms*. Wiley, N.Y., 1975.

[2] M. J. Konopniki, J. H. Eberly, Phys. Rev. A **24**, 2567 (1981).

[3] O. Kocharovskaya, Y. V. Radeonychev, P. Mandel, M. O. Scully, Phys. Rev. A **60,** 3091 (1999).

[4] E. Paspalakis, N. J. Kylstra, P. L. Knight, Phys. RevA **61**, 045802 (2000).

[5] A. I. Maimistov, A. M. Basharov, S. O. Elyutin, Yu. M. Sklyarov, Phys. Rep. C **191**, 1 (1990).

[6] A.I. Maimistov, Quantum Electron. **30**, 287 (2000).

[7] M. A. Kastner, Rev. Mod. Phys. **64**, 849 (1992).

[8] L. Jacak, P. Hawrylak, A. Wojs, *Quantum Dots*. Springer-Verlag, Berlin, 1998.

[9] U.Hohenester, R.DiFelice, E.Molinari, F.Rossi, Appl.Phys.Lett. **75**, 3449 (1999).

[10] J. Li and J.-B. Sia, Phys. Rev. B **61**, 15880 (2000).

[11] M. Pacheco, Z. Barticevic, Phys. Rev. B **64**, 33406 (2001).

[12] O. Keller, T. Garm, J. Opt. Soc. Am. B **13**, 2121 (1996).

[13] T. Brunhes, P. Boucaud, S. Sauvage, et al., Phys. Rev. B **61**, 5562 (2000).

[14] Y. Jiang, J. Xu, W. Wang, et al., Phys. Rev. B **63**, 125308 (2001).

[15] M. Lindberg, R. Binder, Phys. Rev. Lett. **81**, 1477 (1998).

[16] W. Potz, Phys. Rev. Lett. **79**, 3262 (1997).

[17] J. Erland, J. C. Kim, N. H. Bonadeo, et al., Phys. Rev. B **60**, R8497 (1999).

[18] K. Kral, Z. Khas, C. Lin, S. H. Lin, Opt. Commun. **180**, 271 (2000).

[19] A. V. Krasheninnikov, S. N. Molotkov, S. S. Nazin, L. A. Openov, JETP **85**, 682 (1997)

[20] S. O. Elyutin, E. V. Kazantseva, A. I. MaImistov, Optics and Spectrosc. **90**, 439 (2001).

[21] A. I. MaImistov, S. O. Elyutin, Optics and Spectrosc. **93**, 257 (2002).

[22] A. I. MaImistov, Optics and Spectrosc. **93**, 45 (2002).

[23] Y. B. Schrieffer, P. A. Wolff, Phys. Rev. **149**, 491 (1966).

[24] A. M. Basharov, A. I. MaImistov, Optics and Spectrosc. **68**, 649 (1990).

[25] J. Hubbard, Proc. R. Soc. London, Ser. A **276**, 238 (1963).

[26] Yu. A. Izyumov, Phys.Usp. **40**, 433 (1997).

[27] V. M. Agranovich, V. I. Rupasov, Sov. Phys. Solid State **18**, 459 (1976).

[28] S. O. Elyutin, A. I. Maimistov, Proc. SPIE **4605**, 171 (2001).

ENHANCED OPTICAL TRANSMISSION VIA TUNNEL COUPLING IN SURFACE POLARITONIC CRYSTALS

Sergey A. Darmanyan
International Research Centre for Experimental Physics,
The Queen's University of Belfast, Belfast BT7 1NN, United Kingdom, and
Institute of Spectroscopy, Russian Academy of Sciences, Troitsk, Moscow region, Russia
sdarmanyan@yahoo.com

Michel Nevière
Institut Fresnel, Faculté des Sciences et Techniques de Saint Jérome,
13397-262 Marseille Cedex 20, France
michel.neviere@fresnel.fr

Anatoly V. Zayats
School of Mathematics and Physics, The Queen's University of Belfast,
Belfast BT7 1NN, United Kingdom
a.zayats@qub.ac.uk

Abstract Analytical theory of the enhanced optical transmission through a periodically structured metal film capable of supporting surface plasmon polaritons is presented. The spectrum of the surface-polariton Bloch modes of a nanostructured film and their electromagnetic field configuration have been derived. Two resonant regimes have been shown to contribute to the transmission enhancement associated with the surface polariton states of both or at least one of the film interfaces. The enhancement occurs due to the tunnel coupling between the electromagnetic modes on the opposite interfaces. Transmission spectra as well as far- and near-field properties of the reflected and transmitted light are discussed. The obtained results are important for understanding and applications of linear and non-linear optical properties of periodic metallic nanostructures.

F. Kh. Abdullaev and V. V. Konotop (eds.), Nonlinear Waves: Classical and Quantum Aspects, 313–326.

Keywords: Surface plasmon polaritons, nanostructured metal films, enhanced optical transmission.

1. Introduction

Optical properties of metallic films capable of supporting surface plasmon polaritons (SPPs) have recently attracted significant attention due to various unusual electromagnetic effects [1, 2]. An important class of metallic nanostructures for photonic and optoelectronic applications is based on periodically structured metal films. They have been considered in the context of bio- and chemo-sensors, for the enhancement and control of non-linear optical processes, and can lead to the development of all-optical photonic circuits where they can be used as passive as well as active photonic components.

Behaviour of surface plasmon polaritons on a periodically structured surface is governed by the same rules as that of electrons in a crystalline lattice or photons in a photonic crystal. In analogy to this, a nanostructured metal surface has been dubbed a surface-polaritonic crystal. The optical properties of such SPP crystals are determined by surface polariton behaviour in a lattice formed by a nanostructure.

One of the SPP-related optical processes is the enhanced optical transmission through periodic metallic films. After first experimental observations [3], the progress in understanding of this phenomenon has relied on numerical modelling of one- and two-dimensional nanostructures. The effects of the coupling between the electromagnetic modes in the film [4], the role of the SPP Bloch modes and near-field effects [5], the difference between slits and holes in a film [6], the influence of surroundings [7], and other properties have been investigated. In addition to the transmission mechanisms specific to one or the other geometry of a nanostructure, the enhancement related to the photon tunnelling via surface plasmon polariton states is universal for all metallic structures [2, 8]. Further experiments on optical properties of nanostructured metal films addressed non-linear and polarisation effects in transmission [9] as well as temporal behaviour of the transmitted pulses [10].

Very recently, the analytical descriptions of the enhanced transmission in the tunnelling regime were developed [8, 11]. This allowed derivation of analytical expressions for the transmission and reflection of a periodically structured metal film surrounded by dielectric media and analysis of the transmission mechanisms in different regimes. The results provided the understanding of nonnecessity of holes or slits in a film (only one or another kind of periodic modulation is needed, such as topography or dielectric constant variations), the role of the SPP states related to the different branches of the Brillouin zones in photon tunnelling through a

metal film, *etc.* Optically induced enhancement of the transmission of a smooth metal film due to non-linear effects has been suggested [11].

In this paper we have overviewed the theory of the optical transmission of periodically structured metal films related to the resonant light tunnelling via the states of the SPP Bloch modes of surface-polaritonic crystals.

2. SPP modes on a periodically structured surface

Surface plasmon polaritons are collective excitations of electron plasma at a metal surface (surface plasmons) coupled with photons. Surface polaritons have the wavevector k_{SP} exceeding the wavevector of light of the same frequency, $(\omega\epsilon_I^{1/2}/c)$, and therefore, cannot be excited directly by light on a smooth surface. However, light illuminating a periodically structured metal surface (Fig. 1) can excite surface polariton modes since diffraction on a periodic structure can provide the wavevector conservation [12]

$$\vec{k}_{SP} = \frac{\omega}{c}\epsilon_I^{1/2}\sin\theta\vec{u}_x \pm p\vec{q}. \tag{1}$$

Here, light is incident from the medium I and has the electric field component in the incidence plane (x, z), θ is the angle of incidence, $\vec{q} = 2\pi\vec{u}_x/d$ is the reciprocal lattice vector of a periodic structure ($\vec{u}_x$ is the unit reciprocal lattice vector), d is its periodicity, and p is integer number. The SPP propagation through a periodic structure leads to the same effects as for electrons propagating through a crystal lattice or photons propagating through a medium with a periodically modulated refractive index, namely, to modification of their dispersion law $\omega(k_{SP})$ and the band-gap effects [13, 14].

The sketch of the dispersion of surface polaritons on a periodically structured interface between a semi-infinite metal and a dielectric medium I is schematically shown in Fig. 1, where thin solid lines indicate the dispersion of the SPPs on an unstructured surface with $\varepsilon_{II} = \varepsilon_0 < 0$. The SPPs with the wavevector $k_x > \omega\varepsilon_I^{1/2}/c$ being true surface excitations, have an infinite lifetime (with respect to decay in photons), while the SPPs with the wavevector $k_x < \omega\varepsilon_I^{1/2}/c$ (shadowed region in Fig. 1) are believed to be radiative modes because they can directly couple to photons.

If we consider a periodically structured surface illuminated at the normal incidence $\theta = 0$ (the configuration which is most widely used in the experiments), only SPPs in the vicinity of the even-numbered gaps (second $a-b$, forth $c-d$, etc.) can be excited directly with light [Eq. (1)].

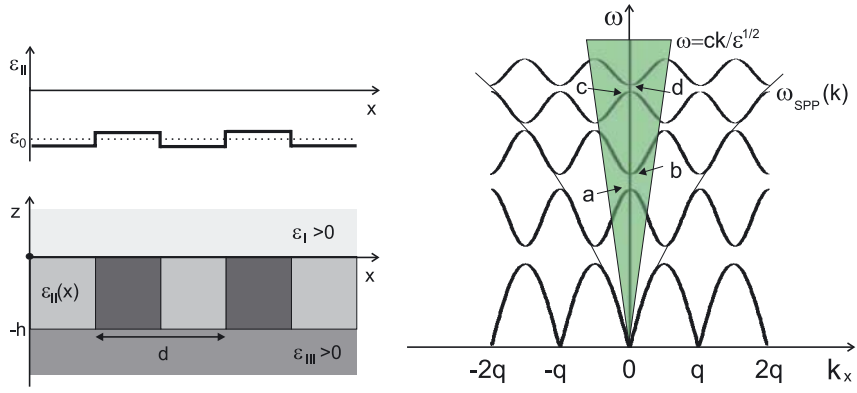

Figure 1. (left) Geometry of a periodically structured metal film. (right) Schematic of the band structure of surface polariton modes on a periodically nanostructured metal surface. The dispersion of SPPs on a smooth surface $\omega_{SP} = \omega(k_x)$ is shown with thin solid lines. Shaded region shows the light cone $\omega = ck/\epsilon^{1/2}$.

These SPPs correspond to the standing SPP Bloch waves on a periodic surface. We have shown in Ref. [8] that the conservation of energy and momentum, or in other words, matching the frequencies and wavevectors of SPPs and bulk light that takes place in the shadowed region in Fig. 1, is not sufficient condition for SPPs to be directly excited by (or converted to) photons. Only the SPP states corresponding to points *a* and *c* (and higher) of the dispersion curve in Fig. 1, which define the SPP Bloch modes near the bottom edges of the even band-gaps, have complex (with an imaginary part) frequencies and, thus, can interact with normally incident photons [8]. In contrast, frequencies corresponding to the top edges of the even band-gaps (points *b*, *d*, and higher in Fig. 1) are real. It means that SPPs at these frequencies have an infinite lifetime and do not interact with photons. This has the important consequences for the understanding of the optical transmission through periodically structured metal films.

3. SPP film modes of a periodic structure

Let us consider a metallic film of a finite thickness with periodic modulation of the dielectric properties throughout the film thickness. This can be either topographic modulation due to slits or holes in the film, metal permittivity modulation, or filling of the slits or holes with other material. The film is placed between two generally different dielectric media (Fig. 1). The structure is characterised by the dielectric con-

stants $\varepsilon_I > 0$ for $z > 0$, $\varepsilon_{III} > 0$ for $z < -h$, and ε_{II} for $-h < z < 0$. The dielectric constant ε_{II} is assumed to be periodic in x-direction, i.e. $\varepsilon_{II}(x) = \varepsilon_{II}(x + nd)$, $n = 1, 2...$, and its average value is negative, $< \varepsilon_{II} >= \varepsilon_0 < 0$. For simplicity we consider the case of the real dielectric functions $\varepsilon_{I,II,III}$.

The structure is illuminated at normal incidence from the medium I and the electromagnetic surface waves can be excited on the structure interfaces due to periodic modulation. In the case of the TM polarised wave propagating along the x-axis, the electromagnetic field has the following form with both transverse and longitudinal components of the electric field

$$\vec{E} = (E_x, 0, E_z)e^{ik_x x - i\omega t} + c.c., \quad \vec{H} = (0, H_y, 0)e^{ik_x x - i\omega t} + c.c. \tag{2}$$

The method of treating the electromagnetic properties of periodic structures is well developed and consists in substitution of the field and dielectric function in the Maxwell equations by their Fourier expansions

$$\vec{E} = \sum_{n=-\infty}^{\infty} \vec{E}_n \exp(ingx), \quad \varepsilon_2 = \sum_{n=-\infty}^{\infty} e_n \exp(ingx), \tag{3}$$

where $g = 2\pi/d$ is the vector of the reciprocal lattice related to the periodic structure. After straightforward algebra one arrives to the set of equations for the field amplitudes that are usually studied numerically.

The first band-gap in the spectrum of SPPs on a periodically structured surface lies in the non-radiative region, therefore, higher SPP band-gaps must be considered for the description of light transmission. We are interested only in the electromagnetic field configuration of the branches of the SPP Bloch modes near the bottom edges of the even band-gaps, since only these states have complex (with imaginary part) frequencies and, thus, can interact with normally incident photons [8]. To get analytical expressions for the dispersion law of the film modes and in particular the width and position of the band-gap edges as well as the field configurations and amplitudes of the reflected and transmitted waves, we restrict ourselves to the simple case of $\varepsilon_{II}(x) = \varepsilon_0 + 2\varepsilon_1 \cos(gx)$. The field configuration near the second band-gap can be calculated by truncating the Fourier series for fields, and the electric field in the metallic medium can be sought in the form

$$\vec{E}_{II} = (\vec{A} + \vec{B}\cos gx + \vec{C}\sin gx)e^{\kappa z}, \tag{4}$$

where $\vec{A}$, $\vec{B}$, $\vec{C}$, and κ are the parameters that should be determined. This is the so-called three-wave approximation which is generalisation of the two-wave approximation commonly used in solid state physics for

the description of the Bloch states near the first band-gap [15]. Being substituted into the Maxwell equations, Eq. (4) leads to the set of six equations for six field amplitudes $A_{x;z}$, $B_{x;z}$, $C_{x;z}$. It is important to note that this set of equations splits into two independent sets for the fields A_x, B_x, C_z and A_z, B_z, C_x. Conditions of solubility of the first set of equations lead to the following expressions for two eigenvalues κ_i:

$$\begin{aligned}\kappa_{1,2}^2 &= \tfrac{1}{2}\left(g^2 - 2\varepsilon_0 k_0^2 \mp \sqrt{g^4 + 8\alpha_1\varepsilon_0 k_0^2(\varepsilon_0 k_0^2 - g^2)}\right) \\ &\approx \left[\begin{array}{l} -\varepsilon_0 k_0^2 - 2\alpha_1\varepsilon_0 k_0^2(\varepsilon_0 k_0^2 - g^2)/g^2 \\ g^2 - \varepsilon_0 k_0^2 + 2\alpha_1\varepsilon_0 k_0^2(\varepsilon_0 k_0^2 - g^2)/g^2 \end{array}\right. ,\end{aligned} \tag{5}$$

while the conditions of solubility of the second set gives the third eigenvalue

$$\kappa_3^2 = -\varepsilon_0 k_0^2 + \frac{g^2}{1-2\alpha_1} \approx -\varepsilon_0 k_0^2 + g^2 + 2\alpha_1 g^2, \tag{6}$$

where $k_0 = \omega/c$. Only three of six eigenvalues κ_i are independent since $\kappa_{4,5,6} = -\kappa_{1,2,3}$.

The approximations made in Eqs. (5) and (6) are valid for $\alpha_1 = \varepsilon_1^2/\varepsilon_0^2 << 1$, or to be more precise in the case of Eq. (5), when the second term in the square root is much smaller than the first one. This condition can be written as

$$8\varepsilon_1^2 \frac{d^2}{\lambda^2}\left(\frac{d^2}{\lambda^2} - \frac{1}{\varepsilon_0}\right) \approx 8\varepsilon_1^2 \frac{d^4}{\lambda^4} << 1. \tag{7}$$

Eq. 7 shows that the absolute value of the dielectric constant modulation depth $|\varepsilon_1|$ is more important than the ratio $|\varepsilon_1/\varepsilon_0|$.

Thus, within the chosen three-wave approximation (Eq. 4), the field in the medium *II* has the following form:

$$\begin{aligned} E_x &= (A_{1;x} + B_{1;x}\cos gx)e^{\kappa_1 z} + (A_{2;x} + B_{2;x}\cos gx)e^{\kappa_2 z} \\ &\quad + C_{3;x}\sin gx\, e^{\kappa_3 z} + (a_{1;x} + b_{1;x}\cos gx)e^{-\kappa_1(z+h)} \\ &\quad + (a_{2;x} + b_{2;x}\cos gx)e^{-\kappa_2(z+h)} + c_{3;x}\sin gx\, e^{-\kappa_3(z+h)}, \\ E_z &= C_{1;z}\sin gx\, e^{\kappa_1 z} + C_{2;z}\sin gx\, e^{\kappa_2 z} + (A_{3;z} + B_{3;z}\cos gx)e^{\kappa_3 z} \\ &\quad + c_{1;z}\sin gx\, e^{-\kappa_1(z+h)} + c_{2;z}\sin gx\, e^{-\kappa_2(z+h)} \\ &\quad + (a_{3;z} + b_{3;z}\cos gx)e^{-\kappa_3(z+h)}, \end{aligned} \tag{8}$$

where the fields of the corresponding eigenmodes are related as

$$A_{1,2;x} = \frac{-\varepsilon_1 k_0^2}{\varepsilon_0 k_0^2 + \kappa_{1,2}^2} B_{1,2;x}, \quad C_{1,2;z} = \frac{g\kappa_{1,2}}{g^2 - \varepsilon_0 k_0^2} B_{1,2;x},$$

$$A_{3;z} = \frac{-\varepsilon_1}{\varepsilon_0} B_{3;z}, \quad C_{3;x} = \frac{\kappa_3}{g}(2\alpha_1 - 1)B_{3;z}. \tag{9}$$

Similar relations hold for the amplitudes a, b, and c with κ_i substituted by $-\kappa_i$.

4. Transmission and reflection coefficients

Light transmission through and reflection from a metal film are determined by the fields in the dielectric media I and III. We take these fields in the form

$$\begin{aligned} E_x &= A_x e^{-ik_I z} + R_x e^{ik_I z} + (B_x \cos gx + C_x \sin gx)\, e^{-\eta_I z}, \\ E_z &= (B_z \cos gx + C_z \sin gx)\, e^{-\eta_I z} \end{aligned} \tag{10}$$

for $z > 0$, where the incident, reflected, and SPP fields are present, and

$$\begin{aligned} E_x &= T_x e^{-ik_{III}(z+h)} + (b_x \cos gx + c_x \sin gx)\, e^{\eta_{III}(z+h)}, \\ E_z &= (b_z \cos gx + c_z \sin gx)\, e^{\eta_{III}(z+h)} \end{aligned} \tag{11}$$

for $z < -h$, where the transmitted and SPP fields exist. Here,

$$k_{I,III}^2 = \varepsilon_{I,III} k_0^2, \quad \eta_{I,III}^2 = g^2 - \varepsilon_{I,III} k_0^2, \tag{12}$$

$$C_z = -\frac{g}{\eta_I} B_x, \quad C_x = \frac{\eta_I}{g} B_z, \quad c_z = \frac{g}{\eta_{III}} b_x, \quad c_x = -\frac{\eta_{III}}{g} b_z, \tag{13}$$

where A, R, and T are the amplitudes of the incident, reflected, and transmitted waves, respectively.

Upon substitution of the expressions (8), (10), and (11) into corresponding boundary conditions, we arrive at two independent sets of equations for the field amplitudes. The set that corresponds to the fields A_x, B_x, and C_z reads as

$$\begin{aligned} &A_x + R_x = A_{1x} + A_{2x} + a_{1x} e^{-\kappa_1 h} + a_{2x} e^{-\kappa_2 h}, \\ &ik_I(R_x - A_x) = \kappa_1 A_{1x} + \kappa_2 A_{2x} - \kappa_1 a_{1x} e^{-\kappa_1 h} - \kappa_2 a_{2x} e^{-\kappa_2 h}, \\ &B_x = B_{1x} + B_{2x} + b_{1x} e^{-\kappa_1 h} + b_{2x} e^{-\kappa_2 h}, \\ &\varepsilon_I C_z = \varepsilon_0 (C_{1z} + C_{2z} + c_{1z} e^{-\kappa_1 h} + c_{2z} e^{-\kappa_2 h}), \\ &T_x = a_{1x} + a_{2x} + A_{1x} e^{-\kappa_1 h} + A_{2x} e^{-\kappa_2 h}, \\ &ik_{III} T_x = \kappa_1 a_{1x} + \kappa_2 a_{2x} - \kappa_1 A_{1x} e^{-\kappa_1 h} - \kappa_2 A_{2x} e^{-\kappa_2 h}, \\ &b_x = b_{1x} + b_{2x} + B_{1x} e^{-\kappa_1 h} + B_{2x} e^{-\kappa_2 h}, \\ &\varepsilon_{III} c_z = \varepsilon_0 (c_{1z} + c_{2z} + C_{1z} e^{-\kappa_1 h} + C_{2z} e^{-\kappa_2 h}). \end{aligned} \tag{14}$$

The set of the boundary conditions Eq. (14) contains the incident amplitude A_x and 18 unknown amplitudes. Using Eqs. (9) and (13) and analogous relations between $a_{1x,2x}, b_{1x,2x}$, and $c_{1z,2z}$, we reduce the full system of equations to the system of four equations defining four amplitudes $A_{1x,2x}$ and $a_{1x,2x}$ in terms of the incident field amplitude A_x:

$$\begin{pmatrix} \Psi_1 & \Psi_2 & \Psi_1^* e^{-\kappa_1 h} & \Psi_2^* e^{-\kappa_2 h} \\ \varphi_1 F_1 & \varphi_2 F_2 & \varphi_1 \bar{F}_1 e^{-\kappa_1 h} & \varphi_2 \bar{F}_2 e^{-\kappa_2 h} \\ \psi_1^* e^{-\kappa_1 h} & \psi_2^* e^{-\kappa_2 h} & \psi_1 & \psi_2 \\ \varphi_1 \bar{f}_1 e^{-\kappa_1 h} & \varphi_2 \bar{f}_2 e^{-\kappa_2 h} & \varphi_1 f_1 & \varphi_2 f_2 \end{pmatrix} \begin{pmatrix} A_{1x} \\ A_{2x} \\ a_{1x} \\ a_{2x} \end{pmatrix} = \begin{pmatrix} 2k_I A_x \\ 0 \\ 0 \\ 0 \end{pmatrix}. \tag{15}$$

In writing down Eq. (15) the following notations were introduced:

$$\begin{aligned} F_{1,2} &= \tfrac{\varepsilon_I}{\eta_I} + \tfrac{\varepsilon_0\kappa_{1,2}}{g^2-\varepsilon_0 k_0^2}, \quad \bar{F}_{1,2} = \tfrac{\varepsilon_I}{\eta_I} - \tfrac{\varepsilon_0\kappa_{1,2}}{g^2-\varepsilon_0 k_0^2}, \\ f_{1,2} &= \tfrac{\varepsilon_{III}}{\eta_{III}} + \tfrac{\varepsilon_0\kappa_{1,2}}{g^2-\varepsilon_0 k_0^2}, \quad \bar{f}_{1,2} = \tfrac{\varepsilon_{III}}{\eta_{III}} - \tfrac{\varepsilon_0\kappa_{1,2}}{g^2-\varepsilon_0 k_0^2}, \end{aligned} \tag{16}$$

and

$$\Psi_{1,2} = k_I + i\kappa_{1,2}, \quad \psi_{1,2} = k_{III} + i\kappa_{1,2}, \quad \varphi_{1,2} = \kappa_{1,2}^2 + \varepsilon_0 k_0^2. \tag{17}$$

Now it is straightforward to get expressions for the fields amplitudes: $A_{1,2x} = d_{1,2}/d$ and $a_{1,2x} = d_{3,4}/d$. Here $d = \det[M]$ is the determinant of the 4×4 matrix defined in the left hand side of Eq. (15) and $d_{1,2,3,4}$ are the determinants of the matrixes obtained from the matrix M by replacing the corresponding column with the column defined in the right hand side of Eq. (15). Using this, one can easily find the transmitted and reflected field amplitudes

$$\begin{aligned} T_x &= \left(d_1 e^{-\kappa_1 h} + d_2 e^{-\kappa_2 h} + d_3 + d_4\right)/d, \\ R_x &= \left(d_1 + d_2 + d_3 e^{-\kappa_1 h} + d_4 e^{-\kappa_2 h}\right)/d \ - A_x. \end{aligned} \tag{18}$$

The equation $d = 0$ defines the dispersion relation of the SPP modes existing on a structured film. In particular case of a single interface, which is given by limit $h \to \infty$, it reproduces the dispersion relation of the surface electromagnetic mode obtained in Ref. [8], while in the case of $\alpha_1 \to 0$ it gives the dispersion relation of the excitations of a homogeneous film [12]. Eqs. (18) together with the corresponding expressions for the determinants d and d_i give the solution of the problem of the light transmission through the periodically nanostructured metal film capable of supporting surface plasmon polaritons.

5. Transmission spectra

We have analysed the transmission spectra of the metallic structures with parametres similar to those studied in the experiments and used for numerical modelling [6, 7, 16]. In particular, we considered a gold film deposited on a quartz substrate ($\varepsilon_{III} = 2.31$). The film was illuminated from the side opposite to the substrate. To model the dielectric function of gold we used the approximation $\varepsilon_0 = 1 - 3 \times 10^{-5}(\lambda[nm])^2$ which is valid in the spectral range λ= 600–1000 nm. A set of permittivities for the adjacent medium was considered ε_I= 1–2.31 in order to clarify the transmission mechanisms related to degenerate and non-degenerate SPP modes on the film interfaces. Only real part of the dielectric constant of gold was taken into account for simplicity, but the influence of the

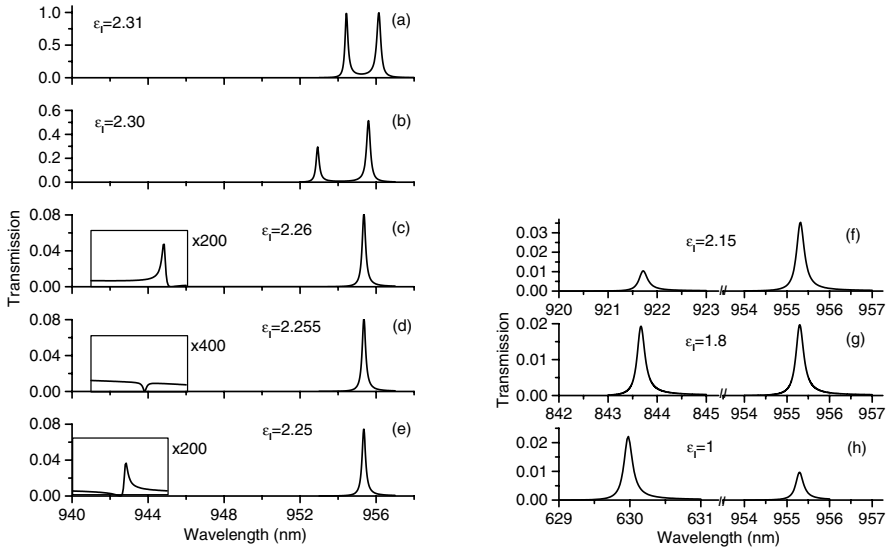

Figure 2. Intensity transmission spectra of the periodically structured gold film deposited on the quartz substrate (ϵ_{III}=2.31) for different dielectric constant of the adjacent medium ϵ_I. The film thickness is 150 nm, the structure periodicity is d=600 nm, and the modulation depth is $|\epsilon_1/\epsilon_0| = 0.1$. TM-polarised electromagnetic wave is incident perpendicularly to a metal surface.

Ohmic losses is also discussed. The analytically calculated transmission spectra $t = |T_x/A_x|^2$ obtained using Eq. (18) are similar to the experimentally observed spectra and numerical calculations. The spectral position, shape of spectral bands as well as their behaviour with refractive index changes and thickness of the film are described well by the analytical expressions.

The transmission spectra are presented in Fig. 2 for different dielectric constants of the adjacent medium ε_I. In the case of a symmetric structure (a metal film sandwiched in quartz), the spectrum consists of two peaks of equal amplitudes. The peak wavelengths are very close in the case of the relatively thick film. For smaller film thicknesses these peaks move in opposite directions with the decrease of the thickness, preserving their amplitudes $t = 1$. With the increase of the thickness, the transmission peaks shift closer, and transmission becomes smaller. These peaks correspond to the film SPP Bloch modes of the nanostructured metal film. In symmetric surroundings, the SPP modes related to the opposite interfaces are degenerated and the interaction leads to splitting of their frequencies and formation of the film SPP modes with symmetric (low-frequency mode) and anti-symmetric (high-frequency mode)

distributions of the field in the film. For relatively thick films, the SPP modes are weakly interacting and thus shifted only slightly from each other. With the decrease of the thickness they are repulsed further.

The transmission is expected to be $t = 1$ in the case of a symmetric structure. This follows from the considerations of the resonant tunnelling between the SPP modes on the opposite film interfaces (double-resonant conditions) [8]. Irrespectively of the film thickness, the full transfer of the excitation energy occurs through the film if the SPP lifetime is long enough, similarly to the tunnelling through a potential barrier via resonant states of quantum wells. However, in the case of very thick films, the decrease in the transmission was observed. This is related to the increase of the interaction time needed to achieve effective tunnelling through a thick film. Although the Ohmic losses are absent, the radiative losses due to coupling back to photons reduce the SPP lifetime. If the imaginary part of the dielectric constant of metal is included into considerations, the amplitude of the peaks drops and they become wider. (In the case of a thick film and thus a weak coupling, these leads to one transmission peak observed which is related to two closely spaced SPP resonances [16].) The decrease of the transmission in both described situations is related to one or another kind of losses in the system leading to the finite SPP lifetime and therefore, reduced tunnelling efficiency.

If the symmetry of the structure is broken (Fig. 2 b–h), the SPP modes are not degenerated by still interact with each other. A short-wavelength mode is related to the interface of the medium with a lower dielectric constant which is varied in the calculations, and shifts to the high frequency range with the decrease of the refractive index. At the same time, the long-wavelength mode related to a quartz interface is shifted much less since it is influenced only by a weak interaction between the SPP modes. For thinner films, this shift is much more pronounced.

Since in the asymmetric case, due to the difference in the position of SPP resonances on opposite interfaces, the double-resonant tunnelling conditions are not satisfied, the transmission becomes smaller in both resonances. In this case, the transmission peaks are related to direct photon tunnelling via one of the SPP resonances. Initially, with the decrease of ε_I the peak transmittance corresponding to the SPP on the interface in contact with the ε_I dielectric is smaller than the other peak. (In the opposite case, with the increase of ε_I, a symmetrical picture is observed with the longer-wavelength resonant transmittance decreasing faster.) However, two distinctively different transmission regimes can be identified with the dielectric constant ε_I variation (cf. Fig. 2 b, c and e–h). The transition between these two regimes is clearly observed at some value of the dielectric constant (Fig. 2 d) which depends on

the film thickness. For close values of the dielectric constants of surroundings (weakly asymmetric case) the SPP Bloch modes of the interfaces "remember" the symmetry of the film SPP modes. With the increase of the asymmetry, the short-wavelength transmission peak becomes smaller and disappears at some value of the dielectric constant at which the transmission at the SPP wavelength is suppressed compared to the transmission of the unstructured film and reaches zero. The physical reason for this behaviour is a crossing of the SPP mode states associated with the two systems of the Bloch modes of surface polaritons on the opposite film interfaces: the radiative SPP branch related to the interface with a lower refractive index medium and the non-radiative branch of the SPP mode on the interface with a higher refractive index medium. The decrease in the transmission and its suppression occurs due to the resonant energy transfer from the radiative SPP Bloch mode to the non-radiative mode (if the Ohmic losses are present, this leads to a significant absorption at this wavelength [16]). With the further increase of the difference in the dielectric constants of surroundings, these SPP modes become separated in energy and the high-frequency transmission peak appears again. However, the shape of the resonance has different symmetry corresponding to the density of states in the Brillouin zone.

Further decrease of the dielectric constant leads to the increase of the short-wavelength peak and the decrease of the long-wavelength transmission until they become equal in the amplitude (Fig. 2 g), then the high-frequency mode becomes dominating (Fig. 2 h). This behaviour is determined by the different behaviour of the $\kappa_{1,2}$ coefficients that describes spatial extension of the two SPP modes with the dielectric constant change. This leads to different tunnelling probabilities related to these modes.

In the case of light incident from the side of a substrate, the transmission coefficient can be calculated by exchanging dielectric constants of a substrate and a neighbouring medium $\varepsilon_{III} \leftrightarrow \varepsilon_I$. The transmittance ratio in this case is determined by the ratio of corresponding dielectric constants $t_{III\to I}/t_{I\to III} = \varepsilon_{III}/\varepsilon_I$. This is a consequence of the fact that the relative transmittance measured as the ratio of the transmitted energy flow (the time averaged Poynting vector) $S_t = \frac{c}{8\pi} n_{I,III} |T|^2$ to the incident energy flow $S_i = \frac{c}{8\pi} n_{III,I} |A|^2$ is equal in both directions. This is valid for the total energy transmitted through the nanostructure. If the structure transmission has, in addition to zero-order, also higher transmitted orders which propagates at some angle to the incident light direction, the transmission in the individual orders might not provide reciprocity with respect to the illumination side of the asymmetric nanostructure. Even if the transmission is the same, the reflection

and absorption of the asymmetric structure depends on the side which is illuminated [16].

6. Near-field and far-field transmission

The expressions (18) describe the field amplitudes in the far-field domain. Knowledge of the near-field is very important for many applications and especially for consideration of non-linear optical properties of the structure if the non-linearity of a metal itself or a thin nonlinear material film deposited on the surface should be taken into account. It is the electromagnetic field enhancement in the near-field region close to a metallic structure that makes possible observation of non-linear optical effects at very low incident light intensities [9, 17].

The analytical approach described above permits determination of the near-field amplitudes as well. According to Eq. (11), the total electromagnetic near-field on the opposite to the illuminated film interface, i.e. at $z = -h - 0$, is described by $E_x = T_x + b_x \cos gx$, and $E_z = c_z \sin gx$, with $c_z = gb_x/\eta_{III}$. The fields proportional to c_x and b_z cannot be excited with normally incident light, as was discussed above, and are omitted from the near-field description.

Thus, in contrast to the far-field region, the near-field of the transmitted light has the component E_z normal to the interface. This effect is responsible for significant polarisation conversion observed in the near-field. The field normal to the surface is related to the non-radiative part of the SPP Bloch wave and cannot be detected in the far-field, where the polarisation of the transmission light is the same as polarisation of the incident light. This polarisation effect is important for scanning near-field microscopy of nanostructured metals since the interpretation of the near-field images depends on the efficiency of coupling of different polarisation components of the field over a surface to a fibre tip and the polarisation dependent electromagnetic field enhancement at the tip apex. Polarisation properties of the transmitted light in the near-field should also be taken into account considering non-linear optical interactions which can exhibit profound polarisation dependencies due to the symmetry properties of the second- and/or third-order nonlinear susceptibilities.

The evanescent field component E_z exhibits a resonant behaviour with the light frequency similar to T_x. However, it is proportional to $\sin(gx)$, and its spatial distribution is out-of-phase compared to the evanescent part of the E_x component. At the same time, the propagating part of the transmitted field (T_x) has no spatial variation linked to the film modulation since the tunnelling through the film as a whole determines

the transmission, the surface periodicity determines only the modes contributing to the tunnelling process.

7. Conclusion

The optical properties of periodically structured metal films are governed by surface polariton behaviour in a surface-polaritonic crystal. The periodic structure modifies the local density of electromagnetic states on the metal film interfaces leading to light tunnelling at the resonant wavelengths of the SPP Bloch waves related to one of or both film interfaces. Due to different structure of the electromagnetic field of the SPP modes in different Brillouin zones, only SPPs in even Brillouin zones contribute to the transmission enhancement at normal incidence.

The presented analytical studies of the enhanced optical transmission through periodically nanostructured metal films allow identification of the origin of the resonances in the spectra, which are related to surface polariton processes. It is shown that the effect of the enhancement arises due to a periodical structure of a film and not necessary requires holes or slits through a film. In fact, the structures of different periodicities on the opposite film interfaces can be advantageous for optimising resonant tunnelling between the SPP states.

Surface polaritonic crystals that intrinsically provides the field enhancement related to SPP modes, are especially advantageous in a combination with optical nonlinear materials. Such non-linear metamaterials can lead to a principally new class of all-optical devices for integrated photonic circuits [2, 9, 17]. Periodically nanostructured metal films provide a possibility to efficiently control the spectrum and intensity of the optical transmission and can find numerous applications in modern photonics and optoelectronics.

Acknowledgments

S.A.D. gratefully acknowledges the support from International Research Centre for Experimental Physics, The Queen's University of Belfast, and NATO Linkage Grant PST CLG 978177. This work was supported in part by EPSRC.

References

[1] W.L. Barnes, A. Dereux, and T.W. Ebbesen, Nature **424**, 824 (2003).

[2] A.V. Zayats and I.I. Smolyaninov, J. Opt. A **5**, S16 (2003).

[3] T.W. Ebbessen, J. Lezec, H.F. Ghaemi, T. Thio, and P.A. Wolff, Nature **391**, 667 (1998).

[4] L. Martin-Moreno, F.J. Garsia-Vidal, H.J. Lezec, K.M. Pellerin, T. Thio, J.B. Pendry, and T.W. Ebbesen, Phys. Rev. Lett. **86**, 1114 (2001).

[5] L. Salomon, F. Grillot, F. de Fornel, and A.V. Zayats, Phys. Rev. Lett. **86**, 1110 (2001).

[6] E. Popov, M. Neviere, S. Enoch, and R. Reinisch, Phys. Rev. B **62**, 16100 (2000).

[7] A. Krishnan, T. Thio, T.J. Kim, H.J. Lezec, T.W. Ebbesen, P.A. Wolf, J. Pendry, L. Martin-Mareno, and F.J. Garsia-Vidal, Opt. Commun. **200**, 1 (2001)

[8] S.A. Darmanyan and A.V. Zayats, Phys. Rev. B **67**, 035424 (2003).

[9] I.I. Smolyaninov, A.V. Zayats, A. Stanishevsky, and C.C. Davis, Phys. Rev. B **66**, 205414 (2002).

[10] A. Dogariu, T. Thio, L.J. Wang, T.W. Ebbessen, and H.J. Lezec, Opt. Lett. **26**, 450 (2001).

[11] A.M. Dykhne, A.K. Sarychev, and V.M. Shalaev, Phys. Rev. B **67**, 195402 (2003).

[12] *Surface Polaritons*, V.M. Agranovich and D.L. Mills, Eds., North-Holland (Amsterdam), 1982.

[13] N.E. Glass and A.A. Maradudin, Phys. Rev. B **29**, 1840 (1984).

[14] W.L. Barnes, T.W. Preist, S.C. Kitson, and J.R. Sambles, Phys. Rev. B **54**, 6227 (1996).

[15] C. Kittel, *Introduction to Solid State Physics*, Wiley (Chichester), 1996.

[16] D. Gérard, L. Salomon, F. de Fornel, and A.V. Zayats, in Proc. 1st International Conference on *Electromagnetic Near-field Characterisation*, Rouen (France), 2003, pp. 221-225.

[17] I.I. Smolyaninov, A.V. Zayats, A. Gungor, and C.C. Davis, Phys. Rev. Lett. **88**, 187402 (2002).

LIQUID LIGHT IN CUBIC-QUINTIC NONLINEAR OPTICAL MATERIALS

Humberto Michinel, Maria J. Paz-Alonso, and Jose R. Salgueiro
Area de Optica, Facultade de Ciencias de Ourense, Universidade de Vigo, As Lagoas s/n, Ourense, ES-32005 Spain.

Abstract For a nonlinear optical material with the adequate dependence of the refractive index with light intensity, a condensation phenomenon takes place for a laser beam. This process can be interpreted as a phase transition from a photon gas to a liquid of light. The physical properties of the resulting state, like surface tension, are similar to those of quantum liquids. Here we report a numerical exploration of the dynamics of these light condensates. We show that, as in the case of superfluids, eternal whirpools can be generated in light droplets. We also stress the deep connections and analogies between this new state of matter and Bose-Einstein condensates.

1. Introduction

It was Albert Einstein, during his *miraculous year* 1905 [1], the first to consider seriously the analogies between a beam of light and a gas. By means of statistical mechanics, he calculated the entropy of a monochromatic gas of light quanta, and applied it to explain the photoelectric effect. Thus, if light can be regarded as a gas of photons, a couple of simple questions are: Would it be possible to obtain a liquid of light? What physical properties will it have? The answers are not trivial. In first place, it is known that even in the quantum world the interactions between photons in vacuum are negligible, thus one could expect that photons will not yield to Van der Waals-like interactions. On the other hand, laser photons are a collection of identical non-massive bosons and thus, a liquid of light would have physical properties similar to those of quantum liquids in a Bose-Einstein condensation.

Concerning the first question, it is interesting to consider the effect on the photon gas of an intensity-dependent refractive index[3]. For nonlinear optical materials with a linear growth of the refractive index with light intensity (optical Kerr effect), only in one-dimensional con-

F. Kh. Abdullaev and V. V. Konotop (eds.), Nonlinear Waves: Classical and Quantum Aspects, 327–351.

figurations stable soliton propagation can be achieved. Two and three-dimensional beams, with powers over a critical value, always collapse to a singularity[6]. This behaviour is quite evident if one takes into account that light directs to the regions with higher refractive index due to Fermat's principle. For these materials this zone corresponds to the center of a gaussian laser beam. Thus, if the refractive index shift is strong enough to counteract the natural curvature of the beam, diffraction is overcame and self-focusing takes place.

2. Physical model

Thus, let us begin by remembering some well-known effects concerning non-resonant laser propagation in nonlinear materials. In optical media presenting linear growth of the refractive index shift with light intensity (optical Kerr effect), envelope solitons [2, 3, 4] can be produced for one-dimensional propagation. They can be obtained as pulses in optical fibers with anomalous dispersion (temporal solitons) or continuous beams in several planar configurations. On the other hand, wild unstable phenomena like blow-up and catastrophic self-focusing take place for intense two-dimensional propagation in bulk Kerr-like materials[5, 6]. However, collapse can be limited if the nonlinear growth of the refractive index saturates for high powers, and thus, stable two-dimensional stationary beams can be obtained [7, 8].

In the present work, we will analyze the dynamical properties of laser beams and pulses propagating through a nonlinear optical material with the following refractive index:

$$n(I) = n_0 + n_2 I - n_4 I^2. \tag{1}$$

Where n_0, n_2 and n_4 are positive constants determining the nonlinear response of the optical material with the intensity (I) of the light beam. This kind of refractive index represents the so-called cubic-quintic optical materials [9, 10, 11, 12, 13, 41] and it can be considered as a Taylor expansion up to I^2 terms of more complicated optical nonlinearities. The above $n(I)$ grows with I for low powers, and diminishes for high powers due to the contribution of the negative $n_4 I^2$ term. A very interesting example of materials which correspond to the previous refractive index are the recently reported nonlinearities of chalcogenide glasses[14], which show an intensity-dependent refractive index that can de fitted by Eq. (1). Our aim in the present paper, will be to show that this change in the sign of the nonlinear response with the intensity, yields to the formation of light condensates with physical properties resembling those of fluids. This light condensates can be obtained as well as continuous or pulsed

beams. Thus, we will use respectively the terms *light streams* or *light drops*, to refer to each case.

We will analyze in first place the propagation along z, in the paraxial regime, of a continuous linearly-polarized laser beam trough a nonlinar optical material with the above refractive index $n(I)$. The dynamics of the envelope of the electromagnetic wave $\Psi(x, y, z)$ is given by a generalized Non Linear Schrdinger Equation (NLSE) of the form[9]:

$$2ikn_0\frac{\partial\Psi}{\partial z} + \nabla_\perp^2\Psi + 2k^2n_0\left(n_2|\Psi|^2 - n_4|\Psi|^4\right)\Psi = 0, \tag{2}$$

where $k = 2\pi/\lambda$ is the wavenumber in vacuum and $\nabla_\perp^2 = \partial^2/\partial x^2 + \partial^2/\partial y^2$ is the transverse Laplacian operator. The previous equation can be interpreted in the light of results obtained for gaseous Bose-Eintein condensates (BEC) where it is called a Gross-Pitaevskii Equation (GPE). In the GPE, the term $\nabla^2\Psi$ represents the kinetic energy that tends to broad the atom gas. The analogous to the optical nonlinearity is the scattering length, which determines whether the interactions between atoms will be attractive (self-focusing) or repulsive (self-defocusing). Thus, a term in the GPE that counteracts the motion of the atoms may be considered as a cooling term. Therefore, coming back to the NLSE, we can conclude that *an optical material with self-focusing nonlinearity acts as a cooling medium for a photon gas.* The key point is that it is neccessary to saturate the growth of the nonlinear shift in order to avoid the collapse of the beam envelope to a singularity. This happens in materials with the cubic-quintic nonlinearity.

Typical values of the above parameters can be chosen to fit usual experimental configurations by taking: $n_0 = 1.8$, $n_2 \approx 2 \cdot 10^{-4} cm^2/GW$ and $n_4 \approx 2 \cdot 10^{-3} cm^4/W^2$, with $\lambda = 1600nm$. Thus, nonlinear effects become significant for values of I in the range of GW/cm^2. The physical picture of the above nonlinearity is evident: for low intensities, propagation remains in a quasi-linear regime. If the power is increased, nonlinear self-focusing tends to counteract diffraction and will overcome it for a critical beam flux. This would yield to blow-up in pure Kerr materials ($n_4 = 0$). However, for high powers, the defocusing effect of the term $n_4 I^2$ will balance collapse, yielding to a stable two-dimensional beam. Thus, for an adequate power, a beam traversing such a nonlinear optical material will yield to a compact state in which light acquires surface tension properties, like droplets of usual liquids.

3. Stationary nodeless states

Before analysing the dynamics of laser beams, it is useful to take a look to the spatial profile of the lowest-order stationary solutions of Eq.

(2), which are nodeless wavefunctions of the form: $\Psi = \psi(r)e^{i\beta z}$, where β is the nonlinear phase shift (propagation constant) and $\Psi(\infty) = 0$. It can be seen in Fig. 1 that the shape and properties of the above states depend crucially on the value of β. To the contrary of linear waveguides (where there is only one fundamental mode with a given β) nonlinear propagation yields to a continuum of nodeless eigenstates. This is evident, as the nonlinear beam generates its own waveguide during propagation. Thus, we have found by numerical integration, the stationary states corresponding to Eq. (2) for increasing values of the nonlinear phase shift, starting from $\beta = 0$. The result is a continuum of stationary states with different shapes and increasing values of the beam power $N = \int |\Psi|^2 dxdy$. Some of these spatial profiles are shown in the insets of Fig. 1.

The form of the stationary solutions of Eq. (2) has been analysed by several authors[15, 16, 17]. It is well known, for instance, that there is a minimum power threshold N_0 to generate a stationary beam. Obviously, this minimum beam flux coincides with the collapse power threshold for a gaussian beam in a bulk Kerr media[18, 19]. We must also point that there is a critical value β_c of the propagation constant for which N diverges. Thus, for $\beta > \beta_c$, no stationary solutions can be obtained. Although there are good analytical approximations for shapes of the previous stationary beams[17], less attention has been paid to investigate the peculiar form of the spatial profiles of Fig. 1 from a physical point of view. Thus, let us try to extract a qualitative picture of the properties of the mentioned stationary beams, by analyzing the changes in the shape of the eigenstates of Eq. (2) for growing values of β.

As it can be appreciated in Fig. 1, low values of the beam flux N (i.e.: $\beta \to 0$) yield to light distributions with quasi-gaussian profiles. Note that the intensity scale in the inset a) is different and thus the corresponding profile is smoother than those in b) and c). As β is incremented, the beam flux grows and the spatial shapes tend to narrow, keeping approximately the gaussian shape and reaches a minimum width and a maximum peak for an intermediate power. For larger values of β, the beam flux grows rapidly and the peak intensity of the light distribution saturates due to the effect of n_4. The light distributions tend to supergaussian profiles and thus, *high power stationary beams yield to wide top flatted profiles ended by sharp decays*. Moreover, as the sharp ends of intense beams are very similar, we can conclude that the shapes of high power beams differ only on the length of the top flat.

Thus, let us reconsider the previous scenario in the light of statistical mechanics of a "photon gas". The situation looks as follows: low powers (i.e.: $\beta \to 0$ quasi-linear regime) yield to smooth gaussian-like spatial

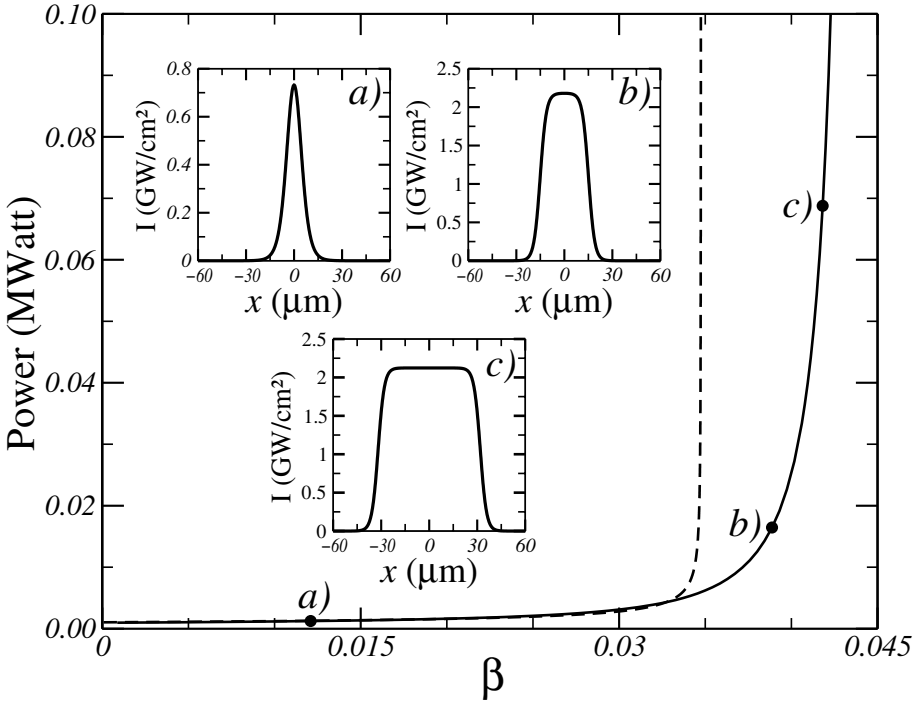

Figure 1. Beam power (N) vs nonlinear phase shift (β)for stationary nodeless states. Solid line: numerical; dashed line: variational. Note that N grows monotonically with β and the gap at $\beta = 0$. Insets: beam shapes corresponding to several powers. Note that the intensity scale in a) is different.

distributions of the "photon gas" and the dominant contribution in Eq. (2) is diffraction ($\nabla^2\psi$) that can be interpreted as a kinetic term (expansion of the photon gas). For stationary beams with higher powers, the Kerr self-focusing term given by n_2, becomes significant and tends to narrow the shape of the light distribution. The beam would collapse for powers over a critical value; however, the defocusing effect of n_4 dominates for high powers and avoids blow-up. The comparison between the low and high power spatial profiles resembles the density distributions of particles inside a gas for low values of N, (smooth quasi-gaussian spatial distribution, representing high delocalization) or a condensed supergaussian shape for high powers (almost constant photon density inside the beam and sharp decay at the boundary). The analogy makes more sense if the nonlinear material is regarded as a "cool region" where the kinetic term $\nabla^2\psi$ of Eq. (2) is balanced by nonlinear effects. Stable "light streams" are formed due to competing effects of diffraction, the Kerr term (n_2) and the self-defocusing nonlinearity (n_4) , in a similar way as Van der Vaals forces form liquid droplets in a gas-liquid condensation. The analogy is more evident in the case of pulsed beams, where "light droplets" will be obtained. We will analyze this case in the last section of the present work.

Thus, if one assumes the previous picture, the following step is to formulate ideal experiments to detect typical properties of liquids in the mentioned liquid light states, like the existence of surface tension properties.

4. Dynamics of collective oscillations

To get a deeper physical insight in the properties of the above light distributions, we have performed a variational analysis of the frequency spectrum of the small amplitude oscillations of slightly perturbed stationary beams. The perturbation can be experimentally implemented with a thin lens, that adds a slight curvature to an input gaussian beam. Thus, we can model the evolution by means of the following trial function:

$$\Psi(r,z) = \psi(z) e^{\left[-\frac{r^2}{2w^2(z)} + ib(z)r^2\right]}, \tag{3}$$

where ψ, w and b are quantities depending on z, corresponding to the peak amplitude, beam width and curvature, respectively. Following the standard variational procedure[42, 15, 16], after minimization of the corresponding Lagrangian density over the set of trial functions from Eq. (3), an ordinary newton-like differential equation is obtained for the above parameter w. These equations can be reformulated in terms of

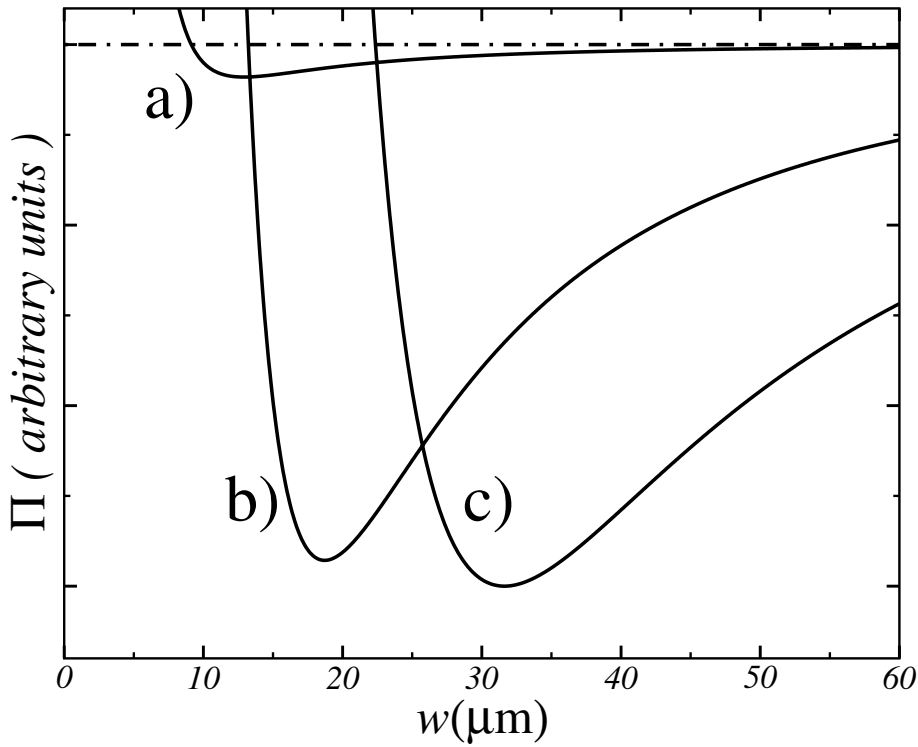

Figure 2. Potential functions given by Eq. 4 of the nodeless states a), b) and c) from Fig. 1 .

effective potentials for equivalent particles in the following form:

$$\Pi = \left(\frac{1}{k^2 n_0^2} - \frac{n_2 N}{2\pi n_0}\right) w^{-2} + \frac{2n_4 N^2}{9\pi^2 n_0} w^{-4}, \tag{4}$$

In Fig. 2, we have plotted the shape of the previous potentials for three different values of the peak power, corresponding to the shapes of the insets in Fig. 1. As it can be seen in the caption, the higher N, the depper Π. The minimum width of the potential is achieved for the b) eigenstate. The widths of the perturbed beams will evolve oscillating around the minimum of Π, as classical particles in potential wells, playing z the role of time. The variational analysis, although not exact, provide the widths of the stationary states w_s, as function of the beam power. They are given as the values of w for which Π is minimum. From a simple inspection of Eq. (4) it is obtained the following value for the width of the beam:

$$w_s^2 = \frac{8n_4}{9n_2} \frac{N^2}{N - N_0},$$

where N_0 is the following critical value for the beam flux:

$$N_0 = \frac{2\pi}{k^2 n_0 n_2}, \tag{5}$$

The value of N is the small gap of the beam power at $\beta = 0$ of Fig. 1. It is straightforward to calculate the minimum width w_m of a stationary beam, which is achieved for $N = 2N_0$ and is given by $w_m = \frac{8}{3k_0 n_2}\sqrt{\frac{\pi n_4}{n_0}}$. For the experimental values given above, it is easily obtained that $w_m \approx 6.4\mu m$, which yields to peak powers in the range of $2GWcm^2$ to generate the stationary states. Thus, the variational model predicts a minimum beam power to generate the stationary states that we calculated above numerically. Obviously, Eq. (5) coincide with the critical collapse threshold for a gaussian beam in a bulk Kerr material [19]. The comparison with direct numerical calculations, as it can be appreciated in Fig. 1, yields to a very good agreement (error below 1%) for low values of β. However, it must be stressed that, as the shape of the stationary states deviates from the gaussian profile, the fit of the theoretical and the numerical curves is only qualitative.

In second place, notice that expanding Π around its minimum, it is possible to obtain the frequencies ν of small amplitude oscillations along z of perturbed stationary states, as functions of the main parameters involved. To get a more physical view of the light condensates, it is interesting to consider ν as a measure of the "rigidity" of the different stationary states. After a trivial Taylor expansion around the minimum of Π, it is obtained:

$$\nu = \frac{9\pi}{4\sqrt{2}k^3 n_0^2 n_4} \frac{\left(\frac{N}{N_0} - 1\right)^{\frac{3}{2}}}{N^2}, \tag{6}$$

As it can be seen in Fig. 3, the variational analysis reveals that a maximum rigidity of the light condensate is achieved for a given value of N (or equivalently β). The critical value of N corresponding to the maximum frequency can be easily calculated by taking $d\nu/dN = 0$, and is given by:

$$N_{cr} = \frac{8\pi}{k^2 n_0 n_2} = 4N_0, \tag{7}$$

In Fig.3, we can observe that the variational method has only a qualitative agreement with the numerical (solid line) calculation. From the shape of the cuves, we can argue that N_{cr} is the critical value over which the surface tension properties of the light beams appear. The reason is that the maximum in the frequency ν_{max} acts as a gap for the excitation

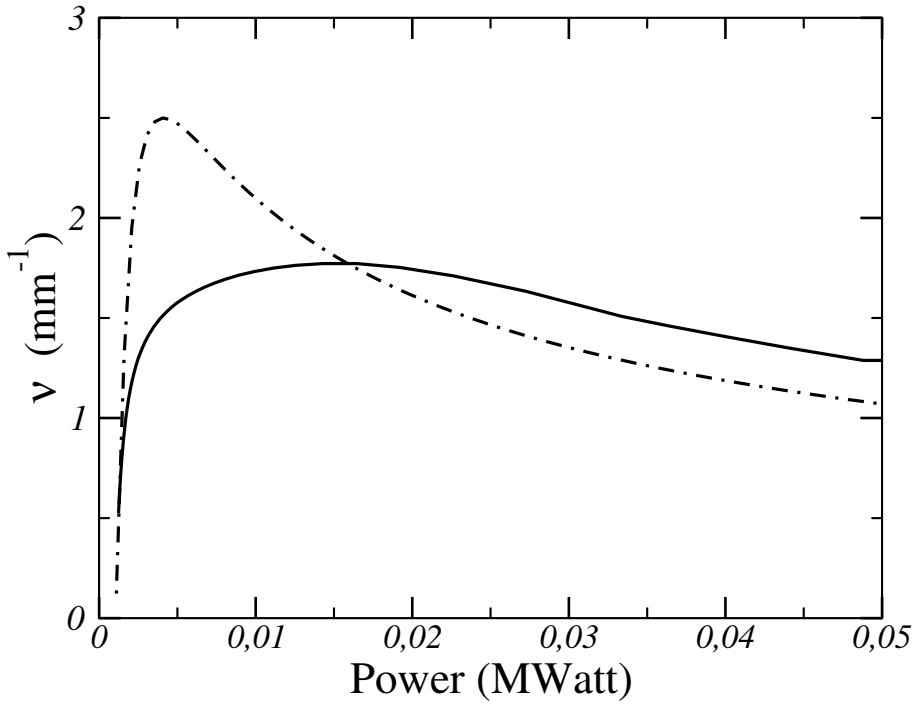

Figure 3. Resonance frequencies (ν) of the nodeless states as a function of the beam power. Dashed (solid) lines correspond to variational (numerical) calculations, as given by Eq. (6).

of linear waves from the stationary state, and thus radiation is blocked for beams with $\nu > \nu_{max}$.

5. Collisional dynamics

In the present section we analyse numerically, the propagation of a light condensates through a bulk cubic-quintic nonlinear optical material in the presence of boundary conditions and localized inhomogeneities (holes). The propagation equation for the above waveguide in the paraxial regime is a generalized NLSE, including the effect of boundaries or holes. The experimental parameters are in the same range as in the previous sections.

Our computer simulations show that there is a deep analogy between incompressible fluid dynamics and interference behavior of light condensates at boundaries and localized discontinuities. This can be understood thinking of light condensates as having some kind of "surface tension", analogous to that of a liquid droplet. Considering that diffraction in

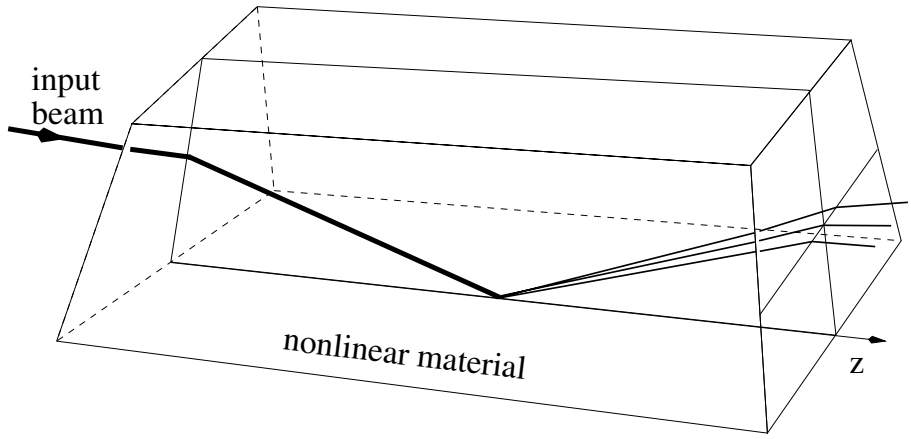

Figure 4. Sketch of the numerical simulation of Fig. 5, showing total reflection at a nonlinear-linear interface.

the NLSE plays the role of a kinetic energy term, a Kerr-like material can be regarded as a "cold medium" that tends to compress the photon gas (i.e.: beam self-focusing). From this point of view, when collapse is stopped due to quintic defocusing terms, the situation is similar to droplet condensation due to Van der Vaals forces.

As in the case of liquids, one can expect surface tension properties from the resulting light condensates. To show this, we present two particular cases from our numerical investigation. Both simulations correspond to a radial stationary fundamental state of the propagation equation. The beam is $25\mu m$ width and its peak intensity is $2.0GW/cm^2$. The numerical simulations has been performed with standard Fourier beam propagation method in a 1024 points grid. In Fig. 4, we show a sketch of the numerical calculations of Fig. 5, where we have simulated internal reflection inside a bulk cubic-quintic material surrounded by air. The interference pattern when the beam reaches the boundary, clearly resembles crushing of a liquid drop thrown towards a solid wall which splits into smaller droplets. We have performed large series of numerical explorations for different angles of incidence, from quasi-elastic to complete inelastic range. Showing that surface tension effect provides the beam a high stability.

In Fig. 6 we have plotted a collision with a $8\mu m$ air hole immersed in the bulk nonlinear material. The role of the surface tension is evident: the beam is strangulated when it intersects the hole. However, it recovers its original form if the angle of incidence is below a critical value. Both simulations show that light condensates behave against collisonal perturbations in a similar fashion as liquids. The raising of surface

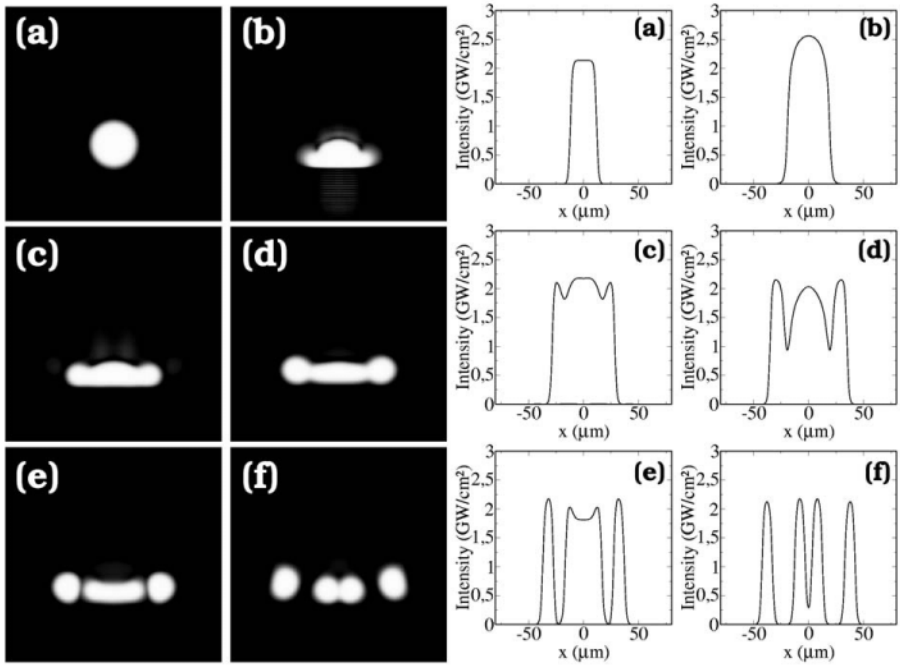

Figure 5. Numerical simulation corresponding to the sketch of 4. Left: grascale images of the transverse xy plane for a) $z = -10$, b) $z = 0$, c) $z = 10$, e) $z = 20$ and f) $z = 40$ (in μm). Right: Maximum intensity profiles along the x axis corresponding to the left images. The scale of the x axis is the same in all the pictures.

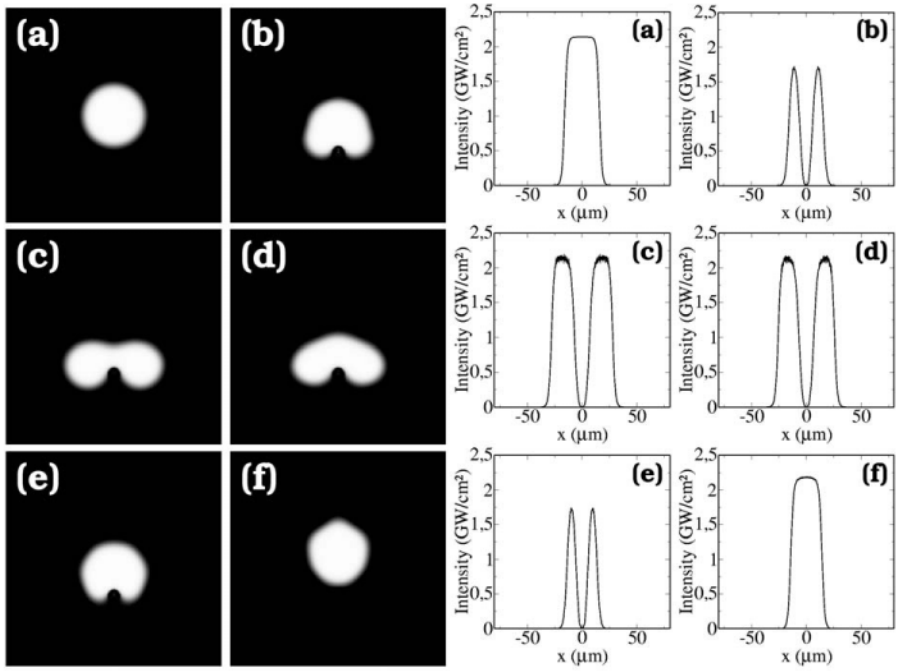

Figure 6. The same as Fig.5 for total reflection at an $8\mu m$ air hole.

tension properties can be qualitatively explained as a balance between the radiation pressure inside and outside the beam. Inside the beam, the refractive index is greater than outside, due to the nonlinear effects. However, a detailed understanding of the phenomenon should start from a thermodynamical point of view, defining quantitative concepts as the temperature and entropy of the beams for a given nonlinearity. This is a deep problem that we address to further research.

6. Pulsed Beams

If the beam is pulsed, time must be included in the simulations. Thus, an extra second derivative with respect to "proper time" should be added to Eq. (2) in order to take into account the effect of second-order dispersion. The corresponding NLSE, becomes 1+3 dimensional, and extra difficulties are added to the numerical simulations. Not only the increase in the length of the calculations is an inconvenient but also the representation of the data obtained. The need for analytical tools as the variational model is more evident in this case.

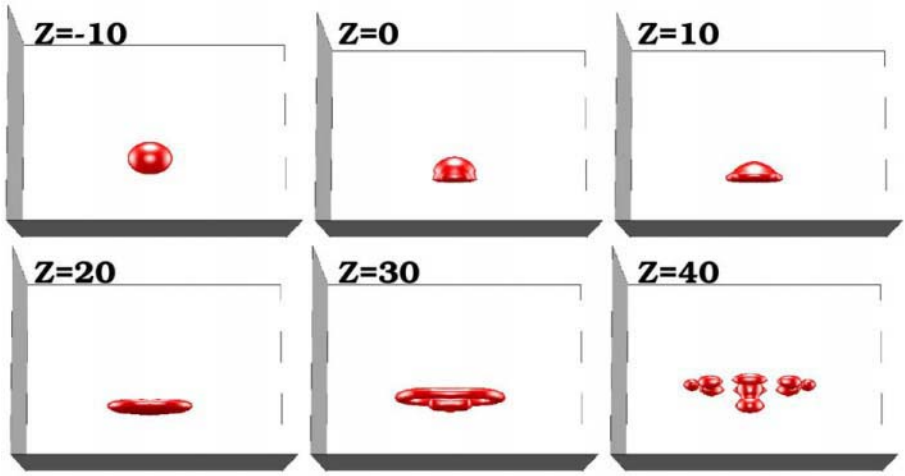

Figure 7. Numerical simulation of the collision of a light drop against a planar boundary (not visible in the graphs). The values of z in each picture are the distances from the center of the pulse to the origin of coordinates. The paper plane is xy and z is perpendicular to the paper plane. The experimental parameters are given in the text.

Thus, taking into account the data obtained for the 2-dimensional case of laser beams, we will analyze the properties of pulsed beams, which propagate in cubic-quintic materials, corresponding to the same material parameters of Fig. 5. The result is plotted in Fig. 7, where it can be seen that the effect of the planar boundary between the non-linear and the linear material (not shown in the captions) is to generate a corona of droplets in a similar fashion as it happens in the crushing of a liquid drop. In fact, the dominant effect in the generation of smaller pulses at the boundary is modulational instability[8, 20] around the rings formed by diffraction.

We must notice the deep connection of this case with the dynamics of Bose-Einstein Condensates (BEC) in alkalii gases. In fact, the collective dynamics of a BEC in the absence of a trapping potential, is given by a NLSE. If three-body elastic interactions are present, the equation for the coherent cloud includes a quintic nonlinear term as in Eq. (2). Thus, it is evident that similar behaviour as shown in Fig. 7 could be expected for BECs with the adequate experimental configuration. In fact, the possibility of gas-liquid phase transitions in Bose Eintein condensates has been recently put forward by several authors[21].

7. Light whirlpools

In wave mechanics, a vortex is a screw phase dislocation, or defect [22] where the amplitude of the field vanishes. The phase around the singularity has an integer number of windings, l, which plays the role of an angular momentum. For fields with non-vanishing boundary conditions, this number is a conserved quantity and governs the interactions between vortices as if they were endowed with electrostatic charges [23]. Thus, l is usually called the "topological charge" of the defect.

Vortices are present in very different branches of physics like fluid mechanics, superconductivity, Bose-Einstein condensation, astrophysics or laser dynamics, among others [24]. In optics, a vortex with charge l takes the form of a black spot surrounded by a light distribution. Around the dark hole, the phase varies from zero to $2l\pi$. This defects appear spontaneously in light propagation through turbulent media and can also be produced by appropriately shining a computer generated hologram [25, 26]. The trace of vortices in a light field is a characteristic "fork-pattern" interferogram produced by superposition with a tilted planar wave. The first experimental works on optical wavefront dislocations were carried out in the 80's, in the context of adaptive systems, where phase singularities were a severe problem for image reconstruction techniques [27, 28]. Since then, they have been studied, among other fields, in optical tweezing [29], particle trapping [30], laser cavities [31], optical interconnectors [32] or even to perform N-bit quantum computers [33].

Concerning light vortices in the nonlinear regime [34], the first theoretical works analysed their stability in Gaussian-like distributions propagating in optical Kerr materials [35]. It was found for a cubic self-focusing refractive index, that a beam of finite size will always filament under the action of a phase dislocation. This also stands for saturable self-focusing nonlinearities. On the other hand, vortex states were predicted and found experimentally for self-defocussing materials both in the Kerr case for continuous background [37] and in the saturable case with finite size beams [39].

It was shown in [15, 38] that stable vortex states with $l = 1$ can be obtained as stationary states of the propagation of a laser beam through cubic-quintic optical materials[9]. This kind of nonlinearity is characterized by the $\chi^{(3)} > 0$ and $\chi^{(5)} < 0$ components of the nonlinear optical susceptibility and changes from self-focusing to self-defocussing at a given intensity[40]. It has been recently shown that a gas-liquid phase transition takes place in light beams propagating in this type of materials[41].

In the next sections we will show that stable vortex states with arbitrary value of the angular momentum exist and its peak amplitude and propagation constant tend asymptotically to values that do not depend on l as the beam flux is increased.

8. Azimuthal eigenstates

For Eq. (2) we have calculated the azimuthal stationary states of the form: $\Psi(r,\theta,z) = \psi(r)e^{i(\beta z + l\theta)}$. The quantity β is the nonlinear phase shift or propagation constant. For a given integer value of l, a continuum of eigenstates can be obtained with β varying between zero and a critical value β_{cr} over which no stationary states can be found[15]. The profiles of the eigenstates for several values of l and β are plotted in Fig. 8. We particularly show states with $l = 3$ and $l = 4$ since these are the first values of l for which all the eigenstates were previously found unstable, as well as two examples of huge angular momentum states ($l = 10$ and $l = 50$). It can be appreciated in the graphs that values of β below $0.5\beta_{cr}$ yield to light distributions with smooth and wide Gaussian-like shapes. As β is incremented, the beam flux grows and the spatial profiles narrow, yielding to a minimum thickness of the ring of the stationary state, for values of β around $0.8\beta_{cr}$ keeping approximately the Gaussian shape. For larger values of β, the beam flux grows rapidly with β and the peak amplitude of the light distribution saturates due to the effect of n_4, reaching asymptotically the value A_{cr}, which is slightly below the maximum amplitude. Thus, high power beams show spatial light distributions with flatted tops in their profiles, similar to those of hyper-Gaussian functions[17] as in the case of nodeless beams.

It also worths to mention that the central hole increases its size with the topological charge, as it can be seen comparing the profiles for $l = 3, 4$ with $l = 10$, 50. However, as the value of β approaches a critical value, the thickness of the external ring grows faster than the internal hole and thus, the final result takes always the asymptotic form of a dark spot surrounded by a larger ring of light of almost constant shape which ends abruptly at a given radius. Close to the origin the profiles follow the linear regime with $\psi \propto r^l$.

Another intriguing fact is that both β_{cr} and A_{cr} do not depend on the value of the topological charge. This is shown in Fig. 9, where the peak value of the intensity has been plotted as a function of β. As it can be appreciated, whatever the value of l all the curves join at the same point. In the inset, it can be seen a detail of the critical zone. This means that the critical value of the propagation constant only depends on the nonlinearity and not on the value of l. Thus, we can deduce

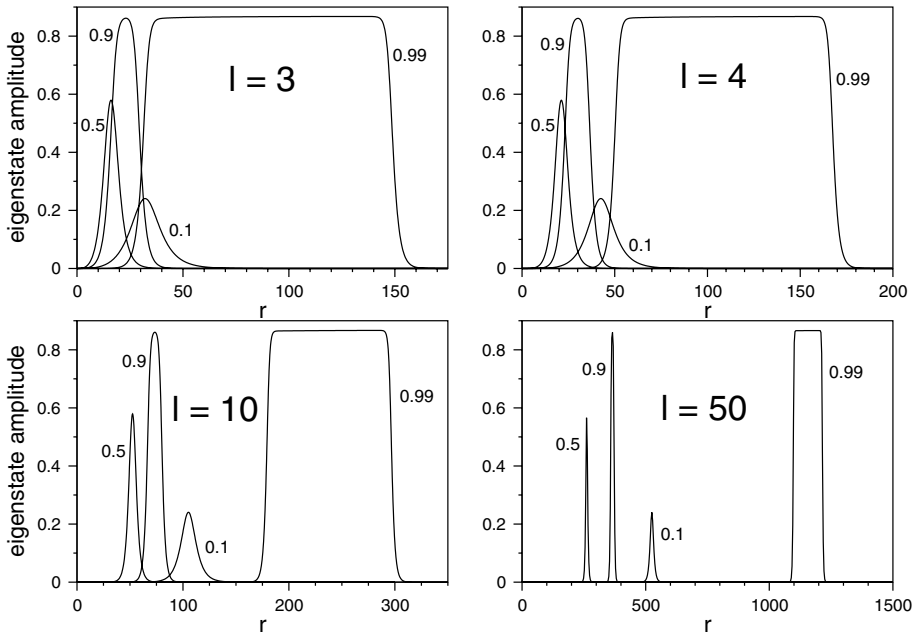

Figure 8. Numerically calculated radial amplitude profiles of the stationary azimuthal states of Eq. (2) for $l = 3, 4, 10$ and 50 with β/β_{cr}=0.1, 0.5, 0.9 and 0.99. We have used a relaxation method and a normalised equation with $n_2 = n_4 = k = 1$, $n_0 = 1/2$.

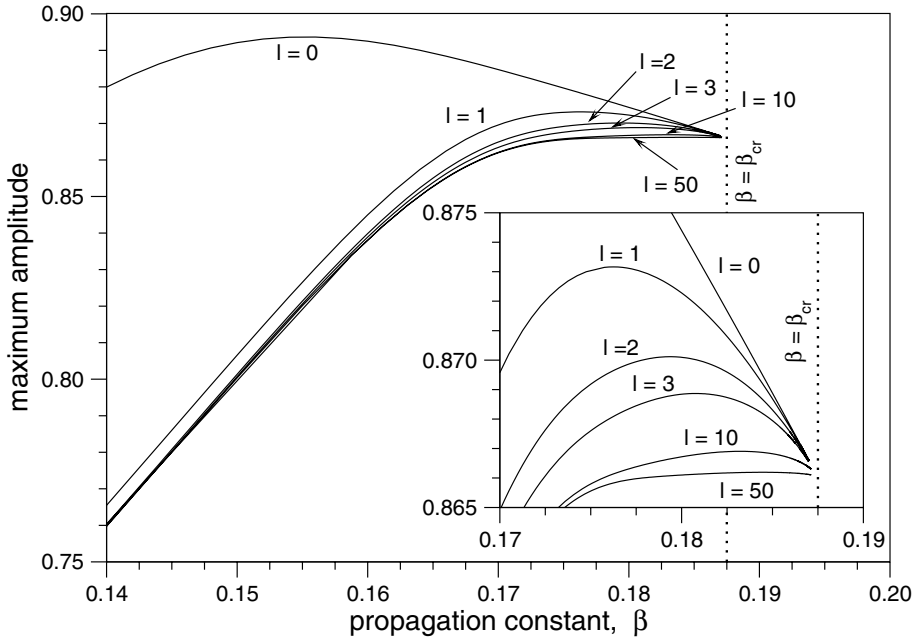

Figure 9. Eigenstates maximum amplitude vs propagation constant for angular momenta l=0, 1, 2, 3, 10 and 50. All the curves join at the point $A = A_{cr} = 0.866$, $\beta = \beta_{cr} = 0.1875$. Inset: detail of the zone close to β_{cr} where the calculations become delicate. The normalisation is the same as in Fig. 8.

that spinning solitons are composite objects: one part is the top-flatted background and the other is the vortex core.

To explain the properties of the above light distributions, we have performed a variational analysis[17] by means of the square-like trial function:

$$\Psi_v(r, \theta, z) = \psi_v(r) \exp[i(\beta z + l\theta)],$$

where $|\psi_v|^2$ takes the constant value $|A|^2$ inside the interval $[(r_0 - w/2), (r_0 + w/2)]$, and zero elsewhere, being w the mean radius of the light ring. As it can be appreciated by comparison with Fig. (8), this square-shaped function is very adequate for the region close to β_{cr}, where the profiles of the stationary states become almost square. Using this trial function and performing the usual average[42] over the lagrangian density associated to Eq.(2), the following relationships are obtained[15]:

$$\beta = k \left(\frac{n_2}{2} |A|^2 - \frac{n_4}{3} |A|^4 \right); \tag{8}$$

$$\left[\beta - k\left(n_2|A|^2 - n_4|A|^4\right)\right] = \frac{l^2}{kn_0}\left(\frac{w^2}{6} + 2r_0^2\right)^{-1}, \tag{9}$$

and thus, in the limit $w, r_0 \to \infty$ the last term of the above equation vanishes and it is obtained the critial value of the amplitude A_{cr}:

$$|A_{cr}|^2 = \frac{3}{4}\frac{n_2}{n_4}, \tag{10}$$

corresponding to $\beta = \beta_{cr} = 3kn_2^2/16n_4$. The comparison of these analytical results with the numerical calculations shows an excellent agreement. Taking the normalised form of Eq. (2), making $n_2 = n_4 = k = 1$ and $n_0 = 1/2$, it is obtained that $\beta_{cr} = 0.1875$ and $A_{cr} = 0.866$, which are exactly the values obtained numerically, as it can be seen in the inset of Fig. (9). This good result is due to the choice of the trial function, which fits very accurately with the exact numerical solution for values close to the critical point.

9. Stability analysis of the azimuthal eigenstates

In order to test the stability of the stationary states, we calculated the growth rates of small azimuthal perturbations to find out the value of β at which they vanish. Additionally, in order to asses the accuracy of the previous analysis, we propagated some eigenstates with a split-step Fourier method and measured the distances at which the unstable states split. The inverse of these values should coincide, except for a constant scale factor, with the dominant perturbation eigenvalues calculated in the azimuthal instability analysis. Finally, we have also simulated other kind of perturbations like total reflection at the boundary between a cubic-quintic material and air. As we will see below, the eigenstates show robust behaviour against these collisions and preserve their angular momentum although strong oscillations are observed.

To carry out the perturbation analysis we add to the original eigenstate a small p-order azimuthal perturbation function[43]:

$$\Psi(r,\theta,z) = [\psi(r) + f(r)e^{\delta_p z + ip\theta} + h(r)e^{\delta_p^* z - ip\theta}]e^{i(l\theta+\beta z)}, \tag{11}$$

where $f(r) = f_1(r) + if_2(r)$ and $h(r) = h_1(r) + ih_2(r)$ are the complex components of the eigenstate of the p-order azimuthal perturbation and δ_p is the corresponding perturbation eigenvalue. In this way, the real part of δ_p constitutes the growth rate of this perturbation. Substitution of this perturbed eigenstate in Eq. (2) leads to the following set of coupled differential equations:

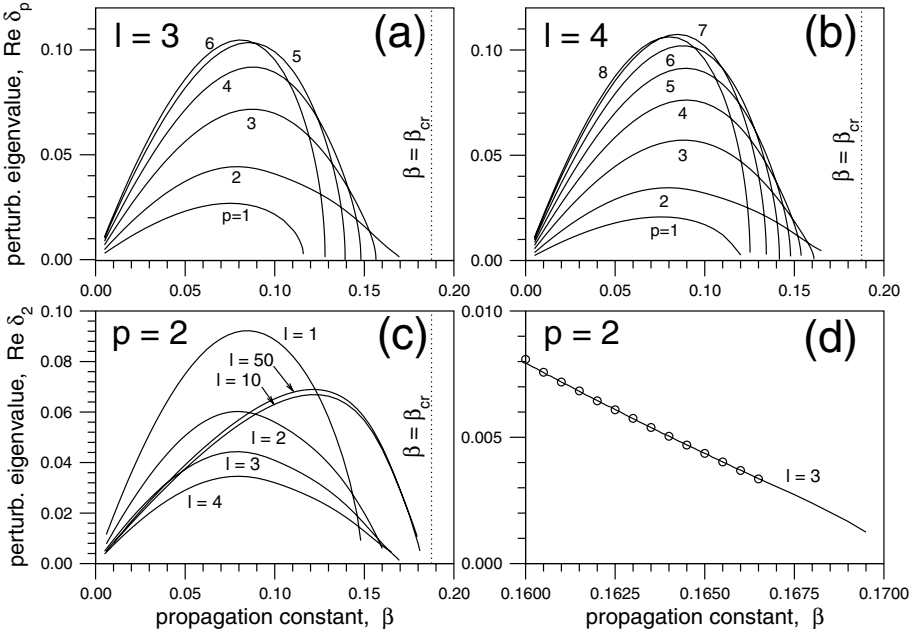

Figure 10. Growth rate of the azimuthal perturbation vs β. In (a) and (b), the angular momentun is fixed (l=3 for (a), l =4 for (b)) and the values of the perturbation order p are indicated by labels near the curves. In (c) the growth rate for the perturbations with p=2 for l=1, 2, 3, 4, 10 and 50 are plotted. In (d), a comparison between the inverse of the splitting distance (dots) and $p = 2$ perturbation eigenvalue for unstable states with $l = 3$ is shown.

$$i\delta_p f + \nabla^2_{rr} f - \frac{(l+p)^2}{r^2} f + Q(\psi) f + R(\psi) h^* = 0 \tag{12a}$$

$$i\delta_p h + \nabla^2_{rr} h - \frac{(l-p)^2}{r^2} h + Q(\psi) h + R(\psi) f^* = 0, \tag{12b}$$

where $\nabla^2_{rr} \equiv \partial^2/\partial r^2 + (1/r)\partial/\partial r$, $Q(\psi) \equiv -\beta + (2 - 3|\psi|^2)|\psi|^2$ and $R(\psi) \equiv (1 - 2|\psi|^2)|\psi|^2$. The solution of this equation system using a Crank-Nicolson propagation scheme [43] yields to the growth rates for different order perturbations versus propagation constant.

The results are illustrated in Fig. (10). Figs. 10(a)-(b) show the growth rates for vortices with angular momentum $l = 3$ and $l = 4$. The maximum growth rate corresponds to perturbation eigenvalues with $p \approx 2l$, while perturbation $l = 2$ has been proved to be the most persistent (the one which remains till highest values of β before vanishing) despite the value of the angular momentum. Hence, in Fig. 10(c) we plot the curve associated to this perturbation for different values of the angular

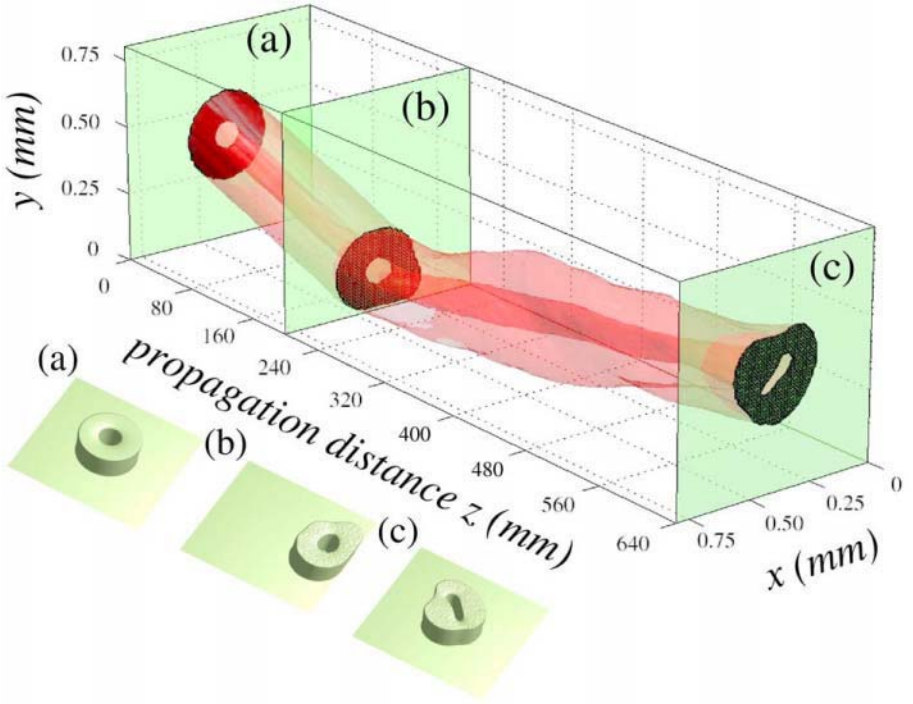

Figure 11. Numerical simulation of the total reflection at a planar boundary of an eigenstate with angular momentum l =4 and $\beta = 0.95\beta_{cr}$. The top image is the isosurface of the beam trayectory. The boundary between the nonlinear material and air is the plane $y = 0$. The images (a)-(c) correspond to intensity profiles of the beam cross section at different points.

momentum, including such high momentum cases as $l = 10$ and $l = 50$. As it is appreciated in these plots, there exists a window between the vanishing point and the limit value for β ($\beta = \beta_{cr}$) which proves the existence of a stability zone close to the critical point. This window narrows for high values of l but it remains finite. As l increases, the point at which the perturbation vanishes tends asymptotically to a value below the critical point. Therefore, whatever the value of l, there always exist a stability window containing an infinite number of stable eigenstates.

We have to stress that close to β_{cr} the azimuthal analysis turns itself very delicate and it has to be carried out in a careful way. In fact, convergence takes a much longer distance and an erroneous final result is obtained if the number of samples and the propagation step are not chosen appropriately. In this sense, combining the analysis with direct calculations of the splitting distance of the unstable eigenstates is definitively useful. In Fig. 10(d) it is zoomed the region of 10(c) where the

perturbation for $l = 3$ drops to zero. They are also plotted the points obtained propagating the eigenstates and taking the inverse of the distance where they split. These values were subsequently scaled by the same constant value to compare with the perturbation eigenvalue curve. It is appreciated that the values obtained from this propagation experiments fall to zero with the same slope as the perturbation eigenvalues do. When the stability analysis is not perform with enough accuracy a more steady behaviour of the curve appears, so that the eigenvalue falls to zero at a higher value of β. In this way, the validity of the perturbation analysis can be assessed.

As a final test of the stability of the eigenstates, we have simulated the total reflection at a planar boundary between a cubic-quintic material and air of beams with different angular momenta as it was done in section 5. For the simulation we have used a split-step Fourier method with a 512×512grid.

As it can be seen in Fig. 11, a beam with $l = 4$ does not split after the total reflection, although a strong oscillation is observed. This is another proof of the stability of these nonlinear waves. We must notice that depending on the incidence angle, a strong deformation of the beam can be induced, which can yield to a split or a decay of the inner vortex into several defects with lower charges.

10. Vortices in pulsed beams

Light whirpools can be induced in pulsed beams as well as in the continuous beams that we have previously studied. From the experimental point of view, it is more interesting to study the possibility of exciting these azimuthal beams starting with pulsed gaussian distributions under adequate conditions.

In Fig.12 we show the numerical simulation of the time evolution of two different light distributions propagating through an optical material with $n_0 = 1.8$, $n_2 = 2 \cdot 10^{-4} cm^2/GW$ and $n_4 = 0.8 \cdot 10^{-3} cm^4/GW^2$. The top-left image a) shows an initial condition consisting on three pulses (i.e.: light droplets) of $100\mu m$ diameter with $\lambda = 1.964nm$ and $I = 1.6GW/cm^2$ that are located at the vertices of a equilateral triangle. The beams are $2\pi/3$ out of phase. With this initial condition it can be seen that the pulses coalesce into a spiral structure b) which finally yields to the asymptotic rotating state c) with a nested vortex with topological charge $l = 1$. The second series of images d) to f) show the direct excitation inside a light droplet of a doubly-charged vortex, with two windings of the phase around the central hole. The experimental parameters are the same as in the previous case, despite the beam width is now $30\mu m$ and $I = 1.4GW$. The images have been rescaled for a better

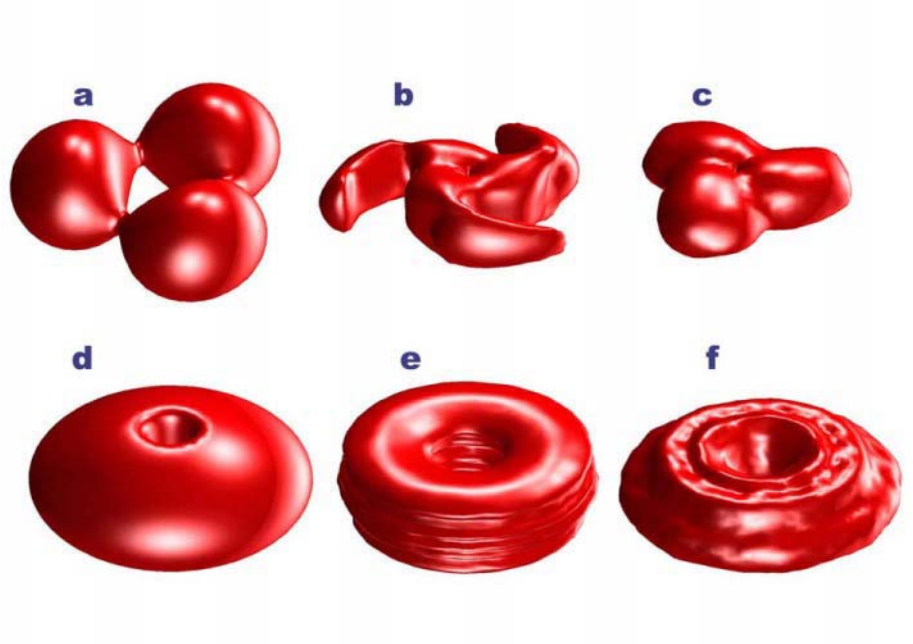

Figure 12. Top: the image a) shows an initial condition consisting on three pulses of $100\mu m$ diameter with $\lambda = 1.964nm$ located at the vertices of a equilateral triangle. The beams are $2\pi/3$ out of phase. The pulses coalesce into a spiral structure b) which finally yields to the asymptotic rotating state c) with a nested vortex with topological charge $l = 1$. Bottom: Evolution of the initial state d) consisting of a gaussian beam which is launched to a holographic phase mask with $l = 2$. After strong oscillations and formation of characteristic surface ripples in e), the beam tends to an asymptotic state with a nested "breathing hole" with topological charge $l = 2$, which is stable over many diffractive lengths. In both examples the material parameters and intensities are the same as for the continuous case.

ilustration. The azimuthal phase can be experimentally implemented with an adequate phase mask. As it can be seen, after strong oscillations and formation of characteristic surface ripples in e), the beam tends to an asymptotic state with a nested "breathing hole" with topological charge $l = 2$, which is stable over many diffractive lengths.

11. Conclusions

We have described the phenomenon of light condensation in nonlinear optical materials with cubic-quintic (C-Q) nonlinearity. To support the analogy between light condensates and quantum liquids, we have tested the surface tension properties of "light streams" and "light drops" by simulating collisions against planar boundaries and localized inhomo-

geneities. We have also shown the existence of a new kind of physical objects: stable azimuthal finite-size beams with arbitrary (integer) angular momentum that can exist in C-Q nonlinear optical materials. The shapes of these beams tend asymptotically to square-like ring profiles with bigger dark holes for higher values of the angular momentum. The critical values of the propagation constant and amplitude do not depend on the angular momentum of the beam. We have also studied the excitation of vortex states in this kind of nonlinear optical materials starting from gaussian beams with an adequate phase distribution. Our predictions open interesting questions about the nature and properties of what we have named "liquid light": a new state of matter-energy formed by nonlinear waves.

Acknowledgments

H. Michinel is partially supported by Ministerio de Ciencia y Tecnologia under grant TIC-2000-1105-C03-01.

References

[1] J. Stachel,(1998) *Einstein's miraculous year: five papers that changed the face of Physics,* Princeton University Press, Princeton.

[2] A. W. Snyder and D. J. Mitchell, "Accesible solitons", Science **276**, 1538-1547 (1997).

[3] G. I. Stegeman and M. Segev, "Optical spatial solitons and their interactions: universality and diversity", Science **286**, 1518-1521 (1999).

[4] *Optical Solitons: Theoretical Challenges and Industrial Perspectives,* edited by V. E. Zakharov and S. Wabnitz (1999). Springer Verlag, Berlin.

[5] *Wave Collapse*, edited by E. Kutnetsov, A. Zakharov, and E. Vladimir (1999) World Scientific, Singapore.

[6] C. Sulem and P. L. Sulem.(1999) *The Nonlinear Schrdinger Equation: Self-Focusing and Wave Collapse*, Springer Verlag, Berlin.

[7] Y. Silberberg, "Collapse of optical pulses", Opt. Lett. **15**, 1282-1285 (1990).

[8] N. N. Akhmediev, D. R. Heatley, G. I. Stegeman, and E. M. Wright, "Pseudorecurrence in two-dimensional modulation instability with a saturable self-focusing nonlinearity", Phys. Rev. Lett **65**, 1423-1426 (1990).

[9] A. H. Piekara, J. S. Moore, and M. S. Feld, "Analysis of self-trapping using the wave equation with high-order nonlinear electric permitivity", Phys. Rev. A **9**, 1403-1407 (1974).

[10] D. E. Edmundson and R. H. Enns, Phys. Rev. A **51**, 2491 (1995).

[11] C. Josserand and S. Rica, "Coalescence and droplets in the subcritical nonlinear Schrdinger equation", Phys. Rev. Lett. **78**, 1215-1218 (1997).

[12] R. McLeod, K. Wagner, and S. Blair, "(3+1)-dimensional optical soliton dragging logic", Phys. Rev. A **52**, 3254-3278 (1995).

[13] Z. Jovanoski, "Light bullet formation in a cubic-quintic nonlinear medium", J. Mod. Opt. **48**, 865-875

[14] F. Smektala, C. Quemard, V. Couderc, and A. Barthelemy, "Non-linear optical properties of chalcogenide glasses measured by Z-scan", J. Non-Cryst. Sol. **274**, 232-237 (2000).

[15] M. Quiroga-Teixeiro and H. Michinel, "Stable azymuthal stationary state in quintic nonlinear optical media", J. Opt. Soc. Am. B **14**, 2004-2009 (1997).

[16] M. Quiroga-Teixeiro, A. Berntson, and H. Michinel, "Internal dynamics of nonlinear beams in their groun states: short and long-lived excitation", J. Opt. Soc. Am. B **16**, 1697-1704 (1999).

[17] K. Dimitrievski, E. Reimhult, E. Svensson, A. hgren, D. Anderson, A. Berntson, M. Lisak, and M. L. Quiroga-Teixeiro, "Analysis of stable self-trapping of laser beams in cubic-quintic nonlinear media", Phys. Lett. A **248**, 369-376 (1998).

[18] V. I. Bespalov and V. I. Talanov, "Filamentary structure of light beams in nonlinear liquids"ZhETF Pis'ma **3**, 471-476 (1966).

[19] A. J. Campillo, S. L. Shapiro, and B. R. Suydam "Periodic breakup of optical beams due to self-focusing", Phys. Rev. Lett **23**,628-630 (1973).

[20] N. B. Abraham and W. J. Firth, "Overview of transverse effects in nonlinear-optical systems", J. Opt. Soc. Am. B **7**, 951-62 (1990).

[21] A. Gammal, T. Frederico, L. Tomio, and P. Chomaz, "Liquid-gas phase transition in Bose-Einstein condensates with time evolution", Phys. Rev. A **61**, 1602-1606 (2000)

[22] J. F. Nye and M. V. Berry, Proc. R. Soc. London A **336,** 165-190 (1974).

[23] D. Rozas, Z. S. Sacks, Jr G. Swartzlander *Phys. Rev. Lett.* **79**, 3399 (1997).

[24] L. Pismen, *Vortices in nonlinear fields*, (Oxford University Press, London, 1999).

[25] N. R. Heckenberg, R. McDuff, C. P. Smith, and A. G. White, Opt. Lett. **17**, 221-223 (1992).

[26] G. Indebetouw, J. Mod. Optics **40** 73 (1993).

[27] N. B. Baranova, B. Ya. Zel'dovich, A. V. Mamaev, N. F. Pilipetslii, and V. V. Shkukov, Pis'ma Zh. Eksp. Teor. Fiz. **33**, 206-209 (1981) [JETP Lett. **33**, 195 (1981)].

[28] N. B. Baranova, A. V. Mamaev, N. P. Pilipetskii, V. V. Shkukov, and B. Ya. Zel'dovich, J. Opt. Soc. Am. **73**, 525-528 (1983).

[29] N. B. Simpson, K. Dholakia, L. Allen, and M. J. Padgett, Opt. Lett **22**, 52-54 (1997).

[30] K. T. Gahagan and G. A. Swartzlander, Jr. , Opt. Lett. **21**, 827 (1996).

[31] C. O. Weiss, M. Vaupel, K. Staliunas, G. Slekys, and V. B Taranenko, Appl. Phys. B **68**, 151-168 (1999).

[32] J. Scheuer and M. Orenstein, Science **285**, 230-233 (1999).

[33] A. Mair, A. Vaziri, G. Weihs and A. Zeilinger, Nature **412**, 313-316 (2001).

[34] Yu. S. Kivshar and E. Ostrovskaia, Opt. Photon. News **12**, 24-28 (2001).

[35] V. I. Kruglov and V. M. Volkov, Phys. Lett. A **111**, 401-404 (1985).

[36] W. J. Firth and A. J. Scroggie 1996 *Phys. Rev. Lett.* **76** 1623.

[37] G. A. Swartzlander, Jr. and C. T. Law, Phys. Rev. Lett. **69**, 2503-2506 (1992).

[38] D. Mihalache, D. Mazilu, L.-C. Crasovan, I. Towers, A. V. Buryak, B. A. Malomed, L. Torner, J. P. Torres and F. Lederer, Phys. Rev. Lett. **88**, 073902-1-4 (2002).

[39] V. Tikhonenko and N. Akhmediev, Opt. Commun. **126**, 108-112 (1996).

[40] G. Fang, Y. Mo, Y. Song, Y. Wang, C. Li, and L. Song, Opt. Commun. **205**, 337-341 (2002).

[41] H. Michinel, J. Campo-Taboas, R. Garcia-Fernandez, J. R. Salgueiro, and M. Quiroga-Teixeiro, Phys. Rev. E **65**, 066604-1-7 (2002).

[42] D. Anderson, "Variational approach to nonlinear pulse propagation in optical fibers", Phys. Rev. A **27**, 3135 (1983).

[43] J. M. Soto-Crespo, D. R. Heatley, E. M. Wright, and N. N. Akhmediev, "Stability of the higher-bound states in a saturable self-focusing medium", Phys. Rev. A **44**, 636-644 (1991).

OPTICAL PULSE EVOLUTION TOWARD LIGHT BULLET AND VORTEX SOLUTION

Vladimir Skarka, Najdan B. Aleksic, and Vazha I. Berezhiani
Laboratoire POMA, UMR 6136 CNRS Universite d'Angers, 49045 Angers, France

Abstract The dynamics of a laser pulse, either with or without phase singularity in media with cubic-quintic nonlinearity, is studied. The stability and the robustness of light bullets predicted by variational approach are confirmed by numerical simulations. Singular beam reaching equilibrium with the power larger than the breaking one, becomes vortex soliton, otherwise it breaks into two filaments running away tangentially. Far from equilibrium pulses with large width may, due to the modulation instability, break into many filaments coalescing and splitting subsequently.

1. Introduction

There is a growing interest for spatiotemporal solitons, characterized by a balance of diffraction and dispersion with respectively nonlinear spatial and temporal self-focusing. Due to their exceptional robustness and their low energy, spatiotemporal solitons, so-called light bullets, appear to be an excellent candidate for carrying the information that has to be treated in all-optical logic circuits. The dynamics of such localized structures is governed by a $(D+1)$-dimensional nonlinear Schrödinger equation (NSE). It turns out that these solitons are unstable for cubic nonlinearity in case of higher transverse dimensions ($D = 2, 3$). However, NSE with the nonlinearity saturation admits multi-dimensional ($D = 2, 3$) soliton solutions that are stable for infinitely small perturbations [1]. Only recently it was shown numerically that under well defined conditions the multidimensional solitons are stable even for large perturbations; their dynamics resemble the ones of soliton solutions in integrable systems [2, 3]. Taking into account that some of materials currently used in optical systems exhibit weak saturation effects, their nonlinearity can be approximated with good accuracy by cubic-quintic model.

F. Kh. Abdullaev and V. V. Konotop (eds.), Nonlinear Waves: Classical and Quantum Aspects, 353–359.

Recent measurements show that the polydiacetylene *para*-toluene sulfonate (PTS) exhibits such a saturating nonlinearity with large nonlinear index of refraction [4]. This kind of nonlinearity has been widely applied in different domains of research not only in nonlinear optics but also in plasma physics as well as in the context of Bose super-fluid [5]. Recently an important development has occurred in the field of nonlinear optics concerning optical vortex solitons (OVS) [6]. These solitons in self-defocusing media are stationary beam structures with phase singularity and nonzero angular momentum proportional to an integer m defined as topological charge. An OVS is a dark spot, i.e., a zero intensity center surrounded by a bright infinite background. Self-focusing media support localized optical vortex solitons (LOVS) with phase dislocation surrounded by one or many bright rings. LOVS are unstable against symmetry breaking perturbations that lead to the breakup of rings into stable filaments [7]. Recently, we demonstrated the possibility to generate both LOVS and OVS in media with cubic-quintic nonlinearity [8, 9].

We will study analytically and numerically the light bullets either with or without a topological charge as well as self-trapped singular beams in saturating nonlinear media.

2. Variational Approach

We will study analytically and numerically the light bullets either with or without a topological charge as well as self-trapped singular beams in saturating nonlinear media.

The evolution of vortices in nonlinear materials is described by a (3+1)-dimensional nonlinear Schrödinger equation (NSE)

$$2ik\left(\frac{\partial \mathcal{E}}{\partial z}+\frac{1}{v_g}\frac{\partial \mathcal{E}}{\partial t}\right)+\Delta_{\perp}\mathcal{E}-kD\frac{\partial^2 \mathcal{E}}{\partial t^2}+2k^2\frac{\delta n(|\mathcal{E}|^2)}{n_0}\mathcal{E}=0, \qquad (1)$$

where $\mathcal{E}$ is a slowly varying field envelope, v_g is the group velocity of the pulse propagating along the z axis, n_0 is the linear optical index, $\Delta_{\perp}=\partial^2/\partial x^2+\partial^2/\partial y^2$ is the two-dimensional Laplacian describing beam diffraction, k is wave vector and $D=d^2k/d\omega^2$ is group velocity dispersion (GVD). In order to prevent the wave collapse the saturating nonlinearity is required. The nonlinear index of refraction (NIR) $\delta n(|\mathcal{E}|^2)$ corresponding for instance to PTS is established to be $\delta n=n_2I+n_4I^2$, where $I=n_0c|\mathcal{E}|^2/4\pi$ is the intensity of the electromagnetic radiation. For the $\lambda=1.6\mu m$ laser radiation the measured values of second and fourth-order optical indices are respectively $n_2=2.2\times10^{-3}cm^2/GW$ and $n_4=-0.8\times10^{-3}cm^4/GW^2$ [4]. The dimensionless form of Eq. (1)

reads

$$i\frac{\partial E}{\partial z} + \Delta_\perp E + s\frac{\partial^2 E}{\partial t^2} + (|E|^2 - |E|^4)E = 0. \tag{2}$$

The field envelope E is $\mathcal{E}$ redefined according to the cubic-quintic nonlinearity under consideration, and $s = \pm 1$ corresponds respectively to the anomalous and normal GVD. For $s = 0$, the NSE reduces to a $(2+1)$-dimensional equation.

General dynamical properties of nonstationary solutions of Eq. (2) are rather complex and numerical simulations are required. Variational approach can serve as a guideline for simulations. In order to study the beam dynamics governed by NSE we first generalize the corresponding variational method for multi-dimensional ($D = 2, 3$) saturating nonlinearitys with arbitrary topological charge m. In the case of cylindrically symmetric pulses, the following Lagrangian density is associated to Eq.(2)

$$L = r\left|\frac{\partial E}{\partial r}\right|^2 - r\left|\frac{\partial E}{\partial t}\right|^2 + \frac{i}{2}r\left(E\frac{\partial E^*}{\partial z} - E^*\frac{\partial E}{\partial z}\right) - \frac{r}{2}|E|^4 + \frac{r}{3}|E|^6 \tag{3}$$

where the radius $r = (x^2 + y^2)^{1/2}$. In the optimization procedure a Gaussian trial functions is chosen

$$E = A_1 r^m \exp\left[-\frac{r^2}{2R^2} - \frac{t^2}{2T^2} + i\left(r^2 b + t^2 c + m\theta + \phi\right)\right] \tag{4}$$

with constant $A_1(z)$, beam width $R(z)$ and temporal width $T(z)$, wave front curvature $b(z)$ and the "temporal curvature" corresponding to the chirp $c(z)$, an integer m known as the topological charge of optical vortex and phase $\phi(z)$ as parameters to optimize variational functional. Substituting trial function into Eq. (3) and integrating over r and t, the average Lagrangian is obtained. It depends only on optimizing z-dependent parameters of this trial function. The condition that the variation of average Lagrangian with respect to each of these parameters is zero, gives corresponding Euler-Lagrange equations [10, 11]. The equations for effective forces following respectively R and T "directions" are

$$2(m+1)\frac{d^2R}{dz^2} = F_R = -\frac{\partial}{\partial R}V(R,T) \quad \text{and} \quad s\frac{d^2T}{dz^2} = F_T = -\frac{\partial}{\partial T}V(R,T) \tag{5}$$

where V is the effective potential

$$V(R,T) = \frac{4(m+1)}{R^2} + \frac{2s}{T^2} - \alpha_1\frac{N}{R^2T} + \alpha_2\frac{N^2}{R^4T^2} \tag{6}$$

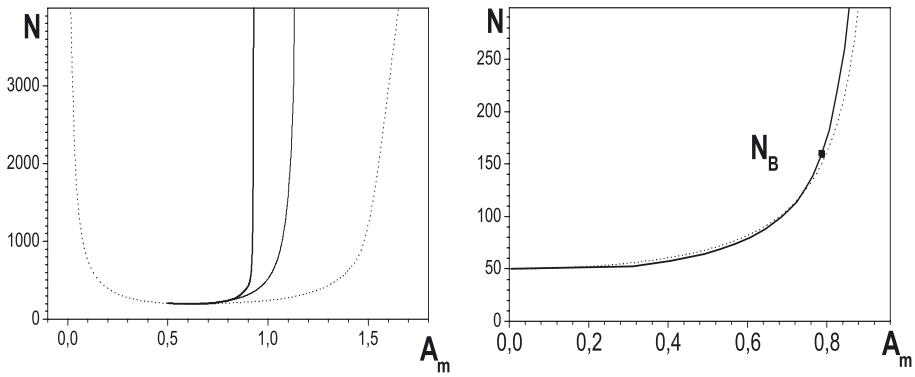

Figure 1. a. Equilibrium energy b. Equilibrium power

with $\alpha_1 = \frac{(2m)!}{2^{2m}\pi\sqrt{2\pi}(m!)^2}$ and $\alpha_2 = \frac{4(3m)!}{3^{3m+2}\sqrt{3}\pi^3(m!)^3}$. The "energy", $N = \alpha A_m^2 R^2 T$ is conserved during the pulse evolution $\left(\alpha = \sqrt{\pi}\pi m! \left(\frac{e}{m}\right)^m\right)$. The wave front curvature is given by the equation $b = (1/4R)dR/dz$, while the chirp parameter is $c = s(1/4T)dT/dz$. The equilibrium "energy" as a function of the amplitude is expressed as

$$N = (m+1)\left(\alpha\alpha_1\right) A_m^{-1}\left(1 - 2\alpha\alpha_2\left(\alpha_1\right)^{-1} A_m^2\right)^{-\frac{3}{2}}. \qquad (7)$$

In the case of the nonsingular light bullet ($m = 0$) the equilibrium curve e is given in Fig. 1.a. For the power larger than the critical one N_c, following variational approach, the pulse is trapped inside the trapping curve t (dotted line in Fig. 1.a) and it oscillates around its stable equilibrium e, as the numerical simulations confirm [3, 10]. Light bullets are generated on the exact equilibrium curve n in Fig. 1.a obtained numerically.

3. Filamentation

An input pulse near the equilibrium undergoes damped oscillations around this curve before becoming light bullet; its "energy" N decreases due to radiative losses. A light bullet is an exceptionally robust pulse resisting to all perturbations. However, very far from equilibrium, a large input pulse (with a small amplitude) even thought in the trapping region may be subject of modulation instability. For instance, a pulse with amplitude $A_m = 0.4$ and "energy" $N = 3545$ will first break into three cells in temporal domain, than the central cells breaks into two filaments in spatial domain, in order to merge back to the initial cell which finally disappears living only other two cells in temporal domain

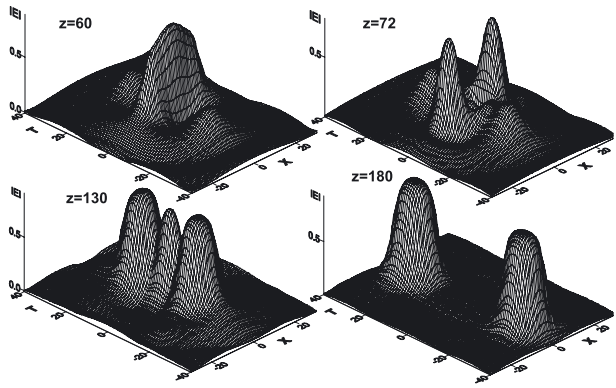

Figure 2. Filaments for N=3545 and A_m=0.4

(see Fig. 2). In the normal group velocity dispersion media ($s = -1$), a laser pulses will never become a light bullets, i.e., a stable completely confined soliton. Since diffraction and dispersion operators are of opposite sign, the laser pulse evolution results from the competition between two main tendencies, the pulse compression in the transverse spatial direction either R (the self focusing) and the pulse stretching along the time axis T (the depression). In media with cubic-quintic nonlinearity that above a critical intensity changes the sign from the positive to the negative one, the supercritical pulse near its peak value undergoes temporal wave collapse while self defocusing, contrary to the behavior for subcritical intensities. However, following our numerical simulations, a catastrophic temporal blow-up is arrested by spatial splitting of pulse into smaller cells [11].

4. Beams carrying phase singularity

Let us consider now the nonlinear dynamics and stability of laser beams carrying phase singularity ($m > 0$) in media with cubic-quintic nonlinearity. Although PTS is self-focusing medium ($d\delta n/dI > 0$), at higher intensity, $I > 0.5I_0$, it can exhibit features of defocusing media since NIR have a negative slope ($d\delta n/dI < 0$). For the peak intensity $I_m > 0.5I_0$ the NIR becomes defocusing at the peak while remains focusing at the wings of the laser beam intensity profile. The NSE admits both LOVS and OVS solutions. The switching from LOVS to OVS and vice versa may be used in information processing. Numerical simulations confirm the stability of such a novel kind of OVS. LOVS are stable to azimuthal perturbations only above breaking power $N_B = 160$ on the equilibrium curve e in Fig. 1.b obtained from Eq. (7) when

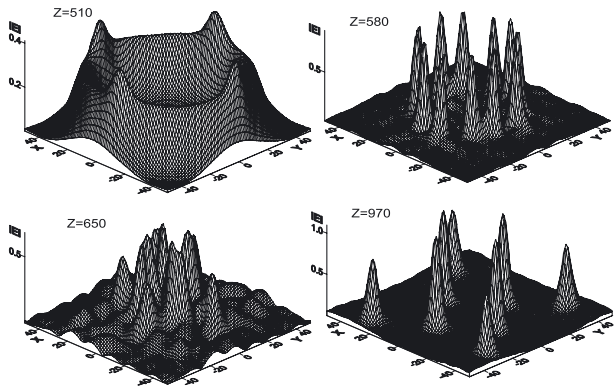

Figure 3. Filamentation for N=300 and A_m=0.1

$s = 0$. This curve nearly coincides with the numerical curve n. Below this power the vortex soliton breaks into two stable bright solitons flying off tangentially to the initial ring conserving total angular momentum $|M| = |m|N$ [8, 9].

In realistic experimental conditions a singular Gaussian input beam is usually generated far from equilibrium, i.e., it differs substantially from the stationary vortex soliton. Even far from equilibrium (for instance, $A_m = 0.5$) input beam power well above the breaking one (N_B) decreases due to radiative losses but will remain above the breaking one. However, a new phenomenon occurs, the beam first breaks into four filaments coalescing subsequently into a ring. For the input amplitude $A_m = 0.4$ at the same power, after resisting to the first splitting into four filaments, the beam finally breaks into two, since the power drops below N_B. An input beam with large width R and therefore, small amplitude (for instance, $A_m = 0.1$) may be subject of the modulation instability that usually leads to the beam breaking in multiple filaments (twelve in Fig. 3).

5. Conclusions

The stability and the robustness of light bullets in media with cubic-quintic nonlinearity, predicted by variational approach are confirmed by numerical simulations. The vortex structure of the laser beam contributes in general, if not to suppress the filamentation generated far from equilibrium, at least to distribute filaments symmetrically around the singularity in order to conserve the angular momentum.

References

[1] N. G. Vakhitov and A. A. Kolokolov, Sov. Radiophys. **16**, 783 (1973).

[2] D. E. Edmundson and R. H. Enns, Opt. Lett. **17**, 536 (1992).

[3] V. Skarka, V. I. Berezhiani, and R. Miklaszewski, Phys. Rev. E **56**, 1081 (1997).

[4] E. M. Wright, B. L. Lawrence, W. Torruellas, Opt. Lett. **20**, (1995) 2481.

[5] E. C. Josserand and S. Rica, Phys. Rev. Lett. **78**, (1997) 1215.

[6] Yu. S. Kivshar and B. Luther-Davies, Phys. Rep. **298**, 81 (1998).

[7] V. Tikhonenko, J. Christou, and B. Luther-Davies, Phys. Rev. Lett. **76**, 2698 (1996).

[8] V. I. Berezhiani, V. Skarka, and N. B. Aleksic, Phys. Rev. E **64**, 057601 (2001).

[9] V. Skarka, V. I. Berezhiani, and N. B. Aleksic, Physics Letters A **291**, 124 (2001).

[10] V. Skarka, V. I. Berezhiani, and N. B. Aleksic, Phys. Rev. E **59**, 1270 (1999).

[11] V. Skarka, V. I. Berezhiani, and N. B. Aleksic, Phys. Rev. E **60**, 7622 (1999).

THE DESCRIPTION OF EXTREMELY SHORT PULSES IN NON-RESONANT MEDIA IN FRAME OF MAXWELL-DUFFING-TYPE MODELS

Elena V. Kazantseva
Department of Solid State Physics, Moscow Engineering Physics Institute, Kashirskoe sh. 31, Moscow, 115409 Russia

Abstract The propagation of extremely short pulses of electromagnetic field (electromagnetic spikes) is considered in the framework of a model where the material medium is represented by anharmonic oscillators with cubic nonlinearities (Duffing model) and waves can propagate in both directions. The system of total Maxwell-Duffing equations admits two families of exact analytical solutions in the form of solitary waves. The single-cycle electromagnetic pulse propagation in a medium whose dispersion and nonlinear properties are described by the cubic-quintic Duffing model (oscillator with third- and fifth-order anharmonicity). A system of equations governing the evolution of a unidirectional electromagnetic wave is analyzed without using the approximation of slowly varying envelopes. Three types of solutions of this system describing stationary propagation of a pulse in such a medium are found. When the signs of the anharmonicity constants are different, the amplitude of a steady-state pulse is limited, but its energy may grow on account of an increase in its duration.

Keywords: extremely short pulses, anharmonic oscillators, Duffing model, steady state pulse, soliton.

1. Introduction

Ultra short nonlinear pulses of an electromagnetic field, which contain as few as one half optical cycle, have recently attracted a great deal of attention [1]-[5]. The description of the evolution of the electromagnetic field was based on Maxwell equations or the subsequent wave equation. To describe a medium where electromagnetic waves propagate, one frequently use an ensemble of oscillators. If the oscillators are linear we obtain the important Lorentz model, which has been very useful to de-

F. Kh. Abdullaev and V. V. Konotop (eds.), Nonlinear Waves: Classical and Quantum Aspects, 361–372.

scribe the propagation of an electromagnetic wave in a linear medium. The simplest generalization of the Lorentz model is obtained by adding an anharmonic term to the equation of the oscillator. This leads to the Duffing model in the case of a cubic nonlinearity [6, 7, 8]. In the framework of the Duffing model it was shown that solitary pulses of a unidirectional electromagnetic field ("electromagnetic bubbles") having an amplitude comparable to the atomic field and a duration down to $\sim 10^{-16}$ s may be expected. These bubbles propagate without dispersion as stable solitary waves. Very short pulses of this kind will be referred to as *extremely short pulses* (ESP). An objective of the present work is to study the propagation of linearly polarized ESPs in a nonlinear dispersive medium modeled by an anharmonic oscillator characterized by the cubic nonlinearities. The evolution of the electric field of ESP will be considered on the base of the Maxwell equations without any unidirectional reduction.

In recent years, much attention has been paid to study of propagation of electromagnetic pulses or beams in media with saturable nonlinearity [9] -[13] and, in particular, media characterized by third- and fifth-order nonlinear susceptibilities with opposite signs [14]- [18]. In the quasi-harmonic approximation, the complex envelope of the pulse will obey the nonlinear Schrödinger equation with third- and fifth-order nonlinear terms. According to conventional terminology, this equation may be called the CQ NSE (cubic-quintic nonlinear Schrödinger equation). On the basis of the Duffing model with cubic nonlinearity, we may suggest that ultimately short electromagnetic pulses in media of this type should be described, in the nonlinear Lorentz model with allowance for the next anharmonic correction. Then, we can obtain the generalization, which take into account the fifth-order anharmonicity. Calculation of the nonlinear susceptibility for this oscillator gives rise to polarization proportional to the third and fifth powers of the amplitude of the electric field strength of the harmonic wave. The subsequent consideration of the second-order group-velocity dispersion leads to the CQ NSE. The oscillator with third- and fifth-order nonlinearities will be called the fifth-order Duffing oscillator or, for brevity, the CQ Duffing oscillator. In this paper, we consider the propagation of USPs in a rarefied medium, when only waves propagating in one direction can be taken into account and the medium is described by an ensemble of identical CQ Duffing oscillators. Contrary to the original Duffing model, in the case under study, a new type of solitary wave arises. This wave resembles the limiting soliton of the Gardner equation [18] and will be referred to as an electromagnetic domain. Such an electromagnetic pulse may occur when the signs of the third- and fifth-order anharmonicity coefficients differ.

2. Constitutive model

The propagation of an extremely short electromagnetic pulse in a nonlinear dispersive medium is described by the total Maxwell wave equation and some model for the medium. Let us consider the standard Lagrangian density for an electromagnetic field taking into account the interaction with an ensemble of nonlinear oscillators:

$$\mathcal{L} = \frac{1}{2c^2}A_{,t}^2 - \frac{1}{2}A_{,z}^2 + 4\pi\sum_a \left\{\frac{1}{2}mX_{a,t}^2 - \frac{1}{2}mX_a^2 - \frac{1}{4}\kappa_{3a}X_a^4 - \frac{e_*}{c}AX_{a,t}\right\} \tag{1}$$

Here a plane electromagnetic wave is considered, it propagate along the z-axis and represented by the vector potential A. An anharmonic oscillators model (Duffing-type model) is used to reproduce the electronic response of an atom located at the spatial point indicated by the symbol a. The electrons are considered as particles in a potential well characterized by the displacements from their equilibrium position X_a. They oscillate with their own frequencies ω_a and are influenced by the electromagnetic field. In expression (1) e_* is the electric charge of the electron and κ_{3a} are anharmonicity coefficients. Hereafter, the symbol m is define the effective mass, which accounts for the local Lorentz field effect. The partial derivatives are denoted as $\partial f/\partial t = f_{,t}, \partial f/\partial z = f_{,z}$ and so on.

The application of the variational procedure to the action related with the Lagrangian density (1) yields equations

$$A_{,zz} - c^{-2}A_{,tt} = (4\pi e_*/c)\sum_a X_{a,t},$$

$$mX_{a,tt} + m\omega_a^2 X_a + \kappa_{3a}X_a^3 = (e_*/c)A_{,t}$$

If one introduces the strength of the electric field $E = c^{-1}A_{,t}$, then the constituent equations of the model under consideration can be written as

$$E_{,zz} - c^{-2}E_{,tt} = (4\pi/c^2)P_{,tt} \tag{2}$$

$$X_{a,tt} + \omega_a^2 X_a + (\kappa_{3a}/m)X_a^3 = (e_*/m)E \tag{3}$$

The polarization P of the nonlinear medium is $P = \sum_a e_* X_a$.

Let us consider the case of a homogeneous broadening medium where all atoms have the same parameters, in particular $\omega_a = \omega_0$. Then we can write the polarization as $P = n_A e_* X$, where n_A is the density of the oscillators (atoms), and the index of the atom can be omitted.

We rescale the variables and fields as $\zeta = z\omega_0/c$, $\tau = \omega_0 t$ and $e = E/E_0$, $q = X/X_0$, where

$$E_0 = m\omega_0^2 X_0/e_* = m\omega_0^3 e_*^{-1}(2\mu/|\kappa_3|)^{1/2}, \quad X_0 = (2\mu m\omega_0^2/|\kappa_3|)^{1/2},$$

and we will also use the following parameters $2\mu = \kappa_3 X_0^2/m\omega_0^2$, $\gamma = \omega_p/\omega_0$, where $\omega_p = (4\pi n_A e_*^2/m)^{1/2}$ is the plasma frequency. In terms of the rescaled variables equations (2) and (3) take the form

$$e_{,\zeta\zeta} - e_{,\tau\tau} = \gamma q_{,\tau\tau} \quad , \quad q_{,\tau\tau} + q + 2\mu q^3 = \gamma e. \tag{4}$$

These equations will be named the *total Maxwell-Duffing equations* (or TMD-equations).

Note that the system of equations (4) can be rewritten in alternative form by introducing the new auxiliary field variable b by the relation $\partial e/\partial\zeta = \partial b/\partial\tau$. In this case the TMD-equations take the following form:

$$e_{,\zeta} = b_{,\tau} \quad , \quad b_{,\zeta} = e_{,\tau} + \gamma p \quad , \quad q_{,\tau} = p \quad , \quad p_{,\tau} + q + 2\mu q^3 = \gamma e. \tag{5}$$

It should be noted that the system of equations (4) can be derived as the Euler-Lagrange equations from the action functional

$$S = \int \mathcal{L}[q, a] d\tau d\zeta,$$

where now the new Lagrangian density is

$$\mathcal{L} = \frac{1}{2}\left(\frac{\partial a}{\partial \zeta}\right)^2 - \frac{1}{2}\left(\frac{\partial a}{\partial \tau}\right)^2 - \frac{1}{2}\left(\frac{\partial q}{\partial \tau}\right)^2 + \frac{1}{2}q^2 + \frac{\mu}{2}q^4 - \gamma q\frac{\partial a}{\partial \tau}. \tag{6}$$

Applying the variational procedure to the action S yields equations

$$\frac{\partial^2 a}{\partial \zeta^2} - \frac{\partial^2 a}{\partial \tau^2} = \gamma\frac{\partial q}{\partial \tau} \quad , \quad \frac{\partial^2 q}{\partial \tau^2} + q + 2\mu q^3 = \gamma\frac{\partial a}{\partial \tau} \tag{7}$$

Identifying a as a potential for the field e, so that $e = a_{,\tau}$, makes these equations identical to Eqs. (4).

From the Lagrangian density (6) we can get the density of moments of the fields a and q:

$$\pi_a(\zeta, \tau) = \frac{\partial \mathcal{L}}{\partial a_{,\zeta}} = a_{,\zeta}(\zeta, \tau) = b(\zeta, \tau) \quad , \quad \pi_q(\zeta, \tau) = \frac{\partial \mathcal{L}}{\partial q_{,\zeta}} = 0. \tag{8}$$

The second expression in (8) indicates that we have a degenerate Lagrangian, which leads to a constrained Hamiltonian system ($\pi_q(\zeta, \tau) = 0$ is a primary constraint) [19, 20].

Now one can get a canonical Hamiltonian density using the Legendre transform

$$\mathcal{H} = a_{,\zeta}\frac{\partial \mathcal{L}}{\partial a_{,\zeta}} - \mathcal{L} = \frac{1}{2}\left(a_{,\zeta}^2 + a_{,\tau}^2 + q_{,\tau}^2 - q^2 - \mu q^4 + 2\gamma q a_{,\tau}\right). \quad (9)$$

The integration of this expression with respect to τ leads to the canonical Hamiltonian which is an integral of motion

$$H = \frac{1}{2}\int\limits_{-\infty}^{\infty}\left(e^2 + b^2 + q_{,\tau}^2 - q^2 - \mu q^4 + 2\gamma q e\right) d\tau. \quad (10)$$

It is worth noting that there are two additional integrals of motion, which follow from the TMD-equations (5):

$$I_1 = \int\limits_{-\infty}^{\infty} e(\zeta,\tau)d\tau = \int\limits_{-\infty}^{\infty} a_{,\tau}(\zeta,\tau)d\tau = a(\zeta,\tau=\infty) - a(\zeta,\tau=-\infty), \quad (11)$$

and

$$I_2 = \int\limits_{-\infty}^{\infty} b(\zeta,\tau)d\tau = \int\limits_{-\infty}^{\infty} \pi_a(\zeta,\tau)d\tau\,. \quad (12)$$

The magnitude of the first integral is defined by the boundary conditions only so that it can be interpreted as a topological charge in the Maxwell-Duffing model. The second integral is the canonical moment in this model.

2.1 Steady state solutions

Let us look for solutions of the TMD-equations as traveling waves with a non-varying profile. To the system of equations (4)should be added the initial conditions:

$$e(\zeta=0,\tau) = e_0(\tau), \quad e_{,\tau}(\zeta=0,\tau) = e_0'(\tau),$$

and the boundary conditions

$$q(\zeta,\tau) = q_{,\tau}(\zeta,\tau) = 0, \quad \text{at} \;\; \tau \to \pm\infty.$$

related to the evolution of an initial electromagnetic solitary wave in a nonlinear dispersive medium.

Substituting $e(\zeta,\tau) = e(\tau - \zeta/v)$, $\quad q(\zeta,\tau) = q(\tau - \zeta/v)$ into the first equation (4) and taking into account the boundary conditions one

finds that it results in $e = \alpha q/\gamma$, where $\alpha = \gamma^2 v^2/(1-v^2)$. The second equation of (4) can be transformed into the ordinary differential equation in the variable $T = \tau - \zeta/v$

$$\frac{d^2q}{dT^2} - (\alpha - 1)q + 2\mu q^3 = 0.$$

A non-singular solution of this equation exists only if $\alpha > 1$ and $\mu > 0$. In this case integrating results in the following expression [2, 7, 8]

$$q_{st}(\zeta, \tau) = \pm\sqrt{(\alpha-1)/\mu}\,\mathrm{sec\,h}\left[\sqrt{(\alpha-1)}\,(\tau - \zeta/v - \tau_0)\right]. \qquad (13)$$

Here the integration constants τ_0 and α are the parameters of this steady state solitary wave. The strength of the electric field of the ESP is given by

$$e_{st}(\zeta, \tau) = \pm\alpha\gamma^{-1}\sqrt{(\alpha-1)/\mu}\,\mathrm{sec\,h}\left[\sqrt{(\alpha-1)}\,(\tau - \zeta/v - \tau_0)\right]. \qquad (14)$$

This solution describes the propagation of an electromagnetic spike with positive (+ sign) or negative (− sign) polarity. The condition for existence of this solution leads to the limitation of it velocity: $1 < v < (1+\gamma^2)^{-1/2}$.

2.2 Bilinear form of the total Maxwell-Duffing equations

The system (5) can be reprezented as the bilinear equations, if the following substitutions

$$e = \frac{g}{h} \quad , \quad b = \frac{j}{h} \quad , \quad q = \frac{f}{h} \qquad (15)$$

are used. Then equations (5) can be rewritten as

$$\begin{gathered}
\frac{1}{h^2}D_\zeta(g\cdot h) - \frac{1}{h^2}D_\tau(j\cdot h) = 0, \\
\frac{1}{h^2}D_\zeta(j\cdot h) - \frac{1}{h^2}D_\tau(g\cdot h) = \gamma\frac{1}{h^2}D_\tau(f\cdot h), \qquad (16) \\
\frac{1}{h^2}D_\tau^2(f\cdot h) - \frac{f}{h^3}D_\tau^2(h\cdot h) + \frac{f}{h} + 2\mu\frac{f^3}{h^3} = \gamma\frac{g}{h},
\end{gathered}$$

where the Hirota D-operators $D_\zeta(a\cdot b) = a_{,\zeta}b - ab_{,\zeta}$, $D_\tau(a\cdot b) = a_{,\tau}b - ab_{,\tau}$ have been introduced [21]. To derive the last equation we follow the rule

$$\frac{\partial^2}{\partial\tau^2}\left(\frac{f}{h}\right) = \frac{1}{h^2}D_\tau^2(f\cdot h) - \frac{f}{h^3}D_\tau^2(h\cdot h).$$

Multiplying the first equation by h^2, the second equation one by h^3, the third one by h^2 and collecting the terms of order h^{-1}, we can write the resulting equations as a system of bilinear ones

$$\begin{aligned} D_\zeta(g\cdot h) &= D_\tau(j\cdot h), &(17)\\ D_\zeta(j\cdot h) &= D_\tau(g\cdot h)+\gamma D_\tau(f\cdot h), &(18)\\ D_\tau^2(f\cdot h) &= (\gamma g-f)h,\\ D_\tau^2(h\cdot h) &= 2\mu f^2 \end{aligned}$$

We will use the usual method [21, 22] to solve equations (18) by writing

$$g=g_1e^\theta,\quad j=j_1e^\theta,\quad f=f_1e^\theta,\quad h=1+h_1e^\theta+h_2e^{2\theta}, \tag{19}$$

where $\theta=k\zeta-\Omega\tau$. Substituting this into (18) results in the equations:

$$\begin{aligned} kg_1e^\theta-kh_2g_1e^{3\theta}+\Omega j_1e^\theta-\Omega h_2j_1e^{3\theta} &= 0,\\ kj_1e^\theta-kh_2j_1e^{3\theta}+\Omega g_1e^\theta-\Omega h_2g_1e^{3\theta}+\Omega\gamma f_1e^\theta-\Omega\gamma h_2f_1e^{3\theta} &= 0,\\ \Omega^2f_1e^\theta+\Omega^2h_2f_1e^{3\theta}-(\gamma g_1-f_1)(e^\theta+h_1e^{2\theta}+h_2e^{3\theta}) &= 0,\\ \Omega^2h_1e^\theta+4\Omega^2h_2e^{2\theta}+\Omega^2h_2h_1e^{3\theta}-\mu f_1^2e^{2\theta} &= 0. \end{aligned}$$

Equating the coefficients of the different powers of e^θ to zero, one obtains the system of equations that define j_1, f_1, g_1, h_1, h_2 :

$$\begin{aligned} kg_1+\Omega j_1 &= 0\ ,\ kj_1+\Omega(g_1+\gamma f_1)=0,\\ \Omega^2f_1-(\gamma g_1-f_1) &= 0\ ,\ 4\Omega^2h_2=\mu f_1^2\ ,\ h_1=0. \end{aligned}$$

From these relations one can get

$$\begin{aligned} h_1 &= 0\ ,\ h_2=\mu f_1^2(2\Omega)^{-2},\\ j_1 &= -\gamma^{-1}(k/\Omega)(1+\Omega^2)f_1\ ,\ g_1=\gamma^{-1}(1+\Omega^2)f_1, \end{aligned}$$

and the "dispersion relation"

$$k^2=\frac{\Omega^2(1+\gamma^2+\Omega^2)}{(1+\Omega^2)}. \tag{20}$$

It should be pointed out that in the low frequency limit this formula yields $k^2=\Omega^2(1+\gamma^2)$, while in the high-frequency limit it yields $k^2=\Omega^2$.

Thus, a one-soliton solution of the bilinear equations (18) is found, which can be written as

$$\begin{aligned} g &= \gamma^{-1}(1+\Omega^2)f_1e^\theta,\\ j &= -\gamma^{-1}(k/\Omega)(1+\Omega^2)f_1e^\theta,\\ f &= f_1e^\theta\ ,\quad h=1+\mu f_1^2(2\Omega)^{-2}e^{2\theta}. \end{aligned}$$

These relations yield a solution of the TMD-equations (6) which is consistent with the steady state solution obtained earlier:

$$\begin{aligned} e_{sol}(\zeta,\tau) &= \frac{\gamma^{-1}(1+\Omega^2)f_1 e^{\theta}}{1+\mu(f/2\Omega)^2 e^{2\theta}}, \\ b_{sol}(\zeta,\tau) &= -\frac{\gamma^{-1}(k/\Omega)(1+\Omega^2)f_1 e^{\theta}}{1+\mu(f/2\Omega)^2 e^{2\theta}}, \\ q_{sol}(\zeta,\tau) &= \frac{f_1 e^{\theta}}{1+\mu(f/2\Omega)^2 e^{2\theta}}. \end{aligned} \tag{21}$$

If we introduce a new constant of integration $\exp\theta_0 = \pm\mu^{1/2} f_1/2\Omega$, then the one-soliton expression for the normalized electric field of ESP can be written as

$$e_{sol}(\zeta,\tau) = \pm\left(\frac{1+\Omega^2}{\mu^{1/2}\gamma}\right)\frac{\Omega}{\cosh(\theta+\theta_0)}. \tag{22}$$

The velocity of this soliton is defined as $v = \Omega/k$. Taking into account the dispersion relation (20) one can obtain

$$v^2 = \frac{1+\Omega^2}{1+\gamma^2+\Omega^2}.$$

The magnitude of this velocity lies in the interval $(1, (1+\gamma^2)^{-1/2})$. This is the same result as for a steady state pulse obtained above. Using the expression for velocity we can see that $\alpha = 1+\Omega^2$, and the expression for the steady state pulse (14) coincides with expression (22).

2.3 Two-component (vector) Duffing model

The simplest generalization of the Duffing model is to consider two-component oscillator with potential

$$U(X,Y) = \frac{1}{2}\omega_1 X^2 + \frac{1}{2}\omega_2 Y^2 + \frac{1}{2}k_2 X^2 Y^2 + \frac{1}{4}k_4\left(X^4+Y^4\right).$$

The wave equations corresponding to the different polarization component of the ESP field can be written as

$$\frac{\partial^2 E_1}{\partial z^2} - \frac{1}{c^2}\frac{\partial^2 E_1}{\partial t^2} = \frac{4\pi n_A e_*}{c^2}\frac{\partial^2 X}{\partial t^2}, \quad \frac{\partial^2 E_2}{\partial z^2} - \frac{1}{c^2}\frac{\partial^2 E_2}{\partial t^2} = \frac{4\pi n_A e_*}{c^2}\frac{\partial^2 Y}{\partial t^2} \tag{23}$$

and the motion equations for the oscillator components are the following

$$\begin{aligned} \frac{\partial^2 X}{\partial t^2} + \omega_1^2 X + \kappa_2 X Y^2 + \kappa_4 X^3 &= \frac{e_*}{m}E_1(z,t), \\ \frac{\partial^2 Y}{\partial t^2} + \omega_2^2 Y + \kappa_2 Y X^2 + \kappa_4 Y^3 &= \frac{e_*}{m}E_2(z,t,). \end{aligned} \tag{24}$$

If the oscillator eigenfrequencies are equal $\omega_1 = \omega_2$, one obtain the steady-state solution corresponding to the linearly polarized pulse whose electric field components

$$E_1(\eta) = E_2(\eta) = E_m\alpha\sqrt{(\alpha-1)}\mathrm{sech}\left[\omega_1\sqrt{(\alpha-1)}\,(\eta-\eta_0)\right]. \qquad (25)$$

with $E_m = \left(m\omega_1^3/e_*\right)\sqrt{2/\left(\kappa_2+\kappa_4\right)}$ are the unipolar.

In the the other case then the the oscillator eigenfrequencies are, but anharmonicity coefficients are equal $\kappa_2 = \kappa_4$, the electic field componens E_1 and E_2 of the corresponding steady-state solution are different

$$E_1(\eta) = \frac{8\pi n_A e\theta\sqrt{2\kappa_2^{-1}}\mu_1\exp(\theta_1)\left\{1+\exp\left(2\theta_2+\mu_{12}\right)\right\}}{1+\exp\left(2\theta_1\right)+\exp\left(2\theta_2\right)+\exp\left(2\theta_1+2\theta_2+\mu_{12}\right)}, \qquad (26)$$

$$E_2(\eta) = \frac{8\pi n_A e\theta\sqrt{2\kappa_2^{-1}}\mu_2\exp(\theta_2)\left\{1+\exp\left(2\theta_1+\mu_{12}\right)\right\}}{1+\exp\left(2\theta_1\right)+\exp\left(2\theta_2\right)+\exp\left(2\theta_1+2\theta_2+\mu_{12}\right)}, \qquad (27)$$

$$\exp(\mu_{12}) = \frac{\mu_1-\mu_2}{\mu_1+\mu_2},\ \mu_{12} = \theta\omega_p^2-\omega_{1,2}^2,\ \theta_{1,2} = \mu_{1,2}\left(\eta-\eta_{1,2}\right). \qquad (28)$$

One of them (E_1) is the unipolar burst of the electric field and the other (E_2) is the solitary wave with changing polarity [23].

3. Quintic Duffing model

Nowadays a considerable attention has been paid to study of propagation of electromagnetic pulses or beams in a medium with third- and fifth-order nonlinearity. Let a plane electromagnetic wave propagate in a transparent low-density medium (a gas of molecules or impurities in a transparent dielectric). In an isotropic dielectric, the Maxwell equation (2) is reduced to one wave equation [24] for the electric field strength

$$E_{,z} + c^{-1}E_{,t} = -(2\pi/c)P_{,t} \qquad (29)$$

On the basis of the Duffing model with cubic nonlinearity, we may suggest that ultimately short electromagnetic pulses in medium should be described with allowance for the next anharmonic correction. Then, we obtain, for isotropic nonlinear medium modeled by an ensemble of identical CQ (cubic-quintic) Duffing oscillators with $\gamma = 1$, the following generalization of (4)

$$\frac{\partial e}{\partial\zeta} = \frac{\partial q}{\partial\tau}, \quad \frac{\partial^2 q}{\partial\tau^2} + q + 2\mu q^3 + 3\varepsilon q^5 = e, \qquad (30)$$

with parameters $\mu = k_3/|k_3| = \pm 1$, $\varepsilon = 4k_5\omega_0^2/3k_3^2$.

In what follows, the reduced system of equations (30) will be referred to as the RM CQD equations.

3.1 Steady state solution

The RM CQD model have a solution in the form of a traveling solitary wave with a constant profile. Let us assume

$$e(\zeta,\tau) = e\left(\eta = \tau - \zeta/\alpha\right)$$

If $\mu = +1$, here two types of solutions are possible:
if $\varepsilon > 0$

$$e^2(\eta, \mu = +1) = \frac{2a(a+1)^2}{1 + \sqrt{1+4a\varepsilon}\cosh\left[2a^{1/2}\left(\eta - \eta_0\right)\right]} \tag{31}$$

and if $\varepsilon < 0$

$$e^2(\eta, \mu = +1) = \frac{2a(a+1)^2}{1 + \sqrt{1-4a|\varepsilon|}\cosh\left[2a^{1/2}\left(\eta - \eta_0\right)\right]} \tag{32}$$

with $a = \alpha - 1$.

Let $\mu = -1$, the only solution is possible, if $\varepsilon > 0$:

$$e^2(\eta, \mu = -1) = \frac{2a(a+1)^2}{\sqrt{1+4a\varepsilon}\cosh\left[2a^{1/2}\left(\eta - \eta_0\right)\right] - 1}. \tag{33}$$

In the other cases we have either singular solutions or a negative value of the squared of the normalized electric field strength.

3.2 Electromagnetic domain

For the steady-state pulse, under the condition that $\mu = 1$, $\varepsilon < 0$ (32) the integral $W(a)$ is given by the expression

$$W\left(a\right) = \int_{-\infty}^{+\infty} e^2(\zeta,\tau)d\tau \sim 4p_c \operatorname{ar\,tanh}\left(\frac{\left(p/p_c\right)^2}{1 + \sqrt{1-\left(p/p_c\right)^2}}\right)$$

with $p = a^{1/2}$. If the critical value of parameter p is $p_c = 1/2|\varepsilon|^{1/2}$, the pulse width can be obtained as

$$\Delta\tau = (1/p)\operatorname{arcosh}\left[2 + \left(1 - \left(p/p_c\right)^2\right)^{1/2}\right]$$

at $p \to p_c$ behave as

$$\Delta\tau \approx \frac{\ln 2p_c - \ln\left(p_c - p\right)}{2p_c}.$$

The steady-state pulse swells, and its amplitude tends to that of the limiting pulse, equal to $(1+p_c^2)$. Such a ESP, almost rectangular in shape with sharp edges, will be referred to as an electromagnetic domain [25].

Therefore, in the vicinity of the domain boundary ($a \to a_c \equiv 1/(4|\varepsilon|)$), we may write an approximate expression for the electric field strength squared

$$e^2(\eta, \mu = +1) = \frac{2a_c(a_c+1)^2}{1 + (b/2)\exp\left[\eta/\sqrt{|\varepsilon|}\right]} \tag{34}$$

It is convenient to define the coordinate of the domain boundary η_1 by the expression $b/2 = \exp\left[-\eta_1/\sqrt{|\varepsilon|}\right]$

The width of the edge of the electromagnetic domain (the domain wall) can be found by noticing that in the vicinity of η_1, the electric field strength rapidly drops from its maximum value to zero. The width of the domain wall $\Delta = 2\ln\left(3+2\sqrt{2}\right)\sqrt{|\varepsilon|}$ may be identified as the derivative of the field strength in the region of the domain wall is a burst whose width at half maximum.

4. Conclusion

A model for the propagation of extremely short unipolar pulses of an electromagnetic field introduced and analyzed for a medium represented by anharmonic oscillators with a cubic nonlinearity. The model takes into account the dispersion properties of both the linear and nonlinear responses of the medium. It is the simplest generalization of the well known Lorenz model used to describe linear optical properties in condensed matter. The cubic nonlinearity is the first type of anharmonic correction to the Lorenz model and it results in the Duffing oscillator. Here we consider the total Maxwell-Duffing model in detail. The Lagrangian picture of the TMD model was considered and three integrals of motion were found. Two families of exact analytical solutions, with positive and negative polarities, have been found as moving solitary pulses. The first kind of steady state ESP is an electromagnetic spike propagating in a nonlinear medium. It was discussed early in [1, 2, 6].

The TMD equations can be represented in bilinear Hirota form. The one-soliton solution of the bilinear equations was obtained. It coincides with the expression of a steady state ESP. Among the solitary waves that have been found in this work, an interesting example is provided by waves propagating in a medium with opposite signs of the third- and fifth order nonlinear susceptibilities. Such pulses, as their energy increases, acquire an almost rectangular shape, with sharp edges. These

pulses look like electromagnetic domains, i.e., regions with a constant electric field strength, propagating as a whole.

Acknowledgments

Author is grateful to Prof. A. I. Maimistov and Dr. J. G. Caputo for the contribution and valuable discussions.

References

[1] K. Akimoto, J. Phys.Soc.Japan **65**, N7, 2020-2032 (1996).

[2] A. E. Kaplan, S.F. Straub and P. L. Shkolnikov, J.Opt.Soc.Amer. B**14**, N11, 3013-3024 (1997).

[3] N. Bloembergen, Rev.Mod.Phys. **71**, N2, S283-S287 (1999).

[4] A.V. Kim, M.Yu. Ryabikin, and A.M. Sergeev, Uspekhi Phys. Nauk **169**, N1, 58-65 (1999).

[5] Th. Brabec and F. Krausz, Rev.Mod.Phys. **72**, N2, 545-591 (2000).

[6] A.D. Vuzha, Fiz.Tverd.Tela (Leningrad) **20**, N1, 272-273 (1978).

[7] A.I. Maimistov and S.O. Elyutin, J.Mod.Opt. **39**, N11, 2201-2208 (1992).

[8] A. E. Kaplan and P. L. Shkolnikov, Phys.Rev.Lett. **75**, N12, 2316-2319 (1995).

[9] E. D. Eugenieva, D. N. Christodoulides, and M. Segev, Opt. Lett. **25**, 972 (2000).

[10] A. Dreischuh, G. G. Paulus, F. Zacher, et al., Phys. Rev. E **60**, 7518 (1999).

[11] N. V. Vysotina, L. A. Nesterov, N. N. Rozanov, and V. A. Smirnov, Opt. Spektrosk. **85**, 239 (1998) [Opt. Spectrosc. 85, 218 (1998)].

[12] N. N. Rosanov, V. E. Semenov, and N. V. Vyssotina, J. Opt. B **3**, S96 (2001).

[13] A. A. Sukhorukov and Yu. S. Kivshar, Pramana, J. Phys. **57**, 1079 (2001).

[14] W. S. Kim and H. T. Moon, Phys. Lett. A **266**, 364 (2000).

[15] A. Desyatnikov, A. Maimistov, and B. Malomed, Phys. Rev. E **61**, 3107 (2000).

[16] D. Mihalache, D. Mazilu, L.-C. Crasovan, et al., Phys. Rev. E **61**, 7142 (2000).

[17] B. A. Malomed, L.-C. Crasovan, and D. Mihalache, Physica D **161**, 187 (2002).

[18] A. V. Slyunyaev and E. N. Pelinovski., Zh. Eksp. Teor. Fiz. **116**, 318 (1999) [JETP 89, 173 (1999)].

[19] P.A.M. Dirac, Canad.J.Math. **2**, N2, 129-148 (1950).

[20] C.A.Hurst, *Recent Developm. in Mathemat. Phys*, Eds. H.Mitter, L.Pittner, Springer-Verlag, Berlin,.(1987), p.18-52.

[21] R. Hirota, and J. Satsuma, Progr.Theor.Phys., Suppl. **59**, 64 (1976).

[22] M.J. Ablowitz, and H. Segur. *Solitons and the Inverse Scattering Transform* (SIAM, Philadelphia, 1981).

[23] A.I.Maimistov, Opt.Spektrosk. **87**, 104-108 (1999).

[24] J. C. Eilbeck and R. K. Bullough, J. Phys. A **5**, 820 (1972).

[25] A. I. Maimistov, Opt. Spektrosk. **94**, No. 2, 281 (2003) [Opt. Spectrosc. 94, No. 2 , 251 (2003)].

STATISTICS OF THREE INTERACTING OPTICAL SOLITONS

Sonia Boscolo, Stanislav A. Derevyanko, and Sergei K. Turitsyn
Photonics Research Group, School of Engineering and Applied Science, Aston University, Birmingham B4 7ET, UK

Abstract We examine the statistics of three interacting optical solitons under the effects of amplifier noise and filtering. We derive rigorously the Fokker-Planck equation that governs the probability distribution of soliton parameters.

1. Introduction

In long-haul fibre-optic soliton communication systems the limitations on the bit rate and error-free transmission distance are set mainly by the amplified spontaneous emission (ASE) noise introduced by in-line optical amplifiers and the interaction of solitons. Even though both noise and interaction are weak effects, in general one cannot use the perturbation approach to obtain the error probability because errors occur when the signal parameters change substantially due to the accumulation of such effects. Large rare fluctuations in a nonlinear system are typically beyond the area of applicability of the usual Gaussian statistics [1, 2]. Recently, rigorous approaches to study non-Gaussian soliton statistics were suggested in [3, 4]. These methods allowed the calculation of the tails of the probability density function (PDF) for soliton parameters that in general are non-Gaussian. However, a straightforward approach is necessary to tackle the problem of determining the exact form of the PDF and not only its tails or halfwidth. One needs the approach that allows to determine the regime of applicability of the classical results based on the assumption of the Gaussian statistics as well as to study the asymptotical behaviour of the tails of the PDF. Such an approach, based on the Fokker-Planck equation (FPE) for the PDF, was initiated in [5] for the single soliton transmission. In this work, we generalize the method to the case of three interacting solitons in the presence of noise. The basic principle of the proposed approach is recognizing the master

F. Kh. Abdullaev and V. V. Konotop (eds.), Nonlinear Waves: Classical and Quantum Aspects, 373–379.

system of stochastic differential equations that govern the dynamics of soliton parameters as a set of generalized Langevin equations with a multiplicative rather than additive noise. Thus the non-Gaussian statistical behaviour of the soliton degrees of freedom becomes somewhat an intrinsic property of the system. We derive the FPE for a transmission system with in-line control by filters. The obtained equation contains exact and complete knowledge of the soliton statistics, and solving this equation analytically or numerically provides one with a complete or marginal PDF for soliton parameters.

2. Basic Model

We start from the nonlinear Schrödinger equation (NLSE) in soliton units, describing the optical pulse propagation in a fibre transmission line under the action of guiding filters and ASE noise,

$$\frac{\partial u}{\partial z} = \frac{i}{2}\frac{\partial^2 u}{\partial t^2} + i|u|^2 u + \alpha u + \beta\frac{\partial^2 u}{\partial t^2} + n. \tag{1}$$

Here, α stands for a required extra gain to compensate for the filter loss, β is the filter strength, and the ASE noise is accounted for as the white noise term n, with the statistical properties: $\langle n(t,z)\rangle = \langle n(t,z)n(t',z')\rangle = 0$ and $\langle n(t,z)n^*(t',z')\rangle = D\delta(t-t')\delta(z-z')$, where D is the noise intensity.

3. Three-Soliton System

To deal with the three-soliton interaction problem we use here the quasi-particle approach [6, 7]. The method is based on the adiabatic approximation, which is valid at least for the solitons with large separation. The main idea of this approach is to view the interaction as a slow deformation of soliton parameters in which only the nearest-neighbor interaction should be taken into account. Following [6, 7], we make the ansatz:

$$u(t,z) = \sum_{j=1}^{3} u_j(t,z), \tag{2}$$

where

$$u_j(t,z) \equiv u_{j0}(t,z) = A_j(z)\mathrm{sech}\{A_j(z)[t-T_j(z)]\}e^{-i\Omega_j(z)[t-T_j(z)]+i\delta_j(z)}. \tag{3}$$

Inserting (2) into Eq. (1) and retaining only first order terms with respect to the overlap in the cubic term of (1), we can write a perturbed NLSE for soliton j,

$$\frac{\partial u_j}{\partial z} = \frac{i}{2}\frac{\partial^2 u_j}{\partial t^2} + i|u_j|^2 u_j + R_j, \tag{4}$$

where the perturbation R_j describes the effects of soliton interaction, filters, and ASE noise:

$$R_j = i \sum_{l=j\pm1} (2|u_j|^2 u_l + u_j^2 u_l^*) + \alpha u_j + \beta \frac{\partial^2 u_j}{\partial t^2} + n. \tag{5}$$

Applying the standard soliton perturbation theory [8, 9] with R_j given by (5), we come up with the following dynamical equations for the jth soliton parameters:

$$\frac{\mathrm{d}A_j}{\mathrm{d}z} = 2\alpha A_j - 2\beta \left(\Omega_j^2 + \frac{A_j^2}{3}\right) A_j + 4A^3 \sum_{l=j\pm1} e^{-A|\Delta T_{j,l}|} \sin \Delta\phi_{j,l} + S_{A_j}(z), \tag{6}$$

$$\frac{\mathrm{d}\Omega_j}{\mathrm{d}z} = -\frac{4}{3}\beta A_j^2 \Omega_j + 4A^3 \sum_{l=j\pm1} s_{j,l} e^{-A|\Delta T_{j,l}|} \cos \Delta\phi_{j,l} + S_{\Omega_j}(z), \tag{7}$$

$$\frac{\mathrm{d}T_j}{\mathrm{d}z} = -\Omega_j + 2A \sum_{l=j\pm1} s_{j,l} e^{-A|\Delta T_{j,l}|} \sin \Delta\phi_{j,l} + S_{T_j}(z), \tag{8}$$

$$\frac{\mathrm{d}\delta_j}{\mathrm{d}z} = \frac{1}{2}(A_j^2 + \Omega_j^2) - 2A\Omega \sum_{l=j\pm1} s_{j,l} e^{-A|\Delta T_{j,l}|} \sin \Delta\phi_{j,l} + 6A^2 \sum_{l=j\pm1} e^{-A|\Delta T_{j,l}|} \cos \Delta\phi_{j,l} + S_{\delta_j}(z). \tag{9}$$

Here $A = \frac{1}{3}\sum_{j=1}^{3} A_j$, $\Omega = \frac{1}{3}\sum_{j=1}^{3} \Omega_j$, $\Delta T_{j,l} = T_j - T_l$, $\Delta\phi_{j,l} = \Omega\Delta T_{j,l} + \Delta\delta_{j,l}$, $\Delta\delta_{j,l} = \delta_j - \delta_l$ and terms S_{y_j},

$$S_{y_j}(z) = \mathrm{Re} \int \mathrm{d}t\, g_{y_j}^*(t,z) n(t,z), \quad y_j = A_j, \Omega_j, T_j, \delta_j, \tag{10}$$

are the projections of the white noise on the perturbation functions g_{y_j},

$$g_{A_j} = u_{j0}, \quad g_{\Omega_j} = -i \tanh[A_j(t - T_j)] u_{j0}, \quad g_{T_j} = \frac{t - T_j}{A_j} u_{j0},$$
$$g_{\delta_j} = \frac{i}{A_j}\{1 - A_j(t - T_j)\tanh[A_j(t - T_j)]\} u_{j0} - \Omega_j g_{T_j}. \tag{11}$$

Moreover, if we assume, e.g., that $T_1 > T_2 > T_3$, then $s_{j,j-1} = -1$ and $s_{j,j+1} = 1$. In deriving Eqs. (6)-(9), we have assumed that, for the differences $\Delta A_{j,l} = A_j - A_l$, $\Delta\Omega_{j,l} = \Omega_j - \Omega_l$, and $\Delta T_{j,l}$,

$$|\Delta A_{j,l}| \ll A, \quad |\Delta\Omega_{j,l}| \ll 1, \quad A|\Delta T_{j,l}| \gg 1, \quad |\Delta A_{j,l}||\Delta T_{j,l}| \ll 1, \tag{12}$$

and we have taken into account only terms of first order with respect to the overlap parameter $e^{-A|\Delta T_{j,l}|}$. From Eqs. (6)-(9), one can derive a system of equations for the variables A, Ω, $\Delta A_{k,k+1}$, $\Delta\Omega_{k,k+1}$, $\Delta T_{k,k+1}$, and $\Delta\phi_{k,k+1}$, $k = 1, 2$, which are, in fact, of interest to us. If we furthemore assume that the noise does not affect significantly the evolution of the average amplitude and frequency, A and Ω, toward the point $(A = A_0, \Omega = 0)$, which gives a stable fixed point in the equations for A and Ω in the absence of noise for the choice $\beta = 3\alpha$, the last system can be further reduced to

$$\frac{\mathrm{d}\Delta A_{1,2}}{\mathrm{d}z} = -4\alpha\Delta A_{1,2} + 4\left(2e^{-\Delta T_{1,2}}\sin\Delta\delta_{1,2} - e^{-\Delta T_{2,3}}\sin\Delta\delta_{2,3}\right) + \Delta S_{A_{1,2}}, \tag{13}$$

$$\frac{\mathrm{d}\Delta A_{2,3}}{\mathrm{d}z} = -4\alpha\Delta A_{2,3} + 4\left(2e^{-\Delta T_{2,3}}\sin\Delta\delta_{2,3} - e^{-\Delta T_{1,2}}\sin\Delta\delta_{1,2}\right) + \Delta S_{A_{2,3}}, \tag{14}$$

$$\frac{\mathrm{d}\Delta\Omega_{1,2}}{\mathrm{d}z} = -4\alpha\Delta\Omega_{1,2} + 4\left(2e^{-\Delta T_{1,2}}\cos\Delta\delta_{1,2} - e^{-\Delta T_{2,3}}\cos\Delta\delta_{2,3}\right) + \Delta S_{\Omega_{1,2}}, \tag{15}$$

$$\frac{\mathrm{d}\Delta\Omega_{2,3}}{\mathrm{d}z} = -4\alpha\Delta\Omega_{2,3} + 4\left(2e^{-\Delta T_{2,3}}\cos\Delta\delta_{2,3} - e^{-\Delta T_{1,2}}\cos\Delta\delta_{1,2}\right) + \Delta S_{\Omega_{2,3}}, \tag{16}$$

$$\frac{\mathrm{d}\Delta T_{1,2}}{\mathrm{d}z} = -\Delta\Omega_{1,2} - 2e^{-\Delta T_{2,3}}\sin\Delta\delta_{2,3} + \Delta S_{T_{1,2}}, \tag{17}$$

$$\frac{\mathrm{d}\Delta T_{2,3}}{\mathrm{d}z} = -\Delta\Omega_{2,3} + 2e^{-\Delta T_{1,2}}\sin\Delta\delta_{1,2} + \Delta S_{T_{2,3}}, \tag{18}$$

$$\frac{\mathrm{d}\Delta\delta_{1,2}}{\mathrm{d}z} = \Delta A_{1,2} - 6e^{-\Delta T_{2,3}}\cos\Delta\delta_{2,3} + \Delta S_{\delta_{1,2}}, \tag{19}$$

$$\frac{\mathrm{d}\Delta\delta_{2,3}}{\mathrm{d}z} = \Delta A_{2,3} + 6e^{-\Delta T_{1,2}}\cos\Delta\delta_{1,2} + \Delta S_{\delta_{2,3}}, \tag{20}$$

where $\Delta S_{y_{k,k+1}} = S_{y_k} - S_{y_{k+1}}$, and we have set $A_0 = 1$. System (13)-(20) is a master set of equations describing the adiabatic stochastic evolution of the differences of soliton parameters. For such a system it is possible to write down a FPE for the joint PDF [10] (see Sec. 4). It is worth noting here that the main results concerning soliton statistics obtained so far have been obtained under the implicit assumption that the functions g_{y_j} do not depend on the soliton parameters, or rather depend on the initial values. Such an approximation is valid only for small propagation distances $z \ll 1$, when the soliton parameters do not change significantly compared to their initial values. Under such an assumption, S_{y_j} become independent additive white noises and one can readily calculate their

variances. However, although the perturbation theory was used to derive Eqs. (13)-(20), these equations are valid even for large deviations from the initial values, i.e., for large distances. Therefore, in order to study soliton statistics for large distances and determine the probabilities of large fluctuations, given by the tails of the PDF, one has to assume that the perturbation functions g_{y_j} depend on the current values of soliton parameters rather than the initial ones. In other words, one needs to recognize system (13)-(20) as a system with multiplicative noise.

4. Fokker-Planck Equation

System (13)-(20) is a special case of a general system with a complex white multiplicative noise,

$$\frac{\mathrm{d}q_i}{\mathrm{d}z} = f_i(\vec{q}) + \mathrm{Re}\int_{-\infty}^{\infty} \mathrm{d}t\,[g_i^*(\vec{q},t) - \tilde{g}_i^*(\vec{q},t)]n(t,z), \quad i = 1,\ldots,N, \quad (21)$$

where $\vec{q}$ is a N-component real field, f_i are deterministic "drift" terms, g_i and $\tilde{g}_i$ are the projection functions which themselves depend on the random field $\vec{q}$, and n is a complex white noise with the statistical properties given in Sec. 2. We are interested in the equation governing the evolution of the PDF:

$$P(\vec{q},z) = \left\langle \prod_{i=1}^{N} \delta(q_i - q_i^s(z)) \right\rangle, \quad (22)$$

where $\vec{q}^s$ is the solution of Langevin system (21). We omit here the calculation details and only present the FPE in a closed form as

$$\frac{\partial P(\vec{q},z)}{\partial z} = -\sum_j \frac{\partial}{\partial q_j}[D_j(\vec{q})P(\vec{q},z)] + \sum_{j,k} \frac{\partial^2}{\partial q_j \partial q_k}[D_{jk}(\vec{q})P(\vec{q},z)]. \quad (23)$$

Here, D_j and D_{jk} are the components of the drift vector and diffusion matrix, respectively, and are given by

$$D_j(\vec{q}) = f_j(\vec{q}) + \frac{D}{4}\sum_k \mathrm{Re}\int_{-\infty}^{\infty} \mathrm{d}t\left[g_k(\vec{q},t)\frac{\partial g_j^*(\vec{q},t)}{\partial q_k} - \tilde{g}_k(\vec{q},t)\frac{\partial \tilde{g}_j^*(\vec{q},t)}{\partial q_k}\right], \quad (24)$$

$$D_{jk}(\vec{q}) = \frac{D}{4}\mathrm{Re}\int_{-\infty}^{\infty} \mathrm{d}t\,[g_j^*(\vec{q},t)g_k(\vec{q},t) - \tilde{g}_j^*(\vec{q},t)\tilde{g}_k(\vec{q},t)]. \quad (25)$$

In our system (13)-(20), we set $\Delta A_{1,2} = q_1$, $\Delta A_{2,3} = q_2$, $\Delta\Omega_{1,2} = q_3$, $\Delta\Omega_{2,3} = q_4$, $\Delta T_{1,2} = q_5$, $\Delta T_{2,3} = q_6$, $\Delta\delta_{1,2} = q_7$, and $\Delta\delta_{2,3} = q_8$,

which yields: $g_1 = g_{A_1}$, $g_2 = \tilde{g}_1 = g_{A_2}$, etc. All that is needed is to calculate functions (24) and (25) using definitions (11). In doing so, we neglect the terms that involve products of g_i and $\tilde{g}_i$ associated with different solitons. This approximation is justified by the small degree of overlap between the solitons. Thus, after some algebra, we end up in the following equation:

$$
\begin{aligned}
\frac{\partial P}{\partial z} = {} & 16\alpha P \\
& - 4(-\alpha q_1 + 2e^{-q_5}\sin q_7 - e^{-q_6}\sin q_8)\frac{\partial P}{\partial q_1} \\
& - 4(-\alpha q_2 + 2e^{-q_6}\sin q_8 - e^{-q_5}\sin q_7)\frac{\partial P}{\partial q_2} \\
& - 4(-\alpha q_3 + 2e^{-q_5}\cos q_7 - e^{-q_6}\cos q_8)\frac{\partial P}{\partial q_3} \\
& - 4(-\alpha q_4 + 2e^{-q_6}\cos q_8 - e^{-q_5}\cos q_7)\frac{\partial P}{\partial q_4} \\
& + (q_3 + 2e^{-q_6}\sin q_8)\frac{\partial P}{\partial q_5} + (q_4 - 2e^{-q_5}\sin q_7)\frac{\partial P}{\partial q_6} \\
& - (q_1 - 6e^{-q_6}\cos q_8)\frac{\partial P}{\partial q_7} - (q_2 + 6e^{-q_5}\cos q_7)\frac{\partial P}{\partial q_8} \\
& + \frac{D}{2}\left(q_1\frac{\partial^2 P}{\partial q_1^2} + q_2\frac{\partial^2 P}{\partial q_2^2}\right) + \frac{D}{6}\left(q_1\frac{\partial^2 P}{\partial q_3^2} + q_2\frac{\partial^2 P}{\partial q_4^2}\right) \\
& + \frac{D\pi^2}{24}\left[\left(\frac{1}{A_1^3} - \frac{1}{A_2^3}\right)\frac{\partial^2 P}{\partial q_5^2} + \left(\frac{1}{A_2^3} - \frac{1}{A_3^3}\right)\frac{\partial^2 P}{\partial q_6^2}\right] \\
& - \frac{D\pi^2}{12}\left[\left(\frac{\Omega_1}{A_1^3} - \frac{\Omega_2}{A_2^3}\right)\frac{\partial^2 P}{\partial q_7 \partial q_5} + \left(\frac{\Omega_2}{A_2^3} - \frac{\Omega_3}{A_3^3}\right)\frac{\partial^2 P}{\partial q_8 \partial q_6}\right] \\
& + \frac{D}{24}\left\{\left[\left(4 + \frac{\pi^2}{3}\right)\left(\frac{1}{A_1} - \frac{1}{A_2}\right) + \pi^2\left(\frac{\Omega_1^2}{A_1^3} - \frac{\Omega_2^2}{A_2^3}\right)\right]\frac{\partial^2 P}{\partial q_7^2}\right. \\
& \left. + \left[\left(4 + \frac{\pi^2}{3}\right)\left(\frac{1}{A_2} - \frac{1}{A_3}\right) + \pi^2\left(\frac{\Omega_2^2}{A_2^3} - \frac{\Omega_3^2}{A_3^3}\right)\right]\frac{\partial^2 P}{\partial q_8^2}\right\}.
\end{aligned}
\tag{26}
$$

Here, $A_1 = 1 + \frac{2}{3}q_1 + \frac{1}{3}q_2$, $A_2 = 1 - \frac{1}{3}q_1 + \frac{1}{3}q_2$, $A_3 = 1 - \frac{1}{3}q_1 - \frac{2}{3}q_2$, $\Omega_1 = \frac{2}{3}q_3 + \frac{1}{3}q_4$, $\Omega_2 = -\frac{1}{3}q_3 + \frac{1}{3}q_4$, and $\Omega_3 = -\frac{1}{3}q_3 - \frac{2}{3}q_4$. Equation (26) is rather complicated and not easy to solve. We point out that neglecting the multiplicative nature of the noise results in constant coefficients of the noise terms, and the resulting equation can be integrated more easily.

5. Summary

We have derived rigorously the FPE governing the evolution of the PDF of soliton parameters for the problem of three interacting optical solitons under the effects of ASE noise and filtering. Solving such an equation in some special cases will be the subject of a future work.

References

[1] C.R. Menyuk, Opt. Lett. **20**, 285 (1995).

[2] T. Georges, Opt. Commun. **123**, 617 (1996).

[3] G.E. Falkovich, I. Kolokov, V. Lebedev, and S.K. Turitsyn, Phys. Rev. E **63**, 025601(R) (2001).

[4] G.E. Falkovich, M.G. Stepanov, and S.K. Turitsyn, Phys. Rev. E **64**, 067602 (2001).

[5] S.A. Derevyanko, S.K. Turitsyn, and D.A. Yakushev, Opt. Lett. **28**, 2097 (2003).

[6] V.I. Karpman and V.V. Solov'ev, Physica D **3**, 487 (1981).

[7] V.S. Gerdjikov, I.M. Uzunov, E.G. Evstatiev, and G.L. Diankov, Phys. Rev. E **55**, 6039 (1997).

[8] V.I. Karpman and E.M. Maslov, Sov. Phys. JETP **46**, 281 (1977).

[9] D.J. Kaup and A.C. Newell, Proc. R. Soc. London Ser. A **361**, 413 (1978).

[10] H. Risken, *The Fokker-Planck Equation* (Springer, 1996).

STATISTICAL STUDY OF RAMAN SCATTERING IN OPTICAL FIBERS AFFECTED BY RANDOM CONDITIONS

J. Villarroel
Faculty of Sciences, University of Salamanca, Plaza de la Merced 37008 Salamanca, Spain

Abstract We study the statistical properties of a model that has been recently suggested to account for the effects of dispersion on stimulated Raman scattering in wavelength division multiplexed systems. We show that if the initial powers are low enough all channels follow a Binomial probability distribution that is the same for channels symmetric with respect to the middle one. This distribution can be approximated by a normal distribution when the number of channels is not too small.

1. Introduction

In recent years, stimulated Raman scattering (SRS) has attracted much attention, as this mechanism is responsible for power transfer from the lowest to the highest wavelengths in wavelength division multiplexed systems (WDM) [1]. This phenomenon is noticeable when a large number of wavelengths or channels is involved. Recently, the exact solution for SRS power exchange in WDM systems was found in the continuous wave (CW) regime [2]. It was shown that for an initially fully loaded WDM system, SRS can lead to an exponential like power distribution among channels, which increases as a function of distance [3, 4]. More recently, a model was proposed to explain the SRS power exchange in high-speed systems [4]. It is assumed that the signal in every channel involves a random sequence of "1" and "0" bits with pulse duration τ_0. In this model, speeds were was supposed to be big enough to allow averaging on statistical quantities (see [4, 5]).

The present model aims to consider statistical deviations from the latter deterministic situation. For previous work in this direction see [6-9]. Mathematically, this involves the problem of determining the distribution of a certain function of a sequence of independent discrete binomial

F. Kh. Abdullaev and V. V. Konotop (eds.), Nonlinear Waves: Classical and Quantum Aspects, 381–388.

random variables $b_{k,1}, ..b_{k,N}$. We show (result 1) that in this case the powers of all channels follow exactly a probability distribution which (up to a linear transformation) is binomial with channel dependent parameters. In most cases, they can be well approximated by Gaussian distributions, unlike what it is claimed in [7, 9]. As the speed tends to ∞ we recover, using the strong law of large numbers, the results of [4, 5].

2. The physical foundations.

Let us assume a WDM system of N channels co-propagating in a single mode fiber, where we assume that each wavelength or channel corresponds to a different group velocity v_k (See [10] for general facts regarding SRS in optical fibers). We take the wavelengths in increasing order, so channel #1 represents the lowest propagating wavelength and $\#N$ the highest. We assume also that every channel is separated by a frequency difference Δf. In that case the group velocities of channel $\#k$ can be written as $v_k^{-1} = \beta_0' + k\beta_0''\Delta\Omega + \frac{k^2}{2}\beta_0'''\Delta\Omega^2$, where $\Omega = k\Delta\Omega$, and $\Delta\Omega = 2\pi\Delta f$ ([2]).

It is assumed that the signal in every channel involves a random sequence of "1" and "0" bits with pulse duration τ_0 and the same probability. A further natural assumption is that the optical power is only exchanged via SRS among bits of "1". We assume that only their ratio of 1 bits with respect to the total number of bits matters and the specific order of the bits "1" in any pattern is irrelevant. Thus the effect of channel $\#k+1$ on channel $\#k$, say, depends only on how many 1 bits of channel $\#k+1$, out of a total of ρ bits, channel $\#k$ sees passing through. Let

$$\delta_{k,m}, \tilde{b}_{k,m} = 0, 1, ..\delta_{k,m} \text{ and } b_{k,m} = \frac{\tilde{b}_{k,m}}{\delta_{k,m}}$$

represent respectively the number of bits in channel $\#m$ passing $\#k$ after a given time τ_0, the total number of "1's" in this sequence, and the ratio of "1 " bits to the total number of bits. Since we assume that that every channel is separated by a constant frequency difference Δf one has $\delta_{k,m} \equiv \rho|k-m|$ where the parameter ρ gives the cross-talk between neighbor channels $\rho = \delta_{m-1,m} = z\beta_0''\Delta\Omega/\tau_0$. We assume that ρ is an integer. Clearly $\tilde{b}_{k,m}$ is a Binomial random variable that may take on the values $j = 0, 1, ..\delta_{k,m}$ with

$$P(\tilde{b}_{k,m} = j) = \left(\begin{array}{c} \delta_{k,m} \\ j \end{array} \right) \frac{1}{2^{\delta_{k,m}}}, \quad 0 \le j \le \delta_{k,m} \tag{1}$$

Variables $\tilde{b}_{k,m}$, $\tilde{b}_{k,n}$ are independent whenever $n \neq m$.

Let $Q_k(z)$ stand for the power in channel $\#k$ at the point z. We shall consider the case of equally loaded channels, i.e., $Q_m(0) = C$ a constant. Then (see [2, 4])

$$Q_k(z) = \frac{Je^{GJkz}}{e^{GJkz} + d\sum_{m\neq k}^{N} b_{k,m}e^{GJmz}} \tag{2}$$

where $G = g'\Delta f/2A$, and g' is the slope of the Raman gain. The effective core area is given by A and G is the Raman gain profile with ω being the angular frequency. J is the total power in the system given by $J = C[\sum_{m=1,n\neq k}^{N} db_{k,m} + 1]$. d represents the fraction of the area under a bit "1" with respect to the total area of the bit slot.

3. Statistical properties of the power

In Ref. [4] ρ was supposed to be very large, in whose case the approximation $b_{k,m} = \frac{1}{2}\forall m, k, m \neq k$ is valid. The present model aims to consider statistical deviations from the latter deterministic situation. In this case, the power $Q_k(z)$ is a random variable, and the problem of determining the probability distribution of Q_k involves determining the distribution of a certain function $Q_k(b_{k,1}, ..b_{k,N})$ of a sequence of independent discrete binomial random variables $b_{k,1}, ..b_{k,N}$. Note that the complicated form of expression (2) renders hopeless the task of determining an exact formula for the probability distribution of this random variable. Even for small SRS cross-talk (i.e., small ρ), Q_k takes a tremendously large number of different values ($N!$ for the simplest case $\rho = 1$); hence numerical simulations become computationally unwieldy as the number of channels N increases.

The situation can be greatly simplified by assuming that $GJkz \ll 1$ is small. This approximation corresponds to low input power levels. The initial power launched in every WDM channel is usually kept relatively low to minimize nonlinear effects. The power levels are in the order of a few mW or even less.

Assume that $GzdCN^2 \ll 1$. Then $GJkz \ll 1$ and one obtains by expansion

$$\begin{aligned} 1 + \sum_{m\neq k}^{N} db_{k,m}e^{GJ(m-k)z} &= \frac{J}{C} + \sum_{m\neq k}^{N} db_{k,m}(e^{GJ(m-k)z} - 1) \\ &\approx \frac{J}{C} + \sum_{m\neq k}^{N} db_{k,m}GJ(m-k)z \end{aligned} \tag{3}$$

We can divide the numerator and denominator of (2) by e^{GJkz}. It follows that

$$\begin{aligned} Q_k(z) &= J[1+\sum_{m\neq k}^{N} db_{k,m}e^{GJ(m-k)z}]^{-1} \\ &\approx C[1-\sum_{m\neq k}^{N} db_{k,m}GC(m-k)z] = \\ &= C[1-\frac{CGzd}{\rho}\sum_{m=1,m\neq k}^{N}\tilde{b}_{k,m}\text{sign }(m-k)] \end{aligned} \tag{4}$$

Let us introduce

$$m_k^+ \equiv \rho\sum_{m>k}^{N}(m-k) = \frac{\rho}{2}(N-k)(N-k+1), m_k^- \equiv \frac{\rho}{2}k(k-1),$$
$$m_k^+ + m_k^- \equiv M_k; \quad k_0 \equiv (N+1)/2 \tag{5}$$

From the latter formula it follows that the mean μ_k and variance σ_k^2 of the power distribution for channel $\#k$ are given by:

$$\mu_k = C[1+\frac{GzdCN}{2}(k-k_0)]$$

$$\sigma_k^2 = \frac{(C^2Gzd)^2}{4\rho^2}M_k,\ M_k = \rho\left((k-k_0)^2+k_0^2-k_0\right)$$

The mean grows linearly with k, but is independent of ρ. The variance σ_k^2 is symmetric with respect to k_0 and attains a minimum for $k=k_0$, i.e. in the middle of the cluster. It first decreases with k, and then grows quadratically again. Besides, it is inversely proportional to the dispersion parameter ρ. Hence

$$\mu_1 \equiv C[1-\frac{GzdC}{4}N(N-1)] \leq \mu_k \leq C[1+\frac{GzdC}{4}N(N-1)] \equiv \mu_N \tag{6}$$

$$\sigma_{k_0}^2 = \frac{(C^2Gzd)^2}{16\rho}(N^2-1) \leq \sigma_k^2 \leq \frac{(C^2Gzd)^2}{8\rho}N(N-1) = \sigma_1^2 = \sigma_N^2 \tag{7}$$

It is remarkable that the expression (5) giving Q_k as a sum of random variables can be simplified further. Note

$$X \equiv \sum_{m=1,m\neq k}^{N}\tilde{b}_{k,m}\text{sign }(m-k) = \left(\sum_{m>k}^{N}-\sum_{m<k}^{N}\right)\tilde{b}_{k,m} \equiv X_+ - X_-$$

where $X_+ \equiv \sum_{m,m>k}^{N} \tilde{b}_{k,m}$ is sum of independent binomial variables $\tilde{b}_{k,m} = B(\rho|m-k|, \frac{1}{2})$. It is well known then that X_+ has also a binomial distribution $B(m_k^+, \frac{1}{2})$. Likewise $X_- \equiv \sum_{m,m<k}^{N} \tilde{b}_{k,m}$ has a binomial distribution $B(m_k^-, \frac{1}{2})$.

To proceed further, let us remind some standard probabilistic notation (see [11] for a basic course in probability theory). Call support of X the set of values X may take with positive probability; let $P(A|B)$ the conditional probability of the event A given that B happened: $P(A|B) = \frac{P(A \cap B)}{P(B)}$. It follows from the above considerations that $X_\pm$, and $X = X_+ - X_-$ have support (i.e., may take on the values) Support $X_\pm = \{0, 1, 2..m_k^\pm\}$, Support $X = \{-m_k^-, ..0, 1, 2..m_k^+\}$. By the theorem on total probabililty one has that for $j \in$ Support X is

$$P(X = j) = \sum_{l=0}^{m_k^-} P(X = j|X_- = l)P(X_- = l) =$$

$$\sum_{l=0}^{m_k^-} P(X_+ = j + l|X_- = l)P(X_- = l) = \sum_{l=0}^{m_k^-} P(X_+ = j + l)P(X_- = l) =$$

$$\frac{1}{2^{M_k}} \sum_{l=0}^{m_k^-} \left(\begin{array}{c} m_k^- \\ l \end{array} \right) \left(\begin{array}{c} m_k^+ \\ j+l \end{array} \right) = \left(\begin{array}{c} M_k \\ m_k^+ - j \end{array} \right) \frac{1}{2^{M_k}}$$

where we have used that X_+, X_- are independent variables and hence $P(X_+ = j|X_- = l) = P(X_+ = j)$ and the well known combinatorial identity:

$$\sum_{l=0}^{n} \left(\begin{array}{c} n \\ l \end{array} \right) \left(\begin{array}{c} m \\ j+l \end{array} \right) = \left(\begin{array}{c} m+n \\ m-j \end{array} \right)$$

Remark. This means that $X \equiv \tilde{X} - m_k^-$ and then $Q_k(z) = C[1 + \frac{C}{\rho} Gzdm_k^- - \frac{C}{\rho} Gzd\tilde{X}]$ are linear functions of a binomial random variable $\tilde{X} = B(M_k, \frac{1}{2})$. We now state our main result

Result 1. Assume that initially all channels are equally loaded , i.e., $Q_m(0) = C$ and that $GzdCN^2 << 1$. Then the random variables Q_k satisfy

(i) For every channel $\#k$, Q_k takes on $M_k + 1$ different values q_j:

$$q_j \equiv C \left[1 - \frac{C}{\rho} Gzdj \right] \text{ for } -m_k^- \leq j \leq m_k^+ \tag{8}$$

(ii) the probability that Q_k takes the value q_j is given by

$$P\{Q_k(z) = q_j\} = \begin{pmatrix} M_k \\ m_k^+ - j \end{pmatrix} \frac{1}{2^{M_k}}, -m_k^- \le j \le m_k^+ \tag{9}$$

(iii) the power distribution is symmetric respect to its mean μ_k where the peak power is attained (which corresponds to $j = [m_k^+ - m_k^-]/2$) in (8); all channels have the same distribution (i.e., binomial up to a linear transformation) but the defining parameters are different; the distance between peaks of different channels is constant and equals $\frac{GzdC^2}{2}$. Finally channels symmetrically positioned with respect to k_0 have the same distribution. □

The study of the dependence on the cross-talk parameter shows interesting features. Using eq. (9) one obtains that while the power's peak is independent of ρ the corresponding probability does depend; assuming for convenience that $M_k \equiv 2\nu_k$ is even and recalling that ρ and ν_k are proportional (see (5)): $\nu_k \equiv \frac{1}{2}\rho R_k; R_k \equiv (k-k_0)^2 + k_0^2 - k_0$, one obtains that the probability of the maximum $\mathcal{P}_{2\nu_k}$ reads

$$\mathcal{P}_{2\nu_k} \equiv P\{Q_k(z) = \mu_k\} = P\{j = m_k - \nu_k\} = \begin{pmatrix} 2\nu_k \\ \nu_k \end{pmatrix} \frac{1}{2^{2\nu_k}} \tag{10}$$

This expression shows that

$$\frac{\mathcal{P}_{2\nu_k+2}}{\mathcal{P}_{2\nu_k}} = \frac{\nu_k + 1/2}{\nu_k + 1} < 1 \tag{11}$$

i.e., that $\mathcal{P}$ decreases as ρ increases. This can be explained by the fact that the interaction between channels takes place over a longer time interval and more SRS exchange can occur. For large ρ, Stirling's approximation shows that for all q_j is

$$P\{Q_k(z) = q_j\} \ \le P\{Q_k(z) = \mu_k\} \approx 1/\sqrt{\pi\nu_k} \overrightarrow{{}_{\rho\to\infty}} 0 \tag{12}$$

However, it is misleading to believe that for very high speed :$\rho \to \infty$, the probability distribution vanishes. Indeed, since $\delta_{k,m} \equiv \rho|k-m|$ one has $\tilde{b}_{k,m} = \sum_{j=1}^{\rho|k-m|} B_j$ where B_j is a sequence of independent Bernouilli variables, i.e., $P(B_j = 0) = P(B_j = 1) = \frac{1}{2}$ and

$$X_+ \equiv \sum_{m,m>k}^{N} \tilde{b}_{k,m} = \sum_{m,m>k}^{N} \sum_{j=1}^{\rho(m-k)} B_j = \sum_{j=1}^{m_k^+} B_j$$

Hence writting $m_k^+ = \frac{\rho}{2}(N-k)(N-k+1) \equiv r_k^+\rho, m_k^- = \frac{\rho}{2}k(k-1) \equiv r_k^-\rho$ one has $X_+/\rho = \sum_{j=1}^{m_k^+} \hat{B}_j/m_k^+$ where $\hat{B}_j \equiv B_j r_k^+$ satisfies $E\hat{B}_j = r_k^+/2; \mathrm{Var}\ B_j = r_k^{+2}/4$.

The series

$$\sum_{j=1}^{\infty} \frac{\text{Var } \hat{B}_j}{j^2} = \pi^2 r_k^{+2}/24$$

is convergent. As $\rho \to \infty$, $m_k^+ \to \infty$. It follows by an application of the strong law of large numbers that $\lim_{\rho\to\infty} X_+/\rho = r_k^+/2$. Likewise

$$Q_k(z) = C[1 - \frac{C}{\rho} GzdX] \underset{\rho\to\infty}{\longrightarrow} C[1 - CGzd(r_k^+ - r_k^-)] \equiv \mu_k$$

or $P\{\lim_{\rho\to\infty} Q_k(z) = \mu_k\} = 1$ i.e., for large speeds $Q_k(z) = C[1 - \frac{GzdC}{4} N(N+1-2k)]$ and we recover the result of [4] (eq. (6) of [4]). We have thus obtained the following result

Result 2. As the cross-talk $\rho \to \infty$ one has

(i)

$$\lim_{\rho\to\infty} P\{Q_k(z) = q_j\} = 0, \ \forall q_j \tag{13}$$

but

$$\text{(ii) } P\{\lim_{\rho\to\infty} Q_k(z) = \mu_k\} = 1 \tag{14}$$

4. Gaussian approximation

The formula (9) gives exactly the distribution of Q_k, independent of whether N is small or large. In the latter case it is well known that the binomial distribution can be approximated by a normal distribution $Q_k(z) = N(\mu_k, \sigma_k^2)$. The normal distribution is applicable if $M_k \geq 50$, even though $M_k \geq 25$ gives very good results. Reminding the reader that $\frac{\rho}{4}(N^2-1) \leq M_k \leq \frac{\rho}{2} N(N-1)$ we see that, the number of channels required for the approximation to hold is $N \geq 10/\sqrt{\rho}$. For example, one needs $N = 5$ for $\rho = 4$ and $N = 10$ for $N = 1$. In this case

$$P\{Q_k(z) = q_j\} \approx \sqrt{\frac{2}{\pi M_k}} \exp\left[-\frac{2(j - M_k/2)^2}{M_k}\right] \tag{15}$$

provided $|j - M_k/2| \approx M_k/4$. This shows that, at least in this regime, the probability distribution is not lognormal as stated in Ref. [9].

Acknowledgments

The suggestion of this problem and fruitful discussions with D. N. Christodoulides and A. Grandpierre are greatly appreciated. This project was supported in part by by DGICYT BFM2002-02609 and Junta de Castilla-Leon SA078/03 in Spain.

References

[1] I. P. Kaminow, and T. L. Koch, Optical Fiber Telecommunications IIIA, Academic Press, San Diego, 1997.

[2] D. N. Christodoulides, and R. B. Jander, "Evolution of Stimulated Raman crosstalk in wavelength division multiplexed systems," IEEE Photon. Technol. Lett., **8**, 1722-1724, (1996).

[3] S. Bigo, S. Gauchard, A. Bertaina, and J.-P. Hamaide, "Experimental investigation of stimulated Raman scattering limitation on WDM transmission over various types of fiber infrastructures," IEEE Photon. Technol. Lett., **11**, 671-673, (1999).

[4] A. G. Grandpierre, D. N. Christodoulides, W. E. Schiesser, C. M. McIntosh, J. Toulouse, "Stimulated Raman scattering crosstalk in massive WDM systems under the action of group velocity dispersion", Opt. Commun. **194**, 319-323, (2001).

[5] A. G. Grandpierre, D. N. Christodoulides, and J. Toulouse, "Theory of stimulated Raman scattering cancellation in wavelength-division-multiplexed systems via spectral inversion," IEEE Photon. Technol. Lett., **11**, 1271-1273, (1999).

[6] D. Cotter and A. M. Hill, "Stimulated Raman crosstalk in optical transmission: effects of group velocity dispersion," Electron. Lett., **20**, 185-187, (1984).

[7] F. Forghieri, R. W. Tkach, and A. R. Chraplyvy, "Effect of modulation statistics on Raman crosstalk in WDM systems," IEEE Photon. Technol. Lett. **7**, 101-103, 1995.

[8] J. Wang, X. Sun, and M. Zhang, "Effect of group velocity dispersion in stimulated Raman crosstalk in multichannel transmission systems," IEEE Photon. Technol. Lett. **10**, 540-542, 1998.

[9] K-Po Ho, "Statistical properties of stimulated Raman crosstalk in WDM systems," J. Lightwave Technol, **18**, 915-921, (2000).

[10] G. P. Agrawal, Nonlinear Fiber Optics, 2nd ed., Academic Press, San Diego, 1995.

[11] A. Papoulis, "Probability, random variables and stochastic processes", Mac-Graw Hill 1965, New York

ELECTROMAGNETICS OF UNHARMONIC WAVES – EXACTLY SOLVABLE MODELS

A. Shvartsburg
Central Design Bureau for Unique Instrumentation Russian Academy of Sciences
p/o 117342, Butlerov Str. 15, Moscow, Russia
alexshvarts@mtu-net.ru

Abstract The non - local dispersion effects, produced by continuous spatial distributions of dielectric susceptibility of the medium, are visualized by means of new exact analytical solutions of Maxwell equations. The broadband antireflection properties of heterogeneous nanolayers, controlled by this artificial dispersion, are shown. The dynamical reflectivity of instantaneous dielectrics, governed by finite relaxation times of their non-stationary dielectric susceptibility, is examined.

Keywords: Heterogeneous nanolayers, unharmonic waveforms, heterogeneity - induced dispersion, broadband antireflection coating, artificial cut - off frequency.

This research is centered on the physical fundamentals and mathematical basis of the electromagnetics of waveforms, whose parameters are varying in the course of propagation in the heterogeneous or instantaneous media. The variable velocity of wave fields propagation in such media can completely change the spectra of wave reflection as well as the spatiotemporal structure of fields, travelling within these media. The dependences of dielectric susceptibility upon coordinates and time, which are described by continuous and smooth functions of these variables, determine the domain of existence of discussed non-local dispersion. Owing to the special types of such dependences these domains can be formed in a frequency ranges remote from the natural resonances and absorption bands of the material. Investigations of these effects are known to give the rise to the series of problems in plasma physics, semiconductor and polymer optics, laser and microwave technologies. Harnessing materials with strong artificial dispersion opens the new avenues for synthesis of optoelectronic and microwave engineering systems, nondestructive test-

F. Kh. Abdullaev and V. V. Konotop (eds.), Nonlinear Waves: Classical and Quantum Aspects, 389–395.

ing of complex materials and optimization of processes of energy and information transfer through stratified and instantaneous media. Moreover, the elaboration of physical insight and the adequate mathematical language for analysis of EM waves interaction with continuous dielectric media can be generalized for the description of wave phenomena of another physical nature.

The effects of artificial non-local dispersion on reflection – refraction phenomena for EM waves in the heterogeneous and non-stationary dielectrics can be considered with the aid of model dependences of dielectric susceptibility upon coordinate $\epsilon(z)$ or time $\epsilon(t)$. These dependences result in the coupled spatiotemporal distortions of waveforms of electric (E) and magnetic (H) field components. In particular, when a wave with harmonic E and H envelops is incidenting on the surface of a heterogeneous medium, the shapes of electric and magnetic envelops of the refracted wave become unharmonic, and, moreover, they are varying in the course of propagation. Herein, the shapes of E and H waveforms can be essentially different. The rate of this distortion is determined by the abovementioned non-local dispersion. The similar effects arise also in the temporal envelops $E(t)$ and $H(t)$ in the non-stationary medium.

Therefore a new branch of the wave theory — electromagnetics of unharmonic waves — is shaping now in the studies of EM fields in continuously heterogeneous and instantaneous media. The following results of this theory are presented:

1 The wide classes of new exact analytical solutions of Maxwell equations, based on the same approach to both heterogeneous and non-stationary dielectrics, are obtained. These results are free from any WKB-like suppositions about smallness or slowness of variations of fields or media.

2 The effects of giant heterogeneity-induced dispersion (HID), exceeding drastically the usual material dispersion, are visualized by means of the aforesaid exact solutions.

3 The broadband antireflection properties of thin heterogeneous films, controlled by the spatial dielectric susceptibility profiles, are examined.

4 The spectral broadening of EM waves, reflected from the media with time-varying dielectric susceptibility is examined, the ratio between the wave period and the medium relaxation time being arbitrary.

5 The crucial role of gradient and curvature of $\epsilon(z)$ and $\epsilon(t)$ profiles in reflectivity of heterogeneous and instantaneous media are shown,

and the relevant 'dynamical' generalizations of classical Fresnel formulae for reflection are presented.

These results are considered below in details:

1. Let us start from the presentation of continuous coordinate-dependent dielectric susceptibility $\epsilon(z)$ in the transparent region($\epsilon > 0$, $z \geq 0$) in a form

$$\epsilon(z) = n_0^2 U^2(z); \quad U|_{z=0} = 1 \tag{1}$$

Here n_0 is the refractive index of the medium at the boundary $z = 0$, and the smooth dimensionless function $U^2(z)$ describes the spatial profile of $\epsilon(z)$. Restricting ourselves by the normal incidence of linearly polarized EM wave on the interface $z = 0$ and expressing the wave field components via some auxiliary function (vector-potential $\overrightarrow{A}$, $A_x = \Psi$, $A_y = A_z = 0$), we'll reduce the system of Maxwell equations to one equation, governing the function Ψ:

$$\frac{\partial^2 \Psi}{\partial z^2} - \frac{n_0^2}{c^2}\frac{\partial^2 \Psi}{\partial t^2} = 0 \tag{2}$$

Introducing the new functions F and Q and new variable η, one can eliminate the unknown function U from the left side of wave equation (2):

$$\Psi_1 = FU^{-1/2}; \quad Q = U^{-1}; \quad \eta(z) = \int_0^z U(z_1)dz_1;$$
$$\frac{\partial^2 F}{\partial \eta^2} - \frac{n_0^2}{c^2}\frac{\partial^2 F}{\partial t^2} = -F\left[\frac{Q}{2}\frac{\partial^2 Q}{\partial z^2} - \frac{1}{4}\left(\frac{\partial Q}{\partial z}\right)^2\right] \tag{3}$$

Let us examine a simple particular solution of eq. (2), which arises in a case, when the expression in brackets at the right side of (2) is equal to some constant p^2 , which will be defined below:

$$\frac{Q}{2}\frac{\partial^2 Q}{\partial z^2} - \frac{1}{4}\left(\frac{\partial Q}{\partial z}\right)^2 = -p^2 \tag{4}$$

Assuming, that the temporal dependence of the field F is harmonic, one can write the solution of (4) in a form of a sinusoidal wave $F = exp\,[i(q\eta - \omega t)]$. Substitution of this solution to (2) brings the explicit expression for dimensionless vector-potential in a form of travelling wave

with spatially modulated amplitude

$$\Psi_1 = \frac{\exp\left[i(q\eta - \omega t)\right]}{\sqrt{U(z)}}; \tag{5}$$

$$q = kN; \quad k = \frac{\omega n_0}{c}; \quad N = \sqrt{1 - \frac{\Omega^2}{\omega^2}}; \quad \Omega^2 = \frac{p^2 c^2}{n_0^2} \tag{6}$$

Factor N in (6) resembles the refractive index for plasma or waveguide with the cut-off frequency Ω. To calculate the EM field components E and H from (2), the dielectric susceptibility profile $U(z)$ has to be found from (4):

$$U^2(z) = \left(1 + s_1 \frac{z}{L_1} + s_2 \frac{z^2}{L_2^2}\right)^{-2}; \tag{7}$$

$$s_1 = 0, \pm 1; \quad s_2 = 0, \pm 1. \tag{8}$$

Here L_1 and L_2 are the free parameters of the model (7); these parameters can be interpreted as the characteristic heterogeneity scales for dielectric susceptibility distribution. The value p^2, determining the cut-off frequency Ω, is obtained due to substitution of (7) to (4)

$$p^2 = \frac{s_1^2}{4L_1^2} - \frac{s_2}{L_2^2} \tag{9}$$

Thus, we found the wide classes of exact analytical solutions of Maxwell equations in a heterogeneous dielectric medium (7). It is necessary to emphasize, that the EM field (5) is presented in a simple form of harmonic travelling wave only in η-space, meanwhile in a real space the spatial waveforms of EM field are unharmonic and the distances between zero-crossing points for field components are varying in the course of propagation. It's interesting, that the classical Rayleigh profile $\epsilon(z) = n_0^2/(1 + z/L)^2$, widely used in the electromagnetics of heterogeneous media, can be considered as a limiting case of (7), related to the limit $L_{1,2} \to \infty$.

2. Formulae (5) – (6) visualize the influence of heterogeneity-induced dispersion (HID) on the wave field structure inside the medium. The salient features of this type of dispersion are:

a. Subject to the correlation of characteristic scales L_1 and L_2 the HID parameter p^2 (9) can assume positive, negative or zero values; respectively, the HID can be both normal and abnormal; in a case $p^2 = 0$ HID doesn't arise.

b. The variations of wave velocity, produced by HID, can exceed in several orders of magnitude the effects of natural material dispersion.

c. Choosing the parameters of heterogeneity profile $U(z)$ one can create the HID phenomena in an arbitrary spectral range, in particular, in a range, far from the material absorption bands.

d. In a case $p^2 > 0$, one can provide the formation of cut-off frequency in the controlled spectral range even in a dispersiveless material.

e. Being derived from exact analytical solutions of Maxwell equations, these results can be scaled from optics to another spectral ranges, e.g., to the microwave phenomena in communication lines with distributed parameters.

3. The reflectivity of heterogeneous media depends critically upon the value of characteristic scales L_1 and L_2. These dependences reveal the new trends in optics of thin heterogeneous dielectric films. These films can be used as the effective frequency-selective interfaces. Several applications of such interfaces, perspective for nano-optics, are discussed:

a. Broadband antireflection coatings and reflectionless barriers. The phase shifts between the waves, reflected from both sides of heterogeneous layer, are dependent upon the spatial profile of $\epsilon(z)$. This dependence is shown to provide the antireflection properties of such layer in a broad spectral range: thus, the layer with thickness $d = 30$ nm ($L_1 = 100$ nm, $L_2 = 200$ nm), made from glass with $n_0 = 1.73$, has the cut-off frequency (6) $\Omega = 1.25 \cdot 10^{14}$ Hz. This layer is characterized by power reflection coefficient, less than 5% over the wavelengths interval 500 nm $< \lambda <$ 1500 nm, covering the visible and near infrared range.

b. The optimized photonic bandgap in an arbitrary spectral range can be created from multilayer coating, containing several heterogeneous films.

c. The artificial skin layer and high-pass filter for the frequencies ω, less than the cut-off frequency Ω (6), can be manufactured in an arbitrary spectral range from the dispersiveless lossless material.

d. The highly dispersive mirror can be synthesized from some combination of the aforesaid heterogeneous films.

e. The thickness of heterogeneous reflectionless coating can be several times smaller, than the thickness of traditional quarter-wave plate, acting in the same spectral range. The relevant optimization of the scales of antireflection coatings opens the new perspectives in the miniaturization of both optical and microwave devices.

4. Temporal variations of the dielectric susceptibility of continuous medium can change drastically the reflection – refraction properties of these media. Unlike the Doppler effect, when the tuning of reflected wave is connected with the reflector's motion, we'll examine here the

temporal evolution of EM fields in the immobile media, whose dielectric susceptibility is time-dependent: $\epsilon = \epsilon(t)$. Both reflected and refracted waves in this case become unharmonic.

The important characteristic of such instantaneous wave processes are the finite relaxation times of electromagnetic parameters of the medium, e.g., its dielectric susceptibility. In a number of problems, both applied and academic, one can face the situation, when the period of oscillations of incidenting field and the relaxation time of the material prove to be of the same order of magnitude, and, thus, the exact analytical solutions of Maxwell equations with time-dependent coefficients are required for analysis of the wave problem. The wide family of such solutions is obtained here for the simple models $\epsilon(t)$, assuming, that the dynamics of medium relaxation is determined by external factors, independent upon the propagating EM field, for instance, by heating, ionization or phase transition. The electric induction D, produced by the field E, can be presented in this model as

$$D(t) = \epsilon(t)E(t); \qquad \epsilon(t) = n_0^2 U^2(t) \tag{10}$$

Let us consider, for simplicity, the normal incidence of linearly polarized EM wave on the plane interface of instantaneous dielectric. Proceeding by analogy with the spatially heterogeneous media, we'll solve the Maxwell equations, expressing the field components by means of an auxiliary function Ψ_2

$$E = \frac{1}{n_0^2 U^2(t)} \frac{\partial \Psi_2}{\partial z}; \qquad H = \frac{1}{c} \frac{\partial \Psi_2}{\partial t} \tag{11}$$

Introducing the new dimensionless function F and the new variable τ, having the dimension of time

$$F = \frac{\Psi_2}{\sqrt{U(t)}}; \qquad \tau = \int_0^t \frac{dt_1}{U(t_1)} \tag{12}$$

and using the model

$$U(t) = 1 + \frac{s_1 t}{T_1} + \frac{s_2 t^2}{T_2^2}, \tag{13}$$

one can derive a simple equation, governing the field F

$$\frac{\partial^2 F}{\partial z^2} - \frac{n_0^2}{c^2} \frac{\partial^2 F}{\partial \tau^2} = \frac{n_0^2}{c^2} \frac{F}{T^2}; \frac{1}{T^2} = \frac{1}{2} \frac{\partial^2 U}{\partial t^2} - \frac{1}{4} \left(\frac{\partial U}{\partial t} \right)^2 = const \tag{14}$$

Combination of (12) and (14) yields an explicit expression for the non-stationary field

$$\Psi_2 = \sqrt{U(t)}\exp\left[i(qz - \omega\tau)\right] \tag{15}$$

$$q = \frac{\omega n_0}{c}N; \quad N = \sqrt{1 - \frac{p^2}{\omega^2}}; \quad p^2 = \frac{1}{T^2} \tag{16}$$

It is remarkable, that the obtained exactly solvable model doesn't contain any suppositions about smallness or slowness of variations of EM fields or media.

5. The results (10) – (16) visualize some important tendencies of EM waves reflection and refraction in the instantaneous dielectrics, resembling the similar tendencies in the electromagnetics of heterogeneous media:

a. Owing to transform (11) the EM field is presented as a travelling harmonic wave in a (z, τ) space, meanwhile in a physical space (z, t) the refracted waveforms are unharmonic and the distances between zero-crossing points are unequal.

b. The non-stationary medium can possess giant non-stationarity–induced dispersion, determined by the ratio between the wave's period and the medium relaxation time. This dispersion, described by factors N (16), can be both normal and abnormal; in particular, in a case $p^2 > 0$ the new cut-off frequency can arise.

c. Generalization of classical Fresnel formulae for the problem of reflectivity of instantaneous dielectrics, obtained by means of exact solutions (15) – (16), reveals the decisive role of the first and second temporal derivatives of the function $\epsilon(t)$ in formation of spatiotemporal structure of both reflected and refracted EM field.

d. The dynamics of EM field in some pump-probe experiments in physics of laser-plasma interactions show the importance of consideration of 'dynamical' models of such interactions, meanwhile the applicability of 'quasistatic' model, operating with usual Fresnel formulae and current value of the function $\epsilon = \epsilon(t)$, is restricted by analysis of 'slow' processes ($\omega T_{1,2} \gg 1$).

e. Formation of EM shock waves and spectral broadening of reflected wave due to fast variations of the dielectric susceptibility are examined.

The next step in development of these models will be the generalization of the developed approach for electromagnetics of lossy media with spatial and temporal variations of losses.

IV

NONLINEAR WAVES IN DISCRETE SYSTEMS

QUANTUM BREATHERS IN AN ATTRACTIVE FERMIONIC HUBBARD MODEL

Quantum breathers in a Hubbard model

J.C. Eilbeck
Department of Mathematics, Heriot-Watt University
Riccarton, Edinburgh, EH14 4AS, UK
J.C.Eilbeck@hw.ac.uk

F. Palmero
Nonlinear Physics Group. Departamento de Fúsica Aplicada I. ETSI Informática,
Universidad de Sevilla, Avda Reina Mercedes s/n, 41012 Sevilla, Spain
palmero@us.es

Abstract In one–dimensional translationally invariant anharmonic lattices, an extended Bloch state with two or more strongly correlated particles is usually called a quantum breather. Here we study an attractive fermionic Hubbard model with two kind of particles of opposite spin. We discuss the existence of breathers, and several effects that break the translational symmetry of the system and localize the breather in the lattice.

Keywords: Anharmonic quantum lattices, Quantum breathers, Quantum lattice solitons

1. Introduction

Recent theoretical developments and improved experimental techniques has led to growing interest in the phenomenon of localization of energy by nonlinearity in anharmonic lattices. The existence and properties of these intrinsic localized modes, known as discrete breathers, have been subject of an much investigation (see, e.g [1] for a number of recent reviews of this topic). At present, discrete breathers in classical systems is a relatively well understood phenomenon, but knowledge of the quan-

F. Kh. Abdullaev and V. V. Konotop (eds.), Nonlinear Waves: Classical and Quantum Aspects, 399–412.

tum equivalent of discrete breathers is not very developed. In particular we restrict ourselves to a study of small lattices and a small number of quanta where some numerically exact solutions can be found. Although of less interest to the study of bulk matter, such studies are relevant to the recent developments in quantum nanotechnology and applications in quantum computing [7].

The quantum equivalent of a discrete breather in a translationally invariant anharmonic lattice is an extended Bloch state with two or more particles in a strongly correlated state. There exist some theoretical results (i.e. [2, 3]), and some experimental observations of these states in different quantum systems, as mixtures of 4–methyl–pyridine [4], in Cu benzoates [5], and in doped alkalihalides [6].

Here we present some results on a quantum one–dimensional lattice problem with a small number of quanta. We study a periodic lattice with f sites containing fermions, described by an attractive fermionic Hubbard model (FH) with two kinds of particles with opposite spins. It is a model of interest in connection with the theory of high-T_c superconductivity [8], and it can be used to describe bound states of electron and holes in some nanostructures as nanorings (excitons) [9]. Many of the results could be extended to a great variety of systems, i.e., we have obtained similar results with a periodic lattice containing bosons and described by the quantum discrete nonlinear Schrödinger equation [10].

This paper is organized as follows: In the next section we present the model, and in Section 3 we study the existence of breathers in the simplest nontrivial case. In Section 4, we consider some modifications that break the translational symmetry of the lattice, and can localize the breather in the lattice. In Section 5 we extend the previous results, obtained in the simplest nontrivial case, to more complicated situations. Finally, in Section 6, we summarize our findings and present our conclusions.

2. The model

We consider an anharmonic lattice with f sites and two kinds of fermions with opposite spins described by an attractive fermionic Hubbard model (FH). The Hamiltonian of the system is given by

$$\hat{H} = -\sum_{j=1}^{f} \gamma_j a_j^\dagger a_j b_j^\dagger b_j + \epsilon_j a_j^\dagger (a_{j-1} + a_{j+1}) + m_e \epsilon_j b_j^\dagger (b_{j-1} + b_{j+1}), \quad (1)$$

where $a_j^\dagger (a_j)$ and $b_j^\dagger (b_j)$ are raising (lowering) operators for different electronic spin states, satisfying the standard fermionic anticommutation re-

lations. The parameter ratio γ_j/ϵ_j represent the ratios of anharmonicity to nearest–neighbor, hopping energy, and m_e is the ratio of the effective mass of one type of fermion to the other. To eliminate the effects related to the finite size of the chain, we consider periodic boundary conditions and, initially, a translational invariant lattice, $\gamma_j = \gamma$ and $\epsilon_j = \epsilon$, independent of j. In general we consider $\epsilon = 1$.

The Hamiltonian (1) conserves the number of quanta N, and it is possible to apply the number–state–method to calculate the eigenvalues and eigenvectors of the Hamiltonian operator [11]. We use a number–state–basis $|\psi_n\rangle = [n_1^a, n_2^a, ..., n_f^a; n_1^b, n_2^b, ..., n_f^b]$, where n_i^a (n_i^b) represents the number of quanta of fermions a (b) at site i. In this case, $N_a = \sum_i n_i^a$, $N_b = \sum_i n_i^b$, and $N = N_a + N_b$. A general wave function is $|\Psi_n\rangle = \sum_n c_n |\psi_n\rangle$. As a first step, we restrict ourselves to study the simplest nontrivial case $N_a = 1$, $N_b = 1$, and as a second step we consider more complicated situations with a small number of quanta, although many of the results are valid for larger values of N_a and N_b. The bound states correspond to exciton states, localized electron/hole states that may appear in nanorings.

3. Quantum breathers in a translational invariant lattice

In a homogeneous quantum lattice with periodic boundary conditions, it is possible to block–diagonalize the Hamiltonian operator using eigenfunctions of the translation operator $\hat{T}$ defined as $\hat{T} b_j^\dagger = b_{j+1}^\dagger \hat{T}$ ($\hat{T} a_j^\dagger = a_{j+1}^\dagger \hat{T}$). In each block, the eigenfunctions have a fixed value of the momentum k, with $\tau = \exp(ik)$ being an eigenvalue of the translation operator [11]. In this way, it is possible to calculate the dispersion relation $E(k)$ with a minimal computational effort. The corresponding matrix in the case $N_a = N_b = 1$ is

$$H_k = - \begin{bmatrix} \gamma & q^* & 0 & . & . & q \\ q & 0 & q^* & 0 & . & 0 \\ 0 & q & 0 & q^* & . & . \\ . & . & . & . & . & . \\ . & . & . & q & 0 & q^* \\ q^* & . & . & . & q & 0 \end{bmatrix},$$

where $q = (m_e + \tau^*)$.

In this simplest non–trivial case, if the anharmonicity parameter is large enough, as Fig 1 shows, there exists an isolated eigenvalue for each k which corresponds to a localized eigenfunction, in the sense that there is a high probability for finding the two quanta at the same site. But due

to the translational invariance of the system, there is an equal probability for finding these two quanta at any site of the system. In these cases, some analytical expressions can be obtained in some asymptotic limits (for a recent discussion see [2, 11, 12]). Note that, qualitatively, the existence of this localized state is independent of the value of parameter m_e.

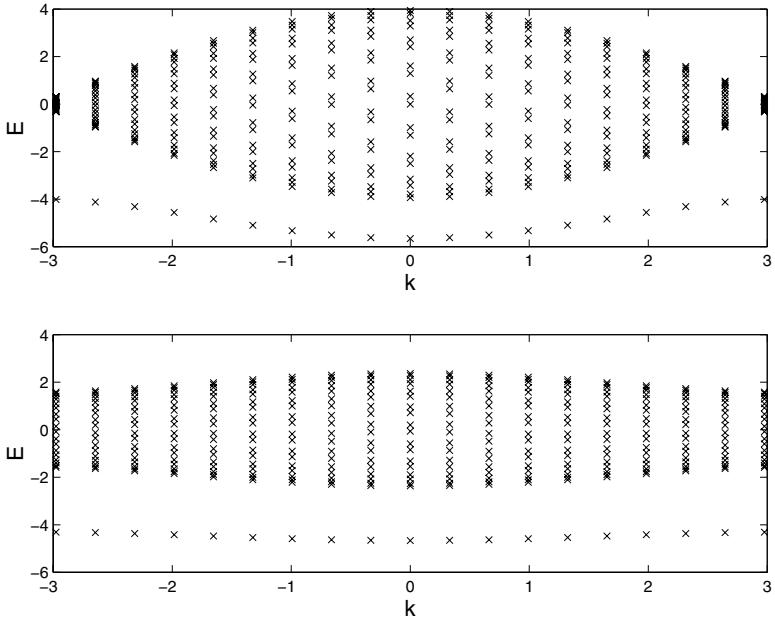

Figure 1. Eigenvalues $E(k)$. $N = 2$, $f = 19$, $\gamma = 4$. $m_e = 1$ (top) and $m_e = 0.2$ (bottom).

If we consider for simplicity the case $k = 0$, the ground state unnormalized eigenfunction is

$$|\Psi\rangle = [10\ldots0;10\ldots0]+[01\ldots0;01\ldots0]+\ldots[0\ldots01;0\ldots01]+O(\gamma^{-1}),$$

i.e. on a lattice of length f, the unnormalized coefficients c_i of the first f terms are equal to unity and the rest are $O(\gamma^{-1})$.

4. Trapping in a lattice with broken translational symmetry

In this section we will consider some modifications that can break the translational invariance of the lattice, changing the coefficients c_i and localize the breather around a particular point of the lattice. In

these cases, the Hamiltonian operator cannot be block-diagonalized using eigenvectors of the translation operator. Although the computational effort increases, it is still possible to calculate its eigenvalues and eigenvectors if f and N are small enough, by using algebraic manipulation methods and numerical eigenvalue solvers. In this section we restrict to the situation $N_a = N_b = 1$.

Perhaps the simplest way to break the translational invariance of the lattice is by considering non–flux boundary conditions to simulate a finite–size chain. In this case, the solution becomes weakly localized around the middle of the lattice. If f is high enough, and we do no take into account boundary effects, this case reduces to the homogeneous lattice case.

A alternative mechanism for breaking the translational invariance can be the existence of local inhomogeneities or impurities. In our model, this can be modeled by making one or more of the γ_j or the ϵ_j dependent on j. This can occur because of localized impurities or long–range interaction between non nearest-neighbors sites due to non–uniform geometries of the lattice chain. The interplay between these two sources of localization, nonlinearity and impurities is important to understand the properties of these bound states.

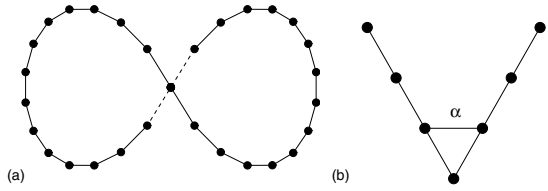

Figure 2. Two non-uniform chain geometries.

Two examples of non–uniform geometries are shown in Fig. 2. In Fig. 2a, a twisted circular geometry causes an interaction between two sites of the chain, which are distant with respect to measurement along the length of the chain. This model has been used in a classical model of a globular protein [13], and it has been shown that moving breathers described by the DNLS equation can be trapped at the cross–over point. Fig. 2b shows another possible geometry, a bent chain, that has been recently studied in the context of the DNLS equation and photonic crystal context [14] and in Klein–Gordon systems [15]. In all these cases, the geometry effects can be modeled by adding a long–range interaction term of the form

$$\alpha_{\ell,m}(b_\ell^\dagger b_m + b_m^\dagger b_\ell), \tag{2}$$

where ℓ and m are the neighbouring sites put brought closer in the twisted–chain case, and $m = m_0 - 1$ and $\ell = m_0 + 1$ in the bent–chain case, where m_0 is the vertex of the chain.

We will analyze in more detail these modifications that break the translational invariance of the system.

4.1 Localization in a chain with impurities

We introduce a local inhomogeneity in the anharmonic parameter in our system and retain periodic boundary conditions, in order to isolate the effect caused by this local inhomogeneity alone. We put $\gamma_\ell = \gamma_{imp}$, and $\gamma_j = \gamma$ for $j \neq l$.

In the homogeneous system, as discussed above, if the anharmonicity parameter is large enough there exists a high probability of finding the two particles at the *same* site of the chain, but with equal probability at *any* site of the chain. If we consider a point impurity, a isolated localized bound state appears, as shown in Fig. 3. This state has minimal energy and corresponds to the ground state.

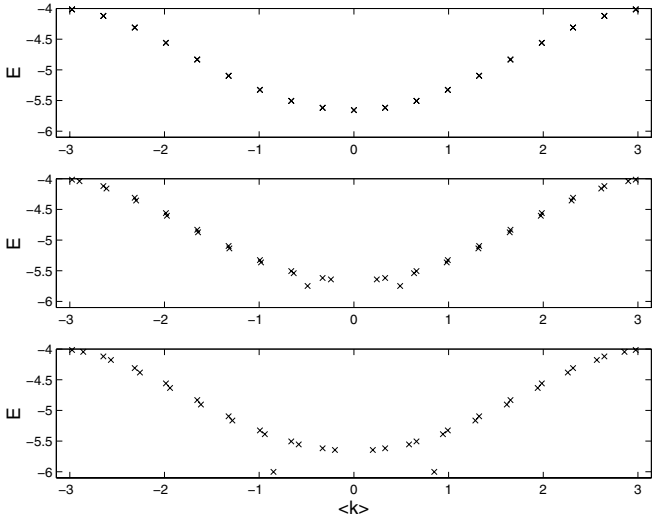

Figure 3. Eigenvalues E as a function of the expected value of k corresponding to the localized eigenfunctions. $N = 2$, $f = 19$, $m_e = 1$ and $\gamma = 4$. Point impurity at the site $\ell = 10$. Homogeneous chain (top). $\gamma_{imp} = 4.5$ (center). $\gamma_{imp} = 5$ (bottom).

If we analyze this ground state, we observe that as γ_{imp} increases, the localization around the impurity increases too, as shown in Fig 4. In particular, the main contribution to the wave function corresponds

to the bound states centered around the impurity. There exists also a small contribution that corresponds to states with particles in adjacent sites around this local inhomogeneity.

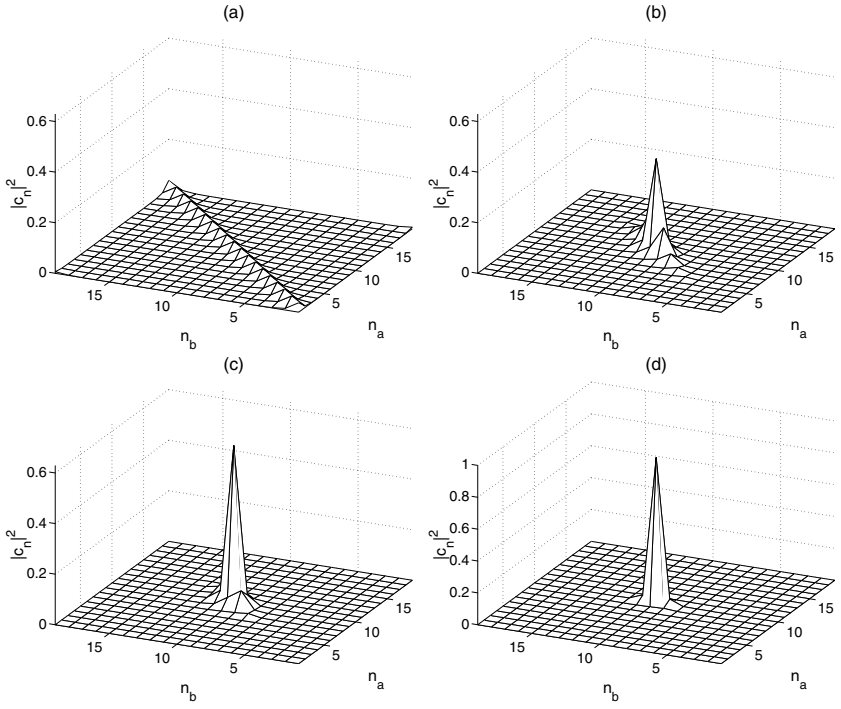

Figure 4. Square wave function amplitudes $|c_n|^2$ corresponding to the ground state as a function of the positions of the two fermions along the chain n_a and n_b. $f = 19$ and $\gamma = 4$. Point impurity at the site $\ell = 10$. (a) Homogeneous chain, $m_e = 1$. (b) $\gamma_{imp} = 4.5$, $m_e = 1$. (c) $\gamma_{imp} = 5$, $m_e = 1$. (d) $\gamma_{imp} = 5$, $m_e = 0.2$.

If we analyze the contribution of the components of the wave function of the ground state corresponding to the two particles centered around the local inhomogeneity in the same site, in adjacent sites, and separated by one site, as shown in Fig 5, we observe that the localization increases very rapidly with the magnitude of the impurity. Varying the value of m_e from unity amplifies this effect even further. We note that, in this case, as harmonic terms are homogeneous (null), there exists no Anderson–like localization.

4.2 Localization in a twisted chain

In order to simulate the twisted chain shown in Fig. 2a, we consider a long–range hopping term between sites m and ℓ given by parameter $\alpha_{m,\ell}$.

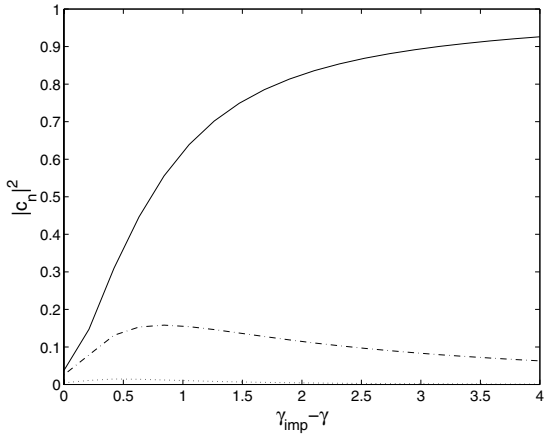

Figure 5. Some components of the wave function corresponding to the ground state. $N = 2$, $f = 19$, $\gamma = 4$ and $m_e = 1$. Two particles centered on the impurity (continuous line). Two particles in adjacent sites with one of them centered on the impurity (dashed–dotted line). Two particles separated by one site and one of them on the impurity (dotted line).

As Fig. 6 shows, this coupling generates a localized bound state around the sites m and ℓ that is a ground state of the system, a phenomenon similar to that shown in Fig 3. Although there exist some degree of localization in the harmonic case ($\gamma = 0$) due to an Anderson–like effect, the existence of bound states due to the anharmonicity parameter γ strongly increases the localization. Similar results have been obtained with different values of the parameter $\alpha_{m\ell}$.

4.3 Localization in a bent chain

To simulate the bend shown in Fig. 2b, we introduce an additional term that takes into account the interaction between the two neighbouring sites of the vertex. In this case, if we suppose that the hopping term varies as the inverse of the square of the distance between sites, the parameter α can be related to the wedge angle θ through $\alpha = \frac{1}{2}/(1-\cos\theta)^{-1}$.

As shown in Fig. 7, due to the existence of this long–range interaction, there exist a localization phenomenon around the vertex of the chain. If the wedge angle is small enough, the ground state is mainly a bound state with the two particles localized in the neighbouring site of the vertex, but when this angle decreases, the contribution of the components corresponding to non–localized states with particles around

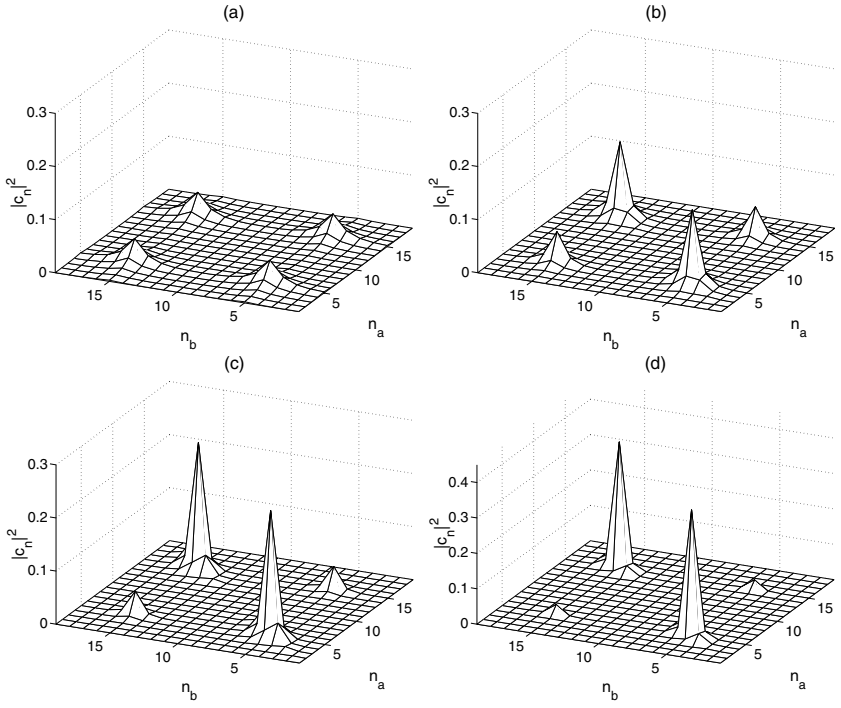

Figure 6. Square wave function amplitudes $|c_n|^2$ corresponding to the ground state as function of the positions of the two fermions n_a and n_b along the twisted chain. Long range interaction between sites $m = 5$ and $\ell = 15$ with $\alpha_{m\ell} = 1$ and $f = 19$. (a) $\gamma = 0$ (harmonic case), $m_e = 1$. (b) $\gamma = 2$, $m_e = 1$. (c) $\gamma = 4$, $m_e = 1$. (d) $\gamma = 4$, $m_e = 0.2$.

the vertex becomes significant. In the limit $\theta \to 0$, the lattice becomes a T-junction. We have found that in this system, the ground state is mainly localized around the junction.

We have compared this localization effect with the Anderson-like localization in the harmonic system ($\gamma = 0$). As shown in Fig. 8, the existence of bound states in the anharmonic case implies that the localization effect due to the curvature of the system increases. This enhancement decreases when θ decreases, although there exists a maximum around $\theta \approx 0.5$.

We note that this model, to give a more realistic approximation of a bent chain, must be improved to take into account the long–range interaction between all sites that becomes significant when the angle θ

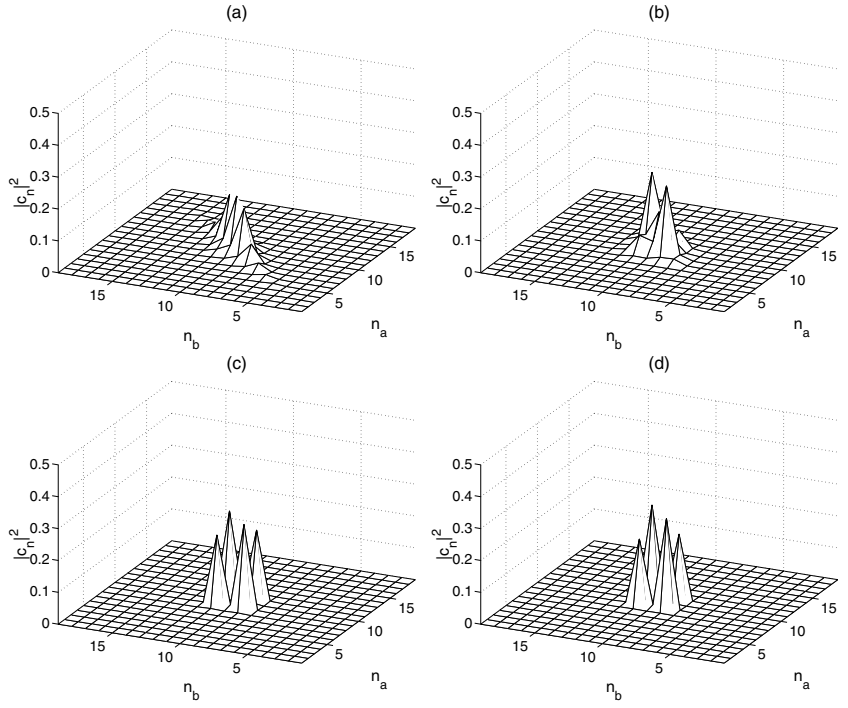

Figure 7. Square wave function amplitudes $|c_n|^2$ corresponding to the ground state as a function of the positions of the two fermions n_a and n_b along the bent chain. $f = 19$ and $\gamma = 4$. (a) $\theta = \pi$, $m_e = 1$. (b) $\theta = \pi/3$, $m_e = 1$. (c) $\theta = \pi/10$, $m_e = 1$. (d) $\theta = \pi/10$, $m_e = 0.2$.

is small enough. We have considered the model given by the Hamiltonian

$$\hat{H} = -\gamma \sum_{j=1}^{f} a_j^\dagger a_j b_j^\dagger b_j - \sum_{j=1}^{f} \sum_{i>j} \frac{1}{d_{ij}^2} (a_i^\dagger a_j + a_j^\dagger a_i) - \sum_{j=1}^{f} \sum_{i>j} \frac{m_e}{d_{ij}^2} (b_i^\dagger b_j + b_j^\dagger b_i), \quad (3)$$

where d_{ij} represents the distance between sites i and j. We have found the same qualitative behavior.

5. Higher number of quanta

In previous sections, we have restricted our studies to the case $N_a = N_b = 1$. Proceeding as the same way, it is possible –in principle– to construct the Hamiltonian matrix for any value of the quantum numbers

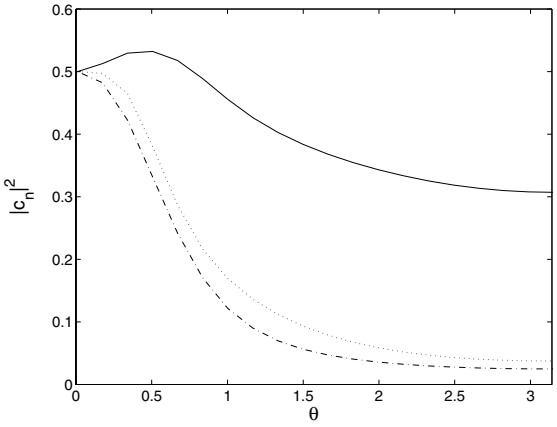

Figure 8. Some components of the wave function corresponding to the ground state. $N = 2$, $f = 19$ and $m_e = 1$. Localized state corresponding to the two particles at the neighbor site of the vertex and $\gamma = 4$ (continuous line). Two particles in a non–localized state at neighbouring sites of the vertex and $\gamma = 4$ (dashed-dotted line). Two particles in a non–localized state at neighbouring sites of the vertex and $\gamma = 0$ (dotted line).

N_a and N_b and to calculate the spectrum. However, the computational effort increases rapidly and can go beyond the limits of computational convenience. Nevertheless, we have studied some cases involving a higher number of fermions. In particular, we have considered the case $N_a = 2$ and $N_b = 1$ and the case $N_a = N_b = 2$.

In general, we have found the same qualitative behavior than in the previous case. In the homogeneous system, if the anharmonic parameter is high enough, the ground state is mainly a localized state, in the sense that there exists a high probability to find two different fermions at the same point of the lattice, but due to the translational invariance of the system, with equal probability of finding these two particles at any site of the system. However, we observe that the main components of the ground state correspond to states where fermions of the same type are as far apart as possible from each other. This is a similar effect as due to the finite–size of the chain where the ground state is weakly localized around the center of the chain. When a fermion is close to other of the same type, the hopping in that direction is limited, as in the case of a finite–size chain.

When we introduce some local inhomogeneities in the system, we have observed similar localization phenomena as noted above. In Fig 9 we show the case $N_a = 2$ and $N_b = 1$ with a point impurity at the

anharmonic parameter. We observe that the ground state is mainly a bound state. The two different fermions are mainly in a localized state centered at the impurity with the other fermion in the other extremum of the chain. We note that there exists a significant contribution of other components corresponding to localized states of the two different fermions in the impurity and the other one in different sites of the chain, this contribution being more significant when it corresponds to states where the two fermions are separated by a large number of sites. This system, in the context of excitons in ring geometries, is usually called ortho–trion, and can be viewed as an exciton plus an additional electron smeared over the ring [16].

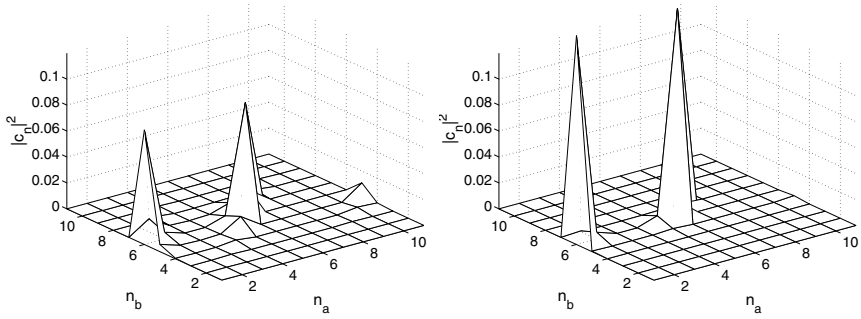

Figure 9. Some components of the wave function of the ground state corresponding to the case $f = 11$, $N_a = 2$, $N_b = 1$, $\gamma = 4$, point impurity at the site $\ell = 6$ and $\gamma_{imp} = 5$. n_a represents the position of one of the fermions of type (a) (the other fermion is located at $n_a + 5$) and n_b the position of the fermion of type (b). $m_e = 1$ (left), $m_e = 0.2$ (right).

In the other cases, when a local inhomogeneity is introduced by means of a long–range interaction term, or $N_a = N_b = 2$ is considered, the behavior is similar. The ground state corresponds to a localized state centered at the local inhomogeneities where different fermions are together and fermions of the same type are located as further apart as possible one from the other.

6. Conclusions

In this work we have shown some results related with the existence and properties of quantum breathers in a fermionic Hubbard model with two kinds of particles of opposite spins. We have studied the existence of localized states due to the nonlinearity and to the influence of local inhomogeneities in these localized states. In particular, we have found that these local inhomogeneities, due to the geometrical factor and to a

long–range interaction or an impurity in the anharmonicity parameter, break the translational invariance of the system and localize the ground state around a particular site of the chain. We expect that these results are rather general, and could be extended to a great variety of systems.

Acknowledgments

The authors are grateful for partial support under the LOCNET EU network HPRN-CT-1999-00163. F. Palmero thanks Heriot-Watt University for hospitality, and the Secretaría de Estado de Educación y Universidades (Spain) for financial support.

References

[1] S. Flach and C.R. Willis, Phys. Rep. **295**, 181 (1998); Physica D **119**, special volume edited by S. Flach and R.S. Mackay (1999): P.G. Kevrekidis, K.Ø. Rasmussen and A.R. Bishop, Int. J. Mod. Phys. B, **15**, 2833 (2001); focus issued edited by Yu. S. Kivshar and S. Flach, Chaos **13**, 586 (2003), *Localization and Energy Transfer in Nonlinear Systems*, eds L. Vázquez, R. S. MacKay, M. P. Zorzano (World Scientific, Singapore, 2003).

[2] A.C. Scott, J.C. Eilbeck and H. Gilhøj, Physica D **78**, 194 (1994).

[3] V. Fleurov, Chaos **13**, 676 (2003); R.S. MacKay, Physica A **288**, 174 (2000).

[4] F. Fillaux and C.J. Carlile, *Phys. Rev. B* 42, 5990 (1990); F. Fillaux, C.J. Carlile and G.J. Kearley, *Phys. Rev. B* 44, 12280 (1991); F. Fillaux, C.J. Carlile and G.J. Kearley, *Phys. Rev. B* 226, 241 (1996); F. Fillaux, C.J. Carlile and G.J. Kearley, *Phys. Rev. B* 58, 11416 (1998).

[5] T. Asano, H. Nojiri, Y. Inagaki, J.P. Boucher, T. Sakon, Y. Ajiro and M. Motokawa, *Phys. Rev. Lett.* 84, 5880 (2000).

[6] L.S. Schulman, E. Mihokova, A. Scardinicchio, P. Facchi, M. Nikl, K. Polak and V. Penne, *Phys. Rev. Lett.* 88, 224101, (2002).

[7] Xiaoqin Li *et al.*, Science **301**, 809 (2003).

[8] R. Micnas, J. Ranninger and S. Robaszkiewicz, *Rev. Mod. Phys.* 62, 113 (1992).

[9] R.A. Römer and A. Punnoose, *Phys. Rev. B* 52, 14809 (1995).

[10] J.C. Eilbeck and F. Palmero. Preprint http://arXiv.org/abs/nlin/0309042, (2003)

[11] A.C. Scott, *Nonlinear Science* (OUP, Oxford 1999, 2003).

[12] J.C. Eilbeck, in *Localization and Energy Transfer in Nonlinear Systems*, eds. L. Vázquez, R.S. MacKay, M.P. Zorzano, World Scientific, Singapore, 177 (2003).

[13] J.C. Eilbeck, in *Computer Analysis for Life Science*, eds. C. Kawabata and A.R Bishop, 12 (Ohmsha: Tokyo 1986).

[14] P.L. Christiansen, Y.B. Gaididei and S.F. Mingaleev, J. Phys. Condens. Matter **13**, 1181 (2001); Yu.S. Kivshar, P.G. Kevrekidis and S. Takeno, Phys. Lett. A **307**, 287 (2003).

[15] J. Cuevas and P.G. Kevrekidis. Preprint http://arxiv.org/abs/nlin.PS/0308022 (2003).

[16] R.A. Römer and M.E. Raikh. Phys. Stat. Sol. (b) **227**, 381 (2001).

ENERGY LOCALIZATION AND FIRST ORDER PHASE TRANSITION IN SOLIDS AND MOLECULES

Shozo Takeno
Institute for Innovative Science and Technology, Nagasaki Institute of Applied Science, Nagasaki 851-0193, Japan
IZK05505@nifty.ne.jp

Tetsuro Suzuki
National Research Institute for Metals, Tsukuba 305-0047, Japan

Abstract An attempt is made to give a unified picture of energy localization as a precursor to the first order phase transition and the Martenthitic transformation in solids and the molecular dissociation in chemistry.

Keywords: Intrinsic localized modes, Energy localization, Melting of solids, Martensitic transformation, Vortices, Bond energy localization, Molecular dissociation, No energy equipartition.

1. Introduction

Despite the strong interest in melting of solids over the past 100 years, its mechanism does not appear to have been well understood. In parallel to this, much debates have been made on natures of Martensitic transformation (MT) in solids. Situations similar to this exist in chemistry, where little is known about dynamics of molecules leading eventually to dissociation and chemical reaction. Let us first pay attention to situations in chemistry, where the familiar normal mode model has long been used to describe vibrations of polyatomic molecules [1]. As a zeroth-order description, it works well as long as the anharmonicity of molecular vibrations is negligibly small compared with harmonic vibrations. A general vibrational state of a given molecule can then be expressed as a superposition of normal-mode-vibrations, in terms of which the standard theory can be formulated both in classical and quantum levels. In

F. Kh. Abdullaev and V. V. Konotop (eds.), Nonlinear Waves: Classical and Quantum Aspects, 413–426.

certain sense, normal coordinates extends equally over whole regions of molecules. On the other hand, local ("bond") modes provide a counter-intuitive contrast to the above situations. The local mode model was put forward long time ago in order to explain the overtone absorption spectra of polyatomic molecules [2], [3]. They are vibrational modes with long lifetimes in which the motion and the energy are more or less confined to a single bond. In spite of its long history and accumulation of a wealth of spectroscopic data, the local mode model itself appears to have remained in conceptual and phenomenological stage. Relevance of the localization of the bond vibrational energy to chemical dissociation does not appear to have been mentioned, to the best of the authors'knowledge. Because the first-order phase transitions including chemical dissociation is initiated by deviations far from equilibrium, there is a good reason to believe that large-amplitude motion of atoms are likely to be involved as a key ingredient among possible mechanisms. Closely connected with this are intrinsic localized modes (ILM) in nonlinear lattice dynamics. [4, 5]

It is the purpose of this paper to show that energy localization (EL) at particular bonds or regions in systems associated with the ILM plays the role of precursor to the first order phase transition including chemical dissociation. Relevance of the EL to the phase transition was previously presumed by Shigenari and his coworkers in their experiments using Raman and fluoresence spectroscopy [6, 7] and by Peyrard theoretically [8, 9]. The result obtained here is different from theirs in the following respect that space-time evolution of atoms exhibiting the EL which subsequently leads to the phase transition or the dissociation was explored both numerically and analytically to illustrate how the EL takes place. Two cases of dynamical systems characterized by soft interatomic potential are considered: (1) An idealized linear 3-atom molecule composed of identical atoms. (2) FCC-type small crystals without internal lattice defects. For case (1) and (2) the Morse potential and a model potential employed empirically for Fe were adopted. In the former, we pay particular attention to large amplitude motion of atoms leads to local breaking of bond and the time-evolution of the bond energy. It is shown that energy localization at a particular bond accompanied with transferring of the bond energy from surroundings induces bond breaking. In the latter we made detailed examination of change of cohesive energy, shape of the model crystal, trajectories of atoms, appearance of BCC phase, etc. Characteristic features were the appearance of vortex-like pattern of trajectories of atoms on the surface of the small crystal as an excited transient state prior to the onset of MT, in which vortices can be considered as a spatially extended version of the ILM.

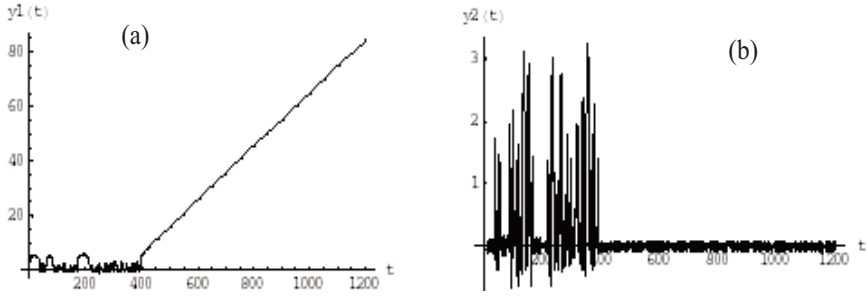

Figure 1. Time evolution for case (i) of $y_1(t)$ (a) (large amplitude) and $y_2(t)$ (b).

Thus, we propose here a unified picture of energy localization as a precursor to the first order phase in solid, the MT transformation and the chemical dissociation.

2. Nonlinear molecular vibrations and chemical dissociation

2.1 Equations of motion

We consider vibrations of molecules. We assume from the outset that the Born-Oppenheimer approximation is satisfied for the electronic, vibrational and rotational states of the molecules. Let the atomic mass and the displacement vector of an i atom from its equilibrium position in a molecule be m_i and $\vec{r}_i$, respectively. The interatomic potential between the i and j atoms, U_{ij} in the molecule is taken to be of the form

$$U_{ij} = U_{ij}(\mid \vec{r}_i - \vec{r}_j \mid) \equiv U_{ij}(\mid \vec{r}_{ij} \mid) \qquad \text{with} \quad U_{ji}(r_{ji}) = U_{ij}(r_{ij}) \tag{1}$$

We first consider vibrations of 3-atom molecules. Let three atoms be 1,2 and 3 with atomic masses m_1, m_2 and m_3, respectively, as depicted in Fig. 1

Let the position vector of an $i(i = 1, 2, 3)$ atom be $\vec{r}_i$. We set

$$\vec{r}_{ij} = \vec{r}_i - \vec{r}_j, \quad r_{ij} = |\vec{r}_i - \vec{r}_j| \quad \text{with} \quad \vec{r}_{ji} = -\vec{r}_{ij}, \quad r_{ji} = r_{ij} \tag{2}$$

Equations of motion for the vibrations of the i atom are written as

$$m_i \frac{d^2\vec{r}_i}{dt^2} = -\sum_{j \neq i} \frac{dU_{ij}(\vec{r}_{ij})}{d\vec{r}_i} \tag{3}$$

We are particularly interested in the dynamics of bonds rather than that of individual constituent atoms. For an i-j bond, the equation of motion takes the form

$$\frac{d^2\vec{r}_{ij}}{dt^2} = -\frac{1}{\mu_{ij}}\frac{dU_{ij}(r_{ij})}{d\vec{r}_{ij}} - \frac{1}{m_i}\sum_{k\neq i}\frac{dU_{ik}(r_{ik})}{d\vec{r}_{ik}} - \frac{1}{m_j}\sum_{\ell\neq j}\frac{dU_{\ell j}(r_{\ell j})}{d\vec{r}_{\ell j}} \tag{4}$$

Such a procedure ensures the conservation of the total momentum of the molecule or the center of gravity of the molecule being at rest, i.e.

$$\sum_i m_i\ddot{\vec{r}}_i = 0 \quad \sum_i m_i\vec{r}_i = \quad \text{const} \tag{5}$$

where

$$\frac{1}{\mu_{ij}} = \frac{1}{m_i} + \frac{1}{m_j} \tag{6}$$

is the reduced mass of the i and j atoms. Multiplying $d\vec{r}_{ij}/dt$ on both sides of Eq.(4) gives equations of motion for the local bond energy h_{ij},

$$h_{ij} = \frac{\mu_{ij}}{2}\left[\frac{d\vec{r}_{ij}}{dt}\right]^2 + U_{ij}(r_{ij}), \tag{7}$$

in the form

$$\frac{dh_{ij}}{dt} = -\frac{\mu_{ij}}{m_i}\sum_{k\neq i}\frac{dU_{ik}(r_{ik})}{d\vec{r}_{ik}}\cdot\frac{d\vec{r}_{ij}}{dt} - \frac{\mu_{ij}}{m_j}\sum_{\ell\neq j}\frac{U_{\ell j}(r_{\ell j})}{d\vec{r}_{\ell j}}\cdot\frac{d\vec{r}_{ij}}{dt} \tag{8}$$

Equation (8) can be rewritten as

$$\frac{dh_{ij}}{dt} = -\frac{\mu_{ij}}{m_i}\sum_{k\neq i}\frac{dU_{ik}(r_{ik})}{dt}\frac{d\vec{r}_{ij}}{d\vec{r}_{ik}} - \frac{\mu_{ij}}{m_j}\sum_{\ell\neq j}\frac{U_{\ell j}(r_{\ell j})}{dt}\frac{d\vec{r}_{ij}}{d\vec{r}_{\ell j}} \tag{9}$$

2.2 Applications: 3-atom molecule

2.2.1 General theory. We first illustrate the above procedure to the case of a 3-atom molecule. Let three atoms be 1,2 and 3 with atomic masses m_1, m_2 and m_3, respectively. Equation (4) then takes

the form

$$\begin{aligned}
\frac{d^2\vec{r}_{12}}{dt^2} &= -\left(\frac{1}{m_1}+\frac{1}{m_2}\right)\nabla_{12}U_{12}(r_{12}) - \frac{1}{m_1}\nabla_{13}U_{13}(r_{13}) \\
&\quad -\frac{1}{m_2}\nabla_{32}U_{32}(r_{32}) \\
\frac{d^2\vec{r}_{13}}{dt^2} &= -\left(\frac{1}{m_1}+\frac{1}{m_3}\right)\nabla_{13}U_{13}(r_{13}) - \frac{1}{m_1}\nabla_{12}U_{12}(r_{12}) \\
&\quad -\frac{1}{m_3}\nabla_{32}U_{32}(r_{32}) \\
\frac{d^2\vec{r}_{32}}{dt^2} &= -\left(\frac{1}{m_2}+\frac{1}{m_3}\right)\nabla_{32}U_{32}(r_{32}) - \frac{1}{m_3}\nabla_{13}U_{13}(r_{13}) \\
&\quad -\frac{1}{m_2}\nabla_{12}U_{12}(r_{12}) \qquad (10)
\end{aligned}$$

Of these three equations, two equations are independent of one another. For example, we can eliminate the relative position vector $\vec{r}_{13}$ in favor of $\vec{r}_{12}$ and $\vec{r}_{32}$ by noting that $\vec{r}_{13} = \vec{r}_{12} - \vec{r}_{32}$, arriving at the equations

$$\frac{d^2\vec{r}_{12}}{dt^2} = -\frac{1}{\mu_{12}}\frac{dU_{12}(r_{12})}{d\vec{r}_{12}} - \frac{1}{m_2}\frac{dU_{32}(r_{32})}{d\vec{r}_{32}} - \frac{1}{m_1}\frac{dU_{13}(|\vec{r}_{12}-\vec{r}_{32}|)}{d\vec{r}_{12}} \qquad (11)$$

$$\frac{d^2\vec{r}_{32}}{dt^2} = -\frac{1}{\mu_{32}}\frac{dU_{32}(r_{32})}{d\vec{r}_{32}} - \frac{1}{m_2}\frac{dU_{12}(r_{12})}{d\vec{r}_{12}} - \frac{1}{m_3}\frac{dU_{31}(|\vec{r}_{32}-\vec{r}_{12}|)}{d\vec{r}_{32}} \qquad (12)$$

Here, we limit our discussion to the case where the last terms in both of Eqs. (11) and (12) can be neglected as compared with the remaining terms, i.e.,

$$\frac{d^2\vec{r}_{12}}{dt^2} = -\frac{1}{\mu_{12}}\frac{dU_{12}(r_{12})}{d\vec{r}_{12}} - \frac{1}{m_2}\frac{dU_{32}(r_{32})}{d\vec{r}_{32}}, \qquad (13)$$

$$\frac{d^2\vec{r}_{32}}{dt^2} = -\frac{1}{\mu_{32}}\frac{dU_{32}(r_{32})}{d\vec{r}_{32}} - \frac{1}{m_2}\frac{dU_{12}(r_{12})}{d\vec{r}_{12}}. \qquad (14)$$

And Eqs. (9) take the form

$$\frac{dh_{12}}{dt} = -\frac{\mu_{12}}{m_2}\frac{dU_{32}(r_{32})}{dt}\frac{d\vec{r}_{12}}{d\vec{r}_{32}}, \qquad (15)$$

$$\frac{dh_{32}}{dt} = -\frac{\mu_{32}}{m_2}\frac{dU_{12}(r_{12})}{dt}\frac{d\vec{r}_{32}}{d\vec{r}_{12}} \qquad (16)$$

From these two equations, we arrive at the equation

$$\frac{dh_{12}}{dt}\frac{dh_{32}}{dt} = \frac{\mu_{12}\mu_{32}}{m_2^2}\frac{dU_{12}(r_{12})}{dt}\frac{dU_{32}(r_{32})}{dt} \tag{17}$$

Conservation of the local bond energy

$$h_{12} = \text{const} \quad \text{or} \qquad h_{32} = \text{const} \quad \text{or} \quad \text{both} \tag{18}$$

provided

$$\frac{dU_{12}(r_{12})}{dt} = 0 \qquad \text{or} \qquad \frac{dU_{32}(r_{32})}{dt} = 0 \tag{19}$$

2.2.2 An illustrative example, a linear 3-atom molecule. Here, we are concerned with stretching vibrations of three atoms in the molecule which are taken to be located on the x-axis. Let x_1, x_2 and x_3 be the displacement of the atoms 1, 2 and 3, respectively, along the x-axis. Then, in terms of

$$r_{12} = x_1 - x_2 \equiv y_1, \qquad r_{32} = x_3 - x_2 \equiv y_2 \tag{20}$$

The inter-atomic potential energy is taken to be of the Morse-potential type

$$U_i(y_i) = c_i[1 - \exp(-a_i y_i)]^2, \quad i = 1, 2 \tag{21}$$

where c_i and a_i are constants. Eqs.(13) and (14) reduce to

$$\frac{d^2y_1}{dt^2} = -\frac{1}{\mu_{12}}\frac{dU_{12}(y_1)}{dy_1} - \frac{1}{m_2}\frac{dU_{32}(y_2)}{dy_2}, \tag{22}$$

$$\frac{d^2y_2}{dt^2} = -\frac{1}{m_2}\frac{dU_{12}(y_1)}{dy_1} - \frac{1}{\mu_{32}}\frac{dU_{32}(y_2)}{dy_2}, \tag{23}$$

$$\frac{dh_{12}}{dt}\frac{dh_{32}}{dt} = \frac{\mu_{12}\mu_{32}}{m_2^2}\frac{dU_{12}(y_1)}{dt}\frac{dU_{32}(r_2)}{dt}. \tag{24}$$

2.2.3 An idealized 3-atom molecule. Equations (22) and (23) constitute a pair of nonlinear differential equations which are generally non-integrable. The basic vibrational properties of the three-particle system under consideration can be understood better by first studying an idealized case where all the three atoms are identical with atomic

mass m. These equations and Eq.(24) then reduce to

$$\frac{d^2y_1}{dt^2} = -\frac{2}{m}\frac{dU_{12}(y_1)}{dy_1} - \frac{1}{m}\frac{dU_{32}(y_2)}{dy_2}, \tag{25}$$

$$\frac{d^2y_2}{dt^2} = -\frac{1}{m}\frac{dU_{12}(y_1)}{dy_1} - \frac{2}{m}\frac{dU_{32}(y_2)}{dy_2}, \tag{26}$$

$$\frac{dh_{12}}{dt}\frac{dh_{32}}{dt} = \frac{1}{4}\frac{dU_{12}(y_1)}{dt}\frac{dU_{32}(r_2}{dt} \tag{27}$$

Small-amplitude regime of these equations are well-known, where their solutions are described by conventional normal modes. We are particularly interested here in the existence of large-amplitude nonlinear modes which leads eventually to dissociation of the molecule. To seek such a mode and inquire into its properties, we solved Eqs. (25) numerically, where we set $c_1 = c_2 = a_1 = a_2 = 1$ for simplicity. For this purpose, for $y_i \equiv y_i(t)$, $\dot{y}_i(t) = dy_i(t)/dt$ $(i = 1, 2)$, we set

$$y_i(0) \equiv u_i, \quad \dot{y}_i(0) \equiv v_i, \tag{28}$$

Two kinds of initial conditions,

$$\begin{aligned} &(i)\ \ u_1 = u_2 = v_2 = 0, \quad v_1 = 1.74 \quad \text{large amplitude regime} \\ &(ii)\ \ u_1 = u_2 = v_2 = 0, \quad v_1 = 0.5 \quad \text{small amplitude regime} \end{aligned} \tag{29}$$

are used here, of which the first one was chosen to observe how molecular dissociation takes place, while the second one was chosen to illustrate the case of small-amplitude vibrations where the conventional normal-mode concepts holds. The result of numerical calculation for case (i) was shown in Fig. 1 and Fig. 2 for $y_i(t)$ and $h_i(t)$, respectively, where we put $U_{12} \equiv U_1(t)$, $U_{32}(t) \equiv U_2(t)$ for simplicity.

The corresponding quantities for case (ii) are shown in Fig. 3 and Fig. 4, respectively.

Figures 1 and 3 shows the how the bond vibrational motion for large-amplitude motions different from the corresponding one for small-amplitude motion. It is seen from Fig. 2a that at the initial stage $t < 400$ equi-partition of energy holds in the bonds 1 and 2, but for $t \geq 400$ almost all energy are localized at bond 1. Here the energy shared by bond 2 is transferred to bond 1. This subsequently induces bond 1 breaking at $t \approx 400$. This is to be compared with the case (ii) where equi-partition of energy takes place between the bonds 1 and 2 as seen from Fig. 4. The physical meaning of the obtained result can be appreciated further

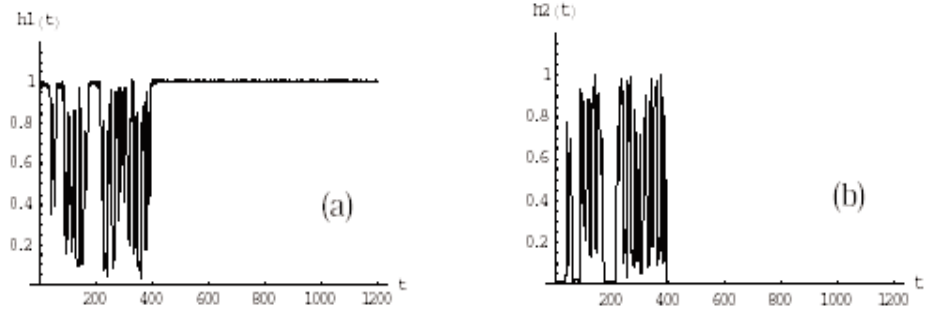

Figure 2. Time evolution for case (i) of $h_1(t)$ (a) and $h_2(t)$ (b).

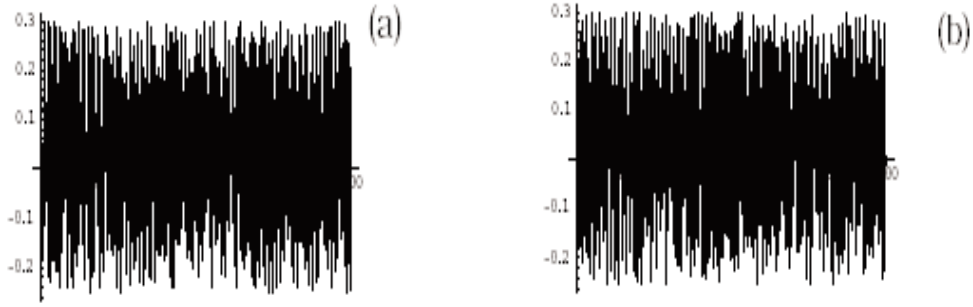

Figure 3. Time evolution for case (ii) of $y_1(t)$ (a) and $y_2(t)$ (b).

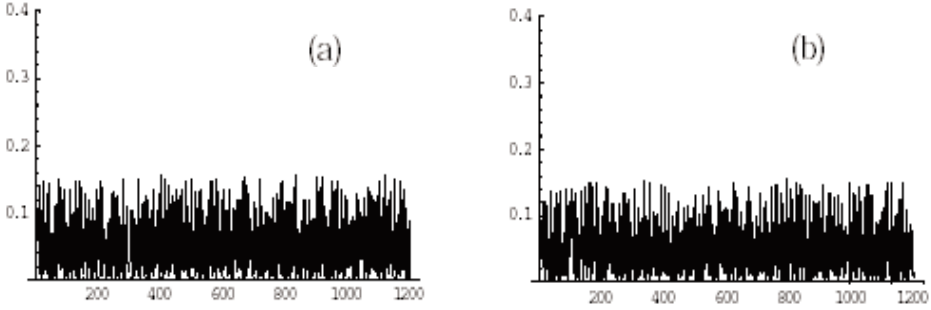

Figure 4. Time evolution for case (ii) of $h_1(t)$ (a) and $h_2(t)$. Small-amplitude vibrations.

by looking at the time evolution of the kinetic energy $K_i(t)$ and the potential energy $U_i(t)$ of the i (=1,2,3) atom defined by

$$K_i(t) = \frac{m}{2}\dot{x_i}(t)^2, \tag{30}$$

$$U_1(t) = (1 - \exp[-y_1])^2, \tag{31}$$

$$U_2(t) = \frac{1}{2}(1 - \exp[-y_1])^2 + \frac{1}{2}(1 - \exp[-y_2])^2, \tag{32}$$

$$U_2(t) = (1 - \exp[-y_2])^2 \tag{33}$$

These quantities are shown in Fig. 5, where Fig.s 5(ai) and 5(bi) (i=1,2,3) stands for $K_i(t)$ and $U_i(t)$, respectively. To make closer examination of the energy localization in molecular vibrations, time evolution of $y_i(t)$ and $h_i(t)$ just before and after dissociation, $390 < t < 400$, was made. The result for the former and the latter was shown in Fig. 6, where Fig.s 6(ai) and 5(bi) (i=1,2,3) stands for $y_i(t)$ and $h_i(t)$, respectively. Comparing these two, we see that breaking of the bond 1 results from accumulation of the vibrational energy there, where the vibrational energy of the bond 2 is transferred to the bond 1.

2.2.4 Implication of the obtained result to melting of solids.

The numerical result for the linear 3-atom molecule obtained above is not directly applicable to the problem of melting of solids. For this purpose, exploring large-amplitude vibrational motion of atoms in three-dimensional (3D) lattice is indispensable, though simpler cases of two-dimensional (2D) lattice gives some useful information on these problems. However, if we look at the motion of atoms in the direction of large-amplitude motion, calculations based on one-dimensional models may be of some use, for which we should modify the original Morse potential by an effective soft potential with several minima.

3. Martensitic transformation of a small pure crystal

Bulk metal crystals are believed to contain dislocations or defects of the order of 10^8 - $10^{10}/\mathrm{cm}^2$. Many discussions have been made to see whether the Martensitic transformation originates from the effects of the defects or the intrinsic properties of the crystals. Keeping this in mind, we performed numerical investigation of the Martensitic transformation (MT) of a small crystal in the range of nm containing any extrinsic defects without using the periodic boundary condition [10]. A molecular dynamics method using the 5th order Gear algorithm was used, where the embedded atom method potential was used [11]. This poten-

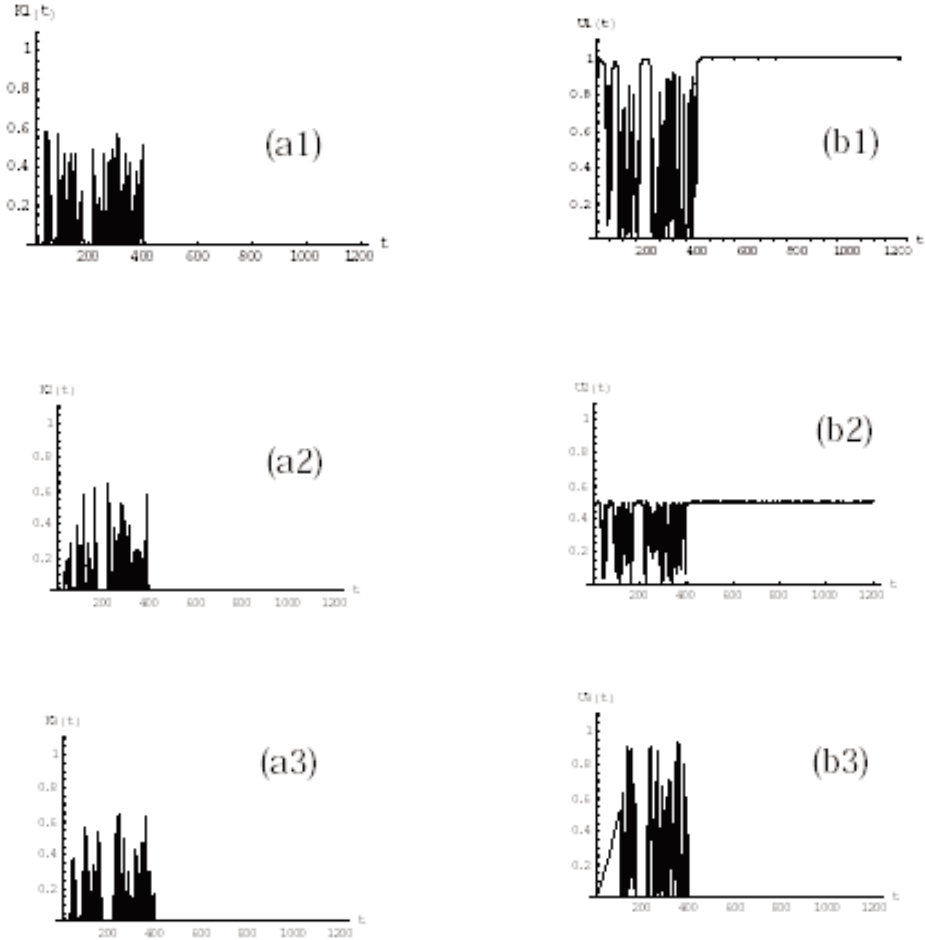

Figure 5. Time evolution of the kintic energy Ki(t) and the potential energy $U_i(t)$ of i-th atom. Case (i).

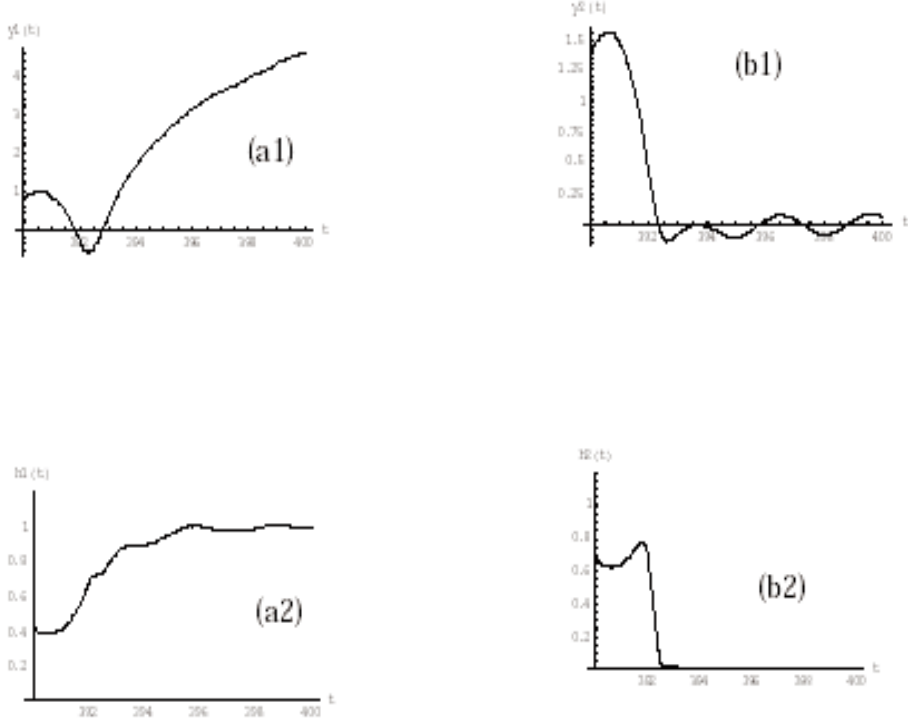

Figure 6. Time-evolution of $y_i(t)$ and $U_i(t)$ $(i = 1, 2)$ in the range $390 < t < 400$ for the case (i).

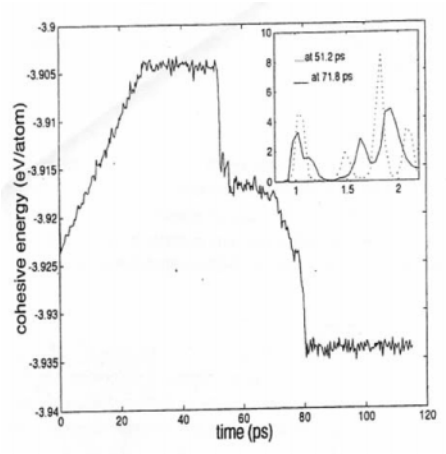

Figure 7 Change of cohesive energy (eV) vs time(ps). Dotted and full lines in the inset corresponds to FCC and BCC, respectively.

tial makes FCC Fe metastable and Bcc stable, it cannot reproduce the reversal of the stability of FCC against Bcc with temperature increase. The study of the MT is therefore carried out by raising the temperature of metastable FCC.

Among many obtained numerical results, the simplest ones, that of a crystal with 453 atoms is presented here. The integration step is 6.4fs. and the total kinetic energy is coled to the temperature at every 10 integration steps. The temperature is raised at constant rate of 4.59K/ps from the initial temperature of 10K up to 200K and held there afterwards. Change of the cohesive energy per one atom is plotted as a function of time in Fig. 7, in which the radial distribution function of the system at 51.2 ps is plotted. It is seen that sudden drop of the cohesive energy close to 51.2 ps signals the MT.

Change of averaged coordinates of the atoms on the surface of the system during the time span from 46 ps to 51 and that from 51 to 56 ps is ps seen from [100] directions is shown in the upper left and right, respect of Fig. 8. The lower left and right show the change of the positions of atoms on the [100] cross section through the center of the crystal during 46 ps to 51 ps and 51 to 56 ps, respectively. It is seen that vortex-like patterns are observed by pairs in the right are found to penetrate gradually in the interior of the crystal as shown in the lower right.

To gain physical picture of vortices as as a precursor of the MT, we explored votex solutions of two-dimensional (2D) sine-Gordon equations [12] as a model field equations for atoms on the surface of system to see

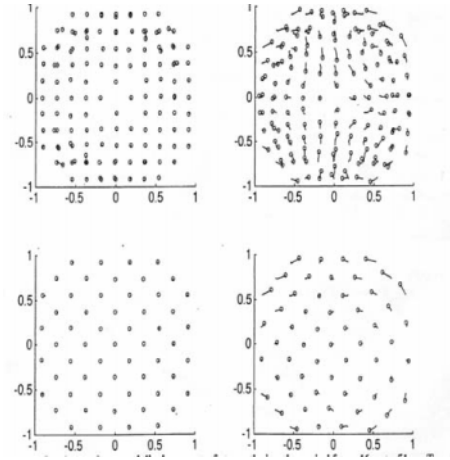

Figure 8. Averaged displacement of atoms.

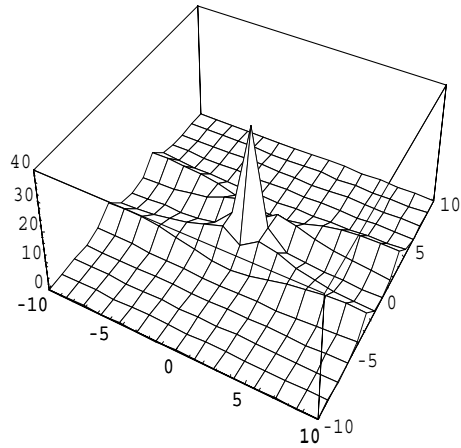

Figure 9. Energy density of vortex solution of 2D SG equations.

that energy localization takes place at the vortex site, though the vortex itself can be considered as an extended defect (see Fig. 9).

References

[1] E.B. Wilson, Jr., J.C. Decius and P.C. Cross, *Molecular vibrations*(McGraw-Hill, New York, 1955), and references cited therein.

[2] M.L. Sage and J. Jortner, Adv. Chem. Phys. **47**, Pt.I, 293(1981) and references cited therein.

[3] R.H. Page, Y.R. Shen and Y.T.Lee, J. Chem. Phys. **88**, 4621(1988) and references cited there.

[4] A.J. Sievers and S. Takeno, Phys. Rev. Lett. **61** 970 (1988); S. Takeno, K. Kisoda and A.J. Sievers, Prog. Theor. Phys. Suppl. No.**94**, 242 (1988).

[5] S. Takeno, and A.J. Sievers, Solid State Commun. **67**,1023(1988).

[6] T. Shigenari, E. Kojima, Y. Ino and and K. Abe, Phys. Rev. Lett. **66**, 2112(1991).

[7] T. Shigenari and K. Abe, in Proc. 2nd Int. Workshop on *Nucleation and Non-Linear Problems in the First Order Phase Transition*, St. Petersburg, Russia, 2002.

[8] M. Peyrard, Acta Phys. Polonica **B25** (1994), 955.

[9] See also, Z.H. Zin, P. Gumbsch, K. Lu and E. Ma, Phys. Rev. Lett. **87**, 055703(1991).

[10] T. Suzuki, M. Shimono and S. Takeno, Phys. Rev. Lett. **82** (1999), 1474.

[11] R.A. Johnson and D.J. Oh, J. Mater. Res. **4** (1989), 1195.

[12] S. Takeno, Prog. Theor. Phys. Prog. Theor. Phys. **68**(1982), 992.

SOLITON DYNAMICS IN RANDOMLY PERTURBED DISCRETE LATTICES

J. Garnier
Laboratoire de Statistique et Probabilités,
Universite Paul Sabatier, 118 Route de Narbonne, 31062 Toulouse Cedex 4, France
garnier@cict.fr

Abstract We consider the propagation of solitons in randomly perturbed nonlinear lattices. We address the Ablowitz-Ladik chain with a random on-site potential and the Toda lattice with a randomly distributed chain of masses. Our approach is based on a perturbation theory of the inverse scattering transform and stochastic calculus. The generation of a soliton gas consisting of a large collection of evanescent solitons is shown to play an important role. The interplay of discreteness, nonlinearity, and randomness is discussed. The interaction is governed by a length-scale competition involving the typical scales of the soliton as well as the correlation length and the lattice step of the medium.

Keywords: Soliton, random media.

1. Introduction

The propagation of nonlinear waves in disordered media was recently the subject of many investigations. Most results concern the dynamics of waves in continuous media. Different scales have been shown to play important roles. One of them is the localization lengthlength,localization characterizing the decay law when the nonlinearity is small. The second one is a nonlinear length, which decays as the wave amplitude increases. Below some amplitude threshold, the localization length is less than the nonlinear length, so that the exponential decay of wave is observed. Above the amplitude threshold the decay law is dramatically reduced which proves that nonlinearity can compete with the exponential localization [1, 2].

When the media are discrete a new length scale is coming into the problem: the distance between two neighboring sites of the lattice. In a periodic chain of masses, interactions between lattice oscillations can take the form of a resonant sequence, leading to the transfer of the

F. Kh. Abdullaev and V. V. Konotop (eds.), Nonlinear Waves: Classical and Quantum Aspects, 427–441.

energies of lattice excitations on large distances. Randomness leads to the detuning of the resonances and to the localization of the energy of an excitation on a finite number of sites. The spectrum of normal modes is pure point [3]. This result is valid for 1D and 2D lattices and occurs in 3D lattices for when the intensity of fluctuations is strong enough [4, 5].

In most nonlinear discrete systems like discrete nonlinear Schrödinger (DNLS) equation, nonlinear Klein-Gordon lattice, Fermi-Pasta-Ulam chain, moving localized modes are absent due to the Peierls-Nabarro barrier and standing localized modes exist. Moving localized solutions exist in integrable nonlinear discrete models. Two models admitting moving discrete solitons are important. The first one is the Ablowitz-Ladik (AL) model, which is the integrable discretized version of the continuum nonlinear Schrödinger (NLS) equation. The wave dynamic in some electric transmission LC lines is modeled by the superposition of DNLS and AL equations with different weights [6]. The second model is the Toda chain, which is used as a model for the dynamics of biopolymers like DNA chains [7], LC transmission lines [8], excitations in anharmonic lattices, lattices of optical solitons in fibers [9].

For disordered nonlinear discrete media few analytical results are available. The first theoretical approach addresses a dilute system of impurities where the distances between impurities are larger than the soliton width and each interaction between soliton and impurity can be considered as isolated [10, 1]. Another approach consists in using the continuum approximation, and studying the stochastically perturbed wave equations [11]. This approach, considering only broad solitons, uses the mean field theory and neglects radiation phenomena that are important for long distance propagation in a random chain, so that it is generally questionable for nonlinear waves in random media [12]. Most papers [13, 14, 15] apply the collective variable approximation or the averaged Lagrangian approach, where the solution is sought in a soliton-like form with time-dependent parameters. The ansatz is substituted into the Lagrangian of the system, so that a finite-dimensional system of ordinary differential equations is obtained for the set of soliton parameters. The most significant drawback of this method is that it neglects radiation effects. Scharf and Bishop [13] show that the collective variable approach is efficient when dealing with a slowly varying potential which is almost constant at the scale of the soliton width. In this paper we consider the AL (resp. Toda) chain with a segment containing a random potential (resp. random masses). We use the Inverse Scattering Transform to take into account both the variations of the soliton parameters and the radiation effects, which are important especially when

the correlation length of the medium is of the same order as the soliton width.

2. The Toda chain

2.1 The homogeneous Toda chain

The model consists of a one-dimensional chain of particles. Each particle with mass 1 interacts through a nearest neighbor exponential potential. The difference equation that governs the dynamics of the lattice is deduced from Newton's law [8]:

$$\ddot{x}_n = \exp(x_{n+1} - x_n) - \exp(x_n - x_{n-1}), \tag{1}$$

where x_n is the longitudinal displacement of the n-th particle from its equilibrium position and the dot stands for a derivative with respect to time.

2.1.1 The inverse scattering transform. Equation (1) can be rewritten as

$$\dot{c}_n = c_n(v_n - v_{n-1}), \qquad \dot{v}_n = c_{n+1} - c_n,$$

where $c_n = \exp(x_n - x_{n-1})$ and $v_n = \dot{x}_n$. The eigenvalue problem for the continuous spectrum filling the interval $-2 \leq \lambda \leq 2$ reads [16]

$$\sqrt{c_{n+1}} f_{n+1}(k) + \sqrt{c_n} f_{n-1}(k) + v_n f_n(k) = \lambda f_n(k), \qquad \lambda = k + k^{-1},$$

where k is the spectral parameter that lies in the unit circle $\mathbb{S}^1 = \{k \in \mathbb{C}, |k| = 1\}$. The Jost function ψ (resp. ϕ) is the eigenfunction that satisfies the boundary condition $\psi_n(k) \simeq k^n$ as $n \to \infty$ (resp. $\phi_n(k) \simeq k^{-n}$ as $n \to -\infty$). The Jost coefficients are connected to the Jost functions through the identities:

$$\phi_n(k) = a(k)\psi_n^*(k) + b(k)\psi_n(k), \qquad \psi_n(k) = a(k)\phi_n^*(k) - b^*(k)\phi_n(k).$$

a admits an analytic continuation inside the unit disk. The points on the real axis k_r, $r = 1, ..., R$, $|k_r| < 1$, at which $a(k_r) = 0$ correspond one-to-one with eigenvalues of the discrete spectrum. At these points we have $\phi_n(k_r) = b_r \psi_n(k_r)$, $\mathrm{Im}(b_r) = 0$. Setting $\rho_r = b_r / a'(k_r)$, the set of scattering data $\left\{a(k), b(k), k \in \mathbb{S}^1, k_r, \rho_r, r = 1, ..., R\right\}$ satisfies two important properties. First it is sufficient to reconstruct the Jost functions and the function $(x_n)_{n \in \mathbb{N}}$ by the Gel'fand-Levitan-Marchenko equation. Second the scattering data satisfy time evolution equations that are uncoupled and integrable: $\dot{a} = 0$, $\dot{b} = \omega(k) b$, and $\dot{\rho_r} = \omega(k_r)\rho_r$, where $\omega(k) = k - 1/k$.

2.1.2 Conserved quantities. As any integrable system the Toda chain possesses conserved quantities that can be expressed either in terms of $(x_n)_{n\in\mathbb{N}}$ or in terms of the density $n(\theta) = -\ln|a(e^{i\theta})|^2$, $\theta \in [0, 2\pi)$. The total displacement

$$\mathcal{D}_0 = \lim_{n\to+\infty} x_n - \lim_{n\to-\infty} x_n = -\frac{1}{2\pi}\int_0^{2\pi} n(\theta)d\theta + 2\sum_{r=1}^{R}\ln(|k_r|)$$

the momentum

$$\mathcal{M}_0 = \sum_{n=-\infty}^{\infty} \dot{x}_n = \frac{1}{2\pi}\int_0^{2\pi} n(\theta)\cos(\theta)d\theta + \sum_{r=1}^{R} k_r - {k_r}^{-1}$$

and the Hamiltonian

$$\begin{aligned}\mathcal{H}_0 &= \sum_{n=-\infty}^{+\infty} \frac{1}{2}\dot{x}_n^2 + [\exp(x_n - x_{n-1}) - (x_n - x_{n-1}) - 1] \\ &= \frac{1}{\pi}\int_0^{2\pi} n(\theta)\sin^2(\theta)d\theta + \sum_{r=1}^{R} {k_r}^2 - {k_r}^{-2} - \ln({k_r}^2)\end{aligned}$$

are three of the infinite number of conserved quantities for the homogeneous Toda chain.

2.1.3 Soliton. The scattering data of a pure soliton are

$$\begin{aligned}&a(k) = \epsilon_0\frac{k-k_0}{kk_0-1}, \quad b(k) = 0, \quad k_0 = \epsilon_0\exp(-q_0), \\ &\rho_0 = \exp(2q_0n_0(t))\sinh(q_0), \quad n_0(t) = n_0(0) - \epsilon_0\sinh(q_0)/q_0t\end{aligned}$$

where $q_0 > 0$, $\epsilon_0 = \pm 1$. The corresponding solution is:

$$x_n(t) = -\ln\left[1 + \frac{e^{q_0}\sinh(q_0)}{\cosh(q_0(n-n_0(t)))}e^{-q_0(n-n_0(t))}\right]. \qquad (2)$$

Note that the soliton solution is negative-valued. Its velocity is negative (resp. positive) if the zero k_0 is positive (resp. negative).

2.2 Propagation with an impure segment

2.2.1 Perturbation model. We assume from now on that the masses of the particles are not equal

$$m_n\ddot{x}_n = (\exp(x_{n+1} - x_n) - \exp(x_n - x_{n-1}))\,, \qquad (3)$$

where m_n is the mass of the particle at site n. A finite segment of impure masses is embedded into a homogeneous infinite chain

$$m_n = \begin{cases} 1 & \text{for } n \leq 0 \text{ and } n \geq N^\varepsilon + 1, \\ 1 + \varepsilon V_n & \text{for } 1 \leq n \leq N^\varepsilon, \end{cases}$$

where the small parameter $\varepsilon \in (0,1)$ characterizes the amplitude of the perturbation. $(V_n)_{n\in\mathbb{N}}$ is a sequence of identically distributed random variables. They are zero-mean $\langle V_n \rangle = 0$; they possess finite moments; the chain is stationary so $\langle V_0 V_n \rangle = \langle V_m V_{m+n} \rangle$. We may think for instance at the discrete white noise, where the random variables V_n are statistically independent $\langle V_m V_n \rangle = 0$ if $m \neq n$ with the variance $\sigma^2 = \langle V_n^2 \rangle$. This configuration has been studied numerically in Refs. [17, 18]. We may also consider a colored noise with a Gaussian autocorrelation function $\langle V_0 V_n \rangle = \sigma^2 \exp(-n^2/l_c^2)$ with variance σ^2 and correlation length l_c.

The length of the impure segment N^ε is assumed to be large, of the order of ε^{-2}, and we set $N^\varepsilon = [l_0/\varepsilon^2]$. We introduce the slow variable l as $n = [l/\varepsilon^2]$. Here the brackets stand for the integral part of a real number. We assume that a pure soliton is incoming from the left. The parameter of the soliton is $k_0 = -e^{-q_0}$. Note that the total displacement, momentum and Hamiltonian are preserved:

$$\mathcal{D} = \lim_{n\to+\infty} x_n - \lim_{n\to-\infty} x_n, \qquad \mathcal{M} = \sum_{n=-\infty}^{\infty} m_n \dot{x}_n, \quad (4)$$

$$\mathcal{H} = \sum_{n=-\infty}^{\infty} \frac{1}{2} m_n \dot{x}_n^2 + \left[\exp(x_n - x_{n-1}) - (x_n - x_{n-1}) - 1\right]. \quad (5)$$

2.2.2 Asymptotic behavior. By applying the method introduced by Karpman [20], the Jost coefficients satisfy the coupled equations:

$$\dot{a} = \varepsilon(k - k^{-1})^{-1} \left(\tilde{\gamma}(t,k) a + \gamma(t,k) b\right), \quad (6)$$

$$\dot{b} = \omega(k) b - \varepsilon(k - k^{-1})^{-1} \left(\gamma^*(t,k) a + \tilde{\gamma}(t,k) b\right), \quad (7)$$

where the coupling terms are $\gamma(t,k) = \sum_n \psi_n^2(t,k) V_n (c_{n+1} - c_n)(t)$ and $\tilde{\gamma}(t,k) = \sum_n |\psi_n|^2(t,k) V_n (c_{n+1} - c_n)(t)$. ψ is the Jost function introduced in Section 2.1.1. The presence of the factor $(k - k^{-1})^{-1}$ in Eqs. (6-7) is important. It means that a resonance exists close to $k = 1$ and $k = -1$, and thus small solitons are likely to be generated, as was observed for the random Korteweg-de Vries equation [21].

The random perturbation induces variations of the spectral data. Calculating these changes we are able to find the effective evolution of the

field and calculate the characteristic parameters of the wave. We are interested in the effective dynamics of the soliton propagating through large impure segments with length $N^\varepsilon = [l_0/\varepsilon^2]$. The total energy is conserved but the discrete and continuous components evolve during the propagation. The evolution of the continuous component corresponding to radiation will be found from the evolution equations of the Jost coefficients. The evolutions of the soliton parameter will then be derived from the conservation of the total energy. However this approach turns out to be a little more tricky than expected because of the generation of new solitons. We can now state the main result [19].

1) With a probability that goes to 1 as $\varepsilon \to 0$, the wave scattered by a large impure segment with length $[l/\varepsilon^2]$ consists of one main soliton with parameter $q^\varepsilon(l)$, a soliton gas, and radiation. A soliton gas is a large collection of small solitons whose total energy is evanescent (as $\varepsilon \to 0$) while the sum of their momenta is non-zero.

2) $q^\varepsilon(l)$ converges in probability to the deterministic function $q_s(l)$ which satisfies the ordinary differential equation

$$\frac{dq_s}{dl} = F(q_s), \tag{8}$$

where

$$F(q) = -\frac{1}{4\pi}\int_0^{2\pi} C^2(q,\theta)\hat{R}(2K(q,\theta))\frac{\sin^2(\theta)}{\sinh^2(q)}d\theta, \tag{9}$$

$C^2(q,\theta)$ is the normalized energy density scattered by the soliton with parameter q per unit distance for a discrete white noise

$$C(q,\theta) = \pi\frac{\sin\left(\theta - \frac{q\sin(\theta)}{\sinh(q)}\right)}{\sinh\left(\frac{\pi\sin(\theta)}{\sinh(q)}\right)}, \tag{10}$$

$\hat{R}(\kappa)$ is the discrete Fourier transform of the autocorrelation function of $(V_n)_{n\in\mathbb{N}}$

$$\hat{R}(\kappa) = \sum_{n=-\infty}^{\infty}\langle V_0 V_n\rangle\cos(\kappa n), \tag{11}$$

and $K(q,\theta)$ is the wavenumber $K(q,\theta) = \theta - \frac{q\sin(\theta)}{\sinh(q)}$. Note that $\hat{R}$ is positive real-valued (Wiener-Khintchine theorem). In case of a discrete white noise $\hat{R}(\kappa)$ is constant and equal to the variance σ^2. In the following sections we shall extend the analysis of equation (8) carried out in [19] by discussing in particular the role of the correlation length.

2.2.3 Small-amplitude soliton regime - white noise. If $q \ll 1$, then the scattered energy density can be analyzed more precisely. It is found that the function C is concentrated around $\theta = \pi$ with a bandwidth of the order of q. This means that the radiation is going backward. Integrating establishes that $q_s(l) = q_0/\sqrt{1 + 2\sigma^2 q_0^2 l/15}$. In terms of energy, the decay rate reads as

$$\mathcal{H}_s(l) = \frac{\mathcal{H}_0}{\left(1 + 2\sigma^2 q_0^2 l/15\right)^{3/2}}. \tag{12}$$

Note that the decay rate as $l^{-3/2}$ for the soliton energy is in agreement with the numerical simulations carried out in [17, 18, 19]. Fig. 1a shows that this behavior of the soliton, obtained theoretically in the asymptotic framework $\varepsilon \to 0$, can be observed in numerical simulations in the case where ε is small, more precisely smaller than any other characteristic scale of the problem.

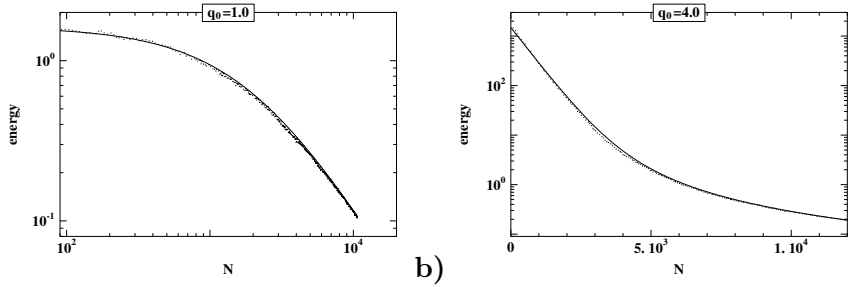

Figure 1. Energy of the transmitted soliton as a function of the length of the impure segment. Different initial values for the soliton parameters are addressed. The solid lines stand for the theoretical values (Eq. (8)), and the dotted lines plot the results of full numerical simulations. We consider random masses $m_n = 1 + \varepsilon V_n$ along the segment $[1, N]$ where V_n are independent random variables with uniform distributions between -1 and 1. We take the value $\varepsilon = 0.1$. The scales are log-log in picture a (so that the $N^{-3/2}$ decay is noticeable), and lin-log in picture b (so that the initial exponential decay is noticeable).

2.2.4 Large-amplitude soliton regime - white noise. The regime when $q_0 \gg 1$ can also be analyzed precisely, as long as $q_s(l) \gg 1$. It is found that the function C becomes independent of θ which means that broadband radiation is emitted. Integrating establishes that the decay rate of q_s is linear $q_s(l) = q_0 - \sigma^2 l/4$, which reads as an exponential decay in terms of the energy:

$$\mathcal{H}_s(l) = \mathcal{H}_0 \exp\left(-\frac{\sigma^2 l}{2}\right). \tag{13}$$

The energy decay rate is also independent of the energy of the incoming soliton. This feature was pointed out by numerical simulations [18, 19] (see also Fig. 1b). When the value q_s becomes of the order of 1, the decay switches to the power law described in the previous section.

It should be noted that the decay rate of a large-amplitude soliton is higher than the one of a small-amplitude soliton. This seems in contradiction with previous analysis of solitons driven by random perturbations for other types of integrable systems, such as the NLS equation [1]. However we cannot extrapolate the results corresponding to the continuous NLS equation to our system for the two following reasons. First the amplitude and velocity of the NLS soliton are not coupled and in the large mass limit the variations of mass is small, but the variation of velocity is important. In the Toda chain the soliton amplitude and velocity are coupled so the deceleration leads to the damping of amplitude. Second discreteness plays a primary role when the soliton amplitude is large and the additional scale order of the lattice step comes into the play. The analysis of the randomly perturbed NLS equation has shown that nonlinearity may reduce the exponential localization. The proposed analysis of the randomly perturbed Toda system shows that the interplay between discreteness, nonlinearity and randomness is more complicated and may lead to an enhanced instability of a large-amplitude soliton. In the large-amplitude regime the soliton width is of the order of one site, and so is the correlation length of the discrete white noise. This involves a strong interaction between the medium and the soliton. This comment will be confirmed in the following section.

2.2.5 Role of the correlation length. Let us assume that $(V_n)_{n\in\mathbb{N}}$ is a colored noise with the autocorrelation function $\langle V_0 V_n\rangle = \sigma^2 \exp(-n^2/l_c^2)$. For an arbitrary l_c the complete expressions (9-11) should be considered. The case $l_c \leq 1$ corresponds to the discrete white noise case. In this section we shall assume that $l_c \geq 1$ to analyze the soliton dynamics and the influence of long-range correlation.

For large-amplitude soliton, the decay rate is independent of the soliton parameter as soon as $q \geq 3$, and that the decay rate is maximal in the white noise case ($l_c \leq 1$). For small-amplitude soliton, the maximal decay rate arises when $ql_c \sim 0.6$ (Fig. 2). Accordingly the interaction between the soliton and the medium is maximal when the soliton width is of the same order as the correlation length of the medium.

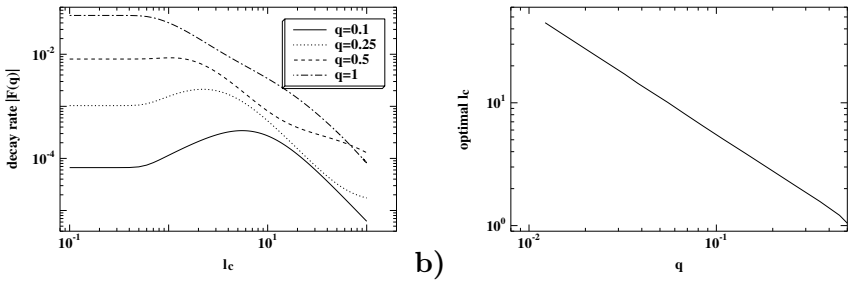

Figure 2. Picture a: Decay rate as a function of the correlation length for a Gaussian correlation function $\langle V_0 V_n \rangle = \sigma^2 \exp(-n^2/l_c^2)$. Picture b: Optimal correlation length involving the maximal decay rate for a given soliton parameter.

3. The Ablowitz-Ladik chain

3.1 The homogeneous Ablowitz-Ladik chain

The integrable discretized version of the continuum NLS equation is the so-called Ablowitz-Ladik (AL) equation [22]:

$$i\dot{q}_n + q_{n+1} + q_{n-1} - 2q_n + |q_n|^2(q_{n+1} + q_{n-1}) = 0. \tag{14}$$

This model can be derived from the Hamiltonian

$$\mathcal{H} = -2\sum_n \mathrm{Re}(q_n q_{n+1}^*) + 2\sum_n \log(1 + |q_n|^2), \tag{15}$$

if we take care to adopt the nonstandard Poisson brackets [23] $\{q_m, q_n^*\} = i(1+|q_n|^2)\delta_{mn}$, $\{q_m, q_n\} = \{q_m^*, q_n^*\} = 0$. This integrable system supports moving nonlinear localized excitations in the form of lattice solitons

$$q_{ns}(t) = \frac{\sinh(\mu)\exp\left[ik(n - x(t)) + i\alpha(t)\right]}{\cosh\left[\mu(n - x(t))\right]}, \tag{16}$$

where

$$x(t) = x_0 + Ut, \qquad \alpha(t) = \alpha_0 + t\left(2\cosh(\mu)\cos(k) - 2 + kU\right),$$

and $U = 2\sin(k)\sinh(\mu)/\mu$ is the velocity of the soliton.

3.2 A randomly perturbed Ablowitz-Ladik chain

3.2.1 The model: A random on-site potential. We consider an AL equation perturbed by a random potential:

$$i\dot{q}_n + q_{n+1} + q_{n-1} - 2q_n + |q_n|^2(q_{n+1} + q_{n-1}) = \varepsilon V_n q_n. \tag{17}$$

The small parameter $\varepsilon \in (0,1)$ characterizes the amplitude of the perturbation. Eq. (17) can be derived from the Hamiltonian

$$\mathcal{H} = -2\sum_n \mathrm{Re}(q_n q_{n+1}^*) + \sum_n (2+\varepsilon V_n)\log(1+|q_n|^2) \tag{18}$$

and the total mass is also conserved

$$\mathcal{N} = \sum_n \log(1+|q_n|^2). \tag{19}$$

The site-dependent potential V is assumed to be a bounded, zero-mean, stationary and ergodic sequence of random variables, of the same type as the one considered in Section 2.2.1. We consider the propagation of a soliton with initial mass $N_0 = 2\mu_0$ and velocity $U_0 = 2\sin(k_0)\sinh(\mu_0)/\mu_0$.

3.2.2 Asymptotic behavior of the soliton parameters. By applying the same method as the one described in Section 2, we come to the following conclusion:

1) With a probability that goes to 1 as $\varepsilon \to 0$, the wave scattered by a large impure segment with length $[l/\varepsilon^2]$ consists of one main soliton with parameters $(\mu^\varepsilon(l), k^\varepsilon(l))$ and radiation. No soliton gas is generated.

2) $(\mu^\varepsilon(l), k^\varepsilon(l))$ converges in probability to the deterministic functions $(\mu_s(l), k_s(l))$ which satisfy the system of ordinary differential equations

$$\frac{d\mu_s}{dl} = F(\mu_s, k_s), \qquad \frac{dk_s}{dl} = G(\mu_s, k_s), \tag{20}$$

starting from $\mu_s(0) = \mu_0$, $k_s(0) = k_0$. The functions F and G are

$$\begin{aligned} F(\mu,k) &= -\int_0^{2\pi} \frac{\sinh(\mu)}{\mu}\sin(k)C(\mu,k,\theta)d\theta, \\ G(\mu,k) &= -\int_0^{2\pi} \frac{\cosh(\mu)\cos(k)-\cos(2\theta)}{\mu}C(\mu,k,\theta)d\theta, \end{aligned}$$

where the function C is the mass density scattered by the soliton with parameters (μ, k) per unit time

$$C(\mu,k,\theta) = \frac{\pi\sinh\mu}{16\mu\cosh\left(\frac{\omega_1\pi}{2\mu}\right)^2\sin(k)} \frac{\sin(\omega_2/2)^4\,\hat{R}(\omega_2)}{(\cosh(\mu)-\cos(2\theta-k))^2}, \tag{21}$$

the functions ω_1 and ω_2 are defined by

$$\omega_1(\mu,k,\theta) = \mu\frac{\cosh(\mu)\cos(k)-\cos(2\theta)}{\sinh(\mu)\sin(k)}, \qquad \omega_2(\mu,k,\theta) = \omega_1 + k - 2\theta,$$

and $\hat{R}$ is the discrete Fourier transform of the autocorrelation function of $(V_n)_{n\in\mathbb{N}}$.

3.2.3 Linear regime in the approximation $\mu_0 \ll 1$. The velocity U of the soliton (equal to $2\sin(k)\sinh(\mu)/\mu \simeq 2\sin(k)$) is almost constant during the propagation, while the mass N (equal to 2μ) decreases exponentially (see Fig. 3a):

$$\mu_s(l) \simeq \mu_0 \exp\left(-\frac{l}{L_{loc}}\right), \quad L_{loc} = \frac{4\sin(k_0)^2}{\hat{R}(2k_0)} \tag{22}$$

The spectrum of the radiation is concentrated around the spectral parameter $\theta = -k_0/2$ (and $-k_0/2 + \pi$) with a bandwidth of the order of μ_0. This means that the radiation oscillates as $\exp(-ik_0 n)$. It can be noticed that, in the limit case $\mu_0 \to 0$, the incoming soliton can be approximated by a linear wavepacket:

$$q_n(t) \simeq \int_{-\infty}^{+\infty} d\kappa \hat{\phi}_0(\kappa) e^{i\kappa n - i4\sin^2(\kappa/2)t},$$

with $\hat{\phi}_0(\kappa) = (1/4)\cosh^{-1}(\pi(\kappa - k_0)/(4\mu_0))$. Note that the dispersion relation for the linear discrete Schrödinger equation reads $\omega(\kappa) = 4\sin^2(\kappa/2)$. The spectrum $\hat{\phi}_0$ of the soliton is sharply peaked about k_0, so that the localization length also reads as $L_{loc} = \omega(2k_0)/\hat{R}(2k_0)$. If $k_0 \ll 1$, then we rediscover the well-known continuum limit. The continuum dispersion relation reads $\omega(\kappa) = \kappa^2$. The spectrum of the soliton has carrier wavenumber k_0, while the one of the scattered wavepacket is $-k_0$. These statements are in agreement with the linear approximation. The localization length $L_{loc} = \omega(2k_0)/\hat{R}(2k_0)$ corresponds to the localization length of a monochromatic wave with wavenumber k_0 scattered by a slab of linear random medium [25].

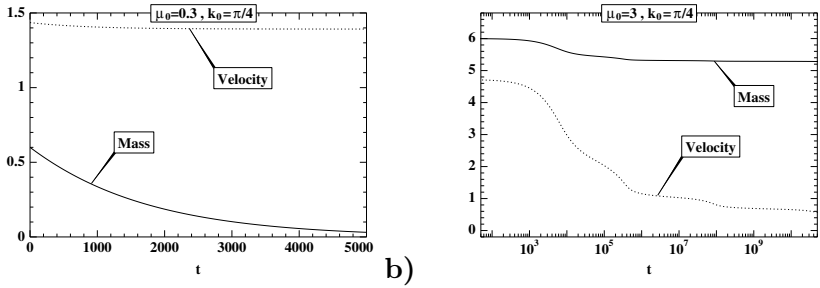

Figure 3. Evolutions of the soliton mass and velocity as predicted by integration of system (20).

3.2.4 Nonlinear regime in the approximation $\mu_0 \gg 1$. The soliton emits radiation whose spectrum covers all frequencies with

a $\sin^4$ form centered at $\mu/\tan(k)+k$. It can be checked that $\exp(\mu)\cos(k)$ is constant during the propagation, which means that the mass of the soliton converges to the limit value N_{lim}

$$N_{lim} = 2\mu_{lim} = 2\mu_0 + 2\log(\cos(k_0)), \tag{23}$$

while the velocity of the soliton decreases to 0 (see Fig. 3d). The limit behavior for large l of the parameter k_s depends on the high frequency behavior of the spectrum of the potential V. An extensive study is performed in [24]. If the spectrum of the potential decays slowly, then k_s decays logarithmically $k_s(l) \simeq \pi/\log l$. This logarithmic rate actually represents the maximal decay of the velocity. Whatever the potential V, $\liminf_{l\to\infty} k_s(l) \times \log(l) \geq \pi$. However the decay rate may be smaller. For instance, if $\langle V_0 V_n\rangle = \sigma^2 \exp(-n^2/l_c^2)$. then the velocity decreases as $k_s(l) \simeq \mu_{lim} l_c/(2\sqrt{\log l})$.

3.2.5 Existence of a critical nonlinearity. In the case where μ_0 is of order 1, then the numerical integration of the system (20) shows that the two above regimes are attractive. There exists a critical value μ_c of μ_0 which determines the behavior of the soliton. If $\mu_0 \leq \mu_c$, then, after a transition period, the velocity becomes constant, and the mass decays exponentially (Fig. 4a). If $\mu_0 \geq \mu_c$, then, after a transition period, the mass becomes constant, and the velocity decays logarithmically (Fig. 4b).

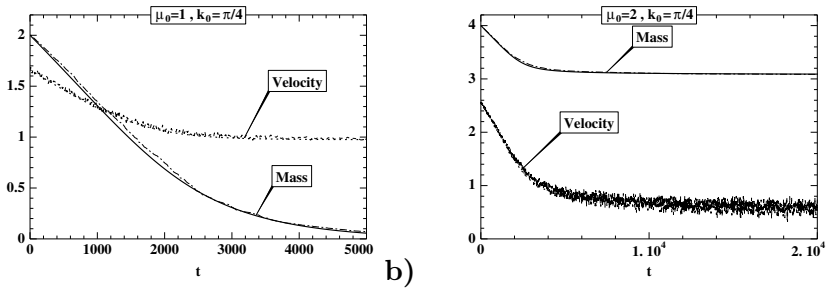

a) b)

Figure 4. Evolutions of the soliton mass and velocity. Two different set of initial values for the soliton parameters are addressed. The solid lines stand for the theoretical values (Eq. (20)), and the dotted lines plot the results of full numerical simulations. V_n is a sequence of independent and identically distributed variables, which obey uniform distributions over the interval $[-1/2, 1/2]$. We take $\varepsilon = 0.1$.

3.2.6 Role of the correlation length. In this section we discuss the dependence of the localization length with respect to the correlation length of the medium. In the case of the Toda chain we have seen

that the interaction between the soliton and the medium is maximal when the correlation length is of the same order as the soliton width. In the AL case the localization length is independent of the amplitude or the width of the soliton, but it depends on the carrier wavenumber k_0. More precisely, let us assume that $(V_n)_{n\in\mathbb{N}}$ is a colored noise with the autocorrelation function $\langle V_0 V_n\rangle = \sigma^2 \exp(-n^2/l_c^2)$. If $0.24\pi \le k_0 \le \pi/2$, then the localization length is minimal (corresponding to maximal interaction) for a discrete white noise. If $k_0 \le 0.24\pi$, then the minimal location length arises when $k_0 l_c \simeq 0.7$ (Fig. 5). This condition corresponds to the maximal interaction between the soliton and the medium. It shows that the soliton carrier wavenumber is the parameter that governs the interaction, which also holds true for the Toda chain as the soliton width and the carrier wavelength are proportional.

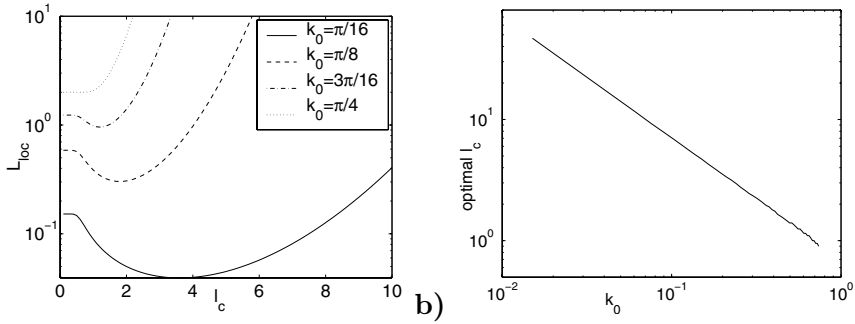

Figure 5. Picture a: Localization length as a function of the correlation length for a Gaussian correlation function $\langle V_0 V_n\rangle = \sigma^2 \exp(-n^2/l_c^2)$. Picture b: Optimal correlation length involving the minimal localization length for a given carrier wavenumber.

4. Conclusion

We have applied random perturbations to two integrable discrete systems. The AL chain has a similar behavior as the continuum NLS equation. We have found that there exists a critical value of the initial mass of the soliton below which we observe an exponential decay of the mass, and above which an original nonlinear regime prevails which involves the convergence of the mass of the soliton to a calculable positive value and the slow decay of the velocity. The overall conclusion is that large-amplitude solitons are more stable than small-amplitude solitons.

In comparison with the random AL chain new phenomena are exhibited for the random Toda chain. First, large-amplitude solitons are less stable than small-amplitude solitons in the random Toda chain. Sec-

ond, the generation of a large number of small quasi-localized solitons in an impure segment is demonstrated. The production of the soliton gas is interesting by itself as a new phenomenon that is not encountered when a random NLS or AL equation is considered, but it should also be pointed out that this production is very important in that we cannot understand correctly the changes in the conservation equations without accounting for soliton production.

Acknowledgments

The author would like to thank Prof. F. Kh. Abdullaev for useful and stimulating discussions.

References

[1] Yu. S. Kivshar, S. A. Gredeskul, A. Sanchez, and L. Vazquez, Phys. Rev. Lett. **64**, 1693 (1990).

[2] *Nonlinearity with Disorder*, Springer Proc. in Physics **67**, F. Kh. Abdullaev, A. R. Bishop, and S. Pnevmatikos (Eds), Springer, Heidelberg, 1992.

[3] K. Ishii, Suppl. Prog. Theor. Phys. Phys. Jpn. **53**, 77 (1977).

[4] P. K. Lee and T. V. Ramakrishran, Rev. Mod. Phys. **57**, 287 (1985).

[5] I. M. Lifshitz, S. Gredeskul, and L. Pastur, *Theory of disordered systems* (Nauka, Moscow, 1988).

[6] P. Marquié, J. M. Bilbault, and M. Remoissenet, Phys. Rev. E **51**, 6127 (1995).

[7] V. Muto, P. S. Lomdahl, and P. L. Christiansen, Phys. Rev. A **42**, 7452 (1990).

[8] M. Toda, *Theory of nonlinear lattices*, (Springer, Heidelberg, 1981).

[9] V. S. Gerdjikov, D. J. Kaup, I. M. Uzunov, and E. G. Evstatiev, Phys. Rev. Lett. **77**, 3943 (1996).

[10] Q. Li, C.M. Soukoulis, St. Pnevmatikos, and E. N. Economou, Phys. Rev. B **38**, 11888 (1988).

[11] T. Ilzuka, T. Nakao, and M. Wadati, J. Phys. Soc. Jap. **60**, 4167 (1991).

[12] F. Kh. Abdullaev, *Theory of solitons in inhomogeneous media* (Wiley, Chichester, 1994).

[13] R. Scharf and A. R. Bishop, Phys. Rev. A **43**, 6535 (1991).

[14] Ch. Claude, Yu. S. Kivshar, O. Kluth, and K. H. Spatschek, Phys. Rev. B **47**, 14228 (1993).

[15] Yu. S. Kivshar and D. K. Campbell, Phys. Rev. E **48**, 3077 (1993).

[16] S. V. Manakov, S. Novikov, L. P. Pitaevskii, and V. E. Zakharov, *Theory of solitons* (Consultants Bureau, New York, 1984).

[17] S. Ishiwata, Y. Okada, S. Watanabe, and H. Tanaka, J. Phys. Soc. Jpn. **59**, 3029 (1990).

[18] Y. Kubota and T. Odagaki, Phys. Rev. E **61**, 3133 (2000).

[19] J. Garnier and F. Kh. Abdullaev, Phys. Rev. E **67**, 026609 (2003).

[20] V. I. Karpman, Phys. Scr. **20**, 462 (1979).

[21] J. Garnier, J. Statist. Phys. **105**, 789 (2001).

[22] M. J. Ablowitz and J. F. Ladik, J. Math. Phys. **16**, 598 (1975); M. J. Ablowitz and J. F. Ladik, Stud. Appl. Math. **55**, 213 (1976).

[23] L. D. Faddeev and L. A. Takhtajan, *Hamiltonian methods in the theory of solitons* (Springer Verlag, Berlin, 1987).

[24] J. Garnier, Phys. Rev. E **63**, 026608 (2001).

[25] L. Arnold, G. Papanicolaou, and V. Wihstutz, SIAM J. Appl. Math. **46**, 427 (1986).

ULTRAFAST ELECTRON TRANSFER: THE STANDARD THEORY REVISITED

A Nonadiabatic and Intrinsically Nonlinear Theory

S. Aubry
Laboratoire Léon Brillouin (CEA-CNRS), CEA Saclay
91191-Gif-sur-Yvette Cedex, France
aubry@llb.saclay.cea.fr

Abstract The vicinity of the Marcus inversion point is the regime where Electron Transfer is expected to become ultrafast in the standard theory but it is also the regime where the validity of the adiabatic approximation used for this theory breaks down and where improvements are needed.

We construct a **non-adiabatic** model for ET where the complex amplitudes of the tight-binding electronic wave function, are the Kramers variables. Because the whole thermalized environment reorganizes during the electron tunnelling, the electron dynamics turns out described by an effective equation which is a discrete nonlinear Shroedinger equation on a dimer with extra dissipative terms and colored Langevin forces. Far from the Marcus inversion point and in the most general case of "soft nonlinearities", our model reproduces essentially the standard results which describe ET as a thermally activated process.

Close to the inversion point where electron transfer is supposed to occur at zero temperature, our model reveals important difference and in particularly a non exponential transfer with long tails. Moreover, our model naturally provides a new approach for understanding catalysis of Ultrafast electron transfer(developed elsewhere).

Keywords: Electron transfer, Catalyst, Ultrafast

1. Introduction

It is known that most chemical and biological processes can be dissected into a few number of elementary processes which are encountered many times in real situations but with different arrangements [1].

F. Kh. Abdullaev and V. V. Konotop (eds.), Nonlinear Waves: Classical and Quantum Aspects, 443–471.

Among these elementary processes, electron transfer (ET) between two molecules (or different parts of the same molecule) is likely the most ubiquitous elementary processes of chemical and biological reactions.

An electron on a donor molecule initially at some energy level is transferred to an acceptor molecule (or to another site of the same molecule). This transfer is accompanied by the relaxation of the density of the other electrons and the nuclear positions in the environment which changes the energy levels on donor and acceptor. Indeed, the transferred electron is generally involved in chemical bonds and also has an electric charge which strongly interact with the other charges and dipoles of its environment. After ET and relaxation, some energy is released in the environment. Thus, a correct description of ET must take into account the reorganization the environment which is induced. This is done in the Marcus theory [2] which describes ETs as thermally activated processes. However, this theory fails in the case of ultrafast ET (precisely in the vicinity of the Marcus inversion point) where some of the hypothesis required for its validity breaks down. It is worthwhile to improve this theory because ultrafast ET have been observed experimentally especially in biosystems and are even faster low temperature. ET in the Photosynthetic Reaction center is a well-studied example[3] which is interpreted as very close to the inversion point [2].

We already presented some details of our nonadiabatic model in [7]. We shall focus mostly in that paper on the fundaments of our model and show that it encompasses the standard model of ET as a limit case. In the case where ET is ultrafast that is close to the inversion point, its is essentially due to a quantum tunneling in a deformable potential. Up to now, this problem was discarded or treated empirically. We show that very generally, the dynamics of the quantum electron during ET can be modeled by a nonlinear discrete Schroedinger equation on a dimer with damping and thermal noise.

The well-known concept of tunnelling which is usually modelled in textbooks by two resonant linear oscillators does not hold for the nonlinear case. Nevertheless, we may have tunnelling when specific conditions for nonlinear resonance are fulfilled. These conditions were only recently made explicit [6] and involve both the coefficients of the linear and nonlinear terms. Moreover, the associated tunnelling process is different from the linear case because first, it is selective on the initial energy and second it is accompanied by frequency (or levels) oscillations. The new terminology Targeted Energy Transfer was used to emphasize the important differences of this phenomena with those of linear resonance. We show that it should naturally play an essential role for a better understanding of ultrafast ET and catalysis.

In section 2, we review the standard theory of ET and explains its inconsistency for ultrafast ET. We propose in section 3, a model which captures the new essential features which should be taken into account at the inversion point that when is the quantum dynamics of the electron wave function cannot be treated within the adiabatic approximation. This new theory is nevertheless equivalent to the Marcus theory far from the inversion point and only differs in the vicinity of the inversion point. In section 4, we derive the master equation for nonadiabatic ET. In section 5, we show our the Marcus theory is recovered by the adiabatic approximation far the inversion point. Section 6 is devoted to the dynamics of ET close to the inversion point, we show that the nonlinearities of the model requires to reconsider the basic concept of linear resonance for electron tunneling. Finally, we conclude 7 by a brief presentation of the mechanism of Targeted Transfer and its application for catalysis of ultrafast ET.

2. Standard theory of ET: A thermally activated process

We describe here the general ideas of the standard theory of ET used in chemistry which was mostly due to Marcus [2]. Considering ET between two molecules (Donor and Acceptor) or two different sites of a molecule, it is assumed that the system has two electronic states. The first one correspond to the initial state where the electron is on the donor molecule and the second one corresponds to the final state where the electron is on the acceptor molecule. The overlap between the redox orbitals associated with these two states is supposed to be small so that they can be considered as eigenstates (except at resonance when their two energy levels are equal). Then, the free energy of the system depends on the many coordinates describing the displacements of nuclei of the molecules and the environment and also on the state of the electron. Thus, there are two free energies surfaces which take into account all contributions to the energy chemical, electrostatic... The first surface describes the reactants (that is when the electron is on the donor molecule) and the second one describes the products (that is when the electron is on the acceptor molecule). These surfaces are well defined within the standard adiabatic (or Born-Oppenheimer) approximation where the electronic energy is only a function of the coordinates of the nuclei which are supposed to move slowly under the effect of the thermal fluctuations.

The minimum versus the nuclear coordinates of the free energy with the electron either in the initial or the final electronic state determines

the initial and the final average configurations respectively of the molecules and their environment supposed to fluctuate under the effect of temperature.

It is next assumed for simplicity that these surfaces are quadratic with the same curvature, which is equivalent to assume that the phonons of these molecules are perfectly harmonics with frequencies independent of the electronic state. These surfaces can be determined in principle from the knowledge of the structures of the molecules and from their normal modes and frequencies. [2]. The difference between the first and the second free energies at the same normal coordinates is just the difference of the electronic levels on the donor and on the acceptor for the same configuration of the environment. Thus, at the intersection of these two quadratic surface which are shifted but identical, the two electronic levels becomes equal. In that situation only, the electron may be transferred from the donor to the acceptor by quantum tunnelling. Standard theory of tunnelling assumes the double well potential due to the environment of the electron is static during the time of tunnelling between the two wells. Actually, the local potentials generated by the thermal fluctuations is not static and because of that the tunneling is supposed to occur only with a certain probability which can be estimated from Landau-Zeener arguments [1].

These resonance events due to random thermal fluctuations are rare but are essential to generate ET. It is equivalent to say that the thermal fluctuations have to bring the system at the top of the lowest energy barrier at the intersection of the two free energy surfaces (see Fig. 1) where electron resonance occurs. Thus, the characteristic time needed for realizing ET is found to obey a standard Arrhenius law (corrected with some prefactor for taking into account the probability of tunneling). This situation is similar to the general theory of chemical reactions described from the pioneering ideas of Kramers [4].

This theory is valid when the characteristic time for producing ET is long at the scale of the phonon frequencies. Two regimes can be defined regarding the tunneling [1]. The adiabatic regime is obtained when the overlap between the redox orbitals (although supposed to be small) is nevertheless sufficiently large (strong reactants) in order when resonance occurs, electron tunnelling is fast at the scale of the phonon frequencies. Thus its probability to occur is almost 1. The diabatic regime is obtained at small overlap (weak reactants). Then, the tunnelling becomes slow at the scale of the phonon characteristic time and has a small probability to occur. In any case, the intrinsic time for tunnelling is usually much shorter than the characteristic time required for the thermal fluctuations

to overcome an energy barrier supposed to be large compared to the thermal energy.

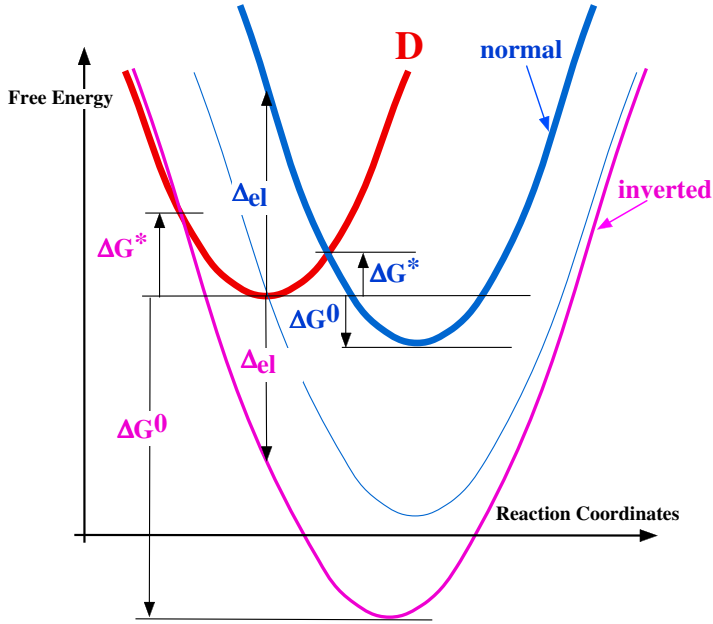

Figure 1. Free Energy versus Reaction Coordinates for the reactants (curve D) and the products for normal reaction (curve A_n), inverted reaction (curve A_i) and at the inversion curve (curve A_c). The electron in the initial state requires a positive excitation energy $\Delta^\star_{el}$ for the normal reaction, a negative excitation energy $-\Delta^\star_{el}$ for the inverted reaction (which could be directly emitted as light). There is a positive energy barrier Δ_n or Δ_i in both cases between the reactants and products which requires thermal activation for the reaction to occur. This energy barrier as well as the energy for a direct electron excitation vanishes for the inversion curve and then the electron transfer becomes ultrafast.

Despite it is based on many assumptions, Marcus theory revealed to be quite successful for describing many observed ET's. Moreover, two different regimes were predicted and are indeed observed. The normal regime where the free energy of the system in the initial atomic configuration and the electron on the donor is smaller than the free energy at the same atomic configuration but with the electron on the acceptor.

The inverted regime is obtained when this inequality is reversed (see Fig. 1). Since the electron may tunnel from the initial state to the final state only when their eigenenergies are degenerate, there exists an energy barrier to overcome by thermal activation in both situations.

However, the inverted situation differs from the normal situation because there is a second pathway for the electron to reach the final state.

The electron may also decay directly from its initial state to its final state which has a lower energy by the direct emission of a photon the energy at fixed nuclei configuration according to the Franck-Condon principle. This inverted regime manifests by the chemiluminescence phenomena which can be observed at low temperature when the first pathway becomes ineffective [2].

This energy barrier precisely vanishes at the Marcus inversion point when the initial electronic state and the final electronic state are degenerate for the initial ground-state atomic configuration. Thus in the close vicinity of this inversion point, there is almost no energy barrier, and ET is expected to become ultrafast even at low temperature. For example, the ultrafast ET which occurs in the phototosynthetic reaction centers of light harvesting cells, is considered to be in the close vicinity to the Marcus inversion point where the energy barrier almost vanishes [2].

In that regime, the absence of energy barrier makes that ET does not require thermal fluctuations and should also occur at zero or almost zero temperature. Moreover, in that case the difference between the almost degenerate electronic states on donor and acceptor being small becomes of the order of the phonon characteristic energies so that the adiabatic hypothesis cannot be fulfilled. The standard ET theory which reduces phenomelogically tunnelling to a probability of transfer is clearly not sufficient for producing the characteristic time of the ET except that ET in that situation can be considered as ultrafast that is much faster than ET requiring thermal activation. This problem is explicitly mentioned in section 3.6 Tunnel Times [1] as an unsolved problem although its relevance in the case of ultrafast Et was not recognized. It should be improved by taking into account explicitly the intrinsic quantum dynamics of the electron without using the adiabatic approximation.

3. Basic hypothesis for an improved theory

We propose a model valid for Ultrafast ET in the vicinity of the inversion point which also reproduce the results of the standard theory away from this inversion point. The hypothesis we use for constructing our model are included in the set of hypothesis used by the Marcus theory except concerning the adiabatic hypothesis. They are

- We consider a model with a single electron which may occupy two states either on the donor molecule (D) or on the acceptor molecule (A) or on two sites of the same molecule. Actually, we may also involve more states α for example three states for a catalytic transfer.

- We assume that the different molecules or states α are weakly interacting. Particularly, there is small overlap between the different redox orbitals α.

- We neglect the possible energy radiation through the electromagnetic field induced by the variation of the spatial distribution of charges during ET. Indeed, the photon emission induced by a direct transition between two electronic quantum states usually requires to consider the electromagnetic field as quantum and is calculated with the Fermi golden rule in the limit of weak coupling [1, 5]. In realistic situations, the characteristic time for a photon emission ranges from ns to longer times. Thus, it is much longer than the time for ET (except at low temperature in the Marcus inverted case which generate chemiluminescence). In any case, it is not relevant when ET is ultrafast where the energy which is released is essentially absorbed by the phonon bath. Consequently, we take into account only the electrostatic energy which varies with the charge distributions discarding any energy loss by radiation.

- For sake of simplicity we consider the environment as a large collection of harmonic oscillators (corresponding to the normal modes of the molecules labelled by i). Each of them is linearly and weakly coupled to the electronic charge distribution so that this system of oscillators acts as a thermal bath. Changes in the charge distribution generate displacements of the rest position of the harmonic oscillators which model the reorganization of the environment [1].

- The averaged number of quantum phonons which are involved by the reorganization of the environment during ET is supposed to be large. In other word, the global displacements of nuclei in the close environment of the electron is much larger than their quantum zero point motion. Then, it is a good approximation to consider the normal modes as non quantum but classical oscillators [2].

Unlike the standard theory, we do not consider tunneling as a probabilistic event which is estimated empirically, but we consider the full quantum dynamics of the electron during tunneling taking into account it evolves in a selfconsistent deformable potential. For that purpose,

[1] Our theory is not valid for small molecules reacting in the vacuum. These small systems have only few modes which cannot play the role of a thermal bath. In addition, in that situation, these modes should be considered as anharmonic.

[2] This approximation may be not valid when only very light nuclei (protons) are involved in the reorganization of the environment. We discard here this possible situation.

it is obviously necessary to consider explicitly electron variables. We consider a system with one electron and two electronic states one on the donor (D) and the second on the acceptor (A). We assume that the overlap between their (redox) orbitals is small so that a tight-binding representation is valid. Then the wave function of the electron is a combination of the (orthogonalized) orbitals on the donor and acceptor with complex amplitudes ψ_D and ψ_A respectively. To be more general, we may also consider a system with one electron and more electronic states α which could be occupied transiently with the normalization condition $\sum_\alpha |\psi_\alpha|^2 = 1$. The total energy $\mathbf{H}$ of the system has to be a function of the electron variables $\{\psi_\alpha\}$, the oscillator coordinates $\{u_i\}$ and their velocities $\{\dot{u}_i\}$. With the assumption that the oscillators are harmonic and the coupling with the electron densities linear, this energy has the general form

$$\mathbf{H} = H_T(\{\psi_\alpha\}) + \frac{1}{2}\sum_i m_i \left(\dot{u}_i^2 + \omega_i^2 (u_i - \sum_\alpha k_{i,\alpha} |\psi_\alpha|^2)^2 \right) \qquad (1)$$

The harmonic oscillators i with mass m_i and frequency ω_i, corresponds to the normal modes not only of the molecules sustaining the electronic states but also of the other molecules of environment which could couple to the electron charge. We assume that there are many oscillators. Each of them is weakly coupled with the coupling constant $k_{i,\alpha}$ to the electric charges $I_\alpha = |\psi_\alpha|^2$ of the electron in the state α. Thus, this collection of harmonic oscillators plays the role of a thermal bath [3]. $H_T(\{\psi_\alpha\})$ is all the rest of the energy which only depends on the complex amplitudes ψ_α. This energy is supposed to include all possible electronic energies in particular the chemical bond energies, the electrostatic energies coming from the charge distribution.... It can be readily checked from (1 that it can be defined as the total energy of the system assuming the amplitudes ψ_α are fixed and minimized with respect to all the nuclei coordinates represented by the displacements of the harmonic oscillators

$$H_T(\{\psi_\alpha\}) = \min_{\{u_i\}} \mathbf{H}(\{\psi_\alpha\}, \{u_i\}) \qquad (2)$$

Thus, H_T would be the Hamiltonian of the electronic system if one assume that all the oscillators adiabatically follow their rest position with respect to the electronic force. This approximation would become valid in case the tunnelling time of the electron would be much longer

[3]The model should be modified in case some special modes would be strongly coupled to the electron but this is left to further works.

than the periods of the oscillators. This is just the limit opposite to the adiabatic limit valid where the electron tunneling is much faster than the phonons and thus we call H_T anti-adiabatic electronic Hamiltonian. Actually, the situation we treat here encompass both the adiabatic limit and the anti-adiabatic limit as limit cases.

Assuming that the oscillators of the thermal bath are nonlinear would be more realistic but the model would not be solvable with the known methods. However, a well-known variational but rough approximation consists in replacing nonlinear oscillators by effective linear oscillators with temperature dependent parameters. Then, the energy form (1) could be interpreted now as the free energy considered in the Marcus theory, if its parameters are considered temperature dependent.

Energy H_T can be written as a sum

$$H_T(\{\psi_\alpha\}) = H_T^d(\{|\psi_\alpha|^2\}) + H_T^{int}(\{\psi_\alpha\}) \tag{3}$$

H_T^d is the component of the energy which is independent of the phase of the complex amplitudes ψ_α (it can be defined by phase averaging H_T). It only depends on the electron densities $|\psi_\alpha|^2$ of the charged molecules. Component H_T^{int} in (3) is the rest of the energy. It also depends on the phase differences of the complex amplitudes ψ_α. It originates from the overlap of the redox orbitals. In most physical situations of ET, this overlap is small but however essential because if zero, ET is not possible. Its role is to trigger electron tunnelling when resonance occurs. This contribution H_T^{int} calculated within the tight binding approximation in the limit of small overlaps has the form

$$H_T^{int}(\{\psi_\alpha\}) = \sum_{\beta\neq\gamma} \lambda_{\beta,\gamma}(\{|\psi_\alpha|^2\})(\psi_\beta\psi_\gamma^\star + \psi_\beta^\star\psi_\gamma) \tag{4}$$

where $\lambda_{\beta,\gamma}(\{|\psi_\alpha|^2\})$ in principle depends on the electronic densities but can be chosen as a constant parameter $\lambda_{\beta,\gamma}$ for simplicity.

The relative displacement of the harmonic oscillator i involved by moving the electron from state α to β is $k_{i,\beta} - k_{i,\alpha}$. Considering this oscillator as quantum, the creation and annihilation operators of phonons for this oscillator are defined as

$$a_i^+ = \sqrt{\frac{m_i\omega_i}{2\hbar}}u_i - \sqrt{\frac{\hbar}{2m_i\omega_i}}\frac{\partial.}{\partial u_i} \quad \text{and} \quad a_i = \sqrt{\frac{m_i\omega_i}{2\hbar}}u_i + \sqrt{\frac{\hbar}{2m_i\omega_i}}\frac{\partial.}{\partial u_i}$$

Then it readily comes out that the total number of phonons $n_i = \langle a_i^+ a_i\rangle$ generated by the displacement $k_{i,\beta} - k_{i,\alpha}$ is $n_i = \frac{m_i\omega_i}{2\hbar}(k_{i,\beta} - k_{i,\alpha})^2$. The condition for considering the thermal bath classical is not that n_i be large but that the total number of phonons $\sum_i n_i$ is large. This

condition validates the meanfield approximation which is equivalent to the classical approximation. We obtain

$$\sum_i m_i\omega_i(k_{i,\beta}-k_{i,\alpha})^2 \gg 2\hbar \tag{5}$$

Thus, the reorganization of the environment after electron transfer is small for each oscillator but large collectively. We shall assume this condition is fulfilled.

4. Dynamical equation for electron transfer and dissipation

We derive the effective equation which governs the ET after elimination of the thermal bath considered as classical. We show that its effect is to dissipate energy and at finite temperature, to generate a random force as for the standard Langevin model. It is essential however to consider that the Fourier spectrum of random force has a cut-off at frequencies larger than the phonon frequencies.

4.1 Hamilton equations

The total energy (1) is the Hamiltonian which yields the dynamics of whole the system by the standard Hamilton equations

$$\frac{\partial \mathbf{H}}{\partial \psi_\alpha^\star} = \frac{\partial H_T}{\partial \psi_\alpha^\star} - \left(\sum_i k_{i,\alpha}m_i\omega_i^2(u_i - \sum_\beta k_{i,\beta}|\psi_\beta|^2)\right)\psi_\alpha \;=\; i\hbar\dot{\psi}_\alpha \tag{6}$$

$$\ddot{u}_i + \omega_i^2(u_i - \sum_\alpha k_{i,\alpha}|\psi_\alpha|^2) \;=\; 0 \tag{7}$$

$u_i(t)$ can be made explicit from the second equation (7) which is linear with respect to u_i. The general solution has the form $u_i = u_i^{(n)} + u_i^{(0)}$ where

$$u_i^{(0)}(t) = \sum_\beta k_{i,\beta}\left(|\psi_\beta(t)|^2 - \int_{-\infty}^{t}\cos\omega_i(t-\tau)\frac{d|\psi_\beta(\tau)|^2}{d\tau}d\tau\right) \tag{8}$$

and $u_i^{(n)} = a_i\cos(\omega_i t - \phi_i)$ is a solution with arbitrary amplitude a_i and phase ϕ_i of (7) without force (i.e. assuming $|\psi_\alpha|^2 = 0$). Substituting $u_i(t)$ as a function of $|\psi_\alpha|^2$ in Eq. (6) yields

$$\frac{\partial H_T}{\partial \psi_\alpha^\star} + \left(\int_{-\infty}^{t}\sum_\beta \Gamma_{\alpha,\beta}(t-\tau)\frac{d|\psi_\beta(\tau)|^2}{d\tau}d\tau + \zeta_\alpha(t)\right)\psi_\alpha = i\hbar\dot{\psi}_\alpha \tag{9}$$

where

$$\Gamma_{\alpha,\beta}(t) = \sum_i k_{i,\alpha} k_{i,\beta} m_i \omega_i^2 \cos \omega_i t \tag{10}$$

will be assumed to be a smooth function because there are many modes i with uniform frequency distribution and

$$\zeta_\alpha(t) = \sum_i k_{i,\alpha} m_i \omega_i^2 u_i^{(n)}(t) \tag{11}$$

is a colored random force.

4.2 Property of the random force

The time correlation function averaged over τ of oscillator i is

$$< u_i^{(n)}(t+\tau) u_j^{(n)}(\tau) >_\tau = \delta_{i,j} < (u_i^{(n)})^2 > \cos \omega_i t \tag{12}$$

If we assume that the harmonic oscillators are thermalized, we have $< (u_i^{(n)})^2 >= k_B T/(m_i \omega_i^2)$ which yields the Langevin relation

$$\begin{aligned} < \zeta_\alpha(\tau) \zeta_\beta(t+\tau) >_\tau &= \sum_i k_{i,\alpha} k_{i,\beta} m_i^2 \omega_i^4 < u_i^{(n)}(\tau) u_i^{(n)}(t+\tau) > \\ &= k_B T \Gamma_{\alpha,\beta}(t) \end{aligned} \tag{13}$$

It can be checked that the total norm $\sum_\alpha |\psi_\alpha|^2 = 1$ is invariant by Eq. (9).

The Fourier transform $\gamma_{\alpha,\beta}(\omega)$ of $\Gamma_{\alpha,\beta}(t)$ defined as

$$\Gamma_{\alpha,\beta}(t) = \frac{1}{\pi} \int_{-\infty}^{+\infty} \gamma_{\alpha,\beta}(\omega) e^{i\omega t} d\omega \tag{14}$$

which by Eq. (13) corresponds also the Fourier transform correlation function of the random force in the master equation (9) corresponds to the weighted phonon spectrum of the thermal bath

$$\gamma_{\alpha,\beta}(\omega) = \sum_i k_{i,\alpha} k_{i,\beta} m_i \omega_i^2 \left(\delta(\omega - \omega_i) + \delta(\omega + \omega_i)\right) \tag{15}$$

Actually, the phonon spectrum does not extend to infinity and has obviously a cut-off at some frequency ω_c. In practice, $\hbar\omega_c$ cannot exceed the largest known phonon quanta energies around 0.3 eV.

At zero temperature, the thermal noise disappears $\zeta_\alpha(t) = 0$. Then, we have

$$\begin{aligned}
\dot{H}_T &= \sum_\alpha \left(\frac{\partial H_T}{\partial \psi_\alpha^\star} \dot{\psi}_\alpha^\star + \frac{\partial H_T}{\partial \psi_\alpha} \dot{\psi}_\alpha \right) \\
&= \sum_\alpha (i\hbar \dot{\psi}_\alpha - \psi_\alpha \int_{-\infty}^{t} \sum_\beta \Gamma_{\alpha,\beta}(t-\tau) \frac{d|\psi_\beta(\tau)|^2}{d\tau} d\tau) \dot{\psi}_\alpha^\star + CC \\
&= -\sum_{\alpha,\beta} \frac{d|\psi_\alpha|^2}{dt} \int_{-\infty}^{t} \Gamma_{\alpha,\beta}(t-\tau) \frac{d|\psi_\beta(\tau)|^2}{d\tau} d\tau \\
&= -\sum_{\alpha,\beta} \frac{d|\psi_\alpha|^2}{dt} \int_{0}^{+\infty} \Gamma_{\alpha,\beta}(\tau) \frac{d|\psi_\beta(t-\tau)|^2}{dt} d\tau \qquad (16)
\end{aligned}$$

using Eq. (9)

4.3 Energy dissipation

The role of the thermal bath is essential for ensuring dissipation of the chemical reaction energy. We show that at zero degree, the dynamical equation (9) yields always energy dissipation after a long time.

If for simplicity, we assume for example that $\Gamma_{\alpha,\beta}(t) = 2\gamma_\alpha \delta_{\alpha,\beta} \delta(t)$ that is $\gamma_{\alpha,\alpha}$ is independent of ω and $\gamma_{\alpha,\beta} = 0$ for $\alpha \neq \beta$. This approximation corresponds to the white noise approximation for ζ_α by Eq. (13). Then, we find

$$\dot{H}_T = -\sum_\alpha \gamma_{\alpha,\alpha} \left(\frac{d|\psi_\alpha|^2}{dt} \right)^2 < 0$$

is necessarily negative because $\gamma_{\alpha,\alpha}(\omega)$ is obviously positive from its definition (15). However, this white noise approximation is not correct physically.

In any case, we can show that there is energy dissipation in average. We consider the energy variation

$$H_T(t_2) - H_T(t_1) = \int_{t_1}^{t_2} \dot{H}_T dt$$

over a long interval of time $[t_1, t_2]$ and consider the Fourier transform

$$\frac{d|\psi_\alpha(t)|^2}{dt} = \dot{I}_\alpha = \int_{-\infty}^{+\infty} \kappa_\alpha(\omega) e^{i\omega t} d\omega \qquad (17)$$

Then, it comes out from Eq. (16)

$$H_T(+\infty) - H_T(-\infty) = -\sum_{\alpha,\beta} \int_0^{+\infty} \Gamma_{\alpha,\beta}(\tau) d\tau$$
$$\times \int_{-\infty}^{+\infty} d\omega \int_{-\infty}^{+\infty} d\omega' \kappa_\alpha(\omega) \kappa_\beta(\omega') \int_{-\infty}^{+\infty} e^{i\omega t} e^{i\omega'(t-\tau)} dt$$
$$= -\sum_{\alpha,\beta} \int_0^{+\infty} \Gamma_{\alpha,\beta}(\tau) d\tau \int_{-\infty}^{+\infty} d\omega \int_{-\infty}^{+\infty} d\omega' \kappa_\alpha(\omega) \kappa_\beta(\omega') e^{-i\omega'\tau}$$
$$\times 2\pi\delta(\omega + \omega')$$
$$= -2\pi \int_{-\infty}^{+\infty} d\omega \int_0^{+\infty} \sum_{\alpha,\beta} \left(\kappa_\alpha(\omega) \Gamma_{\alpha,\beta}(\tau) \kappa_\beta^\star(\omega)\right) e^{i\omega\tau} d\tau \qquad (18)$$

Since $\Gamma_{\alpha,\beta}(\tau) = \Gamma_{\alpha,\beta}(-\tau)$ and since $\sum_{\alpha,\beta} \left(\kappa_\alpha(\omega) \Gamma_{\alpha,\beta}(\tau) \kappa_\beta^\star(\omega)\right)$ is unchanged by changing ω into $-\omega$, it comes out using Eq. (15)

$$H_T(+\infty) - H_T(-\infty) =$$
$$= -\pi \int_{-\infty}^{+\infty} d\omega \int_{-\infty}^{+\infty} \sum_{\alpha,\beta} \left(\kappa_\alpha(\omega) \Gamma_{\alpha,\beta}(\tau) \kappa_\beta^\star(\omega)\right) e^{i\omega\tau} d\tau$$
$$= -2\pi \int_{-\infty}^{+\infty} d\omega \sum_{\alpha,\beta} \left(\kappa_\alpha(\omega) \gamma_{\alpha,\beta}(\omega) \kappa_\beta^\star(\omega)\right) \qquad (19)$$
$$= -2\pi \sum_i m_i \omega_i^2 \left(\sum_\alpha k_{i,\alpha} \kappa_\alpha(\omega_i)\right) \left(\sum_\beta k_{i,\beta} \kappa_\beta^\star(\omega_i)\right) + CC$$
$$= -4\pi \sum_i m_i \omega_i^2 \left| \sum_\alpha k_{i,\alpha} \kappa_\alpha(\omega_i) \right|^2 \qquad (20)$$

which is necessarily negative. Suppose that $\kappa_\alpha(\omega)$ is nonzero only in narrow intervals around $\pm\Omega$ that is the variation of I_α is close to be periodic at frequency Ω. Then $\gamma_{\alpha,\beta}(\omega)$ assumed to be a smooth function of ω can be considered as constant and equal to $\gamma_{\alpha,\beta}(\Omega)$ so that

$$H_T(+\infty) - H_T(-\infty) \approx -2\pi \sum_{\alpha,\beta} \gamma_{\alpha,\beta}(\Omega) \int_{-\infty}^{+\infty} d\omega \kappa_\alpha(\omega) \kappa_\beta^\star(\omega)$$
$$= -\sum_{\alpha,\beta} \gamma_{\alpha,\beta}(\Omega) \int_{-\infty}^{+\infty} \dot{I}_\alpha(t) \dot{I}_\beta(t) dt \qquad (21)$$

This result shows that the effective damping depends on the frequency Ω of the periodic variations of $I_\alpha = |\psi_\alpha(t)|^2$. In the case where $\gamma_{\alpha,\beta}(\Omega)$ is

constant, we recover the case with a white spectrum mentioned above. We shall use the approximation $< \dot{H}_T >= -\sum_{\alpha,\beta} \gamma_{\alpha,\beta}(\Omega) < \dot{I}_\alpha \dot{I}_\beta >$ where $\dot{I}_\gamma(t)$ are time periodic function at frequency Ω which varies slowly in time.

As a result, the effect of the memory function in (9) is always to generate energy dissipation after a long time. Note that the Fourier spectrum of this memory function represents nothing but the local absorption spectrum for ET. The measurements of Infrared Absorption spectrum of the whole system also yields informations but for a uniform field which is non local. However, some peaks associated with the normal modes could appear in both spectrum but with different weights.

Since the total energy H_T always decays in average, the asymptotic behavior of the system at zero degree K (without thermal noise) must be a state without energy dissipation. Eq.18 requires $\kappa_\alpha(\omega) = 0$ when $\gamma_\alpha(\omega)$ is not vanishing that is for ω in the phonon spectrum. If the Fourier spectrum of $|\psi_\alpha(t)|^2$ lies inside the phonon spectrum, that is the characteristic frequencies of the electron dynamics are at the same scale as those of the phonons, this condition implies $d|\psi_\alpha(t)|^2/dt = 0$. Therefore the electron densities $I_\alpha = |\psi_\alpha(t)|^2$ are time constant for the asymptotic states.

5. Recovering the standard Marcus theory

In principle, our model for describing the electron dynamics is valid in the whole non adiabatic regime including the adiabatic regime and the antiadiabatic regime as limit cases. These limit cases are determined by the fact the electron dynamics could be either much faster or much slower than the coupled phonons.

Thus, the standard theory of ET can be recovered as an approximation from the master equation (9) of ET with Eqs. (10) and (13).

If we assume that the electronic variables follow adiabatically the nuclei, instead of eliminating the phonon variables as we did and keep an effective equation for the electron, one could eliminate the electronic degrees of freedom by assuming the electron remains in its initial eigenstate and then obtain an effective potential for the collection of oscillators. The validity of the adiabatic approximation requires that the electron characteristic frequencies $\omega_{\alpha,\beta} = |E_\alpha - E_\beta|/\hbar$ associated with the electronic transitions between pairs of states α, β are much larger than the phonon characteristic energies which have the upper bound $\hbar\omega_c$.

These eigenstates [4] correspond to extrema of $\mathbf{H}$ (1) with respect to $\{\psi_\alpha\}$ under the constraint of fixed norm $\sum_\alpha |\psi_\alpha|^2 = 1$ which yields

$$\frac{\partial \mathbf{H}}{\partial \psi_\alpha^\star} = E_{el} \frac{\partial \sum_\beta |\psi_\beta|^2}{\partial \psi_\alpha^\star} = E_{el} \psi_\alpha \tag{22}$$

where the Lagrange multiplier E_{el} is the electron eigen energy. Note that in the linear case which is more familiar, $\mathbf{H} = \sum_{\alpha,\beta} \psi_\alpha^\star h_{\alpha,\beta} \psi_\beta$ is an Hermitian form of $\{\psi_\alpha\}$, then Eq. (22) becomes linear and one recovers a standard Schroedinger equation (in a tight-binding representation). Otherwise, Eq. (22) is in general a nonlinear equation. Then note that the well-known properties of eigenstates of linear hermitian operators (orthogonality and completeness) are not valid anymore. Nevertheless, according to the dynamical Eq. (6), the time dependence of the eigenstates of of Eq. (22) fulfill $\psi_\alpha(t) = e^{-iE_{el}t/\hbar}\psi_\alpha(0)$.

In any case, far from resonance that is when none of these eigen energies are equal $E_\alpha \neq E_\beta$ for any $\alpha \neq \beta$, the initial states α which were chosen as a base which have been assumed to be weakly coupled yields practically the eigenstates. Thus $\psi_\alpha = 1$ and $\psi_\beta = 0$ for $\beta \neq \alpha$. Moreover, the adiabatic approximation is valid when the energy differences $|E_\alpha - E_\beta|$ are large compared to the phonon energies $\hbar\omega_i$. Thus, in the case this condition is fulfilled, we get one free energy surface for each electronic state but note also that the adiabatic assumption cannot be valid close to the intersection of these free energy surface where $|E_\alpha - E_\beta|$ vanishes.

In the Marcus theory with a donor and an acceptor only $\alpha = D$ or $\alpha = A$, the first free energy surface $G_D(\{u_i\}$ schematized Fig.1 is the quadratic function of the nuclei coordinates $\{u_i\}$ obtained from (1) by fixing the electron on the donor that is $|\psi_D|^2 = 1, |\psi_1|^2 = 0$. The second energy surface $G_A(\{u_i\})$ is obtained similarly by fixing the electron on the acceptor $|\psi_D|^2 = 0$, $|\psi_A|^2 = 1$. We have

$$\begin{aligned} G_D(\{u_i\}) &= \mathbf{H}(\{1,0\},\{u_i\},\{\dot{u}_i = 0\}) \\ &= H_T(1,0) + \frac{1}{2}\sum_i m_i\omega_i^2 (u_i - k_{i,D})^2 \qquad (23) \\ G_A(\{u_i\}) &= \mathbf{H}(\{0,1\},\{u_i\},\{\dot{u}_i = 0\}) \\ &= H_T(0,1) + \frac{1}{2}\sum_i m_i\omega_i^2 (u_i - k_{i,A})^2 \qquad (24) \end{aligned}$$

[4] We use the terminology eigenstate by extension, because in textbook eigenstate are only defined for linear operators.

The minimum of $G_D(\{u_i\})$ is obtained for $u_i = k_{i,D}$. Then, we have

$$\Delta^\star_{el} = G_D(\{k_{i,D}\}) - G_A(\{k_{i,D}\}) = H_T(0,1) - H_T(1,0) + \frac{1}{2}\sum_i m_i\omega_i^2(k_{i,D} - k_{i,A})^2 \qquad (25)$$

(see Fig. 1). The normal regime is defined by the condition $\Delta^\star_{el} > 0$, and the inverted regime by $\Delta^\star_{el} < 0$. The inversion point is obtained when $\Delta^\star_{el} = 0$ or

$$\frac{1}{2}\sum_i m_i\omega_i^2(k_{i,D} - k_{i,A})^2 = H_T(1,0) - H_T(0,1) = \Delta G^0 \qquad (26)$$

Note that the second member of Eq. (26) is ΔG^0 the energy released by the reaction and the first member is the energy released the reorganization.

Marcus theory mostly focuses on the stochastic process for reaching electron resonance and considers electron tunnelling as a probabilistic process with negligible duration. This assumption is generally valid because the energy barrier

$$\Delta G^\star = \frac{1}{4}\frac{{\Delta^\star_{el}}^2}{\Delta G^0 + \Delta^\star_{el}} \qquad (27)$$

is generally much larger than the thermal energy k_BT (this result can be obtained from the graph Fig. 1 or see rRf.[2]).

Clearly, this assumption is not valid at the inversion point where the energy barrier vanishes. Then the characteristic time for ET becomes essentially due to the electron tunnelling which requires a more detailed analysis.

6. Electron transfer from donor to acceptor: a dimer model

Before to describe ET, it is first useful to analyze the form of the energy H_T on the basis of physical arguments.

6.1 Main physical contributions to energy H_T

The precise knowledge of H_T from first principles in realistic situations should require complex and sophisticated ab initio calculations which are still hardly available today. However, we can roughly decompose H_T into several contributions with physical significances. Since we consider ET between weakly interacting units, H_T^d in (3) is mostly the

sum of the energies $H_\alpha(|\psi_\alpha|^2)$ of the isolated (noninteracting) molecules α which depends essentially on the electron occupation density $|\psi_\alpha|^2$ and corrections

$$H_T^d(\{\psi_\alpha\}) = \sum_\alpha H_\alpha(|\psi_\alpha|^2) + H_T^e(\{|\psi_\alpha|^2\}) \tag{28}$$

The small interaction potential $H_T^e(\{|\psi_\alpha|^2\})$ between these charged molecules α supposed to be far apart, may be neglect in a first approach. In principle, they can also be taken into account in the following theory but we shall not do for simplicity.

A good approximation for the energy H_α of the isolated system α is to choose

$$H_\alpha(I_\alpha) = \mu_\alpha I_\alpha + \frac{\chi_\alpha}{2} I_\alpha^2 \tag{29}$$

for capturing the main effect of nonlinearities. Then, μ_α is the energy level of the unoccupied electronic state (the energy $H_\alpha(0)$ when no electron is present is a constant which can dropped for convenience).

We also assume for consistency that the damping function $\Gamma_{\alpha,\beta}$ vanishes when $\alpha \neq \beta$, that is the thermal bath does not mediate significant interactions between the different states α. This is equivalent to assume $k_{i,\alpha}k_{i,\beta} = 0$ if $\alpha \neq \beta$ that is the thermal bath splits into independent thermal baths for each state α with variables $u_{i,\alpha}$ (as we assumed in Ref. [7]). Again, these terms could be taken into account but we shall not do here it for simplicity.

Coefficient χ_α of the nonlinear term is mostly the sum of the two contributions of different physical origin

$$\chi_\alpha = \chi_\alpha^C + \chi_\alpha^R \tag{30}$$

where χ_α^C is a positive coefficient corresponding to the capacitive energy involved by the electrostatic field generated by the electric charge proportional to I_α at site α. It takes into account the relaxation of the surrounding electrons through the dielectric constant ε_∞ but assume that the nuclei remain immobile.

χ_α^R is the negative coefficient corresponding to the energy released by the reorganization of the nuclei of the environment due to the presence of the electron I_α. Actually, this term can be readily calculated from the coupling with the thermal bath in (1) assuming the thermal bath is splitted into independant thermal baths. We have

$$\chi_\alpha^R = -\sum_i m_i \omega_i^2 k_{i,\alpha}^2 = -\Gamma_{\alpha,\alpha}(0) \tag{31}$$

It can be speculated that when the electron occupies a state α involved in chemical bonds, the reorganization energy will be prevalent on the

electrostatic energy so that we shall have χ_α negative. Otherwise, when this state corresponds to an inner orbital of a metallic ion for example, the electrostatic energy may be prevalent on the reorganization energy and thus, we shall χ_α positive.

6.2 The dimer model

Then, a simple Hamiltonian H_T for describing the two states donor-acceptor model ($\alpha = D$ or A) can be written as

$$\begin{aligned} H_T(\psi_D, \psi_A) &= \mu_D|\psi_D|^2 + \frac{1}{2}\chi_D|\psi_D|^4 + \mu_A|\psi_A|^2 + \frac{1}{2}\chi_A|\psi_A|^4 \\ &\quad -\lambda(\psi_D^\star\psi_A + \psi_A^\star\psi_D) \end{aligned} \tag{32}$$

where constant λ is supposed to be small, real (and positive for fixing the ideas). We have $|\psi_D|^2 + |\psi_A|^2 = 1$.

Then, we have from Eq. (9)

$$i\hbar\dot{\psi}_\alpha = \left(\mu_\alpha + \chi_\alpha I_\alpha + \int_{-\infty}^{t} \Gamma_\alpha(t-\tau)\dot{I}_\alpha(\tau)d\tau + \zeta_\alpha(t)\right)\psi_\alpha - \lambda\psi_\beta \tag{33}$$

where $(\alpha, \beta) = (D, A)$ or (A, D) and $\gamma = D$ and A. We also denotes $\Gamma_{\alpha,\alpha}$ as Γ_α for simplicity since the cross terms $\Gamma_{\alpha,\beta}$ have been assumed to be zero for $\alpha \neq \beta$. When the transfer integral is zero $\lambda = 0$ and the temperature zero $\zeta_D = \zeta_A = 0$, there is no coupling between the two units so that I_D and I_A are time constant. Then, $\psi_\alpha(t) = e^{-E_\alpha t/\hbar}\psi_\alpha(0)$, where energy levels E_α depends on $I_\alpha = |\psi_\alpha|^2$ on the donor and the acceptor respectively.

$$E_\alpha(I_\alpha) = \frac{dH_\alpha}{dI_\alpha} = \mu_\alpha + \chi_\alpha I_\alpha \tag{34}$$

These energy levels are those of a very slow electron that is assuming the nuclei has the time to relax adiabatically while the electron density varies. We call these energy levels *antiadiabatic*. The adiabatic energy levels are obtained for the nuclei at fixed position and thus depends on these positions.

It is also convenient to rewrite Eqs. (33) in action-angle representation $\{I_\alpha, \theta_\alpha\}$ defined as

$$\psi_\alpha = \sqrt{I_\alpha}e^{-i\theta_\alpha} \tag{35}$$

We have $I_D + I_A = 1$ time constant and define $\theta = \theta_D - \theta_A$ and $I = (I_D - I_A)/2$. Then, Eqs. (33) yields

$$\begin{aligned} \hbar\dot{\theta} &= (E_D + \zeta_D) - (E_A + \zeta_A) + \frac{4\lambda I}{\sqrt{1-4I^2}}\cos\theta \\ &\quad + \int_{-\infty}^{t} \Gamma(t-\tau)\dot{I}(\tau))d\tau \qquad (36) \\ \hbar\dot{I} &= -2\lambda\sqrt{1-4I^2}\sin\theta \qquad (37) \end{aligned}$$

where $\Gamma = \Gamma_D + \Gamma_A$. When λ is small, Eq. (37) shows that $\dot{I}$ is small and thus I slowly vary as a function of time as well as I_D and I_A.

At zero temperature, $\dot{\theta}$ rotates almost periodically with the frequency $\Omega^0 = (E_D - E_A)/\hbar$ but the integral with kernel Γ may generates "damping". At finite temperature the random force $\zeta_D - \zeta_A$ which corresponds to temperature fluctuations become important but the period $\Omega^T(t) = (E_D + \zeta_D - E_A - \zeta_A)/\hbar$ fluctuates in time with the frequencies of the phonons. Then it can be nevertheless assumed that ζ_D and ζ_A have slow variation at the scale of the average frequency Ω^T.

6.3 Adiabatic electron transfer at nonzero temperature

Let us first analyze the regime where the temperature is prevalent. The existence of a cut-off in frequency range for the phonons, is essential for recovering the adiabatic regime where the Marcus theory holds far away from the inversion point. The time Fourier transforms of $\Gamma_\alpha(t)$ and the random force $\zeta_\alpha(t)$ are zero beyond the cut-off frequency ω_c which corresponds to the largest phonon frequency.

The adiabatic approximation is valid when

$$\hbar\Omega^T(t) = |E_D + \zeta_D - E_A - \zeta_A| \gg \hbar\omega_c \qquad (38)$$

In the most common physical situations, the electronic levels E_D and E_A are not initially at resonance and remains far from resonance during most the ET except at the final stage of tunnelling. The characteristic time for ET is mostly the time for reaching resonance.

Since the Fourier transform $\Gamma(t)$ in Eq. (36) involves the phonon frequencies which are small compared to the frequency variation of $\dot{I}$, the integral in Eq. (36) is practically zero and does not generate damping. Then, the adiabatic equation 33 becomes

$$i\hbar\dot{\psi_\alpha} = (\mu_\alpha + \chi_\alpha I_\alpha + \zeta_\alpha(t))\psi_\alpha - \lambda\psi_\beta \qquad (39)$$

where $(\alpha, \beta) = (D, A)$ or (A, D).

The slow time dependent potential $\zeta_\alpha(t)$, is nothing but the potential generated by the atomic fluctuations (11). $I_\alpha(t)$ is also slow variable, and thus the electronic levels can be assumed to follow adiabatically this external potential $\zeta_\alpha(t)$. Thus, if the electron is initially on the donor, it will stay in the same eigenstate, so that $I_D(t)$ will remain practically constant and equal to 1 while $I_A(t)$ remains equal to zero. No ET is possible while no resonance occurs.

Resonance would occur in the initial state $I_D = 1$, $I_A = 0$ when the electronic levels of Eq. (39) become equal that is when $E_D(1) + \zeta_D \approx E_A(0) + \zeta_A$ (see Fig. 2). Then the adiabatic approximation does not hold. Thus if we forget about the intermediate dynamics of the electron and assume fast tunneling at resonance, our model yields a qualitatively identical behavior to those of Marcus except concerning the definition of parameters as we shall see.

In our model, the inversion point is obtained when there is resonance at zero temperature in the initial state $I_D = 1$ and $I_A = 0$ that is when $\Delta_{el} = E_A(0) - E_D(1) = 0$ or

$$\mu_A = \mu_D + \chi_D \tag{40}$$

Note that $\Delta_{el} \neq \Delta^\star_{el}$. The Marcus condition $\Delta^\star_{el} = 0$ becomes in our model (see 26)

$$\mu_A - \mu_D - \frac{1}{2}\chi_D = \frac{1}{2}(\chi^R_D + \chi^R_A) \tag{41}$$

Actually, rescaling $\mu'_\alpha = \mu_\alpha + \frac{1}{2}\chi^C_\alpha$, the Marcus condition becomes $\mu'_A = \mu'_D + \chi^R_D = 0$ which is formally identical to our condition (40). Moreover, if the capacitive coefficients are supposed to be equal for both sites $\chi^C_D = \chi^C_A$ which is not physically unreasonable if donor and acceptor have similar dielectric environment and similar extension of their charge distribution, the inversion point obtained within our theory is identical to those predicted by Marcus.

Actually, the reason for this discrepancy is obvious because although the Marcus theory does consider electrostatic energies in the global energy, it does not take into account the nonlinearities they induce in the electron dynamics. Indeed in the standard theory, the electronic levels (without lattice reorganization), are supposed to be independent of their occupation density but actually these electronic levels do depend continuously on their occupation density I_α because of the energy variation of the surrounding electric field taking into account the dielectric response ε_∞ of the environment.

When there is resonance, there are two possible situations. Either λ although small is not too small and larger than $\hbar\omega_c$ (strong reactant regime) or it is smaller than $\hbar\omega_c$ (weak reactants). In the strong reactant

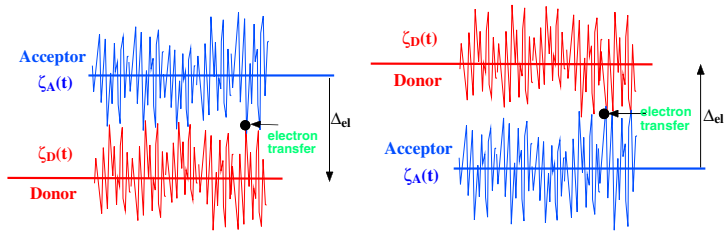

Figure 2. Time-dependent fluctuations (induced by thermal lattice fluctuations) of the Electronic levels of the donor and acceptor in normal regime (a) and in the Marcus inverted regime (b). Within Marcus theory, ET occurs at resonance.

case, the adiabatic approximation remains valid at resonance because the electronic level splitting energy remains larger than the phonon energies and ET occurs adiabatically (in the normal regime only). When ET is in the inverted regime and also in the more frequent weak reactant situation, a correct description requires to return to the non adiabatic equations (33) or (36), (37) for describing properly electron tunnelling.

6.4 Energy barrier during electron transfer

The energy barrier considered in the Marcus theory is not the true barrier in the configuration space because it assumes a discontinuous variation of the electron densities on donor and acceptor 0 or 1. We consider the true energy barrier of the global Hamiltonian (1) for both the electronic and nuclei degrees of freedom. Since H_T is the minimum of $\mathbf{H}$ with respect to the nuclei degrees of freedom. This energy barrier on H_T is also those of the global Hamiltonian. The Marcus energy barrier which is obtained with restrictions, is thus necessarily larger or equal than those obtained for H_T. Actually, the investigation of the energy barrier for ET shall reveals new possible situations in a narrow region close to the inversion point, which are not described in the Marcus theory.

At zero temperature, because of the coupling of the electronic charge with the thermal bath generates only the damping term, the energy H_T of the system is decreasing in average so that the final steady state of the electron is necessarily a local minimum of H_T. Thus, transferring the electron from the donor to the acceptor at zero temperature requires two conditions which are [5]

[5]It may be argued that our argument does not look not rigorous because we have only proved energy dissipation in average. Actually, this energy barrier for H_T is the same as for the initial global Hamiltonian (1) in the full space of variables and cannot passed because of global energy conservation.

- the absence of energy barrier for during ET between the donor and the acceptor
- a nonvanishing energy dissipation

Since $|\psi_D|^2 + |\psi_A|^2 = 1$, the energy variation of the donor-acceptor dimer as a function of the amount of charge $I_A = |\psi_A|^2$ which is transferred onto the acceptor is

$$\begin{aligned} \epsilon_T(I_A) &= H_D(1 - I_A) + H_A(I_A) - H_D(1) - H_A(0) \\ &= (\mu_A - \mu_D - \chi_D)I_A + \frac{1}{2}(\chi_D + \chi_A)I_A^2 \end{aligned} \tag{42}$$

Since the overlap energy between the redox orbitals is small, it could only weakly modify the energy profile (42) and thus we neglect it. Note that this function $\epsilon_T(I_A)$ is nothing but the analogous of the detuning function between two nonlinear oscillators which was defined in [6] for describing the phenomena of Targeted Transfer. (42) can be written again

$$\epsilon_T(I_A) = \Delta_{el} I_A - \frac{1}{2}(\Delta G^0 + \Delta_{el})I_A^2 \tag{43}$$

after redefining $\Delta_{el} = E_A(0) - E_D(1)$ and $\Delta G_0 = H_D(1) + H_A(0) - H_D(0) - H_A(1)$. Please note that this definition for Δ_{el} is different of those of Marcus $\Delta_{el}^\star$ shown Fig. 1 because we take into account the electrostatic nonlinearities through χ_α^C. The definition of the energy ΔG^0 released by ET is the same as in Marcus theory. We assume it is positive.

Within our model, $\epsilon_T(I_A)$ is a quadratic function of I_A which has at most one extrema at $I_A^m = \frac{\Delta_{el}}{2(\Delta G^0 + \Delta_{el})}$ which formally coincides with the Marcus energy barrier (27) if $0 \leq I_A^m \leq 1$. However, it will be a maximum and thus an energy barrier only if

- $0 \leq I_A^m \leq 1$ and
- $\Delta_{el} + \Delta G^0 > 0$

These two conditions requires $\Delta_{el} > 0$ that is to be in the normal Marcus regime. Then, because of the energy barrier, no ET from the donor to the acceptor is possible at zero temperature and λ small. [6].

[6]However, if the barrier is small (small detuning function) it can be shown with the arguments of Ref. [6] that ET may nevertheless occur provided λ be larger than a small critical value.

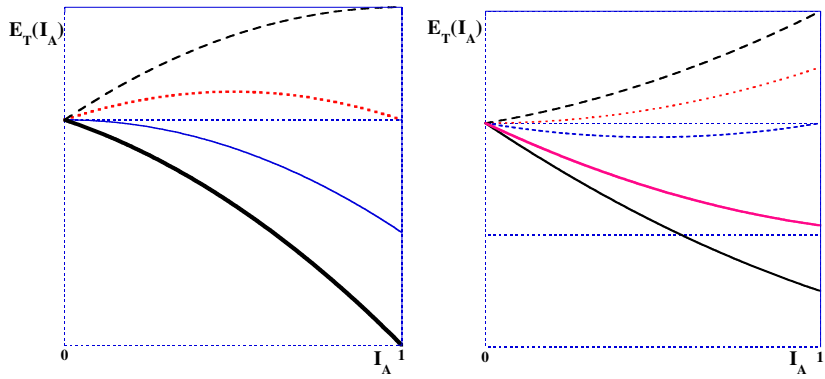

Figure 3. Energy profiles $\epsilon_T(I_A)$ for different values of μ_A versus electron transfer I_A when $\chi_D + \chi_A < 0$ (left) and when $\chi_D + \chi_A > 0$ (right) in the normal regime (top curve) $\mu_A > \mu_D + \chi_D$ (or $\Delta_{el} > 0$), at the Marcus inversion point (middle curve) ($\mu_A = \mu_D + \chi_D$ (or $\Delta_{el} = 0$) and in the inverted regime (bottom curves) $\mu_A < \mu_D + \chi_D$ (or $\Delta_{el} < 0$). ET may occur at zero K only in the inverted regime at the left. This is not sufficient at the right. The minimum should be at $I_A = 1$ that is only for the lowest curve at the right.

On the opposite, there is no energy barrier when $\Delta_{el} < 0$ that is in the inverted regime (in apparent contrast with the Marcus result). Then, the situation is more subtle because one should distinguish two situations according to the curvature of $\epsilon_T(I_A)$ which is given by the sign of $\chi_D + \chi_A = -2(\Delta_{el} + \Delta G_0)$

- When $\chi_D + \chi_A < 0$ or $\Delta G^0 > -\Delta_{el} > 0$ (see Fig. 3 left), the reorganization energy is prevalent on the Coulomb energy.
- When $\chi_D + \chi_A > 0$ or $-\Delta_{el} > \Delta G^0 > 0$ (or (see Fig. 3 right), the electrostatic energy of the system is prevalent on its reorganization energy. (remember Δ_{el} has been redefined and is not those shown Fig. 1). As we already suggested, this physical situations is favored when either the donor or the acceptor involves metallic ions. We have two situations again
  - When, the minimum of $\epsilon_T(I_A)$ is obtained for $0 < I_A^m < 1$ when $d\epsilon_T/dI_A(1) > 0$ that is when $\mu_D < \mu_A + \chi_A$ or $-\Delta_{el} > 2\Delta G^0 > 0$, the ET cannot be complete but partial with a final state where the electronic charge distributed both on the donor and the acceptor. However, the property of this state sharply contrast with those of a standard covalent bond where the charge is also distributed between two sites. The origin of this state is due to the minimization of the electrostatic

energy. This state has the peculiarity that unlike a covalent bond, its energy weakly depends on the phase difference $\theta_D - \theta_A$ because λ is small. There are low frequency electronic modes associated with phase excitation [7].

– When, the minimum of $\epsilon_T(I_A)$ is obtained for $I_A = 1$ (total transfer), that is when $\mu_A + \chi_A < \mu_D$ or $2\Delta G^0 > -\Delta_{el}$, the energy minimum is obtained when the electron is totally transferred to the acceptor as in the previous case.

Although the existence of an energy barrier forbids ET at zero temperature, the absence of energy barrier is nevertheless not sufficient for transferring the electron from the donor to the acceptor at least as an ultrafast process because energy dissipation by the damping terms should be efficient enough. We recover the result that there is practically no ET at zero temperature in the inverted regime but only far enough from the inversion point. On contrary, ET occurs in the inverted regime close to the inversion point as shown by our investigation of the real dynamics of the electron for this transfer.

6.5 Non adiabatic electron transfer at zero temperature close to the inversion point

We consider the weak reactant regime that is the nonadiabatic situation where $\lambda << \hbar\omega_c$. It is clear that when there is a non vanishing energy barrier that is the normal Marcus regime, no ET may occur at zero temperature. Thermal fluctuations are needed.

On the other side of the inversion point but close to it, there is no energy barrier, but the electron dynamics is nonadiabatic because the energy gap between the electronic levels on donor and acceptor still belong to the range of phonon energies. Because of that, ET may occur at zero temperature [8].

We calculate this ET at zero temperature as a function of time in the limit of a small transfer integral λ in the situation corresponding to the right Fig. 3 in the incoherent regime.

[7] Although it is not the purpose of this paper to extend to the discussion of this physical effect, we suggest that it could perhaps be used for the interpretation of intermediate valence systems with transition metals.

[8] Note that in the inverted regime, the adiabatic approximation does not allow ET.

Eqs. (36) and (37) become at zero temperature

$$\hbar\dot{\theta} = \hbar\Omega(\frac{1}{2} - I) + \frac{4\lambda I}{\sqrt{1-4I^2}}\cos\theta + \int_{-\infty}^{t}\Gamma(t-\tau)\dot{I}(\tau))d\tau \tag{44}$$

$$\hbar\dot{I} = -2\lambda\sqrt{1-4I^2}\sin\theta \tag{45}$$

where $\hbar\Omega(I_A) = -\frac{d\epsilon_T(I_A)}{dI_A}$. We have $\hbar\Omega(0) = -\Delta_{el}$

The minimum value of $\Omega(\frac{1}{2} - I) = E_D(\frac{1}{2} + I) - E_A(\frac{1}{2} - I))$ is positive and obtained for $I = 1/2$ (which corresponds to $I_A = 0$). We assume that the negative slope of $\epsilon_T(I_A)$ (42) fulfills $E_D(1 - I_A) - E_A(I_A) = -\Delta_{el} >> |\lambda|$ that is we are close but not very close to the inversion point. Then, the second equation yields $\dot{I}$ is of order λ and the first equation yields at leading order that $\hbar\dot{\theta} \approx E_D(\frac{1}{2} + I) - E_A(\frac{1}{2} - I) = \hbar\Omega(I)$. Consequently, we have over long times $\theta(t) = \Omega(I)t + \Phi + \ldots$ where Φ is an arbitrary phase. Then, $\dot{I}$ is also periodic over long times with frequency $\Omega(I)$.

It is convenient to use Eq. 21 which yields the global energy dissipation. This equation becomes in our dimer model for slow varying frequencies after averaging over a relative long interval of time

$$\begin{aligned} < \frac{dH_T}{dt} > &= -\gamma_D(\Omega(I)) < \dot{I}_D^2 > -\gamma_A(\Omega(I)) < \dot{I}_A^2 > \\ &= -\gamma(\Omega(I)) < \dot{I}^2 > \end{aligned} \tag{46}$$

where $\gamma = \gamma_D + \gamma_A$.

Actually, $I(t)$ can be written explicitly as the sum of two components $\bar{I}(t) + I_p(t)$ where $\bar{I}(t) =< I(t) >$ is averaged on a period of time long compared to the characteristic frequency $\Omega(I)$. This component have large variations but varies slowly. I_p is the fast oscillation at frequency $\Omega(I)$ with a small amplitude of order λ. It can be obtained from Eq. (45) neglecting the fluctuation of I and assuming $\bar{I}$ constant (Φ is an arbitrary phase with slow variation).

$$I_p \approx 2\frac{\lambda}{\hbar}\frac{\sqrt{1-4\bar{I}^2}}{\Omega(\bar{I})}\cos(\Omega(\bar{I})t + \Phi)$$

Then, from Eq. (45), we have at lowest order

$$< \dot{I}^2 > \approx 4\frac{\lambda^2}{\hbar^2}(1-4\bar{I}^2) < \sin^2(\Omega(\bar{I})t + \Phi) >= 2\frac{\lambda^2}{\hbar^2}(1-4\bar{I}^2)$$

which yields in Eq. (46) the rate of decay of the energy averaged on the small amplitude but fast oscillations of I. Neglecting the small

fluctuations of I, we have $H_T(I) \approx H_T(\bar{I})$ and thus, the long term variation equation for $\bar{I}$

$$\dot{\bar{I}} = -2\frac{\lambda^2}{\hbar^2}(1-4\bar{I}^2)\frac{\gamma(\Omega(\bar{I}))}{\Omega(\bar{I})} \tag{47}$$

or

$$\dot{I_A} = \frac{\lambda^2}{2\hbar^2} I_A(1-I_A)F(I_A) \tag{48}$$

where $F(I_A) = \frac{\gamma(\Omega(1/2-I_A))}{\Omega(1/2-I_A}$. Note that in this equation, the phase of the wave function has been averaged out and the equation only concerns their density.

If $F(I_A) = K$ is independent of I_A. This equation has the simple solution

$$I_A(t) = \frac{1}{e^{-\frac{t}{\tau}}+1}$$

with characteristic time $\tau = \frac{2\hbar^2}{K\lambda^2}$. In general this solution is not valid because $F(I_A)$ is not a constant.

There are two opposite limits. If $\Omega(I)$ becomes small or equivalently the electronic gap vanishes, the rate of transfer $\dot{I}_A$ diverges but then we approach resonance and the model is not valid anymore. Then ET also occurs but the phase coherence of the electron wave function plays an essential role and cannot be averaged out.

If $\Omega(I)$ becomes larger than the phonon frequencies, the damping constant $\gamma(\Omega(I))$ vanishes and then ET sharply stops. Actually, it will not stops because γ cannot be strictly zero in physics but it will exhibit a very long tail (stretched exponential?). Thus far from the inversion point in the inverted regime, there is practically no ET at zero temperature despite the absence of any energy barrier.

When, there is no energy barrier that is in the inverted regime, we have ET provided small electronic gaps in the rage of phonon energies which also corresponds to weak reaction energies in the same range. Then, in general, the transfer rate is not simply exponential with a unique characteristic time. ET generally slows down as a function of time because the electronic gap $\hbar\Omega(I_A)$ increases. However, $\Gamma(\Omega(I_A))$ may be non monotone in case of intense absorption bans in the phonon bath.

6.6 Targeted electron transfer, coherent transfer and catalysis

There is a highly interesting situations which is precisely obtained when $\Omega(I_A) = 0$ for all I_A.

This situation corresponds to $\epsilon_T(I_A) = 0$ (42) for all I_A since $d\epsilon_T/dI_A = \hbar\Omega(I_A)$. We have simultaneously $\Delta G_0 = 0$ (no reaction energy) and $\Delta_{el} = 0$ that is we remains permanently at the inversion point. This situation has apparently no physical interest because ET is reversible. Actually, the minimum energy of the system is obtained for a symmetric or antisymmetric electronic state (covalent bond) according to the sign of λ but the binding energy which of the order of λ. This situation requires

$$\chi_A = -\chi_D \tag{49}$$

$$\mu_A = \mu_D + \chi_D \tag{50}$$

which means that the nonlinearities on donor and acceptor have just opposite sign. They seems to cancel each other but on condition the total of electron density on donor and acceptor is just one. Otherwise, if the electron partly occupies other sites, it does not. Eq. (45) becomes

$$\hbar\dot{\theta} = \frac{4\lambda I}{\sqrt{1-4I^2}}\cos\theta + \int_{-\infty}^{t}\Gamma(t-\tau)\dot{I}(\tau))d\tau \tag{51}$$

$$\hbar\dot{I} = -2\lambda\sqrt{1-4I^2}\sin\theta \tag{52}$$

Without damping, this equation can be solved and yields Targeted Transfer [6]. We get the simple solution $\theta = \pm\pi/2$ and $I_A(t) = \sin^2\frac{2\lambda}{\hbar}t$. This solution keeps phase coherence since the phase difference θ is time constant. It correspond to a ultrafast transfer at the order λ since its characteristic time is proportional to $1/\lambda$ instead of $1/\lambda^2$ for the incoherent process described above. Note also that this coherent transfer we call Targeted Electron Transfer is also reversible.

When Γ is not zero, this time periodic solution damps and converges to the covalent solution. The first interesting feature is that these oscillations start only when the electron injected from another source is well focused on the donor where it has reached the density 1 (charge selectivity). Then, the electronic levels $E_D(1-I_A) = E_A(I_A)$ oscillates with the same frequency between two extreme values $\mu_A = \mu_D + \chi_D$ and $\mu_A + \chi_A = \mu_D$. This oscillation damps and finally converge to covalent energy level $\mu_A + \chi_A/2\mu_D + \chi_D/2$.

In such situation, we shall call the acceptor, *catalyst* $\alpha = C$ because it is not really an acceptor for the electron but this oscillating system may induce a spectacular effect when it is weakly coupled to a third unoccupied electronic level.

For λ small, suppose the interaction between such a donor and catalyst generates electronic level oscillations $E_D(t) = E_C(t)$ in an interval

$[\mu_D, \mu_C]$. Then, assume a third unoccupied electronic level initially at energy μ_A in the interval $[\mu_D, \mu_C]$. It is also assumed that this acceptor only coupled with the donor alone would be in the normal Marcus regime (with a energy barrier). Thus, a direct transfer is not possible at zero temperature. However, resonance will necessarily occur at a certain time after TET is initiated when $E_D(t) = \mu_A$. Then, if the acceptor is sufficiently coupled, the immediate effect is to block the oscillation donor-catalyst and to trigger an ultrafast ET from the system donor-catalyst to the acceptor. This very spectacular effect has been numerically observed in [7].

7. Concluding remarks

We have presented here the basic hypothesis of our model but not described some of its applications for example for understanding enzymatic catalysis especially in biology. The reader is referred to [7].

We have demonstrated that the regime of ultrafast ET that is in the vicinity of the Marcus inversion point, requires to take fully into account the nonadiabaticity of the system. We show that this problem cannot be treated within the standard theory of (linear) tunnelling. In the model we obtain, the nonlinearities plays the fundamental role as well damping and thermal noise and cannot be discarded.

The nonlinearity manifests by the fact an electronic energy levels depend on its occupation density both because of the electrostatic effects and the reorganisation of the environment. The special case of Targeted Electron Transfer between donor and catalyst although exceptional present a high physical interest despite in itself it does not produce irreversible ET. A very weak coupling turns out to be sufficient to generate coherent large amplitude oscillation of electronic density associated with a large amplitude oscillation of the corresponding energy level. This phenomena is not an ordinary resonance effect. It relies essentially on the nonlinearities of both electronic energy levels on Donor and Catalyst which must be appropriately tuned. It also requires a specific initial density (i.e., the fully occupied Donor) which yields selectivity. This phenomena is drastically different from linear tunnelling which does not generate oscillations for the electronic levels.

When a third molecule (acceptor) is weakly coupled with such a system donor-catalyst, a resonance may be induced which triggers ultrafast ET to the Acceptor. The presence of the catalyst is not only to suppress the energy barrier between donor and acceptor but also to boost the electron dynamics and generate an ultrafast electron transfer.

There are straightforward extension of this theory, concerning more generally the transfer of quantum excitations and particularly excitons. Other directions concerns the possibility of forming more complex logical devices with many electronic states based of nonlinear coherent electron transfer.

Acknowledgments

This work has been supported by EC under contract HPRN-CT-1999-00163.

References

[1] A.M. Kuznetzov and J. Ulstrup, *Electron Transfer in Chemistry and Biology: An introduction to the theory* Wiley series in Theoretical Chemistry (1999)

[2] R.A. Marcus, Rev.Mod.Phys. **65** (1993) 599-610

[3] X. Hu, A. Damjanovic, T. Ritz and K. Schulten, Proc. Nat. Acad. Sci. (USA) **95** 5935 (1998).

[4] H.A. Kramers, Physica **7** (1940) 284

[5] R. Loudon, *The Quantum Theory of Light* Oxford University Press, Oxford, UK (1979)

[6] S. Aubry, G. Kopidakis, A-M. Morgante and G. Tsironis, Physica **B296** (2001), 222–236

[7] S. Aubry and G. Kopidakis, in *Localization and Energy transfer in Nonlinear systems*, World Scientific Publishing, pp.1-27 (2003)

NONLINEAR SPECTROSCOPY STUDY OF VIBRATIONAL SELF-TRAPPING IN HYDROGEN BONDED CRYSTALS

Julian Edler and Peter Hamm

Physikalisch-Chemisches Institut, Universität Zürich, Winterthurerstrasse 190, CH-8057 Zürich, Switzerland

jedler@pci.unizh.ch; phamm@pci.unizh.ch

Abstract Femtosecond pump probe spectroscopy proves that self-trapping occurs in the NH and amide I band of crystalline acetanilide (ACN). The phonon modes that mediate the self-trapping are identified. Comparison between ACN and N-methylacetamide, both model systems for proteins, shows that self-trapping is a common feature in hydrogen bonded systems.

1. Introduction

It is well known that proteins have the remarkable, yet not well understood capability of storing and transporting efficiently small quanta of energy. Davydov suggested self-localization of vibrational energy as a possible explanation of this phenomena [1]. Crystalline acetanilide (ACN) is considered to be a good model to study vibrational excitations in proteins, since it consists of quasi-one-dimensional chains of hydrogen bonded peptide groups with structural properties that are comparable to those of an α-helix, the most common secondary structural motif in proteins. Self-trapping originates from two coupling mechanisms [2]: (i) dipole-dipole-interaction couples the individual peptide units to form delocalized states, i.e. vibrational molecular excitons. (ii) nonlinear interaction mediated through the hydrogen bonds, which stabilize the crystal structure, couples the excitons to lattice phonons. Thus excitation of an exciton leads to a deformation of the lattice and the initially delocalized state collapses to form a self-localized state.

It is well known that the vibrational spectrum of ACN exhibits interesting anomalies in the region of the amide I (i.e the C=O stretching) and NH stretching band [3]. The amide I mode is observed at 1666 cm^{-1} at

F. Kh. Abdullaev and V. V. Konotop (eds.), Nonlinear Waves: Classical and Quantum Aspects, 473–479.

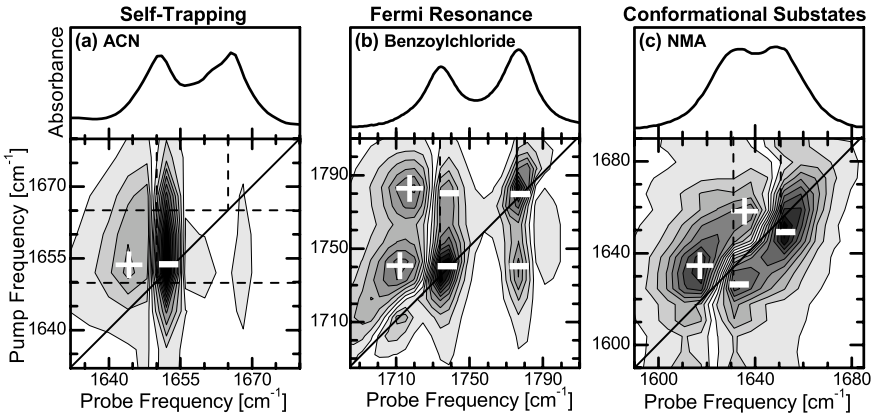

Figure 1. Absorption spectra and 2D-IR pump probe spectra of the C=O mode of (a) crystalline ACN, (b) benzoylchloride and (c) N-methylacetamide (NMA) dissolved in methanol. 2D-IR spectra record the absorption change as a function of probe frequency and the center frequency of a narrow band pump pulse. The contour intervals represent a linear scale. The absorption spectra exhibit the same doublet structure in all three cases, while the 2D-IR spectra are clearly different.

room temperature and splits into two bands at low temperatures with an additional 'anomalous' band at 1650 cm^{-1} (Fig. 2a). The NH stretching mode consists of a main peak at 3295 cm^{-1} accompanied by an almost-regular sequence of satellite peaks towards lower frequencies (Fig. 2b). The anomalies in the CO and NH band have been both explained by self-trapping theory [2, 3], according to which the main peak represents the free exciton and the anomalous side bands represent self-trapped states. In previous works self-trapping was observed through an indirect effect, i.e. through the temperature dependence of the linear absorption spectrum [2, 3]. The temperature dependence is considered to be a signature of anharmonicity of the molecular potential energy surface. We have recently started to use an alternative, more direct approach to investigate anharmonicity, namely nonlinear vibrational spectroscopy [4, 5, 6]. The nonlinear vibrational response is exclusively sensitive to the anharmonic part of the potential energy surface, since the response of a harmonic system vanishes exactly. Anharmonicity at the same time gives also rise to nonlinear dynamics. Hence, nonlinear spectroscopy is extremely valuable to study nonlinear phenomena such as vibrational self-trapping [7].

We performed femtosecond IR pump-probe experiments, using pulses with a bandwidth of 200 cm^{-1} (FWHM). A small fraction of the infrared pulses was split off to obtain a broadband probe pulse, which was spectrally dispersed after interaction with the sample and acquired by a detector array. The remainder was used as a pump pulse, that was

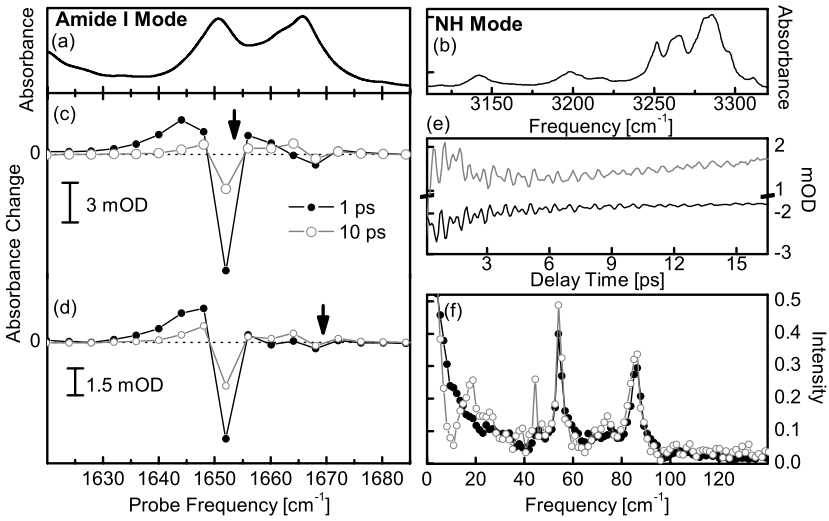

Figure 2. Part of the CO (a) and NH (b) band of crystalline ACN at 90K. Response of the amide I band upon selective excitation of the self-trapped states (c) and the free exciton peak (d) for two different delay times. The arrows indicate the position of the narrow band pump pulse.(e) Coherent Response of the NH mode after impulsive excitation and the Fourier transform spectra (f), for probe frequencies resonant with the absorption peaks in the linear spectrum at 3295 cm^{-1} (grey lines) and 3195 cm^{-1} (black lines).

spectrally filtered to obtain tunable, narrow band pump pulses for some of the experiments. Monocrystalline samples of ACN and deuterated N-methylacetamide (NMA-D6) were placed in a cryostat and experiments were performed with the E-vector parallel to the hydrogen bond chain.

2. Results and Discussion

2.1 The amide I mode

Self-trapping theory is considered to be the most convincing explanation for the observed anomalous amide I band in ACN. However, two alternative explanations, Fermi resonance and conformational substates, have been discussed as well [2]. In a recent study [6] we compared the two-dimensional infrared spectrum (2D-IR) of ACN with that of two molecular systems, which show the same splitting in the amide I band, and which were chosen as simple representatives of the alternative mechanisms (Fig. 1). 2D-IR spectra record the absorption change of the sample as a function of probe frequency and the center frequency of the narrow band pump pulse (spectral width 14 cm^{-1}, pulse duration 700 fs

FWHM) [8]. The three 2D-IR spectra differ completely, albeit in a well understood way. Based on the 2D-IR spectroscopic signature Fermi resonance and conformational sub-states can be definitely excluded as alternative explanations for the anomalous spectra of ACN. Self-trapping of the C=O mode, on the other hand, can naturally explain the observed 2D-IR spectrum of ACN.

Figure 2c,d shows two pump-probe spectra obtained by excitation of either of the two absorption lines of ACN at a temperature of 90 K. These spectra correspond to a horizontal cut through the 2D-IR spectra in Figure 1a. When resonantly pumping the anomalous band (1650 cm^{-1}, Fig. 2c) the band bleaches (negative response) and a positive band emerges at 1644 cm^{-1} (excited state absorption). When resonantly pumping the normal band (1666 cm^{-1}, Fig. 2d), on the other hand, hardly any bleach of the band itself is observed. Coherent broad band excitation experiments show that the lifetime of the normal amide I mode is 1.5 ps [5]. The lack of an observable bleach can therefore only be explained by the cancellation of all contributions to the pump-probe signal (excited state absorption, stimulated emission and bleach), which is the case for a perfect harmonic state [7]. It can be shown that the effective anharmonicity of a vibrational exciton is a direct measure of its degree of delocalization [5]. Thus, we conclude that the free exciton state is almost perfectly delocalized at 90 K. As temperature increases, a bleach signal starts to be observed, pointing to a non-complete cancellation of the different contributions of the total pump-probe signal. Apparently, thermally induced disorder starts to localize the free exciton.

The anharmonicity of the self-trapped state (1650 cm^{-1}), on the other hand, originates from nonlinear interaction between the amide I mode and the phonon system of the crystal. It is mediated through the hydrogen bonds and is nonzero even at low temperatures. With rising temperature, the bleach of the 1650 cm^{-1} band diminishes as the band disappears in the absorption spectrum.

2.2 The NH mode

We used short broadband pump pulses (spectral width 200 cm^{-1}, pulse duration 130 fs FWHM) to excite impulsively the section of the NH absorption spectrum which includes the free-exciton peak and the first three satellite peaks [6](Fig. 2b,e,f). The transient absorbance change signal shows pronounced oscillations that persist up to about 15 ps and contain two distinct frequency components whose temperature dependence and frequencies match perfectly with two phonon bands in the

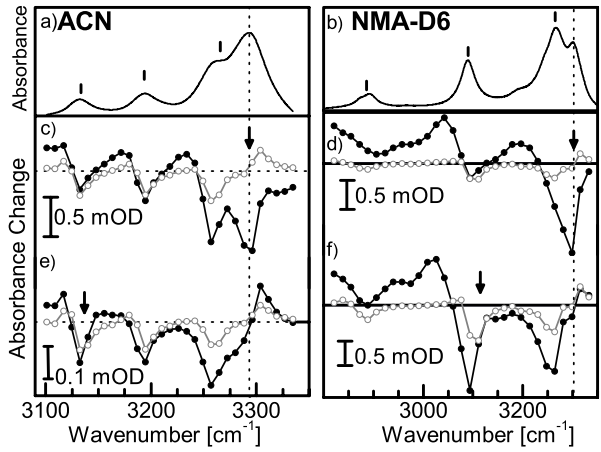

Figure 3. Part of the NH band of crystalline ACN (a) and NMA-D6 (b). The free excitons are marked by dotted lines and the self-trapped states by black bars. Response of the sample upon selective excitation of the free exciton peak (c,d) and the self-trapped states (e,f) for delay times 400 fs (black line) and 4 ps (grey line). The arrows indicate the position of the narrow band pump pulse.

non-resonant electronic Raman spectrum of ACN [3]. Therefore, the beating structure is assigned to a ground state phonon excited through a stimulated impulsive Raman effect, resonantly enhanced by the NH absorption band as a consequence of anharmonic coupling to lattice phonons. These are the phonons which modulate the hydrogen bond distance and thus mediate self-trapping.

In a second experiment, narrow band pump pulses (spectral width 30 cm^{-1}, pulse duration 250 fs FWHM) were used to selectively excite individual sub-levels of the NH band (Fig. 3c, e) [4]. On the sub-picosecond time scale, the free-exciton and the lower lying self-trapped states behave distinctly differently. When exciting the free-exciton (Fig. 3c), a strong bleach and stimulated emission signal is observed which recovers on a 400 fs time scale. Simultaneously, population is transferred into lower lying self-trapped states. On the other hand, when pumping one of the self-trapped states directly (Fig. 3e), population within all self-trapped states equilibrates essentially instantaneously, but the free exciton peak is not back-populated. This is the direct observation of ultrafast self-trapping: Excitation of the free-exciton leads to an irreversible population of self-trapped states, but not vice versa.

2.3 N-methylacetamide

Our studies on the NH and amide I band of ACN prove the self-trapping model and introduce a possible signature of self-trapping in pump probe spectroscopy. So far ACN is the only hydrogen bonded crystal for which vibrational self-trapping has been observed. However, other molecules, such as N-methylacetamide (NMA) are structurally very similar to ACN and form the same type of hydrogen bonded crystals. Therefore they should also exhibit self-trapping, but convincing experimental evidence for self-trapping in NMA has never been reported. Interestingly the NH absorption band in NMA and deuterated NMA (NMA-D6) consists of a main peak at about 3300 cm^{-1} accompanied by a regularly spaced sequence of satellite peaks, which is in fact the same bandshape as in ACN, except that the spacing is three times larger in NMA (see Fig. 3a,b). If one compares the pump probe spectrum of NMA-D6 with ACN one observes essentially the same spectral signature. An excitation of the free exciton state results in negative signals at the position of all bands in the NH mode (Fig. 3c,d), while an excitation of one of the self-trapped states gives only a signal for the self-trapped states(Fig. 3e,f). Consequently, one can use the self-trapping interpretation to explain the spectral data in NMA. The comparison between pump-probe and absorption spectra shows that the highest frequency band corresponds in all three molecules to the free exciton.

3. Conclusion

In the amide I band of ACN we have observed temperature induced localization of the free exciton mode at high temperatures and self-localization at low temperatures. The NH mode self-localizes even at room temperature, due to the larger self-trapping energy. A comparison between ACN and NMA shows that self-trapping is not a unique feature of ACN, but a general property of hydrogen bonded crystals. Hence one might expect that α-helices should also exhibit vibrational self-trapping. We are currently testing this hypothesis.

References

[1] A. S. Davydov, *J. Theor. Biol.* **66**, 379 (1977).

[2] A. C. Scott, *Phys. Reports* **217**, 1 (1992).

[3] G. Careri, U. Buontempo, F. Galluzzi, A. C. Scott, E. Gratton and E. Shyamsunder *Phys. Rev.* **B30**, 4689 (1984).

[4] J. Edler, P. Hamm and A. C. Scott, *Phys. Rev. Lett.* **88**, 067403 (2002).

[5] J. Edler and P. Hamm, *J. Chem. Phys.* **117**, 2415 (2002).

[6] J. Edler and P. Hamm, *J. Chem. Phys.* **119**, 2709 (2003).

[7] Peter Hamm, Julian Edler, in *Energy Localisation and Transfer*; *Advanced Series in Nonlinear Dynamics*; World Scientific (2003); *in press*.

[8] S. Woutersen and P. Hamm, *J. Phys.: Condens. Matter* **14**, R1035 (2002).

QUANTUM ANHARMONIC PHONONS IN THE FERMI-PASTA-ULAM CHAIN

Jacob Szeftel
Université Paris 7, Laboratoire de Physique Théorique de la Matière Condensée, case 7020, 2 Place Jussieu, 75251 Paris Cedex 05, France
szeftel@ccr.jussieu.fr

Abstract By dealing with the classical equation of motion of a Fermi-Pasta-Ulam chain as if the atomic displacement coordinates were quantum operators and requiring that some special linear combinations of the displacements and momenta pertaining to two nearest neighbor atoms obey the Bloch theorem, an effective hermitian one-body potential is worked out at each wave-vector throughout the Brillouin zone. The associated Schrödinger equation is solved to yield the exact full spectrum of quantum anharmonic phonons as the set of bound eigenstates. The anharmonic dispersion curve differs barely from the harmonic one close to the Brillouin zone center even at strong anharmonicity, the deviation being the largest in the middle of the Brillouin zone.

Keywords: anharmonic lattice dynamics, quantum treatment

1. Introduction

The anharmonic part of the interatomic potential has been known for long to be instrumental on a score of issues in solid matter such as heat conduction, thermal expansion and structural changes including melting. The whole gamut of anharmonic lattice dynamics comprises phonons, solitons and breathers. Although the classical treatment of the equation of motion of the solid provides indeed evidence for such stable excitations arising in crystalline matter [1, 2, 3, 4, 5, 6], they prove to be of little use to account for the thermal properties because the energy of classical excitations varying continuously prevents any calculation of the contribution to the free energy associated with the atomic motion.

Dealing with the quantum mechanical counterpart of anharmonic crystal dynamics is a difficult many-body problem for which little has been done[7, 8, 9, 10] beyond perturbation calculations based on harmonic phonons. Consequently the perturbed eigenstates mix phonons

F. Kh. Abdullaev and V. V. Konotop (eds.), Nonlinear Waves: Classical and Quantum Aspects, 481–487.

with different wave-vectors so that they are no longer plane waves, which makes the concept of a dispersion curve meaningless although such dispersion curves have been measured for decades in real anharmonic solids by neutron scattering. In this work an exact diagonalization of the full lattice dynamical Hamiltonian is presented for anharmonic phonons, i.e. these eigenstates are plane waves characterized by a wave-vector. This result has been achieved by requiring that the quantum version of the equation of motion obey the Bloch theorem.

The outline is as follows: the principle of the method is described in section I while an illustrative example is given for the Fermi-Pasta-Ulam (FPU) chain in section II.

2. Working out the Schrödinger equation

As we are looking for plane waves, the crystal dimension is unimportant. Therefore we consider for simplicity an infinite chain of atoms of mass m, distant from one another by the lattice parameter a and coupled by the potential $V = \sum_{j\in\mathbb{Z}} W(u_j - u_{j+1})$ where u_j designates the displacement coordinate of the particle j with respect to its static equibrium position and $W(x)$ is an arbitrary pairwise potential describing the anharmonic coupling between nearest neighbors. The classical equation of motion reads

$$m\ddot{u}_j = W'(u_{j-1} - u_j) - W'(u_j - u_{j+1}) \quad , \quad j \in \mathbb{Z} \quad , \tag{1}$$

where $W' = \frac{dW}{dx}$ and $\ddot{u}_j$ refers to the second derivative of u_j with respect to time. From now on we shall regard the classical variables $u_j, u_{j\pm1}, \ddot{u}_j$ as quantum operators, thus following the footsteps of Heisenberg in his seminal treatment of the quantum harmonic oscillator [11].

Let us introduce now the operators $a_j^\dagger, a_j$ defined as

$$a_j^\dagger = m\omega_0 u_j + ip_j \,, \quad a_j = m\omega_0 u_j - ip_j \,, \tag{2}$$

where ω_0 is a vibrational frequency such that $m\omega_0^2 = \frac{d^2W}{dx^2}(0)$ and $p_j = i\hbar\frac{\partial}{\partial u_j}$ is the canonical momentum attached to the displacement u_j. That $a_j^\dagger, a_j$ are hermitian conjugate of each other ensues from both operators u_j, p_j being hermitian. The identities in Eqs. (2) secure that $a_j^\dagger, a_j$ reduce to the usual boson creation and annihilation operators in the harmonic limit, i.e. $W(x) \propto x^2$.

The main assumption underlying this work consists of requiring that the operators $a_j^\dagger, a_j$ fulfil the Bloch condition consistent with the interatomic potential being periodic

$$a_{j+1}^\dagger = e^{ika} a_j^\dagger \Rightarrow a_{j+1} = e^{-ika} a_j \quad , \quad j \in \mathbb{Z} \quad . \tag{3}$$

The consistency of Eqs. (3) is ensured by $a_j^\dagger, a_j$ being hermitian conjugate of each other. It must be emphasized that Eqs. (3) hold only inside the subset S_k spanned by every anharmonic phonon associated with k. Thence Eqs. (3) characterize S_k and sort S_k out of the whole Hilbert space describing the atomic motion of the crystal. Taking advantage of Eqs. (3), $u_{j\mp1} - u_j$ is inferred to read

$$u_{j\mp1} - u_j = \pm\frac{\sin(ka)}{m\omega_0}p_j - 2\sin^2\left(\frac{ka}{2}\right)u_j \quad .$$

Inserting these expressions into Eqs. (1) results into

$$\begin{aligned} m\ddot{u} = W'\left(\frac{\sin(ka)}{m\omega_0}p - 2\sin^2\left(\frac{ka}{2}\right)u\right) \\ -W'\left(\frac{\sin(ka)}{m\omega_0}p + 2\sin^2\left(\frac{ka}{2}\right)u\right), \end{aligned} \tag{4}$$

wherein the index j has been dropped.

The virtue of the assumption conveyed by the identities in Eqs. (3) is to map exactly the many-body Eqs. (1) into the one-body Eq. (3) but only as far as anharmonic phonons are concerned. Other kinds of nonlinear excitations such as breathers or solitons which do not belong in S_k are thence not taken into account. Eq. (3) will now be used [11] to introduce a one-body effective potential $V_e(k,u)$ valid for anharmonic phonons only

$$\frac{\partial V_e}{\partial u} = -m\ddot{u} \quad . \tag{5}$$

The corresponding Hamiltonian and Schrödinger equation reads

$$H_k = \frac{p^2}{2m} + V_e \quad , \quad (H_k - \varepsilon)\,\psi = 0 \quad , \tag{6}$$

where ε, ψ designate the eigenenergy and eigenfunction and we focus upon the bound eigenstates ψ ($\Rightarrow \int_{-\infty}^{+\infty} |\psi|^2(u)du < \infty$) making up the basis of S_k.

It will be shown now by contradiction that $k \neq k' \Rightarrow S_k \bigcap S_{k'} = \emptyset$. For suppose that $S_k \bigcap S_{k'} \neq \emptyset$. It is then inferred from Eqs. (3) that $a_{j+1} = e^{-ika}a_j = e^{-ik'a}a_j \Rightarrow a_j = 0$, which is wrong provided S_k or $S_{k'}$ are not empty or equivalently Eq. (6) has at least one bound solution. Hence the anharmonic phonon subspace can be defined as $S_\phi = \bigoplus_k S_k$ where the sum is carried out over the whole Brillouin zone. Accordingly the projection of the full anharmonic lattice dynamical Hamiltonian onto S_ϕ reads $H_\phi = \sum_k H_k$. As in the harmonic case, a many-body eigenstate

is made up of a tensor product of phonons, each being labelled by its k. However the many harmonic phonon eigenstates do span the whole Hilbert space describing the crystal motion whereas the many anharmonic phonon subspace S_ϕ fails to include an infinity of eigenstates, e.g. quantum breathers and solitons. Besides the eigenvalues of S_k are in general unequally spaced and the anharmonic phonons have no boson-like property, contrary to the harmonic case. As a matter of fact because the depth of $W(x)$ is finite in real solids ($W(x \to \infty) - W(x = 0) < \infty$) unlike the harmonic case, the sequence of bound states is finite too, for every k and might even be empty, which would hint towards an anharmonicity driven structural instability.

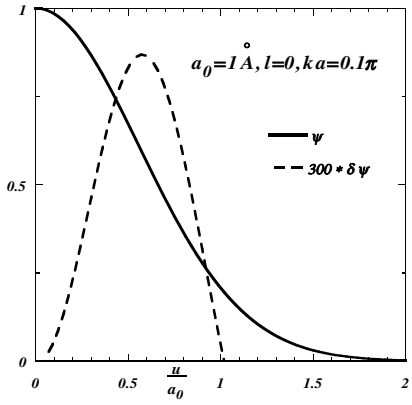

Figure 1. The solid and dashed lines picture $\psi(u)$ and $\delta\psi(u) = \psi(u) - \psi_h(u)$ where ψ, ψ_h refer to the solution of Eq. (8) for given l, k in the anharmonic ($\lambda \neq 0$) and harmonic case ($\lambda = 0$), respectively.

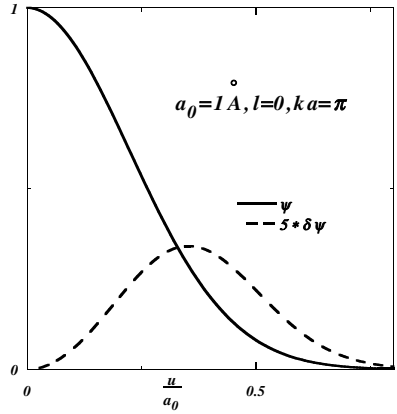

Figure 2. Same as in Fig.1 but for a different k.

3. Results obtained for a FPU chain

The particular FPU pairwise potential chosen here reads

$$W(x) = m\omega_0^2 \left(\frac{x^2}{2} + \lambda \frac{x^4}{4} \right) \quad ,$$

where the parameter λ measures anharmonicity. It is convenient to introduce a_0 such that $\lambda a_0^2 = 2$, which means that the anharmonic $\propto x^4$ and harmonic $\propto x^2$ terms are of equal magnitude for $x = a_0$. It is then seen that the smaller a_0, the larger anharmonicity. Taking advantage of

Eqs. (3,5), it comes for the one-body effective potential $V_e(k,u)$

$$\begin{aligned} V_e &= 2m\omega_0^2 \sin^2(\frac{ka}{2}) \Bigg[u^2 + 2\lambda \sin^4(\frac{ka}{2}) u^4 \\ &+ \lambda \left(\frac{\sin(ka)}{m\omega_0} \right)^2 \left(u^2 p^2 + p u^2 p + p^2 u^2 \right) \Bigg]. \end{aligned} \tag{7}$$

The corresponding Schrödinger equation reads

$$\begin{aligned} \frac{\hbar^2}{m} \Bigg\{ \Bigg[\frac{1}{2} &+ 6\lambda \left(\sin(\frac{ka}{2}) \sin(ka) u \right)^2 \Bigg] \frac{\partial^2 \psi}{\partial u^2} \\ &+ 4\lambda \left(\sin(\frac{ka}{2}) \sin(ka) \right)^2 \left(3u \frac{\partial \psi}{\partial u} + \psi \right) \Bigg\} \\ &= \left\{ 2m\omega_0^2 \sin^2(\frac{ka}{2}) u^2 \left(1 + 2\lambda \sin^4(\frac{ka}{2}) u^2 \right) - \varepsilon \right\} \psi \end{aligned} \tag{8}$$

It can be checked that the harmonic case is retrieved in Eqs. (6), (8) for $\lambda = 0$. A scrutiny of Eq. (8) shows that the effect of anharmonicity is twofold

- similarly to the classical case it adds a term $\propto u^4$ to the harmonic potential $\propto u^2$
- unlike the classical case but in similarity with electron band theory in periodic crystals, it alters the coefficient $\propto \frac{\partial^2 \psi}{\partial u^2}$, which gives rise to a renormalized atomic mass.

Because of $W(-x) = W(x)$, the solutions ψ of Eq. (8) can be assumed to be real and are either even ($\psi(u) = \psi(-u)$) or odd ($\psi(u) = -\psi(-u)$) as for harmonic phonons. It is thence convenient to label each eigenenergy and eigenfunction $\varepsilon(l,k), \psi_{l,k}$ where the integer $l \geq 0$ is a band index, keeping in mind that

$$\varepsilon_h(l,k) = 2\hbar\omega_h(k) \left(l + \frac{1}{2} \right), \qquad \omega_h(k) = 2\omega_0 \sin\left(\frac{ka}{2} \right)$$

for harmonic phonons. Even and odd l values correspond to even and odd eigenfunctions.

In the asymptotic limit $|u| \to \infty$ Eq. (8) entails for a bound eigenstate

$$\psi_{l,k} = u^l e^{-\alpha u^2}, \qquad \alpha = \frac{m\omega_0}{2\hbar\sqrt{6}} \tan\left(\frac{ka}{2} \right)$$

and

$$\psi_{l,k} = u^l e^{-\alpha|u|^3}, \qquad \alpha = \frac{2m\omega_0}{3\hbar}\sqrt{2\lambda}$$

for $ka < \pi$ and $ka = \pi$, respectively. Eq. (8) has been integrated from $u = a_M \gg 1$ down to $u = 0$ by ascribing the relevant asymptotic value to $\frac{\frac{\partial\psi}{\partial u}(a_M)}{\psi(a_M)}$, which yields $\psi(u = 0, \varepsilon)$, $\frac{\partial\psi}{\partial u}(u = 0, \varepsilon)$. The solution ε is then found by requiring $\frac{\partial\psi}{\partial u}(u = 0, \varepsilon) = 0, \psi(u = 0, \varepsilon) = 0$ for even and odd ψ, respectively. The a_M value has been taken large enough so that ε proves independent of a_M and all calculations have been performed with $m = 10^{-26}$Kg, $\omega_0 = 10^{13}$Hz.

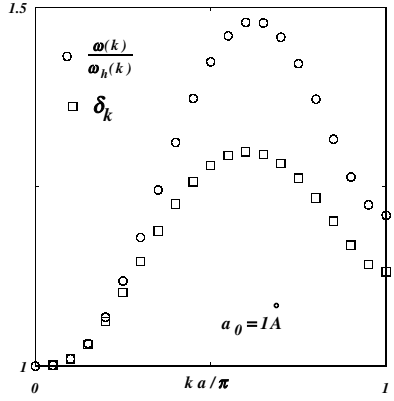

Figure 3. Dispersion data for strongly anharmonic $a_0 = 1$Å phonons.

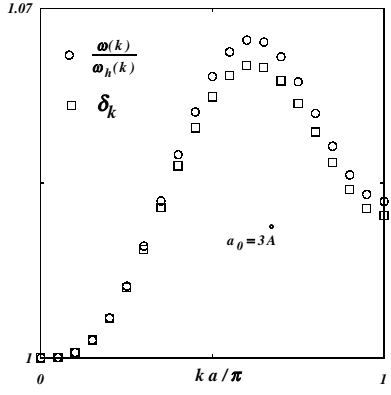

Figure 4. Dispersion data for weakly anharmonic $a_0 = 3$Å phonons.

The eigensolutions $\psi_{l=0,k}$ of Eq. (8), represented in Figs. 1,2 illustrate how little they differ from harmonic eigenfunctions even for subtantial anharmonicity $a_0 = 1$Å. Likewise $\psi_{l,k}(u)$ displays l zeroes. Comparative dispersion data across the Brillouin zone have been depicted for anharmonic and harmonic phonons in Figs. 3,4. The k dependent anharmonic frequency is defined as $\omega(k) = \frac{\varepsilon(l=1,k)-\varepsilon(l=0,k)}{\hbar}$ and the dimensionless parameter $\delta_k = \frac{\varepsilon(l=2,k)-\varepsilon(l=1,k)}{\varepsilon(l=1,k)-\varepsilon(l=0,k)}$. In the harmonic case $\delta_k = 1, \forall k$. It is then realized that the more $\frac{\omega(k)}{\omega_h(k)}, \delta_k$ deviate from unity, the more influential anharmonicity is. This is in accordance with the data in Figs. 3,4 where the difference from unity is indeed larger for smaller a_0. However the deviation is barely noticeable at low k values even for strong anharmonicity, which implies that the sound velocity remains almost unaffected by the anharmonic coupling in contrast with the classical case

[4, 5]. The effect of anharmonicity turns out to be larger in the middle of the Brillouin zone ($ka \simeq 0.6\pi$), which suggests that mass renormalization, vanishing at the zone edge (see Eqs. (6,8)), shows up more efficient than the anharmonic term $\propto u^4$. Accounting for that result within the harmonic theory would require to introduce unreasonably high coupling beyond nearest neighbor atoms.

4. Conclusion

An exact diagonalization procedure has been devised for anharmonic phonons valid for any interatomic coupling. Fitting the measured phonon dispersion should enable one to assess the anharmonic part of the interatomic potential and thereby to compute the partition function of the crystal associated with the atomic motion and additionnally the specific heat, the thermal expansion and the melting temperature. Besides this approach can be extended to study quantum breathers by generalizing the basic assumption in Eq. (3).

Acknowledgments

The author is most indebted to Michel Caffarel, Yuri Gaididei and Vladimir Konotop for invaluable criticisms.

References

[1] J. Szeftel and P. Laurent, Phys.Rev.E, 57, 1134 (1998)
[2] J. Szeftel, P. Laurent and E. Ilisca, Phys.Rev.Lett., 83, 3982 (1999)
[3] J. Szeftel et al., Physica A, 288, 225 (2000)
[4] J. Szeftel et al., Phys. Letters A, 297, 218 (2002)
[5] J. Szeftel and G. Huang, Eur.Phys.J. B, 27, 329 (2002)
[6] J. Szeftel, G. Huang and V. Konotop, Physica D, 181, 215 (2003)
[7] W.Z. Wang et al., Phys.Rev.Lett., 76, 3598 (1996)
[8] W.Z. Wang et al., Phys.Rev.Lett., 80, 3284 (1998)
[9] V.V. Konotop and S. Takeno, Phys.Rev.E, 63, 066606 (2001)
[10] R.S. MacKay, Physica A, 288,174 (2000)
[11] L. Landau and E. Lifchitz, Quantum Mechanics (Mir, Moscow, 1988)

DYNAMICS OF THE PERTURBED ABLOWITZ-LADIK SOLITON BEYOND THE ADIABATIC APPROXIMATION

E.V. Doktorov
B.I. Stepanov Institute of Physics, 220072 Minsk, Belarus

N.P. Matsuka
Institute of Mathematics, 220072 Minsk, Belarus

V.M. Rothos
School of Mathematical Sciences, Queen Mary College, University of London, London E1 4NS, U.K.

Abstract A formalism to account for shape distortion and radiation effects for the perturbed Ablowitz-Ladik soliton is outlined.

1. Introduction

Energy localization phenomena in nonlinear lattices have attracted a great deal of attention [1, 2]. Waves arising as a result of interplay between nonlinearity and lattice discreteness demonstrate a number of novel features as compared with continuous nonlinear systems. Two equations are frequently used to study discrete models - the discrete nonlinear Schrödinger (DNLS) equation and the Ablowitz-Ladik (AL) equation. Being discrete counterparts of the same continuous nonlinear Schrödinger equation, these equations differ drastically in their mathematical properties. The DNLS equation being an adequate model in various applications is nonintegrable [4] and studied numerically, as a rule. Contrary, the AL equation is integrable and admits a complete analytical investigation by means of the inverse spectral method [3]. Moreover, Konotop *et al.* [5] have proved integrability of the inhomogeneous AL system in external field of a particular form.

F. Kh. Abdullaev and V. V. Konotop (eds.), Nonlinear Waves: Classical and Quantum Aspects, 489–495.

It is important that for some region of parameters the DNLS equation can be considered as a perturbed version of the AL equation. In this case, a considerable progress has been achieved in studying the DNLS equation analytically in the framework of the adiabatic approximation of the AL soliton perturbation theory [6, 7, 8, 9, 10]. The adiabatic approximation accounts for a slow perturbation-induced evolution of the soliton parameters, ignoring radiation of small-amplitude dispersive waves and soliton shape distortion. Below we propose a formalism to go beyond the adiabatic approximation. Our approach is based on the Riemann-Hilbert (RH) problem method [11] that has been proved to be efficient for continuous perturbed models [12, 13, 14]. Calculations in the framework of the RH problem do not rely on inconvenient discrete analogs of the Gel'fand-Levitan integral equations, as distinct from the formalism by Konotop *et al.* [8].

2. The matrix Riemann-Hilbert problem and AL soliton solution

The AL equation

$$iu_{nt} + u_{n+1} + u_{n-1} - 2u_n + |u_n|^2(u_{n+1} + u_{n-1}) = 0 \tag{1}$$

for a scalar complex function $u_n(t)$, $-\infty < n < \infty$, admits the Lax representation with the spectral equation [3]

$$\begin{aligned} &J(n+1) = (E + Q_n)J(n)E^{-1}, \\ &Q_n = \begin{pmatrix} 0 & u_n \\ -u_n^* & 0 \end{pmatrix}, \quad E = \begin{pmatrix} z & 0 \\ 0 & z^{-1} \end{pmatrix}, \end{aligned} \tag{2}$$

where z is a spectral parameter. Matrix Jost solutions $J_\pm$ of (1) obey the asymptotics $J_\pm(n) \to I$ as $n \to \pm\infty$ and the conjugation property $J_\pm^\dagger(n, \bar{z}) = v_\pm(n)J_\pm^{-1}(n, z)$. Here $\bar{z} = 1/z^*$, $v_+(n) = \prod_{l=n}^{\infty} \rho_l^{-1}$, $v_-(n) = \prod_{l=-\infty}^{n-1} \rho_l$, $\rho_l = 1 + |u_l|^2$. The scattering matrix

$$S(z) = \begin{pmatrix} a_+ & -b_- \\ b_+ & a_- \end{pmatrix}$$

connects the Jost solutions: $J_-(n) = J_+(n)E^n S(z)E^{-n}$. The spectral problem (1) possesses the $\mathcal{P}$-parity property: if $J(n, z)$ is a solution of the spectral equation, then the function $\mathcal{P}J(n, z) \equiv \sigma_3 J(n, -z)\sigma_3$ is a solution as well. Because $\mathcal{P}S(z) = S(z)$, we have $a_\pm(z) = a_\pm(-z)$, $b_\pm(z) = -b_\pm(-z)$.

It can be shown that the matrix function Ψ_+ (Ψ_-^{-1}) built from columns (rows) of the Jost solutions,

$$\Psi_+(n,z) = \left(J_-^{[1]}, J_+^{[2]}\right)(n,z), \quad \Psi_-^{-1}(n,z) = \begin{pmatrix} (J_-)^{-1}_{[1]} \\ (J_+)^{-1}_{[2]} \end{pmatrix}(n,z),$$

is analytical outside (inside) the unit circle in the z-plane, i.e., in $\mathcal{C}_+$ ($\mathcal{C}_-$) and solves the direct (adjoint) spectral equation. These solutions obey the conjugation relation

$$\Psi_+^{\dagger}(n,z) = B(n)\Psi_-^{-1}(n,\bar{z}), \quad B(n) = \begin{pmatrix} v_-(n) & 0 \\ 0 & v_+(n) \end{pmatrix}.$$

Having matrix functions Ψ_+ and Ψ_-^{-1} analytical in the complementary domains of the z-plane and continuous on the boundary $|z| = 1$, we can formulate the RH problem

$$\Psi_-^{-1}(n,z)\Psi_+(n,z) = E^n G(z) E^{-n}, \quad G = \begin{pmatrix} 1 & b_-/v \\ b_+ & 1 \end{pmatrix}, \quad |z| = 1,$$

as a problem of analytical factorization of the matrix function G defined on the boundary $|z| = 1$ with the normalization condition

$$\Psi_+(n,z) \longrightarrow \begin{pmatrix} 1 & 0 \\ 0 & v_+(n) \end{pmatrix}, \quad z \to \infty. \tag{3}$$

In general, matrices Ψ_+ and Ψ_-^{-1} have zeros in some points z_j and $\bar{z}_j$ in their regions of analyticity, i.e., $\det \Psi_+(z_j) = 0$, $z_j \in \mathcal{C}_+$, and $\det \Psi_-^{-1}(\bar{z}_j) = 0$, $\bar{z}_j \in \mathcal{C}_-$, $j = 1, 2, \ldots, N$. In virtue of the $\mathcal{P}$-parity, zeros appear in pairs $\pm z_j$, $\pm\bar{z}_j$. We will solve the RH problem with zeros by extracting from $\Psi_\pm$ rational factors responsible for zeros. It can be shown [15, 16] that $\Psi_\pm$ is represented as a product $\Psi_\pm = \psi_\pm \Gamma$, where $\psi_\pm$ solve the regular RH problem (i.e., without zeros)

$$\psi_-^{-1}(n,z)\psi_+(n,z) = \Gamma(n,z)E^n G(z) E^{-n}\Gamma^{-1}(n,z), \tag{4}$$

while the rational function $\Gamma(n,z)$ accumulates all zeros of the RH problem and is written as

$$\Gamma(n,z) = I - \sum_{j,k=1}^{2N} \frac{1}{z - \bar{z}_k} |y_j\rangle (D^{-1})_{jk} \langle y_k| B, \quad D_{kj} = \langle y_k| \frac{B}{z_j - \bar{z}_k} |y_j\rangle. \tag{5}$$

Here the vector $|y_j\rangle$ has the form $|y_j\rangle = E^n(z_j) e^{\Omega(z_j)t}|p\rangle$, $|p\rangle = \text{const}$, $\Omega(z_j) = (i/2)(z_j - z_j^{-1})^2 \sigma_3$. Comparing asymptotic expansions for Ψ_+

and Γ, we obtain that the solution of the regular RH problem is given by the leading-order term (3) and the formula to reconstruct a solution of the AL equation has the form

$$u_n(t) = -\frac{\Psi^{(1)}_{+12}}{\Psi^{(0)}_{+22}} = -\frac{\Gamma^{(1)}_{12}}{v_+(n)}. \tag{6}$$

For the soliton solution associated with zeros $\pm z_1$ and $\pm \bar{z}_1$ the vector $|y_j\rangle \equiv |n\rangle$ is written explicitly as

$$|n\rangle = e^{\frac{1}{2}(a+i\varphi)} \begin{pmatrix} e^{\frac{1}{2}(x_n+i\varphi_n)} \\ e^{-\frac{1}{2}(x_n+i\varphi_n)} \end{pmatrix}.$$

Here $z_1 = \exp[(1/2)(\mu + ik)]$, $x_n = \mu n - 2t \sinh\mu \sin k + a$, $\varphi_n = kn + 2t(\cosh\mu\cos k - 1) + \varphi$, a and φ are constants. Substituting this vector into (5) and (6), we obtain soliton of the AL equation:

$$u_n(t) = \exp[ik(n-x) + i\alpha] \frac{\sinh\mu}{\cosh\mu(n-x)}.$$

It depends on four constant parameters μ, k, x_0 and α_0 which determine soliton mass, its group velocity , soliton maximum position and phase.

3. Perturbation-induced evolution of RH data

The perturbed AL equation is written in the form (1) with the r.h.s. ϵr_n, ϵ being a small parameter and r_n is a perturbation. To find corrections to the soliton caused by a perturbation, we first derive the corresponding evolution of the RH data. The perturbation causes a variation δQ_n of the potential which in turn leads to a variation of the analytical solutions:

$$\frac{\delta\Psi_+}{\delta t} = -i\epsilon\Psi_+ E^n \Pi_+ E^{-n}, \quad \frac{\delta\Psi_-^{-1}}{\delta t} = i\epsilon E^n \Pi_- E^{-n}\Psi_-^{-1}. \tag{7}$$

Here the evolution functionals $\Pi_\pm$ are defined by

$$\begin{aligned} \Pi_+(n,z) &= \begin{pmatrix} \Upsilon_{+11}(-\infty, n-1) & -\Upsilon_{+12}(n,\infty) \\ \Upsilon_{+21}(-\infty, n-1) & -\Upsilon_{+22}(n,\infty) \end{pmatrix}, \\ \Pi_-(n,z) &= \begin{pmatrix} \Upsilon_{-11}(-\infty, n-1) & \Upsilon_{-12}(-\infty, n-1) \\ -\Upsilon_{-21}(n,\infty) & -\Upsilon_{-22}(n,\infty) \end{pmatrix} \end{aligned}$$

and we introduce matrix functions

$$\Upsilon_\pm(N_a,N_b) = \sum_{l=N_a}^{N_b} E^{-(l+1)}\Psi_\pm^{-1}(l+1)\hat{R}_l\Psi_\pm(l)E^l, \tag{8}$$

$$\Upsilon_\pm(z) = \Upsilon_\pm(-\infty,\infty), \quad \hat{R}_n = \begin{pmatrix} 0 & r_n \\ r_n^* & 0 \end{pmatrix},$$

which are interrelated by the matrix G entering the RH problem, $\Upsilon_- = G\Upsilon_+G^{-1}$. From (7) we obtain the evolution equation for G in the presence of perturbation:

$$G_t = [\Omega, G] - i\epsilon(G\Pi_+ - \Pi_-G). \tag{9}$$

Perturbation-induced evolution of the discrete RH data is written as

$$z_{1t} = i\epsilon \mathrm{Res}_{z=z_1}\Upsilon_{+11}(z), \quad |p\rangle_t = i\epsilon e^{-\Omega(z_1)t}\begin{pmatrix} \Upsilon_{+11}^{(\mathrm{reg})}(z_1) & 0 \\ \Upsilon_{+21}^{(\mathrm{reg})}(z_1) & 0 \end{pmatrix} e^{\Omega(z_1)t}|p\rangle. \tag{10}$$

Here $\Upsilon^{(\mathrm{reg})}$ is the regular part of the meromorphic function Υ which has simple poles in zeros of the RH problem. Hence, perturbed evolution of the RH data are given by Eqs. (9) and (10). It should be noted that these equations are exact. However, they cannot be directly applied because the matrices $\Pi_\pm$ and $\Upsilon_\pm$ depend on unknown solutions $\Psi_\pm$ of the spectral problem with the perturbed potential. Iterative analysis of these equations w.r.t. ϵ gives consequently the adiabatic and the first-order approximations.

4. The first-order approximation

The adiabatic approximation governed by the discrete data evolution is well known [6]. Below we describe the first-order approximation accounting for the continuous RH data evolution (9). Within this approximation we pose

$$G = I + \epsilon g(z), \qquad \psi_+(n,z) = \psi_+^0(n)(I + \epsilon\phi(n,z)),$$

where ψ_+^0 stands for the solution of the regular RH problem (4) in the adiabatic approximation, whereas the off-diagonal matrices $g(z)$ and $\phi(z)$ describe first-order corrections. Therefore, the reconstruction formula (6) takes now the form

$$u_n = -\Gamma_{12}^{(1)}(n)\Gamma_{22}(n,0) - \epsilon\phi_{12}^{(1)}(n)\Gamma_{22}(n,0).$$

The first term in the r.h.s. represents the soliton solution in the adiabatic approximation and the second one is responsible for radiation (soliton

shape distortion). The matrix $\phi^{(1)}$ is given by the integral

$$\phi^{(1)}(n) = -\frac{1}{2\pi i}\oint_{|z|=1} \mathrm{d}z(\Gamma E^n g E^{-n}\Gamma^{-1})(z)$$

which is simplified considerably at $n \to \infty$,

$$\phi_{12}^{(1)}(n) = -\frac{1}{2\pi i}\oint_{|z|=1} \mathrm{d}z \frac{z^2 - z_1^2}{z^2 - \bar{z}_1^2} z^{2n} g_{12}.$$

Finally, g_{12} entering this integral is obtained from the equation

$$\tilde{g}_{12t} = i \exp\left[-i(z - z^{-1})^2 t\right] \Upsilon_{+12}, \quad \tilde{g} = e^{-\Omega t} g e^{\Omega t}.$$

It is important that because Υ_{+12} corresponds to the first order correction, we can replace in the definition (8) of Υ_+ unknown solution ψ_+ of the regular RH problem (4) by ψ_+^0 known from the adiabatic approximation. Examples of specific perturbations and numerical simulations are considered in our recent paper [17].

Acknowledgments

E.D. and V.R. thank the organizers of the workshop "Nonlinear Waves: Classical and Quantum Aspects" for kind invitation and warm hospitality. This work was partly supported by the Belarussian Foundation for Fundamental Research, Grant No. Φ01-052 and UK-EPSRC, Grant No. GR/S47335/01.

References

[1] Kevrekidis, P.G., Rasmussen, K.Ø., and Bishop, A.R. (2001) The discrete nonlinear Schrödinger equation: A survey of recent results, *Int. J. Mod. Phys. B* **15**, 2833-2900.

[2] Eilbeck, J.C., and Johansson, M. (2002) The discrete nonlinear Schrödinger equation - 20 years on, arXiv:nlin.PS/0211049.

[3] Ablowitz, M.J., and Ladik, J.F. (1976) A nonlinear difference scheme and inverse scattering, *Stud. Appl. Math.*, **55**, 213-229.

[4] Herbst, B.M., and Ablowitz, M.J. (1989) Numerically induced chaos in the nonlinear Schrödinger equation, *Phys. Rev. Lett.*, **62**, 2065-2068.

[5] Konotop, V.V., Chubykalo, O.A., and Vázquez, L. (1993) Dynamics and interaction of solitons on an integrable inhomogeneous lattice, *Phys. Rev. E*, **48**, 563-568.

[6] Vakhnenko, A.A., and Gaididei, Yu.B. (1986) On the motion of solitons in discrete molecular chain, *Theor. Math. Phys.*, **68**, 873-880.

[7] Kivshar, Yu.S., and Campbell, D.K. (1993) Peierls-Nabarro potential barrier for highly localized nonlinear modes, *Phys. Rev. E*, **48**, 3077-3081.

[8] Konotop, V.V., Cai, D., Salerno, M., Bishop, A.R., and Grønbech-Jensen, N. (1993) Interaction of a soliton with point impurities in an inhomogeneous, discrete nonlinear Schrödinger system, *Phys. Rev. E*, **53**, 6476-6485.

[9] Garnier, J. (2001) Propagation of solitons in a randomly perturbed Ablowitz-Ladik chain, *Phys. Rev. E*, **63**, 026608.

[10] Abdullaev, F.Kh, Abdumalikov, A.A., and Umarov, B.A. (2002) Autosoliton in Ablowitz-Ladik chain with linear damping and nonlinear amplification, *Phys. Lett. A*, **305**, 371-376.

[11] Novikov, S.P., Manakov, S.V., Pitaevski, L.P., and Zakharov, V.E. (1984) *Theory of Solitons, the Inverse Scattering Method*, Consultant Bureau, New York.

[12] Kivshar, Yu.S. (1989) Perturbation theory based on the Riemann problem for the Landau-Lifshitz equation, *Physica D*, **40**, 11-32.

[13] Shchesnovich, V.S., and Doktorov, E.V. (1997) Perturbation theory for solitons of the Manakov system, *Phys. Rev. E*, **55**, 7626-7635.

[14] Shchesnovich, V.S., and Doktorov, E.V. (1999) Perturbation theory for the modified nonlinear Schrödinger solitons, *Physica D*, **129**, 115-129.

[15] Kawata, T. (1984) Riemann spectral method for the nonlinear evolution equation, in *Advances in Nonlinear Waves*, edited by L. Debnath, Vol. 1, Pitman Publishing Ltd, London.

[16] Doktorov, E.V., and Rothos, V.M. (2003) Homoclinic orbits for soliton equations solvable via the quadratic bundle, *Phys. Lett. A*, **314**, 59-67.

[17] Doktorov, E.V., Matsuka N.P., and Rothos, V.M. (2004) Perturbation-induced radiation by Ablowitz-Ladik soliton, *Phys. Rev. E*, to be published.

TRAVELLING WAVES IN A PERTURBED DISCRETE SINE-GORDON EQUATION

Vassilis M Rothos
School of Mathematical Sciences Queen Mary Collage, University of London, Mile End London E1 4NS, UK
v.m.rothos@qmul.ac.uk

Michal Feckan
Department of Mathematical Analysis Comenius University, Mlynská dolina, 842 48 Bratislava and Mathematical Institute, Slovak Academy of Sciences, Stefánikova 49, 814 73 Bratislava, Slovakia
Michal.Feckan@fmph.uniba.sk

Abstract The existence of traveling waves is studied analytical for discrete sine-Gordon equation with an inter-site potential. The reduced functional differential equation is formulated as an infinite dimensional differential equation which is reduced by a centre manifold method and to a 4-dimensional singular ODE with certain symmetries and with heteroclinic structure. The bifurcations of solutions from heteroclinic ones are investigated for singular perturbed systems.

Keywords: lattice sine-Gordon, center manifold reduction, normal form theory, bifurcations

1. Introduction

In recent years there has been a flurry of mathematical research arising from condensed matter physics and physical chemistry, namely the study of localised modes in anharmonic molecules and molecular crystals. Using classical approximations, these are described by nonlinear lattice equations. Most nonlinear lattice systems are not integrable even if the PDE model in the continuum limit is; (see [1, 2] and references therein). Prototype models for such nonlinear lattices take the form of various discrete NLS equations or systems, a particularly important class

F. Kh. Abdullaev and V. V. Konotop (eds.), Nonlinear Waves: Classical and Quantum Aspects, 497–501.

of solutions of which are so called *discrete breathers* which are homoclinic in space and oscillatory in time. Other questions involve the existence and propagation of topological defects or *kinks* which mathematically are heteroclinic connections between a ground and an excited steady state. Prototype models here are discrete version of sine-Gordon equations, also known as known as Frenkel-Kontorova (FK) models [3]. There are many outstanding issues for such systems relating to the global existence and dynamics of localised modes for general nonlinearities, away from either continuum or anti-continuum limits [4]. The *kinks* solutions have applications to problems such as dislocation and mass transport in solids, charge-density waves, commensurable-incommensurable phase transitions, Josephson transmission lines etc.

In this paper, we consider a perturbed Hamiltonian chain of coupled oscillators with an Hamiltonian

$$\mathcal{H} = \sum_{n\in\mathbb{Z}} \Big(\frac{1}{2}\dot{u}_n^2 + \frac{1}{2\varepsilon^2}(u_{n+1}-u_n)^2 + H(u_n) + \mu G(u_{n+1}-u_n)\Big) \qquad (1)$$

where $\varepsilon > 0$, μ are small parameters and $h(x) = H'(x)$ and $g(x) = G'(x)$. $H, G \in C^2(\mathbb{R})$. For $H(x) = G(x) = 1 - \cos x$ we obtain the discrete sine-Gordon equation with inter-site potential as perturbation. The Hamiltonian $\mathcal{H}$ gives the nonlinear lattice eqn:

$$\ddot{u}_n - \frac{1}{\varepsilon^2}(u_{n+1}-2u_n+u_{n-1}) + h(u_n) + \mu\Big\{ g(u_n-u_{n-1}) - g(u_{n+1}-u_n)\Big\} = 0 \qquad (2)$$

We suppose for (2) the following conditions

(A1) $h, g \in C^1(\mathbb{R})$ are odd, h is 2π-periodic, $h(x-\pi) = -h(x)$ and g is globally Lipschitz on $\mathbb{R}$.

(A2) $h(0) = h(2\pi) = 0$, $h'(0) = h'(2\pi) = a^2 > 0$ and there is a heteroclinic solution Φ of

$$\ddot{x} - h(x) = 0 : \quad \Phi(t) = 2\pi - \Phi(-t), \quad \Phi(t) \to 2\pi \quad \text{as} t \to +\infty.$$

The continuum limit of eq. (2) for $\mu = 0$

$$u_{tt} - u_{xx} + h(u) = 0$$

admits travelling wave solutions

$$u(x,t) = \Phi\Big(\frac{x-\nu t}{\sqrt{1-\nu^2}}\Big), \quad 0 < \nu < 1\,.$$

We consider for eqn (2) travelling wave solutions of stationary profile in a moving reference with constant velocity ν/ε. One can write

$$u_n(t) = V\Big(n - \frac{\nu}{\varepsilon}t\Big) \equiv V(z), \quad z = n - \frac{\nu}{\varepsilon}t, \quad 0 < \nu < 1\,.$$

Eqn (2) is reduced to the following functional differential equation:

$$\begin{aligned} \nu^2 V''(z) \;&-\; V(z+1) + 2V(z) - V(z-1) + \varepsilon^2 h(V(z)) \\ &+\; \varepsilon^2\mu\Big(g(V(z) - V(z-1)) - g(V(z+1) - V(z))\Big) = 0 \end{aligned} \tag{3}$$

where $'$ represents differentiation with respect to z. In this paper, we review the analytical results about the existence of solutions of eqn (3) near Φ and the relationship between traveling wave solutions of (2) and continuum sine-Gordon for $\varepsilon > 0$, μ small.

2. Periodic travelling waves-bifurcation analysis

We apply center manifold theory to the study of existence of travelling wave solution of eqn (1.8) with small amplitude oscillations on infinite nonlinear lattice.

We introduce a new variable $v \in [-1, 1]$ and functions $X(t, v) = x(t + v)$. The notation $U(t)(v) = \big(x(t), \xi(t), X(t, v)\big)$ indicates our intention to construct V as a map from $\mathbb{R}$ into some function space living on the v-interval $[-1, 1]$. We introduce the Banach spaces $\mathbb{H}$ and $\mathbb{D}$ for $U(v) = \big(x, \xi, X(v)\big)$

$$\mathbb{H} = \mathbb{R}^2 \times C[-1, 1], \quad \mathbb{D} = \Big\{U \in \mathbb{R}^2 \times C^1[-1, 1] \mid X(0) = x\Big\}$$

with the usual maximum norms. Then $L \in \mathcal{L}(\mathbb{D}, \mathbb{H})$ and $M \in C^1(\mathbb{D}, \mathbb{D})$. Eqn (3) can be written as follows [5]

$$U_t = LU + \frac{\varepsilon^2}{\nu^2}M(U) \tag{4}$$

where

$$L = \begin{pmatrix} 0 & 1 & 0 \\ -\frac{2}{\nu^2} & 0 & \frac{1}{\nu^2}\delta^1 + \frac{1}{\nu^2}\delta^{-1} \\ 0 & 0 & \partial_v \end{pmatrix}, \quad \delta^{\pm 1}X(v) = X(\pm 1)$$

$$M(U) = \Big(0, h(x) - \mu\Big\{g(x - \delta^{-1}X(v)) - g(\delta^1 X(v) - x)\Big\}, 0\Big)$$

The spectrum $\sigma(L)$ is given by the resolvent equation $(\lambda I - L)U = F$, $F \in \mathbb{H}, \lambda \in \mathbb{C}\,, U \in \mathbb{D}$. The resolvent equation is solvable if and only if

$N(\lambda) := \lambda^2 + \frac{2}{\nu^2}(1-\cosh\lambda) = 0$. Clearly, $\sigma(L)$ is invariant under $\lambda \to \bar{\lambda}$ and $\lambda \to -\lambda$. The central part $\sigma_0(L) = \sigma(L) \cap \mathrm{i}\,\mathbb{R}$ is determined by the equation $q^2 + \frac{2}{\nu^2}(\cos q - 1) = 0, q \in \mathbb{R}$. We assume that $\nu_1 < \nu < 1$ where $\nu = \nu_1$ is the first value from the left of 1 for which the equations

$$\lambda^2 + \frac{2}{\nu^2}(\cos\lambda - 1) = 0, \quad \lambda - \frac{1}{\nu^2}\sin\lambda = 0$$

have a common nonzero solution $\lambda \neq 0$. Then equation $N(\mathrm{i}\,q) = 0$ has the double root 0 and simple roots $\pm q$. Hence we have $\sigma_0(L) = \{0, \pm\,\mathrm{i}\,q\}$.

The linear operator on the 4th-dimensional central subspace $\mathbb{H}_c$ has the form $L_c = L/\mathbb{H}_c$ in the basis $(\xi_1, \xi_2, \xi_3, \xi_4)$ which satisfies $L\xi_1 = 0$, $L\xi_2 = \xi_1$, $L\xi_3 = -q\xi_4$, $L\xi_4 = q\xi_3$. The projection $P_c\,\mathbb{H} \to \mathbb{H}_c$ is given by $P_c(U) = P_1(U)\xi_1 + P_2(U)\xi_2 + P_3(U)\xi_3 + P_4(U)\xi_4$ [7].Condition (A1) implies that M is globally Lipschitz. We can apply the procedure of a center manifold method to get for ε, μ small the reduced equation of (4) over $\mathbb{H}_c$ given by

$$\dot{u}_c = L_c u_c + \frac{\varepsilon^2}{\nu^2} P_c(M(u_c)) + O(\varepsilon^4), \tag{5}$$

where $u_c = u_1\xi_1 + u_2\xi_2 + u_3\xi_3 + u_4\xi_4$. Introducing the appropriate scaling, we consider the singularly perturbed system of the form:

$$\ddot{x} + h(x) = f_1(x, \dot{x}, y, \varepsilon\dot{y}, \varepsilon) \quad \varepsilon^2\ddot{y} + y = \varepsilon^2 g_1(x, \dot{x}, y, \varepsilon\dot{y}, \varepsilon) \tag{6}$$

Theorem 1 (Feckan & Rothos, 2003) *For any $k_0 \in \mathbb{N}$ there is an $\varepsilon_0 > 0$ such that for any $0 < \varepsilon < \varepsilon_0$, $|\mu| \leq \varepsilon_0\varepsilon^{1/4}$ and $T = \varepsilon\big(k[\varepsilon^{-3/2}]\pi + \tau\big)$ with $k \in \mathbb{N}$, $k \leq k_0$, $\tau \in [\pi/3, \pi/6]$, system (6) has a $4T$-periodic solution $(x_{T,\varepsilon,1}(t), y_{T,\varepsilon,1}(t))$ near $(\phi(t), 0)$, $-T \leq t \leq T$ and has a solution $(x_{T,\varepsilon,2}(t), y_{T,\varepsilon,2}(t))$ on $\mathbb{R}$ near $(\phi(t), 0)$, $-T \leq t \leq T$, such that $x_{T,\varepsilon,\mathrm{i}}$, $y_{T,\varepsilon,\mathrm{i}}$ are odd functions and*

$$x_{T,\varepsilon,\mathrm{i}}(t + 2T) = (-1)^{\mathrm{i}}\, x_{T,\varepsilon,1}(t) + 2\pi(\mathrm{i} - 1),$$

$$y_{T,\varepsilon,\mathrm{i}}(t + 2T) = (-1)^{\mathrm{i}}\, y_{T,\varepsilon,1}(t), \quad \mathrm{i} = 1, 2$$

Theorem 2 (Feckan & Rothos, 2003) *If h, g satisfy the assumptions $(A1 - A2)$ then traveling wave solution $u(x,t) = \Phi\Big(\frac{x-\nu t}{\sqrt{1-\nu^2}}\Big)$ for $0 < \nu_1 < \nu < 1$ of sine-Gordon can be approximated by the both rotational and librational travelling wave solutions of (2) with very large periods and with the velocity ν for $\mu = o(\varepsilon^{1/4})$ small.*

The central part of the spectrum $\sigma(L)$ is $\{0, \pm iq\}$, where 0 has multiplicity two. We can perform a polynomial change of coordinates close to

identity, analytically depending on the parameter $\tilde{\mu}$, $u_c = Y + \Phi(Y, \tilde{\mu})$ such that the reduced system (5) is equivalent in a neighborhood of the origin to

$$\frac{dY}{dt} = N(Y, \tilde{\mu}) + R(Y, \tilde{\mu}) \tag{7}$$

where N is the normal form of order 2 and R represents the new terms of order greater or equal to 3, $Y = (y_1, y_2, y_3, y_4)$ and the system (7) has the following symmetry properties:

$$SN(Y, \tilde{\mu}) = -N(SY, \tilde{\mu}), SR(Y, \tilde{\mu}) = -R(SY, \tilde{\mu})$$

with $S(y_1, y_2, y_3, y_4) = (y_1, -y_2, y_3, -y_4)$.

For studying the dynamics of the initial system near the origin, we perform a polynomial change of coordinates for which the "linear and quadratic" part N is as simple as possible. Next, we analyze the truncated system

$$\frac{dY}{dt} = N(Y, \tilde{\mu}),$$

its heteroclinic orbits close to the origin. We focus on the problem of the persistence for the full system of the heteroclinic connections obtained for the truncated system and emphasize the case of solutions tending to exponentially small oscillations at infinity, (see [6]).

Acknowledgments

VR was partly supported by EPSRC-UK Grant No. GR/R02702/01 and LMS. MF was partly supported by Grant GA-SAV 2/1140/21.

References

[1] S. Flach and C. R. Willis *Discrete breathers*, Phys. Rep. **295**, pp.181-264 (1998)

[2] S. Aubry and R. S. MacKay *Proof of existence of breathers for time-reversible or Hamiltonian networks of weakly coupled oscillators*, Nonlinearity **6**, pp. 1623-1643 (1994).

[3] A. A. Aigner, A. R. Champneys, and V. M. Rothos, *A new barrier to the existence of moving kinks in Frenkel-Kontorova lattices*. Physica D **186**, 148-173 (2003).

[4] G. Iooss and K. Kirchgässner *Traveling waves in a chain of coupled nonlinear oscillators*, Comm. Math. Phys. **211**(2), pp. 439-464 (2000).

[5] M. Feckan and V. M. Rothos *Bifurcations of periodics from homoclinics in singular o.d.e.: Applications to discretizations of traveling waves of p.d.e.*, Comm. Pure Appl. Anal. **1**, pp. 475-483 (2002).

[6] V. M. Rothos and M. Feckan, *Global Normal Form for Travelling Waves in Nonlinear Lattices* (2003) (preprint).

[7] M. Feckan and V. M. Rothos *Travelling Waves for Perturbed Spatial Discretizations of Partial Differential Equations* (2003) (preprint).

DYNAMICS OF MULTICOMPONENT SOLITONS IN PERTURBED LADDER LATTICES

Oleksiy O. Vakhnenko
Bogolyubov Institute for Theoretical Physics, Kyïv UA-03143, Ukraine
vakhnenko@bitp.kiev.ua

Abstract We investigate the interplay between the longitudinal and lateral solitonic modes in perturbed ladder lattices in regard to the transmission of soliton wave packet. (1) In a longitudinal uniform field the lateral and longitudinal solitonic modes are shown to be independent. However, unlike in the unperturbed case the dynamics of soliton center of mass becomes confined within a finite spatial domain via the Bloch mechanism in the longitudinal direction and due to the transverse finiteness of the ladder in the lateral one. (2) We study the impact of the modified transverse bond on the longitudinal soliton dynamics and reveal that this imperfection might act on the soliton either as an attractive or a repulsive potential, depending on the sign of the transverse energy of the ingoing soliton. (3) The segment of zigzag-distributed on-site impurities cause the soliton mode-mode mixing. As a result the soliton exhibits rather complex two-dimensional dynamics accompanied by wave radiation which may give rise to soliton trapping. Nevertheless, under some specific conditions the soliton is able to bypass even the strong impurities slaloming between them.

Keywords: Ladder lattice, soliton, Bloch oscillations, attractive-repulsive alternative, slalom

1. Introduction

The concept of soliton excitations is known to have been arisen originally from the theory of integrable nonlinear evolution systems in one spatial dimension [1, 2]. Moreover, all subsequent history of soliton science has shown that apart from rare exceptions [3, 4] the newly invented integrable nonlinear models turn out to be spatially one-dimensional in true physical (not mathematical) sense of the word. While being admissible on the macrolevel (e.g. to the light pulse propagation in optical

F. Kh. Abdullaev and V. V. Konotop (eds.), Nonlinear Waves: Classical and Quantum Aspects, 503–510.

fibers [5] or to the electric pulse propagation in nonlinear transmission lines [6]) the spatially one-dimensional models can hardly be applied on the microlevel (e.g. to the energy and charge propagation in isolated one-chain samples of long biological molecules [7] or long synthesized molecules [8]) on account of the thermodynamically caused instability of natural one-dimensional structures [9]. On the contrary in the quasi-one-dimensional lattice systems (e.g. in the carbon nanotubes [10] or in the other long molecules consisting of several mutually coupled chains) the effects of structural instability are suppressed and the theoretical description of their nonlinear properties looks more realistic. In addition this type of structures in itself might provide a substantially more rich dynamics of nonlinear excitations [11, 12] as compared with the purely one-dimensional systems to say nothing of pretty interesting or even unexpected ballistic effects stemming from the external fields or specific lattice imperfections unfeasible for the one-chain geometry [13, 14].

2. General model of perturbed ladder lattices

In this communication we summarize the results obtained for the dynamics of multicomponent solitons in perturbed ladder-lattices on an example of generalized Hamiltonian [13, 14]

$$H = \sum_{\alpha=1}^{M}\sum_{\beta=1}^{M}\sum_{n=-\infty}^{\infty}\sum_{m=-\infty}^{\infty} R_\alpha(n)\left[U_{\alpha\beta}(n|\tau|m) - t_{\alpha\beta}\right] Q_\beta(m) \qquad (1)$$
$$- \sum_{\alpha=1}^{M}\sum_{n=-\infty}^{\infty} E(n+1)E(n)\left[R_\alpha(n+1)Q_\alpha(n) + Q_\alpha(n+1)R_\alpha(n)\right],$$

where $E(n) = \sqrt{[\exp(\rho(n)) - 1]/\rho(n)}$ and $\rho(n) = \sum_{\beta=1}^{M} R_\beta(n)Q_\beta(n)$. For the sake of definiteness we associate $Q_\alpha(n)$ and $R_\alpha(n)$ with the probability amplitudes for the lattice site with the longitudinal n and transverse α coordinates to be excited ($R_\alpha(n) \equiv Q^*_\alpha(n)$). Then the term with the matrix $t_{\alpha\beta} \equiv t^*_{\beta\alpha}$ corresponds to the resonant coupling between all M chains of ladder lattice structure, while the term with $E(n+1)E(n)$ describes both the resonant coupling between the sites in longitudinal direction and the nonlinear couplings between the sites in longitudinal and transverse directions. The potential matrix $U_{\alpha\beta}(n|\tau|m) \equiv U^*_{\beta\alpha}(m|\tau|n)$ serves to specify either the external fields or lattice imperfections and besides from the site coordinates may also be dependent on the time τ. It is worth noticing that the amplitudes $Q_\alpha(n)$ and $R_\alpha(n)$ are chosen to be conjugated canonically in order that their evolution being governed

by the dynamical equations in standard Hamiltonian form

$$+idQ_\alpha(n)/d\tau = \partial H/\partial R_\alpha(n), \qquad -idR_\alpha(n)/d\tau = \partial H/\partial Q_\alpha(n). \quad (2)$$

At $t_{\alpha\beta} \equiv 0$ and $U_{\alpha\beta}(n|\tau|m) \equiv 0$ these equations are proven to be one of possible discretizations of famous Manakov system [15] generalized to the case of $2M$ field variables. In contrast to the other known discretizations [16–18, 11] the problem of their integrability remains to be open although the question about the one-soliton solutions has been resolved affirmatively even at $t_{\alpha\beta} \neq 0$. Here we would like to stress that at $t_{\alpha\beta} \neq 0$ and $U_{\alpha\beta}(n|\tau|m) = 0$ and nonzero area of structure cross-section the model (1), (2) is able to describe also the exact one-soliton solutions in the presence of uniform magnetic field directed along the chains [11] and treated within the framework of Peierls substitution [19], supposing of course the excitations to be electrically charged.

3. Three- and two-dimensional solitonic oscillations in uniform longitudinal field

The simplest type of perturbation corresponds to the spatially linear potential [14] when

$$U_{\alpha\beta}(n|\tau|m) = -\delta_{\alpha\beta}\delta_{nm} m\mathscr{E}(\tau). \quad (3)$$

The multicomponent one-soliton solution has the form

$$Q_\alpha(n) = b_\alpha \sqrt{\ln[1 + \sinh^2\mu \ \mathrm{sech}^{\,2}\mu(n-x)]}\ \exp(ikn + i\theta) \quad (4)$$

with $\sum_{\alpha=1}^{M} b_\alpha^* b_\alpha \equiv 1, \quad \alpha = 1, 2, \ldots, M$. Here μ and θ evolve according to the equations $d\mu/d\tau = 0$ and $d\theta/d\tau = 2\cosh\mu\,\cos k$, while the other solitonic parameters form the $M+1$ pairs x, k and b_α, b_α^* of canonically conjugated variables and evolve according to the Hamiltonian equations

$$\frac{dx}{d\tau} = \frac{\partial \mathscr{H}}{\partial k}, \qquad \frac{dk}{d\tau} = -\frac{\partial \mathscr{H}}{\partial x} \quad (5)$$

$$+i\frac{db_\alpha}{d\tau} = \frac{\partial \mathscr{H}}{\partial b_\alpha^*}, \qquad -i\frac{db_\alpha^*}{d\tau} = \frac{\partial \mathscr{H}}{\partial b_\alpha} \quad (6)$$

with the effective Hamiltonian given by

$$\mathscr{H} = -\frac{2}{\mu}\sinh\mu\cos k - x\mathscr{E}(\tau) - \sum_{\alpha=1}^{M}\sum_{\beta=1}^{M} b_\alpha^* t_{\alpha\beta} b_\beta. \quad (7)$$

The collective variables x, k and b_α, b_α^* are responsible respectively for the longitudinal and lateral dynamics of the soliton as a whole. These

two sorts of dynamics are seen to be completely separated. Moreover, the parameter x turns out to coincide with the mean longitudinal coordinate of nonlinear wave packet

$$X = \frac{\sum_{n=-\infty}^{\infty} n\rho(n)}{\sum_{n=-\infty}^{\infty} \rho(n)}$$

calculated on the one-solitonic ansatz (4) and at constant external field $\mathscr{E}(\tau) \equiv \mathscr{E}$ it is bound to be confined within the finite interval of width $(4/\mu\mathscr{E})\sinh\mu$. This effect known as Bloch dynamical localization [20–22] is emanated from the interplay between the finiteness of longitudinal kinetic energy band (the consequence of structure discreteness) and the monotonic dependence of longitudinal potential energy on coordinate x so that the total longitudinal energy to be conserved. The direct integration of dynamical equations confirms this statement and we readily come to the Bloch oscillations with the amplitude $A_{\|} = (2/\mu\mathscr{E})\sinh\mu$ and the cyclic frequency $\omega_{\|} = \mathscr{E}$. As to the lateral dynamics it can be visualized introducing the coordinates for the center of nonlinear wave packet in structure cross-section. Thus, for the two-leg lattice structure ($M = 2$; $t_{\alpha\beta} = (1 - \delta_{\alpha\beta})t$; $\alpha = 1, 2$; $\beta = 1, 2$) the only transverse coordinate

$$Y = \frac{\sum_{\alpha=1}^{2}\sum_{n=-\infty}^{\infty}(-1)^{\alpha}R_{\alpha}(n)Q_{\alpha}(n)}{\sum_{\alpha=1}^{2}\sum_{n=-\infty}^{\infty}R_{\alpha}(n)Q_{\alpha}(n)}$$

is sufficient and the original dynamical equations (2), (1), (3) yield that for harmonic oscillator $d^2Y/d\tau^2 + (2t)^2Y = 0$. The frequency of lateral oscillations is given by $\omega_{\perp} = 2t$, while their amplitude

$$A_{\perp} = \sqrt{\cos^2 2\varphi + \sin^2(\delta_1 - \delta_2)\sin^2 2\varphi}$$

is determined by the initial conditions $b_1(0) = \exp(i\delta_1)\cos\varphi$ and $b_2(0) = \exp(i\delta_2)\sin\varphi$ and never exceeds the half-distance between the chains. At incommensurate frequencies $\omega_{\|}$ and $\omega_{\perp}$ the solitonic centre of mass exhibits unclosed trajectory confined in both spatial directions, although when the frequencies $\omega_{\|}$ and $\omega_{\perp}$ are commensurate the trajectory is reduced to some closed Lissajou one.

The most representative perturbation feasible for the multileg ladder lattices is the local modification of transverse bonds [14]

$$U_{\alpha\beta}(n|\tau|m) = -\delta_{0n}\delta_{m0}h_{\alpha\beta}. \tag{8}$$

Here the parameters $h_{\alpha\beta}$ describe the changes of lateral coupling parameters $t_{\alpha\beta}$ within the zeroth unit cell. In what follows we consider only

the case of proportional modification $h_{\alpha\beta} = wt_{\alpha\beta}$ bearing in mind that it is always justified at least for the two-leg ladder lattice. We will see that such kind of modification might act on the longitudinal soliton dynamics in two absolutely different ways: either as a repulsive or as an attractive potential depending exclusively on the energy of transverse solitonic modes far away from the defect where the longitudinal and transverse solitonic modes prove to be practically uncoupled. The main features of this effect can be understood already within the framework of trial Lagrangian formalism [14]. The standard manipulations with the system Lagrangian and one-solitonic ansatz (4) gives rise to the dynamical equations (5)–(6) for the collective variables x, k and b_α, b^*_α however this time with the effective Hamiltonian [14]

$$\begin{aligned}\mathscr{H} = \; & - \; \frac{2}{\mu}\sinh\mu\cos k \\ & - \; \left[1+\frac{w}{2\mu}\ln\left(1+\sinh^2\mu\,\mathrm{sech}^{\,2}\mu x\right)\right]\sum_{\alpha=1}^{M}\sum_{\beta=1}^{M} b^*_\alpha t_{\alpha\beta} b_\beta, \qquad (9)\end{aligned}$$

where the parameter μ is supposed to be constant. The quantity

$$\eta \equiv \sum_{\alpha=1}^{M}\sum_{\beta=1}^{M} b^*_\alpha t_{\alpha\beta} b_\beta$$

when being conserved happens to be of key importance in the whole problem under study. Its conservation is ensured provided the transverse coupling parameters $t_{\alpha\beta}$ are time independent. Under this assumption the effective equations (5), (9) for the longitudinal dynamics become selfconsistent and the quantity η can be treated as some effective charge of the soliton. Remarkable that through the effective charge η we are capable to regulate the character of the interaction between the soliton and modified transverse bonds from attractive to repulsive and vice versa even at fixed modifying factor w by merely variating the initial parameters of the transverse soliton pattern. We believe this effect might play a crucial role in the phenomena of soliton separation and reflection with respect to the effective transverse energy of the ingoing soliton $-\eta$ since up to the sign it coincides with the effective charge η. Our qualitative theory is certainly valid provided the imperfection-induced effects of wave radiation by soliton and soliton-induced effects of impurity-state excitation are negligible. The qualitative results concerned to the effect of attractive-repulsive alternative in soliton interaction with the modified transverse bonds have been confirmed by the direct numerical simulations of the exact dynamical equations (2), (1), (8) on an example of two-leg ladder lattice [14].

4. Slalom soliton dynamics between zigzag-distributed impurities

In regular two-leg ladder lattice without external fields the trajectory of the soliton as a whole according to the equations $d^2X/d\tau^2 = 0$ and $d^2Y/d\tau^2 + (2t)^2Y = 0$ must be sinusoidal. This simple fact, that the soliton dynamics is essentially two-dimensional, gives rise to the possibility for the soliton to bypass even the strong on-site impurities (the effect which in one-chain lattices is geometrically forbidden). Of course to observe the bypassing effect the impurity locations have to be specially arranged and the soliton initial conditions should be appropriately synchronized. We have verified this hypothesis by the direct computer experiment taking the impurity potential matrix in the form [13, 14]

$$U_{\alpha\beta}(n|\tau|m) = \delta_{\alpha\beta}\delta_{nm}V\sum_{s=0}^{Z-1}\Delta(m - n_i - (\beta-1)l - Mls), \qquad (10)$$

which for the two-leg ladder lattice ($M = 2$; $t_{\alpha\beta} = (1 - \delta_{\alpha\beta})t$; $\alpha = 1, 2$; $\beta = 1, 2$) models the set of $2Z$ on-site impurities arranged in an ideal zigzag-like fashion. Here the constant V characterizes the strength of impurity, n_i marks the longitudinal position of first impurity on first ($\alpha = 1$) chain, $2l$ measures the distance between the neighbouring impurities along the same chain and $\Delta(m - n) \equiv \delta_{mn}$. From the purely geometrical arguments the disturbance of sinusoidal trajectory of ingoing soliton by the segment of zigzag-arranged impurities is expected to be minimal when (i) the spatial period of trajectory $T_\perp v_\parallel$ will be commensurate with the pitch of impurity distribution $2l$ via the relation $(2j + 1)T_\perp v_\parallel = 2l$ ($j = 0, 1, 2, \ldots$), (ii) the amplitude of ingoing soliton will be maximal (i.e. equal to the half distance between the chains), (iii) the trajectory of ingoing soliton will be synchronized to pass through the lattice site $n = n_i$, $\alpha = 2$ just across from the first impurity site $n = n_i$, $\alpha = 1$ and (iv) the soliton longitudinal size d will be narrow as compared with the spatial half period of trajectory $T_\perp v_\parallel/2$. Here $T_\perp = \pi/t$ and $v_\parallel$ are respectively the period of lateral oscillations and the longitudinal velocity of ingoing soliton. The results of numerical simulations are as follows [13, 14]. The above-referred slaloming conditions (i)–(iv) when fulfilled even within few percent windows ensure almost the full transmission of ingoing soliton wave packet through the short ($2Z = 4$) segment of very strong impurities irrespective of their type attractive $V < 0$ or repulsive $V > 0$. However, the substantial break of bypassing conditions (i) and/or (iii) almost inevitably leads to the soliton trapping among impurities accompanied by some low amplitude wave radiation. On the other hand the ingoing soliton with the small

amplitude of sinusoidal trajectory (break of bypassing condition (ii)) is governed by the scenario with the almost total reflection from the strong repulsive impurities. The latter result can be easily understood in view of approximately equal presence of nonlinear excitations on both chains of ladder lattice before the soliton-impurity collision.

5. Conclusion

In conclusion, we have presented a physically corrected model of intramolecular excitations on a multileg ladder lattice supporting both the exact soliton solutions and the standard Hamiltonian formulation. We have subjected this system subsequently to three different types of perturbation and have investigated the corresponding multimode soliton dynamics. In particular, we have paid attention to the uniform longitudinal field, local modification of transverse bonds, and zigzag-distributed on-site impurities and described the effects caused by the nontrivial mixing between the lateral and longitudinal solitonic modes. We expect that transverse-bond imperfection could serve as a filter selecting the solitons with prescribed properties. A similar function is feasible for zigzag-distributed on-site impurities too.

References

[1] C.S. Gardner, J.M. Greene, M.D. Kruskal, and R.M. Miura, Phys. Rev. Lett. **19**, 1095 (1967).

[2] V.E. Zakharov and A.B. Shabat, Zh. Eksp. Teor. Fiz. **61**, 118 (1971).

[3] B.B. Kadomtsev and V.I. Petriashvili, DAN SSSR **192**, 753 (1970).

[4] A. Davey and K. Stewartson, Proc. R. Soc. London A **338**, 101 (1974).

[5] C.R. Menyuk, IEEE J. Quantum Electron. **23**, 174 (1987).

[6] P. Marquie, J.M. Bilbault, and M. Remoissenet, Phys. Rev. E **49**, 828 (1994).

[7] A.S. Davydov, *Solitons in Molecular Systems* (Kluwer Academic, Dordrecht, 1991).

[8] W.P. Su, J.R. Schieffer, and A.J. Heeger, Phys. Rev. B **22**, 2099 (1980).

[9] J.M. Ziman, *Models of Disorder. The Theoretical Physics of Homogeneously Disordered Systems* (Cambridge University Press, Cambridge, 1979).

[10] J.W. Mintmire, B.I. Dunlap, and C.T. White, Phys. Rev. Lett. **68**, 631 (1992).

[11] O.O. Vakhnenko and M.J. Velgakis, Phys. Rev. E **61**, 7110 (2000).

[12] O.O. Vakhnenko, Phys. Rev. E **64**, 067601 (2001).

[13] O.O. Vakhnenko and M.J. Velgakis, Phys. Lett. A **278**, 59 (2000).

[14] O.O. Vakhnenko and M.J. Velgakis, Phys. Rev. E **63**, 016612 (2001).

[15] S.V. Manakov, Zh. Eksp. Teor. Fiz. **65**, 505 (1973).

[16] V.S. Gerdjikov and M.I. Ivanov, Teor. Mat. Fiz. **52**, 89 (1982).

[17] T. Tsuchida, H. Ujino, and M. Wadati, J. Phys. A **32**, 2239 (1999).

[18] M.J. Ablowitz, Y. Ohta, and A.D. Trubatch, Phys. Lett. A **253**, 287 (1999).
[19] R.E. Peierls, Z. Phys. **80**, 763 (1933).
[20] F. Bloch, Z. Phys. **52**, 555 (1928).
[21] R. Scharf and A.R. Bishop, Phys. Rev. A **43**, 6535 (1991).
[22] V.V. Konotop, O.A. Chubykalo, and L. Vázquez, Phys. Rev. E **48**, 563 (1993).

MIWA'S REPRESENTATION OF THE VOLTERRA HIERARCHY

V.E. Vekslerchik
Institute for Radiophysics and Electronics, Kharkov 61085, Ukraine and Universidad de Castilla-La Mancha, 13071 Ciudad Real, Spain
vekslerchik@yahoo.com

Abstract I study the functional representation of the Volterra hierarchy (VH). Using the Miwa's shifts I rewrite the infinite set of Volterra equations as one functional equation. These results are used to derive a formal solution of the associated linear problem and a generating function for the conservation laws and to obtain a new form of the Miura and Backlund transformations. I also discuss some relations between the VH and other integrable systems.

Keywords: Volterra equations, tau-functions, functional equations, conservation laws, Backlund transformations.

1. Introduction

In this work I want to discuss an application of the so-called functional equation approach, or method of the Miwa's shifts, to one of the oldest integrable discrete systems, namely the Volterra model,

$$\dot{u}_n = u_n \left(u_{n+1} - u_{n-1} \right). \tag{1}$$

It was proposed many years ago for the description of the population dynamics [1, 2]. Later it was applied to many physical phenomena, such as, e.g., collapse of Langmuir waves, nonlinear LC nets, Liouville field theory. It is known to be integrable since the paper by Manakov [3] (see also [4]) who developed the corresponding version of the inverse scattering transform (IST).

The IST is a method which drastically changed the theory of PDEs, of nonlinear systems as well as many other fields of nonlinear mathematics and physics. However the practical implementation of its algorithms is not so easy as one might expect. That is why during all the years of the modern theory of integrable systems people were looking for some

F. Kh. Abdullaev and V. V. Konotop (eds.), Nonlinear Waves: Classical and Quantum Aspects, 511–520.

other tools to deal with these particular equations which are called integrable. One of such approaches is the topic of this work. In a few words it can be described as follows: instead of your equation (Volterra equation in our case) you consider an infinite family of similar equations (Volterra hierarchy in our case) and then instead of an infinite number of differential equations you deal with one (or a few) equation of other kind, functional or difference ones. At first glance we complicate the problem. But it turns out that sometimes such complications can make things easier than they were at the beginning.

2. Volterra hierarchy

The Volterra equation is an integrable system. This word, 'integrable', implies the following. First this system possesses an infinite number of constants of motion,

$$\dot{I}_j = 0, \qquad j = 1, 2, 3, ... \tag{2}$$

the simplest of which can be written as

$$\begin{aligned} I_1 &= \sum u_n \\ I_2 &= \sum u_{n+1} u_n + \tfrac{1}{2} u_n^2 \\ &... \end{aligned} \tag{3}$$

Secondly, it is a Hamiltonian system. It can be presented in the form

$$\dot{u}_n = \{\mathcal{H}, u_n\} \tag{4}$$

where the Poisson brackets are given by

$$\{u_m, u_n\} = u_m u_n \left(\delta_{m,n+1} - \delta_{m,n-1}\right) \tag{5}$$

and $\mathcal{H} = I_1$.

The third ingredient of the integrability (the technical, but very important one) is that these constants of motion are in involution:

$$\{I_j, I_k\} = 0. \tag{6}$$

The so-called higher Volterra equations can be obtained by choosing as the Hamiltonian $\mathcal{H}$ not the the simplest constant of motion but one of I_k, $k = 2, 3, ...$ In such a way one can get an infinite number of equations

$$\frac{\partial u_n}{\partial t_k} = \{I_k, u_n\} \qquad k = 1, 2, ... \tag{7}$$

where the simplest ones are given by

$$\partial_1 u_n = \{I_1, u_n\} = u_n\,(u_{n+1} - u_{n-1}) \tag{8}$$

$$\partial_2 u_n = \{I_2, u_n\} = u_n\,\big(u_{n+2}u_{n+1} + u_{n+1}u_n + u_{n+1}^2 \tag{9}$$

$$-u_{n-1}^2 - u_n u_{n-1} - u_{n-1}u_{n-2}\big) \tag{10}$$

with ∂_k standing for $\partial/\partial t_k$ (hereafter I denote different differentiatings using different 'times' t_k). Those who worked with integrable equations and hierarchies know that the difference between these equations is mostly visual. Say, IST for (8) only slightly differs from the IST for (9). This infinite set (7) of equations is called the Volterra hierarchy (VH) by the name of its first representative (1) or (8).

At this point the most important moment for me is that these equations are compatible. In other words, ∂_k are indeed derivatives: they do commute. This fact is a reformulation of the third ingredient of the integrability (6):

$$\{I_j, I_k\} = 0 \qquad \Rightarrow \qquad \partial_j\,\partial_k = \partial_k\,\partial_j. \tag{11}$$

So, one can say that hierarchy is an infinite compatible system. We can find one set of functions u_n that satisfies all equations of the hierarchy. We can find such functions u_n, depending on an infinite number of times

$$u_n = u_n\,(\mathrm{t}) = u_n\,(t_1, t_2, t_3, ...) \tag{12}$$

that, if we differentiate them with respect to t_1 we will get the right-hand side of (8); if we differentiate them with respect to t_2 we will get the right-hand side of (9) and so on.

Hereafter I will discuss mostly not the Volterra equation, but the Volterra hierarchy, and I will try to convince that sometimes to deal with an infinite number of equations can be easier than to deal with only one.

It is known since the pioneering works of Hirota that almost all integrable equations can be rewritten in the bilinear form by introducing the so-called tau-functions. And in some sense these tau-functions are more important objects than the functions in terms of which the original equations were written. For the Volterra equation the tau-function can be introduced by

$$u_n = \frac{\tau_{n+1}\tau_{n-2}}{\tau_n\tau_{n-1}} \tag{13}$$

which transforms (1) to $D_t\ \tau_n \cdot \tau_{n-1} = \tau_{n+1}\tau_{n-2}$ with Hirota's bilinear operators being defined by

$$D_x^a\,D_y^b...\ u \cdot v = \frac{\partial^a}{\partial\xi^a}\,\frac{\partial^b}{\partial\eta^b}\ ...u(x+\xi, y+\eta, ...)v(x-\xi, y-\eta, ...)\Big|_{\xi=\eta=...=0} \tag{14}$$

The first equations of the VH can be presented as

$$D_1\,\tau_n\cdot\tau_{n-1}=\tau_{n+1}\tau_{n-2} \tag{15}$$

$$\left(D_2-D_1^2\right)\,\tau_n\cdot\tau_{n-1}=0 \tag{16}$$

$$\left(D_3-D_1^3\right)\,\tau_n\cdot\tau_{n-1}=3\tau_{n+2}\tau_{n-3} \tag{17}$$

$$\ldots$$

where I use the shortcut $D_k=D_{t_k}$.

Now we face the question: is it possible to present this infinite set of bilinear Volterra equations in some more condensed form? The answer is: yes, if we use the so-called Miwa's shifts.

3. VH in Miwa's representation

The Miwa's shift, which is a simple operation with rather non-trivial consequences, can be described as simultaneous shift of all times t_k according to the rule $t_k\to t_k\pm\zeta^k/k$,

$$f\left(t_1,t_2,t_3,...\right)\to f\left(t_1\pm\zeta,t_2\pm\frac{\zeta^2}{2},t_3\pm\frac{\zeta^3}{3},...\right) \tag{18}$$

or $f\left(\mathrm{t}\right)\to f\left(\mathrm{t}\pm[\zeta]\right)$. In what follows, I will also denote them by the symbols $\mathbb{E}_\zeta$ and $\overline{\mathbb{E}}_\zeta$: $\left(\mathbb{E}_\zeta f\right)\left(\mathrm{t}\right)=f(\mathrm{t}+[\zeta])$, $\left(\overline{\mathbb{E}}_\zeta f\right)\left(\mathrm{t}\right)=f(\mathrm{t}-[\zeta])$.

The main result of this work can be presented as follows: the infinite set of differential Volterra equations (7) is equivalent to one difference equation

$$\zeta\,\tau_{n-2}(\mathrm{t})\,\tau_{n+1}(\mathrm{t}+[\zeta])-\tau_{n-1}(\mathrm{t})\,\tau_n(\mathrm{t}+[\zeta])+\tau_n(\mathrm{t})\,\tau_{n-1}(\mathrm{t}+[\zeta])=0 \tag{19}$$

This equation is closely related to the discrete-time Volterra equation but I will consider it as not a discrete but as a functional (difference) one: all quantities should depend on ζ in such a way that there always exists the $\zeta\to 0$ limit. Moreover, all functions will be analytical in ζ and at any moment one can use the Taylor expansion, returning to the differential equations. So, if we expand (19) in series in ζ using

$$f(\mathrm{t}+[\zeta])=f(\mathrm{t})+\zeta\partial_1\,f(\mathrm{t})+\frac{\zeta^2}{2}\left(\partial_2+\partial_1^2\right)f(\mathrm{t})+... \tag{20}$$

and collect terms with different powers of ζ we will consequently get

$$\zeta^0:\qquad 0=0 \tag{21}$$

$$\zeta^1:\qquad \tau_{n-2}\,\tau_{n+1}-\tau_{n-1}\,\partial_1\tau_n+\tau_n\,\partial_1\tau_{n-1}=0 \tag{22}$$

$$\zeta^2:\qquad 2\tau_{n-2}\,\partial_1\tau_{n+1}-\tau_{n-1}\left(\partial_2+\partial_1^2\right)\tau_n+\tau_n\left(\partial_2+\partial_1^2\right)\tau_{n-1}=0 \tag{23}$$

$$...$$

The ζ^0 term is trivial, the ζ^1 term is nothing but the first Volterra equation (8), the ζ^2 term can be rewritten (with the help of (8)) as the second Volterra equation (9) and so on. In such a way we can get all differential equations of the VH.

Starting from the one-shift formula (19) one can obtain the following relation for the twice shifted functions:

$$a(\xi,\eta)\ \tau_{n-1}\ (\mathbb{E}_\xi \mathbb{E}_\eta \tau_n) = \xi\ (\mathbb{E}_\xi \tau_n)\ (\mathbb{E}_\eta \tau_{n-1}) - \eta\ (\mathbb{E}_\xi \tau_{n-1})\ (\mathbb{E}_\eta \tau_n) \quad (24)$$

where $a(\xi,\eta)$ is some constant (with respect to n) depending on the boundary conditions. These formulae can be extended to the case of arbitrary number of Miwa's shifts,

$$\det \left| \xi_j^{N-k}\, \mathbb{E}_{\xi_j}\, \tau_{n+1-k} \right|_{j,k=1,\dots,N} = a(\xi_1,\dots,\xi_N)\ \tau_{n+1-N} \dots \tau_{n-1}\ (\mathbb{E}_{\xi_1} \dots \mathbb{E}_{\xi_N} \tau_n) \quad (25)$$

with $a(\xi_1,\dots,\xi_N)$ being some kind of generalized Van der Monde determinant:

$$a(\xi_1,\dots,\xi_N) = \prod_{1\le i<j\le N} a(\xi_i,\xi_j). \quad (26)$$

4. Miwa's representation and IST

The Volterra hierarchy is an integrable system that can be analyzed using the IST. So, now I want to present some basic facts about the IST for the VH and then to show how the main ideas, constructions and objects of the inverse scattering approach look like in terms of the functional representation.

The starting point of the IST is the so-called zero-curvature representation, when our nonlinear equation is presented as a compatibility condition for some linear system

$$\Psi_{n+1} = U_n \Psi_n, \qquad \partial_k \Psi_n = V_n^{(k)} \Psi_n \quad (27)$$

with the same matrix U_n (see (28)) but different matrices $V_n^{(k)}$. I will not write down explicit formulae for $V_n^{(k)}$ because, as is known, the main part of the inverse scattering approach is analysis of the first of the linear equations

$$\Psi_{n+1}(\lambda) = U_n(\lambda)\Psi_n(\lambda), \qquad U_n(\lambda) = \begin{pmatrix} \lambda & u_n \\ -1 & 0 \end{pmatrix} \quad (28)$$

which is considered as a scattering problem with λ being the spectral parameter. Functions $\Psi_n(\lambda)$ are the key objects of the IST. They are

used to determine the so-called scattering data, to write down the linear equations from which one can in principle determine solutions of the Volterra equations. Namely $\Psi_n(\lambda)$ are used to construct the generating function for the conservation laws, the Backlund transformations and so on. The main difficulty of this approach is that one cannot find them explicitly or to express them in terms of the u_n's. As a result, for example, one cannot get closed expression for the generating function for the constants of motion, but only an algorithm how to derive it. However it turns out (and it is one of the main results of this work) one can overcome this obstacle if dealing in the framework of the functional representation.

Indeed, rewriting the scattering problem for the VH in the scalar form,

$$\psi_{n+1} - \lambda\psi_n + u_n\psi_{n-1} = 0 \tag{29}$$

where ψ_n is the first element of Ψ_n and comparing it with our basic equation (19) one can conclude that the quantity $\psi_n = \lambda^n \overline{\mathbb{E}}_\zeta \tau_{n-1}/\tau_{n-1}$ is a solution of equation (29). It is a very important moment: now we have a formal solution of the scattering problem given by

$$\Psi_n = \begin{pmatrix} \frac{\overline{\mathbb{E}}_\zeta \tau_{n-1}}{\tau_{n-1}}\,\lambda^n & -\frac{\mathbb{E}_\zeta \tau_{n+1}}{\tau_{n-1}}\,\lambda^{-n-1} \\ -\frac{\overline{\mathbb{E}}_\zeta \tau_{n-2}}{\tau_{n-2}}\,\lambda^{n-1} & \frac{\mathbb{E}_\zeta \tau_n}{\tau_{n-2}}\,\lambda^{-n} \end{pmatrix}, \qquad \zeta = \lambda^{-2} \tag{30}$$

We can use this fact and address the main problems which one usually solves when deals with integrable equations.

5. Conservation laws

As was mentioned above, the VH is known to posses an infinite number of constants of motion:

$$\partial_j J_k = 0, \qquad j = 1, 2, 3, \ldots \quad k = 0, 1, 2, \ldots \tag{31}$$

(hereafter I use, instead of the quantities I_k which were defined above, the constants J_k related to the former by $J_k = (k+1)I_{k+1}$) and the main object of this section is their generating function $J(\zeta)$ and the corresponding density $F_n(\zeta)$,

$$J(\zeta) = \sum_{k=0}^{\infty} \zeta^k J_k = \sum_n F_n(\zeta). \tag{32}$$

In the standard inverse scattering approach this density can be obtained by solving some recurrence which arises from an expansion of the scattering data. It turns out that it is possible to derive a closed formal

expression for F_n (which, I repeat, can hardly be done in the framework of the traditional IST):

$$F_n(\zeta, \mathrm{t}) = \frac{\tau_{n-2}\left(\mathrm{t} - [\zeta]\right)\ \tau_{n+1}\left(\mathrm{t} + [\zeta]\right)}{\tau_{n-1}(\mathrm{t})\tau_n(\mathrm{t})}. \tag{33}$$

Moreover, one can obtain not only the density but the generating function for the conservation laws for the Volterra equations as well. Say, for the first (classical) Volterra equation it can be written as:

$$\partial_1 F_n(\zeta, \mathrm{t}) = G_n^{(1)}(\zeta, \mathrm{t}) - G_{n-1}^{(1)}(\zeta, \mathrm{t}), \tag{34}$$

with

$$G_n^{(1)}(\zeta, \mathrm{t}) = \frac{\tau_{n-2}\left(\mathrm{t} - [\zeta]\right)\ \tau_{n+2}\left(\mathrm{t} + [\zeta]\right)}{\tau_n^2(\mathrm{t})}. \tag{35}$$

In a similar manner we can present other conservation laws (i.e. the ones for the higher Volterra equations) , $\partial_k F_n = G_n^{(k)} - G_{n-1}^{(k)}$, for $k = 2, 3, ...$ and even the generating function for all conservation laws of the VH:

$$\sum_{k=1}^{\infty} \eta^{k-1} \partial_k\ F_n(\zeta, \mathrm{t}) = G_n(\zeta, \eta, \mathrm{t}) - G_{n-1}(\zeta, \eta, \mathrm{t}). \tag{36}$$

Here

$$G_n(\zeta, \eta, \mathrm{t}) = g(\zeta, \eta) \frac{\tau_{n-2}\left(\mathrm{t} - [\zeta] - [\eta]\right)\ \tau_{n+2}\left(\mathrm{t} + [\zeta] + [\eta]\right)}{\tau_n^2(\mathrm{t})} \tag{37}$$

with $g(\zeta, \eta)$ being some constant determined by the boundary conditions. Expansion of this identity in power series in ζ and η leads to

$$\partial_k F_n^{(j)} = G_n^{(jk)} - G_{n-1}^{(jk)} \qquad j = 0, 1, 2, ... \quad k = 1, 2, 3, ... \tag{38}$$

i.e. gives all the conserved densities and conserved currents.

6. Backlund transformations

In discussing the Miura and Backlund transformations I will compare my results with ones obtained earlier by Kajinaga and Wadati [5].

The discrete Miura transformation, given by

$$u_n = \mu^2 \left(1 + q_{n-1}\right)\left(1 - q_n\right), \tag{39}$$

links the Volterra equation (1) and the modified Volterra equation,

$$\dot{q}_n = \mu^2 \left(1 - q_n^2\right)\left(q_{n+1} - q_{n-1}\right). \tag{40}$$

It can be used to construct the Backlund transformation linking different solutions of the Volterra equations: if u_n solves (1) and q_n is defined by (39) then u'_n given by

$$u'_n = \mu^2 \left(1 - q_{n-1}\right)\left(1 + q_n\right) \tag{41}$$

is also a solution of the Volterra equation (and of all equations of the VH).

One can hardly solve (39) in a general case, but it turns out that it is possible to construct its particular solution using the functional representation of the VH. Indeed, it follows from (19) that the functions $q'_n = 1 - 2\tau_{n+1}\left(\mathbb{E}_\zeta \tau_n\right)/\tau_n\left(\mathbb{E}_\zeta \tau_{n+1}\right)$ are related to u_n by $4\zeta u_n = \left(1 + q'_{n-1}\right)\left(1 - q'_n\right)$ i.e. by (39) with $\mu^2 = 1/4\zeta$. Unfortunately this leads to the trivial Backlund transform: $\mathbb{B}' : u_n \to u'_n = \mathbb{E}_\zeta u_{n+1}$. We can construct another Miura transform, $q''_n = 2\left(\overline{\mathbb{E}}_\zeta \tau_n\right)\tau_{n-1}/\left(\overline{\mathbb{E}}_\zeta \tau_{n-1}\right)\tau_n - 1$ corresponding to the same μ. It also leads to a not very interesting result, $\mathbb{B}'' : u_n \to u''_n = \overline{\mathbb{E}}_\zeta u_{n-1}$, but it turns out that their *linear* superposition leads to nontrivial Backlund transformations:

$$\mathbb{B}_\eta : \quad \tau_n(\mathrm{t}) \to \tau_{n+1}\left(\mathrm{t} + [\eta]\right) + \eta^{-n} \exp\left[\chi(\eta, \mathrm{t})\right] \tau_{n-1}\left(\mathrm{t} - [\eta]\right) \tag{42}$$

provided χ solves

$$\chi(\eta, \mathrm{t} + [\zeta]) - \chi(\eta, \mathrm{t}) = \Gamma(\eta, \zeta) - \Gamma(\eta, 0) \tag{43}$$

with $\Gamma(\eta, \zeta) = \ln|\eta - \zeta|/a^2(\eta, \zeta)$. The function χ is a linear function of times

$$\chi(\eta, \mathrm{t}) = \sum_{j=1}^{\infty} c_j(\eta)\, t_j \qquad c_j(\eta) = \frac{1}{j}\, \Gamma_j(\eta) \tag{44}$$

where $\Gamma_j(\eta)$ are the coefficients of the Taylor series

$$\Gamma(\eta, \zeta) = \sum_{j=1}^{\infty} \Gamma_j(\eta)\, \zeta^j.$$

In the case of zero boundary conditions, $u_n \to 0$ as $n \to \infty$ the obtained Backlund transformations can be rewritten as

$$\mathbb{B}_\eta : \quad \tau_n(\mathrm{t}) \to \tau_{n+1}\left(\mathrm{t} + [\eta]\right) + \eta^{-n} \exp\left[\chi(\eta, \mathrm{t})\right] \tau_{n-1}\left(\mathrm{t} - [\eta]\right) \tag{45}$$

with $\chi\left(t_1, t_2, \ldots\right) = \sum_{j=1}^{\infty} \eta^{-j}\, t_j$, i.e. they are nothing but well-known soliton-adding Darboux-Backlund transformations.

7. Volterra and other hierarchies

As the last application of the functional approach I am going to discuss an interesting question of interrelations between different integrable systems. The idea behind examples given below is that starting from the main equation of this work (19) one can derive some other equations which turn out to be closely related to hierarchies different from the VH.

1. Volterra and modified KP hierarchies.
Equation (19) is an functional-difference equation which relates four tau-functions with different index n. However by simple algebra one can derive, as its consequences, equations relating less number of τ_n's. One of them can be written as a *two*-point relation

$$D(\zeta)\ \tau_n \cdot \tau_{n-1} = \left(\overline{\mathbb{E}}_\zeta \tau_{n-1}\right)\left(\mathbb{E}_\zeta \tau_n\right) - \tau_{n-1}\tau_n \tag{46}$$

where $D(\zeta)$ is a "hierarchical" version of the Hirota's bilinear operators: $D(\zeta) = \sum_{j=1}^{\infty} \zeta^j D_j$. Expanding this relation in multidimensional bilinear Taylor series using the identity

$$\left(\overline{\mathbb{E}}_\zeta a\right)\left(\mathbb{E}_\zeta b\right) = F\left(\zeta, D\right)\ a \cdot b \tag{47}$$

where the bilinear operator F is given by

$$F\left(\zeta, D\right) = 1 + \zeta D_1 + \frac{\zeta^2}{2}\left(D_2 + D_{11}\right) + \frac{\zeta^3}{6}\left(2D_3 + 3D_{21} + D_{111}\right) + \ldots \tag{48}$$

(here $D_{j\,k\ldots} = D_j D_k \ldots$) one can get an infinite set of differential equations for the pair τ_n and τ_{n-1}. A few first of them are

$$\left(-D_2 + D_{11}\right)\ \tau_n \cdot \tau_{n-1} = 0 \tag{49}$$

$$\left(-4D_3 + 3D_{21} + D_{111}\right)\ \tau_n \cdot \tau_{n-1} = 0 \tag{50}$$

$$\left(-18D_4 + 8D_{31} + 3D_{22} + 6D_{211} + D_{1111}\right)\ \tau_n \cdot \tau_{n-1} = 0 \tag{51}$$

$$\ldots$$

Comparing these equations with the ones presented in [6] one can conclude that i) equation (46) can be viewed as the Miwa's representation for the 1st modified KP hierarchy (according to the classification of [6]) and that ii) this hierarchy can be "embedded' into the VH.

2. Volterra and KP hierarchies.
Continuing the procedure of decreasing the number of tau-functions involved in our functional relations it is possible to derive the following one:

$$\frac{\zeta}{2}\ D(\zeta) D_1\ \tau_n \cdot \tau_n = \left(\overline{\mathbb{E}}_\zeta \tau_n\right)\left(\mathbb{E}_\zeta \tau_n\right) - \tau_n^2 \tag{52}$$

which contains only *one* tau-function and which can be rewritten as

$$\left[\frac{\zeta}{2}D(\zeta)D_1 + 1 - F(\zeta, D)\right]\ \tau_n \cdot \tau_n = 0 \tag{53}$$

where operator F was defined above. The simplest equation of this infinite set is

$$(-4D_{31} + 3D_{22} + D_{1111})\ \tau_n \cdot \tau_n = 0 \tag{54}$$

nothing but the KP equation. So we have come to an interesting fact: the KP equation can be 'embedded' into the VH and have derived the functional representation (53) for the KP hierarchy.

References

[1] A.J. Lotka. *J. Phys. Chem.* **14** (1910) 271.
A.J. Lotka. *Proc. Nat. Acad. Sci. USA* **6** (1920) 410.

[2] V. Volterra. *Leçons sur la théorie mathématique de la lutte pour la vie.* (Gauthier-Villars, Paris, 1931) 222 p.

[3] S.V. Manakov. *Sov. Phys. JETP* **40** (1974) 269.

[4] M. Kac and P. van Moerbecke. *Adv. Math.* **16** (1975) 160.

[5] Y. Kajinaga and M. Wadati. *J. Phys. Soc. of Japan*, **67** (1998) 2237.
M. Wadati. *Suppl. Progr. Theor. Phys.*, **59** (1976) 36.

[6] M. Jimbo and T. Miwa. *Publ. Res. Inst. Math. Sci.* **19** (1983) 943.

MOVING TOPOLOGICAL SOLITONS IN THE DISCRETE KLEIN-GORDON EQUATION

Yaroslav Zolotaryuk
Bogolyubov Institute for Theoretical Physics, National Academy of Sciences of Ukraine
Kiev 03143, Ukraine
yzolo@nonlin.bitp.kiev.ua

Abstract It is well known that (anti)kink propagation in Klein-Gordon lattices is hampered by the discreteness. However, depending on the shape of the on-site potential, a discrete set of velocities can appear, for which an (anti)kink can propagate freely. On several examples we show that this is a generic effect which takes place for potentials with rather flat barriers and narrow wells.

Keywords: Discrete kinks, topological solitons.

1. Introduction

Studies of the discreteness effects on the topological soliton dynamics have been an important research topic in the last decades because discreteness is a natural feature of many realistic systems like crystals, macro-molecules, or Josephson devices (see [1]). Starting from [2] it is a well-known fact that while propagating along the chain, the (anti)kink radiates small-amplitude waves and finally stops because of the so-called Peierls-Nabarro (PN) potential barrier. However, topological solitons appear to be well-defined traveling waves of stationary profile while they are moving on an oscillating background [3, 4]. On the other hand, the integrable discretisation [5] of the continuous sine-Gordon (SG) equation or discretisations [6] that conserve the Bogomolny's bond yield moving kinks but take us out of the discrete Klein-Gordon (DKG) class. Non-trivial behaviour of static kinks such as the switching of the ground state from the kink solution centered on a chain site to the kink solution, centered in-between two sites and vice-versa depending on the on-site potential convexity was shown to occur in Refs. [7, 8, 4, 9]. This

F. Kh. Abdullaev and V. V. Konotop (eds.), Nonlinear Waves: Classical and Quantum Aspects, 521–528.

observation gives a good reason to believe that for a general nonlinear on-site potential, depending on its convexity, a *transparent* regime of the kink propagation can occur as well. The aim of our paper will be to investigate this possibility.

2. The model

We consider a chain of coupled particles subjected to an external on-site potential. If the particles are coupled via the harmonic potential $U(r) = \kappa r^2/2$, their dynamics is described by the discrete nonlinear Klein-Gordon equation:

$$\ddot{u}_n = \kappa(u_{n+1} - 2u_n + u_{n-1}) - V'(u_n) \ , \quad n \in Z \tag{1}$$

where u_n is the displacement of the nth particle from its equilibrium position. We are going to consider a class of on-site potentials $V(u)$ with the flat barrier and narrow wells. As examples we will take the Peyrard-Remoissenet (PR) potential [8], Eq. (2) and the double-Morse (DM) potential (widely used for modeling the hydrogen bonded systems [9]), Eq. (3):

$$V(u;\alpha) = [(1+2\alpha)(1-\cos u)]/[1+\alpha(1-\cos u)] \ , \ \alpha \geq 0 \ , \tag{2}$$

$$V(u;\beta) = \{ \ [\cosh(\beta a) - \cosh(\beta u)]/[\cosh(\beta a) - 1] \ \}^2 \ , \beta \geq 0 \ . \tag{3}$$

The *shape parameters* α and β measure the convexity of the potential barrier (see Fig. 1): for larger α's the wells of the potential become more narrow and the barrier becomes more flat. The DM potential has two minima at $u = \pm a$, we will take $a = 0.25$ throughout the paper. In

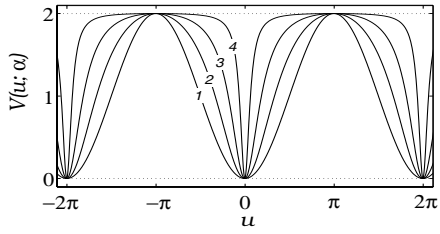

Figure 1 The shape of the PR potential (2) for $\alpha = 0$ (curve 1), $\alpha = 1$ (curve 2), $\alpha = 5$ (curve 3), $\alpha = 20$ (curve 4).

the limit of $\alpha = 0$ the PR potential coincides with the sine-Gordon (SG) potential: $V(u) = 1 - \cos u$. In the opposite limit $V(u; \alpha = \infty) = 2$ if $u = 2\pi k, \ k \in Z$ and $V(u; \alpha = \infty) = 0$ if $u \neq 2\pi k, \ k \in Z$. For the DM potential we obtained the ϕ^4 model in the limit $\beta = 0$: $V(u) = (1 - u^2/a^2)^2$. In the opposite limit of $\beta = \infty$ we have $V(\pm a) = 0$, $V(u) = 1$ if $u \in]-a, a[$ and $V(u) = \infty$ for $u \ni [-a, a]$.

3. Static properties of discrete kinks

We know that for the well-studied DKG models like discrete sine-Gordon (DSG) or ϕ^4 there exist only two stationary (anti)kink solutions: a dynamically unstable one with the central particle n_0 on the potential barrier [see Eq. (4), note, however that a proper shift for u_n's must be added in the case of PR or DSG potentials] and a stable one (a minimum of the potential energy of the system) with two central particles positioned symmetrically with respect to the center of the potential barrier [see Eq. (5)]:

$$u_{n_0-n} = -u_{n_0+n},\ n = 0, \pm 1, \dots\ , \tag{4}$$

$$u_{n_0-n} = -u_{n_0+n-1},\ n = 0, \pm 1, \dots\ . \tag{5}$$

However, for the wider class of potentials this situation changes. First we consider an important limiting case of $\alpha = \infty$ (or $\beta = \infty$), where the static problem is exactly solvable. There exists an infinite countable set of (anti)kink solutions that consist of the the tails where $V(u_n) = 0$ and the core with the finite number of particles, m. We can use this number to numerate the solutions. Then the energy of such an (anti)kink with m particles in the core [or on the barrier of $V(u)$] is given by

$$E_m = E_m(\kappa) = 2m + (\Delta X)^2 \kappa / [2(m+1)]\ . \tag{6}$$

Here ΔX stands for the distance between the two adjacent minima of the on-site potential. Thus, $\Delta X = 2\pi$ for the PR potential potential (2) and $\Delta X = 2a$ for the DM potential (3). From Fig. 2 we see that the dependencies $E_m(\kappa)$ cross each other and for different κ the (anti)kink state with different m has the minimal energy. When moving to large but finite shape parameters (Fig. 3) we see that many features of the limiting case survive. States with larger m's turn into zig-zag-like kinks (curves 4 and 5) and normally are unstable. The most important surviving feature is the switching of the kink state with minimal energy from the state of the symmetry (5) (curve 1) to the state of the symmetry (4) (curve 2) and vice versa as a function of κ. These switchings are accompanied by the change of the linear stability of the respective solutions, as shown in Fig. 3. In the limit when the shape parameter tends to zero, only two states (4) and (5) survive and their energies are always different and this difference tends to zero in the continuum limit. In the inset of Fig. 3 the curve 3 stands for a new type of kink solutions. These kinks do not exhibit any of the symmetries defined by Eqs. (4-5) but are in some sense intermediate configurations between (4) and (5). Their energy is always larger than the energy of the symmetric kinks and they are always unstable. In Fig. 4 we have plotted the position of the $(N/2)$th particle

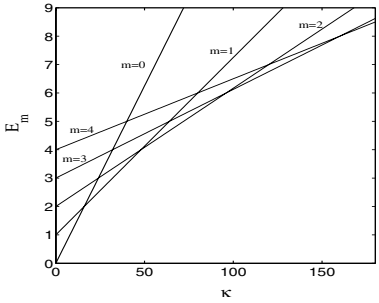

Figure 2. Dependence of the DM kink energy E_m, $m = 0$, 1, 2, 3, and 4, given by Eq. (6), in the exactly solvable limit $\beta = \infty$ on the coupling parameter κ.

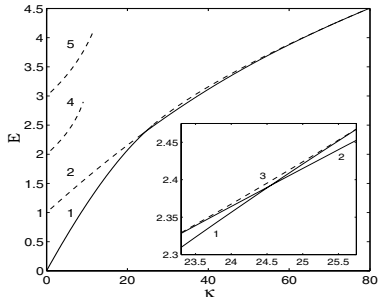

Figure 3. DM kink energy for β=10 as a function of κ for the different types of kinks (see text for details). The inset shows more detailed behavior around the switching point. Solid lines correspond to stable states and dashed lines to unstable ones.

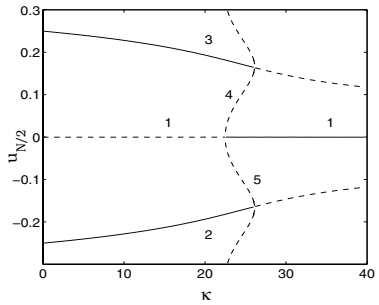

Figure 4. Displacement of the central particle $u_{N/2}$ from equilibrium for the DM model at β=10. Solid lines show stable kinks and dashed lines unstable ones.

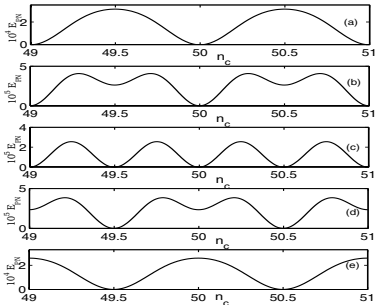

Figure 5. PN potential for $\beta = 10$ and (a) $\kappa = 70.5$, (b) $\kappa = 71.22$, (c) $\kappa = 71.288$, (d) $\kappa = 71.35$, and (e) $\kappa = 72$.

(N is the total number of particles) as a function of the coupling κ. Curve 1 corresponds to the kink of the type (4), centered on the particle $N/2$, so $u_{N/2} \equiv 0$. Curves 2 and 3 correspond to the (5) kinks with centers in-between the particles $N/2$, $N/2+1$ and $N/2-1$,$N/2$, respectively. At a certain value of κ, the pitchfork bifurcation of the kink state, centered on the $N/2$th site takes place. It becomes stable and two new unstable asymmetric solutions (shown by the curves 4 and 5) appear. At the beginning, they look like slightly distorted kinks of Eq. (4), but with the growth of κ, they change more and more toward the configuration (5). The second pitchfork bifurcation takes place at $\kappa \simeq 26.2$. The

asymmetric kinks join the kinks of the type (5) (junction of curves 3 and 4, and curves 2 and 5) and the configuration (5) loses its stability. Thus, this pitchfork bifurcation is nothing but a transition of a kink along the lattice one spacing forward or backwards. In Fig. 5 we show the PN barrier for the DM model in the vicinity of the second switching point $\kappa \simeq 72$. It is important to note that in the point where the energies of two kink configurations coincide [panel (c)] the PN barrier does not disappear but decreases by the order of magnitude. Investigations [8, 4] show that all the above properties of the static kinks also appear in the PR model.

4. Dynamics of discrete kinks

We focus now on the traveling-wave (TW) solutions of stationary profile moving with the constant velocity s, e.g. $u_n(t) = u(n-st) \equiv u(z)$, $z = n-st$. Then Eq. (1) is reduced to the following differential-difference equation:

$$s^2 u''(z) = u(z+1) - 2u(z) + u(z-1) - V'[u(z)] \ , \qquad (7)$$

which has been solved numerically with the so-called pseudo-spectral method [3, 10, 4]. It has been shown that for certain discrete set of velocities it is possible to have moving topological solitons, which are monotonic (see Fig. 6). Anywhere around these selected velocities the moving (anti)kink has a shape of an *nanopteron* (see Ref. [11]), as shown in Fig. 7. Numerical simulations of the dynamics of these solutions,

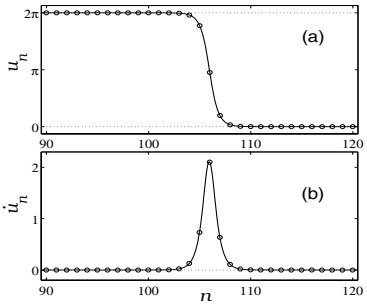

Figure 6. An antikink for the PR model with $\alpha = 1$ and $s = 0.5907$. Solid lines represent the profiles $u(z)$ and $-su'(z)$ obtained by using the pseudo-spectral method. Circles stand for $u_n(t)$ and $\dot{u}_n(t)$ at the time instant $t = 6780$.

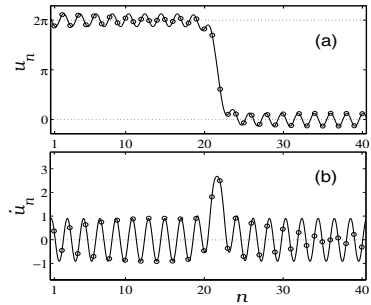

Figure 7. Same as in Fig. 6 for $\alpha = 0$ and $s = 0.73$. Circles represent the final profiles at the time instant $t = 1042$.

performed in [4] have shown their stability. The same results have been

obtained for the DM model in [9]. In the next example we consider the on-site potential, constructed first by Schmidt in [12] for the DKG (1) which has the TW solution $u_n(t) = \tanh[\mu(n-st)]$ (as was shown in [13], it is possible to map an arbitrary kink-like function $u(z)$ into a double-well potential $V(u)$ for which $u(z)$ will be a solution of the corresponding DKG equation). For example, for the potential $V(u) = -u^2/2 - u^4/4 - \ln(2-u^2)$ this kink will move with velocity $s = 1/[\sqrt{2}\ln(1+\sqrt{2})] \simeq 0.8023$. In [13] the DKG equation with the Schmidt potential has been investigated in the vicinity of this velocity using the pseudo-spectral method. In Fig. 8 the amplitude of the oscillation in the tail of the nanopteron is shown to disappear exactly at the above velocity, thus confirming that the phenomenon of discrete kink propagation exists for a selected set of velocities.

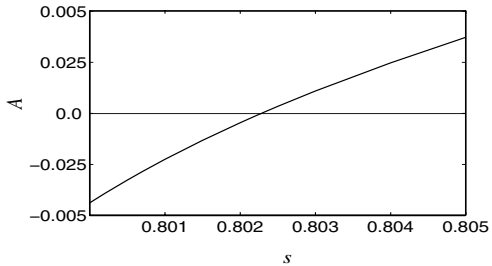

Figure 8 Dependence of the amplitude in the asymptotics of a nanopteron on the velocity for the Schmidt potential.

5. Conclusion

On the different examples we have shown that in the discrete Klein-Gordon (DKG) equation moving topological solitons can exist. Contrary to the continuous Klein-Gordon models, where moving (anti)kinks exist as a one-parametric family of solutions with a *continuous* velocity spectrum, in the DSG the spectrum of the allowed kink velocities is discrete. The existence of moving kinks depends on the shape of the on-site potential. If its barrier is flat enough and its wells are narrow enough, so that the Peierls-Nabarro potential does not decay monotonically with the coupling parameter but can experience deep minima where it decreases by the order of magnitude. Everywhere outside this discrete spectrum of velocities, (anti)kinks couple with phonons, forming a *nanopteron*, or a solitary wave with oscillating tails. In [2] moving non-oscillating kinks have been obtained for DSG for (anti)kinks with topological charges larger then 1. In fact, static properties of these (anti)kinks are similar to the ones, discussed in this paper (see [14]). Similar results, e.g. selected values of velocity for moving (anti)kinks, appearance of nanopterons and moving (anti)kinks with higher topolog-

ical charges has been obtained in [15] for the nonlocal continuous SG equation. Finally we note that anharmonic interparticle interaction can also yield moving topological solitons, as was shown in [10]. However, the mechanism of their appearance was different: they exist as hybrids of acoustic and topological solitons, they are supersonic and while only moving antikinks exist (solitons of contraction) no moving kinks (solitons of rarefaction) have been reported.

References

[1] O.M. Braun and Yu.S. Kivshar. Nonlinear dynamics of the Frenkel-Kontorova model. *Phys. Rep.*, 306:2–108, 1998.

[2] M. Peyrard and M.D. Kruskal. Kink dynamics in the highly discrete sine-Gordon system. *Physica D*, 14:88–102, 1984.

[3] D.B. Duncan *et al.* Solitons on lattices. *Physica D*, 68:1–11, 1993.

[4] A.V. Savin, Y. Zolotaryuk and J.C. Eilbeck. Moving kinks and nanopterons in the nonlinear Klein-Gordon lattice. *Physica D*, 138:265–279, 2000.

[5] S.J. Orfanidis. Discrete sine-Gordon equations. *Phys. Rev. D*, 18:3823–3827, 1978; L. Pilloni and D. Levi. The inverse scattering transform for solving the discrete sine-Gordon equation. *Phys. Lett. A*, 92:5–8, 1982.

[6] J.M. Speight and R.S. Ward. Kink dynamics in a novel discrete sine-Gordon system. *Nonlinearity*, 7:475–484, 1994; J.M. Speight. A discrete ϕ^4 system without a Peierls-Nabarro barrier. *Nonlinearity*, 10: 1615–1625, 1997.

[7] S. Aubry. Ph.D. thesis, private communications; J.H. Weiner and W.T. Sanders. Peierls stress and creep of a linear chain. *Phys. Rev. A*, 134:1007–1015, 1964; J.H. Weiner and A. Askar. Proton migration in hydrogen-bonded chains. *Nature*, 226:842–844, 1970.

[8] M. Peyrard and M. Remoissenet. Solitonlike excitations in a one-dimensional atomic chain with a nonlinear deformable substrate potential. *Phys. Rev. B*, 26: 2886–2899, 1982.

[9] V.M. Karpan, Y. Zolotaryuk, P.L. Christiansen, A.V. Zolotaryuk. Discrete kink dynamics in hydrogen-bonded chains: The one-component model. *Phys. Rev. E*, 66:066603, 2002.

[10] Y. Zolotaryuk, J.C. Eilbeck, and A.V. Savin. Bound states of lattice solitons and their bifurcations. *Physica D*, 108:81–91, 1997.

[11] The term has been introduced first in J. P. Boyd. A numerical calculation of a weakly non-local solitary wave: the ϕ^4 breather. *Nonlinearity*, 3:177–195, 1990.

[12] V.H. Schmidt. Exact solution in the discrete case for solitons propagating in a chain of harmonically coupled particles lying in double-minimum potential wells. *Phys. Rev. B*, 20:4397-4405, 1979.

[13] S. Flach, Y. Zolotaryuk, and K. Kladko. Moving lattice kinks and pulses: An inverse method. *Phys. Rev. E*, 59:6105–6115, 1999.

[14] N.J. Balmforth, R.V. Craster, and P.G. Kevrekidis. Being stable and discrete. *Physica D*, 135:212–232, 2000.

[15] G.L. Alfimov *et al*, Dynamics of topological solitons in models with nonlocal interactions. *CHAOS*, 3:405–414, 1993; G.L. Alfimov, V.M. Eleonsky, L.M. Lerman, Solitary wave solutions of nonlocal sine-Gordon equations. *CHAOS*, 8:257–271, 1998.

DYNAMICS OF DISCRETE SOLITONS IN MEDIA WITH VARYING NONLINEARITY

F. Kh. Abdullaev, E. N. Tsoy
Physical-Technical Institute of the Uzbek Academy of Sciences, Mavlyanov st., 2-B, Tashkent, 700084, Uzbekistan

B. A. Malomed
Department of Interdisciplinary Studies, Faculty of Engineering, Tel Aviv University, Tel-Aviv 69978, Israel

R. A. Kraenkel
Instituto de Física Teórica, UNESP, R. Pamplona 145, 01405-900 São Paulo, Brazil

Abstract The dynamics of discrete solitons under the action of periodic modulations of the nonlinearity is considered. The existence of quasi-stationary states is predicted in the cases of both slow and rapid modulations. A possibility of soliton splitting in the case of resonance modulations is demonstrated.

Keywords: Discrete solitons, perturbations, variational approximation, arrays of waveguides, Bose-Einstein condensate.

1. Introduction

Localized excitations, discrete solitons, are fundamental modes in nonlinear lattices, such as arraysarray of optical waveguides or arrays of droplets of a Bose-Einstein condensate (BEC) in a deep optical lattice. The dynamics of such systems is typically described by the discrete nonlinear Schrödinger (DNLS) equation. Recently different techniques, like the periodic diffraction management [1, 2] and periodic modulation of the coupling constant [3], for a control of soliton parameters are suggested. These cases correspond to a variation of the coefficient at the

F. Kh. Abdullaev and V. V. Konotop (eds.), Nonlinear Waves: Classical and Quantum Aspects, 529–534.

second-finite-difference term in the DNLS equation. However, it is possible to vary the coefficient of the cubic term in the equation. In optics it can be achieved by using an array of waveguides with the strength of the Kerr nonlinearity alternating along the propagation distance. In the case of a BEC the time-variation of the nonlinear coefficient can be realized by ac magnetic field tuned near the Feshbach resonance [4]. On the rest of the paper we study the DNLS equation in the context of the BEC model, though the results obtained can be easily applied to an array of optical waveguides.

The DNLS equation that describes the evolution of a BEC in an optical lattice is written as [5, 6]:

$$i\dot{u}_n + \frac{1}{2}\left(u_{n+1} + u_{n-1} - 2u_n\right) + a(t)\left|u_n\right|^2 u_n = 0\ . \tag{1}$$

where $u_n(t)$ is related to the condensate density at n-th site of the lattice, and $a(t) = a_0 + a_1 \sin(\omega t)$ is a coefficient proportional to the atomic scattering length in the BEC. We set $a_0 = 1$ and $a_0 = -1$ for the cases of the negative and positive scattering lengths (repulsion and attraction between atoms), respectively. Time scale $2K/\hbar$ is related to the tunnel-coupling parameter K between adjacent wells [5]. We study both the case of slow, $\omega \sim 1$, and rapid, $\omega \gg 1$, modulations.

2. Slow modulations

For analysis of the slow modulation case we use the variational approximation [7] based on the Lagrangian:

$$L = \sum_{n=-\infty}^{\infty} \frac{i}{2}\left(u_n^* \dot{u}_n - u_n \dot{u}_n^*\right) - \frac{1}{2}|u_{n+1} - u_n|^2 + \frac{1}{2}a(t)|u_n|^4\ , \tag{2}$$

where u_n^* is a complex conjugate of u_n. We take the following ansatz [7], which describe a pulse-shaped distribution of the BEC:

$$u_n(t) = A \exp(i\phi + ib|n| - \alpha|n|)\ , \tag{3}$$

where $A, \phi, b,$ and α are real functions of time. After substitution of ansatz (3) into Eq. (2) and a variation of the effective Lagrangian, one obtains a set of equations for the distribution parameters:

$$\begin{aligned} W &\equiv A^2 \coth\alpha = \text{const}, \\ \frac{db}{dt} &= 2\left(\cos b\right)\frac{\sinh^3\alpha}{\cosh\left(2\alpha\right)} - \frac{1}{2}Wa(t)\left(\tanh^2\alpha\right)\frac{2\cosh\left(2\alpha\right) - 1}{\cosh\left(2\alpha\right)}, \\ \frac{d\alpha}{dt} &= -\left(\sin b\right)\left(\sinh\alpha\right)\tanh\left(2\alpha\right). \end{aligned} \tag{4}$$

The analysis ot the Eqs. (4) in unperturbed case $a(t) = a_0 = \text{const}$ shows that there exists a non-trivial fixed point (FP), $(\alpha_{\rm FP}, b_{\rm FP})$, with

$$\sinh \alpha_{\rm FP} = \frac{1}{4} W \left(1 + 3 \tanh^2 \alpha_{\rm FP}\right) \ , \tag{5}$$

and $b_{\rm FP} = 0$ for $a_0 = 1$, and $b_{\rm FP} = \pi$ for $a_0 = -1$. A corresponding frequency ω_0 of small oscillations around the FP is found as:

$$\omega_0^2 = \frac{\sinh^3(\alpha_{\rm FP}) \cosh^2(\alpha_{\rm FP})}{\cosh^3(2\alpha_{\rm FP})} \{4 \sinh(\alpha_{\rm FP})[\cosh(2\alpha_{\rm FP}) + 2] - \frac{W}{\cosh^4(\alpha_{\rm FP})} \left[5 \cosh^2(2\alpha_{\rm FP}) - 2 \cosh(2\alpha_{\rm FP}) - 1\right] \Big\} \ . \tag{6}$$

The frequency of small oscillations found from numerical simulations of Eq. (1) is in good agreement with Eq. (6).

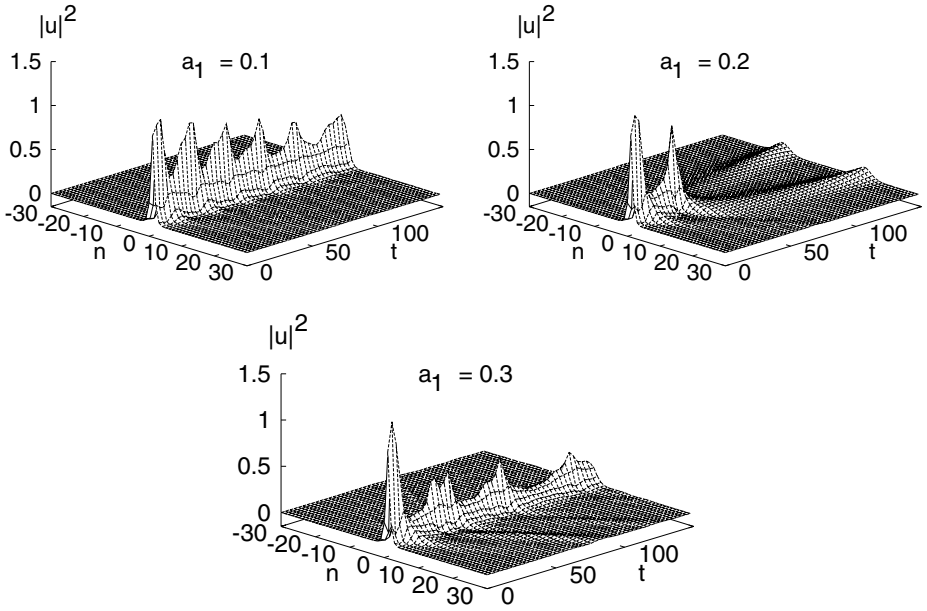

Figure 1. Evolution of a discrete soliton with the initial amplitude $A = 1$ in the periodically modulated system with $a_0 = 1, \omega = 0.5$, and different values of a_1.

In presence of modulations ($a_1 \neq 0$) and relatively small amplitudes $a_1 < \sim 0.1$, Eqs. (4) has a FP of the Poincaré map with the period $T = 2\pi/\omega$. This FP corresponds to a quasi-stationary discrete soliton. The parameters of such a soliton change periodically with period T. This

quasi-stationary soliton can be called a Feshbach-resonance managed (FRM) soliton similarly to dispersion-managed or diffraction-managed [1, 2] optical solitons.

For larger a_1 the dynamics of the parameters, predicted by Eqs. (4), becomes chaotic with asymptotic state $\alpha \to 0$. This indicate a possibility of complex dynamics of the discrete solitons in the case of large modulation amplitudes. Numerical simulations of Eq. (1) show that this chaotic behaviour has transient character, since there is a loss of the soliton energy due to radiation of linear waves. An interplay of the soliton itself, its intrinsic eigenmodes and radiation waves may result in a splitting of the pulse at $a_1 > \sim 0.1$ (see Fig. 1, $a_1 = 0.2$). However, stronger modulations can induce more intensive radiation of linear waves and moving small-amplitude solitons, resulting in a weakening of the resonance influence, so that finally a main part of the condensate is still around $n = 0$ (see Fig. 1, $a_1 = 0.3$).

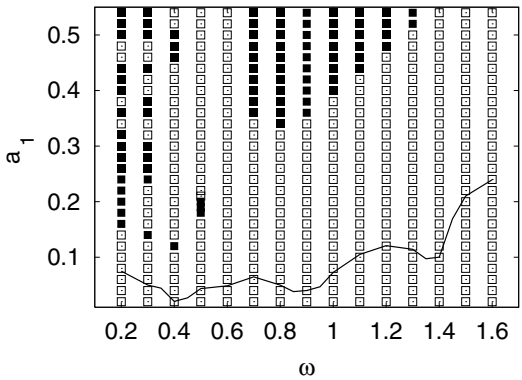

Figure 2. The diagram in the plane (ω, a_1), for the case $a_0 = 1$. Open and solid rectangles correspond to stable and splitting solitons, respectively. The initial soliton's amplitude is $A = 1$. The solid line is the chaos-onset threshold as predicted by the variational equations (4).

Results of the systematic numerical study of the pulse splitting with the initial amplitude $A = 1$ are summarized in Fig. 2. We classify as splitting cases when at least two pulses emerge, moving in opposite directions, and no pulse with an appreciable amplitude stays around $n = 0$. For $a_1 > \sim 0.2$, the modulation results in generation of several moving pulses. However, if a soliton with conspicuous amplitude is eventually found around $n = 0$, this case was classified as a "stable soliton".

Figure 2 also displays the dependence of a chaos threshold a_1 on ω, found from simulations of Eqs. (4). As is seen, the splitting actually occurs far above the threshold in a region of the developed dynamical

chaos. The diagram for the case $a_0 = -1$ looks similar, but not exactly the same.

3. Rapid modulations

For analysis of the case of rapid modulations, $\epsilon \equiv 1/\omega \ll 1$, we introduce a set of time scales $\tau = t/\epsilon$, $t_k = \epsilon^k t$, where $k = 0, 1, 2 \dots$, and look for a solution in the form

$$u_n = U_n + \epsilon u_n^{(1)} + \epsilon^2 u_n^{(2)} + \dots \ , \tag{7}$$

where U_n is a function of the slow variables t_k and $u_n^{(j)} = u_n^{(j)}(\tau, t_1, t_2, \dots)$. Then an application of the multiscale method [8] results in the following equation for an average dynamics of the condensate:

$$\begin{aligned} &i\dot{U}_n + \frac{1}{2}(U_{n+1} + U_{n-1} - 2U_n) + a_0|U_n|^2 U_n = -2Ma_0\epsilon^2|U_n|^6 U_n - \\ &M\epsilon^2 \left[|U_{n+1}|^2(2|U_n|^2 U_{n+1} + U_n^2 U_{n+1}^*) + \right. \\ &\left. |U_{n-1}|^2(2|U_n|^2 U_{n-1} + U_n^2 U_{n-1}^*) - 3|U_n|^4 U_{n+1} - 3|U_n|^4 U_{n-1}\right] \ , \end{aligned} \tag{8}$$

where $M \equiv a_1^2/4$ for the case of the periodic modulation. Equation (8) is the higher-order DNLS equation, which contains extra on-site and intersite (nonlocal) nonlinearities.

A change of variables $q_n \equiv U_n + \epsilon^2 M|U_n|^4 U_n$ and a retention of terms up to $O(\epsilon^2)$ give the dynamical equation for q_n, which can be derived from a Lagrangian

$$L_q = L_0 - \frac{1}{2}\epsilon^2 M \sum_{n=-\infty}^{\infty} (|q_{n+1}|^2 - |q_n|^2)^2 (q_n^* q_{n+1} + q_n q_{n+1}^*) \ , \tag{9}$$

where L_0 is obtained from the underlying Lagrangian (2) by the substitution $u_n \to q_n$ and $a(t) \to a_0$. The existence of the Lagrangian L_q allows one to apply the variational approximation like in Section 2. Such an analysis shows that in presence of rapid modulations there also exists a fixed point, which corresponds to a FRM discrete soliton. One can calculate the parameters of this localized state, for example, the dependence of the total number of particles $\bar{W}$ in the condensate on the distribution maximum amplitude $\bar{A}$ (see Fig 3). As it is suggested by Fig.3, where $\delta \equiv a_1^2/(4\omega^2)$, one can effectively control the soliton by an appropriate choice of the modulation parameters. Increase of the total number of particles in the averaged soliton, as compared to that in the unperturbed soliton with the same amplitude, is clearly seen in Fig. 3.

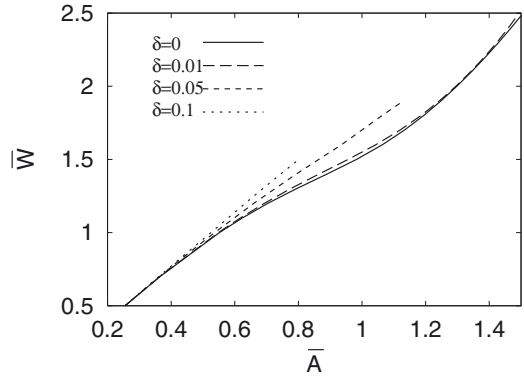

Figure 3. The dependence of $\bar{W}$ vs. $\bar{A}$ of an average soliton (dashed lines) is compared with that of the unperturbed DNLS equation (solid line), $a_0 = 1$.

4. Conclusions

We have studied analytically and numerically the dynamics of discrete solitons in media with alternating nonliearity. By making use of the variational expansion we have demonstrated the existence of quasi-stationary discrete solitons in the case of both slow and rapid modulations. The parameters of such solitons can be controlled by the parameters of modulations. The possibility of the soliton splitting is shown in the case of resonance perturbations.

References

[1] H. S. Eisenberg, Y. Silberberg, R. Morandotti, and J. S. Aitchison, Phys. Rev. Lett. **85**, 1863 (2000).

[2] M. J. Ablowitz and Z. H. Musslimani, Phys. Rev. Lett. **87**, 254102 (2002).

[3] U. Peschel and F. Lederer, J. Opt. Soc. Am. B **19**, 544 (2002).

[4] Y. Kagan, E. L. Surkov, and G. V. Shlyapnikov, Phys. Rev. Lett. **79**, 2604 (1997); S. L. Cornish, N. R. Claussen, J. L. Roberts, E. A. Cornell, and C. E. Wieman, Phys. Rev. Lett. **85**, 1795 (2000).

[5] A. Trombettoni and A. Smerzi, Phys. Rev. Lett. **86**, 2353 (2001).

[6] F. Kh. Abdullaev, B. B. Baizakov, S. A. Darmanyan, V. V. Konotop, and M. Salerno, Phys. Rev. A **64**, 043606 (2001).

[7] See e.g. B. A. Malomed, Progr. Opt. **43**, 71 (2002).

[8] T. S. Yang and W. L. Kath, Opt. Lett. **22**, 985 (1997).

ON CONTINUOUS LIMITS OF SOME GENERALIZED COMPRESSIBLE HEISENBERG SPIN CHAINS

N. S. Serikbaev, Kur. Myrzakul, F. K. Rahimov, and R. Myrzakulov
Institute of Physics and Technology, 480082, Alma-Ata-82, Kazakhstan

Abstract We study the connection between some lattice and continuous Heisenberg spin models. The continuous limits of some generalized compressible Heisenberg spin chains are found. Using the methods of differential geometry of surfaces, the Lakshmanan equivalent counterpart of one of the obtained continuous Heisenberg ferromagnet equation is constructed.

Keywords: Lattice models, Heisenberg spin chains, integrable systems, surfaces, solitons

1. Introduction

In this note we will study the connection between the discrete and continuous compressible Heisenberg spin chains [1-8]. Let us consider the following generalized compressible Heisenberg spin chain

$$\hat{H} = -\sum_{n=1}^{N} J_n \mathbf{S}_n \cdot \mathbf{S}_{n+1} + \hat{H}_l, \tag{1}$$

where $J_n = J(q_{n+1} - q_n)$ and $\hat{H}_l$ is the lattice potential which has the Toda form

$$\hat{H}_l = \sum_{n=1}^{N} \{ \frac{p_n^2}{2m} + [e^{-(q_n - q_{n-1})} - 1] \}. \tag{2}$$

In (1) and (2), $\mathbf{S}_n = (S_n^1, S_n^2, S_n^3)$ is the discrete spin vector in n-th lattice point, $\mathbf{S}_n^2 = s^2 = constant$, q_n, p_n and m are the position, moment and mass of the n-th lattice site. The discrete equations of motion for the Hamiltonian (1) is

$$\mathbf{S}_{nt} = \mathbf{S} \wedge (J_{n-1}\mathbf{S}_{n-1} + J_n \mathbf{S}_{n+1}), \tag{3a}$$

F. Kh. Abdullaev and V. V. Konotop (eds.), Nonlinear Waves: Classical and Quantum Aspects, 535–542.

$$mq_{ntt} = e^{-(q_n - q_{n-1})} - e^{(q_{n+1} - q_n)} + \frac{\partial(J_n \mathbf{S}_n \mathbf{S}_{n+1} + J_{n-1}\mathbf{S}_{n-1}\mathbf{S}_n)}{\partial q_n}. \quad (3b)$$

In the continuous limit, we take $x = na, \quad S_n(t) \to S(na,t) = S(x,t)$ and $S_{n\pm1} \to S(x,t) \pm aS_x + \frac{a^2}{2}S_{xx} + \cdots$. Then in the continuous limit, the system (3) takes the form

$$\mathbf{S}_t = \{(\mu - u)\mathbf{S} \wedge \mathbf{S}_x\}_x, \quad (4a)$$

$$\rho u_{tt} = \nu_0^2 u_{xx} + \alpha(u^2)_{xx} + \beta u_{xxxx} + \lambda(\mathbf{S}_x^2)_{xx}, \quad (4b)$$

which is the Myrzakulov XLIII (M-XLIII) equation [4,12]. Here μ, ν_0, ρ, α, β, λ are constants, $u = q_x$. In the harmonic case ($\alpha = \beta = 0$), instead of the system (4), we obtain the Myrzakulov XLIV (M-XLIV) equation

$$\mathbf{S}_t = \{(\mu - u)\mathbf{S} \wedge \mathbf{S}_x\}_x, \quad \rho u_{tt} = \nu_0^2 u_{xx} + \lambda(\mathbf{S}_x^2)_{xx}. \quad (5)$$

If we take into account the anisotropic interactions, then we get the system

$$\mathbf{S}_t = \{(\mu - u)\mathbf{S} \wedge \mathbf{S}_x\}_x + \mathbf{S} \wedge J\mathbf{S}, \quad (6a)$$

$$\rho u_{tt} = \nu_0^2 u_{xx} + \alpha(u^2)_{xx} + \beta u_{xxxx} + \lambda(\mathbf{S}_x^2)_{xx}, \quad (6b)$$

where $J = \mathrm{diag}(J_1, J_2, J_3)$. Similarly, we can consider the case, when the lattice Hamiltonian $\hat{H}_l$ is the Ablowitz - Ladik potential. In this case, in the continuous limit, after some calculations, we obtain the Myrzakulov LXXIV (M-LXXIV) equation

$$\mathbf{S}_t = \{(\mu|\phi|^2 + \nu)\mathbf{S} \wedge \mathbf{S}_x\}_x + \mathbf{S} \wedge J\mathbf{S}, \quad (7a)$$

$$i\phi_t + \phi_{xx} + 2\alpha|\phi|^2\phi + \lambda\mathbf{S}_x^2\phi = 0, \quad (7b)$$

where μ, ν, α, λ are constants, ϕ is the scalar complex function.

2. A list of some spin systems in 1+1 dimensions

Now we would like to present the list of some spin-phonon systems. At first we give some equations for $\mathbf{S}$ with yet not specified potentials u and then we concretize the form of this potentials.

Here and below, α, β, λ, ν_0, ρ, μ, ν are constants, u, v are the scalar real functions (potentials), $[,]$ ($\{,\}$) is commutator (anticommutator),

$$S = \begin{pmatrix} S_3 & S^- \\ S^+ & -S_3 \end{pmatrix}, \quad S^{\pm} = S_1 \pm iS_2, \quad S^2 = I, \quad \mathbf{S}_x^2 = S_{1x}^2 + S_{2x}^2 + S_{3x}^2.$$

Table 1. Spin systems with the potentials

Name of equation	*Equation of motion*
The M-LVII *equation*	$2iS_t = [S, S_{xx}] + u[S, \sigma_3]$
The M-LVI *equation*	$2iS_t = [S, S_{xx}] + uS_3[S, \sigma_3]$
The M-LV *equation*	$2iS_t = \{(\mu\vec{S}_x^2 - u + m)[S, S_x]\}_x$
The M-LIV *equation*	$2iS_t = n[S, S_{xxxx}] + 2\{(\mu\vec{S}_x^2 - u + m)[S, S_x]\}_x$
The M-LIII *equation*	$2iS_t = [S, S_{xx}] + 2iuS_x$

Table 2. Spin systems of the 1-class

Name of equation	*Equation of motion*
The M-LII *equation*	$2iS_t = [S, S_{xx}] + u[S, \sigma_3]$ $\rho u_{tt} = \nu_0^2 u_{xx} + \lambda(S_3)_{xx}$
The M-LI *equation*	$2iS_t = [S, S_{xx}] + u[S, \sigma_3]$ $\rho u_{tt} = \nu_0^2 u_{xx} + \alpha(u^2)_{xx} + \beta u_{xxxx} + \lambda(S_3)_{xx}$
The M-L *equation*	$2iS_t = [S, S_{xx}] + u[S, \sigma_3]$ $u_t + u_x + \lambda(S_3)_x = 0$
The M-XLIX *equation*	$2iS_t = [S, S_{xx}] + u[S, \sigma_3]$ $u_t + u_x + \alpha(u^2)_x + \beta u_{xxx} + \lambda(S_3)_x = 0$

3. L-equivalent counterparts of spin systems

Now let us we find the Lakshmanan equivalent (L-equivalent) counterpart of one of above presented spin systems [7-12]. To this end, we consider the Gauss-Weingarten equation for surfaces

$$\begin{pmatrix} e_1 \\ e_2 \\ e_3 \end{pmatrix}_x = \begin{pmatrix} 0 & \kappa & -\sigma \\ -\kappa & 0 & \tau \\ \sigma & -\tau & 0 \end{pmatrix} \begin{pmatrix} e_1 \\ e_2 \\ e_3 \end{pmatrix}, \tag{8a}$$

$$\begin{pmatrix} e_1 \\ e_2 \\ e_3 \end{pmatrix}_t = \begin{pmatrix} 0 & \omega_3 & -\omega_2 \\ -\omega_3 & 0 & \omega_1 \\ \omega_2 & -\omega_1 & 0 \end{pmatrix} \begin{pmatrix} e_1 \\ e_2 \\ e_3 \end{pmatrix}. \tag{8b}$$

The corresponding Gauss-Codazzi-Mainardi equation has the form

$$\kappa_t = \omega_{3x} + \tau\omega_2 - \sigma\omega_1, \tag{9a}$$

Table 3. Spin systems of the 2-class

Name of equation	*Equation of motion*
The M-XLVIII *equation*	$2iS_t = [S, S_{xx}] + uS_3[S, \sigma_3]$ $\rho u_{tt} = \nu_0^2 u_{xx} + \lambda(S_3^2)_{xx}$
The M-XLVII *equation*	$2iS_t = [S, S_{xx}] + uS_3[S, \sigma_3]$ $\rho u_{tt} = \nu_0^2 u_{xx} + \alpha(u^2)_{xx} + \beta u_{xxxx} + \lambda(S_3^2)_{xx}$
The M-XLVI *equation*	$2iS_t = [S, S_{xx}] + uS_3[S, \sigma_3]$ $u_t + u_x + \lambda(S_3^2)_x = 0$
The M-XLV *equation*	$2iS_t = [S, S_{xx}] + uS_3[S, \sigma_3]$ $u_t + u_x + \alpha(u^2)_x + \beta u_{xxx} + \lambda(S_3^2)_x = 0$

Table 4. Spin systems of the 3-class

Name of equation	*Equation of motion*
The M-XLIV *equation*	$2iS_t = \{(\mu\vec{S}_x^2 - u + m)[S, S_x]\}_x$ $\rho u_{tt} = \nu_0^2 u_{xx} + \lambda(\vec{S}_x^2)_{xx}$
The M-XLIII *equation*	$2iS_t = \{(\mu\vec{S}_x^2 - u + m)[S, S_x]\}_x$ $\rho u_{tt} = \nu_0^2 u_{xx} + \alpha(u^2)_{xx} + \beta u_{xxxx} + \lambda(\vec{S}_x^2)_{xx}$
The M-XLII *equation*	$2iS_t = \{(\mu\vec{S}_x^2 - u + m)[S, S_x]\}_x$ $u_t + u_x + \lambda(\vec{S}_x^2)_x = 0$
The M-XLI *equation*	$2iS_t = \{(\mu\vec{S}_x^2 - u + m)[S, S_x]\}_x$ $u_t + u_x + \alpha(u^2)_x + \beta u_{xxx} + \lambda(\vec{S}_x^2)_x = 0$

$$\sigma_t = \omega_{2x} + \kappa\omega_1 - \tau\omega_3, \tag{9b}$$

$$\tau_t = \omega_{1x} + \sigma\omega_3 - \kappa\omega_2. \tag{9c}$$

Consider the Myrzakulov LIII (M-LIII) equation

$$\mathbf{S}_t = \mathbf{S} \wedge \mathbf{S}_{xx} + u\mathbf{S}_x. \tag{10}$$

We put $\mathbf{e}_1 \equiv \mathbf{S}$, $\varphi = \frac{1}{2}(i\sigma - \kappa)$. Then the L-equivalent of the M-LIII equation (10) takes the form

$$i\varphi_t + \varphi_{xx} + 2|\varphi|^2\varphi - 2i(u\varphi)_x = 0. \tag{11}$$

Similarly, we can construct the L-equivalents of the other spin systems.

Table 5. Spin systems of the 4-class

Name of equation	*Equation of motion*
The M-XL *equation*	$2iS_t = [S, S_{xxxx}] + 2\{(\mu\vec{S}_x^2 - u + m)[S, S_x]\}_x$ $\rho u_{tt} = \nu_0^2 u_{xx} + \lambda(\vec{S}_x^2)_{xx}$
The M-XXXIX *equation*	$2iS_t = [S, S_{xxxx}] + 2\{(\mu\vec{S}_x^2 - u + m)[S, S_x]\}_x$ $\rho u_{tt} = \nu_0^2 u_{xx} + \alpha(u^2)_{xx} + \beta u_{xxxx} + \lambda(\vec{S}_x^2)_{xx}$
The M-XXXVIII *equation*	$2iS_t = [S, S_{xxxx}] + 2\{(\mu\vec{S}_x^2 - u + m)[S, S_x]\}_x$ $u_t + u_x + \lambda(\vec{S}_x^2)_x = 0$
The M-XXXVII *equation*	$2iS_t = [S, S_{xxxx}] + 2\{(\mu\vec{S}_x^2 - u + m)[S, S_x]\}_x$ $u_t + u_x + \alpha(u^2)_x + \beta u_{xxx} + \lambda(\vec{S}_x^2)_x = 0$

Table 6. Spin systems of the 5-class

Name of equation	*Equation of motion*
The M-XXXVI *equation*	$2iS_t = [S, S_{xx}] + 2iuS_x$ $\rho u_{tt} = \nu_0^2 u_{xx} + \lambda(\mathbf{S}_x^2)_{xx}$
The M-XXXV *equation*	$2iS_t = [S, S_{xx}] + 2iuS_x$ $\rho u_{tt} = \nu_0^2 u_{xx} + \alpha(u^2)_{xx} + \beta u_{xxxx} + \lambda(\mathbf{S}_x^2)_{xx}$
The M-XXXIV *equation*	$2iS_t = [S, S_{xx}] + 2iuS_x$ $u_t + u_x + \lambda(\mathbf{S}_x^2)_x = 0$
The M-XXXIII *equation*	$2iS_t = [S, S_{xx}] + 2iuS_x$ $u_t + u_x + \alpha(u^2)_x + \beta u_{xxx} + \lambda(\mathbf{S}_x^2)_x = 0$

4. Conclusion

To summarize, we have established the connection between the discrete and continuous Heisenberg spin chains. In particular, we obtained a number of nonlinear systems which describe magnetic crystals with account for lattice vibrations. We note that practically all of the presented nonlinear equations admit exact soliton solutions. Also some of these equations are integrable. Investigations of integrability of the other systems is now in progress [7-12].

Table 7. Spin systems of the 6-class

Name of equation	*Equation of motion*
The M-XXXVI *equation*	$2iS_t = [S, S_{xx}] + 2iuS_x$ $\rho u_{tt} = \nu_0^2 u_{xx} + \lambda(\mathbf{S}_x^2)_{xx}$
The M-XXXV *equation*	$2iS_t = [S, S_{xx}] + 2iuS_x$ $\rho u_{tt} = \nu_0^2 u_{xx} + \alpha(u^2)_{xx} + \beta u_{xxxx} + \lambda(\mathbf{S}_x^2)_{xx}$
The M-XXXIV *equation*	$2iS_t = [S, S_{xx}] + 2iuS_x$ $u_t + u_x + \lambda(\mathbf{S}_x^2)_x = 0$
The M-XXXIII *equation*	$2iS_t = [S, S_{xx}] + 2iuS_x$ $u_t + u_x + \alpha(u^2)_x + \beta u_{xxx} + \lambda(\mathbf{S}_x^2)_x = 0$

Table 8. Spin systems of the 7-class

Name of equation	*Equation of motion*
The M-LXIX *equation*	$\mathbf{S}_t = \frac{1}{\sqrt{\mathbf{S}_x^2}}(-\sqrt{\mathbf{S}_x^2 - u^2}\mathbf{S}_x + u\mathbf{S} \wedge \mathbf{S}_x) + \beta\mathbf{S}_x^3$ $u_x = v\sqrt{\mathbf{S}_t^2 - u^2}$ $v_t = -\mathbf{S} \cdot (\mathbf{S}_t \wedge \mathbf{S}_x)$
The M-LXX *equation*	$\mathbf{S}_t = \mathbf{S} \wedge \mathbf{S}_{xx} + \mathbf{H} \wedge \mathbf{S} + \beta\mathbf{S}_x^3$ $\mathbf{H}_t = \mathbf{H} \wedge \mathbf{S}_{xx}$

Table 9. Spin systems of the 8-class

Name of equation	*Equation of motion*
The M-LXXI *equation*	$\mathbf{S}_t = \mathbf{S} \wedge \mathbf{S}_{xx} + \alpha\lvert\phi\rvert^2\mathbf{S}_x + \mathbf{S} \wedge J\mathbf{S}$ $i\phi_t + \phi_{xx} + \lambda\mathbf{S}_x^2\phi = 0$
The M-LXXII *equation*	$\mathbf{S}_t = \mathbf{S} \wedge \mathbf{S}_{xx} + \alpha\lvert\phi\rvert^2\mathbf{S}_x + \mathbf{S} \wedge J\mathbf{S}$ $i\phi_t + \phi_{xx} + i\lambda(\mathbf{S}_x^2\phi)_x = 0$
The M-LXXIII *equation*	$\mathbf{S}_t = \mathbf{S} \wedge \mathbf{S}_{xx} + \alpha\lvert\phi\rvert^2\mathbf{S}_x + \mathbf{S} \wedge J\mathbf{S}$ $i\phi_t + \phi_{xx} + i\lambda\mathbf{S}_x^2\phi_x = 0$

Acknowledgments

RM would like to thank the organizers for hospitality and for a financial support.

Table 10. Spin systems of the 9-class

Name of equation	*Equation of motion*
The M-LXXIV *equation*	$\mathbf{S}_t = \{(\mu\|\phi\|^2 + m)\mathbf{S} \wedge \mathbf{S}_x\}_x + \mathbf{S} \wedge J\mathbf{S}$ $i\phi_t + \phi_{xx} + \lambda\mathbf{S}_x^2\phi = 0$
The M-LXXV *equation*	$\mathbf{S}_t = \{(\mu\|\phi\|^2 + m)\mathbf{S} \wedge \mathbf{S}_x\}_x + \mathbf{S} \wedge J\mathbf{S}$ $i\phi_t + \phi_{xx} + i\lambda(\mathbf{S}_x^2\phi)_x = 0$
The M-LXXVI *equation*	$\mathbf{S}_t = \{(\mu\|\phi\|^2 + m)\mathbf{S} \wedge \mathbf{S}_x\}_x + \mathbf{S} \wedge J\mathbf{S}$ $i\phi_t + \phi_{xx} + i\lambda\mathbf{S}_x^2\phi_x = 0$

Table 11. Spin systems of the 10-class

Name of equation	*Equation of motion*
The M-LXXVII *equation*	$\mathbf{S}_t = n\mathbf{S} \wedge \mathbf{S}_{xxxx} + 2\{(\mu\|\phi\|^2 + m)\mathbf{S} \wedge \mathbf{S}_x\}_x$ $i\phi_t + \phi_{xx} + \lambda\mathbf{S}_x^2\phi = 0$
The M-LXXVIII *equation*	$\mathbf{S}_t = n\mathbf{S} \wedge \mathbf{S}_{xxxx} + 2\{(\mu\|\phi\|^2 + m)\mathbf{S} \wedge \mathbf{S}_x\}_x$ $i\phi_t + \phi_{xx} + i\lambda(\mathbf{S}_x^2\phi)_x = 0$
The M-LXXIX *equation*	$\mathbf{S}_t = n\mathbf{S} \wedge \mathbf{S}_{xxxx} + 2\{(\mu\|\phi\|^2 + m)\mathbf{S} \wedge \mathbf{S}_x\}_x$ $i\phi_t + \phi_{xx} + i\lambda\mathbf{S}_x^2\phi_x = 0$

References

[1] Lakshmanan M. *Phys. Lett. A,* **61**, 53 (1977)

[2] Kosevich A.M., Ivanov B.A., Kovalev A.S. *Nonlinear spin waves. Dynamical and Topological Solitons.* (Naukova Dumka, Kiev, 1983)

[3] Mikhailov A.B. *Integrable Magnetic Models* in Solitons. eds. S.E.Trullinger, V.E.Zakharov, V.L.Pokrovsky. (Elsevier Science Publishers B.V., 1986), 623.

[4] Kozhamkulov T.A., Serikbaev N.S., Koshkinbaev A.D., Myrzakul Kur., Saiymbetova S.K., Rahimov F.K., Myrzakulov R. *On some nonlinear models of magnets.* Preprint JINR P17-2003-171, Dubna, Russia, 2003

[5] Martina L., Kozhamkulov T.A., Myrzakul Kur., Myrzakulov R. *Integrable Heisenberg ferromagnets and soliton geometry of curves and surfaces.* In: Nonlinear Physics: Theory and Experiment. II. Eds. M.J.Ablowits, M.Boiti, F.Pempinelli, B.Prinari. (Singapore: World Scientific, 2003), 248-253

[6] Konotop V.V., Salerno M., Takeno S. *Phys. Rev.,* **58**, 14892 (1998)

[7] Myrzakulov R., Daniel M., Amuda R. *Physica A,* **234**, 715 (1997)

[8] Myrzakulov R., Vijayalakshmi S., Nugmanova G.N., Lakshmanan M. *Phys. Lett.,* **233 A**, 391 (1997)

[9] Martina L., Myrzakul Kur., Myrzakulov R., Soliani G. *J. Math. Phys.,* **39**, 3765 (1998)

[10] Myrzakulov R., Nugmanova G.N., Syzdykova R.N. *Journal of Physics A.: Math. Gen.,* **31**, 9535 (1998)

[11] Myrzakulov R., Danlybaeva A.K., Nugmanova G.N. *Theor. Math. Phys.,* **118**, 347 (1999)

[12] Myrzakulov R. *Spin systems and soliton geometry,* Almaty, 2001

ON THE GEOMETRY OF STATIONARY HEISENBERG FERROMAGNETS

F. K. Rahimov, Kur. Myrzakul, N. S. Serikbaev, and R. Myrzakulov
Institute of Physics and Technology, 480082, Alma-Ata-82, Kazakhstan

Abstract A new class of two-dimensional surfaces generated by formulas which are generalizations of the well known Lelieuvre and Schief formulas is presented. These surfaces are connected with two-dimensional spin systems which are stationary versions of the (2+1)-dimensional classical continuous Heisenberg ferromagnets.

Keywords: nonlinear models, Heisenberg ferromagnets, integrable systems, solitons, differential geometry of surfaces.

1. Introduction

Since a long time surfaces appear in the description of many phenomena in physics: spin glass models, membrane-like polymers, growth of crystals, string theory and so on. On the other hand, there are many very interesting partial differential equations originating from classical differential geometry. The famous Liouville equation, for example, first appeared in differential geometry. After the discovery of soliton theory, people began to recognize the importance of differential geometry in the theory of solitons. Since then, many authors paid attention to the use of methods from differential geometry in theory of solitons [1-12]. The aim of this paper is the investigation of the relation differential geometry of surfaces with the stationary versions of some classical continuous Heisenberg ferromagnets in 2+1 dimensions [13-15].

2. Some formulas on the theory of surfaces

Let $\mathbf{r}$ be the position vector of the surface in three dimensional euclidean space with the parameterization x, y. Then $\mathbf{r}_x$, $\mathbf{r}_y$ are the tangent vectors. Let these tangent vectors, as against existing in the literature, are given by the following Myrzakulov formula (MF) (about our nota-

F. Kh. Abdullaev and V. V. Konotop (eds.), Nonlinear Waves: Classical and Quantum Aspects, 543–549.

tions, see, e.g. Refs. [14-18])

$$\mathbf{r}_x = a_1\mathbf{N}\wedge\mathbf{N}_x + a_2\mathbf{N}\wedge\mathbf{N}_y + a_3\mathbf{N}_x + a_4\mathbf{N}_y + a_5\mathbf{N}, \tag{1a}$$

$$\mathbf{r}_y = b_1\mathbf{N}\wedge\mathbf{N}_x + b_2\mathbf{N}\wedge\mathbf{N}_y + b_3\mathbf{N}_x + b_4\mathbf{N}_y + b_5\mathbf{N}, \tag{1b}$$

where $\mathbf{N}(x,t)$ is some vector function, $a_i(x,t), b_i(x,t)$ are real scalar functions. First of all, we note that the MF (1) contents the following important particular cases:

i) The Rodrigues formula [12]

$$\mathbf{r}_x = -\rho_1\mathbf{N}_x, \quad \mathbf{r}_y = -\rho_2\mathbf{N}_y. \tag{2}$$

as

$$a_1 = a_2 = a_4 = a_5 = b_1 = b_2 = b_3 = b_5 = 0, \quad a_3 = -\rho_1, \quad b_4 = -\rho_2. \tag{3}$$

ii) The Lelieuvre formula [11-12, 19-21]

$$\mathbf{r}_x = \rho\mathbf{N}_x\wedge\mathbf{N}, \quad \mathbf{r}_y = \rho\mathbf{N}\wedge\mathbf{N}_y, \tag{4}$$

as

$$a_2 = a_3 = a_4 = a_5 = b_1 = b_3 = b_4 = b_5 = 0, \quad a_1 = -\rho, \quad b_2 = \rho. \tag{5}$$

iii) The Schief formula [12]

$$\mathbf{r}_x = \rho\mathbf{N}_y\wedge\mathbf{N} + \mu\mathbf{N}_x, \quad \mathbf{r}_y = \rho\mathbf{N}\wedge\mathbf{N}_x + \mu\mathbf{N}_y, \tag{6}$$

as

$$a_1 = a_4 = a_5 = b_2 = b_3 = b_5 = 0, a_2 = -\rho, a_3 = \mu, b_1 = \rho, b_4 = \mu. \tag{7}$$

For us the special interest represents the case, when $\mathbf{N} = \mathbf{S}$, where $\mathbf{S}$ is the spin vector, $\mathbf{S}^2 = 1$. Then the MF (1) takes the form

$$\mathbf{r}_x = a_1\mathbf{S}\wedge\mathbf{S}_x + a_2\mathbf{S}\wedge\mathbf{S}_y + a_3\mathbf{S}_x + a_4\mathbf{S}_y + a_5\mathbf{S}, \tag{8a}$$

$$\mathbf{r}_y = b_1\mathbf{S}\wedge\mathbf{S}_x + b_2\mathbf{S}\wedge\mathbf{S}_y + b_3\mathbf{S}_x + b_4\mathbf{S}_y + b_5\mathbf{S}. \tag{8b}$$

3. Heisenberg ferromagnets associated with the surfaces

Now we find the classical continuous Heisenberg ferromagnets related with the MF (8). We note that the consistency relation of the formulas (8) gives the following spin system

$$(a_{1y} - b_{1x})\mathbf{S}\wedge\mathbf{S}_x + (a_{2y} - b_{2x})\mathbf{S}\wedge\mathbf{S}_y + \mathbf{S}\wedge[a_2\mathbf{S}_{yy} + (a_1 - b_2)\mathbf{S}_{xy} -$$

$$b_1\mathbf{S}_{xx}] + (a_{3y} - b_5 - b_{3x})\mathbf{S}_x + (a_5 + a_{4y} - b_{4x})\mathbf{S}_y + (a_{5y} - b_{5x})\mathbf{S} + (a_1 + b_2)\mathbf{S}_y \wedge \mathbf{S}_x + (a_3 - b_4)\mathbf{S}_{xy} + a_4\mathbf{S}_{yy} - b_3\mathbf{S}_{xx} = 0. \quad (9)$$

From here we obtain

$$a_{5y} - b_{5x} = -(a_1+b_2)\mathbf{S}\cdot(\mathbf{S}_y \wedge \mathbf{S}_x) + \mathbf{S}\cdot[(a_3-b_4)\mathbf{S}_{xy} + a_4\mathbf{S}_{yy} - b_3\mathbf{S}_{xx}]. \quad (10)$$

The topological charge is given by

$$Q = \frac{1}{4\pi}\iint\{-(a_1+b_2)\mathbf{S}\cdot(\mathbf{S}_x\wedge\mathbf{S}_y) + \mathbf{S}\cdot[(a_3-b_4)\mathbf{S}_{xy} + a_4\mathbf{S}_{yy} - b_3\mathbf{S}_{xx}]\}dxdy. \quad (11)$$

We can show that the spin system corresponding to (8) looks like

$$\mathbf{S}\wedge[a_2\mathbf{S}_{yy} + (a_1-b_2)\mathbf{S}_{xy} - b_1\mathbf{S}_{xx}] + (a_{3y}-b_5)\mathbf{S}_x + (a_5-b_{4x})\mathbf{S}_y = 0, \quad (12a)$$

$$a_{5y} - b_{5x} = (a_1 + b_2)\mathbf{S}\cdot(\mathbf{S}_x \wedge \mathbf{S}_y). \quad (12b)$$

It is the stationary version of the following M-XIII equation

$$\mathbf{S}_t = \mathbf{S}\wedge[a_2\mathbf{S}_{yy} + (a_1-b_2)\mathbf{S}_{xy} - b_1\mathbf{S}_{xx}] + (a_{3y}-b_5)\mathbf{S}_x + (a_5-b_{4x})\mathbf{S}_y, \quad (13a)$$

$$a_{5y} - b_{5x} = (a_1 + b_2)\mathbf{S}\cdot(\mathbf{S}_x \wedge \mathbf{S}_y). \quad (13b)$$

Now we present the various special cases of the spin system (12) induced by the formulas (8).

i) Let a_3, b_4 are constants. Then the system (12) pass to the following set of equations

$$\mathbf{S} \wedge [a_2\mathbf{S}_{yy} + (a_1 - b_2)\mathbf{S}_{xy} - b_1\mathbf{S}_{xx}] - b_5\mathbf{S}_x + a_5\mathbf{S}_y = 0, \quad (14a)$$

$$a_{5y} - b_{5x} = (a_1 + b_2)\mathbf{S}\cdot(\mathbf{S}_x \wedge \mathbf{S}_y). \quad (14b)$$

ii) Now we consider the following special case of the system (8), when

$$a_4 = b_3 = 0, \quad a_5 = b_{4x} + \phi_x, \quad b_5 = a_{3y} - \phi_y. \quad (15)$$

In this case, we have

$$\mathbf{r}_x = a_1\mathbf{S} \wedge \mathbf{S}_x + a_2\mathbf{S} \wedge \mathbf{S}_y + a_3\mathbf{S}_x + (b_{4x} + \phi_x)\mathbf{S}, \quad (16a)$$

$$\mathbf{r}_y = b_1\mathbf{S} \wedge \mathbf{S}_x + b_2\mathbf{S} \wedge \mathbf{S}_y + b_4\mathbf{S}_y + (a_{3y} - \phi_y)\mathbf{S}. \quad (16b)$$

The corresponding spin system reads as

$$\mathbf{S} \wedge [a_2\mathbf{S}_{yy} + (a_1 - b_2)\mathbf{S}_{xy} - b_1\mathbf{S}_{xx}] + \phi_y\mathbf{S}_x + \phi_x\mathbf{S}_y = 0, \quad (17a)$$

$$\phi_{xy} = \frac{(a_1 + b_2)}{2}\mathbf{S}\cdot(\mathbf{S}_x \wedge \mathbf{S}_y). \quad (17b)$$

This system is the stationary variant of the following (2+1)-dimensional M-XIIIA equation

$$\mathbf{S}_t = \mathbf{S} \wedge [a_2\mathbf{S}_{yy} + (a_1 - b_2)\mathbf{S}_{xy} - b_1\mathbf{S}_{xx}] + \phi_y\mathbf{S}_x + \phi_x\mathbf{S}_y, \qquad (18a)$$

$$\phi_{xy} = \frac{(a_1 + b_2)}{2}\mathbf{S} \cdot (\mathbf{S}_x \wedge \mathbf{S}_y). \qquad (18b)$$

Now let us consider the properties of the surface corresponding to the system (16) for the simplest case when $a_3 = b_4 = 0$. In this case the formulas for the tangent vectors (16) become simpler

$$\mathbf{r}_x = a_1\mathbf{S} \wedge \mathbf{S}_x + a_2\mathbf{S} \wedge \mathbf{S}_y + \phi_x\mathbf{S}, \quad \mathbf{r}_y = b_1\mathbf{S} \wedge \mathbf{S}_x + b_2\mathbf{S} \wedge \mathbf{S}_y - \phi_y\mathbf{S}. \quad (19)$$

The consistency relation of the equations (19) gives the spin system (17), so that we can speak that the tangent vectors (19) define the some surface associated with the system (17). Consider this surface in detail. Let us calculate the value

$$\mathbf{r}_x \wedge \mathbf{r}_y = (a_1b_2 - a_2b_1)q\mathbf{S} - (b_1\phi_x + a_1\phi_y)\mathbf{S}_x - (b_2\phi_x + a_2\phi_y)\mathbf{S}_y, \quad (20)$$

where $q = \mathbf{S} \cdot (\mathbf{S}_x \wedge \mathbf{S}_y)$. The topological charge is

$$Q = \frac{1}{4\pi}\int\int qdxdy = \frac{1}{4\pi}\int\int dxdy\mathbf{S} \cdot (\mathbf{S}_x \wedge \mathbf{S}_y). \qquad (21)$$

Hence we have

$$|\mathbf{r}_x \wedge \mathbf{r}_y|^2 = (a_1b_2 - a_2b_1)^2q^2 + (b_1\phi_x + a_1\phi_y)^2\mathbf{S}_x^2 + (b_2\phi_x + a_2\phi_y)^2\mathbf{S}_y^2 +$$

$$2(b_1\phi_x + a_1\phi_y)(b_2\phi_x + a_2\phi_y)\mathbf{S}_x\mathbf{S}_y =$$

$$= (a_1b_2 - a_2b_1)^2q^2 + \{(b_1\phi_x + a_1\phi_y)\mathbf{S}_x + (b_2\phi_x + a_2\phi_y)\mathbf{S}_y\}^2. \qquad (22)$$

Using (20) and (22) we can construct the normal vector of the surface. At the same time, the coefficients of the first fundamental form are given by

$$E = a_1^2\mathbf{S}_x^2 + a_2^2\mathbf{S}_y^2 + 2a_1a_2\mathbf{S}_x\mathbf{S}_y + \phi_x^2,$$

$$F = a_1b_1\mathbf{S}_x^2 + (a_2b_1 + a_1b_2)\mathbf{S}_x\mathbf{S}_y + +a_2b_2\mathbf{S}_y^2 - \phi_x\phi_y, \qquad (23)$$

$$G = b_1^2\mathbf{S}_x^2 + b_2^2\mathbf{S}_y^2 + 2b_1b_2\mathbf{S}_x\mathbf{S}_y + \phi_y^2.$$

Similarly we can calculate the coefficients of the second fundamental form and the other parameters of the surface.

v) At last, we consider the reduction of the system (8) correponding to the case

$$a_4 = b_3 = 0, \quad a_5 = \phi_y, \quad b_5 = -\phi_x. \qquad (24)$$

In this case, instead of (8) we have the following formulas

$$\mathbf{r}_x = a_1\mathbf{S}\wedge\mathbf{S}_x + a_2\mathbf{S}\wedge\mathbf{S}_y + \phi_y\mathbf{S},\ \ \mathbf{r}_y = b_1\mathbf{S}\wedge\mathbf{S}_x + b_2\mathbf{S}\wedge\mathbf{S}_y - \phi_x\mathbf{S}. \quad (25)$$

Now the system (12) becomes

$$\mathbf{S}\wedge[a_2\mathbf{S}_{yy} + (a_1 - b_2)\mathbf{S}_{xy} - b_1\mathbf{S}_{xx}] + \phi_x\mathbf{S}_x + \phi_y\mathbf{S}_y = 0, \quad (26a)$$

$$\phi_{xx} + \phi_{yy} = (a_1 + b_2)\mathbf{S}\cdot(\mathbf{S}_x\wedge\mathbf{S}_y). \quad (26b)$$

It is the stationary version of the following M-XIIIB equation

$$\mathbf{S}_t = \mathbf{S}\wedge[a_2\mathbf{S}_{yy} + (a_1 - b_2)\mathbf{S}_{xy} - b_1\mathbf{S}_{xx}] + \phi_x\mathbf{S}_x + \phi_y\mathbf{S}_y, \quad (27a)$$

$$\phi_{xx} + \phi_{yy} = (a_1 + b_2)\mathbf{S}\cdot(\mathbf{S}_x\wedge\mathbf{S}_y). \quad (27b)$$

4. Generalized surfaces

Finally we would like to note that Eq. (1) admits some interesting generalizations. For example, one of possible generalizations of the MF can be written as

$$\mathbf{r}_x = a_1\mathbf{N}\wedge\mathbf{N}_x + a_2\mathbf{N}\wedge\mathbf{N}_y + a_3\mathbf{N}_x + a_4\mathbf{N}_y + a_5\mathbf{N} + \mathbf{A}, \quad (28a)$$

$$\mathbf{r}_y = b_1\mathbf{N}\wedge\mathbf{N}_x + b_2\mathbf{N}\wedge\mathbf{N}_y + b_3\mathbf{N}_x + b_4\mathbf{N}_y + b_5\mathbf{N} + \mathbf{B}. \quad (28b)$$

In this case, from the compatibility of the equations (28), we obtain some spin systems in 1+1 dimensions. The other perspective generalization of the MF, for example, is given by

$$\mathbf{r}_x = a_1\mathbf{S}\wedge\mathbf{S}_x + a_2\mathbf{S}\wedge\mathbf{S}_y + a_3\mathbf{S}_x + a_4\mathbf{S}_y + a_5\mathbf{S},\quad \mathbf{r}_y = b_1\mathbf{S}\wedge\mathbf{S}_x +$$

$$b_2\mathbf{S}\wedge\mathbf{S}_y + b_3\mathbf{S}_x + b_4\mathbf{S}_y + b_5\mathbf{S},\quad \mathbf{r}_t = \mathbf{F}, \quad (29)$$

where $\mathbf{F}$ is the vector function. Hence we get some new class of (2+1)-dimensional spin systems. Investigation of these generalized MF and related spin systems is now in progress.

5. Conclusion

To conclude, in this note, we have considered the relation between differential geometry of surfaces and some stationary versions of the classical continuous Heisenberg ferromagnets in 2+1 dimensions. In particular, we have studied spin systems induced by the new class of two-dimensional surfaces. These surfaces are some generalizations of the surfaces induced by the well-known from the differential geometry Lelieuvre and Schief formulas.

Acknowledgments

RM would like to thank the organizers for hospitality and for financial support.

References

[1] Lakshmanan M. *Phys. Lett. A,* **61**, 53 (1977)

[2] Tsuchida T., Wadati M. *J. Phys. Soc. Jpn.,* **68**, 2241 (1999)

[3] Rogers C., Schief W.K. Backlund and Darboux Transformations: Geometry and Modern Applications in Soliton Theory. London: Cambridge University Press, 2002.

[4] Backlund and Darboux Transformations. The Geometry of Solitons. CRM Proceedings and Lecture Notes. V.29. Eds. A.Coley, D.Levi, R.Milson, C.Rogers, P.Winternitz. Aarms-Crm Workshop. American Mathematical Society, 2001.

[5] Tenenblat K. Transformations of Manifolds and Application to Differential Equations. London: CRC Press, 1998.

[6] Nonlinearity and Geometry. Eds. D.Wojcik, J.Cieslinski. Warszawa: Polish Scientific Publishers, 1998.

[7] Cieslinski J., Goldstein P., Sym A. *J. Phys. A: Math. Gen.,* **27**, 1645(1994)

[8] Balakrishnan R., Guha P. *J. Math. Phys.,* **37** 3651 (1996)

[9] Myrzakulov R. Integrability of the Gauss-Codazzi-Mainardi equation in 2+1 dimensions. In Progress in Nonlinear Science. Proc. of the Int. Conf. (Nizhny Novgorod, July 2-6, 2001). Mathematical Problems of Nonlinear Dynamics. V.I. Eds. L.M.Lerman, L.P.Shil'nikov. Nizhny Novgorod: University of Nizhny Novgorod, 2002. P.314-319.

[10] Sym A. Soliton Surfaces and Their Applications: Soliton Geometry From Spectral Problems. *Lect. Notes in Phys.,* **239**, 154 (1985)

[11] Doliwa A., Nieszporski M. *J. Phys. A: Math. Gen.,* **34**, 10423 (2001)

[12] Schief W.K. *J. Math. Phys.,* **41**, 6566 (2000)

[13] Myrzakulov R., Vijayalakshmi S., Syzdykova R.N., Lakshmanan M. *J. Math. Phys.,* **39**, 2122 (1998)

[14] Lakshmanan M., Vijayalakshmi S., Danlybaeva A.K., Myrzakulov R. *J. Math. Phys.,* **39**, 3765 (1998)

[15] Lakshmanan M. Geometrical interpretation of (2+1)-dimensional integrable nonlinear evolution equations and localized solutions. Mathematisches Forschungsinstitut Oberwolfach. Report/40/97.ps, p.9.

[16] Gutshabash E.Sh. Some notes on Ishimori's magnet model. E-preprint: *nlin.SI/0302002*

[17] Estevez P.G., Hernaez G.A. Lax pair, Darboux Transformations and solitonic solutions for a (2+1) -dimensional nonlinear Schrodinger equation. E-preprint: *solv-int/9910005*

[18] Chou K.S., Qu C.Z. *J. Phys. Soc. Jpn.,* **71**, 1039 (2002)

[19] Konopelchenko B.G. *Stud. Appl. Math.,* **96**, 9 (1996)

[20] Konopelchenko B.G., Pinkall U. *Geometriae Dedicata,* **6**, 11 (1999)

[21] Ferapontov E.V. Surfaces with flat normal bundle: an explicit construction. E-preprint: *math.DG/9805012*

Index